

ACTA PHYSICA

ACADEMIAE SCIENTIARUM
HUNGARICAE

ADIUVANTIBUS

Z. GYULAI, L. JÁNOSSY, I. KOVÁCS, K. NOVOBÁTZKY

REDIGIT

P. GOMBÁS

TOMUS XIII



AKADÉMIAI KIADÓ, BUDAPEST
1961

ACTA PHYS. HUNG.

LES TRAJECTOIRES DU CHAMP UNIFIÉ

JACK LEVY

INSTITUT HENRI-POINCARÉ, PARIS, FRANCE

(Présenté par K. F. Novobátzky. — Soumis le 29. VIII. 1960)

D'un lagrangien unifié déduction est faite d'un système de quatre identités qui par l'intermédiaire des équations des champs conduisent rigoureusement aux équations des trajectoires.

On peut alors identifier un rapport charge/masse.

Introduction

Après un rappel des déterminations classiques de l'équation des trajectoires en relativité générale nous examinerons divers enrichissements heuristiques de la structure du tenseur impulsion énergie, qui caractérise des fluides granuleux avec tension, pression ou viscosité. Nous allons ensuite considérer un lagrangien dont le choix a déjà été justifié, et nous lui appliquerons une variation de LIE-WEYL; ainsi nous serons conduits à des identités rigoureuses. Par l'intermédiaire des équations des champs on retrouve ensuite, complétée, une expression qui rappelle celle donnant les géodésiques d'EISENHART, et qui apparait comme le système différentiel vérifié par un «courant extremum», compte tenu des phénomènes gravitationnels et électromagnétiques. C'est une loi de force plus générale que celle de LORENTZ.

On peut évidemment donner l'expression rigoureuse du tenseur impulsion énergie $\chi T_{\mu\nu}$ de cette théorie, mais pour l'interpréter nous passerons à l'approximation [10] des champs faibles: supposant $\varphi_{\mu\nu}$ petit nous indiquons pour $\chi T_{\mu\nu}$ une structure qui nous renseignera sur la nature profonde du fluide élémentaire.

Nous avons donc fait deux hypothèses:

— les trajectoires des particules chargées, lignes de courant du fluide, peuvent être obtenues comme une condition de stabilité lors d'une libration infinitésimale de l'ensemble des champs et plus spécialement du champ métrique.

— Après l'obtention des résultats rigoureux nous supposons que le champ électromagnétique est faible vis à vis d'un scalaire de la théorie.

La gravitation

Les équations d'EINSTEIN de la relativité générale s'écrivent dans le cas intérieur

$$S_{\alpha\beta} - \chi T_{\alpha\beta} = 0.$$

Le tenseur $S_{\alpha\beta}$ construit à partir de la connexion affine symétrique est d'origine purement géométrique. Seul, il nous a permis de mettre en équation l'évolution des champs. La matière chargée ou non est décrite par le second membre dont la structure caractérise celle du fluide matériel.

Ainsi $\chi T_{\alpha\beta} = \tau_{\alpha\beta}$ représentera¹ un schéma champ électromagnétique pur. Quant à la matière chargée et à l'état de poussière sans pression [8 p. 97] elle s'introduira par un terme en $\varrho u_\alpha u_\beta$

$$\chi T_{\alpha\beta} = \varrho u_\alpha u_\beta + \tau_{\alpha\beta}, \quad u_\alpha = \frac{dx_\alpha}{ds}$$

et le tenseur d'impulsion énergie d'un fluide visqueux s'écrira²

$$\begin{aligned} \chi T_{\alpha\beta} = & (\varrho + p - \lambda \nabla_\varrho C^\varrho) u_\alpha u_\beta - (p - \lambda \nabla_\varrho C^\varrho) g_{\alpha\beta} + \\ & + \frac{\mu}{2} [\nabla_\alpha C_\beta + \nabla_\beta C_\alpha - \bar{C}^\lambda (\nabla_\lambda C_\alpha C_\beta + \nabla_\lambda C_\beta C_\alpha)]. \end{aligned}$$

Cette complication par juxtaposition ne peut évidemment qu'approcher aveuglément la réalité profonde, et ne possède pas l'harmonie d'une déduction partant d'un cadre géométrique.

Les équations des trajectoires sont alors données simplement: le tenseur $S_{\alpha\beta}$ est naturellement conservatif et par le jeu des équations d'EINSTEIN on en déduit la conservation de $\chi T_{\alpha\beta}$. Ce qui dans l'hypothèse du schéma matière pure donne les équations

$$u^\lambda \nabla_\lambda u_\alpha = 0$$

les trajectoires du vecteur vitesse unitaire sont donc des géodésiques. Par contre le schéma matière — champ électromagnétique engendre, en ajoutant une hypothèse de convection de LORENTZ ($J_\alpha = \mu u_\alpha$) analogue à l'hypothèse sur la forme du tenseur impulsion énergie, l'expression suivante:

$$u^\lambda \nabla_\lambda u_\alpha = F_{\alpha\lambda} \frac{J^\lambda}{\varrho} \quad \begin{array}{l} F_{\alpha\beta}: \text{champ électromagnétique;} \\ J_\alpha: \text{courant;} \mu/\varrho: \text{charge/masse.} \end{array}$$

¹ $\tau_{\alpha\beta}$ tenseur de MAXWELL.

² λ, μ sont des coefficients de viscosité, $F = \exp \int_{p_0}^p \frac{dp}{p+p}$ indice du fluide; ∇ dérivation covariante dans la métrique $\overline{g_{\alpha\beta}} = F^2 g_{\alpha\beta}$; ϱ densité propre et p pression scalaire du fluide.

Les trajectoires du champ unifié

Extension qui se veut directe de la relativité générale, la théorie du champ unifié d'EINSTEIN n'a pas réussi à donner des trajectoires de particules ou tout au moins un système différentiel aux lignes de courant.

En relativité générale les équations du champ jouent un rôle fondamental dans la détermination des équations du mouvement. Ou bien l'identité en divergence se répercute dans le cas intérieur et par l'intermédiaire du tenseur impulsion énergie en quatre identités qui donnent l'écart aux géodésiques: ceci étant essentiellement dû à la présence de la charge. Ou bien la méthode des singularités joue sur le flux d'un vecteur qui est directement issu des équations du cas extérieur [9]. Un seul trait commun, l'apport matériel proposé indépendamment de toute géométrie, tient un rôle déterminant.

D'après le théorème de NOETHER [6] il doit exister quatre identités dites de conservation. WEYL [6, p. 200] et EINSTEIN [7, p. 8] ont utilisé une déformation infinitésimale du continuum, dans le cadre d'une unification des théories électromagnétiques et gravitationnelles, et ont bien déterminé ces identités. Mais si le premier réussit une synthèse de l'électromagnétisme, le second échoue devant le champ unifié.

Nous avons déjà donné un exemple intéressant de fonction d'action unifiée et nous avons expliqué [1] pour quelles raisons son expression nous apparaissait comme ne devant pas être réduite:

$$\mathcal{L} \equiv g^{\mu\nu} [R_{\mu\nu}(r) - m\pi_{\mu\nu}^-] + a (g^{\mu\nu} \Gamma_{\mu} \Gamma_{\nu} - 2\alpha^2 \sqrt{|g|}) \quad (1)$$

($R_{\mu\nu}(r)$ tenseur de Ricci dans la connexion $\Gamma_{\beta\gamma}^a$)

$$\Gamma; \Gamma_{\mu} \equiv \Gamma_{\mu 0}^0; \pi_{\mu\nu}^- \equiv \partial_{\mu} \Gamma_{\nu} - \partial_{\nu} \Gamma_{\mu}; g \det. \text{ de } g_{\mu\nu}; g^{\mu\nu} = \sqrt{|g|} g^{\mu\nu}.$$

En effet la suppression³ d'un composant quelconque introduit des restrictions [10] incompatibles avec la nécessité d'une complète généralité de la théorie et nous le verrons, avec la détermination explicite d'identités de conservation.

Nous allons transposer à ce lagrangien une variation du type LIE-WEYL, sans en chercher pour l'instant une signification physique.

Les identités rigoureuses

Appliquons à la fonction d'action I construite sur ce lagrangien des variations quelconques portant sur la connexion affine $\Gamma_{\beta\gamma}^a$, le scalaire a , le ten-

³ Voir [1]. Partant d'une connexion générale (système A) on peut incorporer partiellement $\pi_{\mu\nu}^-$ au tenseur de RIEMANN d'un schéma à vecteur de torsion nul (système B). Alors particulariser m revient à détruire la définition du courant, comme pour a nul.

seur métrique $g^{\mu\nu}$. Supposons-les indépendantes et nulles aux limites d'intégration, on obtient les équations des champs. Ainsi:

$$G'_a{}^{\beta\gamma} = 0$$

qui simplifiées par contraction donnent:

$$G_a{}^{\beta\gamma} = 0, \quad G_a{}^{\beta\gamma} \equiv \partial_a g^{\beta\gamma} - g^{\beta\gamma} \Gamma_{a\sigma}^\sigma + g^{\beta\sigma} \Gamma_{a\sigma}^\gamma + g^{\sigma\gamma} \Gamma_{a\sigma}^\beta - g^{\beta\gamma} \Gamma_a, \quad (2)$$

$$\partial_e g^{\alpha e} = K g^{\alpha e} \Gamma_e, \quad K = \frac{a}{m}, \quad + K \delta_a^\gamma g^{\beta e} \Gamma_e,$$

puis

$$A \equiv g^{\mu\nu} \Gamma_\mu \Gamma_\nu - 2a^2 = 0, \quad (3)$$

$$L_{\mu\nu} \equiv H_{\mu\nu} - a\alpha^2 g_{\mu\nu} \equiv R_{\mu\nu} - m\pi_{\mu\nu}^- + a \Gamma_\mu \Gamma_\nu - a\alpha^2 g_{\mu\nu} = 0. \quad (4)$$

Mais si l'on fait le choix capital d'une transformation de LIE-WEYL sur les êtres géométriques ou phénoménologiques qui constituent notre espace, on détermine quatre identités. Soit la variation de I

$$\delta I = \int_{D, d\tau} G'_a{}^{\beta\gamma} \delta \Gamma_{\beta\gamma}^a + L_{\mu\nu} \delta g^{\mu\nu} + A \delta a,$$

admettons les équations dites de «liaison»

$$G_a{}^{\beta\gamma} = 0$$

et la normalisation

$$A = 0.$$

De cette manière nous particularisons la variation de l'unique champ phénoménologique $g^{\mu\nu}$. Nous avons:

$$\begin{aligned} \delta x^\mu &\equiv x'^\mu - x^\mu, & \delta g^{\mu\nu} &= -g^{\mu\sigma} \partial_\sigma \xi^\nu - g^{\sigma\nu} \partial_\sigma \xi^\mu + \xi^\sigma \partial_\sigma g^{\mu\nu}, \\ \delta \sqrt{|g|} &= \partial_e (\xi^e \sqrt{|g|}). \end{aligned} \quad (5)$$

Avec des intégrations par parties et à cause de nos hypothèses sur le champ ξ^μ (nul aux frontières de D) il vient:

$$\partial_\lambda [L_{\mu e} g^{\mu\lambda} + L_{e\mu} g^{\lambda\mu}] - g^{\mu\nu} \partial_e L_{\mu\nu} \equiv 0. \quad (6)$$

Faisons immédiatement deux remarques. La forme (6) est analogue à celle obtenue dans les théories usuelles (a ou m nuls). Elle est organiquement vérifiée en admettant les équations (4) du champ $g_{\mu\nu}$.

Remplaçons maintenant $L_{\mu\nu}$ par $H_{\mu\nu} - a\alpha^2 g_{\mu\nu}$, il vient:

$$\partial_\lambda [H_{\mu e} g^{\mu\lambda} + H_{e\mu} g^{\lambda\mu}] - g^{\mu\nu} \partial_e H_{\mu\nu} + 2a^2 \sqrt{-g} \partial_e a \equiv 0. \quad (7)$$

Puis exprimons $H_{\mu\nu}$ par sa définition donnée en (4); scindons-le en parties symétrique et antisymétrique:

$$\begin{aligned} \partial_\lambda \left[R_{\mu\varrho} g^{\mu\lambda} - \frac{1}{2} g^{\mu\nu} R_{\mu\nu} \delta_\varrho^\lambda \right] + \frac{1}{2} R_{\mu\nu} \partial_\varrho g^{\mu\nu} + \partial_\lambda \left[a \left(\Gamma_\lambda \Gamma_\varrho g^{\mu\lambda} - \frac{1}{2} g^{\mu\nu} \Gamma_\lambda \Gamma_\nu \delta_\varrho^\lambda \right) \right] + \\ + \alpha^2 \sqrt{-g} \partial_\varrho a + \frac{1}{2} a \Gamma_\mu \Gamma_\nu \partial_\delta g^{\mu\nu} + \partial_\lambda [H_{\mu\nu} g^{\mu\lambda}] - \frac{1}{2} g^{\mu\nu} \partial_\varrho H_{\mu\nu} \equiv 0. \end{aligned} \quad (8)$$

A une capacité scalaire près on sait [5] que les deux premiers termes constituent la divergence dans la métrique

$$\lambda^{\alpha\beta} \equiv \sqrt{\frac{-1}{g}} h^{\alpha\beta} \quad (h^{\alpha\beta} \equiv g^{\alpha\beta}; h \text{ det. de } h_{\alpha\beta}) \quad (9)$$

du tenseur

$$R_{\alpha\beta} - \frac{1}{2} \lambda_{\alpha\beta} R_{\mu\nu} \lambda^{\mu\nu} \quad (10)$$

que nous décomposerons en⁴

$$S_{\alpha\beta} - \chi M_{\alpha\beta}. \quad (10)$$

On a en définitive la formulation rigoureuse suivante:

$$\begin{aligned} \sqrt{-\gamma} \nabla^\lambda (S_{\varrho\lambda} - \chi M_{\varrho\lambda}) + \partial_\lambda \left[a \left(\Gamma_\mu \Gamma_\varrho g^{\mu\lambda} - \frac{1}{2} g^{\mu\nu} \Gamma_\mu \Gamma_\nu \delta_\varrho^\lambda \right) \right] + \\ + \frac{1}{2} a \Gamma_\mu \Gamma_\nu \partial_\varrho g^{\mu\nu} + \alpha^2 \sqrt{-g} \partial_\varrho a + K H_{\mu\nu} g^{\mu\lambda} \Gamma_\lambda - \\ - \frac{1}{2} g^{\mu\nu} [\partial_\varrho H_{\mu\nu} + \partial_\nu H_{\varrho\mu} + \partial_\mu H_{\nu\varrho}] \equiv 0. \end{aligned} \quad (11)$$

Soit encore:

$$\begin{aligned} a \sqrt{-g} \Gamma_{\lambda\mu}^\lambda + K H_{\lambda\mu} g^{\lambda\sigma} \Gamma_\sigma - \frac{1}{2} g^{\lambda\sigma} (\partial_\mu H_{\lambda\sigma} + \partial_\sigma H_{\mu\lambda} + \partial_\lambda H_{\sigma\mu}) + \\ + \sqrt{-\gamma} \nabla^\lambda (-\chi M_{\mu\lambda}) \equiv 0. \end{aligned} \quad (11)$$

On peut obtenir à partir de cette expression celles habituelles aux nombreuses variantes des théories d'EINSTEIN et de SCHRÖDINGER en faisant a nul.

Notons que dans ce cas la condition nécessaire et suffisante d'obtention d'un théorème de conservation est l'annulation du dernier terme de:

$$\sqrt{-\gamma} \nabla^\lambda [S_{\varrho\lambda} - (\chi M_{\varrho\lambda})_{a=0}] - \frac{1}{2} g^{\mu\nu} (\partial_\varrho H_{\mu\nu} + \partial_\nu H_{\varrho\mu} + \partial_\mu H_{\nu\varrho}) \equiv 0 \quad (12)$$

ce qui entraîne l'identification de $H_{\mu\nu}$ à un rotationn e

⁴ $S_{\gamma\beta}$ est le tenseur d'EINSTEIN dans la métrique $\gamma_{\alpha\beta}$; $-\chi M_{\alpha\beta}$ les termes complémentaires.

Nous allons donner une nouvelle forme à (11). Posons par définition

$$\begin{aligned}\mathcal{F}^{\mu\nu} &\equiv \sqrt{-g} f^{\mu\nu}; \quad f^{\mu\nu} \equiv g^{\mu\nu}_{\nu}; \quad \mathcal{F}(\det. \mathcal{F}_{\mu\nu}) = f/g^2; \quad \frac{1}{2} \varepsilon_{\mu\nu\gamma\beta} \mathcal{F}^{\alpha\beta} = \frac{\mathcal{F}^{\mu\nu}}{\sqrt{F}}; \\ \Phi_{\alpha\beta} &\equiv H_{\alpha\beta}; \quad \Phi \det. de \Phi_{\alpha\beta}; \quad \frac{1}{2} \varepsilon^{\alpha\beta\mu\nu} \Phi_{\mu\nu} = \sqrt{\Phi} \Phi^{\alpha\beta}; \\ I^a &\equiv \partial_\sigma (\sqrt{\Phi} \Phi^{\alpha\sigma}); \quad I^a \equiv h^{\lambda\sigma} \Gamma^a_{\sigma}; \quad (h^{\mu\nu} = g^{\mu\nu}).\end{aligned}\quad (13)$$

Il vient alors toujours rigoureusement:

$$a(\sqrt{-g} \Gamma^\lambda) \pi_{\lambda\mu} \equiv k \Phi_{\mu\lambda} (\sqrt{-g} \Gamma^\lambda) + \mathcal{F}^{-1/2} \mathcal{F}_{\mu\lambda} I^\lambda + \nabla^\lambda (\sqrt{-g} \chi M_{\mu\lambda}). \quad (14)$$

Ce sont diverses expressions des quatre identités qui préservent le choix arbitraire d'un référentiel.

La forme du premier membre appelle deux remarques. En associant à la nouvelle théorie des électrons de DIRAC [3] le symbolisme du tenseur tourbillon [2] on retrouve un terme en $\Gamma^\lambda \pi_{\lambda\mu}$ [1]. D'autre part la définition des géodésiques d'EISENHART fait intervenir une équation que l'on peut écrire sous la forme tensorielle suivante:

$$\lambda_\alpha D_\varrho \lambda_\mu - \lambda_\mu D_\varrho \lambda_\alpha = 0. \quad (15)$$

D_ϱ représentant la dérivation covariante dans la connexion générale $\Gamma^a_{\beta\gamma}$ et λ le vecteur déplacé parallèlement à lui-même. Si l'on suppose que le vecteur est conservatif il vient par contraction une condition nécessaire

$$\lambda^\varrho D_\varrho \lambda_\mu = \lambda_\mu D_\varrho \lambda^\varrho = 0. \quad (16)$$

On peut dire que l'expression (11', 14) met en évidence au second membre un écart, dû aux forces d'origine électromagnétique, par rapport aux lignes de courant. Ces lignes donnent pour le cas électromagnétique l'analogie des géodésiques d'un espace déformé par la gravitation seule.

Les identités approchées

Cependant la signification de cette identité n'apparaît pas clairement. Pour en dégager une interprétation plus précise, considérons les équations de la gravitation:

$$R_{\mu\nu} + a \Gamma_\mu \Gamma_\nu = a^2 \gamma_{\mu\nu}. \quad (17)$$

Nous allons supposer successivement que le champ $\varphi_{\mu\nu}$ est faible, de telle façon que l'on puisse négliger les produits au delà d'un certain ordre [5, 10], et que nous sommes dans un domaine où le scalaire a prend de très grandes valeurs par rapport à $\varphi_{\mu\nu}$.

La première hypothèse permet d'exprimer (17) au second ordre par

$$G_{\mu\nu} + G'_{\mu\nu} + a \Gamma_\mu \Gamma_\nu = a a^2 \gamma_{\mu\nu} \quad (18)$$

avec:⁵

$$\begin{aligned} G'_{\mu\nu} = & \frac{1}{2} [\nabla_\mu K S_\nu + \nabla_\nu K S_\mu] - \frac{1}{2} \nabla^\varrho \left[\varphi^\sigma \cdot_\nu (\nabla_\mu \varphi_{\varrho\sigma} - \nabla_\sigma \varphi_{\mu\varrho} + \nabla_\varrho \varphi_{\sigma\mu}) + \right. \\ & \left. + \text{sym en } \mu, \nu \right] + \frac{1}{6} \nabla^\varrho [K S^\lambda (\varphi_{\mu\lambda} \gamma_{\nu\varrho} + \varphi_{\nu\lambda} \gamma_{\mu\varrho} - 3 \varphi_{\varrho\lambda} \gamma_{\mu\nu})] - \frac{K^2}{2} S_\mu S_\nu \\ & - \left(-\frac{1}{2} \varphi_{\lambda\varrho}^\lambda + \nabla^\lambda \varphi_{\mu\varrho} \right) \left(-\frac{1}{2} \varphi_{\lambda\nu}^\varrho + \nabla^\varrho \varphi_{\lambda\nu} \right) \end{aligned}$$

en effet⁶ on a par construction:

$$R_{\underline{\mu\nu}} \equiv G_{\mu\nu} + \nabla_\varrho U_{\mu\nu}^\varrho - \frac{1}{2} \nabla_\mu \nabla_\nu \log g + U_{\mu\nu}^\varrho U_\varrho - (U_{\mu\varrho}^\lambda U_{\lambda\nu}^\varrho + L_{\mu\varrho}^\lambda L_{\lambda\nu}^\varrho). \quad (19)$$

Ces équations comprennent outre $G_{\mu\nu}$ et les termes en $a a^2$ un terme $G'_{\mu\nu}$ au mieux du premier ordre par rapport à $\varphi_{\mu\nu}$. D'après la définition (10) on a l'expression:

$$-\chi M_{\mu\nu} = G'_{\mu\nu} - \frac{1}{2} \gamma_{\mu\nu} G' \quad (20)$$

mais la contribution de cette quantité ne sera négligeable vis à vis des terme

$$KH_{\underline{\nu}}^{\lambda\varrho} g^{\lambda\sigma} \Gamma_\sigma - \frac{1}{2} g^{\mu\nu} [\partial_\varrho H_{\mu\nu}^\varrho + \partial_\nu H_{\varrho\nu}^\mu + \partial_\mu H_{\nu\varrho}^\mu]$$

que dans la mesure où notre seconde hypothèse est valable. Substituons alors cette valeur dans l'identité (11)':

$$\begin{aligned} a \sqrt{-g} \Gamma^\lambda \pi_{\lambda\mu} + KH_{\underline{\nu}}^{\lambda\varrho} \sqrt{-g} \Gamma^\lambda - \frac{1}{2} g^{\lambda\sigma} (\partial_\mu H_{\lambda\sigma} + \partial_\sigma H_{\mu\lambda} + \partial_\lambda H_{\sigma\mu}) \\ + \sqrt{-g} \nabla^\lambda \left(G'_{\mu\lambda} - \frac{1}{2} \gamma_{\mu\lambda} G' \right) = 0. \end{aligned} \quad (21)$$

⁵ Nous utiliserons indifféremment Γ_α ou S_α (voir [1]).

⁶ $u_{\mu\nu}^\varrho$ partie symétrique de la connexion; $\{\varrho_{\mu\nu}\}$ est le symbole de CHRISTOFFEL et $L_{\mu\nu}^\varrho$ la partie antisymétrique:

$$L_{\mu\nu}^\varrho \equiv \{\varrho_{\mu\nu}\} + U_{\mu\nu}^\varrho + L_{\mu\nu}^\varrho, \quad L_{\mu\nu}^\varrho = 0.$$

Les indices pointés sont élevés ou abaissés par la métrique γ .

Ce sont les trajectoires du vecteur Γ_μ .

Notons enfin, et ceci est très important, que l'expression (21) disparaît identiquement avec a nul et se réduit pour Γ_μ isotrope ($a = 0$) à:

$$\dot{I}^\lambda \nabla_\lambda \dot{I}_\mu = 0. \quad (22)$$

Si l'on suppose a constant, $H_{\mu\nu}$ égal à un rotationnel, et une hypothèse de convection:

$$\Gamma_\mu = \sqrt{2} a u_\mu, \quad u_\mu u^\mu = 1, \quad u_\mu = \frac{dx_\mu}{ds}, \quad (23)$$

on retrouve les résultats de la relativité générale

$$u^\lambda \nabla_\lambda u_\mu - \frac{Ka}{\sqrt{2}} \varphi_{\mu\lambda} u^\lambda = 0. \quad (24)$$

L'importante conclusion que nous retiendrons ici est que, avec a présente nécessaire du scalaire a , le terme Ka apparait comme un rapport de charge à masse.

Le tenseur énergie-impulsion

Donnons enfin la structure rigoureuse du tenseur énergie-impulsion $\chi T_{\mu\nu}$ défini par (10') et les équations de la gravitation (17, 18, 19)

$$\begin{aligned} -\chi T_{\mu\nu} \equiv L_{\mu\nu} - \frac{1}{2} \gamma_{\mu\nu} L_{\alpha\beta} \gamma^{\alpha\beta} - S_{\mu\nu} = R_{\mu\nu} - \frac{1}{2} \gamma_{\mu\nu} R - S_{\mu\nu} - aa^2 \gamma_{\mu\nu} + \\ + a \Gamma_\mu \Gamma_\nu - \frac{\gamma_{\mu\nu}}{2} (-4aa^2 + a \Gamma^\lambda \Gamma_\lambda). \end{aligned} \quad (25)$$

Supposons maintenant [10] que le champ $\varphi_{\mu\nu}$ est petit, en négligeant les termes d'ordre supérieur au second il vient:

$$R_{\mu\nu} = G_{\mu\nu} + G'_{\mu\nu}$$

et enfin:

$$-\chi T_{\mu\nu} = G'_{\mu\nu} - \frac{1}{2} \gamma_{\mu\nu} G' + aa^2 \gamma_{\mu\nu} - \frac{a}{2} \gamma_{\mu\nu} \Gamma^\lambda \Gamma_\lambda + a \Gamma_\mu \Gamma_\nu. \quad (26)$$

BIBLIOGRAPHIE

1. J. LÉVY, J. de Phys. et Rad., **20**, 747, 1959.
2. A. LICHNEROWICZ, Théories relativistes de la gravitation et de l'électromagnétisme, Masson, Paris, 1955.
3. P. A. M. DIRAC, Proc. Roy. Soc. **209 A**, 291, 1951; **212 A**, 330, 1952.
4. KENTARO YANO, Theory of Lie Derivatives. Mon. of Pure and Applied Math., 1955.
5. M. A. TONNELAT, Théorie du champ unifié d'Einstein, Gauthiers Villars, Paris, 1955.
6. E. NOETHER, Nachr. der Ges. d. Wissensch. zu Göttingen, 1918, p. 235.
J. WINOGRADSKY, Cahiers de Phys., no 101, Janvier 1959.
7. H. WEYL, Temps espace matière, Blanchard, Paris, 1922.
8. A. EINSTEIN, Prob. cosmologique, Gauthiers Villars, Paris, 1951.
9. A. EINSTEIN, Fondement de la Relativité Générale, Hermann, Paris, 1933.
10. TAN HOANG PHAM, Problèmes actuels en théorie de la Relativité. p. 77. Ed. de la revue d'optique, Paris, 1955.
10. M. A. TONNELAT, Nuovo Cimento, série X, **3**, 902, 1956.

ТРАЕКТОРИИ ОБЪЕДИНЕННОГО ПОЛЯ

Я. ЛЕВИ

Резюме

Из объединенного лагранжиана выводится система четырех идентичностей, которая через промежуточные выражения уравнения поля строго приводит к уравнениям траекторий. Возможно отождествление отношения заряд/масса.

CLASSICAL RELATIVISTIC MOTION OF A POLE PARTICLE UNDER THE ACTION OF EXTERNAL AND PROPER SCALAR FIELDS

By

I. ABONYI

INSTITUTE OF THEORETICAL PHYSICS, ROLAND EÖTVÖS UNIVERSITY, BUDAPEST

(Presented by K. F. Novobátzky. — Received 20. IX. 1960)

The classical relativistic equations of motion of a pole particle subjected to scalar fields are investigated. It can be shown that in the case of a free particle the equations of motion admit a rigorous solution which corresponds to the uniform rectilinear motion. The probable existence of the runaway solutions is mentioned. It is shown that in a special case the particle can move uniformly along a straight line even under the action of a constant external field. The variation of the rest mass is studied on hand of this example and it is pointed out that the proper field of the particle gives no contribution to the rest mass. An analogue of ELIEZER's integral theorem is derived for a particle moving in a central scalar field. Finally it is shown in a certain approximation that the particle cannot perform a uniform circular motion under the action of the force derived from the Yukawa potential.

§ 1. Introduction

The problem of the classical relativistic motion of point particles in external and proper scalar fields has been investigated in many papers. But the main concern of these publications is almost exclusively with the deduction of the equations of motion from general principles. (See e. g. BHABHA [1], HARISH—CHANDRA [2], HAVAS and his co-workers [3, 4, 5, 6]).

The classical relativistic equations of motion of pole particles are deduced from the relativistic non quantized theory of the scalar field. They are more complicated than those describing the motion of pole particles under the action of external and proper electromagnetic fields. This complication has its origin in the fact that a non-vanishing rest mass belongs to the quanta of the scalar field described by the Klein—Gordon equation. The non-vanishing rest mass is the cause of the tail of Green's function of the scalar field — one of the main differences between the scalar and electromagnetic fields. This tail is the consequence of the fact that the interaction transmitted by these quanta may propagate with any velocity smaller than that of the light in vacuum.

The tail of Green's function of the Klein—Gordon equation leads to curious terms in the equations of motion: integrals extended over the whole past portion of the world line of the particle. That is why the equations of motion in the scalar field turn out to be a strongly coupled system of non-linear integro-differential equations.

In spite of the mathematical problems concerning the solution of such a system of equations, there has been a gradually increasing interest in the problems of motion in a scalar field. One may understand this.

The relativistic dynamics was originally based upon the properties of the Lorentz force. Later the physicists observed that there exists an important force of quite different origin and nature, which plays the main role in the nuclear processes. The simplest relativistic model of the nuclear forces — and an example of non-electromagnetic forces at all — can be constructed just by means of the theory of the scalar field.

In the analysis of motion in a scalar field the researchers have in general to introduce drastic approximations (see e. g. P. HAVAS and C. R. MEHL [4], J. SAWICKI [7]). The test-particle approximation systematically expounded by G. MARX and G. SZAMOSI [8] gave important and interesting results (rest-mass variation theorem, theory of the relativistic repulsive core, etc.), but without taking into account the effect of the proper field.

In order to join in this line of the investigations we analysed the possibilities of the solution of the equations of motion in a scalar field.

§ 2. The equations of motion

Let τ denote the proper time, $z^\mu(\tau)$ the world-line, and

$$v^\mu = \frac{dz^\mu(\tau)}{d\tau} = \dot{z}^\mu(\tau) \quad (1)$$

the four-velocity of the pole particle. The Einstein summation convention is understood for Greek indices occurring twice, from 0 to 3, the zero index corresponding to the time component. The velocity of light in vacuum is taken to be unity.

As is well known from the theory of the scalar field, the equations of motion have the general form

$$\frac{d}{d\tau}[(m + U_e + U_p)v^\mu] = F_e^\mu + F_p^\mu, \quad (2)$$

where m is the rest mass, F_e^μ and F_p^μ the external and proper scalar forces, U_e and U_p the respective potentials.

If we restrict ourselves to retarded interactions only, then — according to HAVAS [3] — we arrive at the equations

$$m\dot{v}^\mu - \frac{g^2}{3} (\ddot{v}^\mu + v^\mu \dot{v}_\sigma \dot{v}^\sigma) - \frac{1}{2} g^2 \chi^2 v^\mu + \\ + g^2 \chi^2 \int_{-\infty}^{\tau} \frac{s^\mu}{s^2} J_2(\chi s) d\sigma' + g^2 \chi \frac{d}{d\tau} \left[v^\mu \int_{-\infty}^{\tau} \frac{1}{s} J_1(\chi s) d\tau \right] = gF^\mu + g \frac{d}{d\tau} [v^\mu U]. \quad (3)$$

Here g stands for the coupling constant (mesonic charge) and χ is \hbar^{-1} times the rest mass of the quantum associated with the scalar field. J_n represents the Bessel function of order n . In the integrals we have s^μ and s defined by the relations

$$s^\mu = z^\mu(\tau) - z^\mu(\tau') \quad (4)$$

and

$$s = + (s_\sigma s^\sigma)^{1/2}. \quad (5)$$

Finally U and

$$F^\mu = - \frac{\partial U}{\partial x_\mu} \quad (6)$$

denote the external scalar potential and force, respectively.

In order to attribute physical meaning to the solutions of the equations (3) we must demand that the extra condition

$$\dot{v}_\sigma \dot{v}^\sigma = 1 \quad (7)$$

be satisfied.

§ 3. Rigorous special solutions of the equations of motion

Unfortunately there is no mathematical method which would give directly all the solutions of the equations (3) in the general case. Therefore we must use either some indirect methods (e. g. trial functions) or some approximative methods.

First we consider the rigorous solutions which can be obtained using simple trial functions.

a) Everywhere vanishing external forces, uniform rectilinear motion

The equations to be solved in this case are the following:

$$m\dot{v}^\mu - \frac{g^2}{3} (\ddot{v}^\mu + v^\mu \dot{v}_\sigma \dot{v}^\sigma) - \frac{1}{2} g^2 \chi^2 v^\mu + \\ + g^2 \chi^2 \int_{-\infty}^{\tau} \frac{s^\mu}{s^2} J_2(\chi s) d\tau' + g^2 \chi \frac{d}{d\tau} \left[v^\mu \int_{-\infty}^{\tau} \frac{1}{s} J_1(\chi s) d\tau' \right] = 0 \quad (8a)$$

and

$$v_\sigma \dot{v}^\sigma = 1. \quad (8b)$$

Based on the properties of the Bessel functions one can demonstrate the following statements.

The equations (8a, b) admit a rigorous solution of the form

$$z^\mu(\tau) = a^\mu + b^\mu \tau, \quad (9)$$

where a^μ and b^μ are arbitrary four-vectors, that do not depend on the proper time. They are arbitrary in the sense that

$$b_\sigma b^\sigma = 1 \quad (10)$$

must hold and the other components must be compatible with the prescribed initial values. The solution (9) describes a uniform rectilinear motion corresponding to the initial conditions

$$\left. \begin{aligned} z^\mu(0) &= a^\mu, \\ \dot{z}^\mu(0) &= b^\mu, \\ \ddot{z}^\mu(0) &= 0. \end{aligned} \right\} \quad (11)$$

b) *Everywhere vanishing force, the possible existence of a non-uniform motion*

The problem of self-accelerating, runaway solutions is of great importance in the field theory [10].

It can be shown that considering rectilinear motions only, the world-line of a free particle can be given in the form

$$\left. \begin{aligned} z^0(\tau) &= A^{-1} \operatorname{sh} A\tau + C^0, \\ z^1(\tau) &= A^{-1} \operatorname{ch} A\tau + C^1. \end{aligned} \right\} \quad (12)$$

(C^0 and C^1 are the constants of integration) if and only if A is the root of the equation

$$mA + g^2 \chi^2 I_0(A^{-1} \chi) K_0(A^{-1} \chi) = 0, \quad (13)$$

with I_0 and K_0 representing the modified Bessel and Neumann functions of zero order.

The solution (12) corresponds to the following initial conditions:

$$\left. \begin{aligned} z^\mu(0) &= \{C^0, A^{-1} + C^1, 0, 0\}, \\ \dot{z}^\mu(0) &= \{1, 0, 0, 0\}, \\ \ddot{z}^\mu(0) &= \{0, A, 0, 0\}. \end{aligned} \right\} \quad (14)$$

As we have pointed out in a previous paper the motion described by the solution differs from the self-accelerating solution obtained in the relativistic theory of electron motion, since the characteristic equation (13) has no real roots for A . On the other hand the solutions with complex A probably have

also an oscillatory character superimposed on the runaway character. (In the case of $\chi = 0$ we arrive at the same runaway solution as in the case of the classical electron.)

c) Uniform motion in a special constant external field

Let us consider the motion of a particle in an external field F^μ , which is constant everywhere. Taking

$$U = -F^\sigma x_\sigma,$$

the equations of motion to be solved are:

$$\begin{aligned} m\dot{v}^\mu - \frac{g^2}{3}(\ddot{v}^\mu + v^\mu \dot{v}_\sigma \dot{v}^\sigma) - \frac{1}{2}g^2\chi^2 v^\mu + g^2\chi^2 \int_{-\infty}^{\tau} \frac{s^\mu}{s^2} J_2(\chi s) d\tau' + \\ + g^2\chi \frac{d}{d\tau} \left[v^\mu \int_{-\infty}^{\tau} \frac{1}{2} J_1(\chi s) d\tau' \right] = gF^\mu - gF^\sigma \frac{d}{d\zeta} [v^\mu z_\sigma] \end{aligned} \quad (15a)$$

and

$$\dot{v}_\sigma \dot{v}^\sigma = 1. \quad (15b)$$

It is easy to observe that our statements mentioned in section a) § 3 can be generalized readily to apply in this case.

The equations of motion (15a, b) admit a rigorous solution of the form (9) provided that

$$b_\sigma b^\sigma = 1$$

and

$$F^\mu - b^\mu b_\sigma F^\sigma = 0. \quad (16)$$

In non-trivial cases the latter condition is equivalent to the following:

$$b^\mu = kF^\mu. \quad (17)$$

This shows that this solution exists in the case if the four-vector of the velocity is parallel to that of the force at the initial moment. Then this force will be non-accelerating [8].

In order to elucidate the situation we must study the rest mass variation in the case of the equations of motion containing also the proper field. Rearranging the terms in the equations (3) we write

$$\begin{aligned} \frac{d}{d\tau} \left[\left(m - gU + g^2\chi \int_{-\infty}^{\tau} \frac{1}{s} J_1(\chi s) d\tau' \right) v^\mu \right] - \frac{1}{3}g^2(\ddot{v}^\mu + \dot{v}^\mu \dot{v}_\sigma \dot{v}^\sigma) - \frac{1}{2}g^2\chi^2 v^\mu + \\ + g^2\chi^2 \int_{-\infty}^{\tau} \frac{s^\mu}{s^2} J_2(\chi s) d\tau' = gF^\mu. \end{aligned} \quad (18)$$

Then we introduce

$$M(\tau) = m - gU - g^2 \chi \int_{-\infty}^{\tau} \frac{1}{s} J_1(\chi s) d\tau' \quad (19)$$

as the proper-time dependent dynamical rest mass. Performing the differentiations in (18), we multiply it by v^μ and arrive at

$$\frac{dM}{d\tau} = g v_\sigma F^\sigma + \frac{1}{2} g^2 \chi^2 - g^2 \chi^2 v_\sigma \int_{-\infty}^{\tau} \cdot \frac{s^\sigma}{s^2} J_2(\chi s) d\tau'. \quad (20)$$

Substituting the value of z^μ according to (9) we get from (20)

$$\frac{dM}{d\tau} = gk. \quad (21)$$

This evidently leads to

$$M(\tau) = gk\tau + M_0 \quad (22)$$

with

$$M_0 = m + gkb_\sigma a^\sigma. \quad (23)$$

The equation (22) shows that the action of the force appears only in the change of the rest mass of the particle during its motion in the non-accelerating constant scalar field. The change is monotonously increasing if b^μ and F^μ are parallel ($k > 0$), monotonously decreasing if they are antiparallel ($k < 0$). The second term in (23) corresponds to the mass equivalent of the initial potential energy.

§ 4. On the possibility of a first integral of the equations of motion for central external fields

Let us consider the motion of a particle in a central external field which may be derived from the potential $U = U(r)$, where $r = |r|$, r is the position vector in a three-dimensional Cartesian system of reference, whose origin is at the centre of the attraction or repulsion. We write the equations of motion in the form

$$\begin{aligned} n\ddot{r} - \frac{g^2}{3} (\ddot{r} + \dot{r}(\dot{r}^2 - \ddot{r}^2)) - \frac{1}{2} g^2 \chi^2 \dot{r} + g^2 \chi^2 \int_{-\infty}^{\tau} \frac{\ddot{s}}{s^2} J_2(\chi s) d\tau' + \\ + g^2 \chi \left[\dot{r} \int_{-\infty}^{\tau} \frac{1}{s} J_1(\chi s) d\tau' \right] = -g \frac{dU}{dr} - \frac{r}{r} + r \frac{d}{d\tau} [\dot{r}U], \end{aligned} \quad (24)$$

neglecting the non-independent zero component equation. Here

$$\mathbf{s} = \mathbf{r}(\tau) - \mathbf{r}(\tau') \quad (25)$$

is the three-vector constructed from the last three components of s^μ . Multiplying the equation (24) by the vectorial product $\mathbf{r} \times \dot{\mathbf{r}}$ and re-arranging the terms we obtain

$$\begin{aligned} & \left(m - gU + g^2 \chi \int_{-\infty}^{\tau} \frac{1}{s} J_1(\chi s) d\tau' \right) (\mathbf{r}\ddot{\mathbf{r}}) - \frac{g^2}{3} (\mathbf{r}\ddot{\mathbf{r}}) = \\ & = g^2 \chi \int_{-\infty}^{\tau} \frac{(\mathbf{r}(\tau) \mathbf{r}(\tau') \dot{\mathbf{r}}(\tau))}{s^2} J_2(\chi s) d\tau'. \end{aligned} \quad (26)$$

This integro-differential equation can be considered as the analogue of ELIEZER's integral theorem [11] concerning the motion of electric charges in electromagnetic fields.

If $\mathbf{r}(\tau)$, $\mathbf{r}(\tau')$ and $\dot{\mathbf{r}}(\tau)$ are complanar vectors for all τ and τ' then

$$V(\tau) = (\mathbf{r}\ddot{\mathbf{r}}) \quad (27)$$

satisfies the differential equation

$$\frac{g^2}{3} \dot{V}(\tau) - M(\tau) V(\tau) = 0. \quad (28)$$

The solution of the equation (28) is

$$V(\tau) = V(\tau_0) \exp \left\{ \frac{3}{g^2} \int_{\tau_0}^{\tau} M(\tau') d\tau' \right\}, \quad (29)$$

where $V(\tau_0)$ is the volume of the parallelepiped whose edges are $\mathbf{r}(\tau_0)$, $\dot{\mathbf{r}}(\tau_0)$ and $\ddot{\mathbf{r}}(\tau_0)$. But if $V(\tau_0) = 0$, that is the vectors are complanar at the moment τ_0 , they will remain complanar always. In other words, if the motion starts with complanar \mathbf{r} , $\dot{\mathbf{r}}$ and $\ddot{\mathbf{r}}$, the result will be a motion confined to a plane. Non-complanar start is followed by a motion which deviates from the planar motion according to the equation (28). One cannot draw further inferences without the concrete knowledge of $M(\tau)$ in this case.

In the general case we have the equation

$$\dot{V}(\tau) - \frac{3}{g^2} M(\tau) V(\tau) = 3 \chi^2 \int_{-\infty}^{\tau} \frac{\mathbf{r}(\tau) \dot{\mathbf{r}}(\tau) \dot{\mathbf{r}}(\tau')}{s^2} J_2(\chi s) d\tau'. \quad (30)$$

Its general solution can be given formally by the expression

$$V(\tau) = 3\chi^2 \exp \left[\frac{3}{g^2} \int_{\tau_0}^{\tau} M(\tau') d\tau' \right] \int_{\tau_0}^{\tau} \int_{-\infty}^{\bar{\tau}} \frac{\tau(\tau) \dot{\tau}(\tau) \tau(\tau'')}{s^2(\tau, \tau'')} J_2(\chi s(\bar{\tau}, \tau'')) \cdot \exp \left[-\frac{3}{g^2} \int_{\bar{\tau}_0}^{\bar{\tau}} M(\bar{\tau}) d\bar{\tau} \right] d\bar{\tau} d\tau'', \quad (31)$$

but its physical content cannot be revealed unless we know the actual motion precisely. So in the general case this theorem does not help to solve the equations of motion.

§ 5. On the problem of uniform revolution around a center of attraction

If we are interested in the possibility of the uniform revolution of a particle around a center of attraction, we may start with trial functions of the form:

$$z_0 = t, \quad z^1 = R \sin t, \quad z^2 = R \cos t, \quad z^3 = 0 \quad (32)$$

which do not contradict the theorem deduced in the previous paragraph. The derivation of the "characteristic equations" belonging to the trial functions (32) cannot be done without some simplifying assumptions. The approximations used in the calculations were the following: provided that the main part of the interaction with the proper field can be restricted to a finite time interval $(\tau - \tau')$, the calculations are justified for the values of ω obeying the relation $\omega(\tau - \tau') < 1$. A cumbersome calculation shows that the characteristic equations of the problem do not allow solutions which can be interpreted physically. This shows that the classical two-nucleon problem has no solution of the form (32).

§ 6. Conclusions

The study of the motion of a particle in a scalar field meets with much greater difficulties than those encountered in the (electromagnetic) vector fields. Exact results were obtained in the simplest cases only. Non-trivial problems might be treated — if at all — only by powerful special calculating machines, because the mathematical problems of the solution of coupled non-linear integro-differential equations do not seem to be sufficiently cleared up.

§ 7. Acknowledgements

The author wishes to express his grateful thanks to Prof. G. MARX for suggesting the problem and for his valuable advice. The author is indebted also to Profs. G. SANSONE and F. CONTI (Florence), G. FREUD, F. KÁROLY-HÁZY and M. MIKOLÁS for the interesting discussions on the mathematical problems.

REFERENCES

1. H. J. ВНАВНА, Proc. Roy. Soc. A. **172**, 384, 1939.
2. HARISH-CHANDRA, Proc. Roy. Soc., A. **185**, 269, 1946.
3. P. HAVAS, Phys. Rev., **87**, 309, 1952.
4. C. R. MENL and P. HAVAS, Phys. Rev., **91**, 393, 1953.
5. P. HAVAS, Phys. Rev., **93**, 822, 1954.
6. F. R. CROWNFELD and P. HAVAS, Phys. Rev., **94**, 471, 1954.
7. J. SAWICKI, Acta Phys. Hung., **5**, 381, 1956.
8. G. MARX and G. SZAMOSI, Acta Phys. Hung., **4**, 219, 1954.
9. I. ABONYI, Nuovo Cim., X **15**, 991, 1960.
10. P. A. M. DIRAC, Proc. Roy. Soc., A. **167**, 148, 1938.
11. C. J. ELIEZER, Rev. Mod. Phys., **19**, 147, 1947.

КЛАССИЧЕСКОЕ РЕЛЯТИВИСТИЧЕСКОЕ ДВИЖЕНИЕ ТОЧЕЧНОЙ ЧАСТИЦЫ
ПОД ДЕЙСТВИЕМ ВНЕШНЕГО И СОБСТВЕННОГО СКАЛЯРНОГО ПОЛЯ

И. АБОНИ

Резюме

В статье рассмотрена проблема классического релятивистического движения точечной частицы в скалярном поле. Доказано, что в случае свободной частицы уравнения движения имеют решение, соответствующее равномерному и прямолинейному движению. Упомянуто, что уравнения движения могут иметь автоускорительные решения. Доказывается, что в специальном случае частица может двигаться равномерно и прямолинейно и под действием постоянного внешнего поля. При анализе этой задачи изучена вариация массы покоя и показано, что собственное поле частицы не оказывает влияния на вариацию массы покоя. Интегральная теорема Элиезера обобщена для случая движения в центральном скалярном поле. Наконец, показано в некотором приближении, что частица не может совершать равномерное вращение на постоянном расстоянии от центра силы под действием поля, происходящего от потенциала Юкава.

PROPAGATORS WITH DIPOLE GHOSTS FOR FERMION FIELDS

By

K. L. NAGY

INSTITUTE OF THEORETICAL PHYSICS, ROLAND EÖTVÖS UNIVERSITY, BUDAPEST

(Presented by K. F. Novobátzky — Received: 4. X. 1960)

The spectral representation of propagators for relativistic fermion fields has been calculated in field theories, where the existence of dipole ghost states with $p_0 \geq 0$ are assumed. This general result is compared with a form obtained by MITTER in a certain approximation for a HEISENBERG type of theory.

In the theory of the elementary particles proposed by HEISENBERG [1] the field equations — showing an appropriate transformation character — are completed by using the form

$$\frac{1}{2} S'(p) = \int \varrho(\kappa^2) d\kappa^2 \left\{ \frac{\gamma_\mu p_\mu + i\kappa}{p^2 + \kappa^2} - \frac{\gamma_\mu p_\mu + i\kappa}{p^2} + \frac{\gamma_\mu p_\mu \kappa^2}{(p^2)^2} \right\} \quad (1)$$

for the vacuum expectation value of the propagator

$$S'(x - x') = \langle 0 | \{ \psi(x), \bar{\psi}(x') \} | 0 \rangle, \quad (2)$$

where $|0\rangle$ is the real vacuum state and $\psi(x)$ is the matter field operator in the HEISENBERG picture. The form (1) was stated [1] to be a consequence of the field equations and to correspond to a field theory with an indefinite metric and especially to a theory with indefinite metric with only dipole ghosts [2]. Using, however, the general method of KÄLLÉN and LEHMANN [3], it was shown [4] on the other hand that in a relativistic field theory the relativistic generalization of a dipole ghost state gives a result similar but not identical to that represented in (1).

Recently MITTER [5] — using essentially a Tamm–Dancoff type approximation method — obtained a form for S' different from (1):

$$\frac{1}{2} S'(p) = \int_0^\infty \varrho(\kappa^2) d\kappa^2 \frac{\gamma_\mu p_\mu}{p^2 + \kappa^2}, \quad (3)$$

where a Touschek invariance had been also required and in the first approximation mentioned above

$$\varrho(\kappa^2) = \alpha \lim_{\varepsilon \rightarrow 0} \delta'(\kappa^2 - \varepsilon). \quad (4)$$

Here a is an appropriate constant built up from the universal length occurring in HEISENBERG's field equation and the limes procedure is understood to be performed after the integration. The form (3) and (4) was stated in [5] to correspond to a dipole ghost of zero rest mass.

Here we repeat the general KÄLLÉN—LEHMANN calculations for a fermion field with dipole ghost states, since in [4] the calculations were performed only for a scalar (pseudoscalar) field, and compare the general results thus obtained with MITTER's form of S' . The main line of obtaining the spectral representation of a fermion propagator S' corresponding to a dipole ghost is the same as in [4]. In connection with the indefinite metric the terminology found in [6] is used.

Thus we suppose that there exists an energy-momentum four-vector P_μ with the property

$$[P_\mu, \psi] = i \partial_\mu \psi \quad (5)$$

and treat a field theory with dipole ghost states, according to which one finds states with the properties:

$$\begin{aligned} (P_\mu - p_\mu) |p\rangle &= 0, \langle p | p\rangle = 0; p^2 \leq 0; \\ (P_\mu - p_\mu) |pD\rangle &= C_\mu |p\rangle; \langle pD | pD\rangle = 0. \end{aligned} \quad (6)$$

Here because of relativistic invariance

$$C_\mu = f(p^2) p_\mu. \quad (7)$$

$|pD\rangle$ is the dipole ghost state corresponding to the eigenstate $|p\rangle$ both with zero norm. $|p\rangle$ and $|pD\rangle$ are not orthogonal

$$\langle pD | p'\rangle = a(p^2) \delta p p'. \quad (8)$$

From (6) and (7) $\langle pD | P_\mu | pD\rangle = C_\mu a(p^2)$, thus $f(p^2) a(p^2)$ is real. From (6) and (8) the unit operator is

$$\sum \left\{ |pD\rangle \frac{1}{a^*} \langle p| + |p\rangle \frac{1}{a} \langle pD| \right\} \quad (9)$$

and thus

$$\begin{aligned} S' = \sum \left\{ \langle 0 | \psi(x) | pD\rangle \frac{1}{a^*(p^2)} \langle p | \bar{\psi}(x') | 0\rangle + \right. \\ \left. + \langle 0 | \psi(x) | p\rangle \frac{1}{a(p^2)} \langle pD | \bar{\psi}(x') | 0\rangle \right\} + \{x \leftrightarrow x'\}. \end{aligned} \quad (10)$$

Equations (5), (6), (7) and (10) give

$$\begin{aligned}
 S' = & \sum e^{ip(x-x')} \left\{ \langle 0 | \psi(0) | p D \rangle \frac{1}{a^*(p^2)} \langle p | \bar{\psi}(0) | 0 \rangle + \right. \\
 & + \langle 0 | \psi(0) | p \rangle \frac{1}{a(p^2)} \langle 0 | \bar{\psi}(0) | 0 \rangle \left. \right\} + \\
 & + \sum i p_\mu (x - x')_\mu e^{ip(x-x')} \left\{ \frac{f(p^2) a(p^2)}{a^*(p^2) a(p^2)} \langle 0 | \psi(0) | 0 \rangle \right. \\
 & \left. \langle p | \bar{\psi}(0) | 0 \rangle \right\} + \{x \leftrightarrow x'\}.
 \end{aligned} \tag{11}$$

Introducing

$$\begin{aligned}
 - (2\pi)^3 \sum & \left\{ \langle 0 | \psi(0) | p D \rangle \frac{1}{a^*(p^2)} \langle p | \bar{\psi}(0) | 0 \rangle + \right. \\
 & + \langle 0 | \psi(0) | p \rangle \frac{1}{a(p^2)} \langle p | \bar{\psi}(0) | 0 \rangle = \\
 & = (i\gamma p - \sqrt{-p^2}) \varrho_1(-p^2) + \varrho_2(-p^2),
 \end{aligned}$$

and

$$\begin{aligned}
 - (2\pi)^3 \sum & \left\{ \frac{f(p^2) a(p^2)}{a^*(p^2) a(p^2)} \langle 0 | \psi(0) | p \rangle \langle p | \bar{\psi}(0) | 0 \rangle \right\} = \\
 & = (i\gamma p - \sqrt{-p^2}) \varrho_3(-p^2) + \varrho_4(-p^2),
 \end{aligned}$$

where Lorentz invariance has been required, we finally obtain

$$\begin{aligned}
 S'(x - x') = & \int_0^\infty [S(x - x'; \kappa^2) \varrho_1(\kappa^2) + \Delta(x - x'; \kappa^2) \varrho_2(\kappa^2) + \\
 & + (x - x')_\mu \partial_\mu \{ S(x - x'; \kappa^2) \varrho_3(\kappa^2) + \Delta(x - x'; \kappa^2)^* \varrho_4(\kappa^2) \}] d\kappa^2.
 \end{aligned} \tag{12}$$

Each function ϱ_i is real and may be also negative and LEHMANN's inequality

$$0 \leq \varrho_2(\kappa^2) \leq 2\kappa \varrho_1(\kappa^2)$$

does not hold. Fermion propagators in field theories with ghost states of higher pole order can be calculated in a similar way with the result that there new

and new terms appear containing as many derivatives multiplied by the distances as the dipole order of the ghost state (Cf. [7]).

Requiring an additional Touschek invariance $\varrho_2 \equiv \varrho_4 \equiv 0$ and

$$S'(a - a') = \int_0^\infty \{ \varrho_1(\kappa^2) + \varrho_3(\kappa^2)(x - x')_\mu \partial_\mu \} \gamma_\nu \partial_\nu \Delta(x - x'; \kappa^2) d\kappa^2. \quad (13)$$

Since

$$x_\mu \partial_\mu S(x; \kappa^2) = -2S(x; \kappa^2) - i\gamma_\mu \partial_\mu \Delta(x; \kappa^2) - 2\kappa^2 \frac{\gamma p + i\kappa}{(p^2 + \kappa^2)^2} e^{ikx} dk,$$

these general principles allow MITTER's form of S' (3) and (4) to correspond to dipole ghost states, but the form (1) does not.

The author is greatly indebted to Dr. H. MITTER for sending him a preprint of his interesting article.

REFERENCES

1. W. HEISENBERG, Rev. Mod. Phys., **29**, 269, 1957.
2. W. HEISENBERG, Zeits. Phys., **144**, 1, 1956.
3. G. KÄLLÉN, Helv. Phys. Acta, **25**, 417, 1952; H. LEHMANN, Nuovo Cimento, **11**, 342, 1954.
4. K. L. NAGY, Nuovo Cimento, **15**, 993, 1960.
5. H. MITTER, Zeits. Naturfor., **159**, 753, 1960.
6. K. L. NAGY, Nuovo Cimento Suppl., **17**, 92, 1960.
7. K. L. NAGY, Nuovo Cimento, **17**, 384, 1960.

ФУНКЦИИ РАСПРОСТРАНЕНИЯ С ДИПОЛЬНЫМ ДУХОМ ДЛЯ ФЕРМИОННЫХ ПОЛЕЙ

К. Л. НАДЬ

Резюме

Определяется спектральное представление функций распространения релятивистических фермионных полей в теории поля, в которой предполагается существование состояний дипольных духов $p_0 \geq 0$. Выведенный общий результат сравнивается с формой, полученной Миттером для определенного приближения теории типа Гейзенберга.

MEASUREMENT OF THERMAL NEUTRON DIFFUSION PARAMETERS IN WATER AND IN SOLID DIPHENYL WITH PULSED NEUTRON SOURCE

By

A. ÁDÁM, L. BOD and L. PÁL

CENTRAL RESEARCH INSTITUTE FOR PHYSICS, BUDAPEST

(Presented by L. Jánosy — Received 14. X. 1960)

The diffusion parameters of thermal neutrons were measured in water and in solid diphenyl at room temperature by the pulse method. The results of the measurements in water are consistent within the statistical error with the values known in literature. The diffusion parameters obtained in diphenyl are: $l_0 = 286 \pm 23 \mu \text{ sec}$, $D(T_0) = 42940 \pm 1800 \text{ cm}^2 \text{ sec}^{-1}$, $L_D = 3,50 \pm 0,18 \text{ cm}$, $C = 13300 \pm 2850 \text{ cm}^4 \text{ sec}^{-1}$ and $\lambda_t = 0,515 \text{ cm}$.

Introduction

In investigations into the properties of organic moderators, the development of methods for the measurement of nuclear constants is considered to be of great importance.

In this paper the application of the pulsed neutron technique developed for measuring the diffusion parameters of thermal neutrons will be described. The use of pulsed neutron technique has become extensive, starting in 1953 [1]. This is due to a number of advantages as compared with the stationary method. The diffusion constant D , the mean lifetime l_0 , and the thermalization constant C can be determined by the pulsed neutron technique in a relatively short time and on small quantities of material. For the stationary method usually more material is needed and the parameters D and l_0 can be discriminated only by the "poisoning method" (C is not measurable at all). In addition, the latter procedure is rather lengthy though the values obtained for the diffusion length are more accurate than those determined by the pulse method.

After short theoretical considerations the measuring apparatus will be described and the results obtained for water and solid diphenyl will be given.

Theoretical considerations

Let $t = -t_s$ be the time at which a short burst of fast neutrons occurs in the moderator, then t_s is the time required by the neutrons to reach thermal equilibrium with the nuclei of the moderator. The behaviour of the neutron gas can then be described for $t > 0$ by the diffusion equation

$$\frac{\partial}{\partial t} n(t, \vec{r}) = D(T_n) \Delta n(t, \vec{r}) - \frac{1}{l_0} n(t, \vec{r}), \quad (1)$$

where $n(t, \vec{r})$ is the thermal neutron density at time t in the point \vec{r} , $D(T_n)$ is the diffusion constant for neutrons which have reached thermal equilibrium, l_0 is the mean lifetime of neutrons in an infinite moderator.

The solution of (1) vanishing at the extrapolated boundary of a cylindrical tank with radius R and height H is

$$n(t, \vec{r}) = e^{-t/l_0} \sum_{l,m,n} S_{lmn} J_m \left(\alpha_{ml} \frac{r}{R} \right) \cos m\varphi \cdot \sin \frac{n\pi z}{H} e^{-B_{lmn}^2 D(T_n)t}. \quad (2)$$

Here

$$l, n = 1, 2, 3, \dots,$$

$$m = 0, 1, 2, \dots,$$

α_{ml} is the l -th zero of the m -th order Bessel function of the first kind, and

$$B_{lmn}^2 = \left(\frac{\alpha_{ml}}{R} \right)^2 + \left(\frac{n\pi}{H} \right)^2. \quad (3)$$

The amplitudes S_{lmn} are determined by the initial thermal neutron density.

From (3) it is seen that the lowest indices stand for the lowest value among the constants B_{lmn}^2 . Thus, the variation in neutron density with time becomes exponential a sufficiently long time after the neutron burst and the term involved in the exponent will be precisely B_{101}^2 , that is

$$n(t, \vec{r}) \approx S_{101} J_0 \left(\alpha_{01} \frac{r}{R} \right) \cdot \sin \frac{\pi z}{H} e^{-t/l}$$

and

$$\frac{1}{l} = \frac{1}{l_0} + D(T_n) B_{101}^2. \quad (4)$$

The quantity B_{101}^2 , i. e. the geometric buckling of the cylinder will be denoted from now on by B_0^2 .

Let us now consider more fully the diffusion constant in (4). As previously said, $D(T_n)$ refers to the equilibrium temperature T_n of the neutrons. T_n is known to be in general different from T_0 , the moderator temperature. Physically this is due to the fact that the energy spectrum of the net neutron flux in a given volume element is different from the energy spectrum of the neutrons present at the same time in this volume element. The energy spectrum of the net neutron flux shifts toward the higher velocities. As a result of this the energy distribution of the neutrons present in the volume element ΔV at \vec{r} will change in consequence of two effects:

1. collisions and
2. spatial motion of neutrons.

The collisions will produce in the neutron gas of a temperature above T_0 "cooling", while in that of a temperature below T_0 "heating". Thus, if the collisions alone were responsible for the energy spectrum, the equilibrium neutron temperature T_n would be the same as that of the moderator. There is, however, a second effect which manifests itself when the average flux intensity at the point \vec{r} is different from zero. Then, depending on the influx of neutrons into the volume element under consideration being higher or lower than their outflux, the motion of neutrons will produce heating or cooling, respectively. Since, at time t the net influx of neutrons in the unit volume per unit time is $D \Delta n(t, \vec{r})$, it follows from (4) that

$$D \Delta n(t, \vec{r}) \approx -B_0^2 D(T_n) R(r, z) e^{-t/l} < 0, \quad (5)$$

where

$$R(r, z) = S_{101} J_0 \left(\alpha_{01} \frac{r}{R} \right) \cdot \sin \frac{\pi z}{H}.$$

This means that a certain time after the injection of the neutron burst the net influx in each volume element of the moderator will be negative for finite moderators, i. e. there will be a net outflux, so that eventually the spatial motion produces cooling in the neutron gas. This leads to $T_n < T_0$ for finite moderators. This effect is the so-called diffusion cooling.

From (5) it is apparent that the net outflux per unit volume i. e. the diffusion cooling decreases with decreasing B_0^2 , thus with increasing dimensions. In the extreme case when the moderator is infinite the effect vanishes in the diffusion approximation. Consequently, T_n is such function of B_0^2 for which

$$T_n(B_0^2 = 0) = T_0. \quad (6)$$

It is obvious that through its dependence on the neutron temperature T_n the diffusion constant becomes a function of the geometric buckling. It is also apparent from (6) that

$$\lim_{B_0^2 \rightarrow 0} D(T_n(B_0^2)) = D(T_0). \quad (7)$$

Hence, even if the dimensions are not infinite but still large enough, i. e. B_0^2 is sufficiently small, $D(T_n)$ can be related to $D(T_0)$ in the following way

$$D(T_n) = D(T_0) - C B_0^2 + O(B_0^4). \quad (8)$$

The constant C can be shown to be usually positive and related to the so-called thermalization time. From (4) using (8) for the decay constant the following expression ([2], [3], [4]) can be obtained

$$\frac{1}{l} = \frac{1}{l_0} + D(T_0) B_0^2 - C B_0^4.$$

Measuring now the values of $1/l$ for various moderator dimensions, i. e. for various values of B_0^2 , the experimental points can be fitted to a parabolic curve from which the constants l_0 , $D(T_0)$ and C can be determined. The diffusion length L_D , the transport mean free path λ_t , and the capture cross section σ_a are given by the following expressions

$$L_D = \sqrt{l_0 \cdot D(T_0)}, \quad \lambda_t = \frac{3 D(T_0)}{\bar{v}}, \quad \sigma_a = \frac{1}{l_0 N \bar{v}}. \quad (10)$$

Measuring apparatus

As neutron source a 200 kV accelerator was used which produced fast neutrons emitted in the reaction $T^3(d, n) He^4$ [5]. The ion pulses were obtained by pulsing simultaneously the oscillator and the extraction voltage. The ion

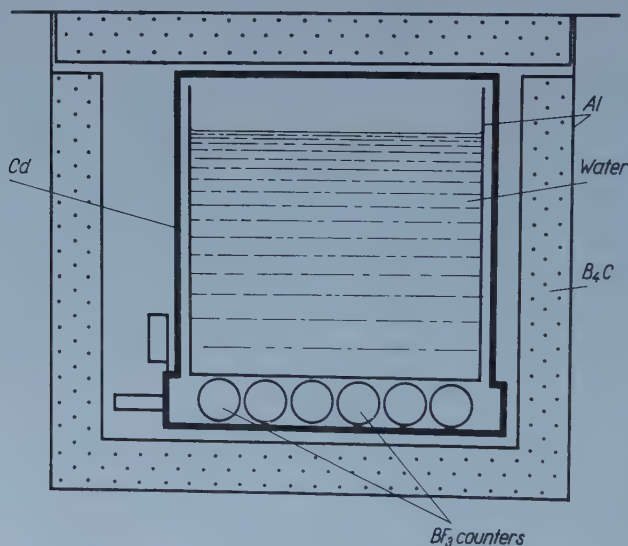
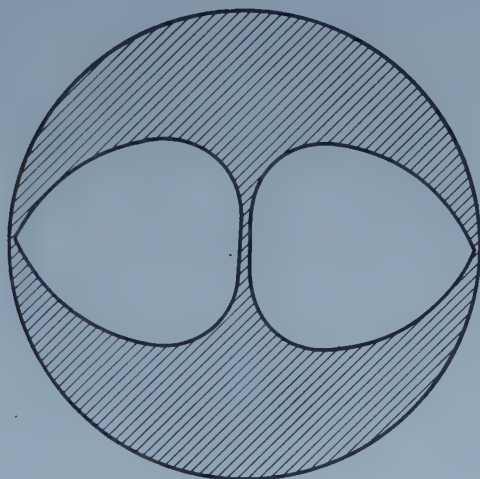


Fig. 1. A schematic view of the experimental arrangement

source was kept in an excited state by the oscillator for 50 μsec while the 10 μsec extracting pulse arrived at the half time of the excitation period. The extracting pulse height was set to be 5 kV. The ion pulse appearing on the target was precisely of the same shape as the extracting pulse, thus the neutron pulse width was also 10 μsec . The pulses succeeded each other in every 1.400 μsec . The neutron yield was adjusted to be $3 \cdot 10^4$ n/pulse. The channel width of the time analyser used in the experiment was varied from 20 to 50 μsec , while the delay varied from 50 to 500 μsec . The timing was achieved by a quartz oscillator precision timer to 0,125 μsec accuracy, that is with an error less than 1 %.

The measuring container (Fig. 1) was an aluminium tank 180 mm in diameter and 170 mm high made of 2,5 mm thick plates apart from the bottom plate which was only 0,5 mm thick. The detectors, five BF_3 filled tubes connected in parallel were mounted below the bottom of the tank. In this way the bottom was virtually completely covered by detectors. The common plateau slope of the five counters was 3% per 100 V. The assembly consisting of



$$\varphi(r) = \text{const. } J_0\left(2,405 \frac{r}{R}\right)$$

Fig. 2. The shape of Cd plate cut according to the function $\varphi(r) = \text{const. } J_0\left(2,405 \frac{r}{R}\right)$

tank and counters was covered by a 1 mm Cd plate. A 4 cm thick B_4C shield was provided to screen the assembly from the scattered neutrons.

The interpretation of the results is based on the assumption that only the fundamental mode is present in the expression (4). The intensity of the higher harmonics is strongly reduced with respect to the intensity of the fundamental mode by starting the measurement with sufficiently long delay. A residue of higher harmonics is usually visible in the decay curve as a deviation from a strictly exponential law observed in the initial part of the measurements.

The influence of the higher harmonics can be reduced by a judicious choice of the experimental conditions. The order of the dying-out of the higher harmonics is determined by ratio R/H . In our case the radial harmonics constituting the chief contamination for low water levels were suppressed by interposing a Cd plate (Fig. 2) cut according to the function $\varphi(r) = \text{const. } J_0\left(2,405 \frac{r}{R}\right)$ between the bottom of the tank and the counters.

Table I
Diffusion parameters of thermal neutrons in water at 22° C

Reference	t_0 [μ sec]	D [$\text{sec}^2 \text{cm}^{-1}$]	L_D [cm]	$C, 10^{-3}$ [$\text{cm}^4 \text{sec}^{-1}$]	Method
V. DARDEL and SJÖSTRAND [6]	$204,4 \pm 2,0$	36340 ± 750	$2,725 \pm 0,03$	$7,3 \pm 1,5$	pulsed source, $B_0^2 = 0,1 - 0,7 \text{ cm}^{-2}$
		35000 ± 1000	$2,7 \pm 0,1$	4 ± 1	pulsed source, $B_0^2 = 0,09 - 0,93 \text{ cm}^{-2}$
ANTONOV et al. [2]	207 ± 6	34850 ± 1100	$2,66 \pm 0,11$	3 ± 1	pulsed source, $B_0^2 = 0,09 - 0,96 \text{ cm}^{-2}$
BRACCI and COCEVA [7]	202 ± 6	34800	$2,70$		pulsed source, $B_0^2 = 0,08 - 1,1 \text{ cm}^{-2}$
CAMPBELL and STELSON [8]	208		$2,71 \pm 0,02$		stationary
BARKOW et al. [9]					
DIO [10]	208 ± 4	35450 ± 600	$2,715 \pm 0,06$	$3,7 \pm 0,7$	pulsed source, $B_0^2 = 0,09 - 0,87 \text{ cm}^{-2}$
BECKURTS and KLÜBER [11]	208 ± 6	35500 ± 1100	$2,72 \pm 0,03$		stationary
KÜCHLE [12]	209 ± 6	35400 ± 700	$2,72 \pm 0,08$	$4,2 \pm 0,8$	pulsed source, $B_0^2 = 0,11 - 0,75 \text{ cm}^{-2}$
ČSIKAI and DEDE [13]			$2,75 \pm 0,08$		stationary, in finite cylinder
Present work	199 ± 10	35550 ± 1550	$2,66 \pm 0,08$	$6,0 \pm 1,8$	pulsed source, $B_0^2 = 0,1 - 0,8 \text{ cm}^{-2}$

In Table I the available experimental values obtained by the pulse method are shown in order of their publication. The results of some of the most accurate stationary measurements are given for comparison as well.

Measurements in water

The mean lifetimes of thermal neutrons were measured for eight different water levels. For these levels the values of B_0^2 varied from 0,802 to 0,102 cm^{-2} . During the measurements the water temperature was kept constant at $21 \pm 1^\circ \text{C}$. The values of $1/l$ obtained in repeated measurements for the same water level were consistent within the statistical error. The values of $1/l$ were computed from the experimental data after subtraction of the background by the

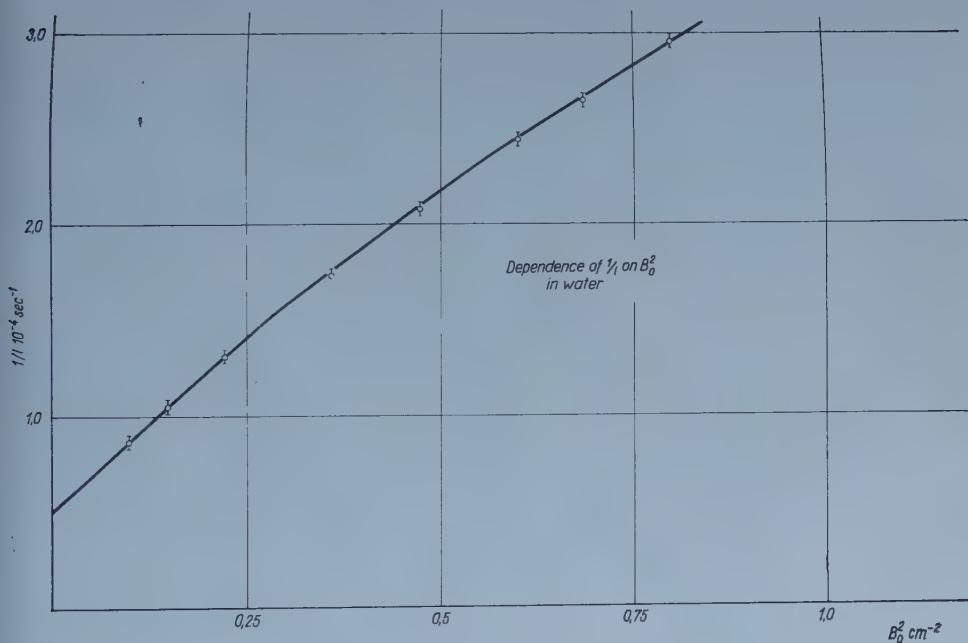


Fig. 3. Dependence of $1/l$ on B_0^2 in water

method of least squares. The background was measured in a particular run before and after each measurement. The correction for background was negligible but for measurements of rather long duration. For the computation of the constants in the parabolic expression (Fig. 3) the method of least squares was used again.

The results of our measurements are shown together with the experimental values of other authors in Table I. It is seen that the results are consistent within the statistical error.

Measurements in solid diphenyl

The diphenyl ($\text{C}_6\text{H}_5 - \text{C}_6\text{H}_5$) used in our measurements was of 1,062 g/cm^3 density and its melting point was 69°C .

The mean lifetimes of thermal neutrons were measured for nine different sizes. The value of B_0^2 varied from 0,671 to 0,111 cm^{-2} . The diphenyl temperature was kept at $21 \pm 1^\circ \text{C}$.

In the evaluation of the experimental data a particular problem arose from our not knowing the value of λ_t for diphenyl. In fact, $\frac{1}{l} = f(B_0^2)$ and $B_0^2 = f(\lambda_t)$ since the terms R and H in the equation

$$B_0^2 = \left(\frac{2,405}{R} \right)^2 + \left(\frac{\pi}{H} \right)^2$$

represent the extrapolated radius and height, respectively, that is $R = R_0 + 0,71 \cdot \lambda_t$ and $H = H_0 + 1,42 \cdot \lambda_t$.

The value of λ_t was determined by iteration (Fig. 4). First, the values of the B_0^2 were computed for $\lambda_t = 0$ and from the parabolic expression thus

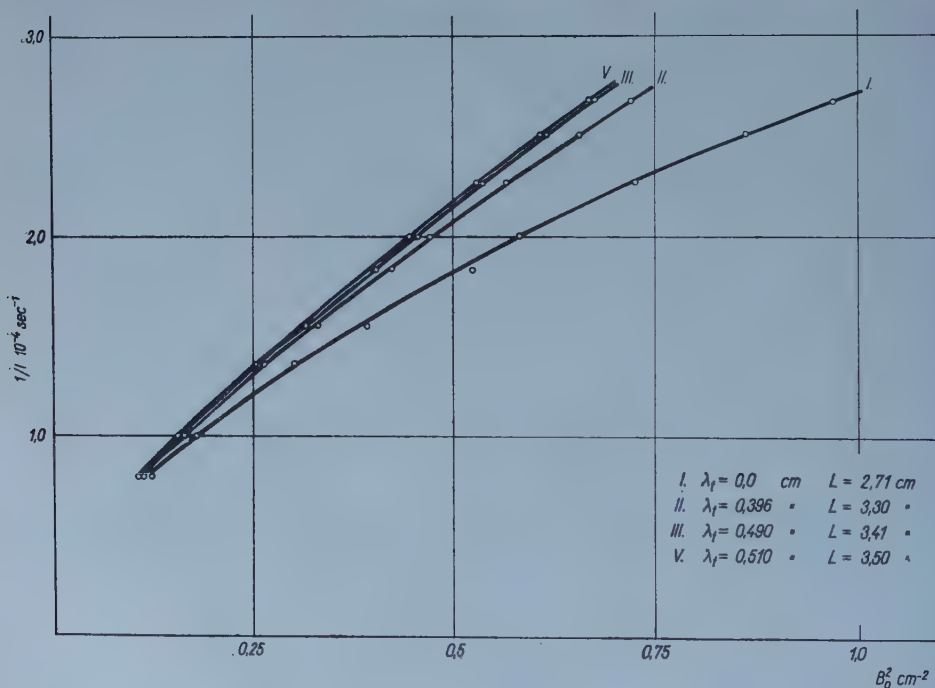


Fig. 4. Determination of λ_t in solid diphenyl

obtained the value of $D(T_0)$ was determined. Making use of the relation $D(T_0) = \frac{\lambda_t \cdot \bar{v}}{3}$ the value of λ_t was computed from this $D(T_0)$. Using now this value of λ_t the values of the B_0^2 were re-calculated and the iteration con-

tinued until consistent results were obtained. Finally, the values in question were found to be

$$\begin{aligned}l_0 &= 286 \pm 23 \text{ } \mu\text{sec}, \\D(T_0) &= 42940 \pm 1800 \text{ cm}^2 \text{ sec}^{-1}, \\I_D &= 3,50 \pm 0,18 \text{ cm}, \\C &= 13300 \pm 2850 \text{ cm}^4 \text{ sec}^{-1}, \\\lambda t &= 0,515 \text{ cm}.\end{aligned}$$

Using now the diphenyl density given above as well as the values of the absorption cross sections for H and C given in the literature it is found from the relation $l_0 = \frac{1}{\bar{v}[\Sigma_{aH} + \Sigma_{aC}]}$ that $l_0 = 290 \text{ } \mu\text{sec}$, which is in good agreement with our experimental results.

REFERENCES

1. G. DARDEL, Trans. Roy. Inst. Techn. Stockh., 75, 1954.
2. A. V. ANTONOV, A. I. ISAKOFF, I. D. MURIN, B. A. NEUPOCOEYEV, I. M. FRANK, F. L. SHAPIRO, I. V. SHTRANICH, Proc. Int. Conf. on Peaceful Uses of Atomic Energy, pp. 5, 3, 82., Geneva, 1955.
3. G. DARDEL, N. G. SJÖSTRAND, Prog. Nucl. Energy, Ser. I, 2, 183, 1958.
4. K. WIRTZ, K. H. BECKURTS, Elementare Neutronenphysik, Springer-Verlag, Berlin—Göttingen—Heidelberg, 1958.
5. A. ADÁM, L. BOD, Z. SZABÓ, L. SZEGHÓ, Acta Phys. Hung., 12, 107, 1960.
6. G. DARDEL, N. G. SJÖSTRAND, Phys. Rev., 96, 1245, 1954.
7. A. BRACCI, C. COCEVA, Nuovo Cim., 4, 59, 1956.
8. E. C. CAMPBELL, P. H. STELSON, ORNL Physics Progress Report, 1956.
9. L. M. BARKOW, V. MAKARIN, K. MUKHIN, J. Nucl. Energy, 4, 94, 1957.
10. W. H. DIO, Nukleonik, 1, 13, 1958.
11. K. H. BECKURTS, D. KLÜBER, Z. Naturforsch, 13a, 822, 1958.
12. M. KÜCHLE, Nukleonik, 2, 131, 1960.
13. GY. CSIKAI, K. DEDE, MFF, 8, 1, 1960.

ОПРЕДЕЛЕНИЕ ПАРАМЕТРОВ ДИФФУЗИИ ТЕПЛОВЫХ НЕЙТРОНОВ В ВОДЕ И В ТВЕРДОМ ДИФЕНИЛЕ ПРИ ПОМОЩИ ИМПУЛЬСНОГО МЕТОДА

А. АДАМ, Л. БОД и Л. ПАЛ

Резюме

При помощи импульсного метода были определены параметры диффузии тепловых нейтронов в воде и в твердом дифениле при комнатной температуре. Полученные данные для воды с достаточной степенью точности совпадают с соответствующими литературными данными. Для твердого дифениля были получены следующие данные: $l_0 = 286 \pm 23 \text{ } \mu\text{sec}$, $D(T_0) = 42940 \pm 1800 \text{ cm}^2 \text{ sec}^{-1}$, $L_D = 3,50 \pm 0,18 \text{ cm}$, $C = 13300 \pm 2850 \text{ cm}^4 \text{ sec}^{-1}$ и $\lambda t = 0,515 \text{ cm}$.

INFORMATIONSTHEORIE, BOHR-ROSENFELDSCHES UNBESTIMMTHEITSRELATIONEN UND DAS PROBLEM DER OPTIMALEN OPTISCHEN ABBILDUNG¹

Von

R. S. INGARDEN

INSTITUT FÜR THEORETISCHE PHYSIK DER UNIVERSITÄT, WROCLAW, POLEN
INSTITUT FÜR PHYSIK DER POLNISCHEN AKADEMIE DER WISSENSCHAFTEN

(Vorgelegt von K. F. Novobátsky. — Eingegangen: 19. X. 1960)

Der fundamentale GABORSche Entwicklungssatz der optischen Informationstheorie wird bewiesen. Es wird die Formel von LINFOOT für den Informationsgehalt des optischen Bildes für vollständig und partiell kohärentes Licht verallgemeinert. Von den BOHR-ROSENFELDSchen Feldunbestimmtheitsrelationen ausgehend wird ein Zusammenhang zwischen der maximalen Zahl der Belichtungsniveaus im Bild und der Anzahl der Freiheitsgrade der optischen Welle gefunden. Aus dieser Tatsache folgt für gegebene äussere Bedingungen die Existenz der optimalen Wellenlänge (oder für gegebene Wellenlänge die Existenz der optimalen Bedingungen, wie Beleuchtung, Belichtungszeit, Öffnungsverhältnis usw.). Alle Betrachtungen werden in der GAUSSschen Annäherung durchgeführt.

Einleitung

Als Einleitung möchte ich über die drei Arbeiten [1], [2], [3] kurz berichten, die mir als besonders wichtig für die Informationstheorie der optischen Instrumente scheinen. Alle drei wurden im Jahre 1955 veröffentlicht.

In der Arbeit von GABOR [1] wird eine sehr einfache und geistreiche Bestimmung des »Signalraumes« der Optik gegeben, d. h. des komplexen Hilbertschen Raumes, in dem man alle optischen Signale von einer bestimmten gegebenen Wellenlänge λ_0 lokalisieren kann (über den Signalraum siehe [4]). Dieser Hilbertsche Raum hat nach GABOR die endliche Dimensionszahl

$$N = \frac{1}{\lambda_0^2} \iint_{S, A} dx d\xi = \frac{1}{\hbar^2} \int_{\Omega} dx dp \quad (1)$$

(siehe Fig. 1). Wir benutzen in dieser Arbeit folgende Bezeichnungen: $\mathbf{x} = (x_1, x_2, z) = (x, z)$; $\mathbf{y} = (y_1, y_2, z) = (y, z)$; $\mathbf{x} = (x_1, x_2)$; $\mathbf{y} = (y_1, y_2)$; $\mathbf{a} = (a_1, a_2)$; $\xi = (\xi_1, \xi_2)$; $\mathbf{k} = (k_1, k_2, k_z) = k_0(\xi, 1 - \xi^2) = (k, k_z)$; $k = (k_1, k_2)$; $k_0 = 2\pi/\lambda_0$; $\mathbf{p} = (p_1, p_2) = \hbar \mathbf{k}$; $\hbar = h/2\pi$, wo h die Plancksche Wirkungskonstante ist. Ferner: $d\mathbf{x} = dx_1 dx_2$; $d\xi = d\xi_1 d\xi_2$; $d\mathbf{k} = dk_1 dk_2$; $d\mathbf{p} = dp_1 dp_2$; $x^2 = x_1^2 + x_2^2$; $k^2 = k_1^2 + k_2^2$; $a^2 = a_1^2 + a_2^2$; $\xi^2 = \xi_1^2 + \xi_2^2$; $r = |\mathbf{x}| = \sqrt{x^2}$; $\varrho =$

¹ Ein Vortrag gehalten an der II. Optischen Konferenz des Optischen und Kinotechnischen Vereins (Optikai és Kinotechnikai Egyesület) in Budapest, 7–11. September 1960. Der vorliegende Text ist etwas ergänzt und mehr ausgearbeitet im Vergleich zu dem Wortlaut des Vortrages.

$= |k| = \sqrt{k^2}$; $xa = x_1a_1 + x_2a_2$; $xk = x_1k_1 + x_2k_2$. S bedeutet die Fläche des Objektes (Bildes) und A den räumlichen Aperturwinkel des Instruments. In dem Fall, der in der Fig. 1 dargestellt ist, gilt angenähert

$$N = \frac{SA}{\lambda_0^2}. \quad (2)$$

Die Formel (1) hat GABOR auf dem Integralinvariantensatz der geometrischen

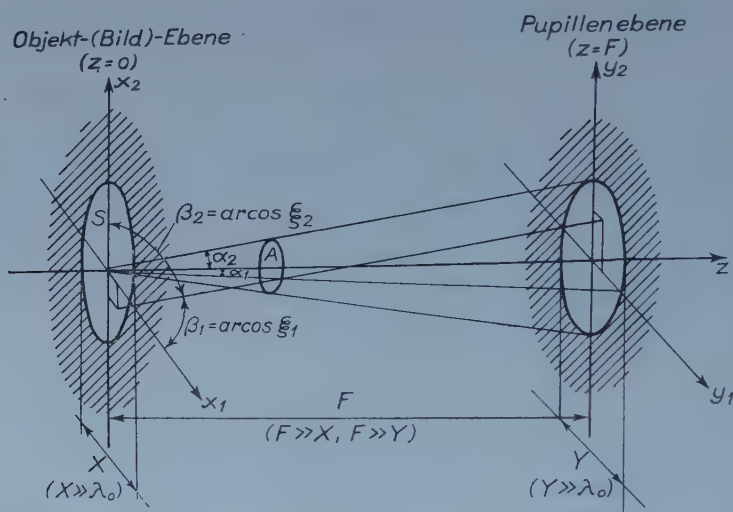


Fig. 1

Optik begründet. Diesen kann man das optische LIOUVILLESche Theorem nennen und in der Form schreiben:

$$\iint dx d\xi = \text{invariant} \quad \text{oder} \quad \iint dx dp = \text{invariant}. \quad (3)$$

In diesem Fall ist die Invarianz gegen optische Transformationen durch Brechungen und Spiegelungen zu verstehen. Ausserdem stützt sich GABOR auf Dimensionsbetrachtungen, wenn er die Existenz der »Quantenzellen« vom Volumen h^2 in dem optischen »Phasenraum« $\Omega = (x, p)$ (oder entsprechend vom Volumen λ_0^2 im »Strahlenraum« (x, ξ)) annimmt.

Mit anderen Worten, GABOR nimmt an, dass jede Lösung der Helmholtz-schen Gleichung

$$(\Delta + k_0^2) u = 0, \quad (4)$$

die auf den schraffierten Gebieten der Objekt(Bild)- und Pupillenebene verschwindet (Fig. 1), in der Form

$$u(\mathbf{x}) = \sum_{i=1}^N c_i u_i(\mathbf{x}) \quad (5)$$

dargestellt werden kann (GABORS »expansion theorem«). Nach dem optischen LIOUVILLESchen Satz haben der Objekt- und der Bildsignalraum die gleiche Dimensionszahl N . Man kann deshalb einen linearen hermiteschen Abbildungsoperator ω_{ij} definieren, der die Objektwelle $\{c_i\}$ in die Bildwelle $\{c'_i\}$ transformiert:

$$c'_i = \sum_{j=1}^N \omega_{ij} c_j, \quad \omega_{ij} = \omega_{ji}^*. \quad (6)$$

Diese Darstellung ist eine Verbindung der GABORSchen mit der alten MANDELSTAMSchen Idee [5]. GABOR selbst gibt sie in einer etwas komplizierteren Form an, die mit dem Begriff der partiellen Kohärenz verbunden ist (einfachheitshalber haben wir oben vollständig kohärentes Licht vorausgesetzt).

Die GABORSchen Betrachtungen sind sehr elegant, bis jetzt sind sie aber wenig mathematisch und physikalisch ausgearbeitet. Kein strenger Beweis des GABORSchen Entwicklungstheorems ist bis jetzt veröffentlicht worden, jedenfalls nach Wissen des Verfassers. Die zweite Quantelung des Lichtes ist in dieser Theorie vernachlässigt, während die erste nur in sehr grober, dimensionsanalytischer Form berücksichtigt ist.

TORALDO DI FRANCIA geht in [2] auf das gleiche Problem von einer anderen Seite ein. Er beschränkt sich aber auch auf klassische Betrachtungen. Er geht von der bekannten Formel für die Beugungswelle im Fall des rechteckigen Spaltes

$$u'(x') = \frac{4a_1 a_2}{\lambda_0^2} \int u(x) \operatorname{sinc} \frac{2a(x-x')}{\lambda_0} dx \quad (7)$$

aus (einfachheitshalber ist die Vergrößerung gleich eins angenommen). Hier ist $u(x)$ die Objektamplitude, $u'(x')$ die Bildamplitude, $\operatorname{sinc} x_1 \equiv \frac{\sin \pi x_1}{\pi x_1}$, $\operatorname{sinc} x \equiv \operatorname{sinc} x_1 \operatorname{sinc} x_2$. Wegen

$$\operatorname{sinc} \frac{2ax}{\lambda_0} = \int_{-\frac{a}{\lambda_0}}^{\frac{a}{\lambda_0}} e^{2\pi i f x} df, \quad (8)$$

wo $f = (f_1, f_2)$ ist, treten im Bild nur die Frequenzen

$$-\frac{a}{\lambda_0} \leq f \leq \frac{a}{\lambda_0} \quad (9)$$

auf. Nach der berühmten GABOR—SHANNONSchen »sampling method« (siehe z. B. [6], Kap. 8, § 7) kann man dann die Funktion $u'(x')$ allein durch ihre

Werte in den diskreten Netzknoten, die in jeder Hauptrichtung jeweils um die Strecke $\lambda_0/2 a_i$ ($i = 1, 2$) entfernt sind, charakterisieren. So, im Fall der rechteckigen Öffnung, bekommt man leicht eine Formel für die Zahl der (komplexen) Freiheitsgrade

$$N = \frac{SA}{\lambda_0^2}, \quad (10)$$

wo $A = 4 a_1 a_2$ ist. Die Formel (10) ist identisch mit (2). Aus dem Gesagten folgt auch unmittelbar für diesen speziellen Fall ein Beweis des GABORSchen Entwicklungssatzes, weil man mit Hilfe der Produkte der SHANNONSchen »sine«-Funktionen leicht die entsprechende Entwicklung aufschreiben kann.

In der Arbeit von LINFOOT [3] werden ein »vereinfachtes« und ein »nicht-vereinfachtes« Modell diskutiert. Wir interessieren uns hier nur für das erste. Ich werde buchstäblich LINFOOTS Worte angeben, weil es schwer ist, dieses einfacher auszudrücken [3] § VIII: »We construct a simplified model of an optical image as follows: The rectangular field is divided up into small cells (squares or hexagons) of diameter comparable with the resolution limit of the system. Each cell is supposed to be capable of a finite number of discrete states or 'brightness levels'. Then, if N is the number of cells and M the number of brightness levels for each cell, the total number of possible images is M^N and, if all these are taken as having equal prior probabilities, the information content of each image (regarded as a message state) is $N \log M$.« (Wir haben die Symbole gemäss unseren Bezeichnungen geändert.) Weil die »Auflösungsgrenze« (resolution limit) angenähert den Wert

$$\delta = \frac{\lambda_0}{\alpha} \quad (11)$$

hat, bekommt man nach LINFOOT genau die angenäherte GABORSche Formel (2), wo $A = \alpha^2$. Für den gesamten (oder maximalen) Informationsgehalt des optischen Bildes ist

$$H_1 = N \log M, \quad (12)$$

wo M die Zahl der »Belichtungs-niveaus« ist.

Verallgemeinerung der Linfoot'schen Formel

Wir haben gesehen, dass in der LINFOOTSchen Arbeit [3] zwei neue Elemente im Vergleich mit [1] und [2] auftreten: die Zahl M der Belichtungs-niveaus und der Informationsgehalt H_1 des optischen Bildes. Physikalisch

entspricht der erste Begriff entweder der Wellenquantelung des Lichtes oder der Kornstruktur der photographischen (bzw. visuellen) Schicht (wenn die Körner grösseren Durchmesser als δ haben, was praktisch nur ausnahmsweise auftritt). Der zweite Begriff entspricht der maximalen Entropie der Lichtverteilung im Bild (»maximal« bedeutet hier, wie auch oben: bei beliebigem Objekt aber gegebenem Gerät). In Verbindung mit diesen Begriffen muss betont werden, dass die Formel (12) nur im Fall der vollständig inkohärenten Belichtung richtig ist, wenn das Licht der einzelnen kohärenten Wellenzüge (die aus verschiedenen Punktquellen ausgehen) prinzipiell unterschieden werden kann, z. B. mit Hilfe einer entsprechenden Ausblendung.

Im Fall des kohärenten Lichtes sind die Photonen ununterscheidbar und die Zahl der möglichen Bilder ist bedeutend kleiner. Statt der Anzahl der Kombinationen mit Wiederholung und mit Berücksichtigung der Anordnung (Variationen) M^N (Boltzmannsche Statistik), wie bei LINFOOT, muss man bei kohärentem Licht die Anzahl der Kombinationen mit Wiederholung aber ohne Berücksichtigung der Anordnung (Bose—Einsteinsche Statistik) nehmen

$$I_0 = \binom{M+N-1}{N} = \frac{(M+N-1)!}{(M-1)! N!}. \quad (13)$$

Da im allgemeinen

$$M \gg 1, N \gg 1 \quad (14)$$

ist, haben wir nach der Stirlingschen Formel für die Fakultätsfunktion

$$I_0 = \frac{1}{\sqrt{2\pi}} \frac{(M+N)^{M+N}}{M^M N^N}. \quad (15)$$

Das gibt für H eine in N und M symmetrische Formel

$$H_0 = \log I_0 = (M+N) \log (M+N) - M \log M - N \log N - \log \sqrt{2\pi}. \quad (16)$$

Zur Unterscheidung haben wir oben das Zeichen H_1 für den inkohärenten Fall und das Zeichen H_0 für den kohärenten Fall benutzt. Wenn die Inkohärenz nur partiell ist, liegt der Informationsgehalt H zwischen H_1 und H_0 . Deshalb kann man bei gegebenen N und M einen neuen Koeffizienten der partiellen Inkohärenz einführen

$$\gamma = \frac{H - H_0}{H_1 - H_0}, \quad (17)$$

der verschwindet, wenn das Licht kohärent ist, und gleich eins ist im Fall der vollständigen Inkohärenz. Nach (17) haben wir

$$H \equiv H_\gamma = H_0 + \gamma (H_1 - H_0) = (1 - \gamma) H_0 + \gamma H_1 \quad (18)$$

oder wegen (12) und (16)

$$H_\gamma = (1 - \gamma) [(M + N) \log (M + N) - M \log M - N \log N - \log \sqrt{2\pi}] + \gamma N \log M, \quad (19)$$

was eine Formel für den allgemeinsten Fall bietet.

Beweis des Gaborschen Entwicklungssatzes

Wir fangen mit der allgemeinen Form der monochromatischen, im leeren Raum in der positiven z -Richtung fortschreitenden Welle an:

$$v(\mathbf{x}, t) = e^{-ik_0 ct} \frac{1}{2\pi} \int_K \psi(k) e^{i(kx + \sqrt{k_0^2 - k^2} z)} dk \equiv e^{-ik_0 ct} u(x), \quad (20)$$

wo c die Lichtgeschwindigkeit ist. Wegen des fortschreitenden Charakters der Welle muss man das Integrationsgebiet in der k -Ebene in (20) auf das Innere des Kreises K mit dem Radius k_0 beschränken:

$$K: k_0^2 - k^2 \geq 0, \text{ oder } \varrho \leq k_0. \quad (21)$$

Wir interessieren uns hier nur für die Werte von $u(x)$ auf der Ebene $z = 0$ (z. B. der Objektebene). Diese Werte werden wir mit $u(x)$ bezeichnen.

Wir führen die polaren Koordinaten in den x - und k -Ebenen ein und bekommen

$$u(r, \varphi) = \frac{1}{2\pi} \int_0^{2\pi} d\vartheta \int_0^{k_0} \psi(\varrho, \vartheta) e^{i\varrho r \cos(\vartheta - \varphi)} \varrho d\varrho. \quad (22)$$

Dann entwickeln wir $\psi(\varrho, \vartheta)$ in eine Fourier-Besselsche Reihe

$$\psi(\varrho, \vartheta) = \sum_{l=1}^{\infty} \sum_{m=-\infty}^{+\infty} A_{lm} e^{im\vartheta} J_0 \left(a_l \frac{\varrho}{k_0} \right), \quad (23)$$

wo a_l die Wurzeln der nullten Besselschen Funktion sind

$$J_0(a_l) = 0. \quad (24)$$

Für grosse l haben wir asymptotisch

$$a_l \approx \pi l. \quad (25)$$

Nach einer kurzen Rechnung bekommen wir

$$u(r, \varphi) = \sum_{l=1}^{\infty} \sum_{m=-\infty}^{\infty} i^m A_{lm} B_{lm}(r) e^{im\varphi}, \quad (26)$$

wo

$$B_{lm}(r) = \int_0^{k_0} J_m(\varrho r) J_0\left(a_l \frac{\varrho}{k_0}\right) \varrho d\varrho \quad (27)$$

ist. Insbesondere

$$B_{l0}(r) = \frac{a_l J_0(k_0 r) J_1(a_l)}{a_l^2 - k_0^2 r^2}. \quad (28)$$

Jede der Funktionen $B_{l0}(r)$ hat ihr Maximum auf dem Umfang des Kreises mit dem Radius

$$r_l = \frac{a_l}{k_0} \approx \frac{l\lambda_0}{2}, \quad (29)$$

das letztere gilt für grosse l wegen (25). Wenn die Welle $u(r, \varphi)$ für $r \geq r_{\max}$ verschwindet (Objekt mit dem Radius r_{\max} oder Lücke mit dem Radius r_{\max} in der Objektebene), müssen alle Koeffizienten A_{lm} für

$$l \geq \frac{2r_{\max}}{\lambda_0} = l_{\max} \quad (30)$$

auch verschwinden. Wenn wir ausserdem fordern, dass $u(r, \varphi)$ in der Umgebung des Koordinatenanfangspunktes keine unendlich grossen Schwankungen in der φ -Richtung hat, müssen für jedes l auch die Koeffizienten A_{lm} mit

$$|m| > l \quad (31)$$

gleich Null sein. Jetzt sehen wir leicht, dass die Anzahl der im allgemeinen nichtverschwindenden Koeffizienten A_{lm} (die ein »Dreieck« bilden) oder die Anzahl der komplexen Freiheitsgrade unseres Problems gleich

$$N = \frac{4r_{\max}^2}{\lambda_0^2} = \frac{4}{\pi} \frac{S}{\lambda_0^2} \quad (32)$$

ist, wo $S = r_{\max}^2 \pi$. Das entspricht dem Fall der freien Welle oder dem Öffnungswinkel $\pi/2$. Wenn man ein Gerät mit einer kreisförmigen Pupille und Lücke und der numerischen Apertur a hat, muss man in (20) nur in dem Kreis

$$K_a: \quad \varrho \leq k_0 a \quad (33)$$

integrieren ($k_0 \rightarrow k_0 a$) und man bekommt endlich statt (32)

$$N = \frac{4}{\pi^2} \frac{SA}{\lambda_0^2}, \quad (34)$$

wo $A = a^2 \pi$. Wir nehmen hier an, dass die Apertur von dem Bildpunkt x nicht abhängt, was selbstverständlich nur eine Annäherung ist und nur für nicht zu grosse Öffnungsverhältnisse und Schwinkel (d. h. im Gauss'schen Gebiet) gilt (siehe Fig. 1).

Wir sehen, dass jetzt die Formel (34) für die Zahl der Freiheitsgrade von der Formel (2) um den numerischen Koeffizienten $4/\pi^2 \approx 0,405$ abweicht. Das ist aber verständlich, weil (2) nur auf Dimensionsbetrachtungen gestützt war, und es ist nicht a priori notwendig, dass N bei gegebenen λ_0 nur von den Oberflächen der Pupille und der Lücke abhängt und nicht von ihrer Gestalt. Darum muss man im allgemeinen in die Formel (2) einen dimensionslosen Koeffizienten einführen, den wir mit G bezeichnen und »Gestaltkoeffizienten« nennen werden:

$$N = G \frac{SA}{\lambda_0^2}. \quad (2')$$

Gleichzeitig haben wir eine nichttriviale Verallgemeinerung der GABOR—SHANNONSchen »sampling method« für zwei Dimensionen erhalten, wesentlich anders als die unmittelbaren Verallgemeinerungen angegeben z. B. in [2] (siehe oben) oder [6] Kap. 8, § 11.

Man muss betonen, dass in allen unseren bisherigen Betrachtungen die Objekt- und Bildwelle in genau gleicher Weise betrachtet waren, d. h. als ob die Objektwelle vom Instrument zurück in Richtung des Objektes projiziert würde. (Mit anderen Worten: wir zählen nur das Licht, welches tatsächlich ins Instrument einfällt.) Deshalb hat die Objektwelle bei uns, wie auch bei GABOR [1], eine endliche Zahl von Freiheitsgraden, und zwar genau so viele wie die Bildwelle. Das steht im Gegensatz zu den Aussagen von TORALDO DI FRANCIA in [2], der über eine unendliche Zahl von Freiheitsgraden der Objektwelle (im Gegensatz zu der Bildwelle) spricht. Nach unseren obigen Betrachtungen würde dann die Objektwelle nicht monochromatisch sein und das Gerät müsste als Monochromator wirken.

Aus dem Obigen ist eine Methode für alle anderen Fälle leicht ersichtlich: man muss nur die entsprechenden Koordinatensysteme in den Pupillen- und Lückenebenen und die mit diesen verbundenen orthogonalen Funktionensysteme benutzen.¹ Gleichzeitig gewinnt man die entsprechende Form der

¹ Auf diese Weise bekommt man auch eine Theorie der Beugungsphänomene, die mit verschiedenen Gestalten der Pupille und der Lücke (des Objekts) verbunden sind und die experimentell so schön von Frau V. BLUMOWA (Prag) an der Budapester Konferenz dargestellt wurden.

GABORSchen endlichen Entwicklung (5) und so den allgemeinen Beweis des »expansion theorem«. Unsere Betrachtungen waren eigentlich nur für den Fall des vollständig kohärenten Lichtes durchgeführt. Es ist aber möglich, sie auch für das vollständig oder partiell inkohärente Licht zu verallgemeinern (siehe [2] für den Spezialfall der rechteckigen Öffnung, wo aber die Betrachtungen nicht ganz komplett sind). Da jedoch diese Erwägungen etwas umständlich sind, und das Endresultat fast genau dasselbe wie oben ist, werden wir hier darauf nicht näher eingehen.

Für unsere weiteren Betrachtungen werden wir die Formeln für den praktisch wichtigsten Fall der kreisförmigen Pupille und Lücke benutzen.

Die grösste Zahl der Belichtungsniveaus

Wir stellen uns jetzt eine weitere Frage: wie kann man die von LINFOOT benutzte Zahl M bestimmen, oder besser: die grösste Zahl M , die man physikalisch realisieren kann? Bei diesem Problem gehen wir von den Bohr—Rosenfeldschen Unbestimmtheitsrelationen für die Messung der Lichtintensität $w = uu^*$ aus (siehe z. B. [6] Kap. 16, § 8)

$$\Delta w \approx \left(-\frac{h}{\varepsilon \tau \Delta x} \right)^2, \quad (35)$$

wo τ die Belichtungszeit, ε die »Probeladung« und Δx die Lageunbestimmtheit bedeuten. (Die »Probeladung« ist die aktive Ladung des elementaren, aber makroskopischen Lichtempfängers, z. B. eines einzigen Bromsilberkristalls.) Dabei muss man voraussetzen

$$\tau \gg \frac{\lambda_0}{c} = T_0, \quad \varepsilon \gg \varepsilon_0, \quad (36)$$

wo ε_0 die Elementarladung ist. Wenn wir annehmen, dass

$$\Delta x = \delta = \frac{1}{2} \sqrt{\frac{SA}{N}} \quad (37)$$

ist (dann müssen die Durchmesser der elementaren Lichtempfänger nicht grösser als δ sein) und mit W die maximale Lichtintensität im Bild bezeichnen,

¹ Für das räumliche Auflösungsvermögen ist nur die Anzahl N der komplexen Freiheitsgrade massgebend, weil die Anzahl $2N$ der reellen Freiheitsgrade noch mit dem Polarisationszustand der Welle verbunden ist (wir benutzen hier die komplexe quasiskalare Lichttheorie von WOLF und GREEN [7]).

bekommen wir

$$M = \frac{W}{\Delta w} = \frac{W \varepsilon^2 \tau^2 S A}{4 h^2 N}, \quad (38)$$

wo noch

$$W \gg \Delta w \quad (39)$$

vorausgesetzt sein muss. Aus (38) folgt unmittelbar

$$M N = \frac{W \varepsilon^2 \tau^2 S A}{4 h^2} \equiv C^2, \quad (40)$$

wo rechts jeweils eine bekannte Grösse steht. Es ist bemerkenswert, dass die dimensionslose Konstante C von der Wellenlänge λ_0 unabhängig ist und nur von der Planckschen Wirkungskonstante h und den äusseren Parametern des Geräts abhängt. Zu den äusseren Parametern gehören: die Objektgrösse S (oder zu ihr proportionaler Sehwinkel), der räumliche Aperturwinkel A (oder die numerische Apertur, oder das Öffnungsverhältnis), die Belichtungszeit τ , die im kleinsten Bildelement maximal mögliche Lichtintensität W (wenn alles Licht dort konzentriert sein würde; darum ist diese Grösse gleich der totalen Lichtintensität des Objekts, die man mit einem Belichtungsmesser bestimmen kann), die aktive Ladung ε des Lichtempfängers (die beim Photographieren dem Volumen des Bromsilberkornes proportional ist und als Mass seiner Lichtempfindlichkeit gelten kann). Es ist aber nichts Wunderliches in dieser Tatsache, weil diese und nur diese Grössen jeder Photographierende messen muss (ausser Konstanten, wie h).

Ein Beispiel

In der Praxis können sich alle äusseren Parameter in (40) in sehr weiten Grenzen ändern. Um aber ein typisches Beispiel zu bekommen und an ihm unsere Resultate mindestens der Grössenordnung nach mit dem Experiment zu vergleichen, betrachten wir die von ROSE in der Arbeit [8] experimentell untersuchten Fälle. ROSE hat eine Serie sechs sehr schöner Aufnahmen veröffentlicht, die ausserordentlich anschaulich die Rolle der Quantenerscheinungen zeigt und in der die Helligkeit des Objektes um 4 Grössenordnungen variiert (bei konstanten Werten aller anderen Parameter). Wir werden hier einfachheitshalber nur zwei extreme Fälle von ROSE diskutieren: der der grössten und der der kleinsten Helligkeit des Objektes (Fig. 1 und 6 in [8]). Nach ROSEschen Angaben können wir folgende äusseren Parameter bestimmen (siehe auch [9]; wir benutzen die CGSE-Einheiten):

$$\begin{aligned} \tau &= 0,2 \text{ sek}, \quad S = 1,5 \cdot 10^3 \text{ cm}^2, \quad A = 2 \cdot 10^{-5}, \\ W &= \begin{cases} 3 \cdot 10^{-22} \text{ erg} \cdot \text{cm}^{-3} \\ 3 \cdot 10^{-18} \text{ erg} \cdot \text{cm}^{-3}. \end{cases} \end{aligned} \quad (41)$$

Dabei sind alle unsere Voraussetzungen (siehe Fig. 1) befriedigt ($X \approx 35$ cm, $Y = 0,6$ cm, $F \approx 125$ cm). Ausserdem ist, wie bekannt,

$$h = 6,6 \cdot 10^{-27} \text{ erg} \cdot \text{sek.} \quad (42)$$

Viel schwieriger ist es, die Probeladung ε zu bestimmen (ROSE gibt selbstverständlich keine Angaben darüber). Wir benutzen eine grobe Schätzung dieser Grösse nach MOTT und GURNEY [10], Kap. VII, § 3, wo man die folgende angenäherte Formel findet:

$$\varepsilon = n \varepsilon_0 \Re = \frac{\kappa \Re R k_B T}{\varepsilon_0} \quad (43)$$

Hier ist n die Anzahl der Elementarladungen in einem aktiven Silberkörnchen des Bromsilberkristalls, \Re ist die Zahl solcher Silberkörnchen pro Kristall, R — der Radius des Silberkörnchen, κ — die Dielektrizitätskonstante für AgBr, $k_B = 1,4 \times 10^{-16}$ erg Grad $^{-1}$ die Boltzmannsche Konstante und T — die absolute Temperatur. Wir setzen nach [10] die typischen Werte

$$\kappa = 12, \Re = 10, R = 5 \cdot 10^{-5} \text{ cm}, T = 300^\circ \text{ K} \quad (44)$$

ein und bekommen

$$\varepsilon = 5 \cdot 10^{-7} \text{ cm}^{3/2} \text{ g}^{1/2} \text{ sek}^{-1} \approx 10^3 \varepsilon_0 \quad (45)$$

in Übereinstimmung mit (36). Endlich haben wir nach (40)

$$C = 2,5 \cdot 10^{16} \text{ cm}^{1/2} \text{ g}^{-1/2} \text{ sek} \sqrt{W} = \begin{cases} 4 \cdot 10^5, \\ 4 \cdot 10^7. \end{cases} \quad (46)$$

Wir sehen, dass jedenfalls

$$C \gg 1 \quad (47)$$

ist.

Die optimale Wellenlänge

Bei unseren Voraussetzungen sind nach (40) die Zahlen M und N nicht unabhängig, wie bei LINFOOT, sondern komplementär oder besser gesagt — reziprok. Für $h \rightarrow 0$ (der klassische Fall) hat man bei konstanten anderen Grössen $MN \rightarrow \infty$, was verständlich ist, weil dann $M \rightarrow \infty$ wird, unabhängig von N , das endlich bleiben kann. Wir sehen, dass die Endlichkeit des Produkts MN eine Folge der Quantenerscheinungen ist. Man bekommt weiter nach (40),

dass jetzt der Informationsgehalt H nur von einer Grösse abhängt (M oder N). Man kann die Frage stellen, für welchen Wert dieser Grösse (z. B. N) H maximal ist?

Für das vollständig inkohärente Licht ($\gamma = 1$) bekommen wir einfach nach (12) die Lage des Maximums des Informationsgehaltes (die unabhängig von der Logarithmenbasis a in (12) ist):

$$N_1^{\text{opt}} = \frac{C^2}{e} \quad (48)$$

(e ist die Nepersche Zahl) oder nach (34)

$$\lambda_0^{\text{opt}}(1) = \frac{2\sqrt{eSA}}{\pi C} = \frac{2h}{\varepsilon\tau\pi} \sqrt{\frac{e}{W}} \quad (49)$$

Das Maximum selbst ist gleich

$$H_1^{\text{max}} = \frac{C^2}{e} \log e \approx 0.553 C^2, \quad (50)$$

das letztere für $a = 2$, wie in der Informationstheorie üblich. Es muss noch nachgeprüft werden, ob für (48) die zweite Ableitung d^2H_1/dN_2 negativ ist. Wir haben, tatsächlich

$$\left(\frac{d^2 H_1}{d N^2} \right)_{N=N_1^{\text{opt}}} = - \frac{e}{C^2 \ln a} < 0 \quad (51)$$

für jedes $a > 1$. Aus (49) sehen wir, dass für $h \rightarrow 0$ $\lambda_0^{\text{opt}} \rightarrow 0$, was verständlich in der klassischen Theorie ist. Wir bemerken weiter, dass $\lambda_0^{\text{opt}}(1)$ unabhängig von S und A ist und nur von ε , τ und W abhängt (alle anderen Grössen sind Konstanten).

Für das vollständig kohärente Licht ($\gamma = 0$) erhalten wir auf dieselbe Weise

$$N_0^{\text{opt}} = \frac{C}{\sqrt{\eta}}, \quad (52)$$

wo η eine Lösung der transzendenten Gleichung

$$\eta \log \eta + (1 - \eta) \log (1 + \eta) = 0 \quad (53)$$

ist, die aus dem Verschwinden der ersten Ableitung dH_0/dN folgt. (Auch hier ist es leicht sichtbar, dass η von a unabhängig ist.) Die Gleichung (53) hat zwei und nur zwei Wurzeln

$$\eta_1 = 0, \eta_2 = 1. \quad (54)$$

Den folgenden kurzen und schönen Beweis, dass (53) nur die Wurzeln (54) hat, hat Herr E. HÓDI dem Verfasser nach seinem Vortrag in Budapest freundlichst mitgeteilt:

Man betrachtet zuerst die Funktion

$$g(\eta) \equiv \eta \ln \eta + (1 - \eta) \ln (1 + \eta) \quad (55)$$

(wir nehmen hier einfachheitshalber $a = e$ an), die — da wir hier nur reelle

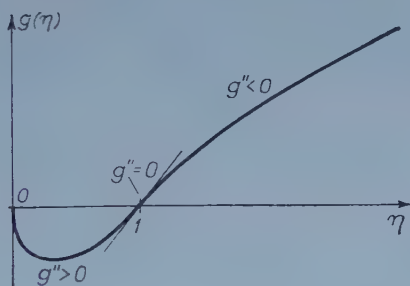


Fig. 2

Argumente und Funktionen betrachten — nur für nichtnegative η definiert ist. Man findet leicht, dass

$$g'(\eta) = \frac{2}{1+\eta} + \ln \frac{\eta}{1+\eta} \quad \text{und} \quad g''(\eta) = \frac{1-\eta}{\eta(1+\eta)^2}. \quad (56)$$

Aus dem letzteren folgt sofort, dass

$$g'' \begin{matrix} \geq \\ \leq \end{matrix} 0 \quad \text{ist, je nachdem ob} \quad \eta \begin{matrix} \leq \\ \geq \end{matrix} 1 \quad (57)$$

ist. Ferner erhält man leicht, dass

$$\lim_{\eta \rightarrow \infty} g(\eta) = \infty. \quad (58)$$

Aus den erwähnten Tatsachen schliesst man unmittelbar auf einen pfeifenförmigen Verlauf der Kurve $g(\eta)$ (siehe Fig. 2) und daraus auch auf die Richtigkeit der obigen Behauptung.

Für $\eta_1 = 0$ haben wir nach (52)

$$N_0^{\text{extr}} = \infty, \quad (59)$$

was aber kein Maximum für $H_0(N)$ gibt. Nach (16) erhalten wir nämlich

$$\lim_{N \rightarrow \infty} H_0(N) = -\log \sqrt{2\pi} \quad (60)$$

und

$$\lim_{N \rightarrow \infty} \frac{d^s H_0}{dN^s} = 0 \quad (61)$$

für jedes $s = 1, 2, 3, \dots$, während die Kurve $H_0(N)$ nicht von unten sondern von oben zu dem Grenzwert (60) strebt (siehe Fig. 3). Wir haben darum für (59) ein (uneigentliches) Minimum für $H_0(N)$.

Für $\eta_2 = 1$ bekommen wir nach (52)

$$N_0^{\text{opt}} = C, \quad (62)$$

was tatsächlich ein Maximum gibt. Wir haben nämlich

$$\left(\frac{d^2 H_0}{dN^2} \right)_{N=N_0^{\text{opt}}} = \frac{2}{C} \left(\log 2 - \frac{1}{\ln a} \right) < 0 \quad (63)$$

für jedes $a > 1$ (z. B. für $a = 2$: $-0,886/C$), weil immer $C > 0$ ist. Nach (34) haben wir dann

$$\lambda_0^{\text{opt}}(0) = \sqrt{\frac{4SA}{\pi C}} = \sqrt{\frac{4h}{\pi \epsilon \tau}} \sqrt{\frac{SA}{W}}. \quad (64)$$

Auch jetzt für $h \rightarrow 0$ $\lambda_0^{\text{opt}} \rightarrow 0$ (der klassische Grenzfall), jedoch jetzt hängt $\lambda_0^{\text{opt}}(0)$ wesentlich von S und A ab. Für den Maximalwert von $H_0(N)$ erhalten wir

$$H_0^{\text{max}} = 2C \log 2 - \log \sqrt{2\pi}. \quad (65)$$

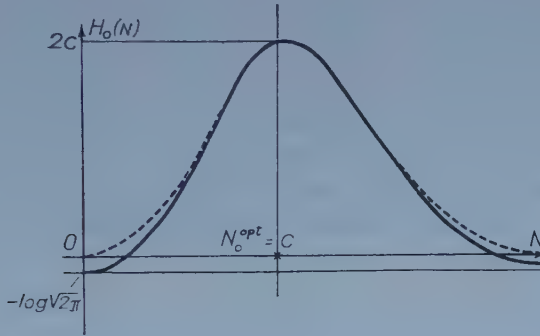
Ferner

$$\lim_{N \rightarrow 0} H_0(N) = -\log \sqrt{2\pi}. \quad (66)$$

Der Verlauf von $H_0(N)$ ist schematisch in der Fig. 3 dargestellt. Es muss dabei betont werden, dass die negativen Werte von $H_0(N)$ bei sehr kleinen und sehr grossen Werten von N (siehe (60) und (66)) nur eine Folge der in diesen Gebieten nicht geltenden Stirlingschen Annäherung (die in (15) benutzt wurde) ist. Wegen dem Zusammenhang (40) sind die Voraussetzungen (14) nicht unabhängig und, obwohl (47) gilt, nicht immer verträglich. Statt (14) haben wir jetzt die Bedingungen

$$1 < N \ll C^2, \quad 1 \ll M \ll C^2 \quad (67)$$

für die Anwendbarkeit der Stirlingschen Formel in (13). Den wirklichen Verlauf von $H_0(N)$ stellt schematisch die gestrichelte Kurve in Fig. 3 dar. Um die durch die Stirlingsche Annäherung verursachte Ungenauigkeit wenigstens teilweise zu kompensieren, kann man einfach das Glied $\log \sqrt{2\pi}$ in allen es



enthaltenen Formeln streichen. Im Gebiet (67), speziell in der Umgebung von $N_0^{\text{opt}} = C$ (62), führt dieses Weglassen zu keinem merklichen Unterschied, wegen (65) und (47). So haben wir jetzt statt (16), (19), (60), (65), (66) die Formeln:

$$\begin{aligned} H_0 &= (M + N) \log (M + N) - M \log M - N \log N = \\ &= \text{wenn (40) gilt: } \frac{C}{\sqrt{\eta}} [-\eta \log \eta + (1 + \eta) \log (1 + \eta)], \end{aligned} \quad (16')$$

$$\begin{aligned} H_\gamma &= (1 - \gamma) [(M + N) \log (M + N) - M \log M - N \log N] + \gamma N \log M = \\ &= \text{wenn (40) gilt: } \frac{C}{\sqrt{\eta}} \left\{ \left[\frac{\gamma}{2} - (1 - \gamma) \eta \right] \log \eta + \right. \\ &\quad \left. + (1 - \gamma) (1 + \eta) \log (1 + \eta) + \gamma \log C \right\}, \end{aligned} \quad (19')$$

$$\lim_{N \rightarrow 0} H_0(N) = \lim_{N \rightarrow \infty} H_0(N) = 0, \quad (66'), (60'), \quad H_0^{\max} = 2C, \quad (65)$$

wo allgemein wie in (52)

$$\eta = \frac{C^2}{N^2}. \quad (52')$$

Ähnlich bekommt man nach (12) für H_1 , wenn (40) gilt,

$$\lim_{N \rightarrow 0} H_1(N) = 0, \quad \lim_{N \rightarrow \infty} H_1(N) = -\infty. \quad (68)$$

und darum auch nach (19') für $0 < \gamma \leq 1$

$$\lim_{N \rightarrow 0} H_\gamma(N) = 0, \quad \lim_{N \rightarrow \infty} H_\gamma(N) = -\infty. \quad (69)$$

Aus (60') und (69) sehen wir, dass wir in dem uneigentlichen Punkt $N = \infty$ eine Unstetigkeit der Funktion $H_\gamma(N)$ (19') bezüglich γ haben, wenn $\gamma \rightarrow 0$. Man muss aber betonen, dass dieses Gebiet keinen eigentlichen physikalischen Sinn hat (weil dann $M \ll 1$) und die Grenzen (66), (60'), (68), (69) sind nur wegen der Vollständigkeit der mathematischen Diskussion nötig.

Im Zwischenfall $0 < \gamma < 1$ ist die Rechnung etwas umständlicher, aber die Resultate sind im allgemeinen qualitativ dieselben. Statt (53) haben wir jetzt die Gleichung

$$q_\gamma(\eta) \equiv g(\eta) + \frac{\gamma}{1-\gamma} \left(\frac{1}{2} \ln \eta + \ln C - 1 \right) = 0 \quad (70)$$

mit $g(\eta)$ nach (55). Wir erhalten einfach

$$\lim_{\eta \rightarrow 0} q_\gamma(\eta) = -\infty, \quad \lim_{\eta \rightarrow \infty} q_\gamma(\eta) = +\infty. \quad (71)$$

Die Grösse $\frac{\gamma}{1-\gamma} \ln C$ in (70) ist eine von η unabhängige additive Konstante und sie beeinflusst nicht die Gestalt der Kurve $q_\gamma(\eta)$, sondern nur ihre Lage bezüglich der Achse $q = 0$. Ähnlich wie in dem HÖDIschen Beweis rechnen wir die zwei ersten Ableitungen von $q_\gamma(\eta)$ aus:

$$q'_\gamma(\eta) = \frac{2}{1+\eta} + \ln \frac{\eta}{1+\eta} + \frac{\gamma}{2(1-\gamma)\eta} \quad \text{und} \quad q''_\gamma(\eta) = \frac{P_\gamma(\eta)}{2(1-\gamma)\eta^2(1+\eta)^2}, \quad (72)$$

wo

$$P_\gamma(\eta) \equiv -(2-\gamma)\eta^2 + 2(1-2\gamma)\eta - \gamma \quad (73)$$

ist. Weil für $0 < \gamma < 1$ der Nenner in (72) immer positiv ist, hängt das Vorzeichen von q''_γ vom Vorzeichen des Polynoms $P_\gamma(\eta)$ ab. Für die Wurzeln der quadratischen Gleichung $P_\gamma(\eta) = 0$ haben wir

$$\eta_{1,2} = \frac{1-2\gamma \mp \sqrt{1-6\gamma+5\gamma^2}}{2-\gamma}. \quad (74)$$

Wir lösen weiter die Gleichung

$$Q(\gamma) \equiv 5\gamma^2 - 6\gamma + 1 = 0 \quad (75)$$

auf und erhalten

$$\gamma_1 = \frac{1}{5}, \quad \gamma_2 = 1. \quad (76)$$

$Q(\gamma)$ ist positiv in den Gebieten $\gamma < \frac{1}{5}$ und $\gamma > 1$. Von diesen ist nur das Gebiet

$$0 < \gamma < \frac{1}{5} \quad (77)$$

für unseres Problem wichtig (weil das andere, $\gamma > 1$, keinen physikalischen Sinn hat). Nur im Gebiet (77) gibt es zwei reelle Wurzeln (74). Sie sind positiv und liegen im Intervall $0 \leq \eta \leq 1$ (d. h. für $N \geq C$ nach (52'), siehe Fig. 4).

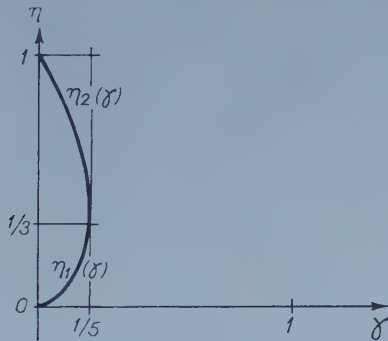


Fig. 4

Nur im Intervall $\eta_1 < \eta < \eta_2$ kann q''_γ sein Vorzeichen vom negativen zum positiven ändern (siehe Fig. 5a, b). In Fig. 5a–e sind die fünf möglichen Typen des Verlaufs der Funktion $q_\gamma(\eta)$ dargestellt. Der Unterschied zwischen den Typen a, b und c in Fig. 5 hängt vom Vorzeichen der Grösse $q'_\gamma(\eta_1(\gamma)) \equiv \omega(\gamma)$ ab. Diese Grösse ist nur eine Funktion von γ (von C ist sie unabhängig), deren Verlauf im uns interessierenden Argumentenintervall (77) die Fig. 6 darstellt. $\omega(\gamma)$ verschwindet für $\gamma = \gamma_0 \approx 0,108$, ist negativ für $0 < \gamma < \gamma_0$ und positiv für $\gamma > \gamma_0$. Aus Fig. 5 sehen wir, dass in den Fällen b, c, d, und e, d. h. für

$$\gamma \geq \gamma_0 \quad (78)$$

nur ein Maximum von $H_\gamma(N)$ möglich ist. Im Fall a, d. h. für

$$0 < \gamma < \gamma_0 \quad (79)$$

sind drei Extrema möglich, aber nur für solche Werte der Konstante C , für

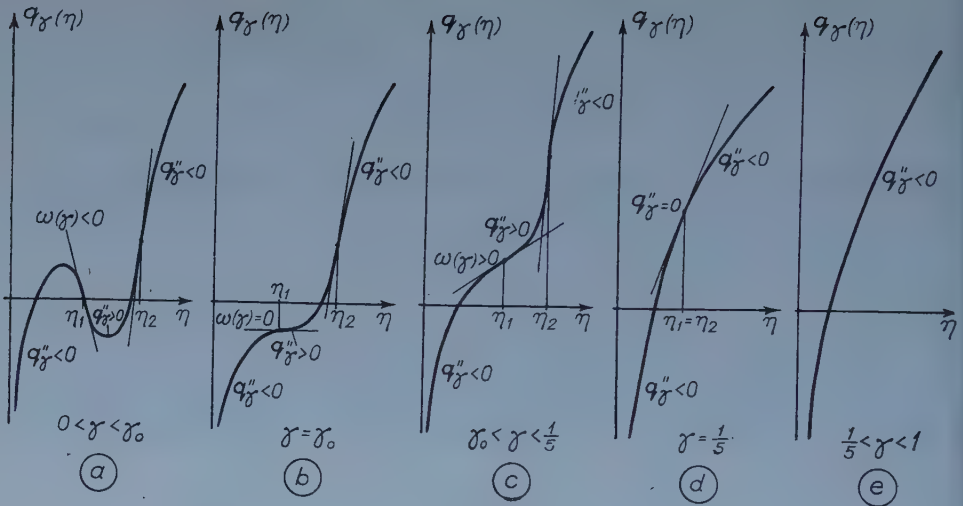


Fig. 5

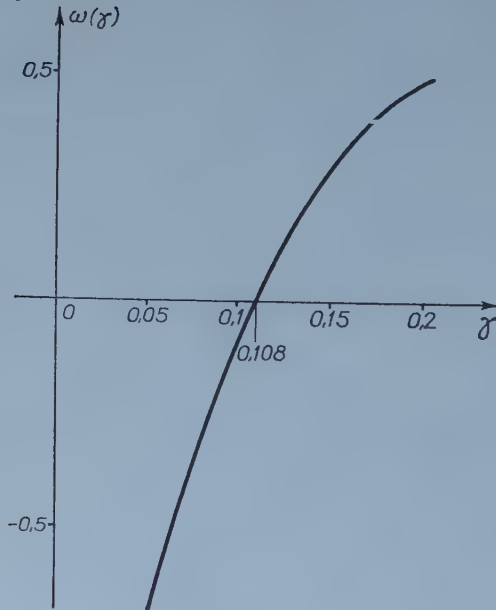


Fig. 6

welche der nach unten eingebogene Teil der Kurve $q_\gamma(\eta)$ die Achse $q = 0$ schneidet. Es gibt daher zwei solche Funktionen $C_1(\gamma)$, $C_2(\gamma)$, dass

$$C_1(\gamma) > C_2(\gamma) \text{ für (79), } C_1(\gamma_0) = C_2(\gamma_0), \quad (80)$$

und dass für die Werte von C im Intervall

$$C_1(\gamma) < C < C_2(\gamma) \quad (81)$$

drei Wurzeln von $q_\gamma(\eta) = 0$ vorkommen. Es folgt aus der Stetigkeit des Pro-

blems und dem Verlauf von q'' , dass die rechte (für das grösste η) der drei Wurzeln ein Maximum von $H_\gamma(N)$ geben wird. Die mittlere Wurzel gibt dann ein Minimum und die linke das zweite Maximum. Wir sind so zum Schluss gekommen, dass im Gebiet (79), (81) (das man ein Ausnahmegebiet nennen kann) zwei Maxima des Informationsgehaltes möglich sind, während ausserhalb dieses Gebietes nur eins auftreten kann. Nur die exakte numerische oder graphische Analyse (die wir hier nicht durchgeführt haben) und ein ausführlicher Vergleich mit dem Experiment kann entscheiden, ob das Ausnahmegebiet von irgendeiner praktischen Bedeutung ist.

Fortsetzung des Beispiels

Wir kehren jetzt zu unserem aus der ROSESchen Arbeit [8] genommenen Beispiel zurück. ROSE gibt keine Angaben über den Kohärenzgrad des vom ihm benutzten Lichtes. Weil aber die aufgenommenen Objekte nicht selbstleuchtend waren, kann man mit guter Annäherung annehmen, dass das Licht ungefähr kohärent war ($\gamma \approx 0$). Mit den C -Werten aus (46) können wir dann nach (64) die optimalen Wellenlängen leicht berechnen. Wir erhalten

$$\lambda_0^{\text{opt}} = \begin{cases} 2 \cdot 10^{-4} \text{ cm,} \\ 2 \cdot 10^{-5} \text{ cm,} \end{cases} \quad (82)$$

wo, wie oben, die obere Zahl der kleinsten und die untere der grössten Beleuchtungsintensität im ROSESchen Experiment entspricht. Unsere Schätzung der numerischen Werte war grob (speziell die von ε nach (43) und (44)), so dass bestenfalls nur die Grössenordnungen gut sind. Bei dieser Genauigkeit haben wir doch einen guten Einklang mit dem Experiment erhalten, weil (im Rahmen des ROSESchen Experiments) der zweite Wert der Wellenlänge dem maximalen Informationsgehalt entspricht und im sichtbaren (bzw. photographischen) Wellengebiet liegt ($\approx 10^{-5}$ cm). Es ist auch vernünftig, dass man für die kleineren Intensitäten des Lichtes die Wellenlänge verlängern muss, um den maximalen Informationsgehalt zu bekommen. Dann würden nämlich die Lichtquanten kleiner und die Quantenzahl grösser (bei gegebener totaler Energie) und deshalb kann das Bild mehr Einzelheiten zeigen.

Schlussbemerkungen

Das ROSESche Experiment hat uns eine grobe Kontrolle der Richtigkeit unserer Betrachtungen ermöglicht. Es würde aber sehr wünschenswert sein, weitere Experimente durchzuführen, um die Übereinstimmung der Theorie mit dem Experiment genauer zu prüfen. Speziell wäre es von grosser Bedeu-

tung, die ROSESche Serie für noch grössere Lichtintensitäten zu erweitern, um sich zu überzeugen, ob es tatsächlich ein Maximum des Informationsgehalts gibt (im ROSESchen Experiment befinden wir uns nur auf der einen Seite des hypothetischen Maximums).

Es muss jedoch bemerkt werden, dass eine sehr genaue Übereinstimmung unserer Resultate mit dem Experiment kaum zu erhoffen ist, da unsere Voraussetzungen ziemlich grobe Annäherungen enthalten. Z. B. gelten die BOHR—ROSENFELDSchen Unbestimmtheitsrelationen eigentlich nur für die freien Ladungen, was bei den realen Lichtrezeptoren nicht genau der Fall ist. Bis jetzt aber sind z. B. die photographischen Prozesse theoretisch nicht ganz geklärt und daher ist es schwer, unsere Betrachtungen zu vervollkommen. Es scheint aber, das die effektive Probeladung ε (die im allgemeinen eine Funktion von λ_0 ist) ohne Theorie, rein experimentell bestimmt werden kann, wenn die Richtigkeit unserer Gesetzmässigkeiten wenigstens in gewissen Grenzen experimentell bewiesen wird.

In unseren obigen Betrachtungen haben wir eigentlich einen Standpunkt eingenommen, der dem in der Praxis üblichen entgegengesetzt ist: wir haben die Parameter der äusseren Bedingungen als gegeben betrachtet und die optimale Wellenlänge gesucht, während normalerweise die Wellenlänge des Lichtes durch die Lichtquellen und Lichtrezeptoren bestimmt ist und nur die Auswahl der äusseren Parameter zur Verfügung steht. Jeder der äusseren Parameter kann bei Festlegung der anderen und bei gegebener Wellenlänge als Optimierungsgrosse benutzt werden. Z. B. das Auge optimalisiert automatisch sein Öffnungsverhältnis zu den jeweiligen äusseren Bedingungen und der Lichtwellenlänge. Ähnlich wählt der Photographierende empirisch die besten äusseren Parameter (wie z. B. Öffnungsverhältnis, Belichtungszeit usw.) für die gegebenen anderen Parameter und die Wellenlänge des Lichtes. Im ROSESchen Experiment diene als Optimisierungsparameter die Beleuchtungsintensität.

Aus der vorliegenden Arbeit sehen wir, dass im Problem der optimalen optischen Abbildung nicht nur die Quantennatur des Lichtes, sondern auch die Natur des Lichtempfängers von Bedeutung ist (Parameter!). Daher sind z. B. die Experimente mit photographischen Schichten im allgemeinen nicht massgebend für das Auge und umgekehrt, wenn auch die anderen Parameter, wie Öffnungsverhältnis usw. dieselben sind (was z. B. ROSE in [8] nicht beachtet, wenn er seine Arbeit »Quantum and Noise Limitations of the Visual Process« betitelt). Im Zusammenhang damit ist es zweckmässig, eine pessimistische Bemerkung von TORALDO DI FRANCIA aus [2] über das Auflösungsvermögen zu zitieren: »After so many investigations about resolving power, one cannot escape the discouraging conclusion that a very common sentence like: 'The resolving power of such instrument has such value' has no meaning. Resolving power is not a well-defined physical quantity.« Nach unseren Be-

trachtungen ist es ganz klar, dass der Begriff des Auflösungsvermögens bezüglich der Rezeptoreigenschaften relativisiert werden muss. Im allgemeinen Fall (d. h. nicht nur in dem Gauss'schen Gebiet) kann auch dieser Begriff von der Gestalt des Objektes wesentlich abhängen. Nach dieser Relativisierung aber kann man schon mit Hilfe der informationstheoretischen Methoden das Auflösungsvermögen eindeutig (*»as a well-defined physical quantity«*) feststellen, z. B. für das Gauss'sche Gebiet als δ^{-1} , siehe oben (37).

In unserer Arbeit haben wir die Bedingungen für die optimale optische Abbildung (oder das optimale optische System) erhalten, welche unabhängig von der Form des Objektes sind. In diese Bedingungen sind nur die äusseren Parameter des optischen Systems eingegangen (russisch *»габариты«*) und nicht die inneren (wie z. B. Krümmungsradien der Brechungsflächen, Brechungskoeffizienten usw.), die zu bestimmen die eigentliche Aufgabe des optischen Rechners ist. Das war eine Folge unseres *»vereinfachten«* Modells, und zwar der Einschränkung auf das Gauss'sche Gebiet (siehe Fig. 1), wo die inneren Parameter belanglos für die optische Abbildung sind. Wenn wir auch nicht-vereinfachte Modelle mit Aberrations-, Rauschproblemen usw. betrachten würden, wie LINFOOT in [3], dann würden wir auch einige Bedingungen für die inneren Parameter erhalten. Dieses Problem ist aber in der von uns oben vorbereiteten Form in aller Allgemeinheit, des Verfassers Wissens nach, bis jetzt noch nicht gelöst und scheint sehr schwierig zu sein. Der Verfasser hat nur ein viel einfacheres Problem gelöst, nämlich das Bestimmen der inneren Parameter des optimalen optischen Systems für ein punktförmiges Objekt, wie dies auf der Stockholmer Konferenz der I. C. O in 1959 berichtet wurde [11], [12].

LITERATUR

1. D. GABOR, Proc. of a Symposium on Astronomical Optics held in the University of Manchester, April 19–22, 1955, North-Holland Publ. Co., Amsterdam, 1956, 17.
2. G. TORALDO DI FRANCA, J. Opt. Soc. Amer., **45**, 497, 1955.
3. E. H. LINFOOT, J. Opt. Soc. Amer., **45**, 808, 1955.
4. C. E. SHANNON, Proc. Inst. Radio Eng., **37**, 10, 1949.
5. L. MANDELSTAM, Weber-Festschrift, 1912, und: Полное собрание сочинений, т. 1, Москва, 1948, 229.
6. L. BRILLOUIN, Science and Information Theory, Academic Press, New York, 1956.
7. H. S. GREEN und E. WOLF, Proc. Phys. Soc. A **66**, 1129, 1953.
8. A. ROSE, J. Opt. Soc. Amer., **43**, 715, 1953.
9. A. ROSE, J. Opt. Soc. Amer., **38**, 196, 1948.
10. N. F. MOTT und R. W. GURNEY, Electronic Processes in Ionic Crystals, Clarendon Press, Oxford, 1948.
11. R. S. INGARDEN, Optica Acta, **7**, 179, 1960.
12. R. S. INGARDEN, Bull. Acad. Polon. Sci. sér. math. astr. phys., **7**, 687, 1959.

ТЕОРИЯ ИНФОРМАЦИИ, СООТНОШЕНИЯ НЕОПРЕДЕЛЕННОСТИ БОРА—
РОЗЕНФЕЛЬДА И ПРОБЛЕМА ОПТИМАЛЬНОГО ОПТИЧЕСКОГО
ИЗОБРАЖЕНИЯ

Р. С. ИНГАРДЕН

Резюме

Доказано основную теорему Габора о разложении в ряд из оптической теории информации. Обобщено формулу Линфута для количества информации в оптическом изображении на случай совершенно и частично когерентного света. Исходя из соотношений неопределенности Бора—Розенфельда найдена связь между максимальным числом уровней освещения в изображении и числом степеней свободы оптической волны. Из этого факта следует для заданных внешних условий существование оптимальной длины волны (или для заданной длины волны существование оптимальных условий, как освещение, время экспозиции, относительное отверстие и т. д.). Все рассуждения проведены в гауссовом приближении.

SOME PRACTICAL REMARKS CONCERNING THE CALCULATION OF THE PHASE SHIFTS OF THE YUKAWA POTENTIAL

By

T. TIETZ

DEPARTMENT OF THEORETICAL PHYSICS, UNIVERSITY ŁÓDŹ, ŁÓDŹ, POLAND

(Presented by A. Kónya. — Received 4. XI. 1960)

In this paper we give some practical formulas making possible the calculation of the phase shifts of the Yukawa potential. The formulas depend on whether the radial quantum number l is large or small. Some numerical values illustrate the accuracy of the mentioned phase shifts.

According to HULTHÉN [1] we write the Schrödinger equation for the Yukawa potential in the following form:

$$\frac{d^2 \Phi}{dx^2} + \left[a + \frac{be^{-x}}{x} - \frac{l(l+1)}{x^2} \right] \Phi = 0, \quad (1)$$

where $x = \kappa r$, $a = M(E/\hbar^2 \kappa^2)$, $M = \frac{1}{2}(M_n + M_p)$; E is the energy in the centre of mass system, M_n the neutron mass, M_p the proton mass and $b = MB^2/\hbar^2 \kappa$. The symbol κ is related to the meson mass M_n as follows; $\kappa = Mmc/\hbar$. The remaining symbols \hbar , c , r and l possess the standard meanings. B appearing in the formula of b is a constant. The solution Φ of eq. (1), as known, fulfils the following boundary conditions:

$$\Phi(0) = 0 \quad \text{and} \quad \Phi(x) \xrightarrow{\lim x \rightarrow \infty} \sin \left(\sqrt{a}x - \frac{l\pi}{2} + \eta_l \right). \quad (2)$$

In order to obtain some formulas concerning the phase shifts of the Schrödinger equation of the Yukawa potential we start from the *WKB* approximation for η_l . This formula applied to eq. (1) takes the form [2]

$$\eta_l = \int_{x_l}^{\infty} \left[a + \frac{be^{-x}}{x} - \frac{\left(l + \frac{1}{2}\right)^2}{x^2} \right]^{1/2} dx - \int_{x_l'}^{\infty} \left[a - \frac{\left(l + \frac{1}{2}\right)^2}{x^2} \right]^{1/2} dx, \quad (3)$$

where the lower limits x_l and x_l' are the largest positive zeros of the respective integrals. When the quantum number l is sufficiently large $(be^{-x_l})/x_l$ is small in comparison with $\left(l + \frac{1}{2}\right)^2/x_l^2$, so that we may consider the lower limits in

the integrals to be equal. Expanding the square roots we obtain for the phase shifts η_l given by eq. (3) the following formula:

$$\eta_l = \frac{b}{2} \int_{(l+\frac{1}{2})/\sqrt{a}}^{\infty} \frac{e^{-x} dx}{\left[a x^2 - \left(l + \frac{1}{2} \right)^2 \right]^{1/2}}. \quad (4)$$

After simple calculations we write formula (4) in the following form:

$$\eta_l = \frac{b}{2\sqrt{a}} \int_1^{\infty} \frac{e^{-\frac{(l+1/2)t}{\sqrt{a}}}}{\sqrt{t^2 - 1}} dt. \quad (5)$$

The integral appearing in formula (5) can be evaluated by means of the following integral [3]:

$$\int_1^{\infty} e^{-zx} (x^2 - 1)^p dx = \frac{1}{\sqrt{\pi}} \left(\frac{z}{2} \right)^{-p-\frac{1}{2}} K_{p+\frac{1}{2}}(z) \Gamma(p+1),$$

where

$$|\arg z| < \frac{\pi}{2} \quad \text{and} \quad \operatorname{Re}(p) > -1. \quad (6)$$

K is the modified Hankel function of zero order and Γ the Euler function. With the last formula we can write the phase shifts η_l given by eq. (5) as follows:

$$\eta_l = \frac{b}{2\sqrt{a}} k_0 \left(\frac{l + \frac{1}{2}}{\sqrt{a}} \right). \quad (7)$$

This simple formula for the phase shifts gives results the more accurate in comparison with the numerical results the larger the quantum numbers. For the first quantum numbers $l=0$, $l=1$ and $l=2$ we must calculate η_l given by eq. (3) numerically if we want to obtain accurate values for η_l . Formula (3) for η_l is not convenient for practical numerical integration because for a given a we must integrate for each l separately. Therefore we write formula (3) at first as follows:

$$\eta_l = \int_{x_l}^{\infty} \omega^{1/2} \left[1 - \frac{\left(l + \frac{1}{2} \right)^2}{\omega x^2} \right]^{1/2} dx - \int_{x_l}^{\infty} \left[a - \frac{\left(l + \frac{1}{2} \right)^2}{x^2} \right]^{1/2} dx. \quad (8)$$

where

$$\omega = a + \frac{be^{-x}}{x}. \quad (9)$$

For small quantum numbers $l = 0, 1, 2$, the term $\left(l + \frac{1}{2}\right)^2 / \omega x^2$ is much smaller than unity over the whole range of x from x_l to infinity. At $x = x_l$ the expression $\left(l + \frac{1}{2}\right)^2 / \omega x_l^2$ is equal to unity but decreases rapidly for $x > x_l$. Expanding the square root appearing in the first integral we obtain

$$\eta_l = \int_{x_l}^{\infty} (\omega^{1/2} - a^{1/2}) dx + \int_{x_l}^{\infty} \omega^{1/2} \left[\frac{\left(l + \frac{1}{2}\right)^2}{\omega x^2} - \frac{1}{8} \frac{\left(l + \frac{1}{2}\right)^4}{\omega^2 x^4} \dots \right] dx \quad (10)$$

$$- \int_{x_l'}^{\infty} \left[a - \frac{\left(l + \frac{1}{2}\right)^2}{x^2} \right]^{1/2} dx.$$

The last integral in formulas (8) and (10) can be calculated analytically.

The lower limit x_l' in this integral is $x_l' = \left(l + \frac{1}{2}\right) / \sqrt{a}$.

The last formula for small l is much more useful for the numerical integration than (3), because the factor containing l may be removed from the integral. The integral in (3) has to be numerically integrated for each value of l . In Table I we have some numerical values for η_1 and η_2 , calculated from formula (7) in comparison with the results obtained by other authors.

Table I shows that formula (7) for η_l for the cases $l = 1$ and $l = 2$ gives results comparable with those obtained by other methods. For quantum numbers $l > 3$ our values for η_l given by the analytical formula (7) will be sufficiently accurate. If we want to obtain accurate numerical values for the phase shifts for lower values of l , e. g. $l = 0$, $l = 1$ and $l = 2$ we must calculate η_l numerically from the formula (10). For quantum numbers $l \geq 3$ our analytical formula for eq. (7) is sufficiently accurate. Thus the formulas (7) and (10) allow calculation of the phase shifts for the Yukawa potential for all quantum numbers l . The problem of the phase shifts for the Yukawa potential for higher quantum numbers l was also considered by the author in a short note [8].

Table I

Comparison of our numerical results for $\text{tg } \eta_l$ from eq. (7) with various other results, for $l = 1$ and $l = 2$

l	$2\sqrt{a}$	b	$\text{tg } \eta_l$
1	1.2	-0.9	$\text{tg } \eta_l \text{ (eq. 7)} = -0.04716$
			$\text{tg } \eta_{lF} = -0.04508$
			$\text{tg } \eta_{lH} = -0.04600$
1	1.6	-0.9	$\text{tg } \eta_l \text{ (eq. 7)} = -0.07430$
			$\text{tg } \eta_{lF} = -0.06775$
			$\text{tg } \eta_{lH} = -0.06906$
			$\text{tg } \eta_{lK} = -0.06850$
1	1.2	2.7	$\text{tg } \eta_l \text{ (eq. 7)} = 0.1414$
			$\text{tg } \eta_{lF} = 0.1479$
			$\text{tg } \eta_{lH} = 0.1925$
2	1.37	2.52	$\text{tg } \eta_l \text{ (eq. 7)} = 0.0306$
			$\text{tg } \eta_{lF} = 0.0305$
			$\text{tg } \eta_{lH} = 0.0368$
			$\text{tg } \eta_{lR} = 0.0366$

FOGEL [4] (η_{lF}); KÄLLÉN [5] (η_{lK}); HANSON [6] (η_{lH}); RAMSEY [7] (η_{lR}).

REFERENCES

1. L. HULTHÉN and H. NAGEL, Phys. Rev., **90**, 62, 1953.
2. P. COMBÁS, Die statistische Theorie des Atoms und ihre Anwendungen, Springer-Verlag, Wien 1949.
3. G. N. WATSON, Theory of Bessel Functions, Cambridge, 1944.
4. K. G. FOGEL, Acta Acad. Aboensis, **19**, 1, 1954.
5. G. KÄLLÉN, Ark. f. Fys., **4**, 42, 1952.
6. K. HANSON, Fysiogr. Sällsk. Lund. Förhandl., **18**, 12, 1948.
7. W. RAMSEY, Proc. Camb. Phil. Soc., **44**, 87, 1948.
8. T. TIETZ, Il Nuovo Cimento, **10**, 553, 1958.

НЕСКОЛЬКО ПРАКТИЧЕСКИХ ЗАМЕЧАНИЙ ОТНОСИТЕЛЬНО ВЫЧИСЛЕНИЯ СДВИГА ФАЗ ПОТЕНЦИАЛА ЮКАВА

Т. ТИТЦ

Резюме

В данной работе предлагается несколько практических формул, позволяющих вычислить сдвиг фаз потенциала Юкава. Формулы зависят от того, что радиальное квантовое число имеет малое или большое значение. Для иллюстрации точности упомянутого сдвига фаз приводятся численные значения.

ELECTROLUMINESCENCE AT LOW VOLTAGE

By

J. WEISZBURG

INDUSTRIAL RESEARCH INSTITUTE FOR TELECOMMUNICATION TECHNIQUE, BUDAPEST

(Presented by G. Szigeti. — Received 11. XI. 1960)

It is usual to distinguish between the intrinsic and the injection electroluminescence, also because of the differences of the threshold voltages of their lightings. There is no foundation for this distinction because the orders of the threshold voltages of the two groups agree with each other. The electroluminescent phenomena of evaporated ZnS layers at low voltages can be well described also by regularities characteristic of the Mott-Shottky-type barriers. The existing measuring data are not detailed enough to serve as check of the correctness of the various theoretical hypotheses.

Dealing in general with the similar features of the intrinsic and the injection electroluminescence we already previously pointed out [1] that the attempt of grouping by which the mechanisms and characteristics of the two phenomena are separated is based on doubtful arguments. In this article the connection between the statements asserting the differences between the exciting voltages of the "two kinds" of electroluminescence on one side and the measured results on the other is examined.

At the very start we note that "low voltage" is a completely undetermined expression and means only that *the voltage put on the examined sample, an unknown part of which produces the electroluminescence, is in absolute value small*. Of course, from this only qualitative conclusions can be drawn as to the voltage causing the electroluminescence. In order to give a better survey of the problem, in Table I we chronologically summed up the data of some characteristic publications.

The so-called intrinsic and injection electroluminescences have formerly [2, 3, 4] been separated — among others — because the field strengths necessary for the excitation in the two cases (really the external exciting voltage put into the sample) have been different. In case of injection electroluminescence in forward direction there is no remarkable threshold field strength. In reverse direction light appears in the range of the breakdown voltage of the material. The field strength necessary for the intrinsic electroluminescence — being an average value — differs from the former ones. It can be seen that in the course of time (with more experience and better detecting devices) the voltage threshold data have decreased in case of the material used for every kind of electroluminescence and generally independently of the material,

Table I

Year	Author	Material		Exciting		Gap width eV	Max. photon energy eV	Ref. No.
		Type	Form	voltage V	frequency			
1928	LOSSEV	SiC	PC	8-R 30-R 2-F	D. C. D. C. D. C.			10
1944	KENDALL	SiC	PC	20	D. C.			11
1947	DESTRIAU	ZnS	P	28 rms	60 c/s			12
1951	LEHOVEC et al.	SiC	PC	30	D. C.	3,0	2,8	13
1952	BRAMLEY et al.	ZnSiO ₄	P	100	60 c/s			14
1953	LEHOVEC et al.	SiC	PC	1,8-F	D. C.	2,9	2,0	15
1953	NEWMAN	Ge		2	350 c/s		0,65	16
1954	SZIGETI	SiC	PC	6-R	D. C.	2,9	2,6	17
1954	NAGY et al.	SiC	PC	1,4-R	D. C.	3,1	2,6	8
1956	HARMAN	BaTiO ₃ TiO ₂ SrTiO ₃ KNbO ₃	P	30 rms	10 c/s— —100 MC/s		2,4	18
1957	JEGES	SnO ₂	PC	3—4	D. C.			19
1958	DESTRIAU et al.			9 rms				20
1959	THORNTON	ZnS	FL	10 rms 20-F 60-R	10 Kc/s D. C. D. C.			5
1959	THORNTON	ZnS	P	2—3 rms	1000 c/s			6
1959	THORNTON	ZnS	FL	1,5 rms	1000 c/s	3,8	2,6	7
1959	KIKUCHI et al.	CdS	SC	20—50 F	D. C.			21
1960	WEISZBURG	SiC	PC	3 rms 4—6-R	1000 c/s D. C.	3,1	2,6	22
1960	LEHMANN	ZnS	P	25 rms	5 Kc/s			23

R. resp. F is the reverse resp. forward direction; SC = single crystal; PC = polycrystal; P = powder; FL = film.

tend to the value of some volts. This voltage value, being presumably a threshold value connected with the measuring technique, seems to be of the same order in the various kinds of electroluminescent excitations. But this does not justify a separation of the theoretical interpretation of the phenomenon.

The measurements of THORNTON are a great help in forming an idea of the phenomenon somewhat freer from contradiction. He effectuated these measurements on ZnS layers and powders [5, 6, 7]. The traditional theoretical contradiction appears the most vividly perhaps in his last-mentioned publication [7]. According to THORNTON low voltage means that there is no impact

excitation, but e. g. charge carrier injection. This is surprising when we consider that from measuring results just in the low voltage range the regularity $B \sim \exp[-V^{-1/2}]$ known as characteristic of the impact ionization excitation is proved through four orders of magnitude (Fig. 1). Here B means the brightness and V the applied voltage.

We should like to show that according to some of our previous observations the results of THORNTON can be interpreted also on another theoretical

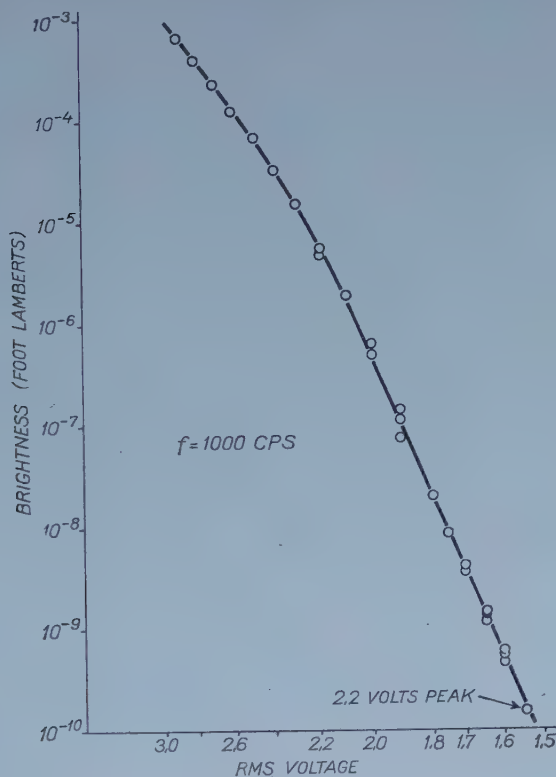


Fig. 1

basis. In the course of our examinations it has been found that the reverse current of the SiC samples is characteristic of the surface barriers and can be well described by the following relation:

$$i = AT^2 \exp \left[-\frac{e}{kT} \left(\Phi - \left[\frac{8\pi e^3 N_0}{\epsilon \eta^2} V \right]^{1/4} \right) \right]. \quad (1)$$

It has also been found and shown by THORNTON too that the measured d. c. is proportional to the emitted electroluminescent light. From this the correctness of

$$B \sim a \cdot \exp[bV^{1/4}] \quad (2)$$

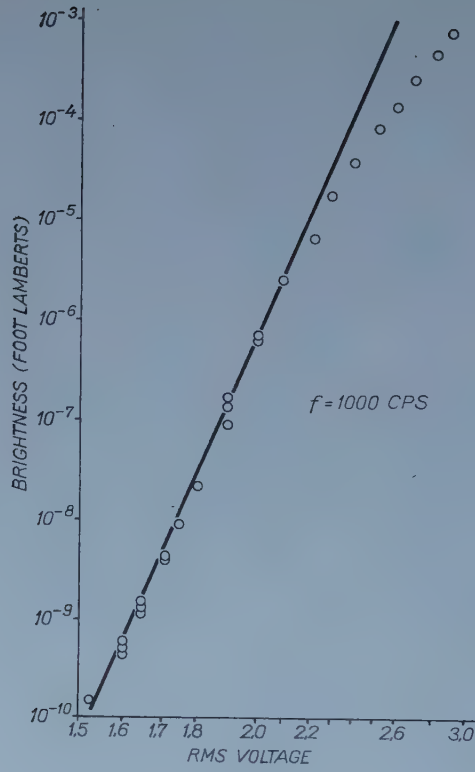


Fig. 2

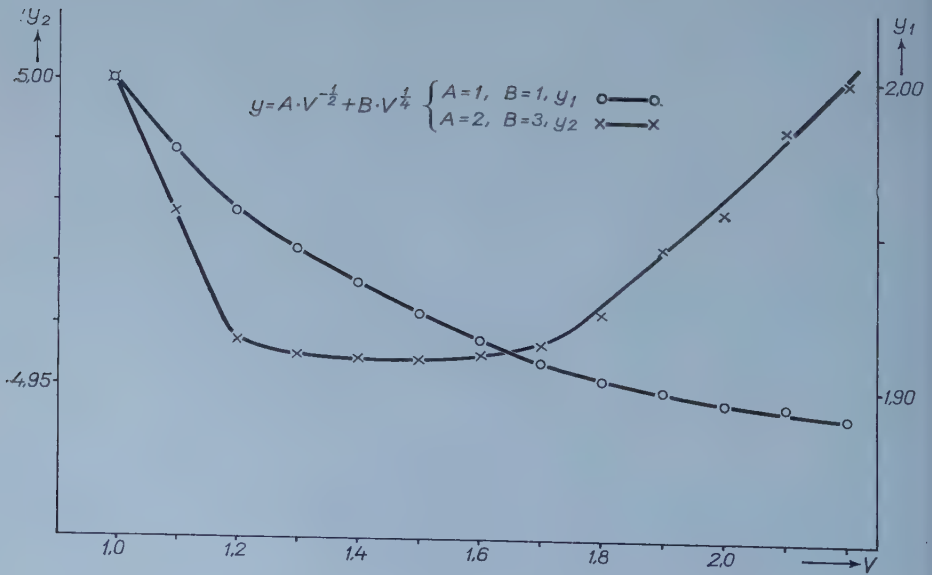


Fig. 3

would follow. Indeed, the measuring data of THORNTON which were re-calculated by us prove also the same fact (Fig. 2). For the sake of comparison the original figure of THORNTON can also be seen (Fig. 1). Both figures seem to prove the assumed regularities, though it is unquestionable that only one notion can be true. The agreement is not surprising taking into consideration that in the voltage range in question the values $-V^{-1/2}$ and $V^{1/4}$ are similarly changing (Fig. 3). In this way it can also be said that every theory in which the relation

$$\log B \propto V^k \quad (3)$$

is valid in case of $-V^{-1/2} < V^k < V^{1/4}$ can be proved by these measurements. This means that inside the given accuracy of measurement only the facts are known and conclusive inferences concerning the mechanism cannot be drawn.

Nevertheless the equations (1) and (2) completed by other considerations seem to be suitable for the description of electroluminescent phenomena. We hope to come back on another occasion [9] to the more detailed discussion of this point.

Summing up one may say that the differences found previously between the threshold voltages of the intrinsic and injection electroluminescences decreased to a high degree by the development of the experimental technique which shows the analogy, resp. identity of the two separate groups of phenomena. Theoretically, the inaccuracy of the measurements known for the time being allows only qualitative statements. Thus the validity of the various theories cannot be proved or refuted only by a better measuring technique or by more comprehensive examinations. The fact that the measurements of THORNTON could be described with fewer contradictions characteristic of the surface barriers shows that there must be a deeper relation between the electroluminescent phenomena experimentally known to differ from each other and these laws.

REFERENCES

1. J. WEISZBURG, *Acta Phys. Hung.*, **10**, 337, 1959.
2. G. DESTRIAU and H. F. IVEY, *Proc. I. R. E.*, **43**, 1911, 1955.
3. F. MATOSI, *Elektrolumineszenz und Elektrophotolumineszenz*. Verl. F. Vieweg & Sohn, Braunschweig, 1957.
4. S. T. HENDERSON, *Brit Journ. Appl. Phys.*, **9**, 45, 1958.
5. W. A. THORNTON, *J. Appl. Phys.*, **30**, 123, 1959.
6. W. A. THORNTON, *Phys. Rev.*, **113**, 1187, 1953.
7. W. A. THORNTON, *Phys. Rev.*, **116**, 893, 1959.
8. E. NAGY and J. WEISZBURG, III. Meeting of R. Eötvös Phys. Soc. Budapest, 1954.
9. J. WEISZBURG, to be published.
10. O. V. LOSSEV, *Phil. Mag.*, **6**, 1024, 1928.
11. J. T. KENDALL, *Proc. Phys. Soc.*, **56**, 123, 1944.

12. G. DESTRIAU, *Phil. Mag.*, **38**, 700, 1947.
13. K. LEHOVEC, C. A. ACCARDO and E. JAMGOCHIAN, *Phys. Rev.*, **83**, 603, 1951.
14. A. BRAMLEY and J. E. ROSENTHAL, *Phys. Rev.*, **87**, 1125, 1952.
15. K. LEHOVEC, C. A. ACCARDO and E. JAMGOCHIAN, *Phys. Rev.*, **89**, 20, 1953.
16. R. NEWMAN, *Phys. Rev.*, **91**, 1313, 1953.
17. G. SZIGETI, *Acta Phys. Hung.*, **4**, 64, 1954.
18. G. G. HARMAN, *Phys. Rev.*, **104**, 1498, 1956.
19. K. JEGES, Pécsi Műszaki Szemle 1957. 4. (In Hungarian.)
20. G. DESTRIAU and L. DOMERGUE, *Proc. Int. Coll. on Semiconductors and Phosphors, Gar-misch-Partenkirchen 1958*. (Interscience Publishers Inc. New York, 1958.)
21. M. KIKUCHI and S. IIZIMA, *J. Phys. Soc. Japan*, **14**, 852, 1959.
22. J. WEISZBURG, *Acta Phys. Hung.*, **11**, 95, 1960.
23. W. LEHMANN, *J. El. chem. Soc.*, **107**, 20, 1960.

ЭЛЕКТРОЛЮМИНЕСЦЕНЦИЯ ПРИ НИЗКОМ НАПРЯЖЕНИИ

Я. ВЕЙСБУРГ

Резюме

Интринсикционную и инъекционную электролюминесценции обычно различают и по расхождению порогового напряжения свечения. Это не имеет основания, так как пороговые напряжения в обеих группах, по порядку величин, совпадают. Электролюминесцентные явления на напыленных слоях ZnS при низком напряжении могут быть достаточно хорошо описаны и закономерностями, характерными для барьеров типа Мотта — Шоттки. Подробности, полнота и точность экспериментальных данных, известных по настоящее время, не достаточны для проверки правильности различных теоретических гипотез.

ON THE REVERSE CHARACTERISTICS OF GERMANIUM JUNCTION DIODES

By

A. LŐRINCZY and G. PATAKI

RESEARCH INSTITUTE FOR TECHNICAL PHYSICS OF THE HUNGARIAN ACADEMY OF SCIENCES,
BUDAPEST

(Presented by G. Szigeti. — Received 7. XII. 1960)

The reverse characteristics of germanium junction diodes have been examined in the temperature range of 200–340° K. It has been found that the reverse current — instead of showing saturation — changes linearly with the voltage. On the basis of the temperature dependence of the slope of the linear section the hypothesis that we have to do here with a shunting effect of the adsorbed water layer of some molecules seems to be justified. Below 0° C an activation energy of 9.1 kcal/mol appears as the conductivity of ice, in good agreement with the corresponding data figuring in the literature. From the temperature dependence of the defined saturation current a value of 0.70 eV was derived as the gap of germanium.

It is already a well-known fact that the reverse characteristics of diodes and transistors are considerably influenced by the ambient atmosphere. This effect, as it is known, means that the diode law

$$I = I_s \left(\exp \frac{eV}{kT} - 1 \right)$$

is not fulfilled in reverse direction, but with increasing voltage also the current rises monotonically. So, apparently, there is no reason for speaking of saturation. But we shall see that in some cases the saturation current can be defined appropriately.

The influence of moisture on the characteristics of $p-n$ junctions has been examined by several researchers and many models have been proposed for the explanation of the appearing excess current. According to A. L. McWHORTER and R. H. KINGSTON [1] the cause of the excess current is the “channel” developing on the surface. But this hypothesis leads to logarithmic voltage-current characteristics. J. T. LAW [2], [3] explains the linear characteristics by the ionic conduction of water adsorbed on the surface. W. T. ERICSEN *et al.* [4] and also E. N. CLARKE [5] suggest an electronic conduction instead of the ionic one. According to the model suggested in article [4] the water layer adsorbed on the surface of the semi-conductor shows hole conduction. The water molecules work their way into the surface states of the semi-conductor and in case of a sufficiently large covering form a “diffuse” band.

The difficulty of proving the ionic conduction model — as has been pointed out also by R. H. KINGSTON [6] — consists in that the gas formation occurring in case of ionic conduction as measured in work [3] could not be reproduced.

In the mechanism described in [4] the transition of the excess current through the oxide layer is not clear.

In our present work the reverse current of encapsulated germanium diodes has been examined as function of the temperature. It seems that the measuring results can be interpreted by supposing ionic conduction. In addition to the work of LAW, the measurement of the 10^{-11} A reverse currents rendered possible the examination of the region below 0°C too and the application of his model also to ionic conduction taking place within ice.

Experimental

The measurements have been performed in the $200\text{--}340^\circ\text{K}$ region. The respective characteristics have generally been plotted in steps of 5 degrees. The adjustment of the temperature happened between $200\text{--}300^\circ\text{K}$, as follows. The diode was placed into a glass recipient filled with paraffine. This

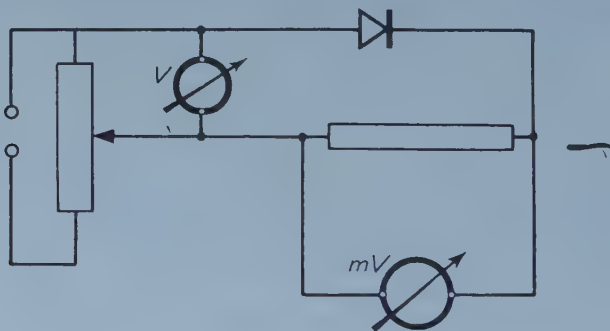


Fig. 1

recipient was immersed in a Dewar vacuum flask filled with acetone and the temperature of the acetone was being reduced by dosages of dry ice. As the diode had the same temperature as the acetone after about 20 minutes, the acetone was maintained for 20 minutes at a constant temperature by the appropriate dosage of solid CO_2 , under steady agitating. The control happened by means of a pentane thermometer. The measurement was effectuated in the direction of the cooling. In the $300\text{--}340^\circ\text{K}$ range a Höppler ultra-thermostat has been used. The temperature measurement took place by means of a calibrated copper-to-constantan thermocouple, fixed to the diode. The electric scheme can be seen in Fig. 1. The measured reverse currents varied between

$5 \cdot 10^{-3} - 10^{-11}$ A, therefore the measurement of the current was performed so that a voltage drop was measured on a known resistance by means of a millivoltmeter of 10^{12} internal resistance.

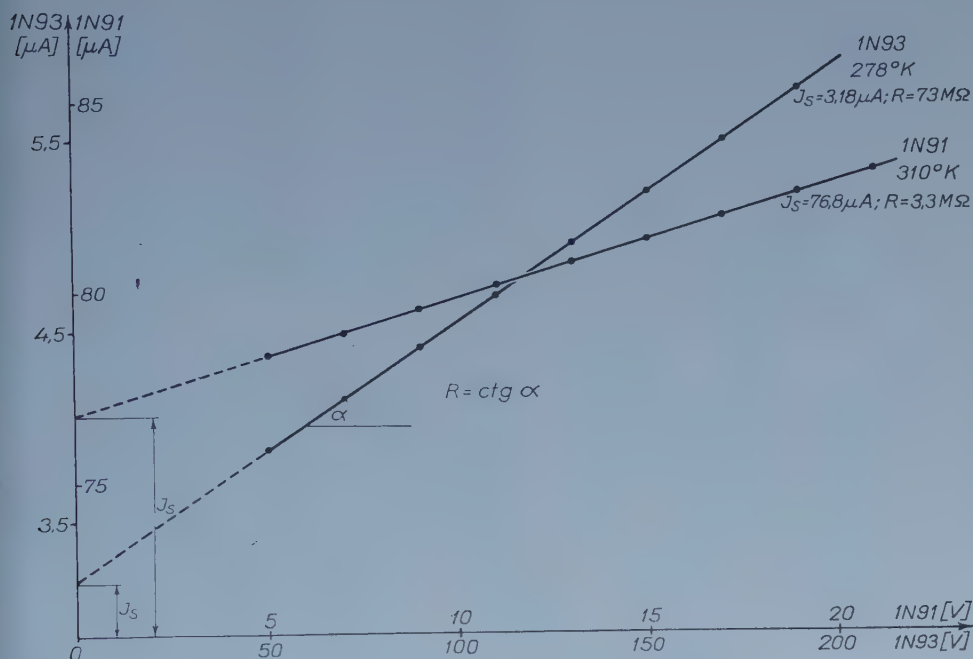


Fig. 2

Experimental results and their interpretation

The measurements have been performed on several germanium junction diodes. In the following we reproduce the measuring data of a 1N91 and a 1N93 diode.

In Fig. 2 a typical $V(I)$ characteristic is visible. Its linear section is conspicuous. In case of such a linear characteristic the saturation current can be defined in the way visible in Fig. 2.*

The temperature dependence of I_s defined in this way can be seen in Fig. 3. On its basis the forbidden band of germanium can be defined and shows generally a value of $E_g = 0.70$ eV, in good agreement with values measured by means of other methods.

On the basis of the model suggested the thin water layer adsorbed on the surface is responsible for the excess current. The resistance of this layer

* This definition of the saturation current has been suggested by Dr. Z. Bodó.

can be defined on the basis of the linear section of Fig. 2. This resistance R is the reciprocal of the incline. It is apparent that in the case of both diodes there is a break of about -8°C in the function $R(T)$ (Fig. 4). The single sections can

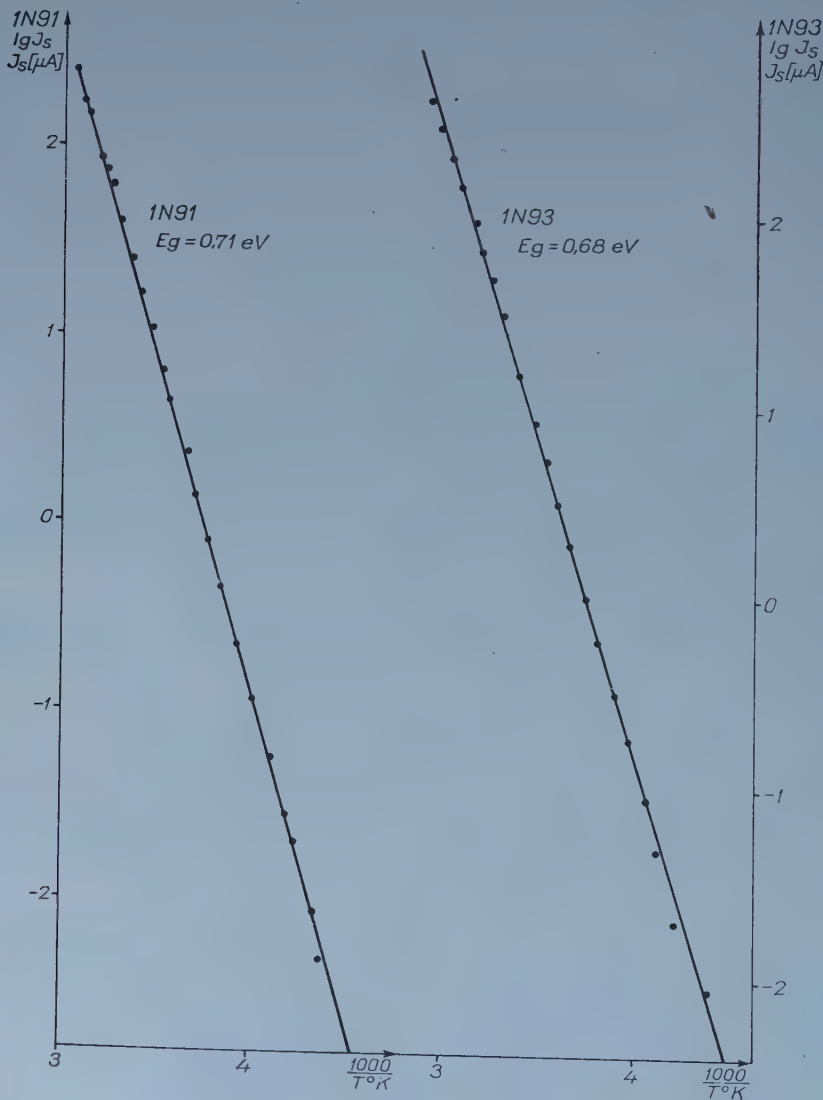


Fig. 3

be characterized by the activation energy which is identical for both diodes, on both sections. The activation energy defined in the low temperature region was found to have a value of 9.1 kcal/mol. Let us compare this value with the activation energy relating to the conductivity of ice.

In the 223—263° C range an activation energy of 21 kcal/mol was obtained by N. V. RIL [7]. A better agreement seems to exist with the work of R. S. BRADLEY [8], who measured a value of 12.3 kcal/mol. A further agreement

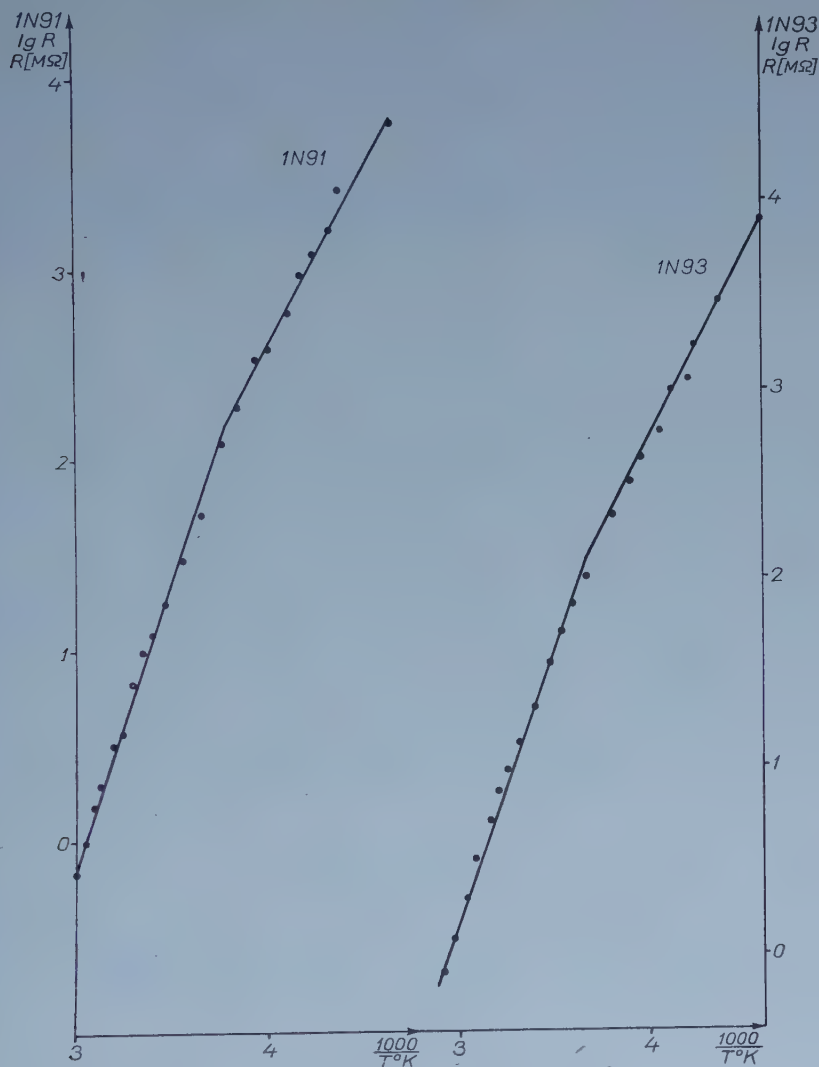


Fig. 4

means the fact that the function $K(T)$ (K -conductivity) of BRADLEY shows at about -6°C a definite break and tends to 0°C more steeply than the incline of the low temperature part. The above-mentioned facts: the linear $V(I)$ characteristics, the incline independent of the diode type and the value

found for the activation energy of ice being in sufficiently good accord with literature data allow to draw the conclusion that the assumption of ionic conduction at least below 0°C is correct.

The above explanation meets with the difficulty that the activation energy of the conductivity of water is according to the literature data smaller than that of ice. In our measurements, however, where we are concerned only with adsorbed water, the activation energy of the conductivity of water would appear greater than that of ice.

In the above-mentioned experiments encapsulated ready diodes have been examined so that the single parameters could not be varied. In further investigations the validity of the above-mentioned model must be examined in open $n-p$ junctions.

Conclusions

On the basis of the temperature dependence of the reverse current of germanium junction diodes the following can be concluded:

- 1) The diodes show in reverse direction instead of saturation, linear characteristics.
- 2) We introduced an I_S saturation current on the basis of the temperature dependence by which the forbidden band of germanium could be determined.
- 3) It seems that the linear characteristics can be interpreted in the region below 0°C by supposing an ionic conduction.
- 4) The above examinations do not determine unambiguously, which of the mechanisms leading to linear characteristics takes place.

Acknowledgements

Finally, the authors wish to express their thanks to Mr. Z. BODÓ, Doctor of Physical Sciences, for his valuable advice and critical remarks.

REFERENCES

1. A. L. MC WHORTER and R. H. KINGSTON, *Proc. IRE*, **42**, 9, 1954.
2. J. T. LAW, *Proc. IRE*, **42**, 9, 1954.
3. J. T. LAW and P. S. MEIGS, *Journ. Appl. Phys.*, **26**, 10, 1955.
4. W. T. ERICSEN, H. STATZ and G. A. DE MARS, *Journ. of Appl. Phys.*, **28**, 1, 133, 1957.
5. E. N. CLARKE, *Phys. Rev.*, **99**, 1899, 1955.
6. R. H. KINGSTON, *Journ. of Appl. Phys.*, **27**, 2, 1956.
7. N. V. RIL, *Journ. Phys. Chem. (USSR)*, **29**, 1372, 1955.
8. R. S. BRADLEY, *Trans. Faraday Soc.*, **53**, 5, 1957.

О ХАРАКТЕРИСТИКЕ ГЕРМАНИЕВЫХ ПЛОСКОСТНЫХ ДИОДОВ
В ЗАПОРНОМ НАПРАВЛЕНИИ

А. ЛЕРИНЦИ и ДЬ. ПАТАКИ

Резюме

Авторами исследована характеристика германиевых плоскостных диодов в запорном направлении в интервале температур 200° — 340° К. Найдено, что ток в запорном направлении не имеет насыщения, а линейно зависит от приложенного напряжения. На основании зависимости крутизны линейной области от температуры очевидно то предположение, что речь идет о шунтирующем действии адсорбированного водяного слоя, состоящего из нескольких молекул. Для проводимости льда ниже температуры 0° С получена энергия активации $9,1 \text{ kcal/mol}$, что хорошо согласуется с литературными данными. Из зависимости тока насыщения от температуры для ширины запрещенной зоны полосы германия получается значение $0,70 \text{ eV}$.



ÜBER EINE KLASSE DYNAMISCHER GRÖSSEN

Von

ARMIN UHLMANN

THEORETISCH-PHYSIKALISCHES INSTITUT DER KARL-MARX-UNIVERSITÄT, LEIPZIG, DDR

(Vorgelegt von K. F. Novobátzky. — Eingegangen: 21. XI. 1960)

Für beliebige Metrik werden allgemeine dynamische Grössen definiert und untersucht. Sie erweisen sich sämtlich als Zustandfunktionale im Sinne von DIRAC. Das Problem der Erhaltungssätze wird diskutiert. Gewisse energieartige dynamische Grössen liefern in zweiter Näherung zwanglos die Newtonsche Gravitationsenergie. Beim Vorliegen von Raum-Zeit-Symmetrien werden einige dynamische Grössen vor den anderen ausgezeichnet. Für die Minkowski-Metrik reduzieren sich diese auf die zehn allgemeinen Integrale der Mechanik. Schliesslich wird gezeigt, dass sich die Vertauschungsregeln der Quantentheorie für diese zehn Integrale in natürlicher Weise auf beliebige dynamische Grössen und beliebige Metrik erweitern lassen.

1. Vorbemerkungen

Wir bezeichnen mit M das Raum-Zeit-Kontinuum und mit Q, Q', \dots seine Punkte (»Raum-Zeit-Punkte«). M trage eine Raum-Zeit-Metrik vom Typ $(+ - - -)$, die wir zunächst nicht näher spezifizieren. Wir legen nur noch zum Zwecke der Normierung fest, dass ds^2 als Verallgemeinerung von

$$c^2 dt^2 - dx^2 - dy^2 - dz^2$$

die physikalische Dimension $[L^2]$ besitze. Lateinische Indizes laufen von 0 bis 3, griechische von 1 bis 3. Die kovariante Ableitung werde mit ∂_i bezeichnet. Das willkürliche Vorzeichen von R_{ik} werde durch $R_{ik} = R_{ink}^n$ festgelegt. Unter dem »Oberflächendifferential« df^k verstehen wir das Vektordifferential

$$df^k = \frac{1}{3!} g^{kl_0} \varepsilon_{l_0 l_1 l_2 l_3} dx^{l_1} \wedge dx^{l_2} \wedge dx^{l_3}.$$

Hierbei bezeichnet \wedge die äussere Multiplikation und $\varepsilon_{l_0 l_1 l_2 l_3}$ den Levi-Civita Tensor. dv sei das vierdimensionale Volumenelement.

Wir verwenden den allgemeinen Stokeschen Satz nur in der folgenden Form: Ist a_i ein beliebiges Vektorfeld, G ein Raum-Zeit-Gebiet und $R(G)$ sein orientierter Rand, so ist

$$\int_{R(G)} a_i df^i = \int_G \partial^i a_i \cdot dv. \quad (1)$$

Sei Ω eine raumartige Hyperfläche. Die Beschränkung der Metrik auf Ω induziert eine Metrik auf Ω , zu der das Volumenelement

$$dv(\Omega) = [-\text{Det}(g_{\nu\mu})]^{1/2} d^3x \quad (2)$$

gehört, falls $x^0 = \text{const.}$ eine Gleichung für Ω ist. Bei richtiger Wahl der (wegen der auftretenden Wurzeln) willkürlichen Vorzeichen ist auf Ω

$$dv(\Omega) = \eta_i df^i, \quad (3)$$

falls η_i die auf 1 normierte Normale von Ω ist. Man findet, dass unter dieser Voraussetzung für ein beliebiges Vektorfeld a_i

$$\int_{\Omega} a_i df^i = \int_{\Omega} a_i \eta^i \cdot dv(\Omega) \quad (4)$$

gilt.

2. Definition einer Klasse dynamischer Grössen

Bekanntlich korrespondieren in der Speziellen Relativitätstheorie (im Folgenden mit SRT abgekürzt) die zehn linear unabhängigen allgemeinen dynamischen Integrale (Impuls, Energie, Drehimpuls, Schwerpunktsgrössen) zu einer linear unabhängigen Basis der infinitesimalen Transformationen der Lorentzgruppe. Die Lorentzgruppe ist die Gruppe der isometrischen Transformationen der Minkowski-Metrik, d. h. einer Metrik, die die Beziehung $R_{iknm} = 0$ erfüllt. Die Isometriegruppe einer genügend allgemein gewählten Metrik besteht jedoch nur aus der Identität.

Die sachgemässe Verallgemeinerung der obigen Korrespondenz für beliebige Metrik ist nach einer Idee von BERGMANN [1] der Übergang zur Gruppe aller eindeutigen Abbildungen von M auf sich. Zu den infinitesimalen Operatoren dieser nur von der Topologie von M und nicht von der Metrik von M abhängenden Gruppe sollten dann geeignete dynamische Grössen korrespondieren.

Bei einem solchen Standpunkt werden natürlich auch im Bereich der SRT ungeheuer viele neue »dynamische Grössen« eingeführt. Jedoch heben sich die zehn allgemeinen Integrale dank der besonderen Symmetrie der Metrik (der sie ihr Dasein überhaupt erst verdanken) aus dieser Menge so stark heraus, dass ihre fast ausschliessliche Verwendung in der SRT ihre natürliche Erklärung finden wird.

Eine eindeutige Abbildung σ von M auf sich ist eine Vorschrift, die jedem Weltpunkt Q einen zweiten Weltpunkt Q^σ zuordnet, wobei wir — wie immer in dieser Arbeit — stillschweigend genügende Regularität voraussetzen. Die Menge der Q^σ soll wieder ganz M sein. Ist $f = f(Q)$ irgendeine Funktion auf (einem Teilgebiet von) M , so ist σf durch

$$\sigma f(Q) = f(Q^\sigma) \quad (5)$$

erklärt. Ist λ ein reeller Parameter und jedem λ eine eindeutige Abbildung von M auf sich zugeordnet, $\lambda \rightarrow \sigma(\lambda)$, so haben wir eine einparametrische, auf einen kanonischen Parameter bezogene Gruppe gerade dann vor uns, wenn

$$\sigma(\lambda_1 + \lambda_2) = \sigma(\lambda_1) \sigma(\lambda_2) \quad (6)$$

ist.

Wir bilden nun einen kontravarianten Vektor wie folgt: Ist $\{x^i\}$ irgendein Koordinatensystem, so sind seine Komponenten ξ^i bezgl. dieses Koordinatensystems durch

$$\xi^i = \lim_{\lambda \rightarrow 0} \frac{\sigma(\lambda) x^i - x^i}{\lambda} \quad (7)$$

gegeben. Man weiss, dass hierdurch wirklich ein Vektorfeld erklärt wird. Es heisst »die zu $\sigma(\lambda)$ gehörende infinitesimale Transformation«.

Man weiss weiter, dass es umgekehrt zu jedem kontravarianten Vektorfeld genau eine auf kanonische Parameter bezogene Gruppe $\sigma(\lambda)$ gibt, die dieses Vektorfeld zu infinitesimalen Transformation hat:

$$\sigma(\lambda) \longleftrightarrow \xi^i. \quad (8)$$

Wir betrachten nun den Energie-Impuls-Tensor T_{ik} , von dem wir zunächst nur die Eigenschaften

$$T_{ik} = T_{ki}, \quad \partial^i T_{ik} = 0 \quad (9)$$

fordern. Mit ihm definieren wir die *dynamischen Grössen*

$$P(\sigma(\lambda), \Omega) \equiv P(\xi^i, \Omega) = \int_{\Omega} \xi^i T_{ik} df^k. \quad (10)$$

Den Ausdruck (10) finden wir erstmalig bei TRAUTMAN [2] im Zusammenhang mit der kovarianten Formulierung der zehn allgemeinen Integrale der SRT.

Der Untersuchung der Ausdrücke (10) ist diese Arbeit gewidmet. Es ist zu beachten, dass wir genauer

$$P = P(\xi^i, \Omega, g_{rs}, T_{nm})$$

schreiben müssten. Jedoch werden nur gerade diejenigen Abhängigkeiten hervorgehoben werden, die gerade interessieren.

3. Die dynamischen Grössen in der Speziellen Relativitätstheorie

Ist g_{ik} die Minkowski-Metrik und ξ_i eine zur Lorentzgruppe gehörende infinitesimale Transformation, so ist $P(\xi^i, \Omega_1) = P(\xi^i, \Omega_2)$ für irgend zwei Hyperflächen Ω_1 und Ω_2 (siehe den nächsten Abschnitt). Wir schreiben daher einfach $P(\xi^i)$.

TRAUTMAN [2] hat bemerkt, dass die $P(\xi^i)$ gerade sämtliche Linearkombinationen der zehn erhalten bleibenden Grössen der SRT darstellen, wenn die ξ^i alle infinitesimalen Lorentztransformationen durchlaufen. Dies sieht man leicht ein, wenn man bedenkt, dass in einem Lorentzischen Koordinatensystem $\{x^i\}$ diese ξ^i durch

$$\xi^i = \alpha^i + \beta_l^i x^l, \quad \beta^{kl} + \beta^{lk} = 0 \quad (11)$$

gegeben sind. Wegen der Unabhängigkeit von Ω kann man nach (3)

$$P(\xi^j) = \int_{x^0=0} \xi^i T_{ik} df^k = \int_{x^0=0} \alpha^i T_{i0} d^3x + \int_{x^0=0} \beta_l^i x^l T_{ik} d^3x \quad (12)$$

schreiben. Die Behauptung ist unmittelbar abzulesen.

TRAUTMAN [2] bemerkte weiter, dass für den Fall $T_i^i = 0$ fünf weitere linear unabhängige und erhalten bleibende Grössen gewonnen werden können, wenn man die ξ^i die infinitesimalen Operationen der konformen Gruppe der Minkowski-Geometrie durchlaufen lässt. Es ergeben sich so gerade die fünfzehn aus der Konforminvarianz der Elektrodynamik folgenden erhalten bleibenden Grössen, wenn T_{ik} der Energie-Impuls-Tensor der Elektrodynamik ist.

Wir wollen zeigen, dass die $P(\xi^i, \Omega)$ die von beliebig bewegten Beobachtern gemessene Energie (mindestens) im Bereich der SRT auszudrücken gestattet. Sei nämlich ein Bündel zeitartiger Weltlinien gegeben, dass wir als Bündel der Weltlinien einer Schar beliebig bewegter Beobachter interpretieren wollen. Sei ξ^i das nach vorwärts gerichtete Feld ihrer auf 1 normierten Tangenten. Dann gehört zu ξ^i eine einparametrische Gruppe $\sigma(\lambda)$, deren Parameter λ die Eigenzeit der Beobachter angibt. Genauer, ist w eine Weltlinie des Bündels und Q ein Weltpunkt auf w , so ist w die »Bahnkurve« von $\sigma(\lambda)$ durch Q , d. h. die Menge aller

$$Q^{(\lambda)}, \quad \lambda \text{ beliebig.}$$

Die Ableitung eines beliebigen Koordinatensystems nach λ in Richtung von w (Gleichung (6)) ergibt deshalb einfach ξ^i und somit

$$ds = (\dot{x}^i \dot{x}^k g_{ik})^{1/2} d\lambda = (\xi^i \xi_i)^{1/2} d\lambda = d\lambda. \quad (13)$$

Die beliebig bewegte Schar von Beobachtern »passiere« nun eine raumartige Hyperfläche Ω und messe zum »Zeitpunkt Ω « die Energie E . Wir behaupten

$$E = \int_{\Omega} \xi^i T_{ik} df^k. \quad (14)$$

Zum Beweis bemerken wir, dass die Energie vom Zustand des Beobachters nur über die Geschwindigkeit abhängig ist. Haben daher zwei Beobachter zum

Zeitpunkt der Messung die Relativgeschwindigkeit Null, so messen sie den gleichen Energiebetrag bzw. die gleiche Energiedichte. Um dies auszunutzen, wählen wir einen beliebigen Weltpunkt Q_0 aus Ω aus. Es gibt dann eine zu einer zeitartigen Lorentz-translation gehörende infinitesimale Lorentztransformation ξ^i , für die

$$\xi^i(Q_0) = \xi^i(Q_0) \quad (15)$$

gilt, und wir können die Bahnkurven dieser Translation als Weltlinien einer Schar von Beobachtern interpretieren, die sich in einem Inertialsystem befinden. Aus (14) und (4) folgt

$$E = \int_{\Omega} \xi^i T_{ik} \eta^k dv(\Omega), \quad P(\xi^j) = \int_{\Omega} \xi^{-i} T_{ik} \eta^k dv(\Omega). \quad (16)$$

Wegen (15) zeigt der Vergleich der beiden Formeln (16), dass im Weltpunkt Q_0 die in den Integralen auftretenden Dichten gleich sind. Nach einer oben gemachten Bemerkung sind aber im Weltpunkt Q_0 auch die beiden zu den verschiedenen Scharen von Beobachtern gehörenden Energiedichten gleich. Überdies steht als Integrand von $P(\xi^i)$ die Energiedichte, die zur Schar der in dem gewählten Inertialsystem sich befindenden Beobachter gehört. Da Q_0 beliebig war, ist

$$\xi^i T_{ik} \eta^k \quad (17)$$

die gesuchte Energiedichte und (14) liefert die Gesamtenergie.

Damit ist gezeigt, dass die Grössen (10) auch einen physikalischen Sinn haben, wenn kein Erhaltungssatz vorliegt.

4. Erhaltungssätze und ihre Klassifizierung

Sei M_0 ein von den Hyperflächen Ω_1 und Ω_2 berandetes Raum-Zeit-Gebiet. (Der orientierte Rand von M_0 sei $\Omega_2 - \Omega_1$.) Dann folgt aus (1)

$$P(\xi^j, \Omega_2) - P(\xi^j, \Omega_1) = \int_{M_0} \partial^i (\xi^k T_{ki}) dv. \quad (18)$$

Unter Berücksichtigung von (9) wird der Integrand zu $T_{ij} \partial^i \xi^j$.

Es folgt, dass $P(\xi^i, \Omega)$ genau dann eine erhalten bleibende Grösse ist (= Unabhängigkeit von Ω), wenn gilt:

$$T_{ik} \partial^i \xi^k = 0. \quad (19)$$

In der Mechanik besitzt ein System von m Freiheitsgraden $2m$ unabhängige Integrale. Jedoch nur einige (nämlich höchstens zehn) dieser Inte-

grale sind *allgemein*, d. h. von den speziellen Eigenschaften des Systems weitgehend unabhängig. Dies kann man so formulieren: Eine dynamische Grösse ist ein *allgemeines* Integral, wenn $P(\xi^i, \Omega)$ eine erhalten bleibende Grösse ist für *jede* mit (9) verträgliche Wahl des Tensors T_{ik} . Die Relation (9) ist offenbar notwendig, damit T_{ik} überhaupt als Energie-Impuls-Tensor eines Systems in Frage kommt.

Da T_{ik} symmetrisch ist, folgt dann aus (19): Damit eine dynamische Grösse $P(\xi^i, \Omega)$ ein allgemeines Integral ist, ist

$$\partial^i \xi^k + \partial^k \xi^i = 0 \quad (20)$$

notwendig und hinreichend (TRAUTMAN [2]).

Ein Vektorfeld, das (20) erfüllt, heisst Killingsch. Die Killingsfelder der SRT sind gerade die infinitesimalen Transformationen der Lorentzgruppe, so dass sich der Kreis schliesst: Obige Definition ist mit der üblichen im Falle der SRT identisch.

Man weiss, dass ein Vektorfeld ξ^i genau dann Killingsch ist, wenn es infinitesimale Transformation einer *isometrischen* einparametrischen Gruppe $\sigma(\lambda)$ ist. Daher sind die allgemeinen Integrale eindeutig mit der Symmetriegruppe der Raum-Zeit-Metrik verknüpft.

Für eine genügend allgemeine Raum-Zeit-Metrik degeneriert jedoch die Isometriegruppe auf die identische Transformation. Wir müssen schliessen, dass allgemeine Integrale bei gekrümmter Raum-Zeit-Mannigfaltigkeit eine seltene Erscheinung sind. D. h. es gibt keine »allgemeinen Erhaltungssätze«, die eine geradlinige Verallgemeinerung der aus der Newtonschen Mechanik und der SRT gewohnten allgemeinen Integrale darstellen.

Es zeigt sich, dass diese auf den ersten Blick merkwürdige Erscheinung sehr natürlich ist. In der Tat, um von (19) auf (20) zu kommen, mussten wir T_{ik} innerhalb der Bedingungen (9) geeignet »variieren« können. Genauer, es musste *genügend viele* T_{ik} mit der Eigenschaft (9) geben, die als Energie-Impuls-Tensoren in Frage kommen. Betrachten wir aber die Allgemeine Relativitätstheorie (»ART«), so gibt es zu jeder Metrik g_{ik} *genau einen* Tensor T_{ik} , der als Energie-Impuls-Tensor in Frage kommt, nämlich den durch die Einsteinschen Gleichungen gegeben:

$$T_{ik} = \kappa^{-1} (1/2 g_{ik} R - R_{ik}). \quad (21)$$

Daher ist eine Variation der T_{ik} nur bei gleichzeitiger Veränderung der Metrik möglich und deshalb ist der Schluss von (19) auf (20) nicht durchführbar: (20) ist hinreichend aber nicht notwendig.

Für die ART scheint daher (19) die angemessenere Forderung für erhalten bleibende Grössen zu sein und die Teilung in allgemeine und spezielle Integrale

wird zumindest formal, wenn nicht sinnlos auf Grund der durch die Einsteinschen Gleichung bewirkten Relation zwischen T_{ik} und Metrik.

Die Forderung (19) ist ungleich schwächer als (20). Tatsächlich gilt, wie einfache Argumente aus der Theorie der partiellen Differentialgleichungen erster Ordnung zeigen, der Satz: Ist ξ^i irgendein Vektorfeld, so gibt es (mindestens) eine reelle Funktion α mit $\alpha > 0$ so, dass $\xi^i = \alpha \hat{\xi}^i$ die Gleichung (19) erfüllt. Erfüllt ξ^i die Gleichung (19), so auch alle Vektorfelder $\beta \xi^i$ mit

$$\xi^i T_i^k \frac{\partial}{\partial x^k} \cdot \beta = 0. \quad (x)$$

Daher ist $\beta = F(\beta_1, \beta_2, \beta_3)$, wobei F beliebig und β_v drei analytisch unabhängige Lösungen von (x) sind. Es gibt also stets »genügend viele« Vektorfelder derart, dass $P(\xi^i, \Omega)$ eine erhalten bleibende Grösse ist.

Bemerken wir noch, dass nach Obigem die Struktur der erhalten bleibenden Grössen $P(\xi^i)$ von der Metrik (bzw. von T_{ik}) abhängt und somit keine »an sich« und unabhängig von jeglicher konkreten physikalischen bzw. geometrischen Struktur gegebene Dinge sind.

5. Zustandsgrössen

Sei Ω eine raumartige Hyperfläche. Ist $\{x^i\}$ ein Koordinatensystem derart, dass x^0 auf Ω konstant ist, so betrachten wir die Funktionen

$$g_{\nu\mu} \quad \text{und} \quad \frac{\partial}{\partial x^0} g_{\nu\mu}. \quad (22)$$

Eine Grösse A heisst eine Zustandsgrösse (bzgl. der Metrik), wenn A aus den Funktionen (22) mit Hilfe von Operationen aufgebaut werden kann, deren Ausführung ohne Verlassen von Ω möglich ist. Beispiele: Integration über Ω , Differentiation nach x^ν . Besonders DIRAC[3] stellte im Hinblick auf den kanonischen Formalismus die Forderung auf, dass die Energie ein Funktional des Zustandes sein müsse.

Ehe wir diese Frage für die Grössen (10) beantworten, wollen wir (22) durch Tensoren ersetzen und somit eine Unabhängigkeit vom Koordinatensystem und eine etwas schärfere Formulierung des Begriffs der Zustandsgrösse erreichen.

Wir sagen, »ein Tensor sei modulo Ω bestimmt«, wenn wir zwei Tensoren $a_{n\dots}^{m\dots}$ und $\hat{a}_{n\dots}^{m\dots}$ bereits dann als gleich betrachten, wenn sie auf Ω übereinstimmen. D. h. es muss

$$a_{n\dots}^{m\dots}(Q) = \hat{a}_{n\dots}^{m\dots}(Q) \quad \text{für alle} \quad Q \in \Omega \quad (23)$$

sein. Zum Beispiel ist das Normalenfeld η_i von Ω nur modulo Ω bestimmt, da bei der Definition dieses Feldes die Frage uninteressant ist, wie es sich für Weltpunkte verhält, die ausserhalb Ω liegen.

Wir ersetzen nun (22) durch zwei modulo Ω bestimmte Tensoren, die nur von Ω und der Metrik abhängen. Wir nennen diese $g_{ik}(\Omega)$ und Ω_{ik} und geben die Konstruktionsvorschrift [4].

Ist η_i das Normalenfeld von Ω , so definieren wir den modulo Ω definierten Tensor $g_{ik}(\Omega)$ durch

$$g_{ik}(\Omega) = g_{mn} r_i^m r_k^n \quad (24a)$$

mit

$$r_i^k = \delta_i^k - \eta_i \eta^k. \quad (24b)$$

Etwas komplizierter ist die Angabe von Ω_{ik} . Sei a_i irgendein Vektorfeld, das auf Ω die Richtung der Normalen hat. D. h. ist η_i das Normalenfeld, so gibt es eine Funktion $\alpha > 0$ auf Ω mit

$$\alpha_i - \alpha \eta_i = 0 \quad \text{für} \quad Q \in \Omega. \quad (25a)$$

Wir setzen dann

$$\Omega_{ik} = r_i^n r_k^m (\partial_n \alpha_m + \partial_m \alpha_n) \cdot \alpha^{-1}. \quad (25b)$$

Wir finden, dass, wie immer wir α_i gemäss (25a) wählen, die entstehenden Tensoren Ω_{ik} modulo Ω übereinstimmen.

Verschwindet der Tensor (25b), so ist nach NEWMAN und JANIS [5] gerade die ROSENsche Starrheitsbedingung für eine Bewegung mit Tangenten η^i erfüllt. Nach BRILL [6] heisst die Metrik »zeitsymmetrisch bezgl. Ω «, wenn (25b) verschwindet. Dieser Fall tritt insbesondere dann ein, wenn man in (25a) α Killingsch wählen kann. Dann ist Ω Niveaufäche einer Gruppe isometrischer Bewegungen, d. h. stationär.

Nach dieser Vorbereitung betrachten wir nun eine beliebige dynamische Grösse

$$P = \int_{\Omega} \xi^i T_{ik} df^k = \int_{\Omega} \xi^i T_{ik} \eta^k \cdot dv(\Omega). \quad (26)$$

Offenbar ist P ein Zustandsfunktional, wenn es die Dichte

$$u = \xi^i T_{ik} \eta^k \quad (27)$$

ist. ξ^i besitzt genau eine Zerlegung

$$\xi^i = \beta \eta^i + \beta^i \quad \text{mit} \quad \beta^i \eta_i = 0. \quad (28)$$

Bei gegebenem Q ist ξ^i durch β und β^i bestimmt. Setzen wir

$$u_1 = \eta^i T_{ik} \eta^k, \quad u_2 = \beta^i T_{ik} \eta^k, \quad (29)$$

so haben wir

$$u = \beta u_1 + u_2. \quad (30)$$

Beim Bestehen der Einsteinschen Gleichungen sind u_1 und u_2 tatsächlich Zustandsgrößen. Indem wir β (und β^i) als vorgegeben, die Grösse P charakterisierend, betrachten, ist daher P eine Zustandsgrösse!

Um dies näher darzulegen, betrachten wir zunächst das Folgende: Die Raum-Zeit-Metrik induziert auf Ω eine Metrik, so dass wir Ω als einen Riemannschen Raum ansehen können. Wir können dann, ohne Ω zu verlassen, auf Ω einen Skalar bilden, den Krümmungsskalar $R(\Omega)$. $R(\Omega)$ ist eine Zustandsgrösse.

Durch Ausrechnen finden wir beim Bestehen der Einsteinschen Gleichungen die folgenden Formeln:

$$u_1 = \frac{1}{2\kappa} R(\Omega) + \frac{1}{8\kappa} (\Omega_i^i \Omega_j^j - \Omega_i^j \Omega_j^i), \quad (31)$$

$$u_2 = \frac{1}{2\kappa} \beta^k (\partial_j \Omega_k^j - \partial_k \Omega_j^j). \quad (32)$$

(31) sieht man sofort an, dass u_1 Zustandsgrösse ist, bei (32) zeigt ein genaueres Betrachten, dass man zur Ausrechnung mit Differentiationen innerhalb Ω auskommt. Eine ausführliche Herleitung findet sich in [4], eine nicht völlig kovariante Formulierung bei BRILL [6]. (Durch ein Versehen hat sich in die Arbeit⁶ ein falscher Zahlenfaktor eingeschlichen. Die Vorzeichenunterschiede entstehen durch andere als die in dieser Arbeit verwendete Konventionen.)

6. Die Gravitationsenergie

Eine Metrik ist statisch, wenn es zwei Funktionen f und h so gibt, dass

$$\xi^i = h \cdot g^{ik} \frac{\partial f}{\partial x^k} \quad \text{mit} \quad \xi^i \xi_i > 0 \quad (33)$$

ein zeitartiges Killingfeld ist. Die durch $f = \text{const.}$ gegebenen Hyperflächen sind dann zeitartig und stationär. Da ξ^i Killingsch ist, hängt die zugehörige dynamische Grösse *nicht* von der Wahl der Hyperfläche ab, weshalb wir eine stationäre zur Berechnung wählen können. Es ist dann $\Omega_{ik} = 0$ und (31) bzw. (32) vereinfacht sich zu

$$u_1 = \frac{1}{2\kappa} R(\Omega), \quad u_2 = 0. \quad (34)$$

Daher ist

$$P(\xi^i) = \frac{1}{2\kappa} \int_{\Omega} \beta R(\Omega) dv(\Omega), \quad \beta = \xi^i \eta_i. \quad (35)$$

Wir wenden dies auf ein in Newtonscher Näherung bestimmtes Linien-element an. Bezeichnet Δ den Laplace-Operator, grad den Gradienten des 3-dimensionalen euklidischen Raumes und ϱ eine vorgegebene Massenverteilung, so ist das Newtonsche Potential durch

$$\Delta\varphi = 4\pi\gamma\varrho, \quad \lim_{r \rightarrow \infty} \varphi = 0 \quad (36)$$

bestimmt. Wir setzen $m = \int \varrho d^3x$. Die verschiedenen Näherungsverfahren liefern dann eine Metrik der Gestalt

$$Adx^{02} - B\delta_{\nu\mu}dx^\nu dx^\mu \quad (37a)$$

mit

$$\begin{aligned} A &= 1 + \psi + \lambda\psi^2 + \dots, \\ B &= 1 - \psi + \mu\psi^2 + \dots, \end{aligned} \quad (37b)$$

$$\psi = \frac{2\varphi}{c^2}.$$

Das Killingfeld ξ^i ist in dem vorliegenden Koordinatensystem einfach durch $\xi^i = \delta_0^i$ gegeben.

Wir berechnen alles bis zur zweiten Ordnung in ψ und vernachlässigen alle Glieder, die in ψ von mindestens dritter Ordnung sind. Da sich zeigt, dass $R(\Omega)$ keine Glieder 0-ter Ordnung besitzt, brauchen wir

$$\beta dV(\Omega) = \sqrt{AB^3} d^3x \quad (38a)$$

nur bis zur ersten Ordnung auszurechnen:

$$\sqrt{AB^3} = 1 - \psi + \dots \quad (38b)$$

Nun ist

$$BR(\Omega) = -2B^{-1}\Delta B + \frac{3}{2}B^{-2}(\text{grad } B)^2, \quad (39a)$$

und daher in unserer Näherung

$$BR(\Omega) = 2\Delta\psi - 2\mu\Delta\psi^2 + 2\psi\Delta\psi + \frac{3}{2}(\text{grad } \psi)^2. \quad (39b)$$

Aus (38b) sehen wir, dass bis zu Gliedern erster Ordnung B gleich $\sqrt{AB^3}$ ist. Da $R(\Omega)$ von erster Ordnung ist, folgt

$$\beta R(\Omega) dv(\Omega) = \left(2\Delta\psi - 2\mu\Delta\psi^2 + 2\psi\Delta\psi + \frac{3}{2}(\text{grad } \psi)^2 \right) d^3x. \quad (40)$$

Unter Beachtung von

$$\Delta\psi^2 = 2\psi \Delta\psi + 2 (\text{grad } \psi)^2 \quad (41)$$

setzen wir (40) in (35) ein und erhalten

$$P(\xi^i) = \frac{1}{x} \int \Delta\psi d^3x + \frac{1}{x} \int [\tau_1 (\text{grad } \psi)^2 + \tau_2 \psi \Delta\psi] d^3x + \dots \quad (42)$$

mit

$$\tau_1 = \frac{3}{4} - 2\mu, \quad \tau_2 = 1 - 2\mu. \quad (42a)$$

Beachten wir

$$\int \psi \Delta\psi d^3x = - \int (\text{grad } \psi)^2 d^3x,$$

so haben wir

$$P(\xi^i) = \frac{1}{x} \int \Delta\psi d^3x - \frac{1}{4x} \int (\text{grad } \psi)^2 d^3x + \dots \quad (43)$$

Da die Koeffizienten λ und μ herausgefallen sind, kommen wir zu dem erstaunlichen Ergebnis: Die Glieder von höherer als der ersten Ordnung in $\psi = 2\varphi/c^2$ der Metrik (37) haben keinen Einfluss auf die Grösse $P(\xi^i)$ bis zur zweiten Ordnung in ψ .

Der Koeffizient μ regelt nach (42) offenbar die lokale Verteilung der zu $P(\xi^i)$ gehörenden Dichte.

Die weitere Ausrechnung von (43) ergibt einfach

$$P(\xi^i) = mc^2 - \frac{1}{8\pi\gamma} \int (\text{grad } \varphi)^2 d^3x + \dots \quad (44)$$

Das nach Obigem durch die Glieder erster Ordnung der Metrik bestimmte Glied zweiter Ordnung von $P(\xi^i)$ ist einfach die Newtonsche Gravitationsenergie.

Formel (43) gestattet eine wesentliche Verallgemeinerung, wenn man als Ausgangspunkt der Approximation nicht die Minkowskische sondern eine beliebige Metrik verwendet. Gilt für die betrachtete Hyperfläche $\Omega_{ik} \neq 0$, so treten in (43) noch zusätzliche Terme auf. Für dieses Problem siehe [4].

7. Vertauschungsregeln der Quantentheorie

Wir haben bereits bei der Definition der Grössen $P(\xi^i, \Omega)$ bemerkt: Durch die Annahme, dass die ξ^i ein beliebiges Vektorfeld bilden, werden mit Notwendigkeit auch im Bereich der SRT neue, üblicherweise nicht definierte

Größen eingeführt. Betrachten wir nun die Quantentheorie und legen uns dabei auf das Heisenberg-Bild fest. Die zehn Operatoren, die zu den allgemeinen dynamischen Erhaltungsgrößen gehören, unterliegen Vertauschungsregeln. Daher müssen, wenn $P(\xi^i, \Omega)$ den zur beobachtbaren Größe $P(\xi^i, \Omega)$ gehörenden Operator bezeichnet, auch die $P(\xi^i, \Omega)$ irgendwelchen Vertauschungsregeln unterliegen. Wenn wir annehmen, dass diese Vertauschungsregeln nicht vom speziellen physikalischen System abhängen, sondern ähnlich wie die zu Energie, Impuls, Drehimpuls und Schwerpunktsgrößen gehörenden nur mit der Geometrie der Raum-Zeit verbunden sind, so scheint es *nur eine* Möglichkeit einer folgerichtigen Verallgemeinerung zu geben.

Nehmen wir zunächst die SRT. Ist ξ^i ein Killingvektor, so ist $P(\xi^i)$ eine Linearkombination des Operators des Energie-Impuls-Vektors P_i und des Drehimpulstensors M_{ik} . Es ist

$$P(\xi^i) = \alpha^n P_n + \beta^{nm} M_{nm} \quad (45)$$

falls

$$\xi^i = \alpha^i + \beta^i_k x^k \quad (11)$$

ist. Da die $iP(\xi^i)$ eine Darstellung der Lie-Algebra der Lorentz-Gruppe sind, ist

$$i[P(\xi^i), P(\eta^j)] = P(\zeta^i) \quad (46)$$

mit einem gewissen Killingfeld ζ^i . Die kontravarianten Killingfelder repräsentieren aber gerade dann die Lie-Algebra der Lorentz-Gruppe, wenn man

$$\zeta^i = \xi^l \frac{\partial}{\partial x^l} \eta^i - \eta^l \frac{\partial}{\partial x^l} \xi^i \quad (47)$$

setzt. Man sieht dies sofort, wenn man die Gleichung

$$\zeta^i \frac{\partial}{\partial x^i} = \left[\xi^l \frac{\partial}{\partial x^l}, \eta^s \frac{\partial}{\partial x^s} \right] \quad (47a)$$

betrachtet; denn die Zuordnung

$$\sigma(\lambda) \rightarrow \xi^i \frac{\partial}{\partial x^i} \varphi$$

ist eine treue Darstellung der Lie-Algebra im Raum der Skalare. Bemerken wir noch, dass (46) und (47) alle Vertauschungsregeln zwischen den P_i und M_{ik} liefern.

Aus (47a) sieht man leicht die folgende Tatsache: Sind ξ^i und η^i beliebige kontravariante Vektorfelder, so wird durch (47) ein kontravariantes Vektorfeld ζ^i gegeben; die Bildung (47) ist koordinatenunabhängig und unabhängig von der Metrik. Tatsächlich kann man zeigen, dass die kontravarianten Vektor-

felder zusammen mit der gewöhnlichen Addition und der Operation (47) (= Lie-Multiplikation) eine treue Darstellung der Lie-Algebra der Gruppe aller eindeutigen (genügend regulären) Abbildungen von M auf sich bilden.

Für eine Feldtheorie mit einem lokalen (pseudo-)skalaren Feld kann man relativ leicht zeigen, dass gilt [4]: Ist Ω eine beliebige raumartige Hyperfläche und ξ^i, η^i zwei beliebige Vektorfelder, so gilt bei beliebiger Metrik

$$i[\mathbf{P}(\xi^j, \Omega), \mathbf{P}(\eta^j, \Omega)] = \mathbf{P}(\zeta^j, \Omega), \quad (48)$$

wobei ζ^i durch (47) gegeben ist. Dabei ist

$$\mathbf{P}(\xi^i, \Omega) = \int_{\Omega} \xi^i \mathbf{T}_{ik} df^k \quad (49a)$$

und die Lagrange-Funktion von der Gestalt

$$L = \partial^i \varphi \cdot \partial_i \varphi + \Sigma \alpha_k \varphi^k \quad (49b)$$

angenommen worden.

Die vermutliche allgemeine Gültigkeit von (48) wird auch dadurch gestützt, dass (wie in der Theorie der geometrischen Objekte gezeigt wird) die Vorschrift (47) die einzige Möglichkeit ist, aus zwei gegebenen Vektorfeldern ohne Zuhilfenahme weiterer Felder (Metrik, affiner Zusammenhang u. ä.) ein drittes kontravariantes Vektorfeld aufzubauen.

Sind ξ^i und η^i Killingsch, so ist auch ζ^i ein Killingfeld und die in (48) stehende Abhängigkeit von Ω ist nur scheinbar.

Zum Schluss wollen wir noch bemerken, dass für ein durch (49) definiertes Feld überdies

$$i[\mathbf{P}(\xi^j, \Omega), \varphi] = \xi^i \frac{\partial}{\partial x^i} \varphi \quad \text{für } Q \in \Omega \quad (50)$$

gilt. (50) besitzt eine Verallgemeinerung für nicht skalare quantisierte Felder, die im Falle der SRT mit den üblichen Regeln identisch ist [4].

LITERATURANGABEN UND HINWEISE

1. P. G. BERGMANN, Phys. Rev., **112**, 287, 1958. Im Sinne der in unserer Arbeit benutzten Definition sind die Koordinaten nur Hilfsgrößen zur Parametrisierung von M .
2. A. TRAUTMAN, Bull. Acad. Pol. Scin. Cl. III, **4**, 671, 1956, sowie **5**, 721, 1957; Lectures on General Relativity, King's College, London, 1958.
3. P. A. M. DIRAC, z. B. Rev. Mod. Phys., **21**, 392, 1949; Phys. Rev. Letters, **2**, 368, 1959.
4. Für den Beweis dieser und vieler anderer hier aus Raumgründen nur referierten Ergebnisse sowie für weitere Literatur siehe: A. UHLMANN, Der Begriff der Energie bei gekrümmter Raum-Zeit-Mannigfaltigkeit, Wiss. Zschr. Friedrich-Schiller-Univ., Jena, **9**, 459, 1960.
5. E. T. NEWMAN, A. I. JANIS, Rigid Frames in Relativity, preprint 1960; N. ROSEN, Phys. Rev., **71**, 54, 1947.
6. D. BRILL, Ann. of Phys., **7**, 466, 1959.

ОБ ОДНОМ КЛАССЕ ДИНАМИЧЕСКИХ ВЕЛИЧИН

А. УЛЬМАНН

Резюме

На некотором множестве пространства времени определяется и исследуется класс динамических величин. Как классически, так и квантовомеханически определяется связь данного класса со специальной теорией относительности. Принимая во внимание канонический формализм, приходим к заключению, что эти величины являются функциями состояния. Найдутся рациональные законы сохранения. В приближении Ньютона однозначно получается сдвиг гравитационной энергии. Координатные системы применяются исключительно для проведения вычислений.

ON THE HIGH ENERGY BEHAVIOUR OF THE PION — NUCLEON ELASTIC SCATTERING AMPLITUDE

By

G. DOMOKOS

CENTRAL RESEARCH INSTITUTE FOR PHYSICS, BUDAPEST

(Presented by L. Jánosy. — Received 15. XII. 1960)

The kinematics of the πN elastic scattering is treated in the quasiclassical approximation. It is shown that if a quasiclassical limit exists, then spin-effects become negligible at sufficiently high pion energies, independently of other details of the interaction. In sec. 3 an asymptotic representation of a function defined by means of a Hilbert transform is given. The latter is made use of to derive the asymptotics of the πN forward scattering amplitude (sec. 4). The possibility of testing the results experimentally is discussed (sec. 5).

1. Introduction

The study of the πN scattering amplitude at high energies, above, say, 2 GeV — is difficult for several reasons. First of all, the high number of partial waves required to describe the scattering renders a usual phase shift analysis almost hopeless. Second — a topic which is of central importance in low energy pion physics — the check of the validity of dispersion relations meets with another difficulty, namely, the numerical evaluation of dispersion integrals is difficult in view of the large energy region involved. Besides of this, there are certain “gaps” in the experimental material available at present (no polarization experiments at high energies etc.) which probably will not be filled in in the very near future.

In the present work we summarize the first results of an investigation which aims at finding some useful expressions which can be calculated numerically and checked experimentally. The main “trick” has always been to find an asymptotic representation for the scattering amplitude and for its real part as expressed by means of a dispersion relation. The basic assumption of our work is the existence of a — finite — semi-classical limit of the phase shifts as the primary energy of incident pions tends to infinity.

The latter is a stronger restriction than the usual one (scil. that total cross sections tend to a constant value), but intuitively it seems to be a rather plausible one and is supported by some experimental evidence: the semi-classical phase shifts calculated by SEBESTYÉN and the author [1] do not show any systematic tendency from 1,4 to 6,8 GeV pion kinetic energy in the L. S.

We have to remark here that the question of convergence of the asymptotic expansions is not even touched at in the present work. We regard them rather as asymptotic representations which must be broken off when the terms cease to decrease. In numerical calculations we never went beyond the leading term of the expansion.

2. Kinematical considerations

The scattering amplitude in the C. M. S. can be written as follows [2]:

$$f = f_1 + \frac{1}{q^2} (\sigma \mathbf{q}') (\sigma \mathbf{q}) f_2. \quad (2,1)$$

(We omitted isobaric indices.)

f_1 and f_2 possess the following partial wave expansion:

$$\left. \begin{aligned} f_1 &= \sum_{l=0}^{\infty} f_{l+} P'_{l+1}(x) - \sum_{l=2}^{\infty} f_l - P'_{l-1}(x), \\ f_2 &= \sum_{l=1}^{\infty} (f_{l-} - f_{l+}) P'_l(x), \\ f_{l\pm} &= (2ig)^{-1} (\exp 2i\delta_{l\pm} - 1). \end{aligned} \right\} \quad (2,2)$$

If both initial and final nucleons are unpolarized, the differential cross section turns out to be

$$\frac{d\sigma}{dl} = |f_1 + x f_2|^2 + \frac{1}{4} (1 - x^2) |f_2|^2. \quad (2,3)$$

In order to investigate the high-energy behaviour of these expressions, we transform the first term of eq. (2, 3) as follows.

Making use of the identities:

$$\begin{aligned} l P_l(x) &= x P'_l(x) - P'_{l-1}(x), \\ (l+1) P_l(x) &= P'_{l+1}(x) - x P'_l(x), \end{aligned}$$

one finds:

$$f_1 + x f_2 = \sum_{l=0}^{\infty} P_l(x) [(l+1) f_{l+} + l f_{l-}] \quad (2,4)$$

with $f_{0-} = f_{0+}$.

We now use the asymptotic representation of the Legendre polynomials and their first derivatives:

$$P_l(\cos \vartheta) \sim J_0 \left[\left(l + \frac{1}{2} \right) \sin \vartheta \right],$$

$$P'_l(\cos \vartheta) \sim \left(l + \frac{1}{2} \right) \operatorname{ctg} \vartheta J_1 \left[\left(l + \frac{1}{2} \right) \sin \vartheta \right]$$

and instead of the variables j, l, ϑ , we go over to the impact parameters (ϱ) and momentum transfer (κ), and integrate over ϱ instead of summing over l :

$$\varrho = q^{-1} \left(l + \frac{1}{2} \right),$$

$$\kappa = 2q \sin \frac{\vartheta}{2} \sim q\vartheta.$$

Thus, $f_{l\pm}$ will depend on two continuous variables instead of j and l , namely one has to replace j by $q\varrho$ and $q(\varrho - q^{-1})$ in f_{l+} and f_{l-} , respectively.

Then:

$$f_{l+} \sim f(\varrho, \varrho),$$

$$f_{l-} \sim f(\varrho, \varrho) - q^{-1} \left(\frac{\partial f(y, \varrho)}{\partial y} \right)_{y=\varrho} + O(q^{-2})$$

and

$$\frac{1}{4}(1-x^2)|f_2|^2 \sim \frac{1}{4}q^2 \left| \int_0^\infty \left(\frac{\partial f(y, \varrho)}{\partial y} \right)_{y=\varrho} J_1(\varrho\kappa) \varrho d\varrho \right|^2 = O(1),$$

while

$$|f_1 + xf_2| \sim 4q^4 \left| \int_0^\infty f(\varrho, \varrho) J_0(\varrho\kappa) \varrho d\varrho \right|^2 = O(q^2).$$

Putting

$$f(\varrho, \varrho) = (2iq)^{-1} [\exp 2i\delta(\varrho) - 1]$$

we find

$$\frac{d\sigma}{d\Omega} \sim q^2 \left| \int_0^\infty (\exp 2i\delta(\varrho) - 1) J_0(\varrho\kappa) \varrho d\varrho \right|^2, \quad (2,5)$$

i. e. we have verified our conjecture expressed in [1] about the spin independence of the differential cross section in the semi-classical limit.

We turn next to the semi-classical wave expansion of the differential cross section. The formula to be found is the analogue of eq. (2.5) of BIEDENHARN, BLATT and ROSE [3].

We write eq. (2, 5) in the following form:

$$\left. \begin{aligned} \frac{d\sigma}{d\Omega} &= q^2 \int_0^\infty \varrho d\varrho \int_0^\infty \varrho' d\varrho' t(\varrho) t^*(\varrho') J_0(\varrho\kappa) J_0(\varrho'\kappa) \\ \text{with} \quad t(\varrho) &\equiv \exp 2i\delta(\varrho) - 1. \end{aligned} \right\} \quad (2,5)$$

Further, we expand the product of the Bessel functions occurring in (2,5) as follows:

$$J_0(\varrho\kappa) J_0(\varrho'\kappa) = \int_0^\infty C(\varrho, \varrho', \xi) J_0(\xi\kappa) \xi d\xi.$$

$C(\varrho, \varrho', \xi)$ can be found with help of WATSON's integral formula [4].

$$C(\varrho, \varrho', \xi) = \begin{cases} (2\pi)^{-1} [(\varrho + \varrho' + \xi)(\varrho + \varrho' - \xi)(\varrho - \varrho' + \xi)(-\varrho + \varrho' + \xi)]^{-1/2} & \text{if } \varrho, \varrho', \xi \text{ form a triangle,} \\ 0 & \text{otherwise.} \end{cases}$$

Inserting this into (8') we obtain the desired expansion for the differential cross section:

$$\left. \begin{aligned} \frac{d\sigma}{d\Omega} &= q^2 \int_0^\infty \xi d\xi T(\xi) J_0(\kappa\xi), \\ T(\xi) &= \int_0^\infty \varrho d\varrho \int_{|\varrho-\xi|}^{\varrho+\xi} \varrho' d\varrho' t(\varrho) t^*(\varrho') C(\varrho, \varrho', \xi). \end{aligned} \right\} \quad (2,6)$$

Eq. (2,6) can be used to extrapolate the differential cross section to forward scattering if one knows it experimentally for small but finite angles [5].

3. Asymptotic representation of Hilbert transforms

We are going to derive an asymptotic representation for a Hilbert transform. The representation to be found will be useful not only for the treatment of the forward scattering amplitude but for more general problems as well,

which we want to deal with in subsequent papers. Therefore we present the material of this section in some detail.

Consider the function $F(x)$ of a real variable defined by the following relation:

$$F(x) = \frac{p}{\pi} \int_0^{\infty} \frac{f(x') dx'}{x' - x}, \quad (3,1)$$

where $f(x')$ is a function such that all occurring integrals exist. (For simplicity we assume that $f(x) = 0(x^{-1})$ as $x \rightarrow \infty$. This condition is sufficient for our purposes.)

Let x_1 be a quantity such that

$$0 < x_1 < x < \infty \quad (3,2)$$

and split the integration interval correspondingly into two parts:

$$F(x) = \frac{1}{\pi} \int_0^{x_1} \frac{f(x') dx'}{x' - x} + \frac{p}{\pi} \int_{x_1}^{\infty} \frac{f(x') dx'}{x' - x}. \quad (3,1')$$

Expanding the denominator of the first integral in a power series gives

$$\frac{1}{\pi} \int_0^{x_1} \frac{f(x') dx'}{x' - x} = -\frac{1}{\pi} \sum_{k=0}^{\infty} x^{-(k+1)} \int_0^{x_1} x'^k f(x') dx'. \quad (3,3)$$

For the treatment of the second integral we assume that $f(x)$ can be expanded into an asymptotic power series around $x = \infty$, and that the latter converges for $x_1 < x < \infty$:

$$f(x') = \sum_{n=1}^{\infty} a_n x'^{1-n} \quad (3,4)$$

and assume that $\sum_{n=1}^{\infty} a_n$ exists.

Inserting this expansion into the second integral, after an elementary term by term integration we are left with the expression

$$\begin{aligned} \frac{p}{\pi} \int_{x_1}^{\infty} \frac{f(x') dx'}{x' - x} &= \frac{1}{\pi} \sum_{n=2}^{\infty} a_n (-x_1)^{-n} \sum_{j=0}^{n-2} \sum_{k=1}^{n-j-1} \frac{C_{j,k}^{n-1}}{n-j-1} \left(-\frac{x}{x_1}\right)^{k-n} - \\ &\quad - \frac{1}{\pi} \ln \frac{x - x_1}{x_1} \sum_{n=1}^{\infty} a_n. \end{aligned}$$

Here $C_{j,k}^n$ is a trinomial coefficient:

$$C_{j,k}^n = \frac{n!}{j! k! (n-j-k)!}.$$

Combining this expression with the previous one, we find the required asymptotic representation for $F(x)$ valid for $x > x_1$:

$$\begin{aligned} F(x) = & -\frac{1}{\pi} \sum_{k=0}^{\infty} x^{-(k+1)} \int_0^{x_1} x'^k f(x') dx' - \frac{1}{\pi} \ln \frac{x-x_1}{x_1} \sum_{n=1}^{\infty} a_n + \\ & + \frac{1}{\pi} \sum_{n=2}^{\infty} a_n (-x_1)^{-n} \sum_{j=0}^{n-2} \sum_{k=1}^{n-j-1} \frac{C_{j,k}^{n-1}}{n-j-1} \left(-\frac{x_1}{x}\right)^{n-k}. \end{aligned} \quad (3,5)$$

In an analogous manner, if $G(x)$ is defined by the relation

$$G(x) = \frac{P}{\pi} \int_{-\infty}^{\infty} dx' g(x') \left(\frac{1}{x' - x} - \frac{1}{x' + x} \right), \quad (3,6)$$

with $g(x) = 0(1)$ as $x \rightarrow \infty$ and for $x > x_1$ it can be expanded into an asymptotic power series

$$g(x) = \sum_{n=0}^{\infty} b_n x^{-n} \quad (3,7)$$

($\sum_{n=0}^{\infty} b_n$ exists), then we find the representation:

$$\begin{aligned} G(x) = & -\frac{2}{\pi} \sum_{k=0}^{\infty} x^{-(2k+1)} \int_0^{x_1} g(x') x'^{2k} dx' + \frac{1}{\pi} \ln \frac{x+x_1}{x-x_1} \sum_{n=0}^{\infty} b_n \\ & + \frac{1}{\pi} \sum_{i=1}^{\infty} b_{2i+1} x_1^{2i+1} \sum_{j=0}^{2i-1} \sum_{n=0}^{\left(\frac{2i-j-1}{2}\right)} \frac{C_{j,2m+1}^{2i}}{2i-j} \left(\frac{x_1}{x}\right)^{2(i-m)}, \end{aligned} \quad (3,8)$$

where $[a]$ is the "integer part of a ", i. e. the largest integer which is less than a , with $[0] = 0$.

One can easily show that if x_1 is in the interior of the convergence domain of (3,4) (resp. (3,7)), then the leading term of the expansion is independent of x_1 .

One can further generalize all the previous results if $f(x)$ is of the form

$$f(x) = \sum_{n=1}^{\infty} \vartheta(x - \xi_n) f_n(x) \quad (3,9)$$

and $f_n(x)$ can be expanded into an asymptotic power series. This generalization is completely trivial and we do not write down the corresponding formulas explicitly.

4. Asymptote of the forward scattering amplitude

We now turn to the investigation of the pion-nucleon forward scattering amplitude.

First of all we remark that asymptotically the total cross sections of π^+p and π^-p scattering are equal, provided both of them tend to a constant if $\sigma_t \rightarrow \infty$. This follows from an obvious generalization of POMERANCHUK's theorem on the asymptotic equality of pp and $\bar{p}p$ total cross sections [6], see also [7].

In consequence of this, the dispersion relation for the charge exchange amplitude needs no subtraction.

So we can write the dispersion relations for the forward scattering amplitude in the $L. S.$ as follows (standard notations are used):

$$\begin{aligned} \operatorname{Re} f_{L.S.}^{(+)}(v) &= \operatorname{Re} f_{L.S.}^{(+)}(\mu) + 2f^2 v_B \left(\frac{1}{v^2 - v_B^2} - \frac{1}{\mu^2 - v_B^2} \right) + \\ &+ \frac{P}{2\pi^2} \int_{\mu}^{\infty} dv' v' q' \sigma^{(+)}(v') \left(\frac{1}{v'^2 - v^2} - \frac{1}{v'^2 - \mu^2} \right) \\ \operatorname{Re} f_{L.S.}^{(-)}(v) &= \frac{2f^2 v}{v^2 - v_B^2} + \frac{vP}{2\pi^2} \int_{\mu}^{\infty} dv' \frac{q' \sigma^{(-)}(v')}{v'^2 - v^2} \end{aligned} \quad (4,1)$$

with $v_B = -\mu^2/2M$.

Let us choose v_1 in such a way that for $v' > v_1$, $\sigma^{(+)}(v') \approx \sigma = \text{const.}$, $\sigma^{(-)}(v') \approx 0$. Then, making use of (3,5) of the previous section the leading terms of the asymptotic expansions of $\operatorname{Re} f_{L.S.}^{(\pm)}(v)$ are given by the following expressions:

$$\begin{aligned} \operatorname{Re} f_{L.S.}^{(+)}(v) &\sim \operatorname{Re} f_{L.S.}^{(+)}(\mu) - \frac{2f^2 v_B}{\mu^2 - v_B^2} - \frac{\mu\sigma}{(2\pi)^2} \ln \left| \frac{\mu + v_1}{\mu - v_1} \right| \\ &- \frac{P}{2\pi^2} \int_{\mu}^{v_1} \frac{dv' q' v' \sigma^{(+)}(v')}{v'^2 - \mu^2} + \frac{\sigma v_1}{2\pi^2}, \end{aligned} \quad (4,2)$$

$$\operatorname{Re} f_{L.S.}^{(-)}(v) \sim v^{-1} \left[2f^2 - \frac{P}{2\pi^2} \int_{\mu}^{v_1} dv' \sigma^{(-)}(v') q' \right]. \quad (4,2)$$

The amplitudes in the C. M. S. are given by $f_{CM} = M \cdot W^{-1} f_{L.S.}$, where W is the total energy in the C. M. S. and M is the nucleon mass. We see at once that $Ref_{CM}^{(+)} = O(W^{-1})$, $Ref_{CM}^{(-)} = (W^{-3})$, i. e. the forward charge exchange amplitude decreases very rapidly with increasing energy. (Note that ν , the energy of the incident pion in the L. S., is connected with W according to the formula

$$\nu = (2M)^{-1}(W^2 - M^2 - \mu^2) \sim W^2/2M).$$

For the numerical evaluation of (4,2) the following values have been chosen:

$$f^2 = 0,08$$

$$\sigma = 28,0 \text{ mb},$$

$$\nu_1 = 15,3 \mu.$$

The values of $f_2^{(+)}(\mu)$ and of the cross sections have been compiled from the papers quoted in [8].

We thus obtain finally:

$$\left. \begin{aligned} Ref_{CM}^{(+)}(W) &\sim -0,62 \frac{M}{\mu W}, \\ Ref_{CM}^{(-)}(W) &\sim -0,031 \frac{2M^2}{W^3}. \end{aligned} \right\} \quad (4,3)$$

We remark, however, that the numerical value of $f^{(-)}$ is rather uncertain, because it arises from the subtraction of two numbers of equal orders of magnitude.

5. Discussion

The results of the present paper allow testing of the dispersion relations at high pion energies. In fact, if a deviation from the predictions of dispersion relations is expected at all, it would manifest itself almost certainly at high energies.

From the experimental point of view, however, the problem of the measurement of the forward scattering amplitude still remains. We believe that the most reliable method for the evaluation of Ref is that suggested in [5]. The method outlined there does not determine the sign of Ref ; this can be measured with help of the Coulomb interference term at small momentum transfers. (In fact, for small momentum transfers the real part is unlikely to change sign.)

It is pointed out, however, in [5] that if we extrapolate to forward scattering from finite angles, where Coulomb scattering is negligible, then the extrapolated quantity is likely to be the nuclear scattering amplitude alone, instead of being the sum of that of nuclear plus Coulomb scattering.

For finite momentum transfers, however, the whole problem of the determination of $\text{Ref}(\nu, \kappa^2)$ becomes much more complicated, since, in general, one needs a whole set of phase shifts instead of total cross sections alone.

We take pleasure in expressing our sincere thanks to Mr. A. FRENKEL for some critical remarks and Miss M. HORVÁTH for having collected the experimental material on total cross sections and for having carried out the numerical computations.

REFERENCES

1. G. DOMOKOS and A. SEBESTYÉN, *Nuc. Phys.*, **21**, 157, 1960.
2. G. CHEW, M. GOLDBERGER, F. LOW and Y. NAMBU, *Phys. Rev.*, **106**, 1337, 1957. In the present paper the same notation is used as in the article quoted here.
3. L. BIEDERHARN, J. BLATT and M. ROSE, *Rev. Mod. Phys.*, **24**, 249, 1952.
4. G. N. WATSON, *A Treatise on Theory of Bessel Functions*, p. 411, Cambridge University Press, 1944.
5. G. DOMOKOS, A. SEBESTYÉN and F. TELBISZ, *Proc. Weimar Conference on High Energy Physics*, Sept. 1960. (to be published).
6. И. Я. Померанчук, *ЖЭТФ*, **34**, 725, 1958.
7. В. С. Барашенков, *Dubna preprint No F-509* (1960).
8. T. J. DEVLIN, B. C. BARISH, W. N. HESS, V. PEREZ-MENDEZ and J. SOLOMON, *Phys. Rev. Letters*, **4**, 242, 1960;
- J. C. BRISSON, J. DETOEF, P. FALK-VAIRANT, L. VAN ROSSUM, G. VALLADA and LUKE C. L. YUAN, *Phys. Rev. Letters*, **3**, 561, 1959;
- M. J. LONGE, J. A. HELLAND, W. N. HESS, B. J. MOYER and V. PEREZ-MENDEZ, *Phys. Rev. Letters*, **3**, 568, 1959;
- H. P. NOYES and D. N. EDWARDS, *Phys. Rev.*, **118**, 1409, 1960.

О ПОВЕДЕНИИ АМПЛИТУДЫ УПРУГОГО π -N РАССЕЯНИЯ ПРИ БОЛЬШИХ ЭНЕРГИЯХ

Г. ДОМОКОШ

Резюме

Рассматривается кинематика упругого π -N рассеяния в квазиклассическом приближении. Доказано, что если квазиклассическое приближение существует, то спинowymi эффектами можно пренебречь при достаточно высокой энергии, независимо от деталей взаимодействия. В § 3 дается асимптотическое представление функции, определенной при помощи трансформации Гильберта. Это представление используется при получении асимптотики амплитуды π -N рассеяния вперед (§ 4). В § 5 обсуждается возможность экспериментальной проверки результатов.

ZUR BERECHNUNG DER GRÜNEISENSCHEN KONSTANTE DES METALLISCHEN SILBERS

Von
I. BÍRÓ

PHYSIKALISCHES INSTITUT DER UNIVERSITÄT FÜR TECHNISCHE WISSENSCHAFTEN, BUDAPEST

(Vorgelegt von A. Kónya. — Eingegangen: 8. II. 1961)

Es wird die GRÜNEISENSCHE Konstante γ als Funktion des Atomvolumens und des Druckes für den absoluten Nullpunkt der Temperatur auf Grund des statistischen Metallmodells von GOMBÁS [2] ohne Zuhilfenahme empirischer oder halbempirischer Parameter berechnet. Für den Druck Null ergibt sich $\gamma = 17/6$ in befriedigender Übereinstimmung mit Werten, die auf halbempirischem Wege berechnet wurden.

§ 1. Einleitung

Die GRÜNEISENSCHE Konstante spielt in der Theorie der Metalle eine wichtige Rolle. Ihre Berechnung ohne empirischer oder halbempirischer Parameter wurde bisher nur für die Alkalimetalle durchgeführt [1]. Wir wollen hier die Berechnung dieser Konstante für das metallische Silber auf Grund des von GOMBÁS entwickelten Metallmodells [2] durchführen, wobei hervorzuheben ist, dass hierbei keinerlei empirische oder halbempirische Parameter benützt werden.

Nach GOMBÁS kann man die Gitterenergie U des metallischen Silbers pro Atom in der Umgebung der Gleichgewichtslage in folgender Form darstellen

$$U = - \frac{A}{R} - \frac{B}{R^n} - C, \quad (1)$$

wo R den Radius der Elementarkugel bezeichnet und A , B sowie C Konstanten mit den folgenden Werten

$$A = 0,85273 e^2, B = 2191,2 e^2 a_0^{10}, C = 0,11693 e^2/a_0 \quad (2)$$

sind, wo e die positive Elementarladung ist, und a_0 den ersten Bohrschen Wasserstoffradius bedeutet; für den Exponenten n des Abstossungsanteiles ist $n = 11$ zu setzen.

Mit dem Ausdruck (1) für die Gitterenergie hat GOMBÁS das Atomvolumen und die Kompressibilität κ als Funktion des Druckes P bestimmt. Aus seinen Berechnungen folgt

$$\kappa_0 P = \frac{3}{n-1} \cdot \frac{1 - q^{\frac{n-1}{3}}}{q^{\frac{n+3}{3}}}, \quad (3)$$

wo κ_0 den Wert der Kompressibilität in der Gleichgewichtslage bezeichnet und q das relative Volumen

$$q = \frac{\Omega}{\Omega_0} = \frac{R}{R_0} \quad (4)$$

ist, wo $\Omega = 4 \pi R^3/3$ das Volumen und R den Radius der Elementarkugel beim Druck P weiterhin Ω_0 sowie R_0 die entsprechenden Grössen beim Druck Null, d. h. in der Gleichgewichtslage bedeuten. Aus (3) ist das relative Volumen als Funktion des Druckes, d. h. die Funktion

$$q = f(\kappa_0, P) \quad (5)$$

eindeutig festgelegt.

Für die Kompressibilität als Funktion des Atomvolumens erhält GOMBÁS

$$\kappa = (n-1) \kappa_0 \frac{q^{\frac{n+3}{3}}}{n+3-4q^{\frac{n-1}{3}}} \quad (6)$$

Mit Hilfe von (5) ergibt sich hiedurch die Kompressibilität als Funktion des Druckes.

Für Drucke, die im Verhältnis zu $1/\kappa_0$ klein sind, erhält GOMBÁS durch eine Reihenentwicklung

$$q = 1 - \kappa_0 P + \frac{n+10}{6} \kappa_0^2 P^2 \quad (7)$$

§ 2. Berechnung der Grüneisenschen Konstante als Funktion des Druckes

Die GRÜNEISENISCHE Konstante γ ist folgendermassen definiert

$$\gamma = \frac{1}{2} \frac{d \ln \kappa}{d \ln \Omega} - \frac{1}{6} = \frac{1}{2} \frac{\Omega}{\kappa} \frac{d \kappa}{d \Omega} - \frac{1}{6} \quad (8)$$

Mit Rücksicht darauf, dass Ω_0 eine Konstante ist, lässt sich dieser Ausdruck auch folgendermassen schreiben

$$\gamma = \frac{1}{2} \frac{q}{\kappa} \frac{d \kappa}{d q} - \frac{1}{6} \quad (9)$$

Nach Einsetzen des Ausdruckes (6) für κ und Durchführung der einfachen Rechnungen ergibt sich

$$\gamma = \frac{1}{6} \frac{(n+2)(n+3) - 12 q^{\frac{n-1}{3}}}{(n+3) - 4 q^{\frac{n-1}{3}}} = \frac{182 - 12 q^{\frac{10}{3}}}{12 \left(7 - 2 q^{\frac{10}{3}} \right)} . \quad (10)$$

Hiermit ist γ als Funktion des Atomvolumens bestimmt. In Verbindung mit (5) erhält man hieraus γ als Funktion des Druckes P bzw. der dimensionslosen

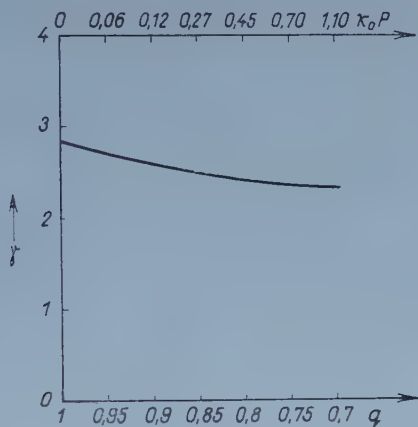


Fig. 1

Grösse $\kappa_0 \cdot P$. Die Beziehung (9) gilt nur für Drucke für die q nicht kleiner wird als 0,8; dies gilt auch für (3), (5) und (6).

Für Drucke, die im Verhältnis zu $1/\kappa_0$ klein sind, ergibt sich durch eine Reihenentwicklung mit Berücksichtigung der Beziehung (7) der Zusammenhang

$$\gamma = \frac{1}{6(n-1)} \left\{ (n+3)(n+2) - 12 - \frac{4}{3} [(n+3)(n+2) - 3(n-1) - 12] \kappa_0 P \right\} = \frac{17}{6} - \frac{28}{9} \kappa_0 P , \quad (11)$$

der jedoch nur für $\kappa_0 P \ll 1$, d. h. etwa im Intervall $1 \geq q \geq 0,95$ gilt. Für kleinere q -Werte hat man die Funktion $\gamma(\kappa_0 \cdot P)$ auf die weiter oben geschilderte Weise zu bestimmen.

Der Verlauf der Funktion $\gamma(q)$, sowie der Funktion $\gamma(\kappa_0 \cdot P)$ ist in der Figur 1 dargestellt. Hierbei ist zu bemerken, dass für κ_0 der von GOMBÁS berechnete Wert

$$\kappa_0 = \frac{12\pi}{(n-1)A} R_0^4 = 0,905 \cdot 10^{-12} \text{ cm}^2/\text{dyn} \quad (12)$$

zu setzen ist.

Für $q = 1$, d. h. $P = 0$, also für die Gleichgewichtslage ergibt sich aus (10) mit dem Wert $n = 11$

$$\gamma = \frac{1}{6} \frac{(n+3)(n+2) - 12}{(n+3) - 4} = \frac{17}{6} = 2,83 \dots \quad (13)$$

Diesen Wert von γ kann man mit den bei SLATER [3] angegebenen halbempirischen Werten vergleichen, die $\gamma = 2,5$ bzw. $\gamma = 2,4$ betragen. Da die Abweichung des von uns berechneten Wertes von diesem nur 10% bis 15% beträgt, kann man die Übereinstimmung als befriedigend bezeichnen.

Für Alkalimetalle beträgt der Exponent des Abstossungsanteiles der Gitterenergie $n = 3$; man erhält [4] somit für diese Metalle $\gamma = 3/2$, also einen fast um die Hälfte kleineren Wert als (13). Dies ist ebenfalls in guter Übereinstimmung mit den bei SLATER angeführten Werten.

LITERATURVERZEICHNIS

1. A. KÓNYA, Journ. Chem. Phys. **17**, 837, 1949 und P. GOMBÁS, Ann. d. Phys. (6) **9**, 70, 1951.
2. P. GOMBÁS, Zs. f. Naturforschung **15a**, 531, 1960.
3. J. C. SLATER, Introduction to Chemical Physics, S. 451, McGraw-Hill Book Comp. Inc., New York, London, 1939.
4. P. GOMBÁS, Ann. d. Phys. (6) **9**, 70, 1951.

ОПРЕДЕЛЕНИЕ ПОСТОЯННОЙ ГРЮНАЙЗЕНА МЕТАЛЛИЧЕСКОГО СЕРЕБРА

И. БИРО

Резюме

В работе определяется постоянная Грюнайзена γ как функция объема атома и давления при температуре абсолютного нуля. В основу вычислений положена статистическая модель металлов Гомбаша [2]; эмпирические или полуэмпирические параметры не используются при определении постоянной γ . Для давления, равного нулю, получается $\gamma = 17/6$, которое удовлетворительно согласуется со значением, вычисленным полуэмпирическим путём.

A POSSIBLE INTERPRETATION OF THE CARCINOGENIC EFFECT OF RADIATIONS AND CARCINOGENIC HYDROCARBONS ON THE BASIS OF THE ELECTRONIC STRUCTURE OF DEOXYRIBONUCLEIC ACID

By

T. A. HOFFMANN

RESEARCH INSTITUTE FOR TELECOMMUNICATION, BUDAPEST

and

J. LADIK

CENTRAL RESEARCH INSTITUTE FOR CHEMISTRY OF THE HUNGARIAN ACADEMY OF SCIENCES, BUDAPEST

(Received 28. IX. 1960)

Numerous attempts have been made to understand the carcinogenic effect of hydrocarbons and radiations of an energy exceeding 3,4 eV [1, 2]. Recently MASON [3] has attempted to explain the process of carcinogenesis on the basis of the electronic structure of proteins. EVANS and GERGELY [4] have shown that if a π -electron interaction is assumed between the parallel polypeptide chains, which are held together by H-bonds and which constitute the protein, the energies of the infinitely long π -electron molecular orbitals so obtained form 3 energy bands. The respective positions of the energy bands are shown in Table I.

Table I

The energy bands of the protein molecule in eV

Band 1	0,00—0,13	Doubly filled
Band 2	3,17—3,43	Doubly filled
Band 3	6,48—6,60	Unfilled

Thus the macromolecule is non-conducting in the ground state, but it assumes conducting properties in the excited state. The width of 3 eV of the forbidden band does not agree exactly with the above value of 3,4 eV, the difference between them is, however, small. With regard to this fact MASON assumes that by irradiating the protein by radiation of suitable energy one electron is raised from the second filled band of the protein into the conduction band. In this way the molecule becomes conductive and this initiates in some way or other the mechanism of carcinogenesis. It should be noted that the theoretical results obtained for the positions of the energy bands have been

confirmed by the experimental investigations carried out to study the photoconduction of proteins [5].

To explain the effect of carcinogenic hydrocarbons MASON [3] assumed that those angularly condensed hydrocarbons are carcinogenically active in which the energy difference between the highest filled molecular orbital and one of the unfilled molecular orbitals is identical with the energy difference between the two filled energy bands of proteins ($3,23 \pm 0,19$ ev). With the aid of this criterion he obtained good agreement with the experimental results. He explained this by the fact that if the energy difference between the energy bands and energy levels is identical, then in the transition complex formed by the protein and the hydrocarbon the hydrocarbon molecule may take up an

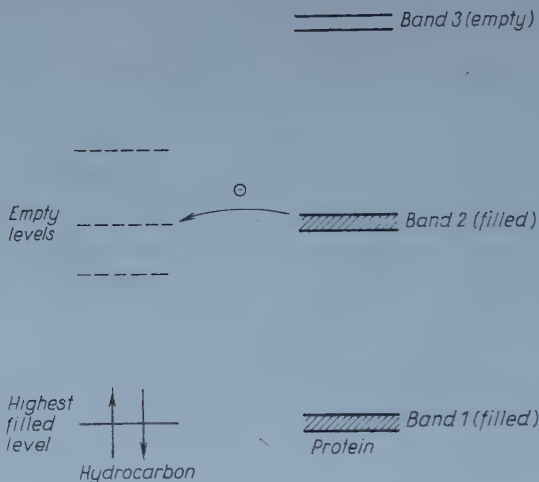


Fig. 1

electron from the protein (see Fig. 1). Owing to this, conduction by π -electrons is induced in the protein with positive-hole mechanism. The appearance of π -electron conduction, as in the case of excitation by radiation, leads in some still unknown way to carcinogenesis.

It should be noted that from the standpoint of quantum chemistry MASON's criterion does not seem to be clarified at all, however, with its aid the carcinogenically active hydrocarbons could be selected from a great number of molecules. It is hoped that it will be possible to formulate a criterion unobjectionable also from the theoretical standpoint.

The results of some recent investigations, however, suggest that in the mechanism of carcinogenesis the primary role should be attributed to deoxyribonucleic acid (DNA) rather than to protein [6]. According to the generally accepted WATSON—CRICK stereo model of the DNA molecule the individual nucleotide bases (adenine, thymine, guanine and cytosine) are situated in the

macromolecule in parallel planes at a distance of 3,36 Å from each other. Between the nucleotide bases having delocalized π -electron systems, i. e. between the π -electrons of the superimposed neighbouring bases there exists a non-negligible interaction, as can be proved by calculating the overlap integrals [8] (see Fig. 2).

For the overlap integral

$$S_{A,B}^{\sigma,\sigma} = \left(\int \psi_A (2p_z) \psi_B (2p_z) d\tau \right)_{R=3,36 \text{ Å}} \quad (1)$$

between two C atoms at a distance of 3,36 Å the value 0,032 was obtained, while the value of the integral (1) in the case of C and N atoms is 0,015. It should be noted that EVANS and GERGELY assume in their calculation for the protein molecule [4] a π -type interaction between the N and O atoms of the neighbouring polypeptide chains. For the N—O distance of 2,65 Å assumed by them, the overlap integral is

$$S_{N,O}^{\pi,\pi} = \left(\int \psi_N (2p_x) \psi_O (2p_x) d\tau \right)_{R=2,65 \text{ Å}} = 0,005. \quad (2)$$

As can be seen this value is about one-sixth of the value of the overlap integral C — C and about one-third of the value of the overlap integral C — N between the nucleotide bases. From this follows that DNA may be equally well described by the energy bands of a common π -electron system, as it was done with protein.

With the aid of the values of the LCAO molecular orbital energies of the individual nucleotide bases found in the literature [9] and calculated by us with somewhat different Coulomb (α_i) and exchange (β_{ij}) integrals [10] the positions of the energy bands can be determined qualitatively.

As in the case of protein, it is found that all bonding bands are completely filled, whereas even the lowest conduction band is entirely empty. Owing to this the molecule (at least the ideal molecule without lattice imperfections and impurities) is non-conducting in the ground state and becomes conductive only by excitation or ionization, via exciton resp. positive-hole mechanism. Knowing the energies of the highest filled and the lowest empty MO-s of the individual nucleotide bases, the width of the forbidden band between the highest valence and the lowest conduction band is calculated to be approximately 3 eV in this case too. The interpretation of the carcinogenic effect of radiation by inducing conduction in the protein molecule can therefore directly be applied also to the DNA. Thus, if the DNA molecule receives radiation of suitable energy, one of its electrons is raised to the conduction band, inducing conducting properties in the DNA molecule.

But, in contrast to the case of protein, if we regard the adenine-thymine and guanine-cytosine base pairs of the WATSON—CRICK model connected

through H-bonds as common π -electron systems interacting through the H-bonds [11], we have to take 5 binding energy bands into account. The width of the forbidden band between the two highest filled energy bands will be much smaller than the value of about 3 eV found for protein. The individual nucleotide bases, however, have such bonding MO-s the energy difference of which does not differ much from the value $3,23 \text{ eV} \pm 0,19 \text{ eV}$ of MASON's criterion. From this follows that the DNA macromolecule will also have (non-successive) bonding energy bands the energy difference of which differs from the value of 3,23 eV only within the limits of the given error. On the basis of

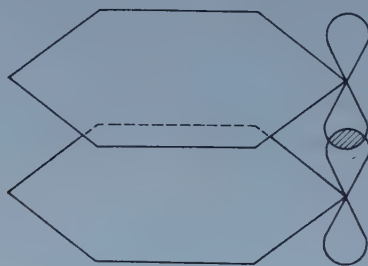


Fig. 2

the data available it is very probable that this condition is fulfilled by the highest bonding energy band of DNA and by the second bonding band under this one. Thus MASON's hypothesis as to the effect of carcinogenic hydrocarbons can be applied also to DNA in the way shown in Fig. 3.

It should be noted that investigations with C-14 suggest that the carcinogenic hydrocarbons interact with protein in the cell in a primary manner [12]. MASON [3] and A. and B. PULLMANN [11], however, also assume the formation of direct nucleotide base — carcinogenic hydrocarbon transition complexes. It can also be imagined that the carcinogen actually interacts with the protein part of the nucleoprotein only, but the π -electron system of the protein and that of DNA also interact in some way or other in the nucleoprotein and thus the carcinogen induces conduction in DNA through the intermediation of the protein.

We intend to return to the more detailed investigation of the problem after having more accurately determined the energy bands of DNA. However, already now it can be stated that it is very probable that the mechanism of carcinogenic hydrocarbons assumed by MASON can be applied in an appropriate way not only to the protein but also to the DNA molecule.

If we assume strong local electric fields within the cell, which is a very plausible assumption, and the symmetry axis of a DNA double helix, in which conduction has been induced by irradiation or by a carcinogen, points in the direction of the field strength, this DNA molecule will be polarized (see Fig. 4).

Thus the production of an excess electric charge at the ends of an excited or ionized DNA molecule has a statistical probability depending on the direction distribution of the axes of the macromolecules.

By realizing that at the ends of the DNA molecule radiation or carcinogen may produce excess charge a relation can be established between the initiation of electronic conduction and that of carcinogenesis. According to the WATSON—CRICK mechanism [7] of DNA duplication, which seems to be the

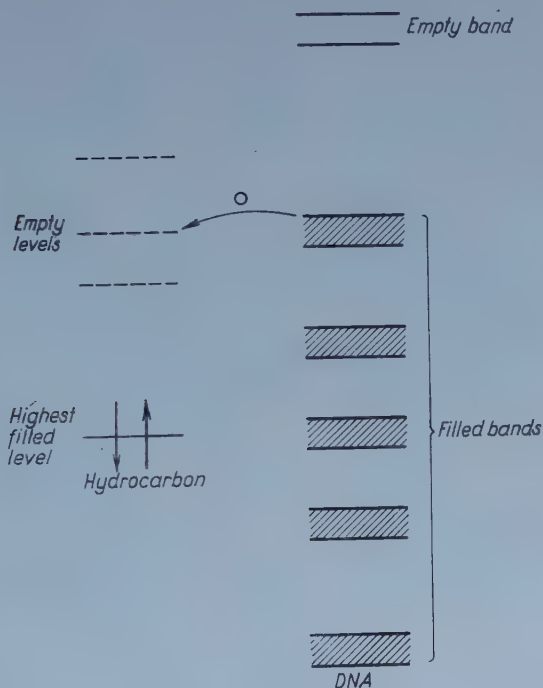


Fig. 3

most probable assumption [13], DNA duplication starts by the unwinding of the double helix constituting the DNA. In the literature, however, no data can be found to explain from where the system obtains the activation energy required to initiate the process. Even if we assume that in the course of duplication the building up of the complementary chain takes place in parallel with the unwinding of the original double helix and so the energy released on account of the formation of the new bonds covers the energy necessary for the original double helix to continue to unwind, for the initiation of the process the system must possess energy sufficient to separate at least one base pair.

To separate the adenine-thymine pair a H-bond of $\text{N}-\text{H} \dots \text{N}$ type of energy of 1,9 kcal/mol and one of $\text{N}-\text{H} \dots \text{O}$ type of an energy of 2,0 kcal/mol

[14] must be broken. The delocalisation energy of the π -electron interaction mentioned above taking place through the H-bonds between the respective base pairs is for adenine-thymine 3,2 kcal/mol, while for guanine-cytosine it is 4,2 kcal/mol [11]. Finally, the mechanical energy of unwinding is 0,3 kcal/mol [15]. With these values we obtain for the energy necessary to separate the adenine-thymine pair

$$\begin{aligned}\Delta E_{A,T} &\approx \varepsilon_{N-H\cdots N} + \varepsilon_{N-H\cdots O} + \varepsilon_{N-H\cdots O} + \varepsilon_{\text{deloc.}} + \varepsilon_{\text{mech.}} = \\ &= 1,9 + 2,0 + 3,2 + 0,3 = 7,4 \text{ kcal/mol.}\end{aligned}\quad (3)$$

In the case of the guanine-cytosine base pair, taking into account that here

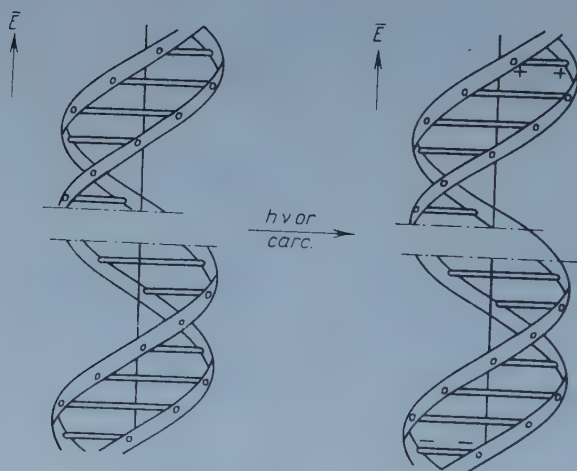


Fig. 4

there are one $N-H\cdots N$ and two $N-H\cdots O$ type H-bonds between the two bases we obtain for the energy of separation

$$\begin{aligned}\Delta E_{G,C} &\approx \varepsilon_{N-H\cdots N} + 2 \varepsilon_{N-H\cdots O} + \varepsilon_{\text{deloc.}} + \varepsilon_{\text{mech.}} = \\ &= 1,9 + 2 \cdot 2,0 + 4,2 + 0,3 = 10,4 \text{ kcal/mol.}\end{aligned}\quad (4)$$

If, owing to irradiation or some carcinogen, the DNA particle undergoes polarization by the mechanism described above, electric repulsion arises between the two halves of the double helix, as shown in Fig. 3. Let us assume e. g. that at the ends of the chains excess charges of a magnitude of $\frac{e_0}{2}$ have appeared, and the centres-of-mass of the charges are approximately at the

central point of the pyrimidine ring, and at the middle-point of the C—C bond in annelation of the purine ring, respectively. Assuming 3,00 Å [16] for the bond distance N—H . . . N binding the rings, for the distance between the centres-of-mass of the two charges we obtain 6,7 Å (see Fig. 5).

With this value we obtain for the potential energy of the repulsion between the two nucleotide bases in the above case

$$V \approx \frac{\left(\frac{e_0}{2}\right)^2}{r} = \frac{4,8^2 \cdot 10^{-20}}{6,7 \cdot 10^{-8}} = 8,6 \cdot 10^{-13} \text{ erg} = 12,5 \text{ kcal/mol.} \quad (5)$$

The value so obtained agrees fairly well with the energy of 10,4 kcal/mol

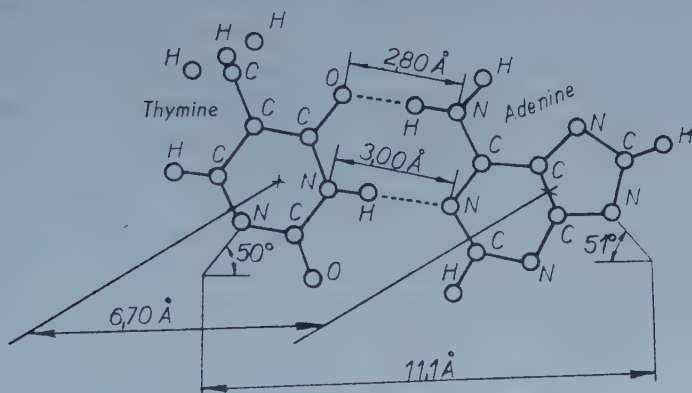


Fig. 5

necessary to separate the guanine-cytosine base pair. Owing to the rough neglects made in the estimation, this of course only means that the potential energy of the repulsion, due to the appearance of an excess charge (of 1 electron) at one of the ends of the double helix, equals in order of magnitude the energy necessary to separate one base pair. Thus it is very probable that the polarization of the chain ends of DNA due to irradiation or carcinogen may start the mechanism of duplication without any other effect on the chain ends. It should be noted that the idea that electric forces play some role in the process of mitosis is not new. It is generally assumed, namely, that electric forces play an essential role in mitosis in the division into two of the cell nucleus [17]. To approach the problem of how the mechanism described may lead to the formation of a macroscopic tumour, we suggest two possibilities. On the one hand in reality photons, or carcinogens may "hit" not only one DNA particle of one single cell, but many DNA particles of many cells of a tissue may be excited or ionized in consequence of such "hits" and each DNA

molecule may also receive several hits. Thus it can be imagined that in the above manner in a time which is not determined by the growth regulation of the organism i. e. at an undesirable time, a great number of new DNA particles may be produced in the cells of some tissue giving rise to their division. It can further be imagined that this process may give rise to a series of irreversible biochemical reactions in the tissue which transform the cells from normal into tumour cells.

On the other hand BURCH [18], on the assumption that radiation may induce cancer by two specific chromosome breaks taking place at different times, developed a statistical theory for the relations between the dose of radiation and the incidence of cancer, which agrees very well with experiment. The mechanism of chromosome break operates according to BUTLER [19] in such a manner that in the chromosome fibril, the morphological basic unit of chromosome, which consists of DNA and nucleohistone particles of the form of small rods standing on the top of each other, the radiation splits the weaker electrostatic bond between the two macromolecules and this causes the chromosome break. The probability, however, that the particle receives the hit just on this spot, is very small. The mechanism described above, however, suggests, that if any part of the DNS molecule is hit, and owing to this the chain ends are polarized, this may lead to the breakage of the electrostatic bond mentioned above and through this to chromosome break. BURCH's theory and our hypothesis thus complete each other.

To support our hypothesis we continue, on the one hand the quantum mechanical investigation of the electronic structure of DNA, and on the other, investigations are being carried out on the behaviour of cancerous tissue cultures placed in electrostatic fields of various intensities over various times. The preliminary experimental data suggest the probability that the electrostatic field somewhat speeds up the metabolism of tumour cells.

A detailed account of these investigations will appear in "Cancer Research".

We express our sincere thanks to Prof. Dr. GY. KISZELY and Dr. I. PATAKY, who called our attention to valuable data in the literature.

REFERENCES

1. O. SCHMIDT, *Z. Physik. Chem.*, **39**, 59, 1938; *ibid*, **42**, 83, 1939; *ibid*, **44**, 185, 1939; *ibid*, **44**, 194, 1939.
2. O. SCHMIDT, *Naturw.*, **29**, 146, 1941.
3. A. PULLMAN, B. PULLMAN, *Adv. Canc. Res.*, New York, Academic Press, **III**, 117, 1955.
4. O. CHALVET, R. DAUDEL, C. MOSER, *Cancer Res.*, **18**, 1033, 1958.
5. C. A. COULSON, *Adv. Canc. Res.*, New York, Academic Press, **I**, 1, 1953.
6. R. MASON, *Nature*, **181**, 820, 1958.
7. R. MASON, *Disc. Far. Soc.*, **27**, 129, 1959.
8. M. G. EVANS, J. GERGELY, *Biochim. Biophys. Acta*, **3**, 188, 1949.
9. D. D. ELEY, C. D. PARFITT, M. J. PERRY, D. H. TAYSUM, *Trans. Far. Soc.*, **49**, 79, 1953.
10. D. D. ELEY, *Disc. Far. Soc.*, **20**, 273, 1955.

- M. H. CARDEW, D. D. ELEY, *Disc. Far. Soc.*, **27**, 115, 1959.
6. See e. g.: D. LAMINANDÉ, *Cancer Res.*, **15**, 329, 1955.
K. C. LEIBMANN, *J. Biol. Chem.*, **216**, 823, 1955.
7. J. D. WATSON, F. H. CRICK, *Nature*, **171**, 737, 1953; *ibid*, **171**, 964, 1953.
F. H. CRICK, J. D. WATSON, *Proc. Roy. Soc.*, **A223**, 80, 1954.
8. J. LADIK, *Acta Phys. Hung.*, **11**, 239, 1960.
9. A. PULLMAN, B. PULLMAN, *Bull. Soc. Chim. France*, 776, 1958; *ibid*, 594, 1959.
10. H. HOFFMANN, T. A. HOFFMANN, J. LADIK, to be published in *Acta Phys. Hung.*
11. A. PULLMAN, B. PULLMAN, *Biochim. Biophys. Acta*, **36**, 343, 1959.
12. P. RONDONI, *Adv. Canc. Res.*, New York, Academic Press, III, 171, 1955.
13. R. C. WILLIAMS, *Rev. Mod. Phys.*, **31**, 233, 1959.
N. SOUKA, *Proc. Nat. Acad. Sci. USA*, **46**, 83, 1960.
14. H. A. STUART, *Die Struktur des freien Moleküls*, p. 49, Springer, Berlin, 1952.
15. M. DELBRÜCK, G. S. STENT, *Symp. on the Chem. Basis of Heredity*, p. 699. Ed. W. D. McElroy, B. Glass, John Hopkins Press, Baltimore, 1957.
16. A. RICH, *Rev. Mod. Phys.*, **31**, 191, 1959.
17. See e. g.: P. GRASSÉ, *Biologie Animale*, p. 107, Masson, Paris, 1957.
18. P. R. J. BURCH, *Nature*, **185**, 135, 1960.
19. J. A. V. BUTLER, *Radiation Res.*, **4**, 20, 1956.

AN ATTEMPT TO EXPLAIN THE ANTICARCINOGENIC ACTIVITY OF SOME NUCLEOTIDE-BASE ANTIMETABOLITES BY THE ELECTRONIC STRUCTURE OF DEOXYRIBONUCLEIC ACID

By

T. A. HOFFMANN

RESEARCH INSTITUTE FOR TELECOMMUNICATION, BUDAPEST

J. LADIK

CENTRAL RESEARCH INSTITUTE FOR CHEMISTRY OF THE HUNGARIAN ACADEMY OF SCIENCES,
BUDAPEST

and

A. UDVARDY

BUDAPEST

(Received 13. X. 1960)

Investigations on the anticarcinogenic activity of numerous nucleotide-base antimetabolites are reported in the literature [1, 2, 3, 4, 5, 6]. These compounds can be divided into two groups: compounds of the purine and of the pyrimidine type (see Fig. 1).

The anticarcinogenic activity of nucleotide-base antimetabolites seems to be subject, in addition to the trivial criterion of ability to build in, to another, electron-structural criterion. It is namely probable that of the compounds substituted in DNA the ones modifying the genuine π -electron distribution of DNA will show anticancer activity. In a previous paper [7] an attempt was made to prove by calculating the overlap integrals between the nucleotide bases the existence of a non-negligible π -electron interaction between the neighbouring nucleotide bases of DNA, located above each other at a separation of 3,36 Å. In other words this means that in DNA a uniform π -electron system describable by energy bands is present. The calculation yielded, among others, the result that certain positions of the nucleotide bases play a distinguished role in the interaction. Thus, as regards overlap, the most important positions are positions 2, 3, 4, 5 and 6 of the purine type, and 2, 5, 6 of the pyrimidine type bases (see numbering in Fig. 1). As further considerations suggest that radiations or carcinogenic hydrocarbons initiate in a primary manner electron mobility along the longitudinal axis of DNA [8] it can be expected that by substituting into the DNA molecule compounds decreasing this electron mobility one may produce anticancer activity. As the electron mobility can be influenced to the greatest extent by substitution at the posi-

tions where the interaction is the strongest, it is probable that the compounds substituted at these positions, if they build in at all, show the strongest activity. This criterion was called above the electron-structural criterion of anticarcinogenic activity.

The most characteristic purine-type antimetabolites are listed in Table I where their activity is also indicated.

It is immediately apparent from the Table that the compounds substituted only at position 2 do not show activity in any of the cases. A purine ring substituted at position 2 (see Fig. 1) can be connected through a H-bond to the pyrimidine-type complementary base corresponding to the WATSON—

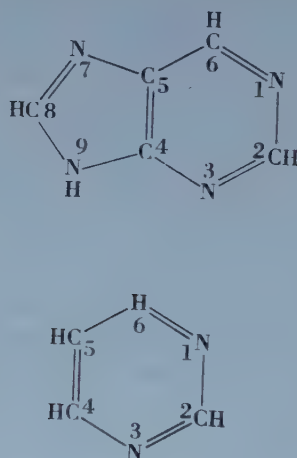


Fig. 1

CRICK model only through the N-atom in the position 1, if the substituent at position 2 is not capable of producing a H-bond with the O-atom attached to the C-atom in position 2 of the thymine or cytosine base (see Fig. 2).

This is just the case with 2-F, 2-Cl and 2-CH₃O-purines and these negative groups even repel the O-atoms of the pyrimidine ring, so that they do not build in at all. The same can be concluded from the fact that 2-F, and 2-Cl—6-NH₂-purines are inactive, but 2-HS—6-NH₂-purine is already slightly active. The substitution of the group NH₂ at position 6 namely facilitates the production of one more H-bond, if the compound is connected to thymine. The energy of this new H-bond is probably not sufficient to counterbalance the repulsion between the F- and Cl-atoms, respectively, substituted at position 2, and the O-atom, but it seems to suffice to counterbalance the repulsion between the less electronegative S- and the O-atom. Thus it can be stated, that although the substitution at position 2 distinguished in respect of the π -electron interaction, satisfies our electron-structural criterion, these compounds are still inactive owing to the restriction of building in.

Table I

The most characteristic purine-type nucleotide-base antimetabolites and their activity

Compound	Activity ¹
Purine	+
2-F-purine	—
2-Cl-purine	—
2-CH ₃ -O-purine	—
2-F-6-NH ₂ -purine	—
2-Cl-6-NH ₂ -purine	—
2-HS-6-NH ₂ -purine	±
6-HS-purine	++
6-Cl-purine	++
6-CH ₃ -purine	+
9-C ₂ H ₅ -purine	—
9-C ₂ H ₅ -6-SH-purine	++

In the case of 6-HS- and 6-CL-purines one more H-bond may be produced between the negative Cl- and S-atoms, respectively, and the cytosine ring of the complementary chain, thus the criterion of building in is fulfilled (see Fig. 2). At the same time the substitution at position 6 of the purine ring, distinguished in respect of the π -electron interaction is likely to influence appreciably the electronic structure of DNA (the configuration of the energy bands) and with it the conditions under which electron mobility is initiated. This seems to account for the strong anticarcinogenic activity of 6-HS- and 6-Cl-purines. In connection with the less active 6-CH₃-purine it should be noted that although some kind of energy-decreasing interaction can be assumed between one of the H-atoms of the CH₃-group and the thymine ring (see Fig. 2), the energy of the "bond" so produced is probably smaller than that of a normal H-bond. Thus the probability of building in will be less than in the former two cases. On the other hand the influence of the CH₃-group by way of hyper-

¹ The signs in the column headed "Activity" of the Table have the following meaning:

—	$Q_t > 0,42 Q_c$,
±	$0,42 Q_c > Q_t < 0,26 Q_c$,
+	$0,26 Q_c > Q_t < 0,06 Q_c$,
++	$Q_t < 0,06 Q_c$.

Here Q_t means the weight of the tumour treated with the compound, Q_c means the weight of the control tumour. The investigations were carried out on Adenocarcinoma 755, which seemed the most suitable for this purpose [1, 2].

conjugate interaction on the delocalized π -electron system of the purine ring is weaker, owing to which the fulfilment of the second criterion of anticarcinogenic activity is less complete. This seems to account for the smaller activity of 6-CH₃-purine.

However, we encounter a difficulty in the interpretation of the 9-C₂H₅- and 9-C₂H₅-6-HS-purines in the last two rows of Table I. (See numbering in Fig. 1). It was assumed [2] that during building in the substituent at position 9 breaks off. In this way the high activity of 9-C₂H₅-6-HS-purine can be well understood, but it remains to be explained that 9-C₂H₅-purine is inactive, whereas the not substituted purine ring is active. It can also be assumed that

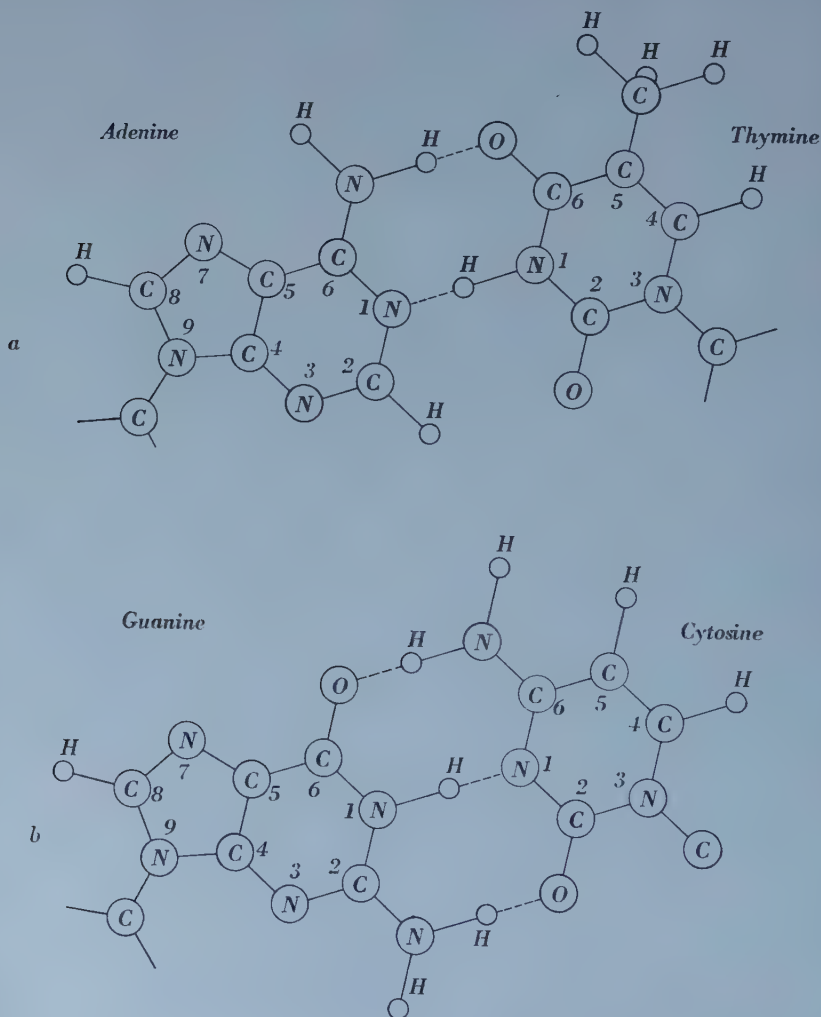


Fig. 2. The adenine-thymine and cytosine-guanine base-pairs

the purine derivatives are attached through their N-atom in position 7 to the deoxyribose, but in this case it is hard to imagine — as Fig. 2 shows — the binding of the molecule so orientated through H-bonds to one of the pyrimidine-type nucleotide bases. The difficulty could perhaps be avoided by assuming that 9-C₂H₅-purine does not build in, but the substitution of the group SH at position 6 in 9-C₂H₅-6-HS-purine influences the reactivity of the C₂H₅ group attached to position 9 of the ring in such a manner that the C₂H₅ group can

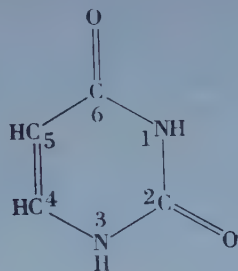


Fig. 3

in this case actually break off during the process of building in. The solution of the problem would of course require more detailed quantum chemical investigations.

In conclusion it should be noted that, as can be seen in Fig. 1, there is no possibility for the substitution into the purine ring at positions 3, 4 and 5 also distinguished with respect to the π -electron interaction between the nucleotide bases.

Comparatively few systematic investigations have been carried out on the anticarcinogenic activity of pyrimidine-type nucleotide-base antimetabolites [10, 11, 12, 13]. 5-F- and 5-Br-uracil (for the formula of uracil see Fig. 3) as well as 5-F-cytosine [11, 12] have been found highly active.

As the C-atom in position 5 of the pyrimidine ring plays an essential role in the interaction between the nucleotide bases located above each other [7], with regard to the above-said it can be understood that the compounds substituted at this position show anticarcinogenic activity. It should be noted that substitution at position 5, as is shown in Fig. 2, does not influence the binding of uracil and cytosine to the corresponding purine-type bases through H-bonds and thus in this case the substitution takes place probably smoothly.

We note that several other pyrimidine derivatives have been produced. However, the investigations on the activity [14] of these compounds have been carried out by so different experimental methods that the results obtained, which cannot be compared, cannot form the basis for the attempt at a theoretical interpretation. We intend to return to the investigation of the problem as soon as the necessary experimental data are available.

REFERENCES

1. H. E. SKIPPER, J. A. MONTGOMERY, J. R. THOMSON and F. M. SCHABEL, *Canc. Res.*, **19**, 425, 1959.
2. J. A. MONTGOMERY, *Canc. Res.*, **19**, 447, 1959.
3. Cancer Chemotherapy Screening Data III, *Canc. Res.*, **19**, No 6, part 2, 287—309, 1959.
4. D. A. CLARKE, G. B. ELION, G. H. HITCHINGS and C. C. STICK, *Canc. Res.*, **18**, 445, 1958.
5. 6-mercaptopurine Conference, Ed. G. H. Hitchings and C. P. Rhead, *Ann. New-York Acad. Sc.*, **60**, 183—503, 1954.
6. D. A. CLARKE, F. S. PHILIPS, S. S. STENBERG and C. C. STOCK, *ibid*, 233.
7. J. LADIK, *Acta Phys. Hung.*, **11**, 239, 1960.
8. T. A. HOFFMANN, J. LADIK, *Canc. Res.*, in the press.
T. A. HOFFMANN, J. LADIK, *Magyar Fizikai Folyóirat*, **3**, 471, 1960.
T. A. HOFFMANN, J. LADIK, *Acta Phys. Hung.*, **13**, 103, 1961.
9. E. CHARGAFF, J. N. DAVIDSON, *The Nucleic Acids I.*, p. 466, Acad. Press, New York, 1955.
10. J. H. BURCHENAL, E. D. HOLMBERG, J. J. FOX, S. C. HEMPHILL and J. A. REPPERT, *Canc. Res.*, **19**, 494, 1959.
11. J. H. BURCHENAL, M. L. MURPHY and C. T. TAN, unpublished observation.
12. C. HEIDELBERGER, N. K. CHAUDHURY, P. DANNEBERG, D. MOOREN, L. GRISBACH, R. DUSCHINSKY, J. R. SCHNITZER, E. PLEVEN, J. SCHEIN, *Nature*, **179**, 663, 1957.
13. C. HEIDELBERGER, L. GRIESBACH, B. J. MONTAG, D. MOOREN, O. CRUZ, J. R. SCHNITZER and E. GRUNBERG, *Canc. Res.*, **18**, 305, 1958.
14. See e. g.: D. W. VISSER, *Antimetabolites and Cancer*, p. 47. Ed. C. P. Rhoad, Washington, D. C. 1955.

APPLICATION OF IRREVERSIBLE THERMODYNAMICS IN THE THEORY OF RECOMBINATION IN SEMICONDUCTORS

By

G. PATAKI

RESEARCH INSTITUTE FOR TECHNICAL PHYSICS OF THE HUNGARIAN ACADEMY OF SCIENCES,
BUDAPEST

(Received 16. II. 1961)

The exact statistical theory of the recombination via traps has been elaborated by W. SHOCKLEY and W. T. READ [1]. They defined the coefficients A_{ik} appearing in the "capture currents", near the equilibrium by

$$U_{cn} = A_{nn} \delta n + A_{np} \delta p, \quad (1)$$

$$U_{cp} = A_{pn} \delta n + A_{pp} \delta p$$

and gave the expressions

$$U_{cn} = \frac{f_{pt} n_0 C_n}{k} \frac{F_n - F_t}{T}, \quad (2)$$

$$U_{cp} = \frac{f_t p_0 C_p}{k} \frac{F_t - F_p}{T},$$

i. e. the relation between the "capture currents" and the quasi Fermi-levels (in the following we use the notations of paper [1]). On the basis of the above equations the theory of recombination can be formulated in terms of irreversible thermodynamics.¹ For the examination of the time dependence of the recombination we write down the equation of motion of thermodynamics in the form given by I. FÉNYES [2] and relating to homogeneous systems near the equilibrium. The equation of conduction (with the usual notations) is as follows:

$$I = LX, \quad (3)$$

where X means the general force and is defined by the equation

$$X = -g a \quad (4)$$

(a being the column vector formed from the extensive quantities: here from δn and δp ,

$$g_{ik} = - \frac{\partial^2 S(a_i, a_k)}{\partial a_i \partial a_k},$$

the symmetrical matrix formed from the entropy).

¹ Note added in proof. From the point of view of fluctuations K. M. VAN VLIET deals with a similar problem. Phys. Rev., **110**, 1, 1958.

Thus we have on the basis of the equations (3) and (4):

$$I = -Lg\alpha.$$

On the other hand the relation between α and I holds as well (assuming homogeneity):

$$\dot{\alpha} \equiv I,$$

i. e.

$$\dot{X} = -g LX; \quad \dot{\alpha} = -Lg\alpha; \quad \dot{I} = -LgI.$$

Let us now introduce the following correspondence, i. e. notation:

$$U_{ci} = -I_{ri}; \quad X_n = -\frac{F_n - F_t}{T}, \quad X_p = -\frac{F_t - F_p}{T}; \quad (Lg)_{ik} = A_{ik},$$

while the conduction matrix becomes diagonal on the basis of the equation (2) and its diagonal elements are $L_{nn} = f_{pi} n_0 C_n/k$, $L_{pp} = f_t p_0 C_p/k$. Matrices $A = -L \cdot g$ and L are then known. From these g can be determined by simple calculations and according to expectation this appears as a symmetrical matrix. According to the above, the equation of motion of the recombination will be as follows:

$$\dot{X} = -AX, \quad \dot{\alpha} = -A\alpha, \quad \dot{I}_r = -A I_r.$$

These matrix equations mean for the components a differential equation of the second order (e. g. for α_i -s):

$$\ddot{\alpha}_i + T(A) \dot{\alpha}_i + D(A) \alpha_i = 0 \quad (i = n, p),$$

where $T(A)$, resp. $D(A)$ mean the trace, resp. the determinant of the matrix A .

Obviously, the form of the solution is

$$\alpha_i(t) = C_{i1} e^{\lambda_r t} + C_{i2} e^{\lambda_l t} \quad (i = n, p), \quad (5)$$

where λ_r and λ_l are the two roots of the characteristic equation

$$\lambda_r = \frac{-T(A) \left[1 - \sqrt{1 - \frac{4D(A)}{T(A)^2}} \right]}{2}; \quad \lambda_l = \frac{-T(A) \left[1 + \sqrt{1 - \frac{4D(A)}{T(A)^2}} \right]}{2}.$$

The equations (5) and (6) describe the time dependence of the recombination

and the quantities $\tau_r = -\frac{1}{\lambda_r}$ resp. $\tau_t = -\frac{1}{\lambda_t}$ give the lifetimes. It is easy to see that expanded in a series in $\frac{4D(A)}{T(A)^2}$ we get in first approximation

$$\tau_r = -\frac{1}{\lambda_r} = \frac{T(A)}{D(A)} = \quad (7)$$

$$= \frac{\tau_{p0} \left[(n_0 + n_1) + N_t \left(1 + \frac{p_1}{p_0} \right)^{-1} \right] + \tau_{n0} \left[(p_0 + p_1) + N_t \left(1 + \frac{p_0}{p_1} \right)^{-1} \right]}{(n_0 + p_0) + N_t \left(1 + \frac{p_2}{p_0} \right)^{-1} \left(1 + \frac{p_0}{p_1} \right)^{-1}},$$

i. e. the stationary lifetime given in paper [1].

For the lifetime τ_t we get in a similar approximation:

$$\tau_t = -\frac{1}{\lambda_r} = \frac{1}{T(A)} = \quad (8)$$

$$= \frac{\tau_{p0} \tau_{n0} N_t}{\tau_{p0} \left[\left(1 + \frac{p_1}{p_0} \right)^{-1} N_t + (n_0 + n_1) \right] + \tau_{n0} \left[\left(1 + \frac{n_1}{n_0} \right)^{-1} N_t + (p_0 + p_1) \right]},$$

which describes a considerably quicker relaxation process than τ_r and corresponds to the filling of the traps.

Summing up what has been said, on the basis of the equations (1) and (2) the irreversible thermodynamic formulation of the recombination is given. From the point of view of irreversible thermodynamics the interesting case occurs where Onsager's cross effect does not appear (L -diagonal), nevertheless, because of the matrix g being off-diagonal, the cross effect found in paper [2] may appear (A off-diagonal).

The non-stationary lifetime τ_r is given and it renders in first approximation the stationary lifetime given in [1]. We have pointed out the mechanism of recombination, giving the relaxation time of the time dependence of the filling of the traps. This relaxation time was given first by D. SANDIFORD [3]. This term may possibly play a part in the time dependence of luminescent phenomena.

REFERENCES

1. W. SHOCKLEY and W. T. READ, Phys. Rev., **87**, 5, 1952.
2. I. FÉNYÉS, Acta Phys. Hung., **11**, 131, 1960.
3. D. SANDIFORD, Phys. Rev., **105**, 2, 1957.

THE GROUND STATE OF THE HYDROGEN MOLECULE ON THE BASIS OF RELATIVISTIC QUANTUM MECHANICS WITH THE AID OF THE WANG WAVE FUNCTION

II. THE RELATIVISTIC CORRECTION ENERGY TERMS

By

J. LADIK

CENTRAL RESEARCH INSTITUTE FOR CHEMISTRY OF THE HUNGARIAN ACADEMY OF SCIENCES, BUDAPEST

(Presented by Z. Gyulai. — Received 17. IX. 1960)

In this paper the expectation values calculated with the Wang approximate wave function of the relativistic correction terms resulting from the treatment of the ground state of the hydrogen molecule on the basis of the BREIT equation are reviewed. The difficulties encountered in the calculation of the part due to retardation of the orbit-orbit magnetic interaction term and the procedure of calculation of another energy term having no non-relativistic counterpart are described. As the spin-orbit interaction terms and the first part of the spin-spin interaction term identically equal zero for any two-electron system of opposite spin, in the ground state of the hydrogen molecule only the second part of the spin-spin interactions term differs from zero. This energy term is shown to be twice as large as one of the terms of the energy having no non-relativistic counterpart.

For the sum of the relativistic correction terms, approximating the value of the magnetic orbit-orbit interaction term by putting it equal to the expectation value of the non-retarded interaction operator, $+1.21 \cdot 10^{-4}$ ev was obtained, which improves the agreement hitherto existing between the experimental and the best theoretical values of the binding energy of the H_2 molecule. The reason for the remaining discrepancy is, in addition to the above neglect, that the expectation values of the correction terms have been calculated instead of with the accurate JAMES—COOLIDGE wave function with the WANG wave function giving a worse approximation, further that the elementary mass correction and the mass polarization corrections have been neglected.

For the treatment of the hydrogen molecule on the basis of relativistic quantum mechanics in a previous paper [1] the reduced BREIT equation of the hydrogen molecule was given. The paper also contained the calculation of the expectation values of three of the relativistic correction energy terms occurring in the ground state of the hydrogen molecule. The calculation was carried out with the aid of the WANG [2] approximate wave function. The purpose of the present paper is to review the remaining relativistic correction energy terms of the ground state of the hydrogen molecule. The expectation values of the respective energy terms calculated by the WANG wave function are also given numerically, except for that part of the magnetic orbit-orbit interaction term which is due to retardation. To determine the expectation value of this energy term proved to be a very intricate mathematical problem. This energy term will be treated in a subsequent paper, after the completion of the calculations now in progress.

1. The magnetic orbit-orbit term

The energy term of the interaction between the magnetic moments due to the motion of the two electrons can be obtained by calculating the expectation value (written in atomic units)

$$\bar{H}_2 = -\frac{1}{2c^2} \int \psi^* \left[\frac{\bar{p}_1 \bar{p}_2}{r_{12}} + \sum_{i,j=1}^3 (x_{1i} - x_{2i})(x_{1j} - x_{2j}) p_{1i} p_{2j} \right] \psi d\tau_1 d\tau_2 \quad (1)$$

of the term H_2 of the Hamiltonian of the reduced BREIT equation (see [1], equation (11)) and by substituting the corresponding parameter values. Here $\bar{p}_k = \frac{1}{i} \text{grad}_k$ ($k=1,2$) is the momentum operator of the k -th electron in atomic units, p_{1i} and p_{2j} are the i -th component of the momentum operator of the first electron, and the j -th component of the momentum operator of the second electron, respectively ($i, j = 1, 2, 3$), $r_{12} = \sqrt{x_{12}^2 + y_{12}^2 + z_{12}^2}$ means the distance between the two electrons, x_{1i} and x_{2j} mean the i -th component of the position vector of the first electron and the j -th component of the position vector of the second electron, respectively ($i, j = 1, 2, 3$) and finally c is the velocity of light. In calculating the expectation value it is again the WANG approximate wave function that has been used for the wave function ψ of the hydrogen molecule.

It should be noted that twice the first half of the term H_2 of the Hamiltonian operator (again in atomic units)

$$H'_2 = \frac{1}{c^2} \left[\frac{\bar{p}_1 \bar{p}_2}{r_{12}} \right], \quad (2)$$

equals the operator obtained for the magnetic orbit-orbit interaction term [3] by reducing to the greater components of the wave function the EDDINGTON—GAUNT relativistic two-electron equation, which uses the non-retarded energy term

$$V_{12} = \frac{e^2}{r_{12}} \left[1 - \frac{\bar{v}_1 \bar{v}_2}{c^2} \right] \quad (3)$$

for the interaction of the two electrons. (In equation (3) \bar{v}_1 and \bar{v}_2 denote the velocity vectors of the first and second electron, respectively). As within the hydrogen molecule the electrons are not too widely separated the value of the non-retarded expression (2) will probably not differ much from the expectation value (1) (at least there will be no difference in order of magnitude bet-

ween them). Therefore, as a first approximation we have calculated the term \bar{H}_2 , which looks simpler, instead of calculating the expectation value

$$\bar{H}_2 = \frac{\bar{H}_2'}{2} + H_2'', \quad (4)$$

where H_2'' is the second term of the expectation value \bar{H}_2 .

In connection with the operator H_2' it should be noted that this operator can also be obtained non-relativistically. Taking the second term of the classical interaction energy between the two moving electrons (3), which is a function of the velocities, as a kinetic energy term, forming the canonically conjugate momenta from the kinetic energy so extended and expressing the velocities \bar{v}_1 and \bar{v}_2 in terms of the momenta \bar{p}_1 and \bar{p}_2 obtained in this way, the result is just the operator H_2' . Following this method [4] for the derivation of operator H_2' the determination of its expectation value for the ground state of the hydrogen molecule has been described in a previous paper [5]. The rather complicated calculation yielded for the expectation value \bar{H}_2' $8,24 \cdot 10^{-4}$ ev, at the nuclear separation of $R = 1,40$ a. u., and the parameter value $a = 1,17$, which results in a maximum binding energy in WANG's original calculation. This value agrees in order of magnitude with the classically estimated value as well as with the approximate value calculated on the basis of the experimental value found by KELLOGG and his collaborators [6] for the interaction of nuclear spins in the H_2 molecule. (For the details see [5]).

Substituting into the second term of (1) the WANG wave function [2]

$$\psi(1,2) = \frac{a^3}{\pi} \frac{[e^{-a(r_{a_1} + r_{b_2})} + e^{-a(r_{a_2} + r_{b_1})}]}{\sqrt{2(1+S^2)}} \quad (5)$$

in atomic units, where

$$\begin{aligned} S^2 &= \frac{a^6}{\pi^2} \left[\int e^{-a(r_{a_1} + r_{b_1})} d\tau_1 \right]^2 = \frac{a^6}{\pi^2} \left[\int e^{-a(r_{a_2} + r_{b_2})} d\tau_2 \right]^2 = \\ &= e^{-2aR} \left(1 + aR + \frac{1}{3} a^2 R^2 \right)^2 \end{aligned}$$

and r_{a_i} and r_{b_i} ($i = 1, 2$) are the distances shown in Fig. 1 the expectation value of the operator H_2'' becomes

$$\begin{aligned} \bar{H}_2'' &= \frac{-a^6}{2\pi^2 c^2} \int \frac{[e^{-a(r_{a_1} + r_{b_2})} + e^{-a(r_{a_2} + r_{b_1})}] \frac{1}{r_{12}^3} \sum_{i,j=1}^3 (x_{1_i} - x_{2_i})(x_{1_j} - x_{2_j}) p_{1_i} p_{2_j}}{2(1+S^2)} \cdot \\ &\quad \cdot [e^{-a(r_{a_1} + r_{b_2})} + e^{-a(r_{a_2} + r_{b_1})}] d\tau_1 d\tau_2. \end{aligned} \quad (6)$$

Writing the operators

$$p_{1k} = \frac{1}{i} \frac{\partial}{\partial x_{1k}}, \quad p_{2k} = \frac{1}{i} \frac{\partial}{\partial x_{2k}} \quad (k = 1, 2, 3)$$

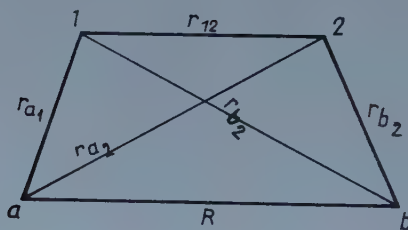


Fig. 1

in atomic units ($\hbar = 1$) and carrying out the multiplications (6) takes the form

$$\begin{aligned} \bar{H}_2'' = \frac{a^6}{2\pi^2 c^2} \int & \frac{[e^{-a(r_{a_1} + r_{b_2})} + e^{-a(r_{a_2} + r_{b_1})}] \frac{1}{r_{12}^3} \left[x_{12}^2 \frac{\partial^2}{\partial x_1 \partial x_2} + y_{12}^2 \frac{\partial^2}{\partial y_1 \partial y_2} + \right.}{2(1 + S^2)} \\ & \left. + z_{12}^2 \frac{\partial^2}{\partial z_1 \partial z_2} + x_{12} y_{12} \left(\frac{\partial^2}{\partial x_1 \partial y_2} + \frac{\partial^2}{\partial y_1 \partial x_2} \right) + \right.}{2(1 + S^2)} \\ & \left. + x_{12} z_{12} \left(\frac{\partial^2}{\partial x_1 \partial z_2} + \frac{\partial^2}{\partial z_1 \partial x_2} \right) + y_{12} z_{12} \left(\frac{\partial^2}{\partial y_1 \partial z_2} + \right. \right. \\ & \left. \left. + \frac{\partial^2}{\partial z_1 \partial y_2} \right) \right] [e^{-a(r_{a_1} + r_{b_2})} + e^{-a(r_{a_2} + r_{b_1})}]}{2(1 + S^2)} \cdot d\tau_1 d\tau_2. \end{aligned} \quad (7)$$

Performing in (7) the differentiations it can be shown that the expression obtained in this way consists of 8 different two-centre integrals. Each one of the hitherto unknown integrals occurring here contains the factor $\frac{1}{r_{12}^3}$, therefore it proved to be a very difficult mathematical problem to evaluate them. For the determination of one of these integrals we have already developed a suitable method [7], so that it may be hoped that it will be possible to evaluate the other integrals too. The results so far obtained also suggest that the determination of the energy term (6) involves, in addition to the mathematical difficulties, a very large amount of numerical work, requiring electronic computing machines. The problem will be discussed in another paper, after the completion of the calculations.

2. The energy term E_4

As in the absence of an external magnetic field the operator H_3 describing the interaction of the magnetic moments belonging to the electron spins with the external magnetic field (see [1], equ. (1)) is equal to zero,

$$H_3 = 0. \quad (8)$$

The next relativistic correction energy term to be considered will be the expectation value of the operator

$$H_4 = \frac{-i}{4c^2} [(\bar{\varepsilon}_1 \bar{p}_1) + (\bar{\varepsilon}_2 \bar{p}_2)] \quad (9)$$

again in atomic units. Here $i = \sqrt{-1}$, c is the velocity of light, \bar{p}_1 and \bar{p}_2 respectively, are the momentum operators of electrons 1 and 2. The expressions of the field intensities $\bar{\varepsilon}_1$ and $\bar{\varepsilon}_2$, respectively, are

$$\bar{\varepsilon}_1 = -\text{grad}_1 V = -\text{grad}_1 \left(\frac{1}{r_{a_1}} + \frac{1}{r_{a_2}} + \frac{1}{r_{b_1}} + \frac{1}{r_{b_2}} - \frac{1}{r_{12}} \right), \quad (10a)$$

$$\bar{\varepsilon}_2 = -\text{grad}_2 V = -\text{grad}_2 \left(\frac{1}{r_{a_1}} + \frac{1}{r_{a_2}} + \frac{1}{r_{b_1}} + \frac{1}{r_{b_2}} - \frac{1}{r_{12}} \right). \quad (10b)$$

It should be noted that the energy term $H_4 = E_4$ has no relativistic counterpart, its appearance is due to the relativistic treatment and it appears already in the one-electron Dirac equation.

It can be shown [8] that the expectation value of the operator H_4 equals the expression

$$\bar{H}_4 = \frac{1}{2} \frac{1}{4c^2} (\overline{\text{div}_1 \bar{\varepsilon}_1} + \overline{\text{div}_2 \bar{\varepsilon}_2}), \quad (11)$$

where

$$\overline{\text{div}_i \bar{\varepsilon}_i} = \int \psi^*_{(1,2)} \text{div}_i \bar{\varepsilon}_i \psi_{(1,2)} d\tau_1 d\tau_2. \quad (i = 1, 2) \quad (12)$$

Substituting the expressions (10a) and (10b) of $\bar{\varepsilon}_1$ and $\bar{\varepsilon}_2$, respectively, into (11) and taking the relations

$$\text{div}_i \bar{\varepsilon}_i = -\Delta_i V, \quad (i = 1, 2)$$

and

$$\Delta \left(\frac{1}{r} \right) = -4\pi\delta(\vec{r})$$

into account [9], where $\delta(\bar{r})$ is the three-dimensional Dirac δ -function, we obtain

$$\bar{H}_4 = \frac{1}{2} \frac{\pi}{c^2} [\delta(\bar{r}_{a_1}) + \delta(\bar{r}_{b_1}) + \delta(\bar{r}_{a_2}) + \delta(\bar{r}_{b_2}) - 2\delta(\bar{r}_{12})]. \quad (13)$$

Using in (13) for the calculation of the expectation values

$$\delta(\bar{r}_{k_i}) = \int \psi^*(1,2) \delta(\bar{r}_{k_i}) \psi(1,2) d\tau_1 d\tau_2, \quad \begin{pmatrix} k = a, b \\ i = 1, 2 \end{pmatrix} \quad (14)$$

again the WANG wave function (5), which is symmetrical with respect to the exchange of the two electrons and the two nuclei, (13) is simplified to the form

$$\bar{H}_4 = \bar{H}'_4 + \bar{H}''_4, \quad (15)$$

where

$$\bar{H}'_4 = 2 \frac{\pi}{c^2} \delta(\bar{r}_{a_1}) \quad (16a)$$

and

$$\bar{H}''_4 = -\frac{\pi}{c^2} \delta(\bar{r}_{12}). \quad (16b)$$

Here

$$\delta(\bar{r}_{12}) = \int \psi^*(1,2) \delta(\bar{r}_{12}) \psi(1,2) d\tau_1 d\tau_2, \quad (17)$$

\bar{r}_{a_1} and \bar{r}_{12} denote the position vectors drawn from the nucleus a to electron 1 and from electron 1 to electron 2, respectively.

In a previous paper [1] the calculation of the expectation values (16a) and (16b) with the WANG wave function has already been described in detail. For these with the parameter values $\alpha = 1,17$ and $R = 1,40$ a. u. have been obtained.

$$E'_4 = [\bar{H}'_4]_{\substack{\alpha=1,17 \\ R=1,40 \text{ a. u.}}} = 20,50 \cdot 10^{-4} \text{ ev}, \quad (18a)$$

$$E''_4 = [\bar{H}''_4]_{\substack{\alpha=1,17 \\ R=1,40 \text{ a. u.}}} = -1,17 \cdot 10^{-4} \text{ ev}, \quad (18b)$$

$$E_4 = E'_4 + E''_4 = (20,50 - 1,17) \cdot 10^{-4} \text{ ev} = 19,33 \cdot 10^{-4} \text{ ev} \quad (18c)$$

(see [1]).

However, the assertion of the above paper that the energy terms (18a) and (18b) are terms of the operator producing the relativistic correction term of the kinetic energy operator is incorrect. These terms are derived from the expectation value of the operator H_4 in the manner described hereabove. The misunderstanding is due to the fact that SUCHER and FOLEY [10] in treating the ground state of the He atom on the basis of the BREIT equation denote

the sum of the correction terms \bar{H}_1 and \bar{H}_4 by \bar{H}_1 . Accordingly, equ. (9) of the previous paper [1] giving the relativistic correction operator of the kinetic energy should be written correctly in the form

$$H_1 = H'_1 = -\frac{1}{8c^2} [(\bar{p}_1^2, \bar{p}_1^2) + (\bar{p}_2^2, \bar{p}_2^2)] \quad (19)$$

instead of the incorrect expression

$$H_1 = H'_1 + H''_1 + H'''_1$$

(see [1] equ. (9)), while the sum of the other two terms is just H_4 . With regard to all this, in Table I of [1], where the relativistic kinetic energy correction terms of the ground state of the He-atom, of the hydrogen molecule and of the two free hydrogen atoms are compared, for the correction term of the kinetic energy only the first row containing the energy term $E'_1 = E_1$ is to be taken into account, whereas the sum of the values in the second and third rows gives the energy term E_4 . It is to be mentioned that in [1] the numerical value of E_1 is also erroneous. The value given in Table I of [1] is to be divided by 2.

3. The spin-orbit interaction terms

The energy of the spin-orbit interaction terms

$$\begin{aligned} H_5 = & \frac{1}{4c^2} \left[\left(\frac{1}{r_{a_1}^3} [\bar{r}_{a_1} \times \bar{p}_1] + \frac{1}{r_{b_1}^3} [\bar{r}_{b_1} \times \bar{p}_1] + \right. \right. \\ & + \frac{1}{r_{12}^3} [\bar{r}_{12} \times (2\bar{p}_2 - \bar{p}_1)] \Big) \sigma_1 + \left(\frac{1}{r_{a_2}^3} [\bar{r}_{a_2} \times \bar{p}_2] + \right. \\ & \left. \left. + \frac{1}{r_{b_2}^3} [\bar{r}_{b_2} \times \bar{p}_2] + \frac{1}{r_{12}^3} [\bar{r}_{21} \times (2\bar{p}_1 - \bar{p}_2)] \right) \sigma_2 \right] \end{aligned} \quad (20)$$

is given by the expectation value of the Hamilton operator

$$\bar{H}_5 = \int {}^1\Phi^* H_5 {}^1\Phi d\tau_1 d\tau_2. \quad (21)$$

The operator H_5 , as is shown in (20), includes the operators $\bar{\sigma}_1$ and $\bar{\sigma}_2$, acting on the spin functions of the first and second electron, respectively, where

$$\bar{\sigma}_1 = \sigma_{1x} \bar{i} + \sigma_{1y} \bar{j} + \sigma_{1z} \bar{k}, \quad (22a)$$

$$\bar{\sigma}_2 = \sigma_{2x} \bar{i} + \sigma_{2y} \bar{j} + \sigma_{2z} \bar{k}, \quad (22b)$$

and

$$\sigma_x = \begin{bmatrix} 0 & 1 \\ 1 & 0 \end{bmatrix}, \sigma_y = \begin{bmatrix} 0 & -i \\ i & 0 \end{bmatrix}, \sigma_z = \begin{bmatrix} 1 & 0 \\ 0 & -1 \end{bmatrix} \quad (23)$$

are the Pauli spin matrices. Thus to calculate the expectation value of the complete, position and wave function of the ground state of the hydrogen molecule

$${}^1\Phi = \psi(\bar{r}_1, \bar{r}_2) \chi(1,2) = \psi(\bar{r}_1, \bar{r}_2) \frac{1}{\sqrt{2}} [\chi_\alpha(1) \chi_\beta(2) - \chi_\alpha(2) \chi_\beta(1)] \quad (24)$$

is to be used. Here the definitions of the orthonormalized spin functions χ_α and χ_β are

$$\chi_\alpha = \begin{pmatrix} 1 \\ 0 \end{pmatrix} \quad \text{and} \quad \chi_\beta = \begin{pmatrix} 0 \\ 1 \end{pmatrix}.$$

The factor of the complete wave function (24), which depends on the spin functions of the two electrons, as can be readily seen from the orthonormalization of χ_α and χ_β , is normalized to 1. This is why no error resulted from neglecting — for the sake of brevity — in the calculation of the expectation values of operators not containing operators acting on the spins the spin-function dependent factors of the wave functions.

It can be shown that the expectation value (21) (see e. g. [11]), independently of what form is used for the factor depending on the position coordinate of the wave function, equals zero for any two-particle system of antiparallel spin. Therefore, as the ground state of the hydrogen molecule is a singlet state the spin-orbit interaction term in the ground state of the hydrogen molecule will be zero,

$$\bar{H}_5 = E_5 = 0. \quad (25)$$

4. Spin-spin interaction terms

It can again be shown [11] that of the operators

$$H_6 = H'_6 + H''_6 \quad (26)$$

giving the spin-spin interaction term, the operator

$$H'_6 = \frac{1}{4c^2} \left[\frac{\delta_1 \delta_2}{r_{12}^3} - \frac{3(\bar{\delta}_1 \bar{r}_{12})(\bar{\delta}_2 \bar{r}_{12})}{r_{12}^5} \right] \quad (27)$$

multiplied by the spin functions from the left and right hand side, i. e.

$$\chi(1,2) H'_6 \chi(1,2) \quad (28)$$

is equal to zero for a singlet two-electron system. Thus in the ground state of the hydrogen molecule the corresponding expectation value will also be zero

$$\bar{H}'_6 = E_6 = 0. \quad (29)$$

The expectation value of the second part of the operator H_6

$$H''_6 = -\frac{8\pi}{3} \frac{1}{4c^2} (\bar{\sigma}_1 \bar{\sigma}_2) \delta(\bar{r}_{12}) \quad (30)$$

(see [1] equ. (9b)), however, will not be zero, not even for the ground state of the hydrogen molecule. For this operator the expression

$$\chi(1,2) H''_6 \chi(1,2)$$

after substituting (30) and $\chi(1,2)$ becomes

$$\begin{aligned} \chi(1,2) H''_6 \chi(1,2) = & -\frac{1}{2} [\chi_\alpha(1) \chi_\beta(2)] - \\ & - \chi_\alpha(2) \chi_\beta(1) \Big] \frac{8\pi}{3} \frac{1}{4c^2} \delta(\bar{r}_{12}) \bar{\sigma}_1 \bar{\sigma}_2 \cdot [\chi_\alpha(1) \chi_\beta(2) - \chi_\alpha(2) \chi_\beta(1)]. \end{aligned} \quad (31)$$

Equ. (31), as can be easily shown, may be simplified to the form

$$\chi(1,2) H''_6 \chi(1,2) = 8\pi \frac{1}{4c^2} \delta(\bar{r}_{12}). \quad (32)$$

A comparison between (32) and the expectation value

$$\bar{H}''_4 = -\frac{\pi}{c^2} \delta(\bar{r}_{12}) \quad (16a)$$

giving the second part of the energy term E_4 , however, shows that for the expectation values the relation

$$\bar{H}''_6 = -2\bar{H}''_4 \quad (33)$$

holds.

On the basis of equation (33) the value of the spin-spin magnetic interaction energy term approximated with the WANG wave function, which also remains in the singlet multiplicity ground state of the hydrogen molecule, can immediately be written down with the aid of the value (18b) of the energy term E_4 ,

$$E''_6 = -2E''_4 = -2(-1,17 \cdot 10^{-4} \text{ ev}) = 2,34 \cdot 10^{-4} \text{ ev}. \quad (34)$$

Comparing this value with the value of $17,38 \cdot 10^{-4}$ ev obtained for this term for the He-atom with a hydrogen-like wave function [10] it can be seen that this is about 13% of the value obtained for He. The value calculated for the electron spin—electron spin interaction energy from the value of the nuclear spin—nuclear spin magnetic interaction energy of the hydrogen molecule, which latter can be determined by the aid of the molecular beam magnetic resonance method, is $3,98 \cdot 10^{-4}$ ev [5]. The good agreement of this value with (34) is very probably accidental. It should be noted that if E_6'' were calculated with the aid of the more accurate JAMES-COOLIDGE wave function, the values so obtained, similar to the case of the He-atom [10], would probably be smaller than the value (34) calculated with the WANG wave function constructed of hydrogen-like wave functions and thus the difference between the theoretical value and the one estimated from the experimental value between the nuclear spins would increase.

Comparing (34) with the value of $8,24 \cdot 10^{-4}$ ev [10] obtained for the magnetic orbit-orbit interaction term it is seen that for the ground state of the hydrogen molecule the orbit-orbit interaction term in the approximation used here is about for times the spin-spin interaction energy. It should be noted that for the He-atom the case is reversed also if the values calculated with the three-parameter Hylleraas wave function are used. Here the spin-spin interaction term is about ten times the magnetic orbit-orbit interaction term ([10], [11]). The difference is due in all probability to the fact that in the case of the He-atom the states of the individual electrons deviate to a small extent from the spherically symmetrical 1s state and thus the value of the magnetic orbit-orbit term is rather small.

Owing to the lack of suitable experimental data, just as in the case of the magnetic orbit-orbit interaction term, the energy value (34) cannot be directly compared with the experiment. If, however, the Zeeman disintegrations of the individual rotational levels of the hydrogen molecule would be investigated in a magnetic field so strong as to cause the uncoupling of the spins of the two electrons and thus the spins of the individual electrons would be quantized with respect to the magnetic field independently of each other it can be imagined that from the spectrum so obtained conclusions could be drawn in some way as regards the spin-spin interaction term E_6'' .

5. The sum of the relativistic correction terms

In Table I the results obtained for the relativistic correction terms of the ground state of the hydrogen molecule with the WANG wave function are summarised.

In the Table E_1 means the relativistic correction term of the kinetic energy, E_2' the non-retarded magnetic orbit-orbit interaction term, E_2'' means

Table I

The energies of the relativistic correction terms
in the ground state of the hydrogen molecule

Energy term	Energy in 10^{-4} ev
E_1	-28,70
E'_2	8,24
E''_2	?
$E_2 = E'_2/2 + E''_2$	4,12 + ?
E_3	0*
E'_4	20,50
E''_4	-1,17
$E_4 = E'_4 + E''_4$	19,33
E_5	0
E'_6	0
E''_6	2,34
$E = E'_6 + E''_6$	2,34
$E_{\text{corr}}^{\text{H}_2} = \sum_{i=1}^6 E_i$	-2,91 + E''_2

* if no external magnetic field is present.

that part of the latter term due to retardation, and $E_2 = E'_2/2 + E''_2$ gives the complete retarded magnetic orbit-orbit interaction term. E_3 is the term resulting from the interaction of the spins with the external magnetic field. The energy term E_4 has no non-relativistic counterpart, E_5 is the spin-orbit interaction term, and $E_6 = E'_6 + E''_6$ gives the energy of interaction between the electron spins. The expression

$$E_{\text{corr}}^{\text{H}_2} = \sum_{i=1}^6 E_i = -2,91 \cdot 10^{-4} \text{ ev} + E''_2 \quad (35)$$

denotes the total energy of all the relativistic correction terms. To determine this, as we have seen above it would also be necessary to calculate the energy term E''_2 which, owing to mathematical difficulties, is not yet possible. Using for E_2 as an approximation the value of $8,24 \cdot 10^{-4}$ ev derived from the expectation value of the non-retarded interaction operator H'_2 we obtain for $E_{\text{corr}}^{\text{H}_2}$ the value

$$E_{\text{corr}}^{\text{H}_2} \approx -1,21 \cdot 10^{-4} \text{ ev.} \quad (36)$$

When it becomes possible to calculate all terms of E_{corr} , the value obtained could be checked as follows. KOLOS and ROTHAAAN [12] taking into

account further terms in the series of the JAMES-COOLIDGE [13] wave function, using altogether 50 terms, have determined the energy of the H_2 molecule to an accuracy of 10^{-4} ev and obtained for the binding energy 4,7467 ev. The expression of the binding energy containing also the relativistic correction terms becomes

$$\begin{aligned}\varepsilon_r &\equiv 2E_r^H - E_r^{H_2} = 2(E_{n,r}^H + E_{corr}^H) - (E_{n,r}^{H_2} + E_{corr}^{H_2}) = \\ &= \varepsilon_{n,r} + 2E_{corr}^H - E_{corr}^{H_2},\end{aligned}\quad (37)$$

where E_{corr}^H and $E_{corr}^{H_2}$, respectively, denote the relativistic correction energy term of the H atom and the H_2 molecule. In the first approximation the relativistic change of the energy of the H atom can be obtained from the expression

$$E_{corr}^H = \frac{-a^2}{8} \text{ a. u.} \quad (38)$$

[14]. Substituting here the value $\frac{1}{137,04}$ of the fine structure constant a we obtain for (38) $-2 \cdot 10^{-4}$ ev. Using this value and for $E_{corr}^{H_2}$ as an approximation (36), we get

$$\varepsilon_r = 4,7467 - 0,0004 - 0,0001 = 4,7462 \text{ ev.} \quad (39)$$

It seems to be interesting to compare the binding energy obtained with the value of the experimental binding energy

$$\varepsilon = D_0^0 + G_0'', \quad (40)$$

where D_0^0 is the dissociation energy and G_0'' is the zero point energy of the vibration of the nuclei. HERZBERG and MONFILS [15], [16] give for G_0'' the value $2179,3 \pm 0,2 \text{ cm}^{-1}$, and they determined the best value of the dissociation energy of the hydrogen molecule, to be $D_0^0 = 36113,0 \pm 0,3 \text{ cm}^{-1}$. The sum of the two values is $38,292,3 \pm 0,5 \text{ cm}^{-1} = 4,74599 \pm 0,0006 \text{ ev}$.

It can be seen that the theoretical non-relativistic value does not agree well with the experimental one, whereas this is not the case with the theoretical relativistic value. The remaining discrepancy can be probably attributed to four main reasons: 1) The use of the value of the non-retarded magnetic orbit-orbit interaction term E_2' instead of $E_2 = \frac{E_2'}{2} + E_2''$. 2) Calculation of the expectation values of the individual operators with the WANG wave function, which gives a rather bad approximation. 3) Neglection of the various radiation correction terms — which can be taken into account in a quantum electrodynamical treatment — in the case of the two free hydrogen atoms as well as for the

ground state of the H_2 molecule. 4) Disregarding the mass correction term due to the motion of the nuclei as well as the so-called mass polarization correction term also due to the motion of the nuclei in many-electron atoms and molecules (in many-electron systems this correction term appears in addition to the elementary mass correction [17]). The values of the retarded and non-retarded magnetic orbit-orbit interaction terms differ probably not much as the inter-electronic distance in the H_2 molecule is not large. The sum of the most important radiation correction energy terms in the ground state of the H_2 molecule is only $-1,8 \cdot 10^{-5}$ ev [18]. The value of the elementary mass correction for two free hydrogen atoms is $+0,0148$ ev, while for the H_2 molecule VAN VLECK's [19] approximate calculation gives $+0,00141$ ev. So this would produce a change of $+0,0007$ ev in the binding energy. However, for the value of the mass polarization term with the best, 38-parameter wave function of the He-atom $+6 \cdot 10^{-4}$ ev was obtained [20]. Taking as approximation this value into account, also for the ground state of the H_2 -molecule, the sum of the two mass correction terms causes a change of only $1 \cdot 10^{-4}$ ev in the binding energy of the H_2 -molecule. With regard to all this it can be expected that the main reason for the discrepancy lies in the fact that the expectation values of the various relativistic correction energy terms are not approximated with sufficient accuracy. Thus, after the completion of the calculation of E_2'' it would seem suitable to repeat the calculations with the JAMES-COOLIDGE wave function, which gives an accurate, non-relativistic binding energy value. Subsequent to this calculation, which probably involves great mathematical difficulties, the mass polarization correction term should be determined for the ground state of the H_2 molecule. It can be hoped that the accurate theoretical value of the binding energy thus obtained will agree with the experimental one just as it was found in the case of the He-atom and He-like ions.

In conclusion it seems to be of interest to compare the approximate value of $+1,21 \cdot 10^{-4}$ ev obtained for the sum of the relativistic corrections with the corresponding value in the He-atom. In the ground state of the He-atom the values obtained for the sum of the relativistic terms are: $(0,73 \cdot 10^{-4}$ ev with hydrogen-like wave function [10, 21], $-17,75 \cdot 10^{-4}$ ev with a HARTREE SCF wave function [10, 22], $-23,46 \cdot 10^{-4}$ ev with a 3-parameter HYLLERAAS wave function [10, 11] and $-28,26 \cdot 10^{-4}$ ev with the KINOSHITA 38-parameter variational trial function [20]. It can be seen that by improving the approximation the absolute value of the relativistic correction energy increases. It can be stated anyway that the values relating to the ground state of the He atom and the H_2 molecule apart from the very bad result obtained by approximating the wave function of the ground state of the He atom by the product of two 1s H-atom functions do not agree in sign and in order of magnitude. The reason for this deviation may be the difference between the one-centre He and the two-centre H_2 problem.

Acknowledgements

I should like to express my gratitude to Prof. C. A. COULSON (Oxford) for his very helpful remarks and suggestions communicated to me by letter, to Academicians G. SCHAY and P. GOMBÁS and to T. A. HOFFMANN, Doctor of Physical Sciences, for encouragement during the progress of this work, to T. MÁTRAI, Candidate of Physical Sciences, for raising my interest in the problems treated above in connection with the non-relativistic deduction of the magnetic orbit-orbit interaction and for helpful discussions, to Dr. J. KOLOS (Warsaw) for helpful discussions and to Dr. A. FRÖMAN (Uppsala) for calling my attention to valuable data in the literature.

REFERENCES

1. J. LADIK, *Acta Phys. Hung.*, **10**, 271, 1959.
2. S. C. WANG, *Phys. Rev. (2)*, **31**, 579, 1928.
3. G. BREIT, *Phys. Rev. (2)*, **34**, 553, 1929.
4. T. MÁTRAI, unpublished work.
5. J. LADIK, A. CSUKÁS, *Acta Phys. Hung.*, **6**, 381, 1957.
6. J. M. B. KELLOGG, L. I. RABl, N. F. RAMSEY JR., J. R. ZACHARIAS, *Phys. Rev. (2)*, **57**, 677, 1940.
7. G. KARDOS, J. LADIK, *Publications of the Mathematical Research Institute Hung. Ac. Sci.*, in the press.
8. See e. g. H. A. BETHE, E. E. SALPETER, *Quantum Mechanics of One and Two-Electron Systems: Handbuch der Physik XXXV*, Springer, 1957, pp. 268—269.
9. H. A. BETHE, E. E. SALPETER, loc. cit., p. 275.
10. J. SUCHER, H. M. FOLEY, *Phys. Rev. (2)*, **95**, 966, 1954.
11. H. A. S. ERIKSSON, *Z. f. Physik*, **109**, 762, 1938.
12. W. KOLOS, C. C. J. Roothan, *Rev. Mod. Phys.*, **32**, 219, 1960.
13. H. M. JAMES, A. S. COOLIDGE, *J. Chem. Phys.*, **1**, 825, 1933.
14. See e. g. H. A. BETHE, E. E. SALPETER, loc. cit. p. 147.
15. G. HERZBERG, A. MONFILS, *J. Mol. Spectr.*, **5**, 482, 1960.
16. A. FRÖMAN, Uppsala Quantum Chemistry Group, Preprint No 54, 1960.
17. See e. g. H. A. BETHE, E. E. SALPETER, loc. cit. p. 254.
18. J. LADIK, *Acta Phys. Hung.*, in the press.
19. F. H. VAN VLECK, *J. Chem. Phys.*, **4**, 327, 1936.
20. H. A. BETHE, E. E. SALPETER, loc. cit. pp. 277—278.
21. H. A. BETHE, *Handbuch der Physik, Quantummeehanik der Ein- und Zwei-Elektronenprobleme*, 24 (II), Springer, 1933, p. 384.
22. A. M. SESSLER, H. M. FOLEY, *Phys. Rev. (2)*, **92**, 1321, 1953.

ТРАКТОВКА ОСНОВНОГО СОСТОЯНИЯ МОЛЕКУЛЫ ВОДОРОДА
НА ОСНОВАНИИ РЕЛЯТИВИСТИЧЕСКОЙ КВАНТОВОЙ МЕХАНИКИ
С ПОМОЩЬЮ ВОЛНОВОЙ ФУНКЦИИ УАНГА II.

Обзор релятивистических коррекционных членов

И. ЛАДИК

[Резюме

В работе дается обзор ожидаемых значений релятивистических коррекционных членов, появляющихся при трактовке основного состояния молекулы водорода на основе уравнения Брейта. Эти члены вычислялись приближенной волновой функцией Уанга. Далее обсуждаются трудности, появляющиеся при вычислении той части члена орбитально-орбитального магнитного взаимодействия, которая обусловлена ретардацией. Кроме этого описывается ход определения члена энергии, не имеющего нерелятивистического аналога. Так как члены спин-орбитального взаимодействия и первая часть члена спин-спинового взаимодействия у всякой двухэлектронной системы с антипараллельными спинами идентично равны нулю, в основном состоянии молекулы водорода лишь вторая часть члена спин-спинового взаимодействия будет отличаться от нуля. По отношению данного члена энергии в работе доказывается, что он в два раза больше одного частного члена энергии, не имеющего нерелятивистического аналога.

Сумма релятивистических коррекционных членов, если значение члена орбитально-орбитального магнитного взаимодействия приближенно брать равным ожидаемому значению неретардированного оператора взаимодействия, равна $+1,21 \cdot 10^{-4}$ eV. Оно улучшит хорошее до этого согласование между экспериментальным и наилучшим нерелятивистическим теоретическим значениями энергии связи молекулы H_2 .

Причина все же имеющегося расхождения заключается в том, что, кроме упомянутых пренебрежений, вычисление ожидаемых значений некоторых коррекционных членов производилось не точной волновой функцией Джемса и Кулиджа, а волновой функцией Уанга, дающей возможность с меньшей точностью аппроксимировать истинное значение, далее в пренебрежении коррекционным членом элементарной массы и членом, учитывающим поляризацию массы.



APPROXIMATE DETERMINATION OF THE MOST IMPORTANT RADIATION CORRECTION ENERGY TERMS FOR THE GROUND STATE OF THE HYDROGEN MOLECULE

By

J. LADIK

CENTRAL RESEARCH INSTITUTE FOR CHEMISTRY OF THE HUNGARIAN ACADEMY OF SCIENCES, BUDAPEST

(Presented by Z. Gyulai. — Received 17. IX. 1960)

The most important radiation correction energy terms for the ground state of the hydrogen molecule can easily be obtained by appropriately modifying the expression for the helium atom. Substituting the results obtained by the approximate WANG wave function for the expectation values occurring in the individual energy terms for the energy term describing the Lamb shift $10,12 \cdot 10^{-5}$ ev, while for the energy term giving approximately the radiation interaction between the two electrons $-0,63 \cdot 10^{-5}$ ev were obtained. Subtracting the sum of these two values from the value of $7,72 \cdot 10^{-5}$ ev giving the Lamb shift for two free hydrogen atoms, for the change of the binding energy due to the appearance of the radiation correction terms $-1,77 \cdot 10^{-5}$ ev is obtained. This value is by one order of magnitude lower than the corresponding value obtained for the ground state of the helium atom, and thus it does not influence the theoretical value of the binding energy of the hydrogen molecule so far determined to an accuracy of 10^{-4} ev.

The expression of the most important radiation correction energy terms for the simplest stable two-electron systems, i. e. the He atom and the ground state of He-like ions can be found in the literature [1]. In the case of a two-electron atom, or ion, just like in the one-electron case, the most important radiation correction terms are the lowest order Lamb shift terms. As is well known these correspond to the emission and reabsorption of a virtual photon by one of the electrons, taking place in such a manner that the electron is scattered between emission and absorption on the potential of the nucleus. For the sum of these terms we find in the literature [1] the expression

$$E_L = \frac{3}{16} \alpha^3 Z \overline{\delta(\bar{r}_1)} \left[\ln \frac{mc^2}{K_0} + \frac{19}{30} - \ln 2 \right] \text{Ry} . \quad (1)$$

Here $\alpha = \frac{1}{137,037}$ is the fine-structure constant, Z is the charge of the nucleus, m stands for the mass of the electron, c for the velocity of light, K_0 is the average excitation energy of the atom averaged over all discrete states [2] and $\overline{\delta(\bar{r}_1)}$ is the following expectation value:

$$\overline{\delta(\bar{r}_1)} = \int \psi^*(\bar{r}_1, \bar{r}_2) \delta(\bar{r}_1) \psi(\bar{r}_1, \bar{r}_2) d\tau_1 d\tau_2 . \quad (2)$$

The vector \bar{r}_1 in the three-dimensional $\delta(\bar{r}_1)$ Dirac delta-function means the position vector drawn from the nucleus to the position of the first electron. Expression (1) yields the value of the energy term [1] in Rydberg energy units (1 Ry = 13,60 ev), if the value of the integral (2) is substituted in atomic units. The value of the average excitation energy K_0 is for the 1S ground state of the He atom 84 Ry and for the states $n = 1, l = 0$ the relation $K_0 = 19,77 Z^2$ Ry is in general valid to a good approximation [3].

In the case of a two-electron system further Lamb-type correction terms appear owing to the fact that the electrons can be scattered between the emission and the reabsorption of the virtual photon not only on the potential of the nucleus, but on that of the other electron as well, and the virtual photon exchange between the two electrons yields a further energy term. For the sum of these terms we find in the literature [1] the approximate expression

$$E'_1 = \frac{28}{3} \alpha^2 \overline{\delta(\bar{r}_{12})} \ln a \text{ Ry}, \quad (3)$$

where the expectation value

$$\overline{\delta(\bar{r}_{12})} = \int \psi^*(\bar{r}_1, \bar{r}_2) \delta(\bar{r}_{12}) \psi(\bar{r}_1, \bar{r}_2) d\tau_1 d\tau_2 \quad (4)$$

is to be substituted in atomic units. The argument $\bar{r}_{12} = \bar{r}_2 - \bar{r}_1$ of the three-dimensional Dirac delta-function means the vector drawn from the position of the first electron to the second.

To determine the change occurring in the ionization energy owing to the most important radiation correction terms the knowledge of the radiation correction terms of the ground state of the He^+ ion is also necessary. In the approximation used for the He atom of these only the energy term

$$E_{L,1} = \frac{8 \alpha^3 Z}{3} \frac{Z^3}{\pi} \left[2 \ln \frac{1}{Za} \frac{K_0}{Z^2 \text{ Ry}} + \frac{19}{30} \right] \text{ Ry} \quad (5)$$

giving the lowest order Lamb shift is to be taken into account. With the aid of this the change of the ionization energy of the He atom due to the radiation correction terms can be expressed approximately in the form

$$\Delta E_J^{\text{He}} = E_{L,1}^{\text{He}^+} - E_L^{\text{He}} - E'_L{}^{\text{He}}. \quad (6)$$

The values of the correction terms $E_{L,1}$, E_L and E'_L for the ground state of the He atom are also given numerically by BETHE and SALPETER [1]. To determine the energy terms E_L and E'_L they used for the expectation values $\overline{\delta(\bar{r}_1)}$ and $\overline{\delta(\bar{r}_{12})}$ the values obtained with the aid of the best 38-parameter

variational function of the ground state of the He atom calculated by KINO-SHITA [4]. They obtained the following results:

$$E_{L,1}^{\text{He}^+} = 4,38 \cdot 10^{-4} \text{ eV}; E_L^{\text{H}^+} = 6,06 \cdot 10^{-4} \text{ eV}; E_L^{\text{H}^+} = -0,26 \cdot 10^{-4} \text{ eV}, \quad (7)$$

and from these

$$\Delta E_J^{\text{H}^+} = (4,38 - 6,06 + 0,26) \cdot 10^{-4} \text{ eV} = -1,42 \cdot 10^{-4} \text{ eV}. \quad (8)$$

Adding this value to the best non-relativistic ionization energy of the He atom and taking into account the values of the various relativistic correction terms due to the BREIT equation as well as the so-called mass-polarization term, the theoretical value so obtained ($J_{\text{th.or.}} = 198310,4 \text{ cm}^{-1}$) agrees excellently with the experimental value ($J_{\text{xp.}} = 198310,5 \pm 1 \text{ cm}^{-1}$) [1].

The change of the energy due to the most important radiation energy terms can be easily determined also for the ground state of the hydrogen molecule. Equation (6) for the ground state of the hydrogen molecule takes the modified form

$$\Delta E_{J^2}^{\text{H}_2} = 2E_{L,1}^{\text{H}} - E_L^{\text{H}_2} - E_L^{\text{H}_2}. \quad (9)$$

$E_{L,1}^{\text{H}}$ can be immediately calculated from equation (5) by substituting $Z = 1$ and $K_0 = 19,77 \text{ Ry}$, which yields

$$E_{L,1} = 3,36 \cdot 10^{-5} \text{ eV}. \quad (10)$$

The expression for $E_L^{\text{H}_2}$ can easily be obtained on the basis of expression (1) for $E_L^{\text{H}^+}$ taking into account that the electrons may be scattered between the emission and the reabsorption of the virtual photon on the potential of not one but two nuclei. Accordingly

$$E_L^{\text{H}_2} = \frac{3}{16} \alpha^3 [\delta(\overline{r_{a_1}}) + \delta(\overline{r_{b_1}})] \left[\ln \frac{mc^2}{K_0} + \frac{19}{30} - \ln 2 \right] \text{ Ry}. \quad (11)$$

Considering that each of the approximate wave functions of the hydrogen molecule is symmetrical with respect to the exchange of the two nuclei, it can be written

$$\delta(\overline{r_{a_1}}) = \delta(\overline{r_{b_1}}), \quad (12)$$

and thus (11) is simplified to the form

$$E_L^{\text{H}_2} = \frac{3}{8} \alpha^3 \delta(\overline{r_{a_1}}) \left[\ln \frac{mc^2}{K_0} + \frac{19}{30} - \ln 2 \right] \text{ Ry}. \quad (13)$$

In the expressions (11)–(13) \bar{r}_{a_1} and \bar{r}_{b_1} denote the vectors drawn to the first electron from the nucleus a and b , respectively. It should be noted that expressions (1) and (11) can be written in just the same way with the aid of the Dirac delta-function containing the position vector of the second electron as argument. Namely, the ground states of both the He atom and the H_2 molecule are symmetrical with respect to the exchange of the two electrons, and thus, should any kind of wave function be used, for the expectation values the relations

$$\overline{\delta(\bar{r}_1)} + \overline{\delta(\bar{r}_2)} = 2 \overline{\delta(\bar{r}_1)} = 2 \overline{\delta(\bar{r}_2)}, \quad (14)$$

and

$$\overline{\delta(\bar{r}_{a_1})} + \overline{\delta(\bar{r}_{b_1})} + \overline{\delta(\bar{r}_{a_2})} + \overline{\delta(\bar{r}_{b_2})} = 4 \overline{\delta(\bar{r}_{a_1})} = 4 \overline{\delta(\bar{r}_{b_1})} = 4 \overline{\delta(\bar{r}_{a_2})} = 4 \overline{\delta(\bar{r}_{b_2})}, \quad (15)$$

respectively, are valid. In deriving expression (1) the relation (14) was obviously used, and taking this into account it was possible to write $E_L^{H_2}$ in the form (11).

To determine the energy term $E_L^{H_2}$ it is necessary to calculate the expectation value

$$\overline{\delta(\bar{r}_{a_1})} = \int \psi^*(\bar{r}_1, \bar{r}_2) \delta(\bar{r}_{a_1}) \psi(\bar{r}_1, \bar{r}_2) d\tau_1 d\tau_2. \quad (16)$$

Approximating the ground state of the hydrogen molecule by the WANG wave function [5]

$$\psi(\bar{r}_1, \bar{r}_2) = \frac{\alpha^3}{\pi} \frac{[e^{-\alpha(r_{a_1} + r_{b_2})} + e^{-\alpha(r_{a_2} + r_{b_1})}]}{\sqrt{2(1 + S^2)}} \quad (17)$$

written in atomic units, where

$$S^2 = \frac{\alpha^6}{\pi^2} \left[\int e^{-\alpha(r_a + r_b)} d\tau \right]^2 = e^{-2\alpha R} \left[1 + \alpha R + \frac{1}{3} \alpha^2 R^2 \right]^2,$$

and R is the internuclear distance, the expectation value $\overline{\delta(\bar{r}_{a_1})}$ was already determined in a previous paper [6]. The result was, using the parameter values $\alpha = 1.17$ and $R = 1.40$ a. u.

$$\overline{\delta(\bar{r}_{a_1})} = 0.224 \text{ a. u.}$$

Substituting this value and $K_0 = 19.77$ Ry into (11) we obtain

$$E_L^{H_2} = 1.012 \cdot 10^{-4} \text{ ev.} \quad (18)$$

Expression (3) of the energy term E'_L remains unchanged if we consider the problem of the two-electron molecule instead of that of the two-electron

atom. To calculate the above expression we now substitute into the expression (4) of the expectation value $\delta \overline{(\bar{r}_{12})}$ the wave function of the ground state of the H_2 molecule. The author also calculated the expectation value $\delta \overline{(\bar{r}_{12})}$ with the aid of WANG's approximate wave function (17) and obtained with the parameter values $a = 1,17$ and $R = 1,40$ a. u.

$$\delta \overline{(\bar{r}_{12})} = 2,58 \cdot 10^{-2} \text{ a. u.}$$

[6]. Substituting this value into (3) results in

$$E_L^{H_2} = -6,25 \cdot 10^{-6} \text{ ev.} \quad (19)$$

Substitution of the values of $E_{L1}^{H_1}$ (10), $E_L^{H_2}$ (18) and $E_L^{H_2}$ (19) into (9) yields for the change of the binding energy of the hydrogen molecule due to the most important radiation correction energy terms

$$\Delta E_J^{H_2} = (2 \cdot 3,36 - 10,12 + 0,63) \cdot 10^{-5} \text{ ev} = -1,77 \cdot 10^{-5} \text{ ev.} \quad (20)$$

As can be seen this value is by one order of magnitude lower than the corresponding value obtained for the ground state of the He atom (see the value (8)).

It is known that the binding energy of the H_2 molecule has been determined by the most accurate non-relativistic calculation already to an accuracy of 10^{-4} ev [7]. As the relativistic correction terms arising from BREIT's equation are for the most part also of the order of 10^{-4} ev in the case of the ground state of the H_2 molecule [6, 8] and the value obtained for the radiation correction terms of the ground state of the He-atom is also of this order, it seemed interesting to investigate whether the values of the radiation correction terms influence the value of the binding energy of the H_2 molecule determined to an accuracy of 10^{-4} ev. It should be noted that the calculation outlined here can only be regarded as first approximation, as it applies for the expectation values the data gained by the inaccurate WANG wave function. However, it does not seem probable that the repetition of the calculations with the more accurate variational function of JAMES and COOLIDGE would result in a change of order of magnitude. Thus it can be stated that in the case of the ground state of the H_2 molecule the values of the radiation correction terms are by one order lower than those obtained within the present accuracy from the theoretical determination of the non-relativistic energy terms giving the largest part of the binding energy.

REFERENCES

1. H. E. HAKANSSON, Ark. Fysik, **1**, 555, 1950; unpublished work of E. E. SALPETER cited by H. A. BETHE and E. E. SALPETER, Handbuch der Physik, **XXXV**, Springer, 1957-276—278.
2. H. A. BETHE and E. E. SALPETER, loc. cit., 185.
3. H. A. BETHE and E. E. SALPETER, loc. cit., 404—406.
4. H. A. BETHE and E. E. SALPETER, loc. cit., 250.
5. S. C. WANG, Phys. Rev. (2), **31**, 579, 1928.
6. J. LADIK, Acta Phys. Hung., **10**, 271, 1959.
7. W. KOLOS and C. C. J. ROTHMAN, Rev. Mod. Phys., **32**, 219, 1960.
8. J. LADIK, Acta Phys. Hung., in the press.

ПРИБЛИЖЕННОЕ ОПРЕДЕЛЕНИЕ
ВАЖНЕЙШИХ КОРРЕКЦИОННЫХ ЧЛЕНОВ ЭНЕРГИИ ИЗЛУЧЕНИЯ
В СЛУЧАЕ ОСНОВНОГО СОСТОЯНИЯ МОЛЕКУЛЫ ВОДОРОДА

И. ЛАДИК

! Резюме!

Важнейшие члены коррекции излучения для основного состояния молекулы водорода могут быть легко получены путем соответствующего изменения выражения, относящегося к атому гелия. Подставляя в фигурирующие в отдельных членах энергии ожидаемые значения — результаты, полученные приближенной волновой функцией Уанга, для энергии, определяющей смещение Ламба, получено значение $10,12 \cdot 10^{-5}$ эв, а для энергии, приближенно определяющей взаимодействие излучения между двумя электронами — $0,63 \cdot 10^{-5}$ эв. Вычитая сумму этих двух величин из $7,72 \cdot 10^{-5}$ эв, определяющего смещение Ламба в случае двух свободных атомов водорода, для изменения энергии связи вследствие появления коррекционных членов излучения получается $1,77 \cdot 10^{-5}$ эв. Эта величина на один порядок меньше соответствующего значения атома гелия, относящегося к его основному состоянию, и таким образом не влияет на теоретическое значение энергии связи молекулы водорода, определенное с точностью 10^{-4} эв.

AN APPROXIMATE SOLUTION OF A GENERALIZED STATISTICAL MODEL

By

K. LADÁNYI

RESEARCH GROUP FOR THEORETICAL PHYSICS OF THE HUNGARIAN ACADEMY OF SCIENCES, BUDAPEST

and

P. SZÉPFALUSY

PHYSICAL INSTITUTE, UNIVERSITY FOR TECHNICAL SCIENCES, BUDAPEST

(Presented by A. Kónya. — Received 19. XI. 1960)

A variational method is presented for the solution of statistical equations derived by the authors independently of each other. A non-linear system of integro-differential equations is given for the radial density D_l of the electrons of azimuthal quantum number l . The variational method introduced here reduces the number of equations. The method has been applied to the determination of the electron density of the Ar atom; the agreement with HARTREE's results is satisfactory.

1. Introduction

The Hartree-Fock method, which constructs the wave function of a system of one-particle wave-functions, can be useful in many cases for the determination of the wave functions and the energies of fermion systems. From the Hartree-Fock method the Thomas-Fermi-Dirac form of the Fermi gas model can be obtained in quasi-classical approximation [1]. The energy of the Fermi gas model is a functional of density; to calculate the energy it is not necessary to know the non-diagonal elements of the density matrix required by the Hartree-Fock method.

Between the results of the Fermi gas model and those of the Hartree-Fock method there are some characteristic deviations. These are due to the fact that the approximation of the kinetic energy with the Fermi zero point kinetic energy is in general not satisfactory. By introducing the WEIZSÄCKER energy term [2] the density function is improved considerably (e. g. for nuclei the model can already take the surface energy into account.) The generalization of the statistical model by GOMBÁS [3] yielded the binding energies in very good agreement with the empirical values.

To derive the statistical model¹ MACKÉ [4] introduced a variational method based on the Hartree-Fock equations. One of us (K. L.) generalized this method for the spherically symmetrical case and obtained the orbitals of

¹ We note that hereafter the term "statistical model" will be used to denote such a simplification of the Hartree-Fock method, in which the energy is a functional of density.

various azimuthal quantum numbers by means of various transformation functions [5]. As a special case the method gives the generalization of the statistical model first derived by HELLMANN [6] by grouping the electrons according to their azimuthal quantum numbers.

One of the authors (P. Sz.) [7] also based the derivation of a statistical model on the Hartree-Fock method. It was shown that the statistical models generalized by introducing the Weizsäcker term and the method proposed by PLASKETT [8] for the determination of the density can be reduced to common bases (at the same time the necessary modification of PLASKETT's method was obtained, which eliminates e. g. the essential shortcoming of the method that its solution is not unique [9]).

The first approximations of the models developed by the authors are identical. The purpose of the present paper is the investigation of the efficiency of this first approximation in the calculation of the electron density and binding energy of the Ar atom.

2. Solution of the generalized statistical equations

The energy expression derived in previous papers of the authors is

$$E = E_W + E_R + E_\varphi + E_Z + E_e, \quad (1)$$

where E_W is the Weizsäcker correction term, E_R and E_φ are the radial and the azimuthal parts of the Fermi energy, respectively, E_Z is the potential energy due to the interaction of the system with the nucleus of charge eZ , E_e is the potential energy due to the Coulomb interaction of the electrons. The energy terms can take the following form²

$$E_W = \frac{1}{2} e^2 a_0 \sum_l \int \left| \frac{du_l}{dr} \right|^2 dr, \quad (2)$$

where a_0 is the first Bohr radius. The summation is to be extended over all azimuthal quantum numbers l , further

$$u_l = D_l^{1/2} = (4\pi r^2 \varrho_l)^{1/2}, \quad (3)$$

where ϱ_l is the density of the electrons of azimuthal quantum number l ,

$$E_R = \sum_l \mathcal{N}_l \int u_l^6 dr, \quad (4)$$

² The notations of paper [5] will be followed.

with

$$\kappa_l = \frac{1}{2} e^2 a_0 \frac{\pi^2}{N_l^3} \sum_i^{(l)} (n_i - 1)^2. \quad (5)$$

In the above relation $\sum_i^{(l)}$ means summation over all filled states of azimuthal quantum number l , n_i is the radial quantum number of the state i , N_l is the number of electrons of azimuthal quantum number l .

$$E_\varphi = \frac{1}{2} e^2 a_0 \sum_l \int \frac{l(l+1)}{r^2} u_l^2 dr, \quad (6)$$

$$E_Z = -e^2 Z \sum_l \int \frac{u_l^2}{r} dr, \quad (7)$$

$$E_e = \frac{e^2}{2} \iint \frac{\varrho(r) \varrho(r')}{|r - r'|} dv dv' - \frac{e^2}{2} \sum_l \frac{1}{N_l} \iint \frac{\varrho_l(r) \varrho_l(r')}{|r - r'|} dv dv'. \quad (8)$$

The second term of the energy E_e is responsible for the consequent elimination of the Coulomb self-interaction. Varying the functions u_l in the energy expression (1) by fixed particle number N_1, \dots, N_l the equations for the determination of the radial densities are obtained.

These equations, however, are much more complicated than the original Thomas-Fermi equation involving only one function of three variables, the electron density ϱ of the system. Therefore we introduce a variational approximation which makes possible to reduce the problem to a single integro-differential equation. The method is presented in the case of the Ar atom and the various generalizations will be discussed later.

For the approximate determination of the radial density u_0^2 of the s -electrons the following variational assumption is used

$$u_0^2 = u_{1s}^2 + \frac{N_0 - 2}{N_1} u_1^2, \quad (9)$$

where u_{1s}^2 is the radial density of the two $1s$ -electrons. The "Ansatz" (9) is based on the assumption that the function $u_0^2 - u_{1s}^2$ and the radial density u_1^2 of the p -electrons are approximately proportional. This assumption is confirmed by the results of the Hartree method. Further, it is very plausible that in the neighbourhood of the nucleus, u_0^2 can be well approximated by the radial density of the hydrogen-like $1s$ -electrons, as in this region the potential of the other electrons is approximately constant, and so the potential energy due to the Coulomb interaction with the nucleus and the Weizsäcker correction term play the most important role. (In the case of s -electrons the Fermi energy has no azimuthal part!) Substituting the variational assumption (9) into the

energy expression (1) and varying the function u_1 by a fixed particle number N_1 we obtain the following equation

$$\begin{aligned} & -\frac{1}{2}e^2a_0\frac{d^2u_1}{dr^2} + 3\kappa_1u_1^5 + e^2a_0\frac{1}{r^2}u_1 - e^2\frac{Z}{r}u_1 + e^2\left(\int\frac{\varrho(r')}{|r-r'|}dv' - \right. \\ & \left. -\frac{1}{N_1}\int\frac{\varrho_1(r')}{|r-r'|}dv'\right)u_1 - \left[-\frac{1}{2}e^2a_0\frac{d^2u_0}{dr^2} + 3\kappa_0u_0^5 - e^2\frac{Z}{r}u_0 \right. \\ & \left. + e^2\left(\int\frac{\varrho(r')}{|r-r'|}dv' - \frac{1}{N_0}\int\frac{\varrho_0(r')}{|r-r'|}dv'\right)u_0\right]\frac{N_0-2}{N_1}\frac{u_1}{u_0} = E_1u_1, \quad (10) \end{aligned}$$

where E_1 is the Lagrange multiplier. It follows immediately from the differential equation for the function u_0 that the expression in square brackets is equal to E_0u_0 (E_0 is a Lagrange multiplier). Thus equation (10) can take the following form

$$-\frac{1}{2}e^2a_0\frac{d^2u_1}{dr^2} + 3\kappa_1u_1^5 + e^2a_0\frac{1}{r^2}u_1 + Vu_1 = \varepsilon_1u_1, \quad (11)$$

with

$$V = e^2\left(-\frac{Z}{r} + \int\frac{\varrho_{1s}(r')}{|r-r'|}dv' + \frac{N-3}{N_1}\int\frac{\varrho_1(r')}{|r-r'|}dv'\right), \quad (12)$$

where ϱ_{1s} is the density of the 1s-electrons, N is the number of electrons in the atom, further

$$\varepsilon_1 = \frac{N_0-2}{N_1}E_0 + E_1. \quad (13)$$

As has been mentioned the density of the 1s-electrons is not influenced appreciably by the potential due to the other electrons, i. e. to a good approximation

$$u_{1s}^2 = 8\lambda_{1s}^2 r^2 e^{-2\lambda_{1s}r}, \quad \lambda_{1s} = Z - \frac{5}{16}. \quad (14)$$

The extension of the procedure is also plausible. If the function u_{1s} is determined from the differential equation derived by varying u_{1s} in the energy expression (1), (9) obviously yields the exact function u_0 .

The advantage of the system of differential equations for the functions u_{1s} and u_1 is that in the case of solution by the iteration method much more rapid convergence can be expected than could be with the system of differential equations for the functions u_0 and u_1 . The solution of equation (11), taking (14) into account, can be regarded as the first step of the iteration method.

For the Ar atom where only s - and p -states are filled, the equation for the functions u_{1s} and u_1 can also be obtained by substitution of (9) into the equation for the functions u_0 and u_1 . The variational method described here is of significance also because its generalization makes possible to reduce the number of functions to be determined. As an example for a larger number of electrons the following variational assumption can be useful

$$u_0^2 = u_{1s}^2 + \frac{N_0 - 2}{N - N_0} u^2, \quad (15)$$

$$u_l^2 = \frac{N_l}{N - N_0} u^2 \text{ if } l \neq 0. \quad (16)$$

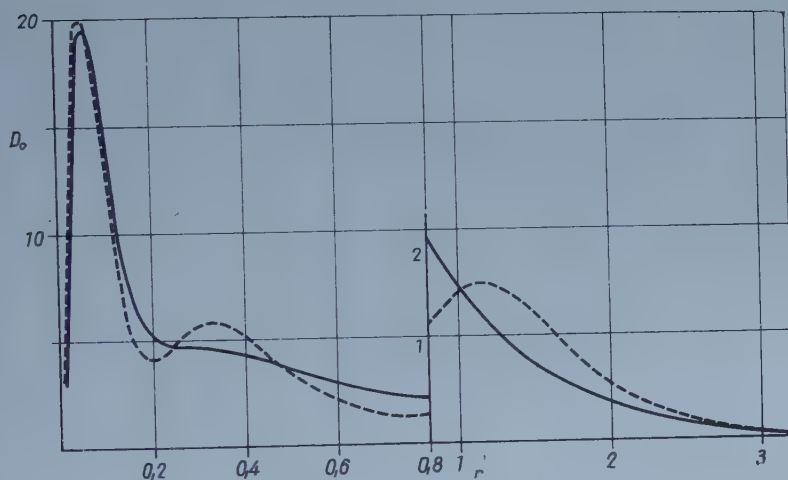


Fig. 1. Radial density of the s -electrons for the Ar atom. r in a_0 units, the radial density D_0 in $1/a_0$ units. The dashed line shows the radial density calculated for these electrons by HARTREE [10]

The energy expression is to be varied with respect to the function u with the following condition:

$$\int_0^{\infty} u^2 dr = N - N_0.$$

The differential equation (11) has been solved numerically with the boundary conditions

$$u_1(0) = u_1(\infty) = 0. \quad (17)$$

The solution is given in Table I. The densities D_0 and D_1 as well as the radial electron density D of the Ar atom are shown in Figs. 1–3.

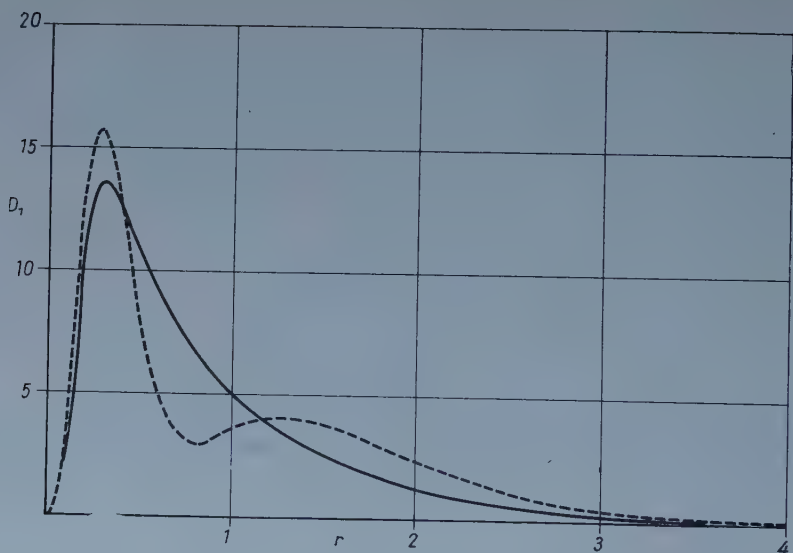


Fig. 2. Radial density of the p -electrons for the Ar atom. r in a_0 units, the radial density D_1 in $1/a_0$ units. The dashed line shows the radial density obtained for these electrons by HARTREE [10]

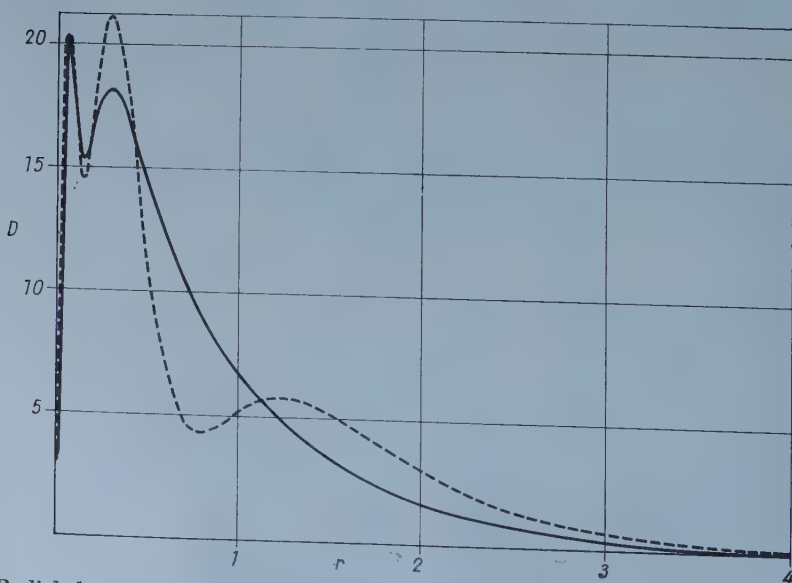


Fig. 3. Radial electron density of the Ar atom. r in a_0 units, the radial density D in $1/a_0$ units. The dashed line shows the radial electron density calculated by HARTREE [10]

Table I

Radial density of the p -electrons for the Ar atom.
 r in a_0 units, the radial density D_1 in $1/a_0$ units

r	D_1	r	D_1
0,001		0,45	11,7012
2		50	10,8616
3		55	10,0495
4	0,0001	60	9,2872
5	2	65	8,5849
6	3	70	7,9411
7	5	75	7,3532
8	7	80	6,8163
9	0,0010	85	6,3267
0,010	0,0016	0,90	5,8773
0,02	0,0217	1,0	5,08550
3	0,0922	1,1	4,41377
4	0,2449	1,2	3,83925
5	0,5036	1,3	3,34378
6	0,8812	1,4	2,91453
7	1,3797	1,5	2,54147
8	1,9916	1,6	2,21474
9	2,7022	1,7	1,92932
0,10	3,4918	1,8	1,67936
		1,9	1,46023
0,12	5,2180	2,0	1,26834
14	6,9886		
16	8,6507	2,2	0,95339
18	10,0991	2,4	0,71297
20	11,2802	2,6	0,53014
22	12,1815	2,8	0,39199
24	12,8207	3,0	0,28804
26	13,2285	3,2	0,21014
28	13,4440	3,4	0,15217
30	13,5049	3,6	0,10908
32	13,4462	3,8	0,07717
34	13,2955	4,0	0,05364
36	13,0776	4,2	0,03637
38	12,8121	4,4	0,02382
0,40	12,5139	4,6	0,01465
		4,8	0,00831
		5,0	0,00412
		5,2	0,00161
		5,4	0,00035
		5,6	0,00007
		5,8	0,00001

3. Discussion

On the basis of Section 2 we may assume that the density and the total ionization energy obtained for the Ar atom by the variational method approximate well the exact solution of the model. The model has been derived from the Hartree-Fock method. In the calculation of the interaction energy between the electrons the exchange energy has not been taken into account so the results of the model are to be compared with those of the Hartree approximation.

The density distribution as can be seen in Fig. 3 approximates well the density obtained with the Hartree method. The total ionization energy obtained here can be compared with the semi-empirical value of SLATER. The latter exceeds the energy calculated by the Hartree approximation. (The semi-empirical value involves the exchange and correlation energies.) The exchange energy for the Ar atom is approximately $-25 e^2/a_0$. Thus the total ionization energy of the Hartree approximation is about $+500 e^2/a_0$, whereas the energy obtained by us is only $+428 e^2/a_0$. The reason for the error can easily be found. The authors followed different ways in constructing the statistical model. The model used here is based in both methods on assumptions satisfied with adequate accuracy only where the potential does not vary appreciably. In the neighbourhood of the nucleus this condition is not fulfilled and it seems necessary to investigate the behaviour of the model in this region separately.

Let us restrict ourselves to a small region of the neighbourhood of the nucleus where the Hartree one-electron wave functions are well approximated by the hydrogen-like wave functions corresponding to the atomic number $Z = 18$. This approximation is justified as long as the screening effect of the electrons on the potential of the nucleus can be neglected. In this region the interaction energy of the electrons as compared to the other energies is negligible. In Table II the following function is given

$$\Delta E(r) = 4\pi \int_0^r [\mathcal{E}^{(H)}(r') - \mathcal{E}^{(S)}(r')] r'^2 dr',$$

where $\mathcal{E}^{(H)}_{(r)}$ is the energy density calculated with the hydrogen-like wave functions and $\mathcal{E}^{(S)}_{(r)}$ is the statistical energy density. The largest radius is $0,08 a_0$, up to which the hydrogen-like wave functions give a good approximation.

Table II

Difference between the wave mechanical and the statistical energy for the regions in the neighbourhood of the nucleus, as a function of the radii of these regions. The energy is given in e^2/a_0 units, the radius of the region in a_0 units

r	ΔE_1	ΔE_2
0,01	0,9017	22,5974
0,02	1,066	24,907
0,03	— 9,2841	11,8539
0,04	— 21,8528	— 3,5998
0,05	— 40,623	— 22,286
0,06	— 62,5065	— 42,7015
0,07	— 84,2969	— 56,5119
0,08	— 108,355	— 73,134

The energies ΔE_1 and ΔE_2 have been calculated with the kinetic energy densities $-\frac{1}{2} \sum_i \psi_i^* \Delta \psi_i$ and $\frac{1}{4} \sum_i |\Delta \psi_i|^2$ respectively; in wave mechanics both are used.

Table II shows that the greater part of the error of the binding energy calculated on the basis of the model is due to the region in the neighbourhood of the nucleus, which could be expected considering the derivation of the model. We note that the variational approximation introduced by one of us (K. L.) [5] eliminates the greater part of the error discussed above by correctly taking into account the electron wave functions (without any averaging of the oscillations). From the above consideration we may conclude that in cases where the potential does not vary appreciably the model yields good results for both the density and the energy. Further, the error of the model in the neighbourhood of the nucleus does not influence the relatively accurate calculation of quantities for which the behaviour of the model is important at the boundary of the atom rather than elsewhere (e. g. ionization energies, electron affinities).

Acknowledgements

The authors are greatly indebted to Mrs. E. HAHN, Miss M. TISZA and, particularly, to Miss O. KUNVÁRI for carrying out the numerical calculations.

REFERENCES

1. See e. g. P. GOMBÁS, *Statistische Behandlung des Atoms* (S. FLÜGGE, *Handbuch der Physik*, Springer, Berlin—Göttingen—Heidelberg, 1956, XXXVI.) p. 171.
2. See e. g. P. GOMBÁS, *l. c.*, p. 151.
3. See e. g. P. GOMBÁS, *l. c.*, p. 153.
4. W. MACKE, *Phys. Rev.*, **100**, 992, 1955; *Ann. d. Phys.*, **17**, 1, 1955; N. H. MARCH, *Proc. Phys. Soc.*, A, **70**, 169, 1957; N. H. MARCH and W. H. YOUNG, *Proc. Phys. Soc.*, A, **72**, 182, 1958.
5. K. LADÁNYI, *Acta Phys. Hung.*, **9**, 115, 1958.
6. See e. g. P. GOMBÁS, *l. c.*, p. 148.
7. P. SZÉFFALUSY, *Acta Phys. Hung.*, **9**, 203, 1958; **9**, 335, 1959.
8. J. S. PLASKETT, *Proc. Phys. Soc.*, A, **66**, 178, 1953.
9. R. A. BALLINGER and N. H. MARCH, *Proc. Phys. Soc.*, A, **67**, 378, 1954.
10. D. R. HARTREE and W. HARTREE, *Proc. Roy. Soc.*, A, **166**, 450, 1938.

ПРИБЛИЖЕННОЕ РЕШЕНИЕ ОБОБЩЕННОЙ СТАТИСТИЧЕСКОЙ МОДЕЛИ

К. ЛАДАНИ и П. СЕПФАЛУШИ

[Резюме

При решении статистического уравнения, выведенного авторами независимо один от другого, применяется вариационный метод. Для радиальной плотности электронов D_l азимутальное квантовое число которых l , дается одно нелинейное интегрально-дифференциальное уравнение. Число уравнений при применении вариационного метода уменьшается. Данным методом была определена плотность электронов атома Ag; результаты удовлетворительно согласуются с результатами Хартри.

ÜBER DIE MÖGLICHKEIT DER BESTIMMUNG MOLEKULARER DIPOLMOMENTE AUS DER STATISTISCHEN THEORIE

Von

M. SCHUBERT und B. WILHELMI

PHYSIKALISCHES INSTITUT DER UNIVERSITÄT JENA, JENA, DDR.

(Vorgelegt von K. F. Novobátzky. — Eingegangen: 21. XII. 1960)

Es wird untersucht, welche Schlüsse sich aus den Grundgleichungen mit Randbedingungen, wie sie aus verschiedenen statistischen Modellen folgen, hinsichtlich der Existenz von Dipolmomenten molekularer Systeme ziehen lassen.

1. Einleitung

Eine näherungsweise Beschreibung atomarer Systeme ist mit der statistischen Theorie [1] möglich, deren Grundlage mit dem Einteilchenansatz der Quantenmechanik im Zusammenhang steht. Anwendungen erfolgten bisher vorzugsweise auf Atome und Ionen [1], [2], wegen der grösseren Schwierigkeiten nur in geringerem Masse auf Moleküle und Kristalle.

Im wesentlichen sind Moleküle behandelt worden, die sich durch niedrige Atomzahl — z. B. N_2 [3], [4], HJ [5], JCl [6], H_2O [7] — oder durch hohe Symmetrie [8], [9] auszeichnen. Unmittelbar aus der Rechnung bei festen Kernabständen folgen die Elektronenverteilung und die Gesamtenergie des Moleküls. Mittelbar lässt sich daraus eine weitere Gruppe von Eigenschaften bestimmen, die im allgemeinen einer experimentellen Prüfung besser zugänglich ist. Es handelt sich bspw. um die Potentialkurve, aus der auch Bindungseigenschaften abgelesen werden können, sowie um das Dipolmoment des Moleküls. Die Lösungen sind nicht in geschlossener Form darstellbar. Die Genauigkeit der Ergebnisse hängt demgemäss von dem Rechenaufwand ab. Daraus resultieren gewisse uneinheitliche Auffassungen in der Literatur über die Grösse und Existenz der Bindung [10], [11] sowie des Dipolmomentes [6], [7] bestimmter Moleküle.

Es erscheint deshalb nützlich, Aussagen über diese Eigenschaften direkt aus den Grundgleichungen zu gewinnen, um so die Unsicherheit der numerischen Rechnung zu vermeiden. Solche Untersuchungen wurden in der vorliegenden Arbeit über die Existenz von Dipolmomenten* unter Berücksichtigung verschiedener statistischer Modelle angestellt. Hierzu erschien es not-

* Die Beantwortung dieser Frage kann einen Hinweis darauf geben, ob es prinzipiell möglich ist, statistische Modelle zur Berechnung der Intensitäten bei Rotations- und Schwingungsspektren heranzuziehen.

wendig, die Ableitung der Grundgleichungen gemeinsam mit den Randbedingungen unter allgemeineren Voraussetzungen vorzunehmen, als sie von SHELDON [10] benutzt worden sind.

2. Bestimmung der Grundgleichungen mit Randbedingungen

Die Gesamtenergie E des Elektronengases im Kernfeld setzt sich aus der kinetischen Energie, der potentiellen Energie der Elektronen im Feld der Kerne, der potentiellen Wechselwirkungsenergie der Elektronen, der Austauschenergie und der Korrelationsenergie zusammen [1]. Es gilt

$$E[\varrho(\vec{r}); B] = \kappa_K \int_B dv \varrho(\vec{r})^{\frac{5}{3}} - e \int_B dv V_K(\vec{r}) \varrho(\vec{r}) + \quad (1)$$

$$+ \frac{1}{2} e^2 \int_B dv \int_B dv' \frac{\varrho(\vec{r}) \varrho(\vec{r}')}{|\vec{r} - \vec{r}'|} - \kappa_a \int_B dv \varrho(\vec{r})^{\frac{4}{3}} + \int_B dv W[\varrho(\vec{r})].$$

Dabei sind κ_K und κ_a zwei universelle Konstanten, e die Elementarladung, \vec{r} der Ortsvektor, $\varrho(\vec{r})$ die Dichte des Elektronengases und W die Dichte der Korrelationsenergie, die ihrerseits von der Dichte des Elektronengases aber nicht explizit von den Ortskoordinaten abhängt. Die additive Konstante im Kernpotential $V_K(\vec{r})$ soll wie üblich so gewählt werden, dass $V_K(\vec{r})$ im Unendlichen verschwindet. $\int_B dv$ bedeutet die Integration über das Raumgebiet, in dem $\varrho(\vec{r})$ ungleich Null ist.

Der Energieausdruck (1) soll bei festen Kernabständen und bei fester Elektronenzahl $N = \int_B dv \varrho(\vec{r})$ zu einem Minimum gemacht werden. Variiert wird gleichzeitig nach der Elektronendichte $\varrho(\vec{r})$ und nach der Begrenzung des Gebietes B . Dieses Verfahren hat GOMBÁS [1] auf Atome und Ionen angewendet. Weil dabei Kugelsymmetrie vorausgesetzt werden konnte, liess sich die Variation der Begrenzung des Gebietes B auf die Festlegung eines optimalen Zahlenwertes für den Radius einer Kugelfläche zurückführen. Da bei Molekülen keinesfalls eine Begrenzungsfläche so hoher Symmetrie vorausgesetzt werden kann, ist die Bestimmung der Randbedingung hier wesentlich schwieriger: Man muss jetzt einen funktionalen Zusammenhang zwischen den Raumkoordinaten finden, der die optimale Berandungsfläche des Gebietes B festlegt. Es zeigt sich, dass die optimale Elektronendichte innerhalb des Gebietes B auch bei Molekülen der von GOMBÁS angegebenen erweiterten Thomas-Fermi-Dirac-Gleichung genügt.

Das optimale Gebiet B_0 werde von der Fläche F_0 begrenzt, die nicht notwendig als zusammenhängend anzunehmen ist. Bei der Ableitung lassen sich eine Reihe mathematischer Schwierigkeiten umgehen, wenn man die physikalisch sinnvolle Annahme macht, dass die Begrenzungsfläche in jedem Punkt ω eine endliche Krümmung hat. Unter ω sollen die Koordinaten eines Punktes auf der Fläche F_0 verstanden werden.

Die Aufstellung der Bestimmungsgleichung für die optimale Elektronendichte $\varrho_0(\vec{r})$ und die optimale Begrenzungsfläche F_0 kann mit den üblichen Mitteln der Variationsrechnung durchgeführt werden. Um die Einhaltung der Nebenbedingung $N = \int_B dv \varrho(\vec{r})$ zu gewährleisten, wird der Ausdruck

$$P[\varrho(\vec{r}); B] = E[\varrho(\vec{r}); B] + e\bar{V} \int_B dv \varrho(\vec{r}) \quad (2)$$

variiert, wobei $e\bar{V}$ als Lagrange-Multiplikator anzusehen ist. Die Bestimmungsgleichungen für $\varrho_0(\vec{r})$ und B_0 gewinnt man folgendermassen: Man ersetzt in P die Grösse $\varrho_0(\vec{r})$ durch $\varrho_0(\vec{r}) + \eta\varrho'(\vec{r})$ und B durch $B_0 + B'(\varepsilon)$. Dabei soll $B'(\varepsilon)$ eine Erweiterung des Integrationsgebietes B_0 sein. Durch $B'(\varepsilon)$ wird eine Schicht gekennzeichnet, die sich an die Fläche F_0 unmittelbar anschliesst. Ihre Dicke sei $\varepsilon h'(\omega)$, wenn diese vom Punkt ω der Fläche F_0 aus in Normalenrichtung gemessen wird. Der Ausdruck $P[\varrho_0(\vec{r}) + \eta\varrho'(\vec{r}); B_0 + B'(\varepsilon)]$ wird nach η und ε entwickelt. Für jede beliebige Funktion $\varrho'(\vec{r})$ und jede beliebige Funktion $h'(\omega)$ muss der Koeffizient von η und ε verschwinden, wenn es sich bei $\varrho_0(\vec{r})$ und B_0 um die optimalen Grössen handeln soll.

Das Verschwinden des Koeffizienten von η führt auf die Bestimmungsgleichung für $\varrho_0(\vec{r})$

$$[V_0(\vec{r}) - \bar{V}]e - \frac{5}{3}\kappa_K\varrho_0(\vec{r})^{\frac{2}{3}} + \frac{4}{3}\kappa_a\varrho_0(\vec{r})^{\frac{1}{3}} - \left\{ \frac{d}{d\varrho} \cdot W(\varrho) \right\}_{\varrho=\varrho_0(\vec{r})} = 0, \quad (3)$$

wobei V_0 die Summe aus Kern- und Elektronenpotential bedeutet. Neben dieser Gleichung muss die Poissonsche Differentialgleichung

$$\Delta V_0(\vec{r}) = 4\pi e\varrho_0(\vec{r}) \quad (4)$$

gelten. Die Lösung beider Gleichungen ist erst eindeutig bestimmt, wenn man ausser der Nebenbedingung $N = \int_B dv \varrho(\vec{r})$ eine Randbedingung vorschreibt.

Diese ergibt sich aus der Variation nach der Berandungsfläche des Gebietes B .

Zur Durchführung dieser Variation muss die Grösse

$$\left\{ \frac{\partial}{\partial \varepsilon} P[\varrho_0(\vec{r}) + \eta\varrho'(\vec{r}); B_0 + B'(\varepsilon)] \right\}_{\eta=0}^{\varepsilon=0} = \left\{ \frac{\partial}{\partial \varepsilon} P[\varrho_0(\vec{r}); B_0 + B'(\varepsilon)] \right\}_{\varepsilon=0}$$

berechnet werden. Nach den Gln. (1) und (2) setzt sich diese Grösse aus Summanden der Form

$$\left\{ \frac{\partial}{\partial \varepsilon} \int_{B_0 + B'(\varepsilon)} dv J[\varrho_0(\vec{r})] \right\}_{\varepsilon=0}$$

und einem Summanden

$$\left\{ \frac{e^2}{2} \frac{\partial}{\partial \varepsilon} \int_{B_0 + B'(\varepsilon)} dv \int_{B_0 + B'(\varepsilon)} dv' \frac{\varrho_0(\vec{r}) \varrho_0(\vec{r}')}{|\vec{r} - \vec{r}'|} \right\}_{\varepsilon=0} = \left\{ \frac{\partial E_e}{\partial \varepsilon} \right\}_{\eta=0}^{\varepsilon=0} \quad (5)$$

zusammen, wobei der letztere Term von der Wechselwirkungsenergie E_e der Elektronen herrührt. Unter Benutzung der Voraussetzung der endlichen Krümmung von F_0 kann man zeigen, dass

$$\left\{ \frac{\partial}{\partial \varepsilon} \int_{B_0 + B'(\varepsilon)} dv J[\varrho_0(\vec{r})] \right\}_{\varepsilon=0} = \int_{F_0} d\omega h'(\omega) J[\varrho_0(\omega)] \quad (6)$$

gilt. Dabei bedeutet $\int_{F_0} d\omega$ eine Integration über die optimale Fläche F_0 . Etwas schwieriger ist der Ausdruck der Gl. (5) zu behandeln. Über die Beziehung

$$\begin{aligned} \left\{ \frac{\partial E_e}{\partial \varepsilon} \right\}_{\eta=0}^{\varepsilon=0} &= \frac{e^2}{2} \left\{ \lim_{\Delta\varepsilon \rightarrow 0} \frac{1}{\Delta\varepsilon} \int_{B_0} dv \varrho_0(\vec{r}) \left[\int_{B'(\varepsilon + \Delta\varepsilon)} dv' \frac{\varrho_0(\vec{r}')}{|\vec{r} - \vec{r}'|} - \int_{B'(\varepsilon)} dv' \frac{\varrho_0(\vec{r}')}{|\vec{r} - \vec{r}'|} \right] + \right. \\ &+ \lim_{\Delta\varepsilon \rightarrow 0} \frac{1}{\Delta\varepsilon} \left[\int_{B'(\varepsilon + \Delta\varepsilon)} dv \varrho_0(\vec{r}) \int_{B_0} dv' \frac{\varrho_0(\vec{r}')}{|\vec{r} - \vec{r}'|} - \int_{B'(\varepsilon)} dv \varrho_0(\vec{r}) \int_{B_0} dv' \frac{\varrho_0(\vec{r}')}{|\vec{r} - \vec{r}'|} \right] + \\ &+ \left. \lim_{\Delta\varepsilon \rightarrow 0} \frac{1}{\Delta\varepsilon} \left[\int_{B'(\varepsilon + \Delta\varepsilon)} dv \varrho_0(\vec{r}) \int_{B'(\varepsilon + \Delta\varepsilon)} dv' \frac{\varrho_0(\vec{r}')}{|\vec{r} - \vec{r}'|} - \int_{B'(\varepsilon)} dv \varrho_0(\vec{r}) \int_{B'(\varepsilon)} dv' \frac{\varrho_0(\vec{r}')}{|\vec{r} - \vec{r}'|} \right] \right\}_{\varepsilon=0} \end{aligned}$$

kommt man unter Benutzung einer ähnlichen Überlegung, wie sie zu Gl. (6) führte, zu

$$\left\{ \frac{\partial E_e}{\partial \varepsilon} \right\}_{\eta=0}^{\varepsilon=0} = -e \int_{F_0} d\omega h'(\omega) V_{e,0}(\omega). \quad (7)$$

$V_{e,0}(\omega)$ bedeutet das Potential der Elektronenwolke auf der Fläche F_0 . Addiert man die einzelnen Summanden entsprechend den Gln. (6) und (7), so erhält man als Koeffizienten von ε

$$\left\{ \frac{\partial P}{\partial \varepsilon} \right\}_{\eta=0}^{\varepsilon=0} = \int_{F_0} d\omega h'(\omega) \left\{ \kappa_K \varrho_0(\omega)^{\frac{5}{3}} - \kappa_a \varrho_0(\omega)^{\frac{4}{3}} - [V_0(\omega) - \bar{V}_0] e \varrho_0(\omega) + W[\varrho_0(\omega)] \right\}.$$

Da $h'(\omega)$ eine willkürliche Funktion ist, folgt aus der Forderung, dass der Koeffizient von ε in einer Entwicklung der Grösse P verschwindet

$$\kappa_K \varrho_0(\omega)^{\frac{5}{3}} - \kappa_a \varrho_0(\omega)^{\frac{4}{3}} - e [V_0(\omega) - V] \varrho_0(\omega) + W[\varrho_0(\omega)] = 0 \quad (8)$$

als Bestimmungsgleichung für die Berandungsfläche.

Die optimalen Grössen müssen die Gln. (3) und (8) sowie die Poisson-Gleichung (4) simultan erfüllen. Aus den Gln. (3) und (8) ergibt sich insbesondere für die Elektronendichte auf dem Rande die Beziehung

$$\frac{2}{3} \kappa_K \varrho_0(\omega)^{\frac{5}{3}} - \frac{1}{3} \kappa_a \varrho_0(\omega)^{\frac{4}{3}} - W[\varrho_0(\omega)] + \varrho_0(\omega) \left\{ \frac{d}{d\varrho} W(\varrho) \right\}_{\varrho=\varrho_0(\omega)} = 0, \quad (9)$$

wenn man $[V_0(\omega) - \bar{V}]$ eliminiert.

3. Diskussion der Grundgleichungen mit Randbedingungen

Die Lösung der Gl. (9) führt auf eine von ω unabhängige Elektronendichte auf dem Rand. Setzt man diesen konstanten Wert (> 0) in Gl. (8) ein, so ergibt sich auch ein konstanter Wert für das Gesamtpotential auf der Fläche F_0 . Diese Ergebnisse, die im 2. Abschnitt ohne Zusatzannahmen lediglich aus der Minimierung der Energie gewonnen worden sind, gelten sowohl für den allgemeinen Fall der Gl. (1), als auch bei Vernachlässigung der Korrelationsenergie, was einer Betrachtung nach Thomas-Fermi-Dirac entspricht.

Es befinden sich demnach alle Ladungen (Kerne und Elektronen) innerhalb eines im Endlichen liegenden Gebietes B_0 , dessen Rand eine Äquipotentialfläche ist. Im Aussenraum darf das Potential kein Extremum annehmen und muss zwischen den Werten $V_0(\omega)$ und $V_0(\vec{r}_1 \rightarrow \infty)$ liegen. Daraus ergibt sich, dass $\frac{\partial V_0(\omega)}{\partial n}$, die Ableitung des optimalen Potentials längs der Normalenrichtung in den Aussenraum hinein, für alle Punkte der Fläche F_0 einheitliches Vorzeichen haben muss.

Wenn die Gesamtladung des Systems Null ist, folgt daraus wegen

$$\int_{F_0} d\omega \frac{\partial V_0(\omega)}{\partial n} = 0$$

das Verschwinden der Normalenableitung des Potentials in jedem Flächenpunkt, d. h. der gesamte Aussenraum ist feldfrei. Dasselbe gilt auch für nichtzusammenhängenden Bereich B_0 . Bei neutralen Molekülen lässt sich also feststellen, dass eine Theorie, die auf Gl. (1) basiert, kein Dipol-

moment* (generell kein Multipolmoment) liefert; diese wichtige Eigenschaft polarer Moleküle kann also mit der vorstehenden Theorie nicht erfasst werden.

Andere Verhältnisse ergeben sich bei Zugrundelegung des Thomas-Fermi-Amaldi-Verfahrens [1]. Die Gesamtenergie wird durch den Ausdruck

$$E = \kappa_K \int_B dv \varrho(\vec{r})^{\frac{5}{3}} + \frac{N-1}{N} \frac{e^2}{2} \int_B dv \int_B dv' \frac{\varrho(\vec{r}) \varrho(\vec{r}')}{|\vec{r} - \vec{r}'|} - e \int_B dv V_K(\vec{r}) \varrho(\vec{r}) \quad (10)$$

dargestellt. Im Vergleich zu Gl. (1) werden hier also Austausch- und Korrelationsenergie durch ein Glied $\frac{1}{N} E_e$ ersetzt, dabei ist N die Zahl der Elektronen.

Die Schwierigkeit der Anwendung des Thomas-Fermi-Amaldi-Modells auf Moleküle liegt in der Definition von N . Baut man das System aus Atomen auf, die man aus unendlicher Entfernung nähert, so setzt man für N die Elektronenzahl jedes einzelnen Atoms. In der gleichen Weise kann N auch bei schwacher Wechselwirkung definiert werden. Die Rechnungen zur Minimierung der Gesamtenergie verlaufen ebenso wie im Anschluss an Gl. (1). Man erhält die Bestimmungsgleichungen

$$[V_0(\vec{r}) - \bar{V}] e - \frac{5}{3} \kappa_K \varrho(\vec{r})^{\frac{2}{3}} - \frac{1}{N} V_{e,0}(\vec{r}) = 0 \quad (11)$$

und

$$\kappa_K \varrho_0(\omega)^{\frac{5}{3}} - [V_0(\omega) - \bar{V}] \varrho_0(\omega) e + \frac{1}{N} V_{e,0}(\omega) = 0, \quad (12)$$

wobei $V_{e,0}$ der von den Elektronen herrührende Potentialanteil ist. Daraus folgt als Randdichte $\varrho_0(\omega) = 0$, woraus jetzt nicht auf ein konstantes Randpotential geschlossen werden kann. Damit wird die Existenz eines Dipolmomentes nicht wie bei den obigen Verfahren von vornherein ausgeschlossen.

Man kann Beispiele angeben, in denen ein von Null verschiedenes Dipolmoment auftritt. Es wird ein elektrisch neutrales System betrachtet, das aus zwei Atomen mit verschwindender Wechselwirkung besteht (die Atome sollen sich dazu in hinreichend grossem Abstand befinden). Wenn man die Elektronenladung des einen Atoms um $(e\Delta N)$, die des anderen um $(-e\Delta N)$ ändert, so erhält man folgende Energieänderung des Gesamtsystems

$$\Delta E = \int_{Z_1}^{Z_1 - \Delta N} dN \left(\frac{\partial E_1}{\partial N} \right)_{Z_1 = \text{const.}} + \int_{Z_2}^{Z_2 + \Delta N} dN \left(\frac{\partial E_2}{\partial N} \right)_{Z_2 = \text{const.}}$$

* Auch die Thomas-Fermi-Theorie (Vernachlässigung des Austauschterms und des Korrelationsterms in Gl. (1)) kann für neutrale Moleküle kein Dipolmoment liefern. Die Entwicklung des Gesamtpotentials in grosser Entfernung R vom Molekülschwerpunkt beginnt mit einem Gliede R^{-m} , wobei $m > 2$ ist. Das Fehlen des Gliedes mit $m = 2$ zeigt unmittelbar an, dass kein Dipolmoment existiert. (Zu dieser Frage s. auch [9].)

Dabei sind E_1, E_2 die Minimalenergien der Einzelatome, wie sie aus Gl. (10) folgen. Die Z_i stellen die Kernladungszahlen dar. Nach HULTHÉN [12] gilt

$$\left(\frac{\partial E_i}{\partial N} \right)_{Z_i = \text{const.}} = -e \bar{V}_{Z_i}(N).$$

Damit ergibt sich ΔE zu

$$\Delta E(Z_1, Z_2; \Delta N) = -e \int_{Z_1}^{Z_1 + \Delta N} dN \bar{V}_{Z_1}(N) - e \int_{Z_2}^{Z_2 + \Delta N} dN \bar{V}_{Z_2}(N).$$

Das Minimum von ΔE bei Variation nach ΔN ergibt sich für

$$\bar{V}_{Z_1}(N = Z_1 - \Delta N) = \bar{V}_{Z_2}(N = Z_2 + \Delta N).$$

Diese Bedingung lässt sich bei $Z_1 \neq Z_2$ nur für $\Delta N \neq 0$ erfüllen. Die Minimierung der Gesamtenergie führt also zu einem von Null verschiedenen Ionisierungsgrad für die beiden Teile des Gesamtsystems. An diesem Ergebnis ändert sich qualitativ nichts, wenn man für endlichen aber sehr grossen Abstand A die Wechselwirkungsenergie der beiden Ionen mit berücksichtigt (für grosses A ist der wesentliche Anteil der Wechselwirkungsenergie durch den Coulombterm $-\frac{(e\Delta N)^2}{A}$ gegeben).

Wendet man das Thomas-Fermi-Dirac-Verfahren auf ein System aus zwei Atomen mit verschwindender Wechselwirkung in gleicher Weise an, so wird jetzt die minimale Gesamtenergie bei $\Delta N = 0$ erreicht. Dieses Ergebnis steht in Einklang mit der oben angegebenen Aussage, dass sich mit einer Behandlung nach Thomas-Fermi-Dirac kein Dipolmoment ergeben kann.

Für fördernde Diskussionen danken wir Herrn Prof. Dr. W. SCHÜTZ

LITERATUR

1. S. dazu etwa P. GOMBÁS. »Die statistische Theorie des Atoms und ihre Anwendungen« Springer, Wien, 1949.
2. N. METROPOLIS und J. R. REITZ, J. Chem. Phys., **19**, 555, 1951.
3. F. HUND, Zs. f. Phys., **77**, 12, 1932.
4. P. GOMBÁS, Acta Phys. Hung., **9**, 461, 1959.
5. R. GÁSPÁR und A. KÓNYA, Acta Phys. Hung., **3**, 31, 1954.
6. H. GLAZER und H. REISS, J. Chem. Phys., **21**, 903, 1953.
7. H. C. BRINKMAN und B. PEPPERZAK, Physica, **21**, 48, 1955.
8. J. D. ALEXANDER und W. A. BOWERS, Phys. Rev., **99**, 1627, 1955.
9. H. GLAZER und H. REISS, J. Chem. Phys., **23**, 937, 1955.
10. J. W. SHELDON, Phys. Rev., **99**, 1291, 1955.
11. J. R. TOWNSEND und G. S. HANDLER, J. Chem. Phys., **31**, 1689, 1959.
12. L. HULTHÉN, ZS. f. Phys., **95**, 789, 1935.

О ВОЗМОЖНОСТЯХ ОПРЕДЕЛЕНИЯ ДИПОЛЬНЫХ МОМЕНТОВ МОЛЕКУЛ В СТАТИСТИЧЕСКОЙ ТЕОРИИ

М. ШУБЕРТ и Б. ВИЛЬГЕЛЬМИ

Резюме

В работе исследуется, какие следствия вытекают из основных уравнений статистической модели, принимая во внимание существование дипольных моментов молекулярных систем. Уравнения применяются с темиграничными условиями, которые следуют из разных статистических моделей.

RANGE OF PROTONS IN THE AGFA K2 NUCLEAR EMULSION

By

L. MEDVECZKY and G. SOMOGYI*

INSTITUTE OF NUCLEAR RESEARCH OF THE HUNGARIAN ACADEMY OF SCIENCES, DEBRECEN

(Presented by A. Szalay. — Received 11. XI. 1960)

By measuring the range-energy curve of recoil protons produced in the nuclear emulsion by reactions $\text{H}^2(d, n) \text{He}^3$ and $\text{H}^3(d, n) \text{He}^4$, calibration points were obtained to determine the range-energy relation of the Agfa K2 emulsion. The measured ranges showed good agreement within the error limits with results of calculations for Agfa K2 emulsion containing 60% relative humidity [1].

The photoemulsion method cannot be applied to determine the energy of particles without precise knowledge of their range-energy relation. Therefore it is not surprising that in the literature such a great number of both calculated and measured data can be found on emulsions of different make and type.

The range-energy relation of Agfa K2 emulsions was investigated by LANIUS [2] and BEBEL [1]. Both authors carried out calculations for protons, and obtained the calibration points by measuring and reducing the range of alpha-particles from the decay series of Th. Experimental data on protons were reported only by LANIUS, who measured the range of 0,58 MeV protons from the reaction $\text{N}^{14}(n, p) \text{C}^{14}$. Both measurements were made in air of 60% relative humidity, and the calculations were also made for emulsions of this kind. There is a substantial difference in the atomic composition reported by the two authors and accordingly also in the density of emulsions. According to BEBEL's recent data the latter is $3,38 \text{ gcm}^{-3}$ as against the previous $3,84 \text{ gcm}^{-3}$. LANIUS carried out the calculations as described by CÜER [3], while BEBEL made them with the method developed by VIGNERON [4] using — in addition to the composition of the emulsion — new data also for the average ionization potential value.

On the basis of the above it can be expected and also understood that the discrepancy in the range of protons with identical energy is considerably greater between the data of the two authors referred to than the usual error in measurement. The data of measurement and calculated values of both authors — on the other hand — show good agreement. The reason for this, besides the use of emulsions with different stopping power, is to be found in the fact that

* Now at the Institute of Experimental Physics of the Kossuth University, Debrecen.

the range of particles in the investigated region is shorter than 50μ , and at lower energies, the straggling of ranges in emulsions is greater [5] than in air because of the small number of grains constituting the tracks.

Table I

Range of alpha-particles from decay series of Th measured in Agfa K2 emulsion

E_α MeV	Mean ranges in μ and relative mean errors		
	LANIUS [2]	BEBEL [1]	BUJDOSÓ—MEDVECZKY [6]
5,68	$24,6 \pm 4,2$	$25,5_5 \pm 4,1$	$25,5 \pm 2,0$
6,28	$28,5 \pm 4,0$	$29,8_6 \pm 3,5$	$29,5 \pm 1,7$
6,78	$32,0 \pm 3,1$	$33,3_2 \pm 3,2$	$33,0 \pm 1,51$
8,78	$47,7 \pm 1,3$	$49,7_6 \pm 1,8$	$49,0 \pm 1,0$

In measurements for alpha-particles from decay series of Th [6], we took into consideration only tracks falling in the plane of the emulsion. As it can be seen in Table I, values similar to those of BEBEL were obtained, yet for the sake of accuracy in other investigations, the testing of the range of protons by means of longer tracks was needed. In this manner, it was possible to obtain calibration points at higher energies.

The proton tracks used in our measurements were produced by neutrons obtained from reaction (d, n) , with H^2 and H^3 targets, respectively.

In relation to deuterons accelerated by 0,1 MeV the irradiated plates formed with them an angle of 0° in the case of reaction D—D and an angle of 90° in the case of reaction D + T. Accordingly, the energies of the obtained neutrons were $2,850 \pm 0,001$ and $14,06 \pm 0,02$ MeV, respectively. The plates wrapped in aluminium foil and then in paper were placed at distances of 120 and 350 mm respectively from the target, which was approximately 8 mm in diameter. In reaction D — D, plates of 100μ layer thickness were used, and the time of irradiation was 40 hours, whereas with D — T, the layer thickness was 200μ and the time of exposure 2 hours. The emulsions were processed by temperature development with amidol [7]. The tracks from reaction D — D were measured under a magnification of approximately 1000X, while the measurements on the longer tracks were made under a magnification of approximately 420X. Transverse displacement of the tracks was measured by an eyepiece micrometer and the dip displacement by the finefocus motion of the microscope. For the calculation of track lengths, nomograms [8] were used. Only such tracks were considered, where the angle between the direction of the track and the straight line connecting its initial point with the centre of the target was less than 10° . The results of measurement are shown in Figs. 1 and 2. Both spectra are corrected for the variation with energy of the neutron-proton scattering cross section and for the escape of protons from the emulsion.

The errors indicated in the Figures are statistical errors only. Fig. 1 represents the range distribution of 2,85 MeV protons in 450 measured tracks. The mean range of the tracks is $70 \pm 3 \mu$. The mean value calculated from the corrected range distribution of the measured 971 recoil protons of 14,06 MeV energy is $1075 \pm 43 \mu$ (Fig. 2).

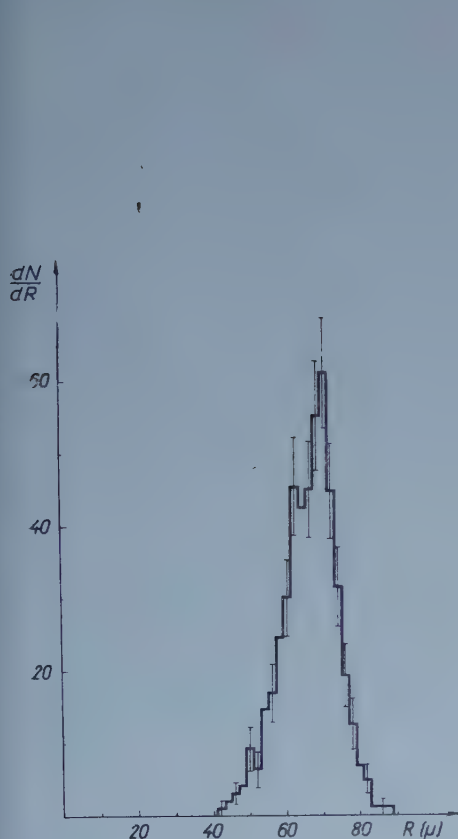


Fig. 1

Range distribution of 2,85 MeV protons

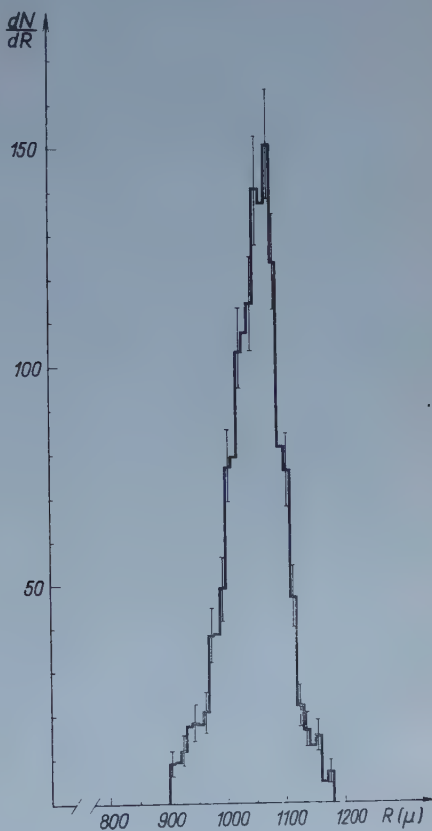


Fig. 2

Range distribution of 14,06 MeV protons

In Fig. 3 the results of our investigations are compared with range-energy relations reported by LANIUS and BEBEL, respectively. As it can be seen, the results of our measurements fall systematically between the two range-energy curves. Taking the limits of error in measurement into consideration, the agreement in the mean ranges with BEBEL's figures is satisfactory, (there is even full agreement in the case of extrapolated ranges). The ranges are in all cases, greater than those reported by LANIUS. In our opinion, the following facts are responsible for the slight systematic deviation from BEBEL's

data: a) our investigations were carried out in air containing exactly less than 60% relative humidity, b) the composition of emulsions is not completely identical in the different preparations [1].

Summing up our investigations, it can be stated that in Agfa K2 nuclear emulsions, it is BEBEL's calculated values that correspond to the range-

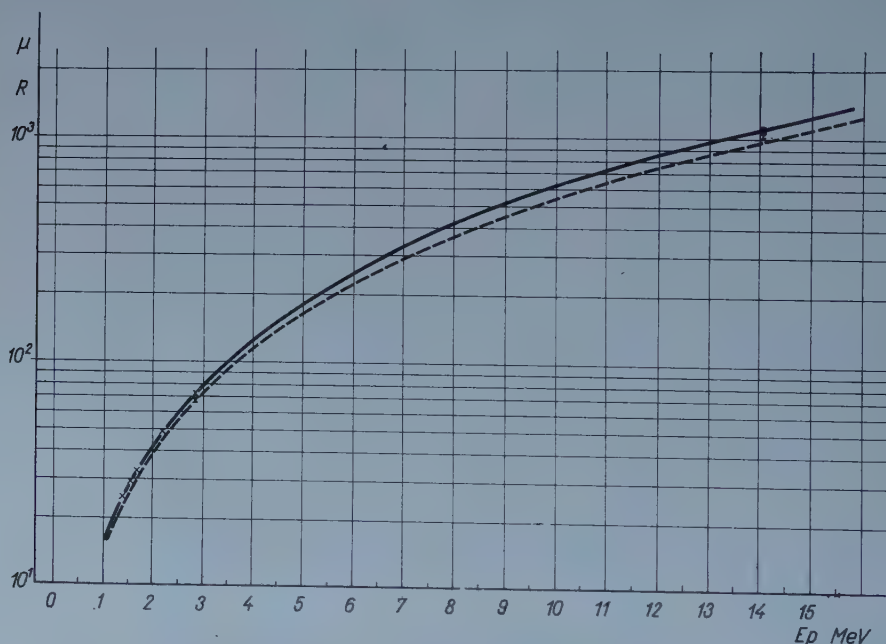


Fig. 3. Range-energy relation of Agfa K2 nuclear emulsions for protons. The uninterrupted curve represents BEBEL's calculations [1] and the dotted curve those of LANIUS [2]
 × designates data measured on and reduced from Th stars [6]
 ⊥ designates data measured on tracks of recoil protons

energy relation of protons. It is, however desirable to carry out the calibration also at energies not yet investigated.

*

We wish to thank Professor A. SZALAY, Director of the Institute of Nuclear Research in Debrecen, for his help and his interest in our work.

Acknowledgement is due also to Mrs. G. BORNEMISZA for having carried out the irradiation, as well as to the microscopists for their thorough work.

*

REFERENCES

1. D. BEBEL, Ann. Physik (7), **5**, 144, 1960.
2. K. LANIUS, Z. wiss. Photogr., **48**, 243, 1953.
3. P. CÜER, Comptes Rendus, **223**, 1121, 1946.
4. L. VIGNERON, J. Physique et le Radium, **14**, 145, 1953.
5. J. ROTBLAT, Nature, **165**, 387, 1950.
6. E. BUJDOSÓ and L. MEDVECZKY, unpublished measurement (1955).
7. E. BUJDOSÓ and L. MEDVECZKY, Nuclear Instruments, **2**, 270, 1958.
8. E. BUJDOSÓ, L. MEDVECZKY and S. TÖRÖK, Acta Phys. Hung., **7**, 373, 1957.

ПРОБЕГ ПРОТОНОВ В ЯДЕРНОЙ ЭМУЛЬСИИ AGFA K2

Л. МЕДВЕЦКИ и Д. ШОМОДЬИ

Резюме

Измерением пробега рассеянных протонов, созданных в ядерной эмульсии нейтронами, полученными от ядерных процессов $\text{H}^2(d,n)\text{He}^3$ и $\text{H}^3(d,n)\text{H}^4$ были получены калибрационные точки для определения зависимости пробега-энергии в эмульсии Agfa K2. Измеренные в пределах погрешности пробеги показывают хорошее совпадение с результатами [1] вычислений, относящимися к эмульсии Agfa K2 с 60% относительной влажностью.



EXAMINATION OF TANTALUM MONOCRYSTAL TIPS BY MEANS OF A FIELD EMISSION MICROSCOPE

By

L. ERNST

INDUSTRIAL RESEARCH INSTITUTE FOR TELECOMMUNICATION TECHNIQUE, BUDAPEST

(Presented by E. Winter. — Received 28. XII. 1960)

We examined by means of a field emission microscope the degassing process of tantalum tips and the deformation of pure tips, on the one hand under the influence of heating only, and on the other under the influence of both heating and electric field. In the former case we observed a behaviour similar to that of tungsten, in the other case a behaviour different from it. We observed also the formation of twin crystals under the influence of heat.

1. Introduction

The principle of the field emission microscope is as follows [1].

To a very fine metal tip in vacuum a negative voltage is connected, which is high relative to the fluorescent screen surrounding it. Under the influence of the high field intensity around it, the tip emits electrons and in consequence a considerably enlarged emission image of the surface of the tip appears, on which the bright spots correspond to surface parts of low work function and the dark spots to surface parts of high work function. Taking into consideration that the dimensions of the tip are usually smaller than the grains of the polycrystalline metal the obtained image is characteristic of the monocrystalline structure.

As yet tantalum tips have been examined by relatively few researchers [2, 3, 4] by means of a field emission microscope and DRECHSLER was the very first who was able to produce the field emission image of an absolutely pure tantalum surface.

As we were able to reproduce the simplest field emission microscopic experiments on tungsten tips we began to study tantalum, a metal which has been relatively little examined but which is of great practical importance.

2. Experimental device and method

The field emission microscope can be seen in Fig. 1. The borosilicate-glass sphere of 3,5 cm radius was covered on the inside by a tin dioxide conducting layer serving as anode, to which the tungsten terminal *b* was connected. The willemite fluorescent layer was put on the conducting layer. The tantalum tip was welded on a mesh made also of tantalum wire. By means of electric heating

of the mesh the tip can be made free from both adsorbed and absorbed impurities. The mesh must be made of tantalum, in order to avoid alloying during the heating process. The tip was made of a wire of 0,1 mm diam. produced by electrolytic etching in a 40 % fluorhydric acid solution at 30 V d. c.

Before incorporation the tip was examined under the microscope to ascertain whether its surface was perfectly smooth and whether its radius of curvature was smaller than 1μ . Namely, the radius of curvature must be smaller than this value if we wish to obtain from the tip a comparatively large field emission current at an anode voltage of some kV-s. During operation the tip was earthed and to the terminal *b* a positive voltage was connected from a high voltage supply which could be regulated from 1 to 15 kV.

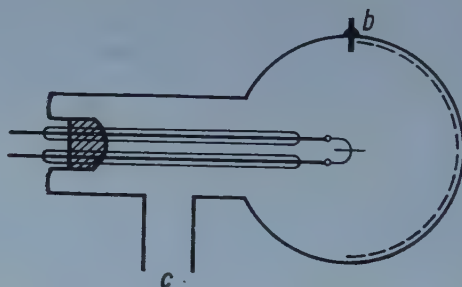


Fig. 1. Schematic structure of a field emission microscope

The field emission valve was connected at *c* to the ultra-high vacuum pump. Ultra-high vacuum was produced by a procedure which essentially is a kind of ALPERT-technique [5]. The structure of our vacuum system was as follows: after a glass mercury diffusion pump and a liquid air double trap followed a two-stage ultra-high vacuum pump; connected to each stage was a BAYARD—ALPERT ion meter and a COMSA—MUSA ion pump [6]. The two stages were separated from each other and from the trap by magnetically controllable glass valves. The field emission microscope was connected to the second stage. After keeping the ionic pump-part for some hours at 450°C in a furnace and degassing the electrodes by heating them up by means of electron bombardment, we measured in the second stage an air-equivalent pressure of $1 \cdot 10^{-9}$ mm. After heating for one or two days we could reduce this value to $5-6 \cdot 10^{-10}$ mm.

If the vacuum is suitable the degassing of the tip can be performed by heating it gradually at increasingly higher temperatures. The heating process was at times interrupted and the field emission image produced and photographed. At the same time the field emission current and the voltage belonging to it was measured. This is useful because the voltage belonging to a given current at a given radius of curvature is characteristic of the work function,

respectively of the form of the tip. The current was measured by means of a microammeter, the voltage by an electrostatic voltmeter of 10, respectively 15 kV range of measurement. The measurement of the heating temperature of the tip was carried out by means of a disappearing-filament optical micropyrometer. The temperature of the tip itself, which was of submicroscopic dimensions, could not directly be measured in this way. The temperature can only be measured near the welding spot and from this, taking the radiation loss into consideration, the temperature of the tip itself can be calculated [7]. The two values differ from each other only above 1500°C to any greater extent. In case of the first tip examined by us we determined the temperatures over 1850°C by means of extrapolation of the heating current — tip temperature curve, therefore the accuracy of these values is rather limited.

3. Preparation of a pure tantalum tip

Two tips were examined, one after the other, by means of a field emission microscope. Under the influence of the heat treatments they behaved essentially in an analogous way only on the second tip formation of a twin crystal could be observed; concerning this observation we give a more detailed account in section 6. Fig. 2 shows the typical images obtained of the first tip after heating at various temperatures. At the time of photographing the tip was naturally at room temperature and the pressure generally did not rise above the value of $3 \cdot 10^{-9}$ mm, but in most cases it was about $1 \cdot 10^{-9}$ mm.

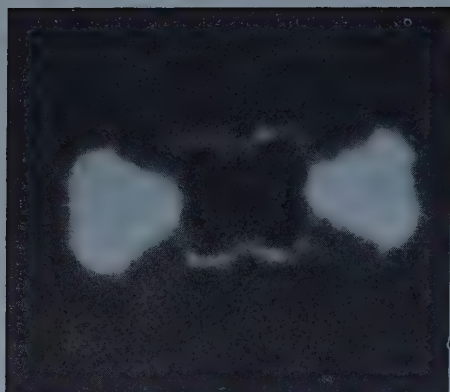
(In the Figure the following denotation is used: t_n = temperature of heating, τ_n = the heating time belonging to it, V = voltage necessary to gain a current of 1 μA .)

Fig. 2/a agrees with the image of a tantalum tip made and considered as pure by GOMER [2] and Fig. 2/d with that studied by HAEFER and al. [3]. On the other hand, Fig. 2/e agrees essentially with the really pure tantalum image of DRECHSLER and VANSELOW [4].

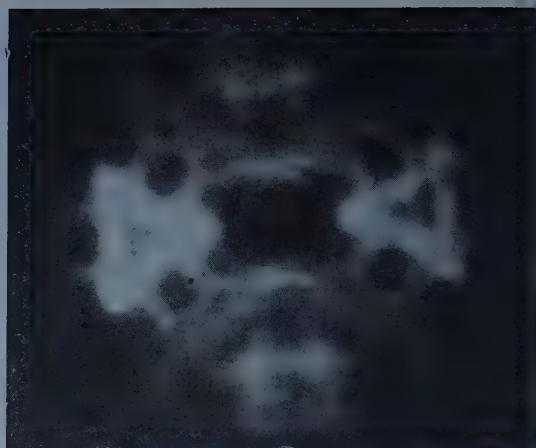
The criterion whether a surface is pure from the point of view of field emission microscopy, i. e. from a point of view making the most exacting demands is that the image of the material in question should not change up to the highest attainable temperatures.

As we shall see further on, though the image changed during the further heating, this was due to the diffusion of the solved impurities from the inside of the tip, so that after all Fig. 2/e can indeed be regarded as the field emission image of the pure tantalum tip.

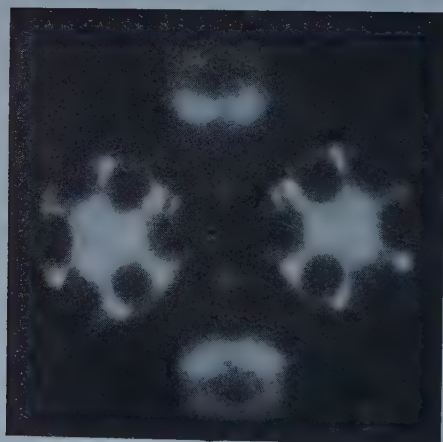
The photographs presented correspond to the mean phases of the degassing process and besides these some transitional images were also observed. The image of the pure tantalum tip is characteristic of body-centered cubic lattice metals. The central dark spot corresponds to the surface 011, the two



a)



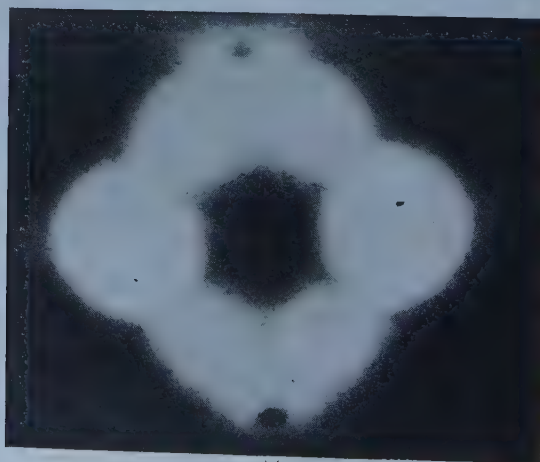
b)



c)



d)



e)

little round spots correspond to the surface 001, respectively 010. Making a comparison with the image of the tungsten tip (Fig. 3) we see that the most essential difference between them is that on the latter image the surfaces 112 appear too (four dark spots placed in the form of an X), while in case of tantalum they do not appear. From this point of view tantalum behaves according to the theory and tungsten does not. Namely, according to STRANSKI's theory for the appearance of 112 faces on the surface of the body-centered cubic lattice also a force between the third neighbours must be effective. But in this case also 111 faces must appear [8]. This is not the case either for tungsten or

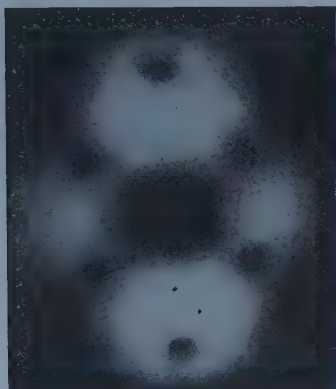


Fig. 3. Field emission microscopic image of a tungsten tip

for tantalum, so in case of these metals the force acting between the third neighbours can already be neglected. The reason why in the case of tungsten the 112 faces do appear has as far not entirely been cleared up.

On the basis of the FOWLER—NORDHEIM equation for field emission the radius of curvature of the tip can be calculated if the work function, the current intensity and the corresponding voltage are known. For this calculation the following formula was given by DRECHSLER and HENKEL [9]:

$$r = \frac{0.15}{\varphi^2} V^{3/2},$$

where φ means the work function in electron volts, V the voltage in volts necessary to gain $10 \mu\text{A}$ current and r the radius of curvature in Ångströms,

Fig. 2. Degassing of a tantalum tip

a) $t = 1750^\circ \text{C}$	$\tau = \text{some minutes}$	$V = 7,07 \text{ kV}$
b) $t_1 = 1900^\circ \text{C}$	$\tau_1 = 10 \text{ sec.}$	$t_2 = 1830^\circ \text{C}$ $\tau_2 = 2 \text{ m.}$ $V = 9,50 \text{ kV}$
c) $t_1 = 1880^\circ \text{C}$	$\tau_1 = 1,5 \text{ m.}$	$t_2 = 1920^\circ \text{C}$ $\tau_2 = 10 \text{ sec.}$ $V = 8,50 \text{ kV}$
d) $t = 1920^\circ \text{C}$	$\tau_1 = 1,5 \text{ m.}$	$V = 8,35 \text{ kV}$
e) $t_1 = 1880^\circ \text{C}$	$\tau_1 = 1 \text{ m.}$	$t_2 = 1920^\circ \text{C}$ $\tau_2 = 2 \text{ m.}$ $V = 8,70 \text{ kV}$

From this formula r is obtained with an error of about 20%. Converting to relation to 1 μA current we obtained for the constant 0,17 instead of 0,1. As the work function of tantalum is 4,1 eV [10], the radius of curvature of the tantalum tip reproduced in Fig. 2/e was found to be $8 \cdot 10^{-5}$ cm. In our case this value corresponds to a magnification of about 30 000 times.

Raising the temperature of the already pure tip for some seconds at 2000°C the image visible in Fig. 4 appears. After further heatings above 2000°C we obtained only images similar to that of Fig. 2/e. We have often observed this also in cases when the already pure tip had rested for a long time in poor vacuum and was then degassed by heating in ultra-high vacuum.



Fig. 4. Impurity migrated onto the surface of a tantalum tip

Also in such cases when the image of pure tantalum already had appeared we obtained after raising the temperature again an image of impurity but after further heating for an adequate time we obtained at any temperature only images of the pure tip. From this we can conclude that during the degassing process the cleaning of the surface happens with a greater velocity than the diffusion of the solved impurities onto the surface and thus near the surface a high concentration gradient arises. At higher temperature further impurities come to the surface and if these impurities are of an appropriate quantity we obtain an impurity image. This repeats itself until the inside of the metal becomes clean too. Also in this respect the behaviour of tantalum differs from that of tungsten. If once the surface of the tungsten tip has become clean it remains so, to whatever temperature it is heated as we could convince ourselves from the images on the screen of the field emission microscope. This is easy to understand, considering that tungsten practically does not solve gases while the good solution power of tantalum for gas is well-known, its getter capacity being based upon just this property.

Unfortunately we could not define by which impurities certain characteristic images were brought about. But it seems to be probable that oxygen plays the most important part among the impurity gases. The entirely pure tip was left for 40 hours in the air and after this it was heated to 1400°C . The result was the image reproduced in Fig. 2/c.

The appearance of the individual characteristic images is not bound up with certain temperatures. E. g. the image shown in Fig. 4 could be observed not only after heating to 2000°C but also at 1150°C . The fact which kind of images will appear is determined rather by the surface concentration of impu-

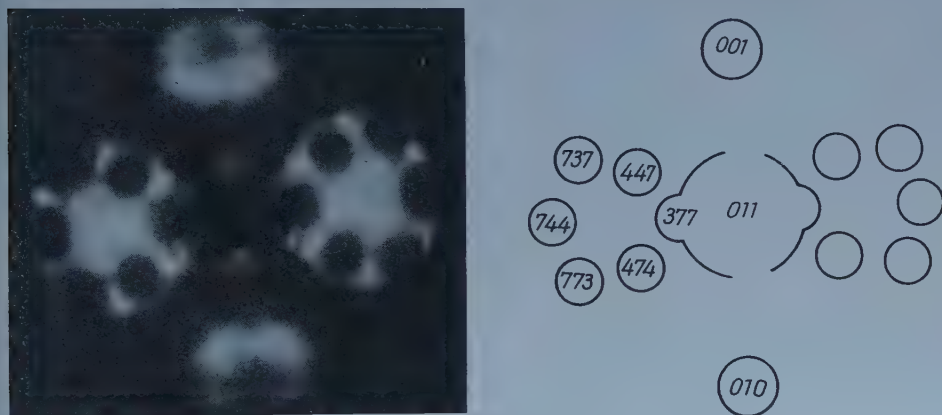


Fig. 5. Miller indices of faces appearing on a contaminated tantalum tip

rities and this is a function of the ratio of the diffusion towards the surface and the evaporation from the surface. Simultaneously with the heating of the tip certain reactions will take place between the absorbed gases present on the surface and the tantalum, while new surface phases are arising and various faces are growing.

The Miller indices of the faces which mostly were appearing in the form of dark spots were determined (Fig. 5). Besides the faces shown in the figure, on the almost clean tip near 111 often appear the 779 surfaces, as it is visible e. g. in Figs. 4 and 8. Most frequently the 447 faces appear and they probably correspond to some oxide. We remark that HAEFER et al. regarded the 447 faces visible also on their photographs [3] as 112 faces and on the basis of this they stated that the field emission image of tantalum agrees with that of tungsten. In fact — as we have already mentioned — the image of tantalum on their photograph was partly contaminated and not 112 but 447 faces occur on their photographs.

The usual procedure to determine some index is the following. On the screen or on the photograph the distance of the centre of the spot in question

from a point of known index is measured and from this the index is calculated. It must, however, be taken into consideration that the image — because of the field not being perfectly spherically symmetrical — is distorted. Therefore the angular distance of the two hexahedric faces immediately recognizable on the images is measured on the screen. Suppose this to be a , then the correct angular distance can be obtained by multiplying the measured values by a factor of $90/a$. In this way one generally gets correct values, however, in our case we could not obtain correctly the angular distance of the points of known indices determined for the sake of control. E. g. in case of the first tantalum tip for the angular distance 111—011 we obtained $33,7^\circ \pm 0,4$, instead of $35,3^\circ$. The discrepancy may have several causes, e. g. the screen or as it was observed by DRECHSLER the end of the tip may not be exactly spherical [11].

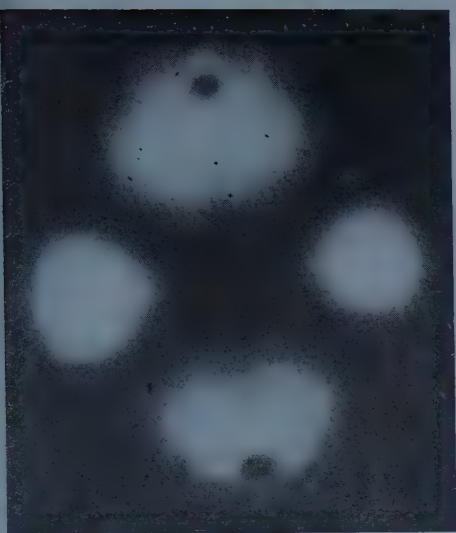
In order to eliminate these errors we made the indexing in that way that we measured on the photographs the angle of inclination between the straight line connecting the point in question with the centre of the face 011 with the line connecting face 010 with 011. From this the indices in question can be calculated. By this method we obtained exact values even if the system is not spherically but only cylindrically symmetrical.

4. Dependence of the form of tantalum tips on the temperature

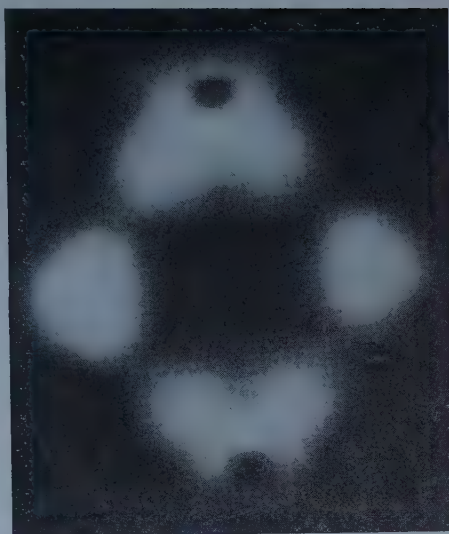
BECKER observed that some surfaces of a tungsten tip already heated to 2300°C grow after a reheating at 900°C . A similar symptom can be observed on tantalum tips too. In Fig. 6 it can be seen that after heating at lower temperatures the surfaces 011 and 001 enlarge. Heating the tip again to 2000°C we regain essentially the starting image. The photographs, naturally, were taken at room temperature.

This phenomenon can be explained by the fact that at higher temperatures crystals become gradually more isotropic [13]. The tip has the form of a hyperboloid of revolution and is cut by the crystal faces in the directions in which the surface free energy shows a sharp minimum. These are equilibrium surfaces of small Miller-indices, i. e. in our case of 001 and 011. By increasing the temperature, the sharp minimum gradually disappears and consequently the size of the faces decreases.

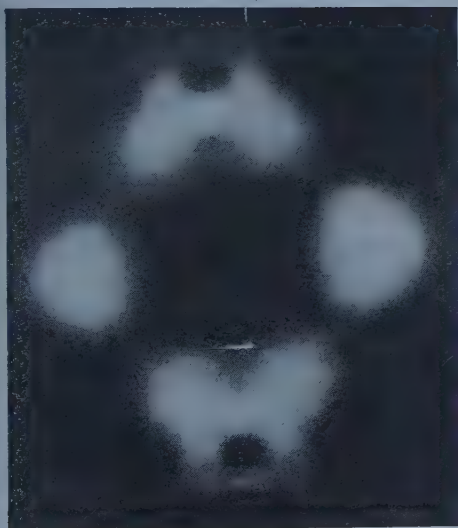
At higher temperatures the dark bands placed in the form of an X along the zone 111 are wider than at lower temperatures. This is connected with the fact that when heating at lower temperatures in the zone 111 a stepped structure takes shape which is especially well visible in Fig. 6/b. According to BECKER's observation this is the case also for tungsten. The formation of steps can be understood, namely with the decrease of the temperature the surface energy minimum of 011 becomes deeper relative to the surroundings and this condition is favourable to the formation of lattice steps.



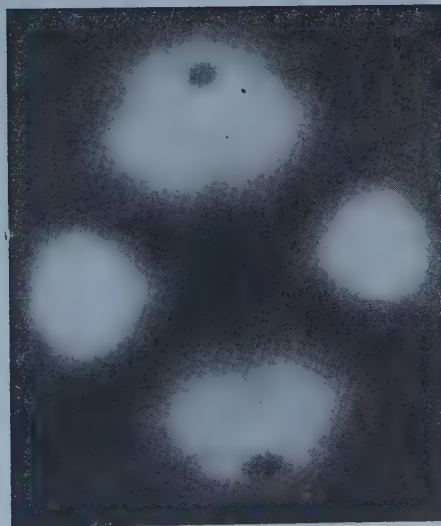
a)



b)



c)



d)

Fig. 6. Influence of the heat treatment on the form of a tantalum tip

a)	$t = 2000^{\circ} \text{C}$	$\tau = 20 \text{ sec}$	$V = 9,45 \text{ kV}$
b)	$t = 1400^{\circ} \text{C}$	$\tau = 30 \text{ sec}$	$V = 9,35 \text{ kV}$
c)	$t = 1170^{\circ} \text{C}$	$\tau = 30 \text{ sec}$	$V = 9,35 \text{ kV}$
d)	$t = 2000^{\circ} \text{C}$	$\tau = 30 \text{ sec}$	$V = 9,45 \text{ kV}$

We remark that apart from the local deformation at temperatures above 1000°C , similarly to tungsten, the radius of curvature of the tip grows because from the end of the tip surface migration takes place towards the places of greater radius of curvature and then the surface free energy of the whole tip decreases. This roughening of the tip appears the most markedly in the decrease of the field emission current, respectively in the increase of the voltage at a constant current.

5. Deformation of tantalum tips under the common influence of high temperature and electric field

The form of the tip examined at room temperature by means of a field emission microscope is constant. Namely, the activation energy of the surface atom migration causing the deformation is generally so high that it cannot arise under the influence of an electric field only. But heating the tip to such a high temperature at which surface migration takes already place and also switching on an electric field, the phenomenon appears which is called in the Anglo-American literature "build-up" and which means that the tip which till then was rounded off and almost rotationally symmetrical becomes polyhedral and sharp edges and angles are formed on it. On tungsten this has already been studied by several researchers [12, 14, 15]. In such cases essentially two processes can take place: at lower field intensities the equilibrium surfaces enlarge, because atoms are migrating to their edges and are further building the face. At higher field intensities, however, rather smaller steps are forming first of all in the places where plate faces had originally not been. Both processes follow from the fact that atoms are polarizable and that their potential energy is lower if they are placed on the edges and angles, i. e. on places of higher field intensity. At the place with field strength E the increase in the atomic bonding energy is $\frac{1}{2} aE^2$, where a is the polarisability [14]. From this it follows that the activation energy of the surface migration decreases proportional to E^2 and so, if during the build-up high field intensity maxima are forming, the migration will primarily tend towards these places.

Fig. 7 shows the process taking place at 900°C on a tantalum tip in the field emission microscope. Under the individual images we indicated the voltage belonging to the $1\mu\text{A}$ current which in the course of the process decreases, as was to be expected. The surfaces 011 and 001 do not grow to any considerable degree, rather the step formation predominates. First a concentric step system arises the most markedly near 111, where the step heights remain below the resolving power. At the same time the bright crosses with hexahedric faces in their centres, which appear also on the tip when in the normal state, protrude better from their surroundings. In the further process the tapering of 111

becomes pronounced, a high field intensity maximum appears and the whole emission current derives essentially from the two 111 tips. Disconnecting the voltage and heating the tip to 1200° C for one minute, we obtain again the image 7/a.

From the quoted literature it can be established that for tungsten build-ups of a similar type could be observed only in case of field intensities above $5 \cdot 10^{-7}$ V/cm. Below this field intensity the surfaces 011, 001 and 112 enlarged until they met with definite edges. The field intensity in the starting state was in our case — as can be calculated from the voltage necessary to obtain a gain of 1 μ A current, $-2,4 \cdot 10^7$ V/cm.

As to what kind of process generally will ensue, one can suppose that it will be like that of tungsten at low field intensities, if $\Delta Q_0 > \frac{1}{2} a E^2$, where ΔQ_0 means the increase of the average bonding energy arising from the enlargement of the equilibrium surfaces of the surface atoms. Namely, in such cases, in the first place ΔQ_0 contributes to the minimization of the surface energy and only secondly $\frac{1}{2} a E^2$, in such a way that the equilibrium faces will have definite edges and in consequence part of the atoms will work their way into places of high field intensities. In case $\Delta Q_0 < \frac{1}{2} a E^2$ and especially if $\Delta Q_0 \ll \frac{1}{2} a E^2$ the build-up will be of the same type as that which was observed in case of tantalum, i. e. the influence of the field will be effective in the first place. The bonding energy of the surface atoms of tantalum and hereby also ΔQ_0 , is because of the higher lattice constant, lower by 30% than the corresponding values of tungsten, supposing that the bonding energy changes with the distance according to the law r^{-6} . The polarizability of the tantalum atom must be greater than that of the tungsten atom but as to how much we did not find any data. By no means can it be so much higher that hereby the difference between the tungsten and tantalum build-ups could be explained if for field intensity the average field strengths calculated for a tip of the starting state is accepted. Tantalum is probably more susceptible to step formation, even without a field, than is tungsten, to which also other signs point, and taking into consideration that on the edges of the steps the field intensity may be considerably higher than the average intensity on these places only the influence of the field will after all be effective.

6. Formation of tantalum twin crystals

During the degassing process of the second tip studied, having heated it to 1900° C, we reached the state, to which the image 2/c corresponds. Having further heated the tip for about 1,5 minutes at the same temperature we obtained the image 8/a and after another heating for one minute the image 8/b was visible. 8/b is the image of the "almost pure" tantalum tip. Near 001 there

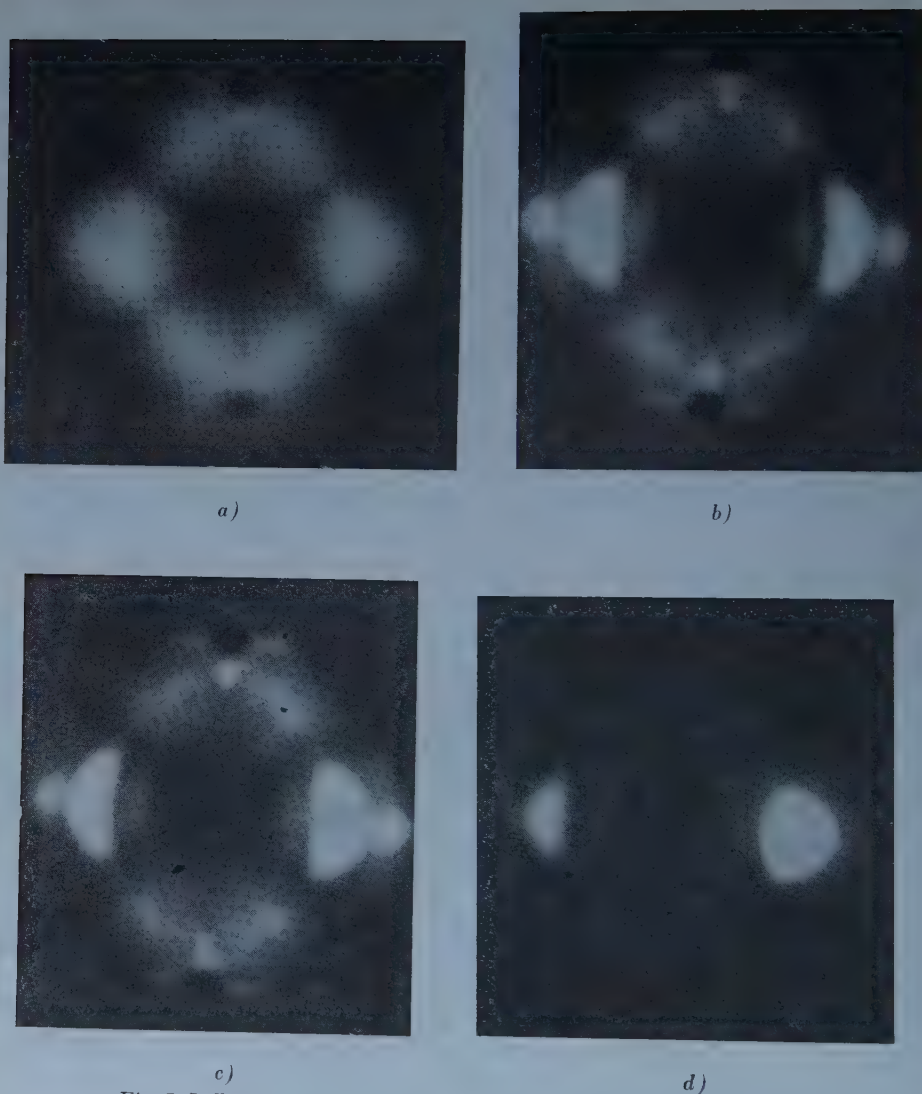


Fig. 7. Influence of the electric field on a tantalum tip at 900°C

- | | |
|-------------------|------------------------|
| a) starting state | $V = 11,3 \text{ kV}$ |
| b) 2 m | $V = 10,85 \text{ kV}$ |
| c) 4 m | $V = 10,4 \text{ kV}$ |
| d) 6 m | $V = 8,9 \text{ kV}$ |

is still a dark band and around 111 also the faces 779 appear which used to come forth, as we have already mentioned, on the "almost pure" tips. In this state a twin crystal was temporarily formed, namely a penetration twin. The twin plane as can be seen intersects the plane 011 along one arm of the dark X appearing in the tantalum images, and is in effect nothing else than the plane

111 perpendicular to it. This kind of twin appears most often in the case of crystals belonging to the cubic system. According to TERTSCH more than 70% of cubic twin crystals are ingeminated with respect to the face 111 [16].

As to the question what has brought about the formation of twin crystals and what produced afterwards their reversion into normal crystals, we could not find anything. It is evident, that heating played a role in it. In this connection further examinations would be necessary.

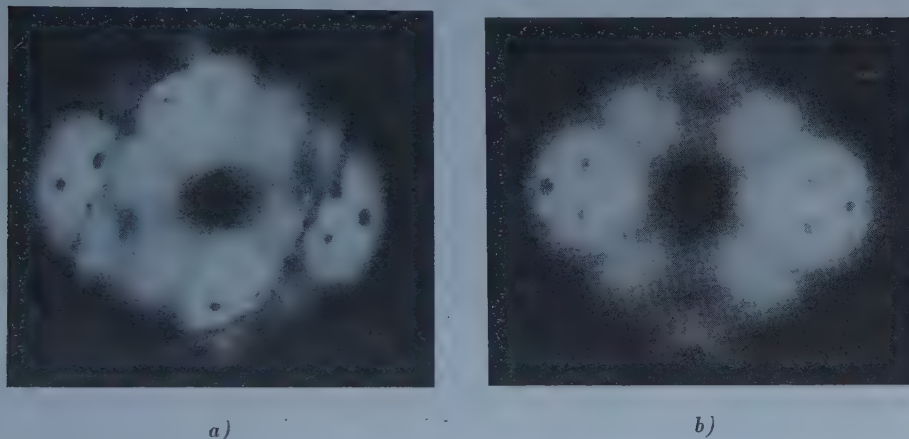


Fig. 8. Twin crystal transformation on a tantalum tip
a) tantalum twin crystal
b) after reversing into a normal crystal

Acknowledgements

I wish to thank Prof. Dr. I. P. VALKÓ, Head of the Electronic Laboratory of the Industrial Research Institute for Telecommunication Technique and Mr. F. FISCHER, Deputy Director of the Laboratory, for their continuous help and interest in this work, and Mr. E. VÁRBIRÓ Sr., glass technician, for the preparation of the glass components of the experimental device.

REFERENCES

1. R. H. GOOD and E. W. MÜLLER, *Handbuch d. Phys.* **XXI**, Springer Verlag, 1956, p. 176.
2. R. GOMER, *J. Chem. Phys.*, **20**, 1500, 1952.
3. H. BIRKENSCHENKEL, R. HAEFER und P. MEZGER, *Acta Phys. Aust.*, **7**, 402, 1953.
4. M. DRECHSLER and R. VANSELOW, *Z. f. Kristallogr.*, **107**, 161, 1956.
5. D. ALPERT, *J. Appl. Phys.*, **24**, 860, 1953.
6. G. COMSA and G. MUSA, *J. Sci. Instr.*, **34**, 291, 1957.
7. E. W. MÜLLER, *Z. f. Phys.*, **126**, 642, 1949.
8. I. N. STRANSKI and R. SUHRMANN, *FIAT Rep.*, 1030, 1947.

9. M. DRECHSLER and E. HENKEL, *Z. f. angew. Phys.*, **6**, 341, 1954.
10. H. B. MICHAELSON, *J. Appl. Phys.*, **21**, 536, 1950.
11. M. DRECHSLER and P. WOLF, IV. Int. Kongr. f. Elektron Mikr. Berlin, 1958.
12. J. A. BECKER, *Bell Syst. Techn. Journ.*, **30**, 907, 1951.
13. C. HEARING, *Structure and Properties of Solid Surfaces*, Chicago Univ. Press, 1953.
14. M. DRECHSLER, *Z. f. Elektrochem.*, **61**, 48, 1957.
15. P. C. BETTLER and F. M. CHARBONNIER, *Phys. Rev.*, **119**, 85, 1960.
16. H. TERTSCH, *Z. f. Kristallogr.*, **94**, 461, 1936.

ИССЛЕДОВАНИЕ ВЕРШИН ТАНТАЛОВЫХ МОНОКРИСТАЛЛОВ ПРОСТРАНСТВЕННО-ЭМИССИОННЫМ МИКРОСКОПОМ

Л. ЭРНСТ

Резюме

Пространственно-эмиссионным микроскопом исследовались процесс дегазирования танталовых вершин и деформация чистых вершин под влиянием нагревания, а с другой стороны нагревания и электрического поля. В первом случае наблюдалось поведение, аналогичное наблюдаемому у вольфрама, а во втором — отличное от этого. Наблюдалось образование двойниковых кристаллов под влиянием тепла.

ПРИМЕЧАНИЯ К ЭЛЕКТРОЛЮМИНЕСЦЕНЦИИ $\text{ZnS} \cdot \text{Cu} : \text{Mn}$ НА ПОСТОЯННОМ И ПЕРЕМЕННОМ ТОКЕ

Э. ЛЕНДВАИ, Я. ШАНДА и Я. ВЕЙСБУРГ

ФИЗИКО-ТЕХНИЧЕСКИЙ ИНСТИТУТ АКАДЕМИИ НАУК ВЕНГРИИ

и

НАУЧНО-ИССЛЕДОВАТЕЛЬСКИЙ ИНСТИТУТ ПРОМЫШЛЕННОСТИ СВЯЗИ,
БУДАПЕШТ

(Представлено Д. Сигети. — Поступило 10. I. 1961.)

Авторы, анализируя данные работ В. Н. Фаворина и других по исследованию электролюминесцентных свойств электролюминофора $\text{ZnS} \cdot \text{Cu} \cdot \text{Mn}$, приходят к выводу, что наблюдаемое в спектре перераспределение интенсивностей при применении постоянного и переменного напряжений можно объяснить локальным нагреванием ячейки. Это нагревание связано с «dc» компонентом одновременно присутствующей «ac-dc» электролюминесценции, т. е. температурным тушением зеленых центров. Таким образом, в данном случае изменение спектра электролюминесценции связано не с изменением напряженности, как предполагается в работах [1, 2], а является следствием изменения температуры, т. к. температурные зависимости полосы меди и полосы марганца различны.

В работах [1, 2] была исследована электролюминесценция твердых конденсаторов на основе люминофора $\text{ZnS} \cdot \text{Cu} : \text{Mn}$. Авторы пришли к выводу, что относительная интенсивность двух присутствующих в спектре электролюминесцентных полос (зеленая полоса Cu и желтая полоса Mn (зависит не только от частоты применяемого поля, но и от его напряжения. При возбуждении постоянным полем в спектре появляется только желтая полоса, тогда как при возбуждении переменным полем появляются и желтая, и зеленая. Интенсивности отдельных полос отсчитывались в местах, заданных в работах [1, 2]. Эти величины приведены в табл. I. (G — интенсивность зеленой полосы, Y — желтой.)

В. Н. Фавориным и его сотрудниками [1] было также исследовано и излучение люминофора $\text{ZnS} \cdot \text{Cu} : \text{Mn}$ при одновременном возбуждении постоянным и переменным токами. Их основные данные по этому вопросу приведены в таблице II. (G и Y — также как в таблице I — относительная интенсивность желтой и зеленой полос в указанных местах максимума.)

В настоящем сообщении дается анализ экспериментальных данных работ [1, 2]. На основе такого анализа можно было прийти к выводам, отличающимся от выводов В. Н. Фаворина и его сотрудников. Показано, что данные вышеуказанных авторов хорошо согласуются с одной стороны с люминесцентными эффектами, вызванными действием одновременно приложенного постоянного и переменного напряжения, с другой стороны с изменениями температуры, возникающими вследствие увеличивающейся мощности, вызванной увеличением напряжения.

Таблица I

Значения интенсивностей максимумов полос, определенных из кривых спектрального распределения энергии в произвольных единицах (определены по рис 1, 2 и 3 [2])

На- пряжения V	Частота					
	60 гц		600 гц		2000 гц	
	Y	G	Y	G	Y	G
300	—	—	—	—	36,1	71,2
400	—	—	36,2	55,0	—	—
500	71,5	49,7	—	—	39,8	71,2
600	—	—	42,2	55,0	—	—
700	71,5	44,7	—	—	48,1	71,2
800	71,5	39,0	53,5	53,0	—	—
900	71,5	31,6	55,0	48,0	57,2	71,2
1000	71,5	27,5	55,0	41,0	69,8	71,2
1100	71,5	21,0	55,0	31,0	—	—

Таблица II

Данные В. Н. Фаворина [1]

Y — относительная интенсивность желтой и G — зеленой полос

	Напряжение (V)		Ток dc μA	Относительная интенсивность максимумов		R
	ac 500 гц	dc V		Y	G	
1	0	1100	100	5	0	∞
	220	1100	100	11,5	9,2	1,25
	280	1100	100	15,6	23,5	0,665
	400	1100	100	24,0	47,5	0,506
	220	0	0	2,65	9,2	0,288
	280	0	0	5,8	23,5	0,247
	400	0	0	13,3	47,5	0,280
2	0	1050	55	9,0	0	∞
	0	1200	100	23,8	0	∞
	0	1400	200	32,5	0	∞
	280	1050	55	33,0	91,0	0,362
	280	1200	100	47,0	85,6	0,55
	280	1400	200	62,2	80,1	0,773

§ 1

Для обработки данных, приведенных в таблице I мы рассчитали отношения максимумов интенсивностей желтой и зеленой полосы для всех значений напряжения и частоты:

$$R = \frac{Y}{G} = \frac{(\text{интенсивность при } 580 \text{ ммк})}{(\text{интенсивность при } 520 \text{ ммк})} \quad (1)$$

Эти данные содержатся в таблице III.

Таблица III

Зависимость R от частоты и от напряжения

Напряжение (V)	300	400	500	600	700	800	900	1000	1100
$R/60$ гц	—	—	1,445	—	1,600	1,805	2,260	2,600	3,414
$R/600$ гц	—	0,658	—	0,767	—	0,935	1,145	1,342	1,775
$R/2000$ гц	0,507	—	0,559	—	0,676	—	0,804	0,980	—

Как видно из приведенных данных значение R , т. е. относительная интенсивность желтой полосы к зеленой полосе при увеличении напряжения растет, а при увеличении частоты — уменьшается.

Далее исследовалась зависимость R от напряжении при разных частотах. Как видно из табл. IV соотношения R , определенные при разных двух частотах (с точностью нескольких процентов) не зависят от напряжения. То есть изменение значений R имеет одинаковый характер при разных примененных частотах. Таблица IV содержит значения соотношения

$$C_{f_2}^{f_1} = R_{f_1}/R_{f_2}.$$

Среднее значение $C_{600}^{60} = 1,94 \pm 1\%$; $C_{2000}^{60} = 2,6 \pm 8\%$.

Таблица IV

Значения R , вычисленные при различных частотах, но при одинаковых напряжениях

Напряжение (V)	300	400	500	600	700	800	900	1000	1100
$\frac{R/60 \text{ гц}}{R/600 \text{ гц}}$	—	—	—	—	—	1,93	1,97	1,94	1,92
$\frac{R/60 \text{ гц}}{R/2000 \text{ гц}}$	—	—	2,58	—	2,37	—	2,8	2,65	—

Для выяснения зависимости R от напряжения мы составили график этой зависимости на основе данных, приведенных в таблице IV. Мы получили возможность охарактеризовать одной кривой экспериментальные данные, полученные при различных частотах. Умножив R_{60} и R_{2000} со средними значениями факторов C_{60}^{60} и C_{2000}^{60} и изображая полученные данные, мы получили хорошее совпадение с экспериментальными данными, полученными в работе [2]. Общий характер найденной закономерности еще больше выясняется из того факта, что кроме нами уже ранее использованных трех частот, измеренные данные при частоте 2000 гц хорошо согласуются с данными, полученными при частотах 60 и 600 гц. Также вероятно, что данные, полученные из опытов в другой установке, могут быть согласованы, если их умножить на постоянную. (На рисунке эти данные отмечены знаком*.)

Ход кривой можно выразить уравнением:

$$R = A \cdot V^\alpha + B, \quad (2)$$

где A , α и B постоянные.

§ 2

При рассмотрении данных работы [2], полученных при одновременном действии полей постоянного и переменного тока, можно указать на следующие закономерности. На основе данных, приведенных в табл. II, выявляется, что при возбуждении постоянным напряжением появляется только желтая полоса, а при возбуждении переменным напряжением появляются и желтая и зеленая полосы. При сравнении данных, полученных при возбуждении только постоянным или только переменным напряжением с данными, полученными при одновременном воздействии постоянного и переменного напряжений, оказывается, что при равенстве интенсивностей зеленых полос интенсивность желтой полосы всегда больше, чем сумма интенсивностей желтой полосы при отдельном воздействии полей.

Если обозначать интенсивность желтой полосы при воздействии только постоянным напряжением через Y_1 , а только переменным напряжением через Y_2 , тогда на добавочный желтый свет (Y_3) мы получаем следующую формулу:

$$Y_3 \equiv Y - (Y_1 + Y_2) > 0. \quad (3)$$

По нашему мнению добавочный свет, Y_3 пропорционален переменному напряжению, и значения Y_3^* , рассчитанные из следующей формулы, хорошо совпадают со значениями Y_3

$$Y_2^* = \frac{V_{ac}}{V_0} (Y - (Y_1 + Y_2)), \quad (4)$$

где V_{ac} — приложенное переменное напряжение, а V_0 то напряжение, с которым мы сравниваем. (В дальнейшем $V_0 = 220 \text{ V.}$)

Вышеуказанные результаты и основные данные содержатся в табл. V.

Таблица V
Анализ данных 1-ой группы таблицы II

Напряжение ас 500 гц μ	Ток		Относительная интенсивность максимумов					
	dc V	dc μA	Y_1	Y_2	Y_3	Y^*	Y	G
0	1100	100	5,0	—	—	5,0	5,0	—
220	1100	100	5,0	2,65	3,85	11,5	11,5	9,2
280	1100	100	5,0	5,8	4,9	15,7	15,6	23,5
400	1100	100	5,0	13,3	7,0	25,3	24,0	47,5

Для облегчения сравнения полученных результатов мы ввели обозначение Y^* , равное

$$Y^* = Y_1 + Y_2 + Y_3^* \quad (5)$$

хорошее совпадение которого со значениями Y подтверждает правильность вышеуказанного разложения. Правильность сравнения с данными, полученными при применении только переменного напряжения подтверждается тем, что значения R , рассчитанные из данных, полученных при приложении только переменного напряжения хорошо совпадают с наблюдаемой зависимостью $R(V)$ в данной области напряжения. Это значит, что желтое свечение, возникающее при приложении только постоянного напряжения, в том отличается от свечения при одновременном действии постоянного и переменного напряжения, что в последнем случае возрастает (пропорционально с напряжением) излучение не только желтых центров, которые могут возбуждаться и постоянным полем, но возбуждаются и дальнейшие такие центры (большой частью зеленые, меньшей желтые), которые в данных условиях возбуждаются только под действием переменного напряжения. Из изменения интенсивностей можем получить дальнейшие выводы по данным группы 2. таблица II. Отсюда выясняется, что вычитая желтое свечение, возникающее под действием только постоянного напряжения из свечения, которое возникает под действием одновременно переменного постоянного и переменного напряжений, мы получаем практически постоянное добавочное желтое свечение. Отношение максимумов интенсивностей этого добавочного желтого свечения к зеленому свечению хорошо совпадает с отношением максимумов интенсивностей желтого к зеленому свечению, возникающему при возбуждении только переменным

напряжением. (Значения этих отношений при напряжении возбуждения 280V — 500 гц. без постоянного напряжения — 0,247; при постоянном напряжении 1050 V — 0,264; при 1200 V — 0,273; и при постоянном напряжении 1400 V — 0,367).

§ 3

На рисунке 2. заметно, насколько быстро растет использованная мощность с увеличением напряжения. Это может вызвать сильное локальное

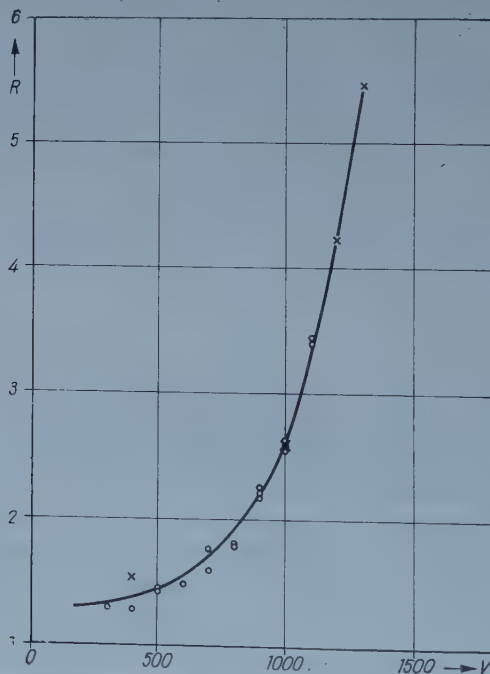


Рис. 1. Зависимость R от напряжения (o-): измерения на 60, 600, 2000 гц, нормируя на 60 гц. -x-: измерение на 2000 гц нормируя при 1000 V.

нагревание, и этим может объясняться ненормальное значение точки при напряжении постоянного тока 1400 V. Если умножить значения относительных чисел R , полученных при одновременном действии постоянного и переменного напряжений, соответствующим коэффициентом и изобразить эти значения в зависимости от суммарного напряжения (рис. 3.), то получаем хорошее совпадение с зависимостью, изображенной на рис. 1. Это указывает на то, что нагревание также играет роль при появлении изменений, возникающих только под действием переменного напряжения. С учетом термических действий открывается возможность простого объяснения изменений отношений интенсивностей в спектре. Достаточно указать на тот известный факт, что свечение активаторных центров меди (зеленый свет) при уве-

личении температуры выше комнатной быстро падает, тогда как активаторные центры марганца (желтый свет) в этой же области менее чувствительны.

Познание того, что термические действия одинаково играют роль при различных типах возбуждения, с учетом того, что часть центров может быть возбуждена и постоянным напряжением (другая часть возбуждается только переменным напряжением) подтверждает то предположение, что в выше

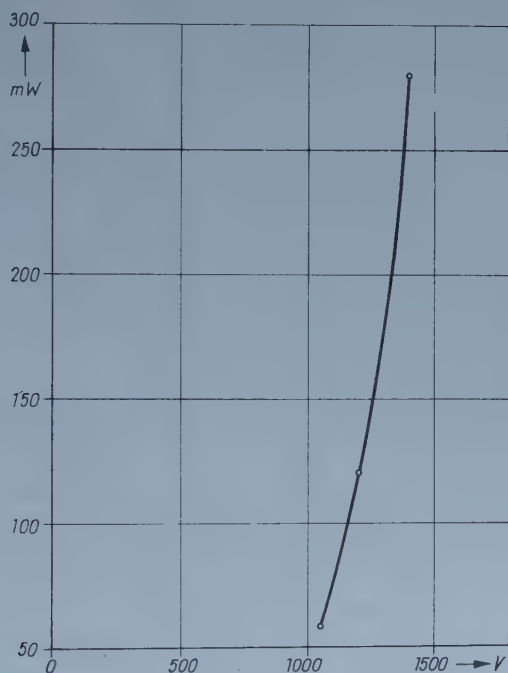


Рис. 2. Зависимость потребляемой мощности постоянного тока от напряжения, в случае электролюминесцентного конденсатора

цитированных измерениях на самом деле, даже в случае только переменного напряжения, излучение возникает как излучение при одновременном «ас - dc» возбуждении.

Выводы

Из вышесказанного следует, что в опытах В. Н. Фаворина и его сотрудников

1. Изменение соотношений интенсивностей желтой и зеленой полос при возбуждении переменным напряжением, независимо от частоты возбуждения, при изменении напряжения (3), хорошо описывается зависимостью на рис. 1.

2. Излучение под действием переменного напряжения можно разложить на «ас-дс» компоненты.

3. Мощность (при постоянном токе) использованная ячейкой, сильно возрастает при увеличении напряжения, что приводит к локальному нагреванию.

4. Увеличение соотношений желтого к зеленому излучению, наблюдаемое при увеличении напряжения переменного тока, объясняется известным температурным тушением зеленых центров.

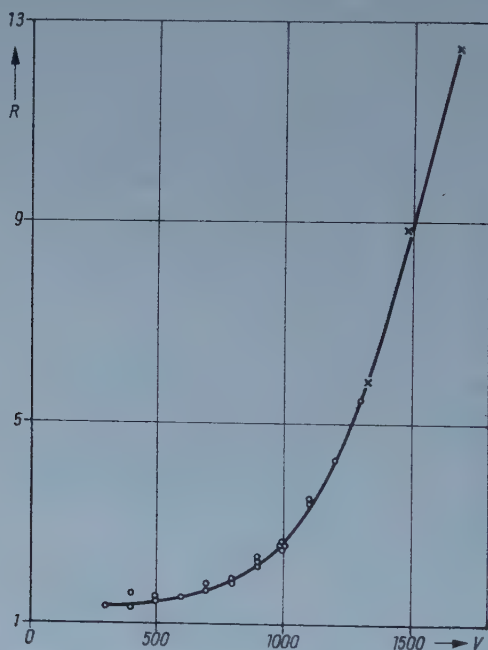


Рис. 3. Зависимость между значениями R полученных при применении одновременно приложенных полей постоянного и переменного тока, а также при приложении только полей переменного тока (R)

(-o-: значения, полученные при возбуждении переменным напряжением; -x-: значения, полученные при одновременном приложении постоянного и переменного напряжения),

5. В уменьшении соотношения желтого излучения к зеленому, при увеличении частоты переменного напряжения, также играет роль температурное тушение, возникающее вследствие локального нагревания. Точнее: при увеличении частоты «ас» компонент свечения относительно к компоненту «дс» увеличивается, уменьшается относительное нагревание зеленых центров, так как меньшая часть использованной мощности преобразуется в тепло.

6. Используемые в измерении электролюминесцентные ячейки являются нелинейными. Это может указать на возможность существования внутренних барьеров.

ЛИТЕРАТУРА

1. В. Н. Фаворин, Г. С. Козина, Л. Тихонова, *Опт. и Спектр*, **7**, 703, 1959.
2. В. Н. Фаворин, Л. П. Паскачев, *Опт. и Спектр*, **7**, 706, 1959.
3. Z. Bodó, J. WEISZBURG, J. SCHANDA, *Arbeitstagung »Festkörperphysik« Balatonfüred*, 14—19, Sept. 1959.

SOME REMARKS ON THE D. C. AND A. C. ELECTROLUMINESCENCE OF ZnS·Cu:Mn

By

E. LENDVAY, J. SCHANDA and J. WEISZBURG

Abstract

Analysing the results of FAVORIN et al. [1, 2] the authors came to the conclusion that the alterations observed in the spectrum can be explained by the local heating due to the d. c. component of the a. c. — d. c. electroluminescence appearing simultaneously in the cells, respectively by the thermal quenching effect found in the green light. In this case the spectra are not voltage- but heat-dependent. the temperature dependences of the bands differing from each other.

ON MOVING STRIATIONS OF LOW-PRESSURE MERCURY DISCHARGES*

By

G. LAKATOS and J. BITÓ

INDUSTRIAL RESEARCH INSTITUTE FOR TELECOMMUNICATION TECHNIQUE, BUDAPEST

(Presented by G. Szigeti. — Received: 30. I. 1961)

The authors examined the propagation velocity of the moving striations appearing in low-pressure mercury vapour discharge tubes in the case of direct current. They studied also the influence of the pressure of argon applied besides mercury on the mentioned velocity, when the vapour pressure of mercury was kept at an approximately constant value.

In the positive column of discharges, also in case of d. c. ones, appear oscillations, time instabilities, concerning the origin of which various opinions have been put forward [1—4]. In certain current regions, at certain gas pressures also space charge waves moving in the plasma of the positive column can be detected [5] and optically observed as moving striations.

According to DONAHUE et al. [5] in case of d. c. discharges characterized by constant electric and external parameters (temperature, geometry, etc.) the appearing striation can be regarded as superposition of two space charge waves, the origins of which can be interpreted in terms of the phenomena occurring in the vicinity of the cathode and the anode [6, 7].

These space charge waves are moving in the discharge tube in the direction corresponding to the sign of the moving charges. Among these waves the negative electron waves have the greater velocity.

The aim of the experiments here described is the examination of some characteristic properties of the space charge waves moving with greater velocities at various pressures and given discharge current intensities.

The experimental arrangement used in course of the experiments corresponds to the arrangement described by DONAHUE et al. [5]. The block diagram can be seen in Fig. 1.

Data of the discharge tube:

1200 mm length, 38 mm outer diameter; it was filled with 1—4 mm Hg argon and about 100 mg mercury. During the experiments the discharge tube was put in a thermostatic water jacket so that the temperature of the bulb wall regulating the mercury vapour pressure could be held within narrow limits. The tube operated without any external cathode heating and was fed

* A report on research conducted under contract with the United Incandescent Lamp and Electrical Co. Ltd.

from the stabilized d. c. power supply PS and during the experiments it worked generally under a symmetric ohmic loading. The tube voltage was measured by the static voltmeter V_s and the net voltage by the instrument V_n . The discharge current of the tube could be read on the ammeter I. The instrument V_s could for the time of measurement be inserted by means of the switch S.

The photo-electric cell P with suitably adjusted slit could be moved along the discharge tube and the current from it came through an amplifier to the vertical input of the oscilloscope O, according to the arrangement shown in Fig. 1. By means of the photo-electric cell the light oscillation representing

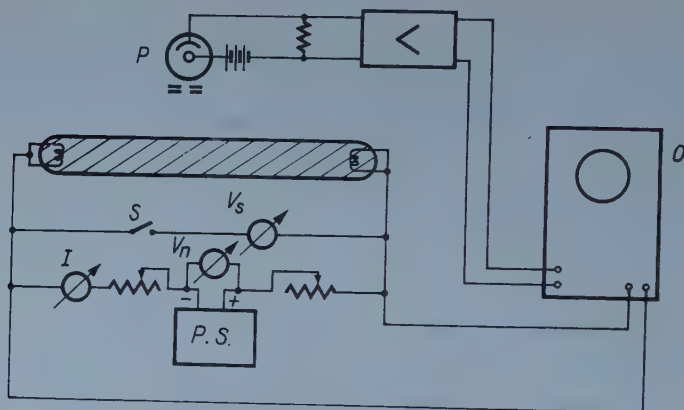


Fig. 1. Experimental arrangement for the examination of moving striations

the moving striation could be indicated and its frequency, shape and amplitude variations examined.

In each case it was advisable to apply the tube voltage variations to the horizontal input of the oscilloscope for the sake of synchronization and thus generally a standing wave form appeared on the screen of the oscilloscope.

In order to reduce the accidental disturbing frequency infiltrations, the wirings were made of shielded cables.

The testing method applied in course of the measurements essentially agreed with the method described by DONAHUE et al. [5] and YOSHIMOTO et al. [8] with the difference that whilst YOSHIMOTO et al. have held constant the temperature of the ambient air, in the experiments described above — as we have already mentioned — the temperature of the water jacket around the discharge tube was maintained at a constant value.

It is known that the propagation of the space charge wave is also shown by the shifting of the excitation processes appearing at the wavefront [9]. This means also that the light maximum is moving with a certain velocity and this can be well detected by a photo-electric cell arrangement. If the photo-electric cell is placed somewhere along the discharge tube, it shows light oscillations

which are connected with the axial propagation velocity of the light maxima (wave fronts) passing before the slit of the cell. Each wave maximum — light maximum — propagates with a definite velocity, in case of a given frequency and under constant conditions and this is one of the parameters characteristic of the striation.

The determination of this parameter was carried through by means of the photoelectric cell P, as follows. As the oscillation of the tube voltage regarding its frequency generally agreed with that of the light oscillations, the light wave could be synchronized in the above-mentioned way and so, on the screen of the oscilloscope a standing wave form appeared. Then, at given discharge parameters the wave form is stable in time and its characteristics depend only on the position of the photo-electric cell along the tube.

Changing the position of the photo-electric cell along the longitudinal axis of the discharge tube the amplitude of the arbitrarily chosen phase point is modified too. The wavelength l of the moving striation is defined by the smallest shifting of the photo-electric cell at which the amplitudes belonging to the given phase angle agree with each other.

In this case the wavelength was determined by choosing a phase point of a well-observable maximum amplitude. The frequency n of the moving striation could be determined by comparison of the voltage oscillations arising from the light oscillations recorded by the photo-electric cell and the oscillation of known frequency of a tone frequency generator on an oscilloscope by means of the method of the Lissajous curve. Thus, the wavelength l and the frequency n of the striation could be given and knowing these data the propagation velocity c could be calculated.

The measurements took place in a discharge current region from 20 to 400 mA at argon pressures of 1, 2, 3 and 4 mm Hg. When the tube was switched on, a stabilization time of about 20 minutes was allowed before the measurements were started.

In order to ensure the correctness of the measured values it was advisable to allow a setup time of 2 minutes after the adjustment for the various current values. Without this the effect of the discharge current previously adjusted could still be detected.

It was observable that generally the light oscillation within the tube followed the oscillations of the tube voltage. A difference occurred only, when the reading took place immediately after the readjustment to new discharge conditions (e. g. after varying the current). In such a case the tube voltage oscillations settled down quicker to the constant values determined by the particular conditions than the frequency of the light oscillation which — according to this experiment — needs a longer time of stabilization. Presumably, this is connected with the attenuation effect occurring in the tube, resp. with the relaxation time of the positive column.

As it was already mentioned above, the experimental tube was surrounded by a water jacket. The temperature of the water was held at $25 \pm 0.1^\circ \text{C}$. The reason for applying a water jacket was that the temperature fluctuations on the walls of the discharge tube were to be kept small — in spite of the fact that different heat quantities had to be extracted in the case of the various current intensities.

This aim can be achieved when using a thermostatic water jacket (instead of air surroundings) on account of the higher heat transfer factor of water. The smaller temperature fluctuations thus attained result namely in a smaller variation of the mercury vapour pressure.

Having fixed the photo-electric cell to a given point of the tube, the curve of the shape visible in Fig. 2 appeared on the oscilloscope. Modifying

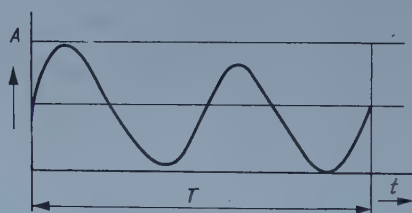


Fig. 2. Characteristic wave form of the light oscillation A — Amplitude, t — time, T — period

the positions of the photo-electric cell also the form of the wave somewhat changed.

Starting from the anode and taking the photographs in steps of 0.5 cm, the wave forms changed in the way shown in Fig. 3. Comparing the curves with each other it follows that the characteristic maximum remains all the time in the same phase. This conclusion gave the starting point for the choice of the method for the determination of the velocities.

It is also evident that moving away from the anode the wave form shown in Fig. 3 gets a steeper slope and its secondary maximum increases up to a certain value, though it attains nowhere the value of the primary maximum.

The photographs were taken at an operating current of 50 mA and a tube wall temperature of $25 \pm 0.1^\circ \text{C}$ adjusted by a thermostatic water jacket. The frequency of the oscillations appearing under such conditions was 620 cycles per second.

In the further measurements a tube was used, at one end of which there were several glass opening extensions [10], so that the difference of the geometric conditions and of the electrodes should not influence the process to be examined. By means of these extensions gases of various pressures could be filled into the same tube. The electrodes of the discharge tube were mounted identically, they consisted of a tungsten helix coated with an electron emitting

material and of an auxiliary anode surrounding the helix. During the measurement the terminals of the electrodes were short-circuited.

It is well-known that in case of mercury vapour discharge tubes the parameters characteristic of the discharge depend to a high degree on the mercury vapour pressure. But the mercury vapour pressure within the tube is always

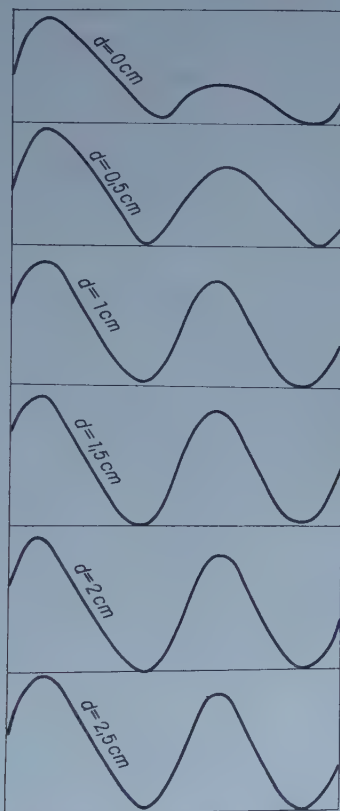


Fig. 3. Dependence of the wave form of the light oscillation on the distance d measured from the anode

determined by the temperature of the coldest part of the tube wall. As the opening extensions at the end of the tube were not inside the water jacket, in order to eliminate the deposition of mercury it was necessary to keep them by external electric heating at a higher temperature than that of the water jacket.

To avoid mercury diffusion along the longitudinal axis of the tube, before the measurements it was also necessary to ensure that all the liquid mercury of the tube collects at the inlet port of the water of the thermostat.

In the above circumstances, by means of the described method the striation frequencies belonging to the various discharge currents at different pres-

tures could be determined. The dependence of the frequency on the current at various pressures as parameters can be seen in Fig. 4. Here it is shown that with increasing pressure of the filling gas the striation frequency decreases monotonously. (During the experiments the pressure of the mercury vapour remained approximately constant at a value corresponding to the temperature of the thermostatic jacket.) The frequencies appear in the range of 300–1500 cycles per second. The forms of the curves — except the curve belonging to the pressure of 1 mmHg — are characterized by a breaking point. This

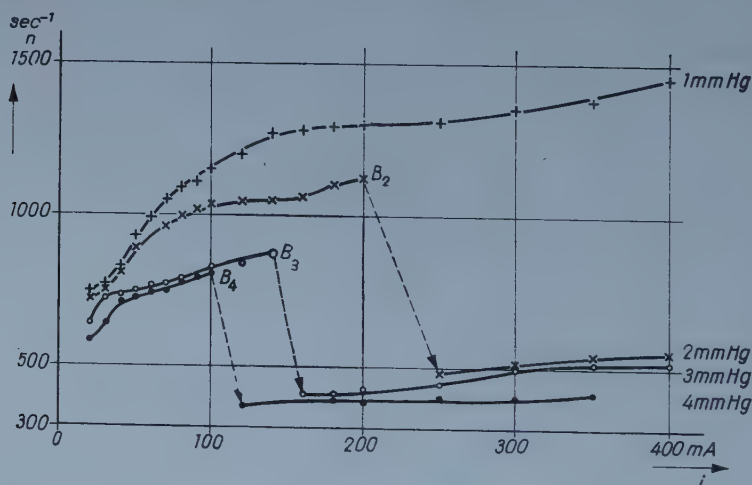


Fig. 4. Dependence of the frequency n of the moving striation on the discharge current i at various argon pressures. B_2 , B_3 , B_4 breaking points

breaking point is displaced towards the lower current values. The value of this frequency decrease may reach many hundreds of cycles per second. The dependence of the breaking point of the frequency on the pressure and the shifting of the current values characteristic of the breaking point as function of the applied gas pressure are shown in Fig. 5.

After the determination of the wavelength and the frequency of the striation the propagation velocity of the latter could be calculated. In Fig. 6 the propagation velocity of the moving striation can be seen as function of the discharge current, at various pressures.

It can be seen that at constant current intensity, decreasing the pressure, the propagation velocity increases. The velocities in the examined range fall generally between 10^3 and 10^4 cm/sec. At the pressure of 4 mm Hg in the current region between 120 and 180 mA no velocity value is given, because here the wavelength determination gave very uncertain values.

The velocity vs current intensity curves belonging to the various pressures are of similar character. It is typical that at low current intensities the

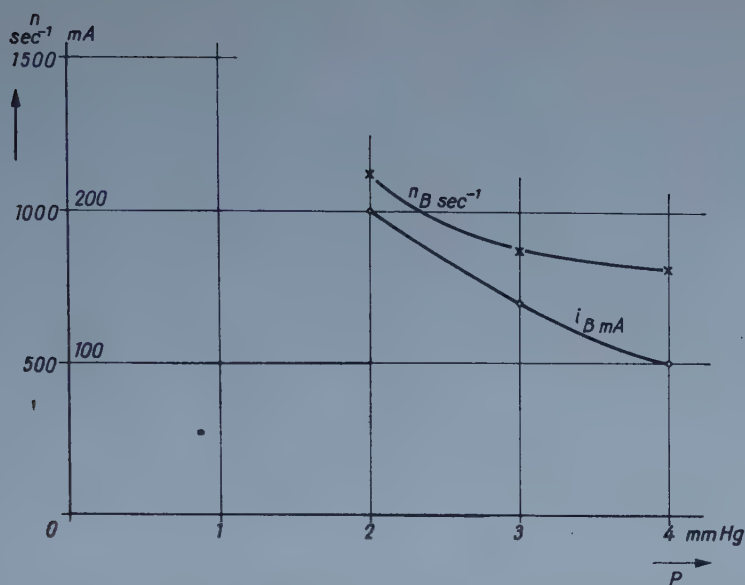


Fig. 5. Dependence of the frequency n_B and the current intensity i_B belonging to the breaking points B_2 , B_3 and B_4 shown in Fig. 4 on the argon pressure p

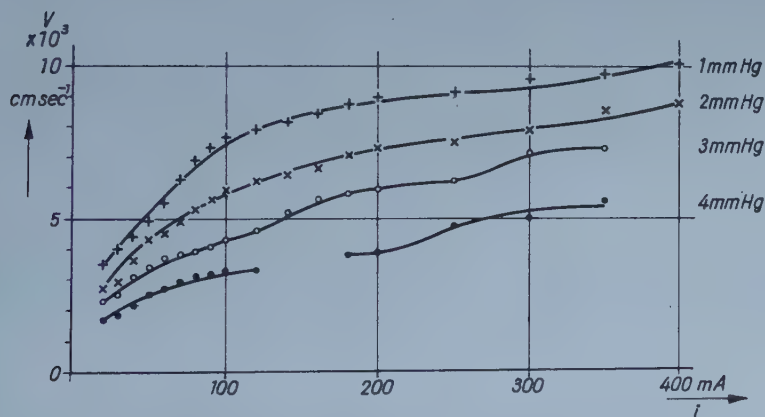


Fig. 6. Dependence of the propagation velocity v of the moving striation on the discharge current i , at various argon pressures p

velocity increases steeply with increasing current and further, at higher current values the curves become flat.

The dependence of the velocities on the pressure is shown in Fig. 7 for several values of the discharge current. It can be seen that in the case of the 20–100 mA current region and the 1–4 mm Hg pressure region, the dependence of the propagation velocity v on the pressure p in case of various current intensities i can be described by curves of similar character.

At currents higher than 100 mA the dependence of the velocity on the pressure is already different, presumably because of the increase of the mercury vapour pressure. Namely, according to the measurements increasing the current intensity the tube voltage changed only little and thus the power consumed by the tube increased approximately proportional to the current intensity.

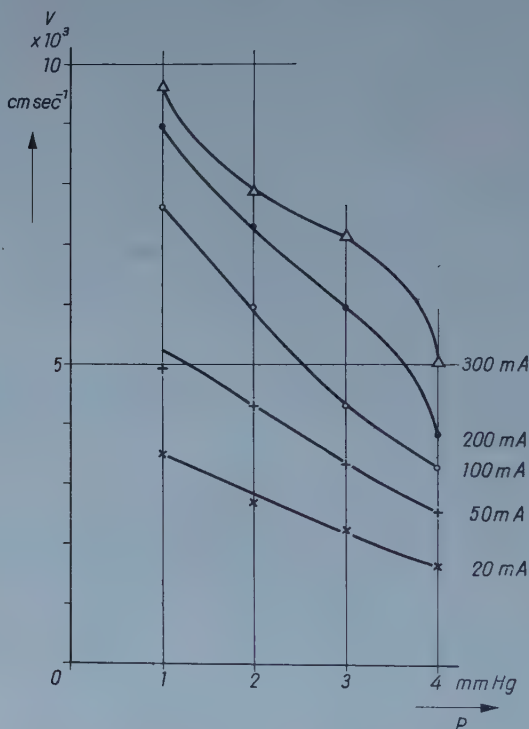


Fig. 7. Dependence of the propagation velocity v of the moving striation on the argon pressure p , at various current intensities i

As the input power transfers mainly into heat, the energy emitted in the form of heat is also nearly proportional to the current intensity. Thus, increasing the current intensity, the temperature difference between the mercury and the water jacket must also increase.

We note that the experiments performed with two different tubes which were of the same geometry, resulted in different velocities v for the moving striations although the same pressure was applied.

REFERENCES

1. W. PUPP, Phys. Z., **34**, 756, 1933.
2. K. WOJACZEK, Acta Phys. Hung., **11**, 35, 1960.
3. G. SZIGETI and J. BITÓ, Acta Phys. Hung., **11**, 103, 1960.
4. J. BITÓ, Magyar Híradástechnika, **11**, 23, 1960.
5. T. DONAHUE and G. H. DIEKE, Phys. Rev., **81**, 248, 1951.
6. L. PEKAREK, Czechosl. J. Phys., **8**, 32, 1958.
7. H. S. ROBERTSON and M. A. HAKEEM, Plasma Phys. Bulletin of Department of Physics. Univ. of Miami, **1—2**, 2, 1960.
8. H. YOSHIMOTO, M. SATO and Y. NAKAO, J. of the Phys. Soc. Jap., **13**, 734, 1958.
9. A. V. NEDOSPASOV, G. I. PANKOVA and V. F. KONAИ, Journ. Techn. Phys., **30**, 125, 1960.
10. J. SZABÓ and G. LAKATOS, Hungarian Patent Nr. 146.209.

О ДВИЖЕНИИ СЛОЕВ В РАЗРЯДНОЙ ТРУБКЕ РТУТНЫХ ПАРОВ
НИЗКОГО ДАВЛЕНИЯ

Г. ЛАКАТОШЫ — Я. БИТО

Резюме

Авторами статьи исследована поступательная скорость движущихся слоев, появляющихся в разрядной трубке ртутных паров низкого давления в случае постоянного тока. Исследованы влияния силы тока и давления аргона, использованного при ртути, на данную скорость. При этом давление ртутных паров было приблизительно постоянным.

КВАНТОВО-МЕХАНИЧЕСКИЙ РАСЧЁТ ПРОТОННОГО СРОДСТВА

Н. А. ИЗМАЙЛОВ и Ю. А. КРУГЛЯК

ХАРЬКОВСКИЙ ГОСУДАРСТВЕННЫЙ УНИВЕРСИТЕТ ИМ. А. М. ГОРЬКОГО, КАФЕДРА ФИЗИЧЕСКОЙ ХИМИИ, ХАРЬКОВ, СОВЕТСКИЙ СОЮЗ

Р. ГАШПАР и ТАМАШШИ-ЛЕНТЕИ

УНИВЕРСИТЕТ ИМ. ЛАЙОША КОШУТА, ИНСТИТУТ ТЕОРЕТИЧЕСКОЙ ФИЗИКИ, ДЕБРЕЦЕН

(Представлено: А. Конья. — Поступило 10. II. 1961.)

Некоторые недостатки электростатической теории образования сольватов могут быть устранены предположением более общего механизма сольватации ионов, рассматривая сольватацию как образование комплексов. Электростатические соображения содержатся в нем в качестве специального случая. Механизм сольватации протона и значение его сольватационной энергии отличаются от соответствующих данных для других ионов. Были проведены вычисления для определения протонного аффинитета молекулы воды и некоторых ионов квантовомеханическим путем, ввиду того, что эти данные имеют большое значение и с точки зрения теории кислотно-базисного взаимодействия, так же как и при оценке кислотности растворов. На основе объединенной атомной модели были определены энергии систем HF , F^- , HO^- , O^- , HO , O^+ , H_2O и H_3O^+ , протонный аффинитет ионов F^- , O^{--} , O^- , HO^- , и молекулы H_2O , также и теплота образования молекулы воды из ионов HO^- и H_3O^+ . Результаты вычислений хорошо согласуются с экспериментальными и литературными данными.

Выяснение природы связей в сольватах является одной из основных проблем теории растворов электролитов. В настоящее время в большей части работ образование сольватов рассматривается с точки зрения электростатической теории [1, 2]. Однако существует ряд экспериментальных фактов и теоретических соображений, которые не могут быть объяснены электростатической теорией.

Н. А. Измайлов [3, 4], используя предложенный им метод экстраполяции, вычислил значения энергий сольватации ряда ионов в таких растворителях, как аммиак, вода, метанол, этанол и муравьиная кислота. Оказалось, что энергия (изменение изобарно-изотермического потенциала) сольватации ΔZ_s^i какого-либо однозарядного иона группы щелочных или галоидных элементов практически не зависит от типа растворителя (в пределах указанной группы растворителей). Этот факт находится в глубоком противоречии с электростатической теорией.

В электростатической теории молекулы и ионы рассматриваются, как сферически симметричные частицы, что является довольно грубым приближением к действительности.

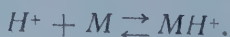
Силы взаимодействия между составляющими сольват частицами можно было бы аппроксимировать мультипольным взаимодействием, если бы расстояния между взаимодействующими частицами значительно превышали бы собственные размеры самих частиц, что не справедливо для растворов.

Выражение для энергии, используемое в электростатической теории, не обеспечивает сходимости на малых расстояниях. Таким образом, электростатическая теория фактически описывает сильно разрыхленные сольваты, в то время как в действительности комплексы, образующиеся при первичной сольватации, имеют довольно плотно упакованную структуру.

Недавно одними из нас [5] был предложен более общий механизм сольватации ионов, включающий как частный случай и электростатические представления. Для объяснения природы связей в сольватах были привлечены представления о донорно-акцепторном взаимодействии. Волновая функция связывающих электронов может быть построена из волновых функций вакантных орбит ионов и электронов таких атомов молекул растворителей, как азот, кислород. Рассмотрение симметрии орбит, принимающих участие в образовании связей, позволяет предсказать структуру образующихся сольватов. Плотная упаковка молекул растворителя в сольватах учитывается естественным образом в теории молекулярных орбит, существенным преимуществом которой является возможность описания как ковалентных, так и ионных связей. Предлагаемый механизм образования связей позволяет удовлетворительно объяснить ряд экспериментальных фактов, относящихся к сольватации ионов.

Развиваемые представления касаются первичной сольватации ионов, тогда как энергия вторичной сольватации, возможно, имеет электростатическую природу.

Сольватация протонов отличается от сольватации остальных ионов как по механизму, так и по величине энергии сольватации. Так например, если энергия сольватации однозарядных ионов составляет 60—130 ккал/г-ион, то для протона энергия гидратации составляет 258 ккал/г-ион [4]. Сольватацию протона можно рассматривать протекающей в три стадии. Сначала образуется ион лиония



Энергетический эффект этой реакции в пустоте называют протонным сродством молекулы растворителя M . Заметим, что протонное сродство следует определять изменением изобарно-изотермического потенциала. Однако из-за отсутствия достаточно надёжных данных по величинам ΔZ и вследствие близости¹ значений ΔZ и ΔH , протонное сродство обычно оценивают изменением энтальпии.

Вторая стадия заключается в присоединении к иону лиония молекул растворителя с образованием «первичной» сольватной оболочки. Затем происходит дальнейшее взаимодействие образовавшегося комплекса с моле-

¹ — см. напр., осылки [3, 4, 5].

кулами растворителя (третья стадия), соответствующая вторичной сольватации всех других ионов. Между второй и третьей стадией невозможно провести такую резкую границу, как между первой и второй.

Присоединение протона к первой молекуле воды происходит за счёт образования координационной связи между вакантной орбитой протона $1s$ и одной из гибридных орбит типа sp^3 атома кислорода молекулы воды. В процессе образования иона гидроксония атом кислорода молекулы воды играет роль донора электронов, при дальнейшей же гидратации образовавшегося иона — акцептора. В этом смысле ион гидроксония похож на ион натрия. Обращает на себя внимание близость энергии гидратации иона гидроксония и натрия [4]. Величины протонного сродства молекулы воды и ионов имеют большое значение и для построения теории кислотно-основного взаимодействия, т. к. основной акт этого процесса состоит в переносе протона от молекулы кислоты к молекуле основания. Степень кислотно-основного взаимодействия зависит в основном от разности протонного сродства аниона кислоты и протонного сродства молекулы основания. Мерой собственной кислотности любой кислоты является протонное сродство соответствующего ей основания.

Как известно, кислотность водных растворов, характеризующаяся величиной pH , определяется активностью гидратированных ионов гидроксония. Н. А. Измайлов [3, 6], обобщая определение величины pH на неводные растворы, предложил относительную кислотность pH_p в пределах одного растворителя оценивать активностью ионов лиония MH^+ данного растворителя M , а именно: $pH_p = -\lg a^*_{MH^+}$, где активность $a^*_{MH^+}$ отнесена к бесконечно разбавленному раствору в данном растворителе.

Сравнение кислотности в различных растворителях, другими словами, приведение шкал pH_p к единому началу отсчёта принципиально отличается от сравнения кислотности в пределах одного растворителя, т. к. в этом случае приходится сравнивать между собой кислотность, созданную различными ионами лиония. Как указал ещё Брэнстэд, единая кислотность растворов однозначно определяется активностью протонов в растворах. Для оценки единой кислотности следует не только определить активность ионов лиония, но и установить относительную активность протонов в различных ионах лиония. По предложению Н. А. Измайлова [6], единая кислотность pA определяется следующим образом: $pA = -\lg a_{H^+} = -\lg a^*_{MH^+} - \lg \gamma_{0H^+} = pH_p - \lg \gamma_{0H^+}$, где активность a_{H^+} и единый нулевой коэффициент активности протонов γ_{0H^+} отнесены к бесконечно разбавленному водному раствору, выбранному в качестве наиболее удобного стандартного состояния. Единый нулевой коэффициент активности γ_{0H^+} определяется изменением изобарно-изотермического потенциала протонов при их переносе из бесконечно разбавленного неводного раствора в бесконечно разбавленный водный раствор. Эта энергия определяется раз-

ностью химических энергий сольватации ΔZ_{XH^+} протонов в воде и в неводном растворителе: $\lg \gamma_{0H^+} = (\Delta Z_{XH^+}^M - \Delta Z_{XH^+}^{H_2O})/2, 3 RT$.

Исходя из указанной недостаточности электростатической схемы сольватации ионов, а тем более протона, любые попытки расчёта энергии сольватации протона на основе электростатической теории (см. напр., ссылку [7]) мы считаем грубо приближенными и не соответствующими действительной природе связи между протоном и молекулой растворителя.

Учитывая важность величин протонного сродства, небезинтересно рассчитать последние квантово-механическим путём. Для определения протонного сродства F^- , O^{--} , O^- и HO^- были использованы результаты расчётов энергии HF , O^- , HO^- , HO , F^- , O^{--} и H_2O , выполненных Р. Гашпаром и И. Тамашши-Лентеи [8] методом объединённого атома. Волновая функция системы строилась по методу Фока—Слэтэра из следующих ортонормированных одноэлектронных волновых функций:

$$\Phi(1s) = (a^3/\pi)^{1/2} \cdot \exp(-a_1),$$

$$\Phi(2s) = [3b^5/\pi(a^2 - ab + b^2)]^{1/2} [1 - r(a + b)/3] \cdot \exp(-br),$$

$$\Phi(2p_x) = (c^5/32\pi)^{1/2} r \cdot \sin \theta \cdot \cos \varphi \exp(-cr/2),$$

$$\Phi(2p_y) = (c^5/32\pi)^{1/2} r \cdot \sin \theta \cdot \sin \varphi \exp(-c'r/2),$$

$$\Phi(2p_z) = (d^5/32\pi)^{1/2} r \cdot \cos \theta \cdot \exp(-dr/2)$$

и из спиновых функций α и β . В вышеприведенных выражениях для Φ r обозначает расстояние от электрона до наиболее тяжелого ядра рассматриваемой частицы. Энергия системы $E = \int \Phi^* H \Psi d\tau$, где оператор Гамильтона² H в случае N центров и n электронов имеет вид:

$$H = -\frac{1}{2} \sum_{i=1}^n \Delta_i - \sum_{\lambda=1}^N \sum_{i=1}^n \frac{Z_{\lambda}}{r_{\lambda i}} + \sum_{i=1}^n \sum_{K=1}^N \frac{1}{r_{iK}} + \sum_{\mu=1}^N \sum_{\lambda=1}^N \frac{Z_{\lambda} Z_{\mu}}{R_{\mu\lambda}}.$$

Z_{λ} — заряд ядра λ . $R_{\mu\lambda}$ и $r_{\lambda i}$ обозначают расстояния между центрами μ и λ и, соответственно, между центром λ и электроном i . a , b , c , c' и d — вариационные параметры. Межъядерное расстояние также было выбрано в качестве вариационного параметра. Так как волновая функция системы строилась из одноцентровых волновых функций, при расчёте энергии необходимо было вычислять только одно- и двухцентровые интегралы. Следует заметить, что используемая модель объединённого атома не отражает направленный характер связей в молекуле воды. Энергия минимальна при валентном угле 180° . Однако, можно ожидать, что учёт конфигурационного

² — в дальнейшем используются атомные единицы Хартри.

взаимодействия улучшит соответствие с экспериментальными данными, в связи с чем энергия молекулы воды была рассчитана при валентных углах 180° , $104^\circ 27'$ и 90° . Вычисленные и полученные из экспериментальных данных (9) значения полной энергии E систем HF , HO^- , HO , F^- , O^{--} , O^- и H_2O представлены в таблице 1.

Из таблицы 1 видно, что соответствие между вычисленными и полученными из экспериментальных данных значениями энергии E вполне удовлетворительное.

Недавно нами [10] этим же методом был рассчитан ион гидроксония. В рассматриваемой здесь форме модель объединённого атома предполагает плоскую структуру иона гидроксония с валентным углом 120° .

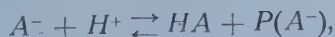
Таблица 1

Вычисленные и полученные из экспериментальных данных [9] значения полной энергии E систем HF , HO , HO^- , F^- , O^- , O^{--} и H_2O . В случае молекулы воды в скобках указаны валентные углы, при которых производился расчёт.

	— E , ат. ед.			— E , ат. ед.	
	выч.	эксп.		выч.	эксп.
HF	99,016	100,489	H_2O	75,113	
F^-	98,468	99,905		(180°)	
HO^-	74,404	75,690		75,031	76,3065
O^{--}	73,422	74,718		($104^\circ 27'$)	
HO	74,658	75,617		74,985	
O^-	74,126	75,043		(90°)	

Результаты расчёта иона гидроксония следующие: $a = 7,7$; $b = 2,6$; $c = 3,8$; $d = 4,3$; $E = -75,412$ (валентный угол 120°); $R_{\text{OH}} = 1,71$; $R_{\text{HH}} = R_{\text{OH}} \sqrt{3}$. Известно, что структура иона гидроксония подобна структуре молекулы аммиака, имеющей валентный угол $106^\circ 46'$. Полная энергия иона гидроксония с валентным углом $106^\circ 46'$ оказывается равной $-75,332$.

Исходя из рассчитанных величин полной энергии E , можно вычислить протонное сродство $P(A^-)$ системы A^- , т. е. энергетический эффект происходящей в пустоте реакции



где $P(A^-) = -E(A^-) + E(\text{HA})$. При расчёте протонного сродства гидроксильного иона и молекулы воды предполагалось, что валентные углы молекулы воды и иона гидроксония равны $104^\circ 27'$ и $106^\circ 46'$, соответственно. В таблице 2 представлены вычисленные по вышеприведённому уравнению

³ — энергии E даны в отрицательной шкале.

значения протонного сродства систем F^- , O^{--} , O^- , HO^- и H_2O , а также результаты расчётов других исследователей.

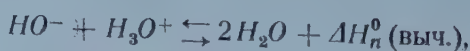
Учитывая, что метод расчёта, основанный на модели объединённого атома, является довольно приближенным, можно считать соответствие между вычисленными и литературными значениями протонного сродства иона F^- и молекулы воды вполне удовлетворительным, не говоря уже о прекрасном соответствии для ионов O^{--} и HO^- . Какие-либо данные по протонному сродству иона O^- нам не известны.

Таблица 2

Вычисленные и имеющиеся в литературе значения протонного сродства систем F^- , O^{--} , O^- , HO^- и H_2O .

		протонное сродство ккал/г-ион	$-P(A^-)$
	по данным авторов	литературные данные	
F^-	343,9	361 [11], 363 [12], 366 [13]	
O^{--}	616,4	615 [12], 612 [14]	
O^-	333,9		
HO^-	393,6	392 [15], 386 [14], 383 [12], 370 [13]	
H_2O	188,9	188,6 [16], 182 [17, 18], 184 [15], 200 [12, 19], 180 [20], 170 [13], 169 [21], 155 ⁴	

Нами была также вычислена теплота реакции образования молекул воды из ионов гидроксония и гидроксила:



где

$$\Delta H_n^0 \text{ (выч.)} = -E(HO^-) - E(H_3O^+) + 2E(H_2O).$$

Подставляя вычисленные значения E , получаем, что $\Delta H_n^0 \text{ (выч.)} = -204,63$ ккал/г-ион.

Теплота реакции нейтрализации в жидкой фазе хорошо известна [22] и составляет $\Delta H_n^{\text{экс}} = -13,7$ ккал/г-ион. Для сравнения экспериментальной величины $\Delta H_n^{\text{экс}}$ с вычисленной $\Delta H_n^0 \text{ (выч.)}$ был произведен пересчёт $\Delta H_n^{\text{экс}}$ в $\Delta H_n^0(\Gamma-B)$ по циклу Габера—Борна, из которого следует, что $\Delta H_n^0(\Gamma-B) = \Delta H_n(H_3O^+) + \Delta H_n(HO^-) + \Delta H_n^{\text{экс}} + 2p$, где $\Delta H_n(H_3O^+) = \Delta H_n(H^+) - P(H_2O)$. Принимая, что $\Delta H_n(H^+) = -265$ ккал/г-ион⁴, $P(H_2O) =$

⁴ — см. ссылку [3], табл. 31.

$= -175$ ккал/г-ион [3], $\Delta H_n(\text{HO}^-) = -122$ ккал/г-ион⁵, $\Delta H_n^{\text{эс}} = -13,7$ ккал/г-ион и «истинная» теплота испарения 1 г-моля воды при 25° $p = 9,899$ ккал/г-ион [23], находим, что $\Delta H_n^0(\text{Г—Б}) = -205,9$ ккал/г-ион. Соответствие между $\Delta H_n^0(\text{Г—Б})$ и вычисленным значением ΔH_n^0 (выч.) более чем удовлетворительное.

Из приведенных выше данных следует, что в пустоте из двух конкурирующих реакций



и



вероятнее вторая. Таким образом, и в этих условиях, как и в растворах, более вероятными являются реакции переноса протонов, а не реакции выделения протонов.

Подводя итоги проведенных вычислений, можно сказать, что метод объединённого атома является подходящим для расчёта таких энергетических характеристик, как протонное сродство и тепловые эффекты некоторых простых реакций.

Выводы

1. Рассмотрены некоторые из существующих недостатков электростатической теории образования сольватов. Предложен более общий механизм сольватации ионов, основанный на представлении о сольватации, как комплексообразовании, и включающий как частный случай электростатические представления.

2. Рассмотрена значимость величин протонного сродства в теории сольватации ионов, в теории кислотно-основного взаимодействия и в оценке кислотности растворов.

3. Изложены основы метода объединённого атома в приложении к гидридам типа XH_n и приведены результаты расчёта энергии E систем HF , F^- , HO^- , O^{--} , HO , O^- , H_2O и H_3O^+ .

4. Исходя из вычисленных значений энергии E вышеприведенных систем, рассчитано протонное сродство ионов F^- , O^{--} , O^- , HO^- и молекулы воды и теплота реакции нейтрализации в пустоте ΔH_n^0 (выч.). Рассчитанные значения протонного сродства и ΔH_n^0 (выч.) удовлетворительно согласуются с экспериментальными и литературными данными.

⁵ — см. ссылку [3], табл. 31.

ЛИТЕРАТУРА

1. К. П. Мищенко, А. М. Сухотин, Журнал физич. химии, **27**, 26, 1953.
2. A. D. BUSKINGHAM, *Discussions Faraday soc.*, **24**, 151, 1957.
3. Н. А. Измайлов, Электрохимия растворов, Издательство Харьковского университета, Харьков, 1959.
4. Н. А. Измайлов, Доклады Акад. Наук СССР, **126**, 1033, 1959.
5. Н. А. Измайлов, Ю. А. Кругляк, Доклады Акад. Наук СССР, **134**, 1390, 1960.
6. Н. А. Измайлов, Доклады Акад. Наук СССР, **127**, 104, 1959.
7. Стефан Минц, Термодинамика и строение растворов (Труды совещания 27—30 января 1958 г.), Изд. АН СССР, М., 1959, стр. 152.
8. R. GÁSPÁR, I. TAMÁSSY-LENTEI, *Ann. d. Phys.* 7. Folge **2**, 208, 1958; *Acta Phys. Hung.*, **10**, 149, 1959.
9. G. HERZBERG, *Molecular Spectra and Molecular Structure. I. Spectra of Diatomic Molecules*, D. van Nostrand Company, Inc., New York, 1953.
10. Р. Гашпар, И. Тамашши-Лентеи, Ю. А. Кругляк, находится в редакции «Журнала структурной химии» АН СССР.
11. C. D. WEST, *J. Phys. Chem.*, **39**, 493, 1935.
12. К. Б. Яцимирский, Термохимия комплексных соединений, Изд. АН СССР, М., 1951.
13. R. JUSA, *Z. allg. anorg. ch.*, **231**, 121, 1937.
14. А. Ф. Капустинский, И. А. Маколкин, Л. И. Кришталек, Журнал физич. химии, **21**, 125, 1947.
15. G. BRIGLEB, *Naturwissenschaft*, **30**, 436, 469, 1942.
16. В. Н. Кондратьев, Н. Д. Соколов, Журнал физич. химии, **29**, 1265, 1955.
17. B. E. CONWAY, *Proc. Roy. Soc., A* **247**, 400, 1958.
18. J. SHERMAN, *Chem. Reviews*, **II**, 93, 1932.
19. О. К. Райс, Электронное строение и химическая связь в неорганической химии, ИИЛ, М., 1949 г., стр. 430.
20. Я. К. Сыркин, М. Е. Дяткина, Химическая связь и строение молекул, Госхимиздат, М.—Л., 1946 г., стр. 138.
21. В. Л. Талрозе, Е. Л. Франкевич, Доклады Акад. Наук СССР, **111**, 376, 1956; *J. Amer. Chem. Soc.*, **80**, 2344, 1958.
22. С. Глестон, Введение в электрохимию, ИИЛ, М., 1951 г., стр. 26—27.
23. *Handbook of Chemistry and Physics*, 37th ed., 1955—1956, p. 2260.

QUANTUM MECHANICAL CALCULATION OF PROTON AFFINITY

By

N. A. ISMAILOV, J. A. KRUGLIAK, R. GÁSPÁR and I. TAMÁSSY-LENTEI

Abstract

Some deficiencies of the electrostatical theory of the formation of solvates can be eliminated by supposing a more general mechanism of the solvation of ions, the solvation being considered as the formation of complexes. This hypothesis comprises as a special case also the electrostatical conception. The mechanism of solvation of the proton and the value of its energy of solvation are different from those of the other ions. Computations based on quantum theory have been effected in order to determine the proton affinity of the water molecule and of some ions since these data are of great importance for the theory of acid-basis interaction, and in estimating the acidity of solutions. On the basis of the united atom model the energy of the systems HF , F^- , HO^- , O^{--} , HO^- , H_2O and H_3O^+ has been determined, as well as the proton affinity of the ions F^- , O^{--} , O^- , HO^- and of the molecule H_2O , and moreover the heat of formation of the water molecule from the ions HO^- and H_3O^+ . The computed values show good agreement with those obtained experimentally resp. from the literature.

DIE BESTIMMUNG DER ELEKTRONENDICHTE DES J-ATOMS AUF GRUND DES STATISTISCHEN ATOMMODELLS

Von

Z. FÜZESSY

PHYSIKALISCHES INSTITUT DER TECHNISCHEN UNIVERSITÄT, BUDAPEST

(Vorgelegt von A. Kónya. — Eingegangen 16. II. 1961)

In der vorliegenden Arbeit wird die Elektronenverteilung des J-Atoms auf Grund des statistischen Atommodells ermittelt. Für die Berechnung der Elektronendichte wird die durch die Weizsäckersche kinetische Energiekorrektur erweiterte statistische Grundgleichung gelöst. Die Elektronenverteilung stimmt mit der für die äusseren Gebiete des Atoms zu erwartenden wellenmechanischen Verteilung überein. Die erhaltenen Resultate werden mit der aus der Thomas-Fermischen Gleichung berechneten Elektronenverteilung verglichen.

Einleitung

Unter den bei der Berechnung atomarer Systeme angewandten Methoden gibt die statistische Behandlungsweise der Atome eines der am leichtesten zu handhabenden Verfahren.

Die ursprüngliche Form der statistischen Behandlungsweise — das Thomas-Fermische Atommodell — näherte wegen seiner Unvollständigkeit die Potential-, bzw. die Dichteverteilung der Elektronen des Atoms nur sehr grob an. Die eingeführten Korrekturen [1], [2] verbesserten den Verlauf der Elektronendichteverteilung in bedeutendem Masse. Die Weizsäckersche kinetische Energiekorrektur, die die Inhomogenität der Dichteverteilung berücksichtigt, kann als eine wichtige Abänderung betrachtet werden. Auch die durch GOMBÁS eingeführte kinetische Energiekorrektur brachte bedeutende positive Ergebnisse [4].

Wir führten unsere Rechnungen für die Bestimmung der Elektronendichte des J-Atoms ohne die GOMBÁSSche Korrektur auf Grund des durch die ursprüngliche Weizsäckersche Korrektur erweiterten Atommodells durch. Wir vernachlässigten die erwähnte Korrektur — um die Rechnungen zu erleichtern — in der Hoffnung, dass sich die Bindung des J_2 -Moleküls auch bei einer in dieser Näherung berechneten Elektronendichte ergibt. Dies bildet den Gegenstand eines nachfolgenden Aufsatzes.

Die Lösung der statistischen Grundgleichung für das J-Atom

Die durch die ursprüngliche Weizsäckersche Korrektur erweiterte statistische Grundgleichung kann in der Form

$$4\kappa_w \Delta\psi - \frac{10}{3} \kappa_0 \psi^{7/3} + \frac{4}{3} \kappa_a \psi^{5/3} + (V - V_0) \psi = 0 \quad (1)$$

geschrieben werden. Der Zusammenhang zwischen ψ und der Elektronendichte ρ wird durch die Gleichung

$$\psi = \rho^{1/2}$$

ausgedrückt, ferner

$$\kappa_w = \frac{1}{8} e^2 a_0; \quad \kappa_0 = \frac{3}{20} (3\pi^2)^{2/3} e^2 a_0; \quad \kappa_a = \frac{3}{4} \left(\frac{3}{\pi}\right)^{1/3} e^2,$$

wo a_0 — der erste Bohrsche Wasserstoffradius und e — die positive Elementarladung ist. Das in der Gleichung (1) auftretende V ist das vom Kern und von den Elektronen herrührende Potential, V_0 ist eine Konstante.

ψ muss der Nebenbedingung

$$\int \psi^2 dv = N \quad (2)$$

genügen, mit deren Hilfe auch die Konstante V_0 bestimmt werden kann. Das in (1) vorkommende elektrostatische Potential V setzt sich — wie bekannt — aus zwei Teilen zusammen: der eine Teil ist das von dem Kern und der andere das von den Elektronen herrührende Potential

$$V_k = \frac{Ze}{r}$$

bzw.

$$V_e = -e \int \frac{\psi^2(r')}{|r - r'|} dv',$$

wo r und r' Ortsvektoren sind. Das Gesamtpotential $V = V_k + V_e$ befriedigt auch die Poisson-Gleichung

$$\Delta V = 4\pi e \psi^2 \quad (3)$$

und somit stehen zur Bestimmung der Elektronendichte zwei Differentialgleichungen zur Verfügung.

Da wir eine kugelsymmetrische Verteilung annehmen, ist es zweckmässig die Bezeichnungen

$$y = r\psi \quad \text{und} \quad U = rV$$

einzuführen. y'' und U'' sollen ferner die zweiten Ableitungen von y und U nach r bedeuten. Mit diesen Bezeichnungen können wir die Gleichungen (1), (3) und die Nebenbedingung (2) in folgender Form schreiben:

$$4\kappa_w y'' - \frac{10}{3} \kappa_0 y^{7/3} \frac{1}{r^{4/3}} + \frac{4}{3} \kappa_a y^{5/3} \frac{1}{r^{2/3}} + U \frac{1}{r} ey - V_0 ey = 0, \quad (4)$$

$$U'' = 4\pi e y^2 \frac{1}{r}, \quad (5)$$

$$4\pi \int_0^\infty y^2 dr = N. \quad (6)$$

Wir führten die Integration des obigen Gleichungssystems wie bereits erwähnt, für das J-Atom auf numerischem Wege durch. Die Integration wurde nicht an der Stelle $r = 0$ angefangen, weil der Verlauf der Kurve $y(r)$ in grosser Entfernung von dem Kern dann nur mit grosser Schwierigkeit bestimmt werden kann; die Integration wurde deshalb bei einem grossen Wert ($r \sim 12a_0$) begonnen und in der Richtung des abnehmenden r bis zum Punkt $r = 0$ weitergeführt. Zu diesem Zwecke war es notwendig festzustellen, durch welche Funktionen y und U , in grosser Entfernung vom Kern dargestellt werden können. Mit Hinsicht darauf, dass im Falle von grossen r , die 2., 3. und 4. Glieder der Gleichung (4) schneller nach Null streben, als das erste und das letzte, lösten wir anstatt (4) die asymptotische Gleichung

$$4\kappa_w y'' - V_0 ey = 0, \quad (7)$$

deren Lösungen

$$y = ae^{-\gamma r} \quad (8)$$

mit

$$\gamma = \left(\frac{V_0 e}{4\kappa_w} \right)^{1/2} \quad (9)$$

sind. a und γ sind hier Konstanten. Diese Konstanten müssen so gewählt werden, dass y an der Stelle $r = 0$ verschwindet, und dass die Nebenbedingung (2) erfüllt ist. Wird γ entsprechend gewählt, so kann von Ne bis X die Grundgleichung (4) an den Stellen $r \geq 12a_0$ praktisch durch (7) ersetzt werden, was auch durch die Lösungen der exakten Gleichung, sowie durch die für mehrere Atome von GOMBÁS auf Grund des statistischen Atommodells ermittelten Werte bewiesen wird. Gemäss der Gleichung (7) verschwindet die Elektronen-

dichte in grosser Entfernung vom Kern exponentiell, dies entspricht den Ergebnissen der Wellenmechanik; weiter wird dies auch durch die Tatsache bewiesen, dass die mit der Dichteverteilung berechneten Atom-, bzw. Molekülkonstanten mit den Erfahrungswerten gut übereinstimmen.

Den Ausdruck für U bestimmen wir in grosser Entfernung von dem Kern durch Anwendung der Gleichung (7).

Auf Grund einfacher elektrostatischer Erwägungen gewinnen wir für $U = rV$ die Gleichung

$$U = \frac{4\pi\gamma^2}{2\gamma} [1 - H(-x)] \quad (10)$$

wo $x = 2\gamma r$, H dagegen mit Hilfe der Reihenentwicklung

$$H(-x) = 0,9999965 - \frac{0,9989710}{x} + \frac{1,9487646}{x^2} - \frac{4,9482092}{x^3} + \\ + \frac{11,7850792}{x^4} - \frac{20,4523840}{x^5} + \frac{21,1491469}{x^6} - \dots$$

ermittelt werden kann.

Die auf diesem Wege bestimmten Werte von γ und U befriedigen unsere Bedingungen in den äusseren Gebieten des Atoms. Mit Hilfe von diesen kann die Integration auf numerischem Wege angefangen werden. Wir ermittelten die in den Gleichungen (7)–(9) vorkommenden Konstanten a und γ durch wiederholtes Probieren und zwar mit den folgenden zwei Nebenbedingungen: 1. die Kurve $y(r)$ soll durch den Anfangspunkt des Koordinatensystems gehen, d. h. an der Stelle $r = 0$ soll $y = 0$ sein, 2. die Nebenbedingung (6) soll erfüllt sein.

Das mit Hilfe unserer Rechnungen ermittelte γ erfüllt gut die erwähnten zwei Bedingungen: die Kurve $y(r)$ schneidet die r -Achse zwischen $r = 0$ und $r = -0,001$ (siehe Tabelle 2) und die Integration des Ausdrucks (6) gibt die Anzahl der Elektronen mit einer Genauigkeit von 99,89%.

Tabelle 1

Die Werte der Parameter a , γ und V_0
 a in $1/a_0^{1/2}$, γ in $1/a_0$ und V_0 in e/a_0 -Einheiten

J	a	γ	V_0
	3,00463	0,65437	0,21410

Die Lösungen der durch die ursprüngliche Weizsäckersche Korrektur erweiterten Gleichung sind in der Tabelle 2 wiedergegeben. Die Werte von a , γ und V_0 sind in der Tabelle 1 zusammengefasst.

In der Abb. 1 wurde die radiale Elektronendichte

$$D = 4\pi r^2 \rho = 4\pi \gamma^2$$

des J-Atoms als Funktion von r aufgezeichnet. Bei der Darstellung der Dichte wählten wir für die Ordinate eine pseudologarithmische Skala, und zwar wurde auf der Ordinatenachse der Wert $\lg(1 + Da_0)$ aufgetragen. Die Zahlen auf der Ordinatenachse bedeuten jedoch die Werte von D . Zum Vergleich führten wir

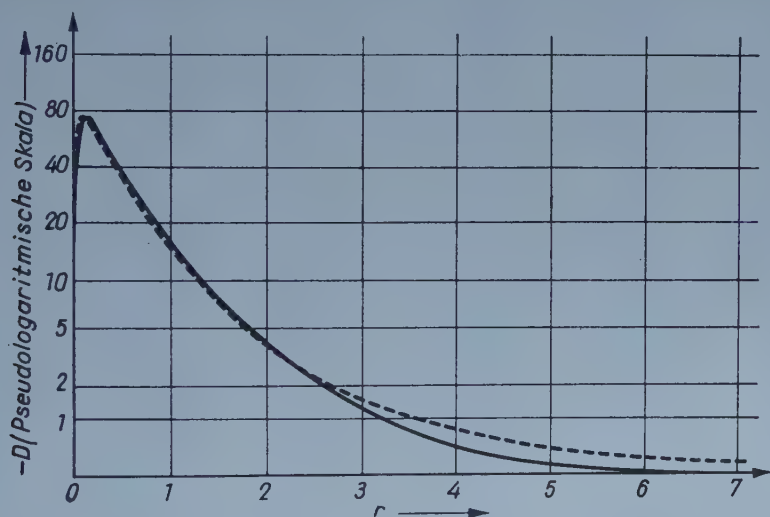


Abb. 1. Die radiale Elektronendichte $D = 4\pi \gamma^2$ für das J-Atom. r in a_0 . D in $1/a_0$ -Einheiten — mit der ursprünglichen Weizsäckerschen Korrektur berechnet, - - - nach der Thomas—Fermi-Grundgleichung

in der Abb. 1 in derselben pseudologarithmischen Skala auch die mit der Thomas-Fermischen Grundgleichung bestimmte Elektronendichte des J-Atoms an. Aus dem Vergleich geht hervor, dass die zwei Kurven im Gebiete zwischen $r = 0$ und $r \sim 2 - 3a_0$ ungefähr den gleichen Verlauf haben, die auf Grund der Thomas-Fermischen Gleichung berechnete Elektronendichte aber im Gebiete $r > 3a_0$ viel grösser ist, als die von uns ermittelte Elektronendichte.

Dieser Unterschied ist in der Abb. 2 besonders auffallend, wo wir die Elektronenverteilung des J-Atoms in den äusseren Gebieten des Atoms vergrößert darstellten. In der Abb. 2 wurden auf die Ordinatenachse die Werte von D aufgetragen.

Tabelle 2

Lösung der Grundgleichung (1) für das J-Atom

Die Funktion $y = r\psi$ und die radiale Dichteverteilung der Elektronen $D = 4\pi r^2 \cdot$
 Die Funktion y in $1/a_0^{1/2}$ - und D in $1/a_0$ - Einheiten.

r	y	D	r	y	D
0,000	0,00000	0,0000	0,348	2,03820	52,1775
0,001	0,22600	0,6415	0,380	1,97356	48,9204
0,002	0,37363	1,7534	0,412	1,91095	45,8657
0,003	0,50534	3,2074	0,444	1,85055	43,0122
0,004	0,62989	4,9833	0,476	1,79245	40,3538
0,005	0,74315	6,9365	0,508	1,73669	37,8821
0,006	0,84659	9,0019	0,540	1,68321	35,5850
0,007	0,94141	11,1313	0,572	1,63196	33,4509
0,008	1,02862	13,2892	0,604	1,58289	31,4696
0,009	1,10906	15,4489	0,636	1,53586	29,6274
0,010	1,18345	17,5909	0,668	1,49083	27,9155
			0,700	1,44770	26,3238
0,012	1,31653	21,7696	0,732	1,40637	24,8421
0,014	1,43193	25,7533	0,764	1,36676	23,4625
0,016	1,53275	29,5075	0,796	1,32877	22,1763
0,018	1,62143	33,0207	0,828	1,29233	20,9767
0,020	1,69989	36,2938	0,860	1,25735	19,8565
			0,892	1,22376	18,8097
0,024	1,83204	42,1560	0,924	1,19150	17,8311
0,028	1,93843	47,1943	0,956	1,16049	16,9151
0,032	2,02529	51,5186	0,988	1,13066	16,0566
0,036	2,09700	55,2315	1,020	1,10196	15,2519
0,040	2,15675	58,4237	1,052	1,07433	14,4965
0,044	2,20688	61,1712	1,084	1,04772	13,7874
0,048	2,24917	63,5382	1,116	1,02208	13,1208
0,052	2,28498	65,5774	1,148	0,99734	12,4933
0,056	2,31537	67,3334	1,180	0,97349	11,9029
0,060	2,34119	68,8435	1,212	0,95047	11,3466
			1,244	0,92823	10,8218
0,068	2,38175	71,2495	1,276	0,90675	10,3268
0,076	2,41068	72,9909			
0,084	2,43074	74,2108	1,340	0,86589	9,4170
0,092	2,44393	75,0182	1,404	0,82764	8,6034
0,100	2,45166	75,4936	1,468	0,79176	7,8737
0,108	2,45503	75,7013	1,532	0,75806	7,2177
0,116	2,45485	75,6902	1,596	0,72632	6,6259
0,124	2,45177	75,5004	1,660	0,69640	6,0913
			1,724	0,66814	5,6069
0,140	2,43886	74,7073	1,788	0,64140	5,1671
0,156	2,41925	73,5108	1,852	0,61607	4,7670
0,172	2,39491	72,0390	1,916	0,59206	4,4028
0,188	2,36727	70,3859	1,980	0,56923	4,0697
0,204	2,33730	68,6149	2,044	0,54752	3,7652
0,220	2,30571	66,7727	2,108	0,52684	3,4862
0,236	2,27303	64,8934			
0,252	2,23967	63,0025	2,236	0,48829	2,9946
0,268	2,20594	61,1191	2,364	0,45309	2,5784
0,284	2,17207	59,2567	2,492	0,42082	2,2242
0,300	2,13824	57,4252	2,620	0,39114	1,9216
0,316	2,10459	55,6320	2,748	0,36375	1,6618

r	y	D	r	y	D
2,876	0,33839	1,4382	7,484	0,021688	0,005908
3,004	0,31489	1,2454	7,740	0,018433	0,004268
3,132	0,29306	1,0787	7,996	0,015658	0,003079
			8,252	0,013294	0,002220
3,388	0,25383	0,8092	8,508	0,011282	0,001599
3,644	0,21976	0,6066	8,764	0,0095703	0,001150
3,900	0,19007	0,4538	9,020	0,0081157	0,0008273
4,156	0,16419	0,3386	9,276	0,0068799	0,0005945
4,412	0,14165	0,2520	9,532	0,0058306	0,0004270
4,668	0,12201	0,1870	9,788	0,0049400	0,0003065
4,924	0,10494	0,1383	10,044	0,0041844	0,0002199
5,180	0,090114	0,1020	10,300	0,0035435	0,0001577
5,436	0,077275	0,07500	10,556	0,0030001	0,0001130
5,692	0,066175	0,05500	10,812	0,0025395	0,00008100
5,948	0,056597	0,04023	11,068	0,0021490	0,00005800
6,204	0,048350	0,02936	11,324	0,0018182	0,00004152
6,460	0,041260	0,02138	11,580	0,0015377	0,00002970
6,716	0,035175	0,01554	11,836	0,0013006	0,00002125
6,972	0,029961	0,01127	12,092	0,0010999	0,00001519
7,228	0,025500	0,008167	12,348	0,0009303	0,00001087

Unseres Wissens sind aus der Literatur die Verteilung der Elektronendichte des J-Atoms und die damit zusammenhängenden Rechnungen nicht bekannt, deshalb können wir die Richtigkeit unseres Ergebnisses vorderhand nur

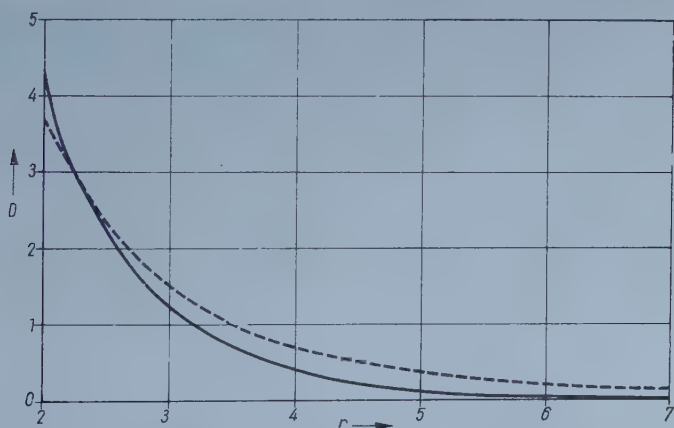


Abb. 2. Die radiale Dichteverteilung der Elektronen $D = 4\pi y^2$ in den äusseren Gebieten des J-Atoms. r in a_0 -, D in $1/a_0$ -Einheiten. — mit der ursprünglichen Weizsäckerschen Korrektur berechnet, - - - - nach der Thomas—Fermi-Gleichung

durch qualitative Schätzungen bestätigen. Eine Frage, wie gute Näherung der wirklichen Elektronendichte die auf Grund des obenerwähnten Atommodells berechnete Elektronendichte darstellt, kann natürlich nur auf Grund der Übereinstimmung der mit ihr berechneten Atom- bzw. Molekülkonstanten mit

den Erfahrungswerten bestimmt werden. Wir können aber schon jetzt soviel feststellen, dass der Dichteverlauf in qualitativer Hinsicht befriedigend ist.

Ich möchte Herrn Prof. P. GOMBÁS an dieser Stelle meinen besten Dank für seine Hilfe und für seine nützlichen Unterweisungen ausdrücken.

Weiterhin danke ich Frl. E. MÁGORI und Frl. O. KUNVÁRI für ihre Hilfe bei den numerischen Rechnungen.

LITERATUR

1. P. GOMBÁS, Die statistische Theorie des Atoms und ihre Anwendungen, Springer, Wien, 1949.
2. П. Гомбаш, Проблемы современной физики, **1**, 72, 1958.
3. P. GOMBÁS, Acta Phys. Hung., **5**, 483, 1956.
4. P. GOMBÁS, Magyar Fizikai Folyóirat, **II**, 63, 1954.
5. Handbuch der Physik XXXVI, Springer, Berlin—Göttingen—Heidelberg, 1956.

ОПРЕДЕЛЕНИЕ ПЛОТНОСТИ ЭЛЕКТРОНОВ АТОМА J НА ОСНОВЕ СТАТИСТИЧЕСКОЙ ТЕОРИИ АТОМА

З. ФЮЗЕШИ

Резюме

В работе определяется распределение электронов атома J на основе статистической теории атома. Плотность электронов получается решением основного уравнения статистической теории, расширенного коррекцией Вайцзеккера к кинетической энергии. Распределение плотности электронов качественно согласуется с квантово-механическим, предполагаемым для внешней области атома. Результаты сравниваются с плотностью, полученной по уравнению Томаса—Ферми.

ÜBER DIE REIHENFOLGE DER BESETZUNG DER QUANTENZUSTÄNDE IN ATOMEN

Von

A. KÓNYA

FORSCHUNGSGRUPPE FÜR THEORETISCHE PHYSIK
DER UNGARISCHEN AKADEMIE DER WISSENSCHAFTEN, BUDAPEST

(Eingegangen 4. V. 1961)

Aus der statistischen Theorie des Atoms kann man die Mittelwerte des Drehimpulsquadrats der Elektronen, des absoluten Betrags des Drehimpulsvektors und des absoluten Betrags der Komponente dieses Vektors in einer Achsenrichtung als Funktionen der Ordnungszahl bestimmen. Es ist auch möglich, aus dem wellenmechanischen Schalenmodell für dieselben Mittelwerte asymptotische Formeln herzuleiten. In diesen Formeln werden die Koeffizienten von der Reihenfolge abhängig sein, die wir für die Besetzung der Eielektronquantenzustände der Atome annehmen. Aus dem Vergleich der Ergebnisse gelangt man zu der Folgerung, dass das Thomas-Fermische statistische Atommodell die verspätete Besetzung der Quantenzustände mit höheren Nebenquantenzahlen richtig wiedergibt.

Eines der frühesten unter den vielseitigen Anwendungen der statistischen Theorie des Atoms war — von FERMI [1] ausgearbeitet — die Behandlung der Elektronengruppen mit verschiedenen Nebenquantenzahlen im periodischen System der Elemente und auf dieser Grundlage die Erklärung der Anomalien in der Besetzung der Eielektronquantenzustände.

JENSEN und LUTTINGER [2] haben darauf hingewiesen, dass die Gruppierung der Elektronen des statistischen Modells nach der Nebenquantenzahl und besonders die Bestimmung der Ordnungszahlen, bei welchen s -, p -, d -, f -, ... — Elektronen erstmalig auftreten, nach der Methode von FERMI mit einer gewissen Willkür behaftet sind, da die Drehimpulse der Elektronen im statistischen Modell nicht diskrete quantisierte Werte aufnehmen, sondern sich kontinuierlich ändern. Nach ihrer Meinung ist es dem Charakter der statistischen Behandlungsweise mehr angemessen, wenn man nur durch das statistische Modell eindeutig bestimmte Mittelwerte — wie z. B. das mittlere Drehimpulsquadrat — berechnet und diese mit den entsprechenden Grössen des quantenmechanischen Schalenmodells vergleicht.

Später hat THEIS in einer Arbeit [3] gezeigt, dass es möglich ist, die Gruppierung der Elektronen nach der Nebenquantenzahl ganz ohne Willkür eindeutig zu begründen. Aus seinen Ergebnissen folgt auch, dass — innerhalb der Grenzen der Genauigkeit, die man von diesem Modell sinngemäss fordern kann — auch die verspätete Besetzung der Quantenzustände mit höheren Nebenquantenzahlen durch das statistische Atommodell gut erfasst wird. Zu demselben Ergebnis sind IVANENKO und LARIN [4] auf einem anderen Wege

für das erste Auftreten der Elektronen mit verschiedenen Nebenquantenzahlen gekommen.

Unser Ziel ist zu zeigen, dass es

1. auf Grund der statistischen Mittelwerte, wie sie von JENSEN und LUTTINGER vorgeschlagen wurden, auch möglich ist, auf die Reihenfolge der Besetzung der Quantenzustände des Atoms zu schliessen — ohne jede Einteilung der Elektronen in Gruppen und dass

2. diese Reihenfolge der Besetzung für grosse Ordnungszahlen der anomalen Besetzung bedeutend näher kommt als der Reihenfolge der regelmässigen Besetzung, welche der Reihenfolge der wasserstoffähnlichen Terme entspricht.

I. Berechnung der Mittelwerte mit dem statistischen Atommodell

Um mehrere Vergleiche zu ermöglichen, wollen wir folgende Mittelwerte bestimmen

den Mittelwert des Drehimpulsquadrats $\langle L^2 \rangle$,

den Mittelwert des Betrags des Drehimpulsvektors $\langle L \rangle$ und den Mittelwert des absoluten Betrags der Drehimpulskomponente L_z in der Richtung der z -Achse (magnetische Quantenzahl) $\langle |L_z| \rangle$.

Die ersten zwei Mittelwerte können wir nach den Ergebnissen von FERMI und JENSEN—LUTTINGER sofort aufschreiben. Die Zahl der Elektronen, welche einen Drehimpulsbetrag zwischen L und $L + dL$ haben, ist nämlich nach FERMI

$$n(L) dL = \frac{4}{\pi} L dL \int_{L \leq Pr} (P^2 r^2 - L^2)^{1/2} \frac{dr}{r}, \quad (1)$$

wo

$$P = (3\pi^2)^{1/3} \varrho^{1/3} \text{ at. Einh.} \quad (2)$$

und $\varrho = \varrho(r)$ die Elektronendichte des statistischen Atommodells ist. Zu integrieren ist in Gl. (1) im Bereich, wo $P^2 r^2 - L^2 \geq 0$ ist.

Eine charakteristische Eigenschaft der Verteilungsfunktion $n(L)$ ist, dass sie nur in dem endlichen Intervall $0 \leq L \leq L_{\max}$ von Null verschieden ist, wo

$$L_{\max} = (Pr)_{\max}$$

und $(Pr)_{\max}$ das Maximum von Pr im Atomvolumen bedeuten.

Mit Hilfe der Gl. (1) bekommen wir nach JENSEN—LUTTINGER

$$\langle L^2 \rangle = \frac{1}{Z} \int_0^{L_{\max}} L^2 n(L) dL = \frac{8}{15\pi Z} \int_0^\infty \frac{dr}{r} (Pr)^5. \quad (3)$$

Ganz ähnlich ergibt sich der Wert für $\langle L \rangle$:

$$\langle L \rangle = \frac{1}{Z} \int_0^{L_{\max}} L n(L) dL = \frac{1}{4Z} \int_0^{\infty} \frac{dr}{r} (Pr)^4. \quad (4)$$

Mit der Bestimmung von $\langle |L_z| \rangle$ müssen wir uns ausführlich beschäftigen. Vor allem wollen wir die Definition der magnetischen Quantenzahl im statistischen Atommodell geben und weiterhin die Verteilungsfunktion $p(L_z)$ der Elektronen im Wertebereich der Drehimpulskomponente L_z herleiten.

Die magnetische Quantenzahl können wir in die statistische Theorie des Atoms auf dieselbe Weise einführen, in der FERMI die Nebenquantenzahl definiert hat. Betrachten wir die Komponente des Drehimpulsvektors in der Richtung der z -Achse, die wir mit L_z bezeichnen wollen. Da im statistischen Modell der Wert von L sich kontinuierlich ändert und der Drehimpulsvektor mit der z -Achse einen beliebigen Winkel einschliessen kann, ändert sich der Wert der Komponente L_z auch kontinuierlich.

Die Elektronen mit kontinuierlich veränderlichen L_z -Werten lassen sich in Gruppen einteilen, wenn wir gewisse L_z -Intervalle definieren. Damit ist es dann möglich, den einzelnen Elektronengruppen die diskreten magnetischen Quantenzahlwerte der Quantenmechanik zuzuordnen. (Mit dem Problem der Gruppierung der Elektronen nach der magnetischen Quantenzahl wollen wir uns in einer späteren Arbeit ausführlich beschäftigen. Da wir jetzt nur Mittelwerte berechnen wollen, werden wir diese Gruppierung hier nicht benutzen.)

Im folgenden bezeichnen wir mit $p(L_z) dL_z$ die Zahl der Elektronen im Atom, die einen L_z -Wert zwischen L_z und $L_z + dL_z$ haben. Wir können die Verteilungsfunktion $p(L_z)$ folgendermassen mit Hilfe der in (1) gegebenen Funktion $n(L)$ bestimmen.

Betrachten wir die aus $n(L) dL$ Elektronen bestehende Gruppe, bei welcher alle Drehimpulse einen Betrag zwischen L und $L + dL$ haben. Die L_z -Komponenten dieser Elektronen liegen alle zwischen $+L$ und $-L$ und zwar gleichmässig verteilt zwischen den beiden Grenzwerten (Fig. 1), weil die Elektronenverteilung des statistischen Atommodells sowohl im Koordinatenraum wie im Impulsraum [5] kugelsymmetrisch ist.

Wählen wir nun ein Intervall der L_z -Komponente zwischen L_z und $L_z + dL_z$ ($0 \leq L_z \leq L$). Von den $n(L) dL$ Elektronen werden $\frac{dL_z}{2L} n(L) dL$ eine Komponente zwischen L_z und $L_z + dL_z$ haben. Zur Anzahl $p(L_z) dL_z$ der Elektronen liefert jede Elektronengruppe $n(L) dL$ einen Beitrag, für welche $L \geq L_z$ ist. So erhält man den einfachen Zusammenhang

$$p(L_z) = \frac{1}{2} \int_{L_z}^{L_{\max}} \frac{dL}{L} n(L) dL, \quad (5)$$

wenn $L_z \geq 0$ ist und aus Symmetriegründen

$$p(-L_z) = p(L_z). \quad (6)$$

Wir haben also die Funktion $p(L_z)$ — wenn wir noch $n(L)$ gemäss (1) einsetzen — durch ein Doppelintegral dargestellt. Die Integration nach L können wir auf elementarem Wege durchführen. So bekommen wir für die Verteilungsfunktion $p(L_z)$ folgende Grundformel: für positive L_z -Werte ist

$$p(L_z) = \frac{1}{2\pi} \int_{L_z \leq Pr} (Pr)^2 \left(\pi - 2 \arcsin \frac{L_z}{Pr} \right) \frac{dr}{r} - \frac{1}{4} n(L_z). \quad (7)$$

Auf Grund der Gln. (6)–(7) wäre es möglich, den Mittelwert der L_z -Komponente zu berechnen. Hierzu ist aber noch folgendes zu beachten. Wie

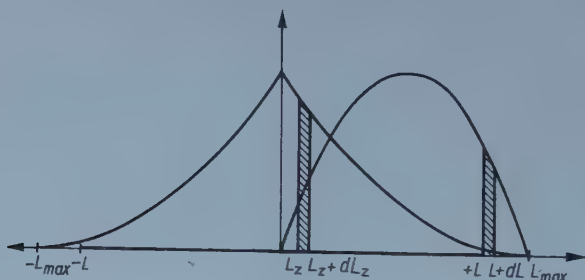


Fig. 1

aus Gl. (6) ersichtlich ist, ist die Funktion $p(L_z)$ eine gerade Funktion der Veränderlichen L_z . Demzufolge ist für jede Ordnungszahl stets

$$\int_{-L_{\max}}^{+L_{\max}} L_z p(L_z) dL_z = 0.$$

In dieser Relation spiegelt sich die Eigenschaft des statistischen Modells, dass im Falle des Auftretens eines Drehimpulsbetrags L gleichzeitig auch alle Komponentenwerte zwischen $+L$ und $-L$ auftreten und zwar mit gleichmässiger Verteilung, so dass ihr Mittelwert gleich Null ist. Bei dem Schalenmodell der Quantenmechanik gilt eine solche Relation im allgemeinen nur im Falle vollständig besetzter Unterschalen. Diese Eigenschaft des statistischen Atommodells rührt daher, dass der Drehimpulsvektor keinerlei Richtungsquantelung unterworfen ist.

Eine Grösse, welche für beide Modelle definierbar und wenigstens im Falle vollbesetzter Unterschalen eindeutig vergleichbar ist, wird also nur der

Mittelwert des absoluten Betrags der L_z -Komponenten bzw. der magnetischen Quantenzahlen sein. Wir definieren diese Grösse in Anbetracht auf (6) folgendermassen:

$$\langle |L_z| \rangle = \frac{2}{Z} \int_0^{L_{\max}} L_z p(L_z) dL_z. \quad (8)$$

Wenn wir hier $p(L_z)$ gemäss (7) einsetzen, ergibt sich nach der Integration nach L_z

$$\langle |L_z| \rangle = \frac{1}{8Z} \int_0^{\infty} \frac{dr}{r} (Pr)^4, \quad (9)$$

also mit (4) verglichen

$$\langle |L_z| \rangle = \frac{1}{2} \langle L \rangle. \quad (10)$$

Die Elektronendichte des Thomas-Fermischen Atommodells im Falle von neutralen Atomen gibt uns den Ausdruck [6]

$$\varrho = \frac{Z}{4\pi\mu^3} \left(\frac{\varphi_0}{x} \right)^{3,2}, \quad (11)$$

wo

$$x = \frac{r}{\mu}, \quad \mu = \frac{1}{4} \left(\frac{9\pi^2}{2Z} \right)^{1/3} \text{ at. Einh.}, \quad (12)$$

φ_0 die Lösung der Thomas-Fermischen Differentialgleichung für neutrale Atome und Z die Ordnungszahl bedeuten. Mit Rücksicht auf Gl. (2) erhalten wir aus Gl. (3)

$$\langle L^2 \rangle = \frac{2}{5} \left(\frac{3\pi}{4} \right)^{2/3} Z^{2/3} \int_0^{\infty} \frac{dx}{x} (x\varphi_0)^{5,2} = 0,262 Z^{2/3}, \quad (13)$$

ähnlich wie in [2], aus Gl. (4)

$$\langle L \rangle = \frac{1}{4} \left(\frac{3\pi}{4} \right)^{4/3} Z^{1/3} \int_0^{\infty} \frac{dx}{x} (x\varphi_0)^2 = 0,468 Z^{1/3}, \quad (14)$$

und aus Gl. (9) bzw. (10)

$$\langle |L_z| \rangle = 0,234 Z^{1/3}. \quad (15)$$

Für die Integrale in Gl. (13) und (14) erhalten wir nämlich durch numerische Integration

$$\int_0^{\infty} \frac{dx}{x} (x \varphi_0)^{5/2} = 0,370 \quad \text{und} \quad \int_0^{\infty} \frac{dx}{x} (x \varphi_0)^2 = 0,596. \quad (16)$$

Wie die Fig. 2 zeigt, geben die Zusammenhänge (13), (14) und (15) durchschnittlich eine sehr gute Näherung der entsprechenden Grössen des

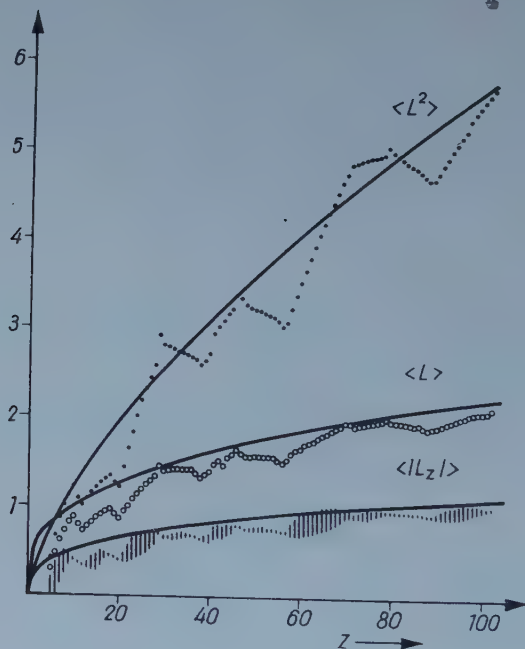


Fig. 2

Schalenmodells, welche wir aus der Elektronenkonfiguration der Grundzustände der Atome berechnet haben. Für kleine Ordnungszahlen liegen die berechneten Kurven höher als die empirischen Werte, mit wachsender Ordnungszahl nimmt aber die Differenz ab.

II. Berechnung der Mittelwerte mit dem Schalenmodell

Charakteristisch für die Mittelwerte (13), (14) und (15) des statistischen Atommodells sind der Exponent der Ordnungszahl und der Koeffizient dieser Potenz. Unsere Ergebnisse können wir — ausser in der in der Fig. 2 dargestellten Weise — mit den entsprechenden Grössen des Schalenmodells auch dadurch

vergleichen, dass wir diese Grössen als Funktionen der Ordnungszahl bestimmen. Das Resultat dieser Rechnung wird natürlich davon abhängig sein, was für eine Elektronenkonfiguration wir für den Grundzustand der Atome annehmen. Im folgenden wollen wir die Rechnungen für zwei Fälle durchführen: für die vollständig regelmässige Besetzung der Zustände der Atome und für eine Besetzung, welche eine triviale Verallgemeinerung der anomalen Besetzung der Stoner-Tabelle ist.

Prinzipiell gibt das statistische Atommodell eine gute Näherung für grosse Ordnungszahlwerte und für edelgasähnliche Atome mit vollständig besetzten Unterschalen. Wir werden daher im folgenden asymptotische Formeln für die Mittelwerte von Atomen mit ähnlicher Elektronenkonfiguration herleiten.'

1. *Fall der vollständig regelmässigen Besetzung.* Nehmen wir jetzt an, dass die Elektronen die Eielektronquantenzustände der Atome streng in der Reihenfolge der wasserstoffähnlichen Terme, also in der Reihenfolge

$$1s; 2s, 2p; 3s, 3p, 3d; 4s, 4p, 4d; 4f; 5s, 5p, 5d, 5f, 5g; \dots \quad (17)$$

besetzen. Die sukzessive Besetzung geschieht also nach unserer jetzigen Annahme in der Reihenfolge der zunehmenden Hauptquantenzahlen und innerhalb einer Hauptquantenzahl in der Reihenfolge der zunehmenden Nebenquantenzahlen.

Wir wollen nun die Mittelwerte für solche Ordnungszahlwerte berechnen, bei welchen die Besetzung einer Elektronenschale eben beendet ist. Aus dem Pauli-Prinzip und aus den möglichen Werten der Quantenzahlen folgt, dass bei solchen Atomen die Ordnungszahl Z und die grösste Hauptquantenzahl N , welche zu der äussersten, noch besetzten Elektronenschale gehört, der Relation

$$\sum_{n=1}^N 2n^2 = Z \quad (18)$$

genügen. Durch Aufsummieren bekommt man daraus

$$\frac{N(N+1)(2N+1)}{3} = Z. \quad (19)$$

In einem Atom mit der angenommenen Elektronenkonfiguration befinden sich in einer Unterschale $2(2l+1)$ Elektronen mit der Nebenquantenzahl l . Jedes dieser Elektronen hat das Drehimpulsquadrat $l(l+1)$, den Drehimpulsbetrag $[l(l+1)]^{1/2}$, während der absolute Betrag ihrer magnetischen

Quantenzahlen die Werte $0, 1, 2, \dots, l$ annimmt. Es ist also für eine Unterschale mit der Nebenquantenzahl l

$$\Sigma L^2 = 2(2l + 1) l(l + 1), \quad (20)$$

$$\Sigma L = 2(2l + 1) [l(l + 1)]^{1/2} \cong 2(2l + 1) l, \quad (21)$$

$$\Sigma |m| = 4(1 + 2 + \dots + l) = 2l(l + 1). \quad (22)$$

Die in (21) angewandte Näherung ist anscheinend zu grob. Da wir aber bei dem Übergang zu den asymptotischen Formeln nur die höchste Potenz der in (21) stehenden Grösse behalten, ist der hier begangene Fehler ganz belanglos.

Wenn wir eine Elektronenschale mit der Hauptquantenzahl n betrachten, gewinnen wir die Summe der Grössen (20), (21) bzw. (22) durch eine Summierung über l von $l = 0$ bis $l = n - 1$.

Für ein Atom mit der Ordnungszahl Z , bei welchem die äusserste vollbesetzte Elektronenschale die Hauptquantenzahl N hat, müssen wir über n von $n = 1$ bis $n = N$ nochmals summieren. Zu den gesuchten Mittelwerten gelangen wir, wenn wir die so gewonnenen Summenwerte durch Z dividieren. Es ist also

$$\langle L^2 \rangle = \frac{2}{Z} \sum_{n=1}^N \sum_{l=0}^{n-1} l(l + 1) (2l + 1), \quad (23)$$

$$\langle L \rangle = \frac{2}{Z} \sum_{n=1}^N \sum_{l=0}^{n-1} l(2l + 1), \quad (24)$$

$$\langle |m| \rangle = \frac{2}{Z} \sum_{n=1}^N \sum_{l=0}^{n-1} l(l + 1). \quad (25)$$

Wir können alle hier auftretende Doppelsummen auf einfache Form bringen. Nach Einsetzen von Z gemäss Gl. (19) bekommen wir folgende Ausdrücke für die Mittelwerte ausgedrückt mittels der höchsten Hauptquantenzahl N :

$$\langle L^2 \rangle \cong \frac{3}{10} (N^2 + N - 2), \quad (26)$$

$$\langle L \rangle = \frac{N^2 - 1}{2N + 1}, \quad (27)$$

$$\langle |m| \rangle = \frac{1}{2} \frac{N^2 + N - 2}{2N + 1}. \quad (28)$$

Nehmen wir an, dass Z — gleichzeitig mit N — sehr gross ist. Dann folgt aus Gl. (19)

$$N \cong \left(\frac{3}{2} \right)^{1/3} Z^{1/3}, \quad (29)$$

wodurch

$$\langle L^2 \rangle \cong \frac{3}{10} N^2 \cong 0,393 Z^{2/3}, \quad (30)$$

$$\langle L \rangle \cong \frac{1}{2} N \cong 0,572 Z^{1/3}, \quad (31)$$

$$\langle m \rangle \cong \frac{1}{4} N \cong 0,286 Z^{1/3} = \frac{1}{2} \langle L \rangle. \quad (32)$$

wird.

2. *Fall der anomalen Besetzung.* Die empirischen Ergebnisse betreffs der Besetzung der Eielektronquantenzustände im periodischen System sind in der Stoner-Tabelle zusammengefasst. Hiernach werden die Terme nicht in der regelmässigen Folge von (17) besetzt, sondern nach dem Schema

$$1s; 2s, 2p; 3s, 3p; 4s, 3d, 4p; 5s, 4d, 5p; 6s, 4f, 5d, 6p; 7s, 5f, 6d, 7p; \dots \quad (33)$$

Wir wollen nun die Mittelwerte auf Grund dieser anomalen Besetzung berechnen. Wir verallgemeinern das Schema in (33) folgendermassen. Bei dem Auftreten der Hauptquantenzahl n kommen die ns - und np -Zustände gleichzeitig zur Besetzung, dann die d -Zustände der vorletzten, die f -Zustände der vorvorletzten Schale usw. Das verallgemeinerte Schema für die Besetzung der Zustände ist also folgendes:

Hauptquantenzahl	Nebenquantenzahl	
n	$l = 0$	s
n	$l = 1$	p
$n - 1$	$l = 2$	d
$n - 2$	$l = 3$	f
.	.	.
.	.	.
.	.	.
$n - l + 1$	l	.
.	.	.
.	.	.
.	.	.
$n - x + 1$	x	.

Für gegebenes n geht diese Folge bis zu dem Nebenquantenzahlwert x , für welchen

$$x = (n - x + 1) - 1$$

ist, woraus

$$x = \frac{n}{2} \quad (34)$$

folgt. Wenn n eine ungerade Zahl ist, müssen wir den ganzen Teil von $\frac{n}{2}$ nehmen, den wir — wie üblich — mit $\left[\frac{n}{2}\right]$ bezeichnen.

Bei einem Atom mit edelgasähnlicher Elektronenkonfiguration gibt also das Auftreten der neuen Hauptquantenzahl n eine Möglichkeit für die Besetzung von nur $\left[\frac{n}{2}\right]$ Unterschalen und nicht für die Besetzung von $n-1$ Unterschalen, wie wir es früher aus (17) gefolgert haben. Nach der Besetzung dieser $\left[\frac{n}{2}\right]$ Unterschalen gelangen wir wieder zu einem edelgasähnlichen Atom in dem periodischen System der Elemente.

Da in einer Unterschale mit der Nebenquantenzahl l wieder $2(2l+1)$ Elektronen Platz finden können, werden sich nach unserer jetzigen Annahme mit dem Auftreten der Hauptquantenzahl n insgesamt

$$2 \sum_{l=0}^{\left[\frac{n}{2}\right]} (2l+1)$$

Elektronen einbauen. (Dieser Ausdruck gibt uns die Differenz der Ordnungszahlen zweier benachbarter edelgasähnlicher Atome, und zwar der Reihe nach 2, 8, 8, 18, 18, 32, 32, 50, 50, ...).

Nehmen wir jetzt das edelgasähnliche Atom mit der Ordnungszahl Z , bei welchem die grösste Hauptquantenzahl N ist. Wir bekommen jetzt statt (18) den Zusammenhang

$$2 \sum_{n=1}^N \sum_{l=0}^{\left[\frac{n}{2}\right]} (2l+1) = Z. \quad (35)$$

Wir wollen wieder nur asymptotische Formeln herleiten, und dabei ist die Unterscheidung zwischen geraden und ungeraden n -Werten überflüssig. Wir werden also im folgenden die Rechnungen statt mit $\left[\frac{n}{2}\right]$ nur mit $\frac{n}{2}$ weiterführen.

Durch Aufsummieren von (35) ergibt sich der Ausdruck

$$N(N+1)(2N+13) + 12N = 12Z, \quad (36)$$

und daraus

$$N \cong 6^{1/3} Z^{1/3}. \quad (37)$$

Die Mittelwerte können wir mit derselben Methode durch Summieren berechnen wie im Falle der regelmässigen Besetzung. Der einzige Unterschied

ist der, dass das Summieren über l jetzt von $l = 0$ nur bis $l = \frac{n}{2}$ auszudehnen ist. Es ist also

$$\langle L^2 \rangle = \frac{2}{Z} \sum_{n=1}^N \sum_{l=0}^{\frac{n}{2}} l(l+1)(2l+1), \quad (38)$$

$$\langle L \rangle = \frac{2}{Z} \sum_{n=1}^N \sum_{l=0}^{\frac{n}{2}} l(2l+1), \quad (39)$$

$$\langle |m| \rangle = \frac{2}{Z} \sum_{n=1}^N \sum_{l=0}^{\frac{n}{2}} l(l+1). \quad (40)$$

Die Doppelsummen können wir wieder elementar ausdrücken, wodurch wir die Formeln

$$\langle L^2 \rangle = \frac{1}{480 Z} N(N+1)(6N^3 + 61N^2 + 261N + 239), \quad (41)$$

$$\langle L \rangle = \frac{1}{24 Z} N(N+1)(N^2 + 7N + 13), \quad (42)$$

$$\langle |m| \rangle = \frac{1}{48 Z} N(N+1)(N^2 + 9N + 20) \quad (43)$$

erhalten. Wenn wir noch Z aus Gl. (36) einsetzen, erhalten wir mit Hilfe von Gl. (37) sofort die asymptotischen Formeln

$$\langle L^2 \rangle \cong \frac{3}{40} N^2 \cong 0,248 Z^2{}^3, \quad (44)$$

$$\langle L \rangle \cong \frac{1}{4} N \cong 0,454 Z^{1/3}, \quad (45)$$

$$\langle |m| \rangle \cong \frac{1}{8} N \cong 0,228 Z^{1/3} = \frac{1}{2} \langle L \rangle. \quad (46)$$

III. Diskussion

Die Resultate (13), (14) und (15) aus der statistischen Theorie des Atoms wollen wir jetzt mit den Ausdrücken (30), (31) und (32) bzw. (44), (45) und (46) vergleichen.

Man sieht, dass die Abhängigkeit von der Ordnungszahl in allen Fällen die gleiche ist, ein Unterschied tritt nur zwischen den Werten der Koeffizienten, welche wir in der Tabelle I zusammengestellt haben, auf.

Tabelle 1

		$\langle L^2 \rangle / Z^{1,3}$		$\langle L \rangle / Z^{1,3}$		$\langle m \rangle / Z^{1,3}$	
Thomas—Fermisches Modell		0,262		0,468		0,234	
Schalenmodell	regelmässige Besetzung	0,393	50%	0,572	22%	0,286	22%
	anomale Besetzung	0,248	5%	0,454	3%	0,228	3%

Die mit Hilfe des Thomas-Fermischen statistischen Modells gewonnenen Koeffizienten liegen alle zwischen den Koeffizienten der beiden wellenmechanischen Schalenmodelle — und zwar bedeutend näher zu den Werten, welche wir auf Grund der anomalen Besetzung gewonnen haben. Die prozentuellen Fehler in der Tabelle 1 geben die relativen Unterschiede zu den Ergebnissen des statistischen Modells. Wie man sieht, sind diese Fehler im Falle der anomalen Besetzung nur etwa 1/10 der Fehler der regelmässigen Besetzung. Wir können also behaupten, dass das Thomas-Fermische statistische Atommodell eine sehr gute Näherung der anomalen Besetzung gibt, während es sich von dem Schalenmodell mit regelmässiger Besetzung wesentlich unterscheidet.

Zusammenfassend können wir also aus unseren Ergebnissen folgern, dass das statistische Atommodell für grosse Ordnungszahlen im wesentlichen die Anomalien in der Besetzung der Einelektronquantenzustände wiedergibt. Der Beweis dieser Behauptung, wie er mit der hier vorgelegten Methode geführt wurde, entspricht nach unserer Meinung besser dem Charakter des statistischen Modells als die Untersuchung des ersten Auftretens einer Nebenquantenzahl bei relativ kleinen Ordnungszahlen. Wir haben hier aus dem Verhalten des Modells bei grossen Ordnungszahlen Folgerungen gezogen und haben keine Gruppierung der Elektronen nach der Nebenquantenzahl verwendet. In dieser Hinsicht ist unsere Methode mit der Methode von IVANENKO und LARIN [4] verwandt.

LITERATUR

1. E. FERMI, Z. Physik, **48**, 73, 1928; Nature, **121**, 502, 1928.
2. J. H. D. JENSEN and J. M. LUTTINGER, Phys. Rev, **86**, 907, 1952.
3. W. R. THEIS, Z. Physik, **140**, 1, 1955.
4. Д. Д. ИВАНЕНКО и С. И. ЛАРИН, Д. А. Н. **33**, 45, 1953; С. И. Ларин, Ж. Э. Т. Ф. **28**, 498, 1955.
5. A. KÓNYA, Hung. Acta Phys., **1**, 12, 1949.
6. P. GOMBÁS, »Statistische Behandlung des Atoms« in dem Hb. d. Phys., Bd. XXXVI, Springer, Berlin—Göttingen—Heidelberg, Ss. 125 u. 127.

О ПОРЯДКЕ ОЧЕРЕДИ ЗАПОЛНЕНИЯ КВАНТОВЫХ СОСТОЯНИЙ В АТОМЕ

А. КОНЯ

Резюме

На основе статистической теории атома возможно определить среднее значение квадрата количества движения электрона, абсолютного значения суммы момента количества движения и абсолютное значение суммы компонентов данного вектора по одной координатной оси как функцию порядкового номера. Кроме этого имеется возможность для вывода на основании квантовомеханической оболочечной модели для этих же средних значений асимптотической формулы.

В этих формулах коэффициенты зависят от порядка очереди заполнения состояний, которые предполагаются при заполнении одноэлектронных квантовых состояний в атоме. Сравнивая результаты, можно прийти к заключению, что статистической атомной моделью Томаса—Ферми верно отражается опаздывающее заполнение квантовых состояний с более высоким орбитальным квантовым числом.

ÜBER DIE KORRELATIONSENERGIE UND DAS KORRELATIONSPOTENTIAL EINES ELEKTRONENGASES

Von

P. GOMBÁS

PHYSIKALISCHES INSTITUT DER UNIVERSITÄT FÜR TECHNISCHE WISSENSCHAFTEN, BUDAPEST

(Eingegangen 10. V. 1961)

Für die Korrelationsenergie eines Elektronengases wird eine für den ganzen Dichtebereich gültige Interpolationsformel hergeleitet. An Hand dieser lässt sich die Korrelationswechselwirkung des Elektrons im höchsten besetzten Energiezustand mit den übrigen Elektronen durch ein Korrelationspotential darstellen.

I. Einleitung

Mit dem Problem der Berechnung der Korrelationsenergie eines freien Elektronengases befassen sich besonders in neuerer Zeit viele Arbeiten[1]. Dieses Problem, das für mehrere Gebiete der Quantenphysik eine wichtige Rolle spielt, konnte jedoch bis jetzt wegen mathematischer Schwierigkeiten nicht vollständig gelöst werden; eine Lösung konnte nur für sehr kleine und sehr grosse Elektronendichten und für Elektronendichten von der Grössenordnung der Elektronengasdichten in Metallen erzielt werden. Das Ziel der vorliegenden Arbeit ist für die Korrelationsenergie des freien Elektronengases mit Hilfe der vorliegenden Lösungen eine Interpolationsformel herzuleiten, die für alle Dichten des Elektronengases eine gute Näherung darstellt.

Kürzlich wurde von LEWIS[2] eine Interpolationsformel angegeben, die für sehr kleine Elektronendichten das richtige Verhalten aufweist, bei grossen Elektronendichten unterscheidet sie sich jedoch vom tatsächlichen Verlauf durch eine Konstante. Diese Interpolationsformel ist demzufolge für Elektronendichten von der Grössenordnung $\varrho \sim 1/a_0^3$ (a_0 = erster Bohrscher Wasserstoffradius) mit einem bedeutenden Fehler behaftet, der sich auch noch auf Elektronendichten von der Grössenordnung der Dichten des Metallelektronengases auswirkt.

2. Herleitung der Interpolationsformel

Wir befassen uns zunächst mit den drei Ausdrücken für die Korrelationsenergie pro Elektron, w_m , auf die sich unsere Interpolationsformel gründet.

Als ersten ziehen wir den für sehr kleine ϱ gültigen Ausdruck in Betracht, der von WIGNER [3] hergeleitet und später von PINES [4] korrigiert wurde.

Dieser lautet

$$w_m^{(1)} = -g_1(\varrho^{1/3}) = -0,44 \frac{e^2}{r_s} = -0,44 \left(\frac{4\pi}{3} \right)^{1/3} e^2 \varrho^{1/3} = -0,709 e^2 \varrho^{1/3} \quad (1)$$

für

$$r_s \gtrsim 20a_0, \text{ d. h. } \varrho^{1/3} \lesssim 0,03/a_0,$$

wo e die positive Elementarladung bezeichnet, a_0 den ersten Bohrschen Wasserstoffradius bedeutet und r_s der Radius der 1 Elektron enthaltenden Elementarkugel ist, der mit der Elektronendichte folgendermassen zusammenhängt

$$\varrho = \frac{3}{4\pi r_s^3}. \quad (2)$$

Der Ausdruck (1) gilt für $\varrho \rightarrow 0$ exakt.

Als zweiten betrachten wir einen von PINES [5] für Elektronendichten von der Grössenordnung der Dichten des Metallelektronengases hergeleiteten Ausdruck

$$\begin{aligned} w_m^{(2)} &= -g_2(\varrho^{1/3}) = -0,0155 \frac{e^2}{a_0} \ln \left(\frac{r_s}{a_0} \right) + 0,0575 \frac{e^2}{a_0} = \\ &= 0,0155 \frac{e^2}{a_0} \ln(\varrho^{1/3} a_0) + 0,0649 \frac{e^2}{a_0}, \end{aligned} \quad (3)$$

der für

$$1,8 a_0 \lesssim r_s \lesssim 5,6 a_0, \text{ d. h. } 0,10/a_0 \lesssim \varrho^{1/3} \lesssim 0,35/a_0$$

gültig ist.

Schliesslich als dritten ziehen wir den von GELL-MANN und BRUECKNER [6] für sehr grosse Elektronendichten hergeleiteten Ausdruck

$$\begin{aligned} w_m^{(3)} &= -g_3(\varrho^{1/3}) = -0,0311 \frac{e^2}{a_0} \ln \left(\frac{r_s}{a_0} \right) + 0,048 \frac{e^2}{a_0} = \\ &= 0,0311 \frac{e^2}{a_0} \ln(\varrho^{1/3} a_0) + 0,0628 \frac{e^2}{a_0} \end{aligned} \quad (4)$$

heran, der für

$$r_s \lesssim 1a_0, \text{ d. h. } \varrho^{1/3} \gtrsim 0,6/a_0$$

Gültigkeit hat. Für $\varrho \rightarrow \infty$ gilt dieser Ausdruck exakt.

Die Gültigkeitsbereiche der verschiedenen Ausdrücke für die Korrelationsenergie wurden sehr ausführlich von NOZIÈRES und PINES [7] untersucht;

die weiter oben gemachten Angaben über die Gültigkeitsbereiche der einzelnen Ausdrücke entsprechen ihren Feststellungen.

Wie man sich an Hand von Fig. 1 oder der Formeln (1), (3) und (4) überzeugt, gibt keine dieser Formeln im ganzen Bereich von $\varrho = 0$ bis $\varrho = \infty$ eine brauchbare Näherung, die Formeln werden ausserhalb ihres Gültigkeitsbereiches unbrauchbar. Um im ganzen Bereich von ϱ eine brauchbare

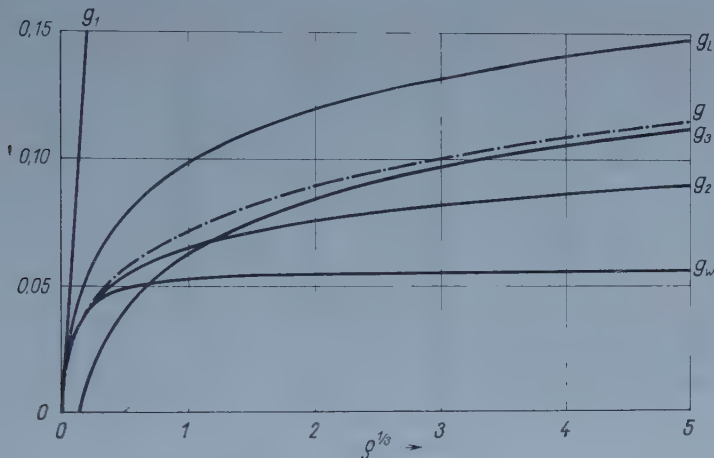


Fig. 1. Der Verlauf von g_1, g_2, g_3, g, g_W und g_L als Funktion von $\varrho^{1/3}$. Die Funktion g_2 wird bei $\text{cca } \varrho^{1/3} \cong 0,02/a_0$ negativ; dies konnte jedoch in der Figur nicht dargestellt werden.
Einheiten: Abszisse $1/a_0$, Ordinate e^2/a_0 .

Näherung zu erhalten, ist es zwäckmässig eine Interpolationsformel zu konstruieren. Wie sich zeigt, eignet sich für diese folgende Form

$$w_m = -g(\varrho^{1/3}) = -\frac{\alpha_1}{\alpha_2 + \varrho^{1/3}} \varrho^{1/3} - \beta_1 \ln(1 + \beta_2 \varrho^{1/3}), \quad (5)$$

in welcher die Konstanten $\alpha_1, \alpha_2, \beta_1$ und β_2 so gewählt werden, dass w_m für $\varrho = 0$ in den dort exakt gültigen Ausdruck (1), für $\varrho = \infty$ in den für diesen Dichtewert ebenfalls exakt gültigen Ausdruck (4) übergehe und für den Dichtewert $\varrho^{1/3} = 0,15/a_0$, der in den Gültigkeitsbereich des Ausdruckes (3) fällt (und der approximativ der Randdichte des statistischen Atoms entspricht) mit (3) übereinstimme. Es ergeben sich so folgende Bedingungsgleichungen

$$\frac{\alpha_1}{\alpha_2} + \beta_1 \beta_2 = 0,709 e^2, \quad (6)$$

$$\beta_1 = 0,0311 \frac{e^3}{a_0}, \quad (7)$$

$$\alpha_1 + \beta_1 \ln \left(\frac{\beta_2}{a_0} \right) = 0,0628 \frac{e^2}{a_0}, \quad (8)$$

$$-\frac{\alpha_1}{a_2 a_0 + 0,15} \cdot 0,15 + \beta_1 \ln \left(1 + \beta_2 \frac{0,15}{a_0} \right) = g_2(0,15/a_0). \quad (9)$$

Hieraus erhält man für die Konstanten α_1 , α_2 , β_1 und β_2 die folgenden Werte

$$\left. \begin{aligned} \alpha_1 &= 0,0357_0 \frac{e^2}{a_0}, & \alpha_2 &= 0,0562_5 \frac{1}{a_0}, \\ \beta_1 &= 0,0311_0 \frac{e^2}{a_0}, & \beta_2 &= 2,39_0 a_0. \end{aligned} \right\} \quad (10)$$

Es existiert auch noch eine andere Lösung des Gleichungssystems (6)–(9), bei der α_1 einen negativen Wert hat. Mit dieser Lösung zeigt jedoch der Interpolations-Ausdruck (5) praktisch denselben Verlauf wie mit der Lösung (10).

Mit den Konstanten (10) dominiert in (5) für sehr kleine ϱ das erste Glied und für sehr grosse ϱ das zweite Glied. Dieses erste Glied hat die Form eines von WIGNER [8] angegebenen und später von PINES [9] korrigierten Interpolationsausdruckes g_W , der für $\varrho \rightarrow 0$ in (1) übergeht und für grosse ϱ Werte annimmt, die von WIGNER zur Zeit der Herleitung dieses Interpolationsausdruckes festgestellt wurden und die sich nach Bekanntwerden des für grosse ϱ exakt gültigen Ausdruckes (4) als ziemlich ungenau erwiesen. Dieser WIGNERsche Ausdruck für g lautet

$$g_W = \frac{\gamma_1}{\gamma_2 + \varrho^{1,3}} \varrho^{1/3} \quad (11)$$

mit $\gamma_1 = 0,0564e^2/a_0$ und $\gamma_2 = 0,0795/a_0$.

Das zweite Glied in (5) hat die Form eines von LEWIS [10] angegebenen Interpolationsausdruckes

$$g_L = \varepsilon_1 \ln(1 + \varepsilon_2 \varrho^{1/3}), \quad (12)$$

wo $\varepsilon_1 = 0,0311e^2/a_0$ und $\varepsilon_2 = 22,80a_0$ ist und der sich für sehr grosse ϱ — wie weiter oben schon erwähnt wurde — durch eine Konstante von dem durch (4) gegebenen exakten Verlauf von g unterscheidet. Die dieser entsprechende für grosse ϱ fehlende Konstante wird in unserer Interpolationsformel durch

das erste Glied geliefert, das für sehr grosse ϱ gerade in diese Konstante übergeht.

Zum Vergleich ist der Verlauf von g_1, g_2, g_3 sowie von g und weiterhin der Verlauf von g_w und g_L als Funktion von $\varrho^{1/3}$ in Fig. 1 dargestellt. Wir schätzen, dass der Fehler von g auch in den Interpolationsgebieten, wo der Fehler am grössten ist, 10% nicht überschreitet.

Für die Korrelationsenergie pro Volumeneinheit, d. h. die Dichte der Korrelationsenergie erhält man mit unserem Ausdruck (5) für g

$$W_K = \varrho \quad w_m = - \varrho \cdot g(\varrho^{1/3}). \quad (13)$$

Die Korrelationsenergie E_K des gesamten Elektronengases, z. B. der Elektronenwolke des Atoms ergibt sich durch eine Integration dieses Ausdruckes auf den ganzen Raum; man hat also

$$E_K = - \int \varrho g(\varrho^{1/3}) dv, \quad (14)$$

wo dv das Volumenelement bezeichnet.

3. Das Korrelationspotential

Zur näherungsweisen Berechnung der exakt sehr schwer zu erfassenden Korrelationswechselwirkung der Elektronen lässt sich — wie in vorangehenden Arbeiten[11] gezeigt wurde — ein Korrelationspotential herleiten. Für die Korrelationswechselwirkung des Elektrons mit der höchsten Energie gestaltet sich dieses folgendermassen

$$V_K = - \frac{1}{e} \frac{\partial W_K}{\partial \varrho}. \quad (15)$$

Mit Rücksicht auf (13) ergibt sich hieraus mit unserem Ausdruck (5)

$$V_K = \frac{a_1}{3e} \frac{4a_2 + 3\varrho^{1/3}}{(\alpha_2 + \varrho^{1/3})^2} \varrho^{1/3} + \frac{\beta_1}{e} \ln(1 + \beta_2 \varrho^{1/3}) + \frac{\beta_1 \beta_2}{3e} \frac{\varrho^{1/3}}{1 + \beta_2 \varrho^{1/3}}. \quad (16)$$

Das Korrelationspotential wird also für $\varrho \rightarrow 0$ gleich Null und für $\varrho \rightarrow \infty$ logarithmisch unendlich. Der Verlauf von V_K als Funktion von $\varrho^{1/3}$ ist in Fig. 2 dargestellt.

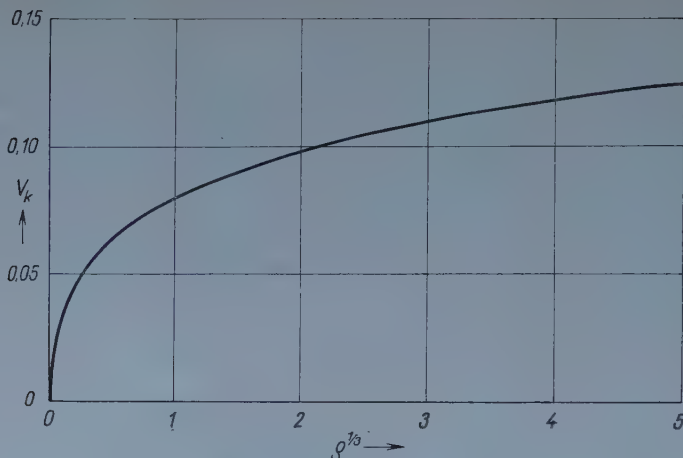


Fig. 2. Verlauf des Korrelationspotentials V_K als Funktion von $q^{1/3}$
Einheiten: Abszisse $1/a_0$, Ordinate e/a_0 .

Die Korrelationsenergie u_k des Elektrons mit höchster Energie im Atom, d. h. eines Valenzelektrons im Atom, die aus der Korrelations-Wechselwirkung dieses Elektrons mit den Rumpfelektronen resultiert, ergibt sich mit Hilfe von V_K folgendermassen

$$u_k = - \int V_K |\psi_n|^2 e dv, \quad (17)$$

wo ψ_n die auf 1 normierte Ein-Elektron-Eigenfunktion des Valenzelektrons im Atom und dv das Volumenelement bezeichnet; die Integration ist auf den ganzen Raum auszudehnen.

Auf einige Anwendungen der Ausdrücke (5), (14) bzw. (17) kommen wir in folgenden Arbeiten zu sprechen.

LITERATURVERZEICHNIS

1. Man vgl. z. B. den Artikel von D. PINES in Solid State Physics Vol. I (herausgegeben von F. Seitz u. D. Turnbull), Academic Press Inc., New York, 1955, sowie den Artikel von P. NOZIÈRES u. D. PINES, Phys. Rev. **III**, 442, 1958.
2. H. W. LEWIS, Phys. Rev. **III**, 1554, 1958.
3. E. P. WIGNER, Phys. Rev. **46**, 1002, 1934.
4. D. PINES, Solid State Physics Vol. I (herausgegeben von F. Seitz u. D. Turnbull), S. 374, 375, Academic Press Inc., New York, 1955.
5. P. NOZIÈRES u. D. PINES, Phys. Rev. **III**, 442, 1958.
6. M. GELL-MANN u. K. A. BRUECKNER, Phys. Rev. **106**, 364, 1957.
7. P. NOZIÈRES u. D. PINES, Phys. Rev. **III**, 442, 1958.
8. E. P. WIGNER, Phys. Rev. **46**, 1002, 1934.
9. D. PINES, Solid State Physics Vol. I (herausgegeben von F. Seitz u. D. Turnbull), S. 374, 375, Academic Press Inc., New York, 1955.
10. H. W. LEWIS, Phys. Rev. **III**, 1554, 1958.
11. P. GOMBÁS, Acta Phys. Hung. **4**, 187, 1954; J. CALLAWAY, Phys. Rev. **95**, 656, 1954.

О КОРРЕЛЯЦИОННОЙ ЭНЕРГИИ И КОРРЕЛЯЦИОННОМ ПОТЕНЦИАЛЕ
ЭЛЕКТРОННОГО ГАЗА

П. ГОМБАШ

Резюме

Для корреляционной энергии электронного газа выводится интерполяционная формула, действительная для всей области плотности. Данная формула дает возможность для представления корреляционного взаимодействия электрона, находящегося в наивысшем энергетическом состоянии, с другими электронами через корреляционный потенциал.

DIE IMPULSVERTEILUNG DER NUKLEONEN IM ATOMKERN

Von
Zs. CSOMA

PHYSIKALISCHES INSTITUT DER UNIVERSITÄT FÜR TECHNISCHE WISSENSCHAFTEN, BUDAPEST

(Eingegangen: 12. XII. 1960)

Die Impulsverteilung der Nukleonen im Atomkern kann ähnlich der Impulsverteilung der Atomelektronen berechnet werden, da die Nukleonen ebenfalls der Fermi-Statistik gehorchen. Nach dem statistischen Atommodell von GOMBÁS [1] ist die durchschnittliche Nukleonendichte durch eine im allgemeinen nicht monotone Funktion des vom Kernzentrum gemessenen Abstandes darstellbar. Für die Wechselwirkungsenergie soll die Gestalt

$$J = -\varepsilon \cdot \exp \left[-\frac{|r - r_0|}{r_0} \right]$$

angenommen werden [2], wo ε eine Konstante mit der Dimension einer Energie, jedoch r_0 die durch 2π dividierte Compton-Wellenlänge des π -Mesons ist, $r_0 = 1,355 \cdot 10^{-13}$ cm soll im folgenden als Längeneinheit dienen. Misst man nun die Entfernung mit dieser Einheit, dann nimmt die Nukleonendichte in zweiter Näherung folgende Gestalt an:

$$\varrho = \frac{A \cdot a^3}{\pi^{3/2} \cdot p_0} \cdot e^{-a^2 r^2} \cdot \left[1 + \frac{1}{3} \gamma a^2 r^2 \right]^3 r_0^{-3},$$

worin A die Massenzahl

$$a = \frac{c_0}{2^{2/3} (9\pi)^{1/6} A^{1/3}}; \quad p_0 = 1 + \frac{3}{2} \gamma + \frac{5}{4} \gamma^2 + \frac{35}{72} \gamma^3,$$

und c_0 und γ Variationsparameter sind, deren Werte die folgende Tabelle enthält

A	16	80	200
c_0	4,73	5,85	5,95
γ	0,54	1,4	1,8

Den zu einem gegebenen ϱ -Wert gehörenden maximalen Impuls liefert die aus der statistischen Theorie des Atoms [3] bekannte Formel

$$p = \frac{1}{2} \left(\frac{3}{\pi} \right)^{1/3} \cdot h \cdot \varrho^{1/3}.$$

Im Falle von $A = 16$ sind ϱ und deshalb auch p monoton abnehmende Funktionen von r . So können die Nukleonen mit gegebenem Impuls vom Absolutwert p nur in einer solchen Kugel vorkommen, die einen zu diesem p gehörenden Radius r besitzt. Alle Nukleonen, deren absolute Impulswerte zwischen p

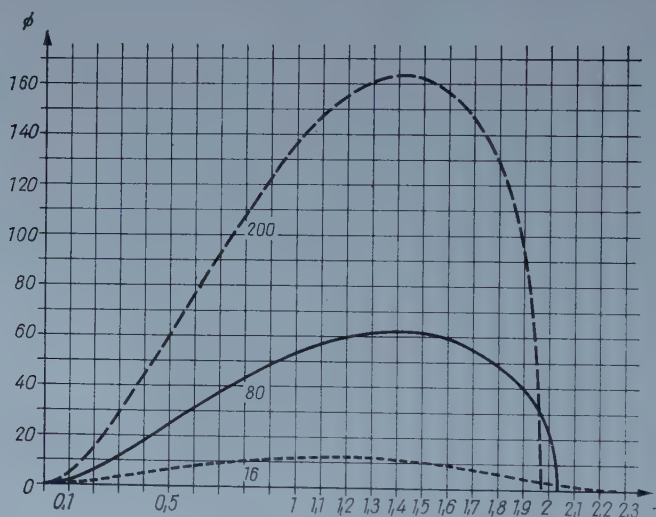


Fig. 1

und $p + dp$ fallen, besetzen demzufolge im Impulsraum einen Bereich der Grösse $4 \pi p^2 dp$, im Koordinatenraum jedoch einen solchen der Grösse $\frac{4\pi}{3} r^3$, im Phasenraum füllen sie daher ein Phasenvolumen der Grösse

$$\frac{4\pi}{3} [r(p)]^3 \cdot 4\pi p^2 dp$$

aus. Wenn im Falle des tiefsten Energiezustandes sich in jeder Phasenzelle der Grösse h^3 zwei Nukleonen mit entgegengesetztem Spin aufhalten, dann ist die Zahl der Nukleonen, deren Impulswerte zwischen p und $p + dp$ fallen [4],

$$\Phi(p) dp = 2 \frac{16 \pi^2}{3 h^3} r^3 p^2 dp.$$

Im Falle von $A = 80$ bzw. 200 nehmen ρ und p mit r bis zu einer maximalen Dichte monoton zu und danach monoton ab, deshalb gehören in der Nähe des Maximums von p zu einem p -Wert zwei r -Werte: r_1 und r_2 . Nehmen wir nun an, dass $r_2 > r_1$, dann ist

$$\Phi(p) = \frac{4}{3\pi} (r_2^3 - r_1^3) p^2,$$

worin die Einheit der vom Kernzentrum gemessenen Entfernung r_0 und die Einheit des Impulses $\frac{h}{2\pi r_0}$ ist.

Der Verlauf der drei Verteilungsfunktionen wird durch Fig. 1 wiedergegeben. In den drei Fällen sind die Werte des maximalen und des Impulses, in dessen Nähe sich die meisten Nukleonen befinden (»wahrscheinlichster Impuls«: p_e), in den erwähnten Einheiten die folgenden:

A	p_{\max}	p_e
16	2,2736	1,1827
80	2,0382	1,4033
200	1,9702	1,4263

Zum Schluss möchte ich auch an dieser Stelle Herrn Professor Dr. P. GOMBÁS für wertvolle Ratschläge danken.

LITERATUR

1. P. GOMBÁS, Acta Phys. Hung., **1**, 329, 1952.
2. P. GOMBÁS, E. MÁGORI, B. MOLNÁR und É. SZABÓ, Acta Phys. Hung., **4**, 267, 1954.
3. P. GOMBÁS, Die statistische Theorie des Atoms und ihre Anwendungen, Verlag Springer Wien, 1949, S. 5.
4. G. BURKHARDT, Ann. Phys., **26**, 567, 1936.

THE INFLUENCE OF EXTERNAL RESISTANCE ON THE MOVING STRIATIONS OF THE POSITIVE COLUMN*

By

G. LAKATOS and J. BITÓ

INDUSTRIAL RESEARCH INSTITUTE FOR TELECOMMUNICATION TECHNIQUE, BUDAPEST

(Received 10. I. 1961)

On the basis of SZIGETI's previous statement [1] one of the authors [2] examined the influence of some internal anodic side parameters of the discharge tube on the moving striations in the positive column of a gas discharge of low pressure. The influence exercised by the external parameters of the gas discharge tube on the moving striations was examined by several authors. According to YOSHIMOTO et al. [3] the velocity of moving striations can be sensitively influenced by external conditions (ambient temperature, external resistance, etc. . .). Also PEKAREK [4] mentions the weak influence exercised by the parameters of the external circuit on moving striations. According to NEDOSPASOV et al. [5] the external effects have an influence not only on the velocity of the striations, but on their wavelength too.

The authors have examined the dependence of the frequency and other parameters of moving striations arising in the gas discharge of low pressure on the magnitude and kind of the external limiting element.

The experimental tube had a 36 mm internal diameter, 1200 mm length, and was filled with argon and mercury vapour of 3 mmHg total pressure. The cathode of the tube was an oxide cathode and its anode a nickel disk. The discharge tube was placed in a water jacket, whose temperature was kept at $25 \pm 0,1^\circ \text{C}$. In the course of the experiments no external magnetic field was employed.

The power supply of the discharge tube was a stabilized dc electrical source; the arc current was 100 mA, without the external heating of the cathode. In the first part of the experiments a variable ohmic resistance, whose inductive resistance was negligible, was used as an external limiting element. The external ohmic resistance was so adjusted that for the different values of the supply voltage (200, 300, 400 V) the current always remained 100 mA. The different parameters of the moving striations were determined with the

* A report on research conducted under contract with the United Incandescent Lamp and Electrical Co. Ltd.

measuring method used by DONAHUE et al. [6] and the results of the measurement are shown in the following Figure 1.

The parameters in Fig. 1 refer, from among the two waves of striations of different speed detectable in the discharge, to the wave of greater speed.

In the second part of the experiments as an external limiting element, beside the ohmic resistance, connected in series, there was also used an insertable or disconnectable inductive resistance, connected similarly in series. The magnitude of the inductive resistance was 1,5 H and its ohmic resistance

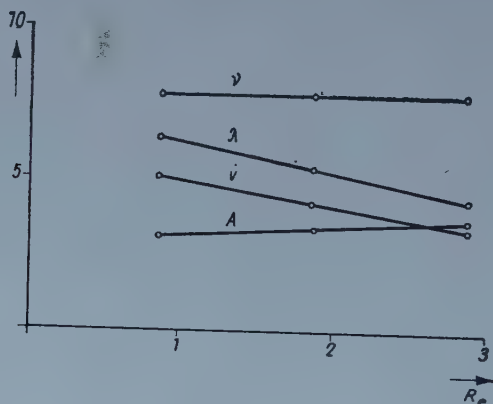


Fig. 1

The dependence of the different parameters of moving striations on the size of the employed external ohmic resistance at 100 mA current.

A — amplitude of the oscillation of the light intensity in arb. units; v — speed of the moving striations in 10^3 cmsec^{-1} units; λ — wavelength in cm; ν — frequency in 10^2 sec^{-1} units

10 ohm. In case of insertion of the inductive element, so as to keep the resulting ohmic resistance of the external limiting circuit unchanged, the original variable resistance was reduced by 10 ohm. The influence of the inductive resistance on the frequency of the moving striations at 20 mA arc current is shown in the following Table 1.

Table 1

	Inductive resistance	
	Disconnected	Inserted
Frequency (sec^{-1})	541	498

From the Figure it is clear that in the examined range at constant arc current the magnitude of the external limiting ohmic resistance influences the amplitude (A) of the oscillation of the light intensity of the moving striations and similarly its speed (v) and wavelength (λ) — as it was also stated by the

above mentioned authors — but does not influence its frequency (ν). It follows that in the investigated range the frequency of the moving striations is determined only by the internal parameters of the discharge.

On the other side, from Table 1 it can be seen that under suitable conditions the frequency of the moving striations is influenced by the presence of the inductive part of the external limiting element; consequently in this case this frequency is determined not only by the internal parameters of the discharge.

The influence of external ohmic resistance on the frequency, light intensity and current oscillations will be described in a following paper [7].

REFERENCES

1. G. SZICETI and J. BITÓ, *Acta Phys. Hung.*, **11**, 103, 1960.
2. J. BITÓ, *Magyar Híradástechnika*, **11**, 23, 1960.
3. H. YOSHIMOTO, M. SATO and Y. NAKAO, *Journ. of the Phys. Soc. Jap.*, **13**, 734, 1958.
4. L. PEKAREK, *Czechosl. Journ. Phys.*, **8**, 32, 1958.
5. A. V. NEDOSPASOV, G. J. PANKOVA and V. F. KONAĤ, *Journ. Tech. Phys.*, **30**, 125, 1960.
6. T. DONAHUE and G. H. DIEKE, *Phys. Rev.*, **81**, 248, 1951.
7. G. LAKATOS, to be published.

LUMINESCENCE OF ADSORBED FLUORESC EIN

(PRELIMINARY COMMUNICATION)

By

E. LENDVAY

RESEARCH INSTITUTE FOR TECHNICAL PHYSICS OF THE HUNGARIAN ACADEMY OF SCIENCES,
BUDAPEST

(Received 2. III. 1961)

It is well known that fluorescein luminesces very intensively in various polar solvents or in a rigid medium (e. g. in boric acid glass) etc., but our knowledge of its lighting in the adsorbed state is very poor.

We examined the behaviour of fluorescein adsorbed on different surfaces and observed that the luminous characteristic of fluorescein, adsorbed on Al_2O_3 hydrogels are well measurable.

We prepared the adsorbent by anodic oxydation. The "adsorbat" phosphors were prepared by adsorption of fluorescein on Al_2O_3 films, previously treated with basic solutions. The spectra of the emission depended on the method of chemical treatment. Some characteristic spectra are shown in Fig. 1.

We can conclude from the connection existing between the conversion of the oxyde to hydroxydes (which occurs when oxyde is treated with basic reagents) and the spectral energy distribution of the luminescence that the emitting molecules are joined to the surface with H-bridges. This supposition was provable by chemisorption of methylalcohol, resp. water which was followed by the adsorption of fluorescein. (In the second case twice the number of $-\text{OH}$ groups were originated from the oxyde, as in the first one, therefore the intensity of lighting of the second phosphor was also twice that of the first one.)

As mentioned above the spectra changed with the chemical treatment. From this we supposed that the $-\text{OH}$ groups on the surface are of different natures. All hydroxyl groups, which are of equal acidity, contribute to the same elementary band in the spectra. The elementary bands corresponding to different $-\text{OH}$ groups differ from each other chiefly in the wavelength of the maximum.

It can be shown that there are four elementary bands in the spectra, the maxima of these lying at 520, 527, 558 and 593 $\text{m}\mu$.

The intensity of an elementary band can be calculated theoretically, however, only if the centers are identical and the phosphors differ only in their

concentrations. If these suppositions are assumed to be valid, it follows that

$$\frac{W_1(\lambda)}{W_2(\lambda)} = \frac{N_1}{N_2}, \quad (1)$$

where N_1 and N_2 are the concentrations of the emitting molecules adsorbed on the surface and $W_1(\lambda)$ and $W_2(\lambda)$ the wavelength dependence of the emitted

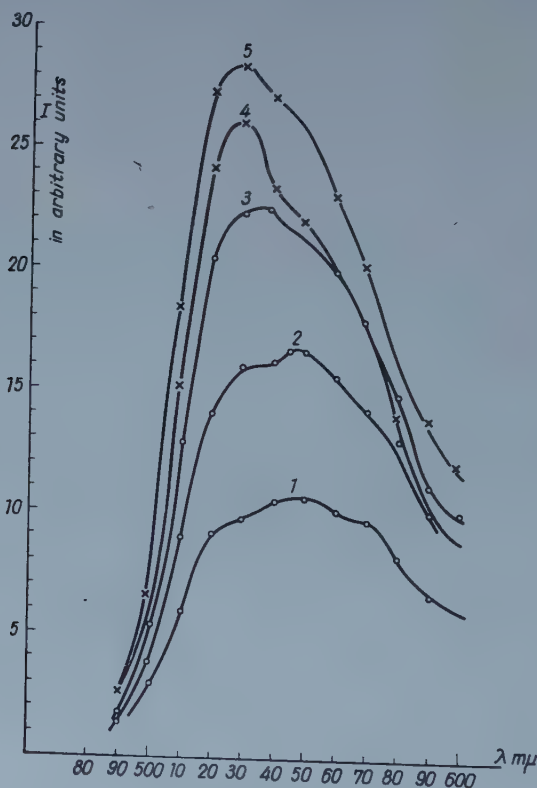


Fig 1. Luminescent spectra of $\text{Al}_2\text{O}_3 \cdot x\text{H}_2\text{O}$ phosphors. The different spectra belong to the different surface treatments

energy. With the above mentioned equation the changes in the spectra can be explained. If the rates of generation of the various $-\text{OH}$ groups are different, the places of maxima and the intensities of the spectra vary, because the intensity of the elementary bands also varies, as this depends on the chemical treatment of the Al_2O_3 film.

To demonstrate the correctness of the above mentioned conception, we examined the behaviour of the Al_2O_3 films, which were exposed to the same reagent for various times and in each case fluorescein was adsorbed on them. In the mentioned cases the spectra shown in Fig. 2 were obtained.

It can be shown that the changes occurring in Fig. 1 and Fig. 2 are very similar. Examining layer phosphors, which were treated by the same method and which differed from each other only in the time of adsorption of the fluorescein, we found that their spectra are also similar.

These experiments verify that the surface contains different emitting centers, which come into existence because surface —OH groups of different characters are present.

According to the suppositions mentioned above we are of the opinion that the luminescence originates from different centers, and that its intensity

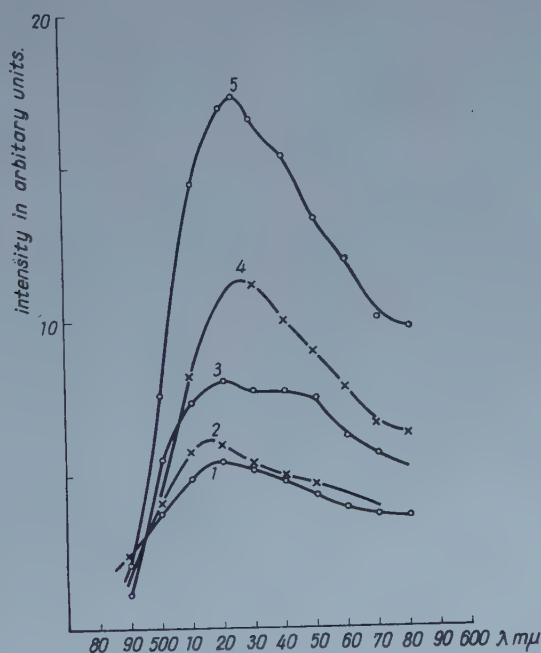


Fig. 2. The influence of the adsorption time on the shape of the luminescent spectra. The intensity of the spectra increases with the duration of adsorption

under excitation can therefore be represented as a function of wavelength by an equation of the type

$$W^L(\lambda, T) = \sum_{i=1}^n W^{Li}(\lambda, T_i) = \frac{1}{\lambda^5} \sum_{i=1}^n \varepsilon_i(\lambda, T) d_i(T) \exp \left| -\frac{c'}{kT\lambda} \right|, \quad (2)$$

where $W^{Li}(\lambda, T_i)$ is the energy distribution of an elementary band, T_i the "temperature" of the i -th center, which is defined by the equation of ALENCEV [1], T the ambient temperature, $\varepsilon_i(\lambda, T)$ the absorption band of the corresponding center, $d_i(T)$ a constant, which is independent of λ , and c' the constant of Wien's formula.

If we take into consideration what we have said above we can describe quantitatively the change in the emission as function of the hydration of the Al_2O_3 film because the adsorbing groups originate in a series of reactions following each other.

Supposing three kinds of adsorbing centers with different acidity (Al_2O_3 , AlOOH and $\text{Al}(\text{OH})_3$) the intensity of the first band can be written as a simple exponential decay

$$I_A(t) = I_A^0 \exp(-k_A t), \quad (3)$$

where I_A^0 is the intensity of the adsorbed fluorescein on a clean surface of Al_2O_3 , t the duration of the chemical treatment and k_A the specific rate of the reaction.

The dependence of the second band on the period of the chemical reaction was derived from formula (3). The equation can be expressed in the form

$$I_B(t) = C \frac{k_A}{k_B - k_A} I_A^0 [\exp(-k_A t) - \exp(-k_B t)], \quad (4)$$

where k_A and k_B are the specific rates of reactions, C a constant, and t the duration of the chemical reaction. The equation for the intensity of the third band takes the form

$$I_Q(t) = C^* \frac{I_A^0}{k_B - k_A} \{k_B [1 - \exp(-k_A t)] - k_A [1 - \exp(-k_B t)]\}, \quad (5)$$

where C^* a constant. The fourth band appears because of the polifunctional character of fluorescein.

In the case of the same adsorbent and different adsorbing times the change of the luminescent intensity can be expressed in a similar way. The increase of the luminescent intensity can be represented for these elementary bands in the following form:

$$I_i(t_A) = \frac{C_0 [\exp(\Delta k_i t) - 1]}{D \exp(\Delta k_i t) - 1}. \quad (6)$$

In the equation (6) C_0 is the total concentration of the fluorescein in the solution, when $t = 0$. $\Delta = C_0 - N_i$, where N_i is the concentration of the active spots on the surface, and $D = C_0/N_i$. Equation (6) tends toward the limit N_i , when the value of t becomes very large.

These equations are in good agreement with the experimental data. This agreement shows that the assumptions which we made in connection with the nature of adsorbat phosphors are justified.

We hope to return later to the more exact description and detailed explanation of these phenomena.

REFERENCE

1. A. H. Алленцев, *Опт. и Спектр.* **4**, 690, 1959.

E. v. ANGERER: Technische Kunstgriffe bei physikalischen Untersuchungen

Herausgegeben von H. EBERT. Friedr. Vieweg & Sohn, Braunschweig, 1959.
12. Auflage. 464 Seiten, 172 Abbildungen.

Die 12. völlig neubearbeitete Auflage des »Angerer« ist, so wie es dieses Werk seit seiner ersten Auflage immer war, ein nützlicher Wegweiser für die jüngeren und ein sehr wertvoller Ratgeber für die älteren Experimentatoren.

Seit beinahe 40 Jahren ist der »Angerer« ein Standardhilfswerk von physikalischen Laboratorien und Generationen von Experimentalphysikern benutzten und benutzen auch heute noch fast täglich dieses kleine Büchlein in ihrer Laboratoriumsarbeit.

Die Neuauflage enthält neben dem stark umgearbeiteten alten Stoff als gesonderten Abschnitt ein sehr erweitertes Literaturverzeichnis. Ausserdem werden in dem neuen Abschnitt IV einige allgemeine Grundprobleme einer gut organisierten Arbeit im Laboratorium besprochen.

Obwohl auch in dieser Neuauflage verschiedene ausgezeichnete Fachwissenschaftler die einzelnen Teilgebiete bearbeitet haben, hat das Buch durch sorgfältige Redaktion seine Einheitlichkeit weiterhin bewahrt.

Das erste Kapitel behandelt die Werkstoffe und gibt Hinweise auf Kunstgriffe bei deren Be- und Verarbeitung. Zuerst werden die Metalle, Legierungen und Karbide besprochen (B. SCHARNOW, H. EBERT). Dann folgen die Nichtmetalle: H. EBERT gibt eine Zusammenfassung von nichtmetallischen Elementen und deren Verbindungen und W. GROTH bespricht die Anreicherung gasförmiger Isotope. Die Kunststoffe werden von J. MOLL (organische Stoffe), H. LÖBER (Glas) und H. EBERT (keramische Massen) besprochen. Es folgt weiter ein Abschnitt geschrieben von J. MOLL über die Kitt- und Klebstoffe und deren praktische Verwendung.

In der Bearbeitung der Werkstoffe werden das Löten und Schweißen (G. LEHNERT), die Oberflächenbehandlung sowie Beläge und Überzüge (H. EBERT) und die Bearbeitung von Glas (H. LÖBER) behandelt.

Der Abschnitt »Verarbeitung« enthält Artikel über Metallschichten (H. EBERT, R. RITSCHL), dünne Folien (H. MAHL), dünne

Drähte (H. EBERT) und feine Fäden (H. EBERT).

Das zweite Kapitel wird der Behandlung verschiedener wichtiger Verfahren gewidmet. J. GIELESSEN bespricht das Abdichten und den Aufbau von Hochdruckapparateteilen. W. LOTTERMOSER berichtet über akustische Verfahren. Es folgen die Arbeiten über das Abschirmen hochfrequenter elektromagnetischer Felde von E. W. HELMHOLZ, über das Elektromikroskopieren von H. MAHL, über erschütterungsfreies Aufstellen geschrieben von G. TINGWALDT. K. DIELS und R. JAECKEL geben eine sehr gute und brauchbare Zusammenstellung über das Evakuieren und die wichtigsten vakuumtechnischen Verfahren. H. EBERT behandelt das Füllen von Spektralaröhren und R. OCHSENFELD einige magnetische Verfahren. Über optische Verfahren berichten G. CARIO, H. EBERT und H. KORTE, über Photographie W. MEIDINGER. Die praktischen Probleme der Regelungstechnik werden besprochen, u. zwar das Regeln der Drehzahlen (W. v. MEYEREN) des Druckes (J. GIELESSEN), der Feuchtigkeit und der Temperatur (H. EBERT), der Spannung (E. W. HELMHOLZ) und Temperatur allein (J. GIELESSEN). H. SCHARDIN gibt eine Zusammenfassung über das Sichtbarmachen von Schlieren und H. EBERT behandelt endlich Verfahren zur Handhabung verschiedener Geräte.

Der dritte Teil enthält Arbeiten über einige Geräte und Zubehörteile. Hier werden akustische Geräte (W. LOTTERMOSER), Elektroden (H. EBERT, E. W. HELMHOLZ), Elektronenröhren (E. W. HELMHOLZ) besprochen, sowie Fenster an Entladungsröhren (R. JAEGER), Ionenquellen (H. EBERT), Ionisationskammern und Zählrohre (R. JAEGER), Hochohmwiderstände, Isolatoren (W. v. MEYEREN), Messblenden (R. JAEGER) und Nernststifte- und -röhren (C. TINGWALDT), optische Geräte (H. EBERT, H. KORTE, C. TINGWALDT), Röntgenröhren für Weitwinkelaufnahmen und Doppel-Lochkamera-Aufnahmen (R. JAEGER). Über thermische Geräte berichten H. EBERT, A. SCHULZE, H. MEISSNER

und W. HEUSE und zwar über Temperaturindikatoren, Thermoelemente, tiefe Temperaturen und Widerstandsthermometer. E. RIECKMANN's Artikel behandelt die Uhren und R. JAEGER den Uralkompensator zur Messung schwacher Ionisationsströme.

Die Zählrohre und die Nebelkammer beschreiben H. FRÄNZ (GM-Zähler und Wilsonsche Nebelkammer) und S. WAGNER (Szintillationszähler).

Am Ende des Kapitels berichten E. FÜNFER, W. LEO und H. EBERT über verschiedene Zellen (Kernzellen, Photozellen, usw.).

Der vierte Teil gibt Ratschläge für die Einrichtung eines Laboratoriums und behandelt einige Kunstgriffe beim Arbeiten. H. EBERT bespricht die Laboratoriumseinrich-

tung und Geräte, W. KALLENBACH dagegen die Messwagen. Ein wichtiger Artikel ist der von H. EBERT und R. JAEGER über die Sicherheitsmassnahmen im Laboratorium und endlich folgen nützliche Ratschläge von H. EBERT über das Arbeiten im Laboratorium.

Das Buch hat ein sehr reiches Literaturverzeichnis von fast 50 Seiten und enthält es am Ende ein Geräte-, Sach-, Werkstoff- und Bezugsquellenverzeichnis.

Ein sehr umfangreiches Buch, von der ersten bis zur letzten Seite sehr klar und wohl lesbar geschrieben. Daneben hat es eine schöne Ausstattung und ist als solche eine sehr gute typographische Arbeit.

J. ANTAL

Printed in Hungary

A kiadásért felel az Akadémiai Kiadó igazgatója

Műszaki szerkesztő: Farkas Sándor

A kézirat nyomdába érkezett: 1961. VI. 14 — Terjedelem: 11,50 (A/5) ív, 48 ábra

1961.53617 — Akadémiai Nyomda, Budapest — Felelős vezető: Bernát György

MANY-BODY PROPAGATORS OF A SELF-COUPLED SPINOR FIELD IN EDWARDS—LIEB'S APPROXIMATION

By

G. PÓCSIK

INSTITUTE FOR THEORETICAL PHYSICS, ROLAND EÖTVÖS UNIVERSITY, BUDAPEST

(Presented by K. F. Novobátzky — Received: 10. I. 1961)

The continuous integral representation of the complete, many-body propagators of a self-coupled spinor field is deduced and investigated. The continuous integrals are calculated by means of EDWARDS—LIEB's non-perturbative approximation method. In first approximation, the physical one-body propagator agrees with the propagator of a free, dressed particle and the physical two-body propagator corresponds to the one obtained in the "closed-loop chain" approximation of ABRIKOSOV et al.

§ 1. Introduction

As is well known, the physical Green's functions (Δ'_F , S'_F) play an important role in the quantum field theory, they determine such quantities as the self-mass, the scattering amplitudes etc. It is also known that in many cases the application of the perturbative approach to problems connected with Green's functions leads to meaningless results. Therefore, it seems to be necessary to discuss other methods, too.

The present work deals with the Green's functions of the scalar Fermi self-coupling. Lately, an exact method (Schwinger's formalism [1]) was proposed for the calculation of the Green's functions of a self-coupled spinor field [2, 3]. The fundamental idea of Schwinger's method is the introduction of external spinor sources into the Green's function. By this means, for the Green's function as a functional of the external sources a functional differential equation can be deduced. For example, in our case the one-body propagator satisfies an inhomogeneous, non-linear functional differential equation of second order [3]. In general, from the Schwinger equation we can arrive at the continuous integral representation of the propagator, which can be evaluated in simpler cases [4].

In the first part of this paper (§ 2) it will be shown that the Schwinger equation of the self-coupled Fermi field is integrable, too. (Practically, it is simpler to integrate the differential equation of the vacuum functional.)

In the second part the one- and two-body propagators, respectively, are investigated in detail (§ 3 and § 4, resp.). As there is a quartic part in the Lagrangian, EDWARDS—LIEB's non-perturbative approach [5] (as the only

possible one) has to be applied.* We have obtained the following results: the physical one-body Green's function is in first approximation identical with the free neutrino propagator supposing that the bare mass vanishes (essentially because of the γ_5 invariance) and it is identical with a free, dressed one-particle propagator in the case of non-vanishing bare mass. The self-mass depending on the observed mass contains also the cut-off momentum square. In second approximation an unrenormalizable equation is obtained which makes further investigations impossible.

For the physical two-body propagator, in first approximation an integral equation (in momentum space) is deduced which can be exactly solved. It is found that the vertex part of our Green's function can be obtained by summing up chains of closed loops. Thus, the approximation used here corresponds to the approach of ABRIKOSOV et al. [6]. On the other hand, the asymptotic behaviour of this approximation is not correct [2]. Consequently, in the case of the two-body propagator EDWARDS—LIEB's first approximation means a rather weak one. This seems to explain the fact why in LIEB's corresponding case ghost states appear in the two-body propagator.

§ 2. Continuous integral representation of the vacuum functional

In this § we shall show that the Schwinger equations of a self-coupled spinor field [3] can be integrated and that there does exist the continuous integral representation of the propagators. As we mentioned, it is more expedient to integrate the equation written down for the vacuum functional $\langle 0|S|0\rangle$, therefore, first of all we must deal with the deduction of the equation of $\langle 0|S|0\rangle$.

Let us consider the field equation

$$(i\gamma^\mu \partial_\mu - m + 2g\bar{\psi}(x)\psi(x))\psi(x) + \eta(x) = 0 \quad (2.1)$$

characterizing the interaction of the field ψ with itself and the external sources η , $\bar{\eta}$ and define the source-free Heisenberg picture in which the field $\varphi(x)$ (picture of $\psi(x)$) and the vacuum $|0\rangle$ do not contain the sources η , $\bar{\eta}$. At η , $\bar{\eta} = 0$ $\varphi(x)$ satisfies (2.1); $|0\rangle$ is the physical vacuum. Then the operator S of the interaction of the self-acting Fermi particle and the external sources has the form

$$S = T \exp \left(i \int_{-\infty}^{\infty} dx (\bar{\eta} \varphi + \bar{\varphi} \eta) \right). \quad (2.2)$$

* LIEB has investigated a self-coupled scalar meson field. According to his calculations, in first approximation the field energy is always given correctly to within 16%, the second approximation, however, yields worse results.

Let us consider the expectation value of (2.1) in the Heisenberg vacuum. Turning to the source-free Heisenberg picture, we get

$$(i\gamma^\mu \partial_\mu - m) \langle 0 | T(\varphi(x) S) | 0 \rangle + 2g \langle 0 | T((\bar{\varphi}(x) \varphi(x)) \varphi(x) S) | 0 \rangle + \eta(x) \langle 0 | S | 0 \rangle = 0. \quad (2.3)$$

Using the relations

$$\frac{\delta \langle 0 | S | 0 \rangle}{\delta \eta(x)} = i \langle 0 | T(\bar{\varphi}(x) S) | 0 \rangle, \quad \frac{\delta \langle 0 | S | 0 \rangle}{\delta \bar{\eta}(x)} = i \langle 0 | T(\varphi(x) S) | 0 \rangle \quad (2.4)$$

and the similar ones following from (2.2), in (2.3) the vacuum expectation values can be expressed by the vacuum functional

$$\left[(i\gamma^\mu \partial_\mu - m) \frac{\delta}{\delta \bar{\eta}(x)} + 2g \frac{\delta^3}{\delta \bar{\eta}(x) (\delta \bar{\eta}(x) \delta \eta(x))} + i\eta(x) \right] \langle 0 | S | 0 \rangle = 0. \quad (2.5)$$

Starting from (2.5) we can easily arrive at the desired representation of $\langle 0 | S | 0 \rangle$. Because of the linear character of (2.5), $\langle 0 | S | 0 \rangle$ may be determined by using the functional Fourier-transform

$$\langle 0 | S | 0 \rangle = \int \delta\psi \delta\bar{\psi} s(\psi, \bar{\psi}) \exp \left[i \int_{-\infty}^{\infty} dx (\bar{\eta}\psi + \bar{\psi}\eta) \right], \quad (2.6)$$

where $s(\psi, \bar{\psi})$ means the functional Fourier transform of $\langle 0 | S | 0 \rangle$. After MATTHEWS and SALAM [7] the functional integrals appearing in this work are defined as multiple integrals taken over all the expansion coefficients of the c -number fermion fields $\psi, \bar{\psi}$. Furthermore, we prescribe the anticommutation of ψ and $\bar{\psi}$. It must be noted that this definition is not quite correct, it is important, however, that also in the cases which could be investigated by the correct definition (bilinear exponentials) other results have not been obtained [8].

Now, we write down the equation that is satisfied by $s(\psi, \bar{\psi})$. Substituting (2.6) into (2.5) we find

$$(i\gamma_\mu \partial^\mu - m + 2g \bar{\psi}(x) \psi(x)) \psi(x) s(\psi, \bar{\psi}) = -i \frac{\delta s(\psi, \bar{\psi})}{\delta \bar{\psi}(x)}. \quad (2.7)$$

The solution of (2.7) can be immediately written down:

$$s(\psi, \bar{\psi}) = N^{-1} \exp \left\{ i \int_{-\infty}^{\infty} dx [\bar{\psi}(x) (i\gamma^\mu \partial_\mu - m) \psi(x) + g \bar{\psi}(x) (\bar{\psi}(x) \psi(x)) \psi(x)] \right\}, \quad (2.8)$$

where N^{-1} is a constant. N^{-1} must be determined from the boundary condition $\lim_{\bar{\eta}, \eta \rightarrow 0} \langle 0 | S | 0 \rangle = 1$ therefore, we may choose

$$N = \int \delta\psi \delta\bar{\psi} \exp [i I]. \quad (2.9)$$

Here I means the action

$$I = - \int_{-\infty}^{\infty} dx dy \bar{\psi}(x) S_F^{-1}(x, y) \psi(y) + g \int_{-\infty}^{\infty} dx \bar{\psi}(x) (\bar{\psi}(x) \psi(x)) \psi(x), \quad (2.10)$$

$$S_F^{-1}(x, y) = -\delta(x - y) (i \gamma^\mu \partial_\mu - m).$$

(2.6), (2.8) and (2.9) give the continuous integral representation of the vacuum functional

$$\langle 0 | S | 0 \rangle = (\int \delta\psi \delta\bar{\psi} \exp [iI])^{-1} \int \delta\psi \delta\bar{\psi} \exp [iI + i \int_{-\infty}^{\infty} dx (\bar{\eta}\psi + \bar{\psi}\eta)]. \quad (2.11)$$

(2.11) has an important role. Using (2.11) the physical propagators can be obtained by differentiations. For example, in the case of the one-body propagator, we get the following representation

$$S_F^{-1}(x, y) = -\delta(x - y) (i \gamma^\mu \partial_\mu - m).$$

$$S'_F(x, y) = \left[\frac{1}{i \langle 0 | S | 0 \rangle} \frac{\delta^2 \langle 0 | S | 0 \rangle}{\delta \bar{\eta}(x) \delta \eta(y)} \right]_{\bar{\eta}, \eta = 0} = \quad (2.12)$$

$$= i (\int \delta\psi \delta\bar{\psi} \exp [iI])^{-1} \int \delta\psi \delta\bar{\psi} \psi(x) \bar{\psi}(y) \exp [iI].$$

The possibility of representation of the Green's functions in a form similar to (2.12) seems to be a general law of the quantum field theory, expressed by the Feynman principle of the quantum field theory [7].

§ 3. One-particle propagator

It is clear that the parts characterizing the self-action in (2.11) and (2.12) have the form $\exp (ig \int_{-\infty}^{\infty} dx \bar{\psi}(\bar{\psi}\psi))$, therefore, to evaluate our functional integrals some kind of approximation method has to be sought. If we expand the exponential function mentioned above, the unrenormalizable divergences of the perturbation method appear. At present, the only other possibility is to use EDWARDS and LIEB's nonperturbative method. In this part after having surveyed the general formulation of the method, the one-body propagator will be examined in first approximation.

Now we define the functional V of the sources $\eta, \bar{\eta}$ which represent the vacuum functional in the form

$$\langle 0 | S | 0 \rangle = \exp \left(i \int_{-\infty}^{\infty} dx dy \bar{\eta}(x) V(x, y) \eta(y) \right). \quad (3.1)$$

Then, first of all from (2.11) and (3.1) follows the property $\lim_{\eta, \bar{\eta} \rightarrow 0} V(x, y) = S'_F(x, y)$. We assume that the relations concerning the free, many-particle propagators are valid for both S_F and V , for example

$$V(x, y) = i \left[\int \delta\psi \delta\bar{\psi} \exp \left[-i \int_{-\infty}^{\infty} d\xi d\xi \bar{\psi} V^{-1} \psi \right] \right]^{-1} \int \delta\psi d\bar{\psi} \psi(x) \bar{\psi}(y) \cdot \\ \exp \left[-i \int_{-\infty}^{\infty} d\xi d\xi \bar{\psi} V^{-1} \psi \right].$$

This means that we assume the conditions

$$\gamma^0 V^+(x, y) \gamma^0 = V(y, x), \quad \gamma^0 (V^{-1}(x, y))^+ \gamma^0 = V^{-1}(y, x). \quad (3.2)$$

(For example, S_F and S_F^{-1} , respectively, satisfy (3.2). As it will be seen, V determined by LIEB's method satisfies (3.2)). Then, in the case of the exponentials containing also linear expressions, the linear substitution

$$\psi(x) = \psi'(x) + \int_{-\infty}^{\infty} dy V(x, y) \eta(y), \quad \delta\psi' = \delta\psi, \\ \bar{\psi}(x) = \bar{\psi}'(x) + \int_{-\infty}^{\infty} dy \bar{\eta}(y) V(y, x), \quad \delta\bar{\psi}' = \delta\bar{\psi} \quad (3.3)$$

may be applied, for example

$$\left(\int \delta\psi \delta\bar{\psi} \exp \left[-i \int_{-\infty}^{\infty} dx dy \bar{\psi} V^{-1} \psi \right] \right)^{-1} \int \delta\psi d\bar{\psi} \exp \left[-i \int_{-\infty}^{\infty} dx dy \bar{\psi} V^{-1} \psi + \right. \\ \left. + i \int_{-\infty}^{\infty} dx (\bar{\eta}\psi + \bar{\psi}\eta) \right] = \exp \left(i \int_{-\infty}^{\infty} dx dx \bar{\eta} V \eta \right) = \langle 0 | S | 0 \rangle.$$

After these rearrangements let us consider the equation satisfied by V . Writing (2.11) as

$$\langle 0 | S | 0 \rangle = \left\{ \int \delta\psi \delta\bar{\psi} \exp \left(-i \int_{-\infty}^{\infty} dx dy \bar{\psi} V^{-1} \psi \right) \exp \left[i \int_{-\infty}^{\infty} dx dy \bar{\psi} \text{II} \psi + \right. \right. \\ \left. + i g \int_{-\infty}^{\infty} dx \bar{\psi} (\bar{\psi}\psi) \psi \right] \right\}^{-1} \int \delta\psi d\bar{\psi} \exp \left(-i \int_{-\infty}^{\infty} dx dy \bar{\psi} V^{-1} \psi + i \int_{-\infty}^{\infty} dx (\bar{\eta}\psi + \bar{\psi}\eta) \right) \cdot \\ \cdot \exp \left[i \int_{-\infty}^{\infty} dx dy \bar{\psi} \text{II} \psi + i g \int_{-\infty}^{\infty} dx \bar{\psi} (\bar{\psi}\psi) \psi \right], \quad (3.4)$$

where

$$\int_{-\infty}^{\infty} dz V^{-1}(x, z) V(z, y) = \delta(x, y), \quad II(x, y) = V^{-1}(x, y) - S_F^{-1}(x - y)$$

and expanding the $\exp [\dots]$ in (3.4) from the first term and the first two terms, respectively, follows an identity or an equation concerning V (first approximation). Namely, substituting (3.3) into the nominator of (3.4) from the nominator the vacuum functional and the denominator can be separated. Thus, the first approximation means the vanishing of the remainder

$$\begin{aligned} & \int_{-\infty}^{\infty} dx_1 dx_2 dx_3 dx_4 \bar{\eta}(1) V(1, 2) [i II(2, 3) + 2g(V(3, 3) - Sp V(3, 3)) \delta(3 - 2) + \\ & + ig \int_{-\infty}^{\infty} dv_5 dx_6 \bar{\eta}(5) V(5, 3) V(3, 6) \eta(6) \delta(3 - 2)] V(3, 4) \eta(4) = 0. \end{aligned}$$

Hence we get in first approximation

$$\begin{aligned} & i II(1, 2) + 2g\delta(1 - 2)(V(1, 1) - Sp V(1, 1)) + \\ & + ig\delta(1 - 2) \int_{-\infty}^{\infty} dx_3 dx_4 \bar{\eta}(3) V(3, 1) V(1, 4) \eta(4) = 0. \end{aligned} \quad (3.5)$$

Finally, from the definition of II and (3.5) we get the fundamental equation of V in first approximation

$$\begin{aligned} & \left[i \gamma^\mu \frac{\partial}{\partial \gamma_1^\mu} - m + 2ig(Sp V(1, 1) - V(1, 1)) + \right. \\ & \left. + g \int_{-\infty}^{\infty} dx_3 dx_4 \bar{\eta}(3) V(3, 1) V(1, 4) \eta(4) \right] V(1, 2) = -\delta(1 - 2). \end{aligned} \quad (3.6)$$

As we want to deal with the one-body propagator take (3.6) in the limit $\eta, \bar{\eta} \rightarrow 0$,

$$[i \gamma^\mu \partial_\mu - m - 2ig(S'_F(0) - Sp S'_F(0))] S'_F(x - y) = -\delta(x - y). \quad (3.7)$$

This gives the one-body Green's function in LIEB's first approximation. (3.7) is compatible with the first order perturbation equation, in which case $S_F(0)$ stands instead of $S'_F(0)$ in (3.7). Now, supposing that the bare mass does not vanish, $S'_F(0)$ is equal to constant \times unity matrix which follows from the well-known LEHMANN representation [9]

$$S'_F(0) = -\frac{1}{(2\pi)^4} \int_0^\infty dm^2 \int_{-\infty}^\infty d^4p (\varrho_1(m^2)m + \varrho_2(m^2))(p^2 - m^2 + i\varepsilon)^{-1}. \quad (3.8)$$

ϱ_1 and ϱ_2 are real density functions. Furthermore, $iS'_F(0)$ is real, namely, integrating over p_0 the relation

$$S'_F(0) = i \frac{1}{8\pi^2} \int_0^\infty dm^2 (\varrho_1 m + \varrho_2) \int_0^\infty \frac{p^3 dp}{p^2 + m^2} \quad (3.9)$$

can be obtained. Therefore, (3.7) can be made finite by mass renormalization. The observable mass is defined by the quantity

$$m_R = m + \delta m = m + 2ig(S'_F(0) - S_P S'_F(0)) > 0. \quad (3.10)$$

Thus, in case of $m \neq 0$ S'_F is identical with the propagator of a free, dressed particle, as shown by (3.7), (3.9) and (3.10). The self-action creates the quadratically diverging self-mass

$$\delta m = 3ig m_R (8\pi^4)^{-1} \int_{-\infty}^{\infty} d^4 p (p^2 - m_R^2 + i\varepsilon)^{-1} = 3g m_R (8\pi^2)^{-1} \cdot \\ \cdot \lim_{\Lambda \rightarrow \infty} \left[\Lambda^2 - m_R^2 \ln \left(\frac{\Lambda^2}{m_R^2} + 1 \right) \right],$$

where Λ is the cut-off momentum.

Comparing these results with the first-order perturbation approximation, two differences can be seen: we have not used the fact that the coupling is weak and the self-mass depends on the observable mass.

We have a different case when the bare mass m vanishes. In this case, in consequence of the γ_5 invariance $S'_F(0)$ and δm also vanish, therefore, $S'_F(x, y)$ is identical with the free neutrino propagator.*

Naturally, the procedure used above can be applied also to the representation (2.12) of $S'_F(x, y)$. The first approximation leads to the same results, but in second approximation (which is worse according to its definition) we get an unrenormalizable equation.

§ 4. Two-particle propagator

Compare the coefficients of $\frac{i^2}{4} \int_{-\infty}^{\infty} dx_1 \dots dx_4 \bar{\eta}_e(1) \bar{\eta}_a(2) \eta_\beta(3) \eta_\sigma(4)$ in (2.11)

and (3.1). It follows that the two-body propagator can be expressed as

$$S_{\varrho\alpha\beta\sigma}^{(2)'}(1, 2, 3, 4) = - \sum (S'_{F\varrho\sigma}(1, 3) S'_{F\alpha\sigma}(2, 4) + i V_{\varrho\alpha\beta\sigma}(1, 2, 3, 4)),$$

*Nevertheless, if we do not use for $S'_F(0)$ the γ -invariant form, we have the NAMBU solution which leads to the Hilbert spaces corresponding to the solutions $m=0$ and $m \neq 0$ [0].

where

$$V_{\varrho\sigma}(1,2) = S'_{F\varrho\sigma}(1,2) + W_{\varrho\tau}(1,2), \quad (4.1)$$

$$W_{\varrho\sigma}(1,2) = \int_{-\infty}^{\infty} dx_3 dx_4 \bar{\eta}_\alpha(3) V_{\varrho\alpha\beta\sigma}(1,3,4,2) \eta_\beta(4)$$

and Σ means a suitable antisymmetrization. The first part of the Σ characterizes two free particles, $V_{\varrho\alpha\beta\sigma}$ is responsible for the two-particle scattering. $V_{\varrho\alpha\beta\sigma}$ will be considered in first order.

Instead of (3.6) we examine the integral equation

$$\begin{aligned} V(1,2) = S'_F(1,2) + \int_{-\infty}^{\infty} dx_3 S'_F(1,3) \left[2ig(S_P W(3,3) - W(3,3)) + \right. \\ \left. + g \int_{-\infty}^{\infty} dx_4 dx_5 \bar{\eta}(4) V(4,3) V(3,5) \eta(5) \right] V(3,2). \end{aligned} \quad (4.2)$$

As we want to treat only the two-body propagator, it is quite satisfactory to consider the equation

$$\begin{aligned} W(1,2) = \int_{-\infty}^{\infty} dx_3 S'_F(1,3) [2ig(S_P W(3,3) - W(3,3)) + \\ + g \int_{-\infty}^{\infty} dx_4 dx_5 \bar{\eta}(4) S'_F(4,3) S'_F(3,5) \eta(5)] S'_F(3,2). \end{aligned} \quad (4.3)$$

Substituting (4.1) into (4.3) we get

$$\begin{aligned} V_{\varrho\alpha\beta\sigma}(1,2,3,4) = g \int_{-\infty}^{\infty} dx_5 (S'_F(1,5) S'_F(5,4))_{\varrho\sigma} (S'_F(2,5) S'_F(5,3))_{\alpha\beta} + \\ + 2ig \int_{-\infty}^{\infty} dx_5 S'_{F\varrho\tau}(1,5) (\delta_{\tau\omega} V_{\nu\alpha\beta\nu}(5,2,3,5) - V_{\tau\alpha\beta\omega}(5,2,3,5)) S'_{F\omega\sigma}(5,4). \end{aligned} \quad (4.4)$$

Let us turn to the momentum space. Define $V(p_1, p_2, p_3, p_4)$ as

$$\begin{aligned} V(x_1, x_2, x_3, x_4) = \int_{-\infty}^{\infty} dp_1 dp_2 dp_3 dp_4 V(p_1, p_2, p_3, p_4) \\ \exp \cdot [-i(p_1 x_1 + p_2 x_2 - p_3 x_3 - p_4 x_4)], \end{aligned}$$

then instead of (4.4) the equation

$$V_{\alpha\beta\sigma}(p_1, p_2, p_3, p_4) = g(2\pi)^4 \delta(p_1 + p_2 - p_3 - p_4) (S'_F(p_1) S'_F(p_4))_{\alpha\sigma} \cdot \\ (S'_F(p_2) S'_F(p_3))_{\alpha\beta} + 2ig(2\pi)^4 \int_{-\infty}^{\infty} dq S'_{F\varrho\tau}(p_1) (\delta_{\tau\omega} V_{\alpha\beta\nu}(q, p_2, p_3, q + p_4 - p_1) - \\ - V_{\tau\alpha\beta\omega}(q, p_2, p_3, q + p_4 - p_1)) S'_{F\omega\sigma}(p_4) \quad (4.5)$$

can be written, where

$$S'_F = - (2\pi)^{-4} \frac{\gamma^\mu p_\mu + m_R}{p^2 - m_R^2 + i\varepsilon}.$$

Our integral equation is illustrated in Fig. 1. Fig. 1 is reminiscent of the approximation of ABRIKOSOV et al. [6].

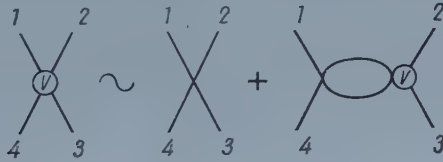


Fig. 1

It is very important that (4.5) can be solved exactly. By using successive approximation we arrive at the series

$$V_{\alpha\beta\sigma}(p_1, p_2, p_3, p_4) = g(2\pi)^4 \delta(p_1 + p_2 - p_3 - p_4) (S'_F(p_2) S'_F(p_3))_{\alpha\beta} \cdot \\ [(S'_F(p_1) \cdot 1 \cdot S'_F(p_4))_{\alpha\sigma} + \dots], \quad (4.6)$$

where the high-order approximations can be obtained by the substitution

$$1 \rightarrow (2\pi)^4 2ig \int_{-\infty}^{\infty} dq [S_F(S'_F(q) \cdot 1 \cdot S'_F(q + p_4 + p_1)) - \\ - S'_F(q) \cdot 1 \cdot S'_F(q + p_4 - p_1)]. \quad (4.7)$$

(4.6) and (4.7) show that the two-body Green's function contains not only a point scattering, but also graphs of the type drawn in Fig. 2. Now we shall prove that (4.6) means actually the chain approximation of ABRIKOSOV et al. Namely, the second integral in (4.7) can be written as

$$\int_{-\infty}^{\infty} dq S'_F(q) S'_F(q - p) = (2\pi)^{-4} \int_{-\infty}^{\infty} dx \left(i \gamma_\mu \frac{\partial \Delta_F^R(x)}{\partial x_\mu} + m_R \right) \left(i \gamma_\mu \frac{\partial \Delta_F^R(-x)}{\partial (-x_\mu)} + m_R \right) e^{ipx}.$$

Accordingly, the part containing a single γ^μ will vanish from the integral. Consequently, the series (4.6) can be summed up

$$V_{\alpha\beta\sigma}(p_1, p_2, p_3, p_4) = (2\pi)^4 g \delta(p_1 + p_2 - p_3 - p_4) (S'_F(p_2) S'_F(p_3))_{\alpha\beta}, \quad (4.8)$$

$$(S'_F(p_1) S'_F(p_4))_{\sigma\sigma} \left[1 - \frac{3}{2} i g (2\pi)^4 \int_{-\infty}^{\infty} dq S p (S'_F(q) S'_F(q + p_4 - p_1)) \right]^{-1}.$$

(4.8) is in accordance with the first-order perturbation theory.

The scattering characterized by the self-action $g \bar{\psi}(\bar{\psi} \psi) \psi$ in EDWARDS—LIEB's first approximation is a point scattering which is made nonlocal. The



Fig. 2

vertex part depending on the relative momentum has been investigated by ABRIKOSOV et al. (using a cut-off in momentum space), it is a very important circumstance, however, that the asymptotic behaviour of their vertex function is not correct [2]. Hence, it is not at all satisfactory to sum only over the "most divergent" diagrams, thus, the EDWARDS—LIEB approximation of the two-body propagator is a rather weak one. It seems that this is the reason why ghost states have appeared in LIEB's two-body propagator.

REFERENCES

1. H. UMEZAWA, Quantum Field Theory, North-Holland Publ. Co., Amsterdam, 1956; Chapt. 18.
2. T. YOSHIMURA, Progr. Theor. Phys., **23**, 569, 1960.
3. G. PÓCSIK, Acta Phys. Hung., **12**, 181, 1960.
4. S. F. EDWARDS and R. E. PEIERLS, Proc. Roy. Soc., (A) **224**, 24, 1954.
5. E. H. LIEB, Proc. Roy. Soc., (A) **241**, 339, 1957.
6. A. A. ABRIKOSOV et al., Phys. Rev., **131**, 321, 1958.
7. P. T. MATTHEWS and A. SALAM, Nuovo Cim., **2**, 130, 1955.
8. W. K. BURTON and A. H. DE BORDE, Nuovo Cim., **4**, 254, 1956.
9. H. LEHMANN, Nuovo Cim., **11**, 342, 1954.
10. Y. NAMBU and G. JONA—LASINIO, Phys. Rev., **122**, 345, 1961.

ФУНКЦИИ РАСПРОСТРАНЕНИЯ МНОГИХ ТЕЛ САМОСВЯЗАННОГО СПИНОРНОГО ПОЛЯ В ПРИБЛИЖЕНИИ ЭДВАРДСА—ЛИБСА

Г. ПОЧИК

Резюме

В работе выводится и исследуется непрерывное интегральное представление полных функций распространения многих тел самосвязанного спинорного поля. Непрерывный интеграл определяется непertурбированным приближенным методом Эдвардса—Либса. В первом приближении физическая функция распространения одного тела совпадает с функцией распространения свободной неодетой частицы, а физическая функция распространения двух тел — с функцией распространения, полученной в приближении «замкнутой петельной цепи» Абрикосова и др.

DIE EINDEUTIGKEIT DER MAGNETOHYDRODYNAMISCHEN STRÖMUNG BAROTROPER, LEITENDER MEDIEN

Von

J. SZABÓ und Cs. HARGITAI

INSTITUT FÜR THEORETISCHE PHYSIK DER ROLAND-EÖTVÖS-UNIVERSITÄT, BUDAPEST

(Vorgelegt von K. F. Novobátzky. — Eingegangen: 1. II. 1961)

Es wird mit einer direkten Methode die Eindeutigkeit der Lösung der magnetohydrodynamischen Grundgleichungen für barotrope, leitende Flüssigkeiten bei den folgenden Voraussetzungen bewiesen: A) Der die Flüssigkeit enthaltende Bereich ist durch eine glatte Fläche berandet und seine Punkte liegen alle im Endlichen. B) Der Druck hängt eindeutig und nur von der Dichte der Flüssigkeit ab. C) Die elektrische Leitfähigkeit und die beiden Viskositätskoeffizienten des Mediums sind konstant. D) Die Rand- und Anfangsbedingungen sind durch stetige Funktionen vorgegeben. E) Die magnetohydrodynamischen Größen haben für $t > 0$ stetige partielle Ableitungen, der minimale Wert der Massendichte aber ist in dem ganzen Strömungsbereich endlich.

Nach den neueren theoretischen und experimentellen Ergebnissen können die magnetohydrodynamischen Stosswellen bei der Heizung von Plasmen eine wichtige Rolle spielen. Besonders im Hinblick auf die Entstehung von Stosswellen mag die Untersuchung der Eindeutigkeit der magnetohydrodynamischen Strömungen Interesse haben.

In einer vorangehenden Arbeit haben wir die Eindeutigkeit des magnetohydrodynamischen Randwertproblems für inkompressible Flüssigkeiten bewiesen [1]. In der vorliegenden Arbeit wird der Beweis auf die magnetohydrodynamischen Strömungen barotroper Flüssigkeiten verallgemeinert.

Wir betrachten die Bewegung der leitenden Flüssigkeiten in einem Bereich τ , der durch eine glatte Fläche F berandet ist, und dessen Punkte alle im Endlichen liegen. Es wird vorausgesetzt, dass die Flüssigkeit barotrop ist, d.h. dass der Druck eindeutig und nur von der Massendichte der Flüssigkeit abhängt. Die elektrische Leitfähigkeit und die beiden Reibungskoeffizienten werden als (positive) Konstanten betrachtet. Die magnetohydrodynamischen Größen sind für $t > 0$ auf der Randfläche F , für $t = 0$ aber in dem ganzen Bereich τ durch stetige Funktionen vorgegeben. Es wird weiter vorausgesetzt, dass die magnetohydrodynamischen Größen für $t > 0$ in dem ganzen Bereich τ stetige partielle Ableitungen besitzen und dass die Massendichte der Flüssigkeit in keinem Punkt des Bereiches τ Null ist.

In barotropen, leitenden Flüssigkeiten genügen die hydrodynamische Geschwindigkeit \mathbf{v} , die magnetische Feldstärke \mathfrak{H} , der Druck p und die Massendichte ρ den folgenden Gleichungen:

$$\frac{\partial \mathfrak{H}}{\partial t} = \text{rot} [\mathbf{v} \times \mathfrak{H}] + \nu_m \Delta \mathfrak{H}, \quad (1)$$

$$\operatorname{div} \mathfrak{H} = 0, \quad (2)$$

$$\varrho \frac{\partial \mathfrak{v}}{\partial t} + \varrho (\mathfrak{v} \operatorname{grad}) \mathfrak{v} = - \operatorname{grad} p + \mu \Delta \mathfrak{v} + \mu' \operatorname{grad} \operatorname{div} \mathfrak{v} - \frac{1}{4\pi} [\mathfrak{H} \times \operatorname{rot} \mathfrak{H}], \quad (3)$$

$$\frac{\partial \varrho}{\partial t} + \operatorname{div} (\varrho \mathfrak{v}) = 0, \quad (4)$$

$$p = p(\varrho), \quad (5)$$

wo μ und μ' die beiden Reibungskoeffizienten und ν_m der sogenannte magnetische Viskositätskoeffizient sind.

Nehmen wir an, dass das magnetohydrodynamische Problem zwei Lösungen: $\mathfrak{H}_1, \mathfrak{v}_1, p_1, \varrho_1$ bzw. $\mathfrak{H}_2, \mathfrak{v}_2, p_2, \varrho_2$ hat, die den gleichen Rand- und Anfangsbedingungen genügen. D. E. DOLIDSE [2] hat bewiesen, dass die Kontinuitätsgleichung (4) für die Funktion $\varrho(t, x, y, z)$ eine eindeutige Lösung hat, wenn die Grösse $\frac{1}{\varrho_0} \operatorname{div} (\varrho_1 \mathfrak{v}_0)$ in dem ganzen Strömungsbereich beschränkt ist, wo $\varrho_0 = \varrho_2 - \varrho_1$ und $\mathfrak{v}_0 = \mathfrak{v}_2 - \mathfrak{v}_1$ sind. Dann folgt aber aus der Eindeutigkeit der Dichte die Eindeutigkeit von p . Es bleibt also noch zu beweisen, dass das magnetohydrodynamische Gleichungssystem (1) bis (4) bei den erwähnten Voraussetzungen für \mathfrak{H} und \mathfrak{v} eine eindeutige Lösung hat.

Setzt man die Grössen $\mathfrak{H}_1, \mathfrak{v}_1, p, \varrho$ bzw. $\mathfrak{H}_2, \mathfrak{v}_2, p, \varrho$ in das Gleichungssystem (1) bis (3) ein und bildet dann die Differenz der entsprechenden Gleichungen, so bekommt man das folgende Gleichungssystem:

$$\frac{\partial \mathfrak{H}_0}{\partial t} = \operatorname{rot} [\mathfrak{v}_1 \times \mathfrak{H}_0] + \operatorname{rot} [\mathfrak{v}_0 \times \mathfrak{H}_2] + \nu_m \Delta \mathfrak{H}_0, \quad (6)$$

$$\operatorname{div} \mathfrak{H}_0 = 0, \quad (7)$$

$$\begin{aligned} \varrho \frac{\partial \mathfrak{v}_0}{\partial t} + \varrho (\mathfrak{v}_1 \operatorname{grad}) \mathfrak{v}_0 + \varrho (\mathfrak{v}_0 \operatorname{grad}) \mathfrak{v}_2 = \mu \Delta \mathfrak{v}_0 + \\ + \mu' \operatorname{grad} \operatorname{div} \mathfrak{v}_0 - \frac{1}{4\pi} [\mathfrak{H}_0 \times \operatorname{rot} \mathfrak{H}_1] - \frac{1}{4\pi} [\mathfrak{H}_2 \times \operatorname{rot} \mathfrak{H}_0], \end{aligned} \quad (8)$$

wo $\mathfrak{H}_0 = \mathfrak{H}_2 - \mathfrak{H}_1$ und $\mathfrak{v}_0 = \mathfrak{v}_2 - \mathfrak{v}_1$ sind.

Zuerst wollen wir uns mit der Umformung der Gl. (8) beschäftigen. Multiplizieren wir diese Gleichung skalar mit \mathfrak{v}_0 , so erhalten wir:

$$\begin{aligned} 2\pi\varrho \frac{\partial \mathfrak{v}_0^2}{\partial t} + 4\pi\varrho \mathfrak{v}_0 \{(\mathfrak{v}_1 \operatorname{grad}) \mathfrak{v}_0\} + 4\pi\varrho \mathfrak{v}_0 \{(\mathfrak{v}_0 \operatorname{grad}) \mathfrak{v}_2\} = 4\pi\mu \mathfrak{v}_0 \Delta \mathfrak{v}_0 + \\ + 4\pi\mu' \mathfrak{v}_0 \operatorname{grad} \operatorname{div} \mathfrak{v}_0 - \mathfrak{v}_0 [\mathfrak{H}_0 \times \operatorname{rot} \mathfrak{H}_1] - \mathfrak{v}_0 [\mathfrak{H}_2 \times \operatorname{rot} \mathfrak{H}_0]. \end{aligned} \quad (9)$$

Es ist leicht, die folgende Identität zu beweisen:

$$\varrho v_0 \{ (v_1 \text{ grad}) v_0 \} = \frac{1}{2} \operatorname{div} (\varrho v_0^2 v_1) - \frac{1}{2} v_0^2 \operatorname{div} (\varrho v_1). \quad (10)$$

Da aber ϱ und v_1 der Gl. (4) genügen, so ist

$$\operatorname{div} (\varrho v_1) = - \frac{\partial \varrho}{\partial t}. \quad (11)$$

Mit der Hilfe der Gln. (10) und (11) können wir die Gl. (9) folgendermassen umformen:

$$\begin{aligned} 2\pi \frac{\partial}{\partial t} (\varrho v_0^2) + 2\pi \operatorname{div} (\varrho v_0^2 v_1 - 2\mu' v_0 \operatorname{div} v_0) + 4\pi \varrho v_0 \{ (v_0 \text{ grad}) v_2 \} = \\ = 4\pi \mu v_0 \triangle v_0 - 4\pi \mu' (\operatorname{div} v_0)^2 - v_0 [\xi_0 \times \operatorname{rot} \xi_1] - v_0 [\xi_2 \times \operatorname{rot} \xi_0]. \end{aligned} \quad (12)$$

Jetzt wollen wir die Gl. (6) umformen. Wenn wir diese Gleichung skalar mit ξ_0 multiplizieren, bekommen wir die folgende Gleichung:

$$\frac{1}{2} \frac{\partial \xi_0^2}{\partial t} = \xi_0 \operatorname{rot} [v_1 \times \xi_0] + \xi_0 \operatorname{rot} [v_0 \times \xi_2] + v_m \xi_0 \triangle \xi_0. \quad (13)$$

Integriert man die Summe der Gln. (12) und (13) über das Volumen τ , so verschwinden die die Operation Divergenz enthaltenden Glieder nach dem Satz von Gauss wegen des Verschwindens von v_0 und ξ_0 auf der Randfläche F . Wenn wir dann noch die den Laplaceschen Operator \triangle enthaltenden Glieder mit der Hilfe des Greenschen Satzes umformen, so erhalten wir aus den Gln. (12) und (13):

$$\begin{aligned} 4\pi \frac{d}{dt} \int_{\tau} \left(\frac{\varrho v_0^2}{2} + \frac{\xi_0^2}{8\pi} \right) d\tau + I = \int_{\tau} 4\pi \varrho v_0 \{ (v_0 \text{ grad}) v_2 \} d\tau - \\ - \int_{\tau} \{ v_0 [\xi_0 \times \operatorname{rot} \xi_1] + v_0 [\xi_2 \times \operatorname{rot} \xi_0] - \xi_0 \operatorname{rot} [v_1 \times \xi_0] - \xi_0 \operatorname{rot} [v_0 \times \xi_2] \} d\tau, \end{aligned} \quad (14)$$

wo

$$I = 4\pi \mu \int_{\tau} \sum_{i=1}^3 \sum_{k=1}^3 \left(\frac{\partial v_{0i}}{\partial x_k} \right) d\tau + v_m \int_{\tau} \sum_{i=1}^3 \sum_{k=1}^3 \left(\frac{\partial H_{0i}}{\partial x_k} \right)^2 d\tau + 4\pi \mu' \int_{\tau} (\operatorname{div} v_0)^2 d\tau \quad (15)$$

ist. In der Gl. (15) sind v_{0i} und H_{0i} die rechtwinkligen Komponenten der Vektoren v_0 und ξ_0 , und die Bezeichnung $x = x_1, y = x_2, z = x_3$ wurde zur Vereinfachung der Schreibweise gebraucht. Es ist wichtig, dass I eine nicht-negative Grösse ist.

Wir wollen jetzt die Glieder in dem letzten Integral in der Gl. (14) umformen. Bei der Umformung dieser Glieder brauchen wir ausser der Gl. (7) die folgenden Identitäten:

$$\mathfrak{S}_0 \operatorname{rot} [v_0 \times \mathfrak{S}_2] = [v_0 \times \mathfrak{S}_2] \operatorname{rot} \mathfrak{S}_0 - \operatorname{div} [\mathfrak{S}_0 \times [v_0 \times \mathfrak{S}_2]], \quad (16)$$

$$\mathfrak{S}_0 \operatorname{rot} [v_1 \times \mathfrak{S}_0] = \mathfrak{S}_0 \{(\mathfrak{S}_0 \operatorname{grad}) v_1\} - \frac{1}{2} \operatorname{div} (\mathfrak{S}_0^2 v_1) - \frac{1}{2} \mathfrak{S}_0^2 \operatorname{div} v_1. \quad (17)$$

Wenn wir noch berücksichtigen, dass die die Operation Divergenz enthaltenden Glieder nach der Integration wiederum verschwinden, so erhalten wir mit der Hilfe von (16) und (17) aus der Gl. (14):

$$\begin{aligned} 4\pi \frac{d}{dt} \int_{\tau} \left(\frac{\varrho v_0^2}{2} + \frac{\mathfrak{S}_0^2}{8\pi} \right) d\tau + I = \int_{\tau} 4\pi \varrho v_0 \{ (v_0 \operatorname{grad}) v_2 \} d\tau - \\ - \int_{\tau} v_0 [\mathfrak{S}_0 \times \operatorname{rot} \mathfrak{S}_1] d\tau + \int_{\tau} \mathfrak{S}_0 \{ (\mathfrak{S}_0 \operatorname{grad}) v_1 \} d\tau - \frac{1}{2} \int_{\tau} \mathfrak{S}_0^2 \operatorname{div} v_1 d\tau. \end{aligned} \quad (18)$$

Da im Zeitpunkt $t = 0$ die Grössen v_0 und \mathfrak{S}_0 in dem ganzen Bereich τ verschwinden, so ist das erste Integral auf der linken Seite der Gl. (18) für $t = 0$ gleich Null. Sein Wert kann aber auch für $t > 0$ nicht negativ sein. Es gibt also einen endlichen Zeitraum $< 0, t_0 >$, wo

$$\frac{d}{dt} \int_{\tau} \left(\frac{\varrho v_0^2}{2} + \frac{\mathfrak{S}_0^2}{8\pi} \right) d\tau \geq 0 \quad (19)$$

ist. Wenn wir noch berücksichtigen, dass $I \geq 0$ ist, so ergibt sich aus (18) die folgende Ungleichung:

$$\begin{aligned} \frac{d}{dt} \int_{\tau} \left(\frac{\varrho v_0^2}{2} + \frac{\mathfrak{S}_0^2}{8\pi} \right) d\tau \leq \left| \int_{\tau} \varrho v_0 \{ (v_0 \operatorname{grad}) v_2 \} d\tau \right| + \frac{1}{4\pi} \left| \int_{\tau} v_0 [\mathfrak{S}_0 \times \operatorname{rot} \mathfrak{S}_1] d\tau \right| + \\ + \frac{1}{4\pi} \left| \int_{\tau} \mathfrak{S}_0 \{ (\mathfrak{S}_0 \operatorname{grad}) v_1 \} d\tau \right| + \frac{1}{8\pi} \left| \int_{\tau} \mathfrak{S}_0^2 \operatorname{div} v_1 d\tau \right|. \end{aligned} \quad (20)$$

Sind die partiellen Ableitungen von v_1 , v_2 und \mathfrak{S}_1 in τ stetig, so kann man zwei positive Grössen K und L angeben, so dass

$$|\operatorname{grad} v_{1i}| \leq K; \quad |\operatorname{grad} v_{2i}| \leq K; \quad |\operatorname{div} v_1| \leq K; \quad |\operatorname{rot} \mathfrak{S}_1| \leq L \quad (21)$$

sind, wo v_{1i} und v_{2i} die rechtwinkligen Komponenten der Vektoren v_1 und v_2 sind. In diesem Fall können wir schreiben:

$$\left| \int_{\tau} \varrho v_0 \{ (v_0 \text{ grad}) v_2 \} d\tau \right| + \frac{1}{4\pi} \left| \int_{\tau} \xi_0 \{ (\xi_0 \text{ grad}) v_1 \} d\tau \right| + \frac{1}{4\pi} \left| \int_{\tau} v_0 [\xi_0 \times \text{rot } \xi_1] d\tau \right| + \\ + \frac{1}{8\pi} \left| \int_{\tau} \xi_0^2 \text{div } v_1 d\tau \right| \leq 3K \int_{\tau} \varrho v_0^2 d\tau + \frac{7K}{8\pi} \int_{\tau} \xi_0^2 d\tau + \frac{L}{4\pi} \int_{\tau} |v_0| |\xi_0| d\tau. \quad (22)$$

Ist die Massendichte ϱ in dem ganzen Strömungsbereich endlich, d. h. existiert eine positive Grösse M , so dass

$$\min \sqrt{\varrho} = M(4\pi)^{1/2} > 0 \quad \text{in } \tau$$

gilt, so ist

$$\int_{\tau} |v_0| |\xi_0| d\tau \leq \frac{1}{M\sqrt{4\pi}} \int_{\tau} \sqrt{\varrho} |v_0| |\xi_0| d\tau. \quad (23)$$

Nach der Cauchyschen Ungleichung ist aber

$$\int_{\tau} \sqrt{\varrho} |v_0| \frac{|\xi_0|}{\sqrt{4\pi}} d\tau \leq \frac{1}{2} \int_{\tau} \varrho v_0^2 d\tau + \frac{1}{8\pi} \int_{\tau} \xi_0^2 d\tau. \quad (24)$$

Unter Heranziehung von (22) bis (24) bekommt man aus (20):

$$\frac{d}{dt} \int_{\tau} \left(\frac{\varrho v_0^2}{2} + \frac{\xi_0^2}{8\pi} \right) d\tau \leq N \int_{\tau} \left(\frac{\varrho v_0^2}{2} + \frac{\xi_0^2}{8\pi} \right) d\tau, \quad (25)$$

wo

$$N = 7K + \frac{L}{4\pi M} \quad (26)$$

ist. In dem Zeitintervall $< 0, t_0 >$ nimmt also das Integral in (25) nicht schneller zu, als in dem Fall der Gleichung

$$\frac{d}{dt} \int_{\tau} \left(\frac{\varrho v_0^2}{2} + \frac{\xi_0^2}{8\pi} \right) d\tau = N \int_{\tau} \left(\frac{\varrho v_0^2}{2} + \frac{\xi_0^2}{8\pi} \right) d\tau. \quad (27)$$

Die Lösung der Gl. (27) ist

$$\int_{\tau} \left(\frac{\varrho v_0^2}{2} + \frac{\xi_0^2}{8\pi} \right) d\tau = C e^{Nt}, \quad (28)$$

woraus das identische Verschwinden von v_0 und ξ_0 in dem ganzen Bereich τ folgt, da das Integral in (28) nach der Anfangsbedingung für $t = 0$ verschwinden muss.

Die Verfasser danken Herrn Gy. KARVASZ für wertvolle Diskussionen.

LITERATUR

1. Cs. HARGITAI und J. SZABÓ, Z. Naturf. **16a**, 92, 1961.
2. Д. Е. Долидзе, Труды Тбилисского Матем. Инст. **21**, 261, 1955.

ЕДИНСТВЕННОСТЬ МАГНИТОГИДРОДИНАМИЧЕСКОГО ТЕЧЕНИЯ БАРОТРОПНОЙ, ПРОВОДЯЩЕЙ СРЕДЫ

Й. САБО и Ч. ХАРГИТАИ

Резюме

В работе прямым методом показывается единственность решения основных уравнений магнитогидродинамики для баротропной, проводящей жидкости при следующих условиях:

- а) область, занятая жидкостью, ограничивается кусочно-гладкой плоскостью, все точки предыдущей лежат в конечной области;
- б) давление зависит исключительно от плотности жидкости;
- в) электрическая проводимость и оба коэффициента вязкости среды постоянны;
- г) граничные и начальные условия даны в виде непрерывных функций;
- д) магнитогидродинамические величины для $t > 0$ имеют непрерывные частные производные, однако, минимальное значение плотности массы по всей области течения является конечным.

TIME DEPENDENCE OF SOME PARAMETERS OF A. C. DISCHARGES*

By

G. LAKATOS and J. BITÓ

INDUSTRIAL RESEARCH INSTITUTE FOR TELECOMMUNICATION TECHNIQUE, BUDAPEST

(Presented by G. Szigeti. — Received 21. II. 1961)

The time dependence of the various discharge parameters in a hot-cathode a. c. low pressure mercury vapour argon discharge was investigated. The authors applied FAJT and KONCZ's a. c. probe measurement method based on the LANGMUIR probe theorem. They describe the time dependence of the field strength, electron temperature, electron concentration, recombination velocity, cathode- and anode-fall. In the experiments the cathode was not heated by any external source.

Introduction

The plasma of the low pressure, d. c. gas discharge has often been examined by means of the LANGMUIR probe measuring principle [1] in mercury vapour and in a mixture of mercury vapour and argon [2]. LANGMUIR's method has been used by some workers also in case of an a. c. gas discharge [3, 4, 5].

The authors examined the time dependence of some parameters of the a. c. gas discharge in a mixture of mercury vapour and argon of 3 mm Hg pressure, at an ambient temperature of 22,5—24 °C. In all measurements an oxide-coated cathode was used which was heated by the discharge only, no external heating being applied.

From the probe characteristics they obtained the time dependence of the axial field strength, the electron temperature, the electron concentration, the recombination velocity and the cathode- and anode-fall.

Measuring method and arrangement

LANGMUIR [1] obtained in case of an increasing probe-potential an increasing electron current on the probe, according to the equation:

$$i_e = 1/4 \cdot e \cdot n_e \cdot v_e f \cdot \exp \left(- \frac{eV}{kT_e} \right), \quad (1)$$

* A report on research conducted under contract with the United Incandescent Lamp and Electrical Co. Ltd.

where i_e is the electron current on the probe, e the electron charge, n_e the electron concentration in the plasma, v_e the mean velocity of the electrons in the plasma, f the effective surface of the probe, V the difference of the plasma and probe potentials, k the Boltzmann constant and T_e the electron temperature in the plasma, in the probe region.

Representing the logarithm of the probe current as function of the probe potential, the electron current i_e is characterized by a straight line. The straight line has a break at a certain potential value, this breaking point gives the potential in the examined point of the plasma. The electron temperature T_e can be determined from the slope of the straight line:

$$\frac{2,303 \Delta \log i_e}{\Delta V} = \frac{11600}{T_e} \quad (2)$$

and the electron concentration n_e from the equation

$$n_e = \frac{4 \cdot i_e}{f \cdot e \left(\frac{8 k T_e}{\pi \cdot m_e} \right)^{1/2}} \cdot \exp \left(\frac{eV}{k T_e} \right), \quad (3)$$

where m_e means the mass of the electron.

The FAJT—KONCZ method [4] of the measurement of the a. c. discharge based on LANGMUIR probes and applied by the authors consists in the following: the probe is held on a constant potential with respect to one of the electrodes and the probe current is applied to the vertical input of an oscilloscope.

Taking photographs of the screen of the oscilloscope at various probe potentials and reading off the current values of these photographs belonging to one and the same value of the time base, the probe current vs. probe potential characteristics can be plotted with the time value as parameter.

The examined gas discharge tube was of the hot-cathode type, with an internal diameter of 38 mm, and an electrode spacing of 1130 mm, filled with a mixture of mercury and argon of 3 mm Hg pressure. The hot cathode was not heated by any external source.

The internal wall of the tube was coated with a luminescent phosphor. The cathodes were of the oxide-cathode type, made of the oxides of alkaline-earth metals. In the gas discharge tube there were three probes: one in the middle of the positive column and from this at a distance of 400 mm one probe towards the one end and another probe towards the other end of the positive column.

The probes reached into the axis of the discharge tube. Their length were 2 mm and their diameters 0.2 mm, each. The feed of the tube happened from an a. c. network of 50 cycles/sec frequency, with a discharge current I_t of 430 mA. The measurements were carried out in an ambient temperature of 22,5—24 °C.

The scheme of the device used for the measurement is shown in Fig. 1. In order to avoid too high electron currents, the potential of the probe was kept at a lower value than that of one of the electrodes.

In the half period in which the electrode in question is negative, only an ion current passes through the probe, the intensity of which compared to the electron current can be neglected.

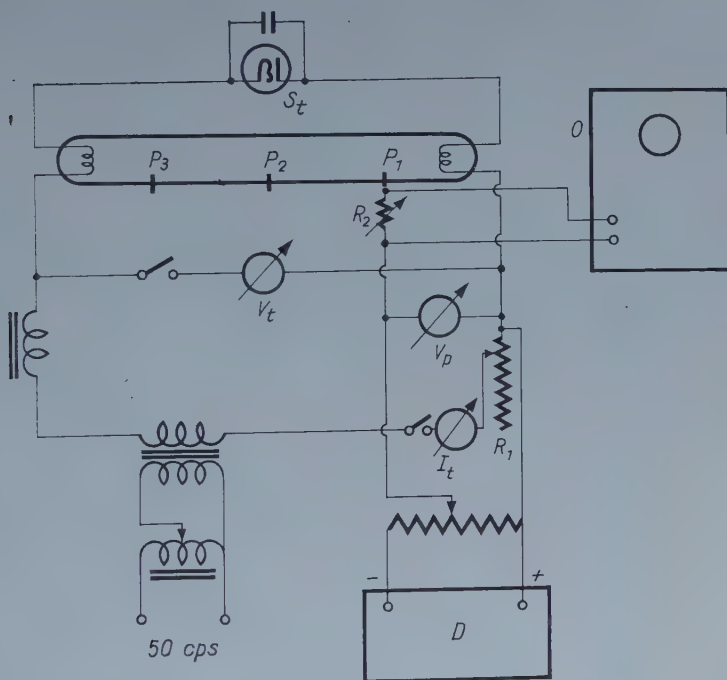


Fig. 1. Block diagram of the device used in the probe measurement of the a. c. discharge tube. P_1 , P_2 , P_3 = probes; S_t = starter; O = oscilloscope, V_p = probe voltage; V_t = tube voltage; I_t = discharge current; R_2 = measuring resistance of the probe current; D = d. c. voltage source

In the other half period when the electrode is positive, an electron current flows, which depends on the d. c. voltage applied to the probe. The intensity of the current could be measured by means of the voltage taken from the resistance R_2 on one of the vertical inputs of a double ray oscilloscope, while the horizontal input was fed by a sweep frequency of 50 cycles/sec, corresponding to the a. c. to be measured. To the other vertical input a voltage proportional to the current of the discharge tube was applied in order to make the phase relations identical. The oscillogram taken of the time dependence of the probe current can be seen in Fig. 2, it relates to the probe nearest to the cathode.

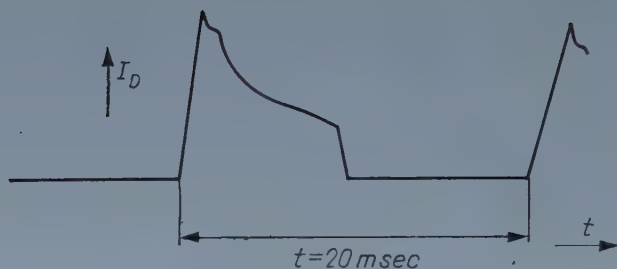


Fig. 2. Probe current vs. time

Measuring results

The calculated values of the electron temperature of the a.c. gas discharge as a function of the phase angle of the a.c. are shown in Fig. 3. In the region $c-d$ of the phase angle the Figure shows no values as the oscillo-

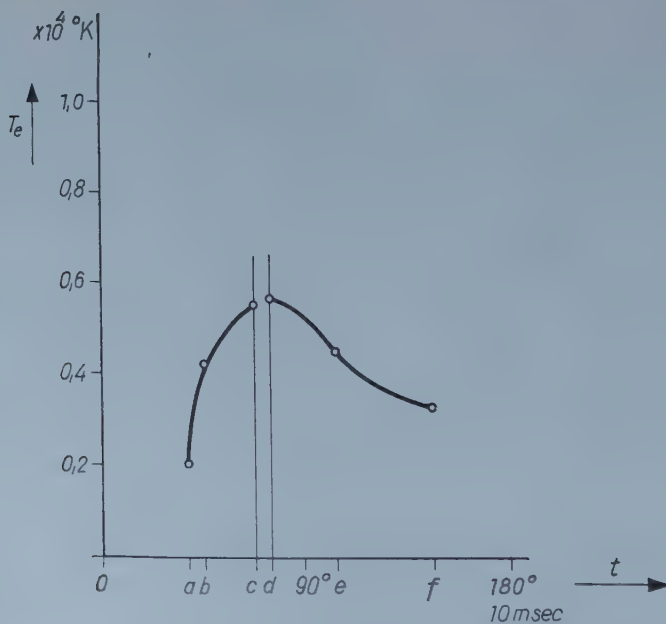


Fig. 3. Electron temperature vs. time

grams in this region could not be well evaluated. The region $c-d$ is visible also in Fig. 4, which represents the time dependence of the tube voltage. From this it can be seen that the region in question coincides with that of the voltage breakdown. From Fig. 3 it can be seen that the electron temperature within

the examined region is the highest at the phase angles belonging to the points *c* and *d*.

The time dependence of the electron concentration n is shown in Fig. 5. According to this, the electron concentration within this region, at the begin-

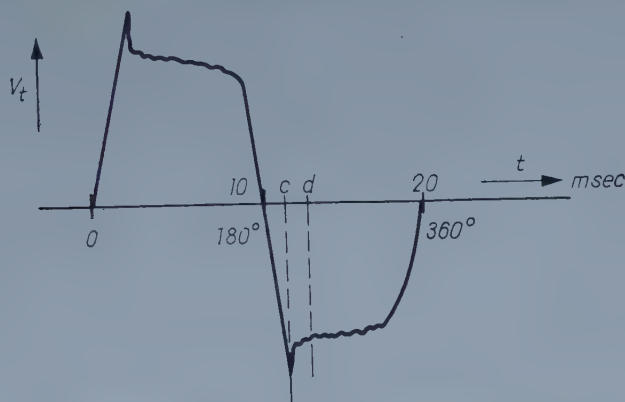


Fig. 4. Tube voltage vs. time, *c*—*d* voltage breaking phase

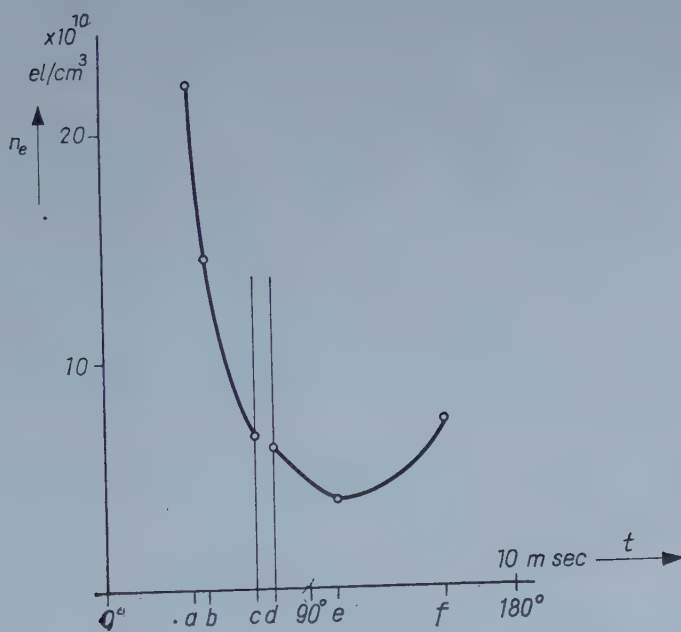


Fig. 5. Electron concentration vs. time

ning of the half period is still the highest in the phase before the breakdown and it decreases gradually till the middle phase of the half period, where there is a minimum in the neighbourhood of the phase angle *e*. The slope

of the curve in the region $a-c$, where presumably there is as yet no ionization, gives the recombination velocity

$$v_r = \frac{dn_e}{dt}. \quad (4)$$

The time dependence of the recombination velocity v_r in the region $a-c$ calculated from the data of Fig. 5 is shown in Fig. 6. It can be seen that the

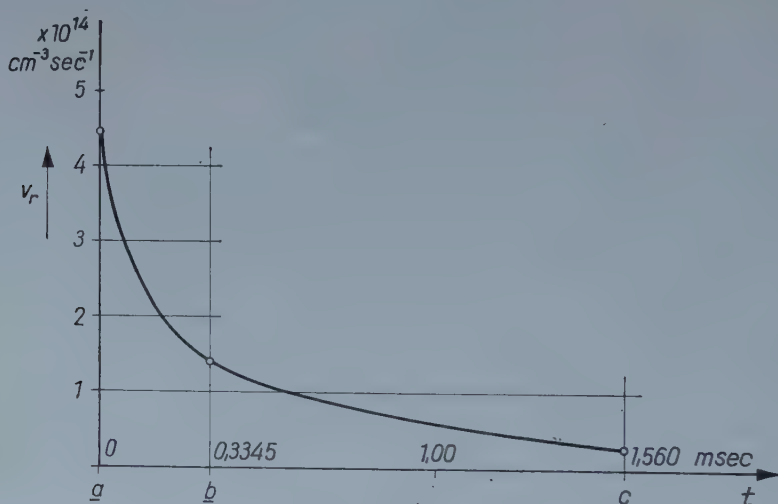


Fig. 6. Recombination velocity vs. time; points a , b and c see in Fig. 5

recombination velocity decreases with the time similarly to the electron concentration. The region $a-c$ of the curve plotted in Fig. 5 can be described by the following empirical formula:

$$n_e = n_{e0} \exp(\beta t), \quad (5)$$

where n_{e0} means the electron concentration belonging to the phase point a , t the time and $\beta = f(t)$, the value of which at the phase b amounts to 766 sec^{-1} and at the phase point c to 1425 sec^{-1} .

Applying the equations (4) and (5) the recombination velocity v_r in the region $a-c$ can be given by the following equation:

$$\frac{dn_e}{dt} = -\beta n_{e0} \exp(-\beta t). \quad (6)$$

From the relations of the recombination occurring in the region $a-c$, i. e. equs. (5) and (6), and the equation of the volume recombination [6]

$$-\frac{dn_e}{dt} = \varrho_e n_e^2, \quad (7)$$

in which ϱ_e is the coefficient of the volume recombination, the surface recombination can be determined, if ϱ_e is known.

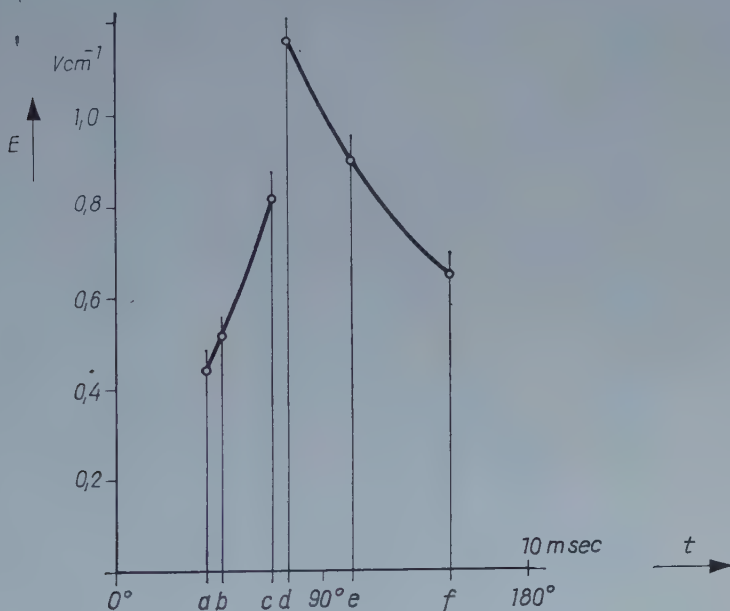


Fig. 7. Electric field strength vs. time

In this way information can be obtained concerning the relation between the tube diameter and the surface recombination which — as is known [7] — influences the value of the gradient. Some further experiments are still required to clear this point.

By determining the value of the plasma potential in the above-mentioned way around more probes the gradient of the positive column could be determined from the potential difference between the plasma points and the distances between them. The calculated values of this for the examined region $a-f$ are shown in Fig. 7, from which it is apparent that the time dependence of the gradient is similar to that of the voltage of the gas discharge tube (Fig. 4).

Finally, from the time dependence of the plasma potential measured at all the three probes in the way known from the literature [8] also the time dependence of the anode- and cathode-fall could be determined. For this determination it was necessary to measure the extension of the cathode dark space in the direction of the axis of the discharge tube. The time dependence of the cathode- and anode-fall can be seen in Fig. 8, from which it is evident

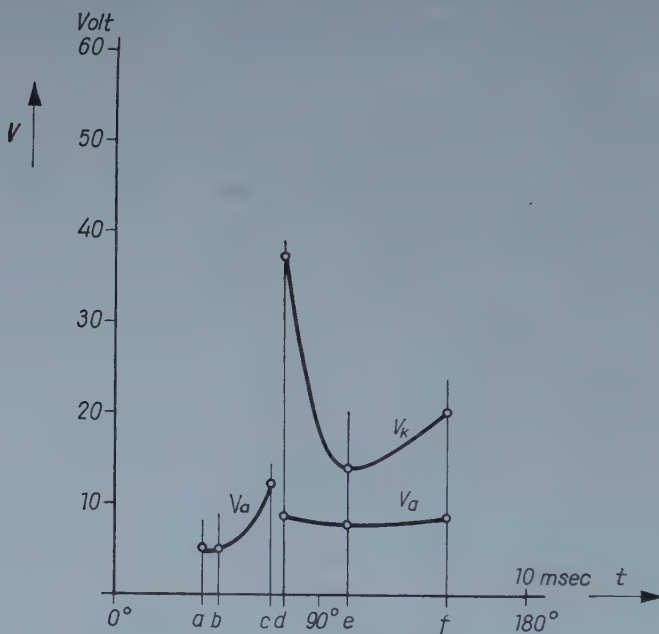


Fig. 8. Time dependence of the cathode- and anode-fall

that the anode-fall in the examined regions changes to a smaller degree and is of a lower value than the cathode-fall.

The measurements described above and their further extensions to the surface recombination can contribute to the widening of our knowledge concerning the physical processes occurring in a. c. discharges.

REFERENCES

1. I. LANGMUIR and H. MOTT-SMITH, General Electric Review, **27**, 449, 538, 616, 762, 1924.
2. W. VERWEIJ, Physica, **25**, 980, 1959.
3. R. A. LEDRUS, Appl. Sci. Res. Sec. B **5**, 151, 1955.
4. J. FAJT and J. KONCZ, Meeting on Gas Discharges. Balatonvilágos, 1958.
5. J. F. WAYMOUTH, J. Appl. Phys., **30**, 1404, 1959.
6. A. VON ENGEL, Ionized Gases, Oxford, Clarendon Press, 1955.
7. E. NEUMANN, Die physikalischen Grundlagen der Leuchtstofflampen und Leuchtröhren, VEB Verl. Technik, Berlin, 1954.
8. E. NÖLLE, Technisch-wissenschaftliche Abhandlungen der Osram Gesellschaft, **7**, 65, 1958.

ЗАВИСИМОСТЬ НЕКОТОРЫХ ПАРАМЕТРОВ ГАЗОВОГО РАЗРЯДА
ПЕРЕМЕННОГО ТОКА ОТ ВРЕМЕНИ

Г. ЛАКАТОШ и Я. БИТО

Резюме

Авторами исследуется зависимость разных параметров разряда от времени в смеси ртутных паров и аргона в разрядной трубке с горячим катодом переменного тока низкого давления.

При исследовании данной зависимости применялся метод измерения зондами переменного тока Файта и Конца, основанный на методе Лэнгмюра. Для случая, когда катод не нагревается извне, определяется зависимость от времени, напряженности поля, электронной температуры, концентрации электронов, скорости рекомбинации, катодного и анодного падений. Приводятся соответствующие диаграммы.



FISSION PRODUCT PRECIPITATION FROM THE ATMOSPHERE IN DEBRECEN, HUNGARY, BETWEEN 1958 AND 1960

By

A. SZALAY and A. KOVÁCH

INSTITUTE OF NUCLEAR RESEARCH OF THE HUNGARIAN ACADEMY OF SCIENCES, DEBRECEN, HUNGARY

(Received 27. II. 1961)

Observations concerning the atmospherical precipitation of fission products were continued during 1958—1960.

The cessation of nuclear test explosions since Nov. 1958 made it possible to approximately measure the clean up rate of fission products in the atmosphere. A mean residence time of 0,45 years and a clean up half period of 0,3 years were observed. Owing to this, a reduction of fission product contamination of the atmosphere to one hundredth of its original value can be expected within two years.

The clean up therefore is much quicker, and the rate of mixing between stratosphere and troposphere seems to be more intense than anticipated. The fission product contamination decreases to 10% of its original value within one year. In this reduction the effect of the mixing between the air masses of the stratosphere and troposphere and the radioactive decay are included. The mixing rate of the air masses of the stratosphere (or at least that of the lower layers of it) is about 75% per year.

The atmospheric precipitation has been observed without interruption and by the same methods at this Institute since 1952 [1], [2], [3], [4], [5]. The measurements we are dealing with in this paper were made between 1958 and 1960 and indicate a very rapid decrease of contamination since the cessation of nuclear test explosions in November 1958.

The atmospheric precipitation has been collected each morning, whenever there was any precipitation in an ombrometer with a PVC funnel 40 cm in diameter. We suppose — in agreement with other authors [6] — that by such a sampling method practically the total fallout can be gathered. Most of the fallout is brought down by rain and snow. Dust fallout deposited on the funnel is mostly washed into the bottle by the next rain. The total water sample containing the dust and soot particles is removed from the bottle and concentrated by evaporation in a porcelain dish, then carried into a sample measuring glass cup of 25 mm inner diameter and 8 mm high. (For detailed description of methodics see Ref. [4].)

The sample is measured about 48 hours after collection by an end-window GM counter 25 mm in diameter with an aluminium window thickness of 0,1 mm.

The quantity of water and the measured activity is then reduced so as to refer to the dimensions of a normal meteorological ombrometer, i. e. to a surface of $1/50 \text{ m}^2$. In the earliest measurements (in 1952) a normal meteorological ombrometer was used, but later experience warranted a

change over to the collection method described above. In the earlier measurements (1952—53) activity was partly adsorbed by the zinc funnel of the meteorological ombrometer and the quantity of water was often too low because of the small amount of precipitation.

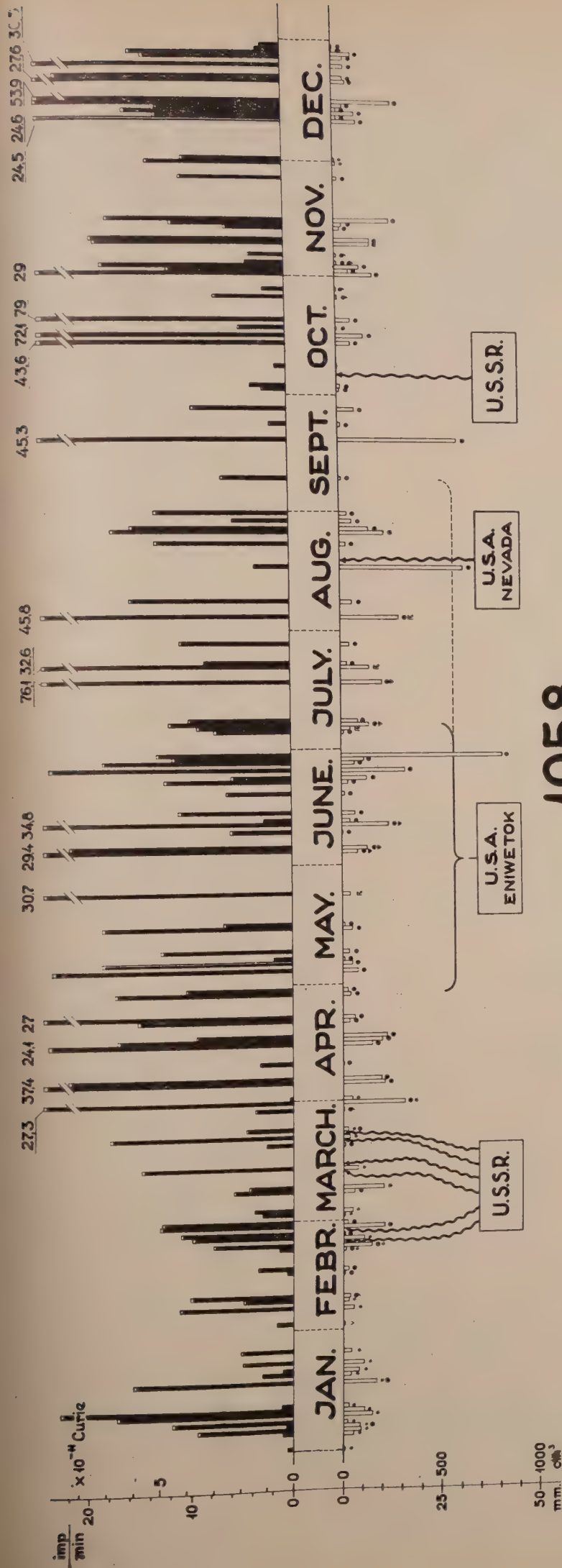
The GM counter was calibrated with an uranium oxide standard placed in the same type of glass measuring cup and in the same geometrical arrangement. No corrections were made either for the standards or for the atmospheric precipitation samples for the absorption in the Al-window of the GM counter tube.

Fig. 1 represents the measured activities as the function of calendar time. Black lines denote the measured activities. The ordinate shows the activity in actual counts/min., but reduced to a $1/50 \text{ m}^2$ ombrometer surface. On the right side of the ordinate the activity is denoted by 10^{-11} Curie units. Considering that during the year 1958, like in preceding years, activity was sometimes so high that the height of the black lines could not be represented proportionally, these were not drawn fully and the activity was presented in counts/min. above them. Empty downward lines represent the quantity of collected precipitation in mm and in volume, respectively, reduced to a normal ombrometer surface of $1/50 \text{ m}^2$. The type of meteorological precipitation is marked by the usual meteorological key.

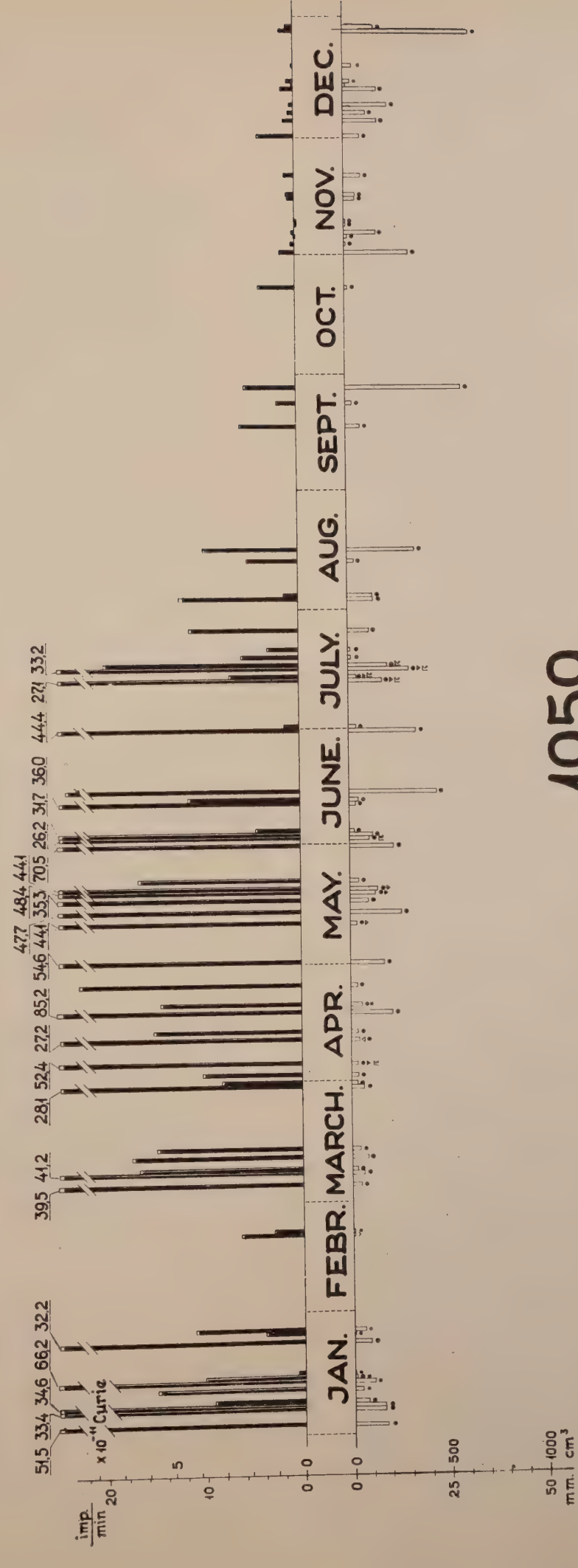
Known atomic bomb tests are marked on the calendar time abscissae as precisely as possible, but owing to the fact that information concerning atomic bomb tests has been scanty, accuracy and fullness of the records cannot be guaranteed.

If the activity of the years 1959 and 1960 is compared with earlier measurements at this Institute, a very large decrease can be observed since the middle of 1959. The cessation of the tests, dating from November 1958, has led to a quicker decontamination of the atmosphere than was anticipated [7], [8], [9].

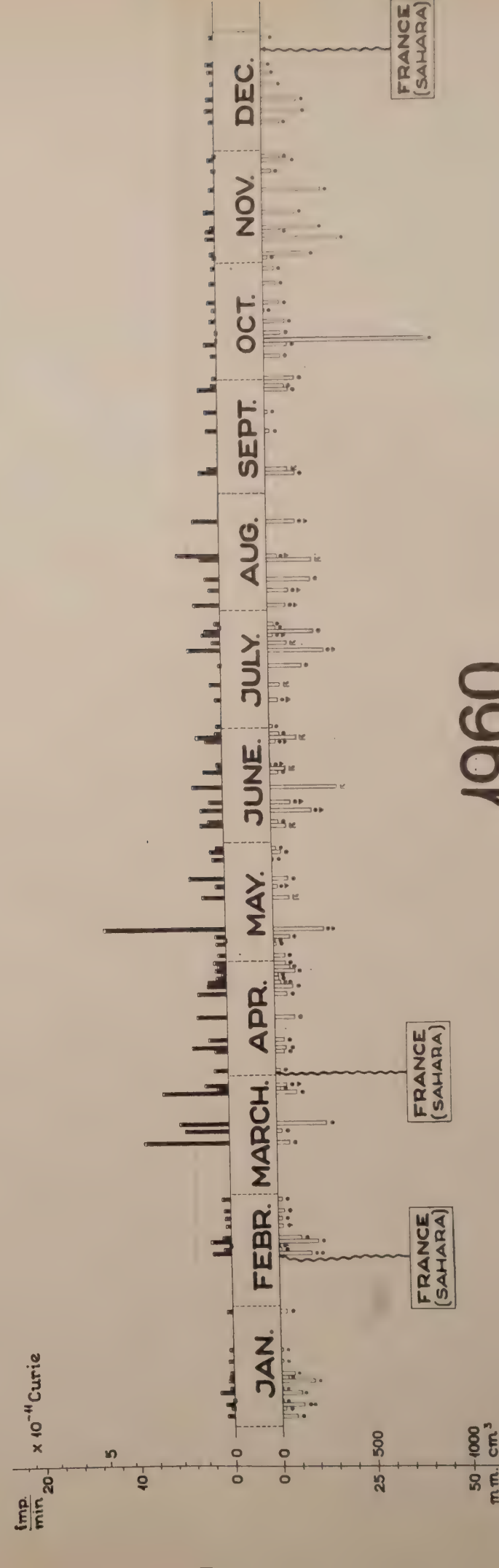
It is well known that in an atomic bomb explosion in the air the fission products are distributed between the troposphere and the stratosphere, and the distribution quotient depends upon the energy and height of the explosion, etc. The fission products of the troposphere are carried down within about one month by the atmospheric precipitation [6], [10]. Smoke particles of nuclear explosions (in diameter less than some tenths of a micron) may float in the stratosphere for many years, as they are not markedly influenced by gravitation. Since there is no water and precipitation in the stratosphere, the only process which carries down the activity from the stratosphere is the mixing of the air masses between the stratosphere and troposphere. It was assumed [7], [8] that this mixing process is very slow and that it would take 10 or at least 4 years for the fission products of the stratosphere to come down to the surface of the Earth.



1958



1959.



1960.

METEOROLOGICAL KEY USED: • RAIN, • FOG, ▴ SHOWER, ▽ THUNDERSTORM, ▴ HAILSTORM, ▽ RIME,

Fig. 1. Fission product precipitation from the atmosphere in Debrecen, Hungary, between 1958 and 1960. Ordinate upwards, right: Activity observed, in 10^{-11} Curies, corrected for the geometry of the counting equipment. Ordinate downwards, left: Activity observed, in cpm reduced to $1/50 \text{ m}^2$ ombrometer surface. Very large activities are not shown linearly but by numbers indicating observed cpm . Ordinate downwards, right: One day's rainfall expressed as volume collected from an exposed area of $1/50 \text{ m}^2$. Ordinate downwards, left: One day's rainfall, in mm . Abscissa: Calendar time



Considering that the last nuclear test explosions took place in October 1958, it can be assumed that all measurements since the end of 1958 have actually concerned fission products coming down from the stratosphere.

In contradiction to all expectations, activity decreased rather quickly in the second half of 1959. A further marked decrease was observable during 1960, and at present activity is nearly negligible.

As it is well known, the cessation of nuclear test explosions was interrupted in 1960 by 3 French bomb tests carried out in the Sahara. These tests

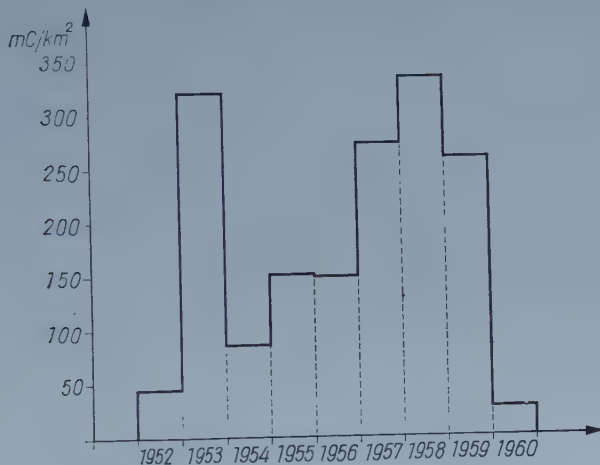


Fig. 2. Total yearly fallout of fission products in Debrecen, Hungary. Ordinate: Total yearly fallout, not corrected for radioactive decay, in millicuries/km². Abscissa: Calendar time. (Note the rapid decrease in 1959 and 1960, since the cessation of nuclear test explosions.)

did not remarkably affect the contamination of the atmosphere, at least not above Debrecen.

Fig. 2 shows the total yearly fallout calculated from our measurements, in millicurie/km² units, since 1952. The decrease of atmospheric contamination since the cessation of nuclear test explosions seems to have been very quick. If we assume that the total fallout of 1959 and 1960 came from the stratosphere, we can calculate a decontamination half period ($T_{1/2}$) of the stratosphere as well as the "mean residence time" (τ) of the involved fission products. This half period is defined as the time necessary for the stratosphere to loose half of its fission product contamination.

For this calculation the following assumptions are to be made:

a) At the end of 1958, the fission products were uniformly distributed in the air masses of the stratosphere.

b) By the same time, the fission products of the troposphere originating immediately from explosion tests (so-called "tropospheric fallout") had already

been cleaned up by atmospheric precipitation, thus the activities measured in 1959 and 1960 came entirely from the stratosphere.

c) The mixing of the air masses of the stratosphere and troposphere in the years 1959 and 1960 was not exceptional. We assume that it was of about the usual extent, and each year about the same fraction of the air masses is being mixed.

d) Activities produced by the French atomic tests are neglected.

According to these assumptions, the total measured fallout of the year 1959, denoted by A_1 , is proportional to the fission product content of the stratosphere for that year, A_2 for 1960 and so on. With assumption c) we can expect $A_2/A_1 = A_3/A_2 = A_4/A_3$ etc. for the subsequent years.

Let us denote by (M) the total air mass of the stratosphere, by (A) its total activity (supposed to be uniformly distributed) and by (dM) and (dA) , respectively, their fraction carried down into the troposphere during the time interval (dt) . We can define a constant (τ) , the "mean residence time", of the activity in the stratosphere, so that the following equation is valid according to the assumptions made above:

$$\frac{dM}{M} = \frac{dA}{A} = -\frac{dt}{\tau}.$$

The solution of this equation is

$A = A_0 e^{-\frac{t}{\tau}}$, where A_0 is the total activity at time $t = 0$, and A is the same at time t .

The observed yearly total fallout was $A_1 = 261$ mC/km² during the year 1959 and $A_2 = 27,7$ mC/km² during 1960 (Fig. 2) with an interval of one year ($t = 1$), in between, thus

$$\frac{A_2}{A_1} = e^{-1/\tau} \quad \text{and} \quad \ln \frac{A_2}{A_1} = -1/\tau.$$

Inserting the numerical values for A_1 and A_2 , $\tau = 0,45$ years is obtained for the "mean residence time" of the activity in the stratosphere. The activity of the stratosphere decreases by a factor e during this time interval, that is to 37% of its previous value. Similarly, the time necessary for a decrease to one half ($T_{1/2}$ or to one tenth ($T_{1/10}$) can be computed:

$$T_{1/2} = 0,3 \text{ year and } T_{1/10} = 1,0 \text{ year.}$$

The total fission product contamination of the atmosphere is reduced within one year to one tenth and within two years to one hundredth of its original value.

These observations show that the clean up rate of the fission products of the whole atmosphere is quicker than supposed, the mixing between the troposphere and stratosphere being more intense than anticipated.

In the calculations above, no corrections have been made for the radioactive decay of fission products, hence the clean up rate of the atmosphere determined above includes also the effect of radioactive decay of the products. This is not objectionable from the point of view of public health, but perhaps it would be so if from it we tried to determine the mixing rate of the troposphere and atmosphere. From the calculations above, the mixing rate of the stratosphere and troposphere would be about 90% per year, at least in the lower layers of the stratosphere. This value is probably higher than the real one, because the radioactive decay of fission products has the effect of a seemingly larger mixing rate. This error could be avoided by selecting long-lived fission products (e. g. Sr—90, Cs—137) from the total fallout. Unfortunately, this possibility has been neglected and the quantity of samples collected was not sufficient for this purpose.

The effect of radioactive decay can be taken into consideration by applying for correction the WAY—WIGNER formula, which describes the collective decay of fission product as follows:

$$A(t) = A(1) \cdot t^{-1,2}$$

where t denotes the time, which has elapsed since the nuclear explosion, $A(t)$ is the activity at the time t , and $A(1)$ the activity at the first unit of time after the bomb test.

By a simplifying approximation, we can consider the activity of the stratosphere in the years after the cessation of atomic bomb tests as if it had been produced by a single hypothetical nuclear explosion in the year 1958. This simplification is justified by the fact that the preceding calculation indicates a rather high mixing rate between the stratosphere and the troposphere, so that fission products from explosions earlier than 1958 represent only a small percentage of the fallout of the years 1959 and 1960.

Now taking one year for the unit of time, the total activity of the stratosphere (without mixing and fallout) one year after the hypothetical single explosion, that is in 1959, would be $A(1)$ and in 1959 it would be $A(2)$. According to the WAY—WIGNER formula

$$\frac{A(2)}{A(1)} = 2^{-1,2} = 0,435 = 1/2,3.$$

On this assumption, the amount of fission products must have decayed from 1959 to 1960 (within one year, two years after the hypothetical explosion) to 43,5%. Therefore, if we want to correct the value of A_2 for radioactive

decay, we must multiply it by the factor 2,3. In computing the real mixing rate between the air masses of the stratosphere and the troposphere, we must use this corrected value for A_2 . The corrected values for this calculation are $A'_1 = 261,5 \text{ mC/km}^2$ (as before) and $A'_2 = 2,3 \cdot 27,7 = 63,71 \text{ mC/km}^2$. Now by a calculation similar to the above, we can calculate the "mean residence time" (τ') of the air mass M in the stratosphere, with the result

$$\tau' = 0,71 \text{ years,}$$

and consequently $T'_{1/2} = 0,49$ years. This means, that the mixing rate between the stratosphere and troposphere is about 50% in half a year, and about 75% in one year.

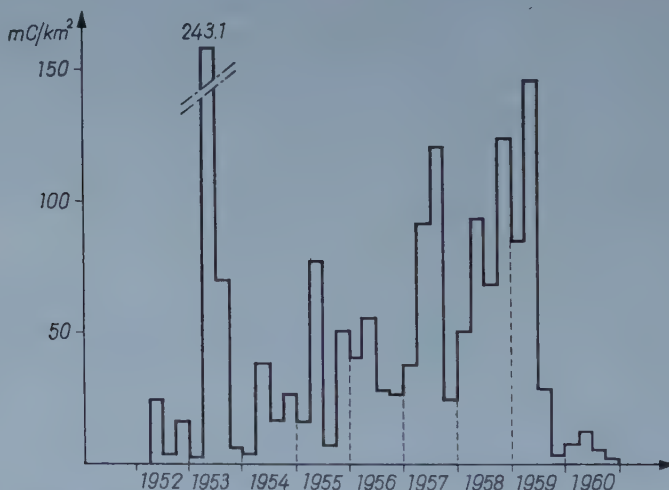


Fig. 3. Total fallout above Debrecen, Hungary, in quarterly distribution. Ordinate: Total fallout, not corrected for radioactive decay, in millicuries/km². Abscissa: Calendar time. (Note the relative maximum of fallout in the Spring of each year.)

Fig. 3 represents the fallout in quarterly distribution. As stated by STEWART and others [11], [12] it can be seen that the rate of mixing between stratosphere and troposphere is the most intense in the second quarter of the year.

REFERENCES

1. A. SZALAY and D. BERÉNYI sen., *Acta Phys. Acad. Sci. Hung.*, **5**, 1, 1955.
2. A. SZALAY and D. BERÉNYI sen., *MTA III. Oszt. Közl.* **5**, 89, 1955.
3. A. SZALAY and D. BERÉNYI sen., *MTA III. Oszt. Közl.* **9**, 175, 1959.
4. A. SZALAY—D. BERÉNYI, *Proc. 2nd Geneva Conf.*, P/1953, Vol. 18. p. 570.
5. A. KOVÁCH and A. SZALAY, *ATOMKI Közlemények*, **2**, 229, 1960.
6. W. ANDERSON et al., *Nature*, **186**, 925, 1960.

7. F. W. LIBBY, Proc. US. Natl. Acad. Sci., **42**, 365, 1956.
8. F. W. LIBBY, Proc. US. Natl. Acad. Sci., **45**, 738, 1957.
9. H. W. FEELY, Science, **131**, 645, 1960.
10. N. G. STEWART, et al., AERE Publ. No. AERE HP/R 1701, 1955.
11. N. G. STEWART et al., AERE Publ. No. AERE HP/R 2354, 1957.
12. P. K. KURODA et al., Science, **132**, 742, 1960.

ОСАЖДЕНИЕ ПРОДУКТОВ ДЕЛЕНИЯ ИЗ АТМОСФЕРЫ В Г. ДЕБРЕЦЕН В ВЕНГРИИ В 1958—1960 Г. Г.

А. САЛАИ и А. КОВАЧ

Резюме

Наблюдения атмосферных осадков по отношению продуктов деления последовательно проводились и в 1958—1960 г. г.

Прекращение опытных атомных взрывов в ноябре 1958 года дало возможность для приближенной оценки скорости уменьшения продуктов деления в атмосфере. Для среднего времени сохранения продуктов в стратосфере было получено 0,45 года, а для времени половинного очищения — 0,3 года.

Согласно этому можно ожидать, что загрязнение атмосферы радиоактивными продуктами за два года уменьшается до одной сотой доли его первоначального значения.

Поэтому очистка происходит намного быстрее и смешивание между слоями тропосферы и стратосферы происходит в больших масштабах, как это предполагалось раньше.

Загрязнение продуктами деления за один год уменьшается до 10% его первоначального значения. В данной очистке играют роль как и радиоактивный распад, так и смешивание между воздушными слоями тропосферы и стратосферы.

Мера обмена воздушных слоев тропосферы и стратосферы (по крайней мере, ее низших слоев) составляет примерно 75% ежегодно.



LUMINESCENCE OF FLUORESCEIN ACTIVATED LAYER PHOSPHORS

By

E. LENDVAY

RESEARCH INSTITUTE FOR TECHNICAL PHYSICS OF THE HUNGARIAN ACADEMY OF SCIENCES, BUDAPEST

(Presented by G. Szigeti. — Received: 2. III. 1961)

The sodium fluorescein adsorption of oxide layers formed on aluminium surfaces gives layer phosphors emitting green light under the excitation of high-pressure mercury vapour lamps. The intensity and energy distribution of the light depends on the physical and chemical structure of the layer. It has been established that the activation of the oxide hydrate layers happens by chemisorption and that there is a relation between the hydration of the oxide surface and the energy distribution of the emission.

§ 1. Introduction

There are many organic compounds showing an intense luminescence in solution. Not so often, an effect of similar intensity appears also in case of solid solutions or on molecules adsorbed on solid bodies [1—9].

Several of the above-mentioned systems, containing practically only the solid phase, are called "organophosphors". The properties of these organophosphors arising by adsorption are determined chiefly by the surface properties of the adsorbent. The relation between surface phenomena and luminescent light emission justifies to distinguish these phosphors by the name of "adsorbate phosphors".

The so-called two-dimensional phosphors belong to the adsorbate phosphors. They can be prepared by means of organic compounds adsorbed on thin layers or films. CHOMSE et al. dealt with the properties of these phosphors.

The authors referred to above, examined the luminescence of 1-oxi-2-naphthonic acid, therephtalic acid, salicylic acid and tryptaflavine on aluminium, magnesium and zinc oxide, resp. hydroxide layers. In the course of their experiments they established that luminescent lighting appears only under certain conditions. This fact shows that not every adsorption process leads to the formation of layer phosphors, therefore all adsorption processes producing a luminescent system will further be called active adsorption.

The extraordinary low intensity of the lighting of the CHOMSE phosphors (the original publication does not contain data concerning either the intensity or the energy distribution) necessitated — by means of the choice of an adequate activator — the preparation of such a layer phosphor the spectral

examination of which can be effectuated. Such an activator is e. g. the fluorescein ion having in solution a well-known luminescence, but the data concerning its adsorbed state are very deficient.

In the following we report our experiments made on aluminium oxide layers where we have used the above-mentioned activator.

§ 2. Preparation of adsorbent layers

The oxide films on aluminium were prepared chemically or by means of the known methods of anodic oxidation [11—15]. The natural oxide film and the thin layers made by chemical and thermic methods proved to be unsuited to the preparation of layer phosphors. A fluorescent effect could

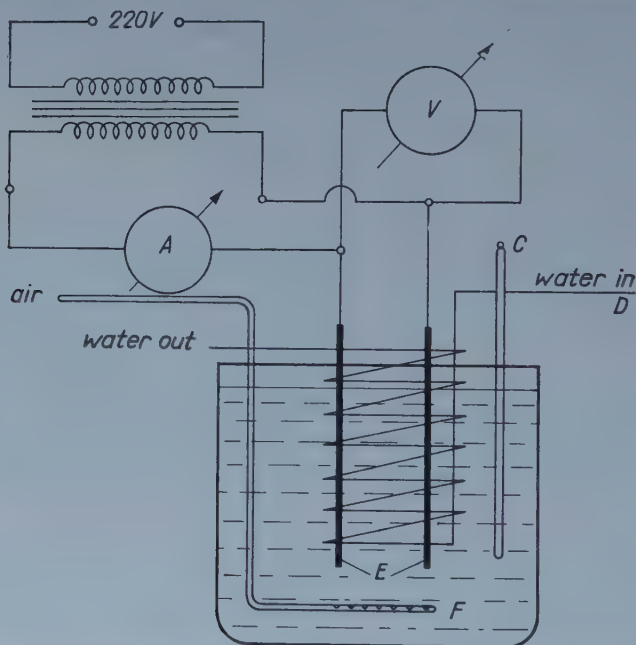


Fig. 1. A simple sketch of the apparatus for the electrolytic oxidation. A—ampermeter, V—voltmeter, D—glass-cooling coil, F—mixer, C—thermometer, E—aluminium samples

be demonstrated only in the latter case, however, the emitted green light was of such a low intensity that the spectral examination of the system did not succeed.

A similar observation was made by CHOMSE, who made a comparison between the normal boron phosphor and his layer phosphors. According to his statement concerning chemically-formed thin layers, when oxinaphthonic acid and terephthalic acid were used as activators, only 0.7—3% of the luminescent intensity of the boron phosphor made with the same activator could be detected [10].

The layers made by anodic oxidation showed more favourable properties, therefore we used them for the preparation of the layer phosphors. The samples to be oxidized were made of 99,9% pure aluminium sheets in the form of squares. Their surface was 100 cm² large of which 60 cm² was oxidized. Their cleaning before the oxidation happened by washing with solvent (CCl₄) and etching. The etching took place either with 5% NaOH at 35°C during two minutes or with a mixture of sulfuric acid — phosphoric acid — water at 100° C for one minute [16]. For the oxidation we used as electrolyte either 5% sulfuric acid or 7% oxalic acid. The grade of the used chemicals was reagent. The water used for washing the samples, preparing the electrolyte etc. was purified by ion exchange resin. In the majority of cases the oxidation happened by a. c. in the arrangement shown in Fig. 1 with a constant voltage value. The voltage switched on the cell was 18, resp. 40 V and depended on whether the oxidation happened in sulphuric acid or in an oxalic acid bath. The initial density of the current passing through the aluminium electrodes put into the glass tub was about 25 mA/cm². The constant temperature of the electrolyte was assured by a glass cooling coil and by a mixer by means of which the system could be held at 20° C during the period of the oxidation. The supply source was a TR 100 transformer. The time of oxidation was between 15 and 60 minutes according to the thickness of the layer. The formed layers were slightly coloured, their thickness was between 5 and 20 μ .

§ 3. Preparation of layer phosphors

The oxide layers made in the manner described above were washed thoroughly with cold ion-exchanged water and dried at 110° C. The oxide films obtained in this way — although they behaved favourably from the point of view of the adsorption, — in their active adsorption hardly surpassed the properties of the chemically produced thin layers. The hydrothermal after-treatment of the layers described by CHOMSE et al. [10] advanced the active adsorption but the order of magnitude of the emission hardly exceeded the lower limit of the intensity necessary for spectral examination. After the chemical treatment of the oxide films a satisfying result was obtained. The layers arising in the course of the treatment of the oxide films with alkaline solutions showed after the activation and under the influence of a 3650 Å ultraviolet excitation a uniform lighting of the same order of magnitude as that of the solutions, resp. exceeded it.

For after-treatment purposes a 0.1—5% soda solution seemed to be the most appropriate. The treatment took place during periods lasting from 1 to 60 minutes in a temperature interval between 20 and 80° C, without any pressure. When in a cold or warm soda solution for a longer time the layers first lost their yellowish colour and then under a stronger action, the

originally intensively reflecting surface became dull. The deterioration of the reflection properties did not influence the adsorption capacity of the layers to any considerable degree. After the treatment the elution of the electrolyte was followed by drying at 100° C.

Also with ammonium hydroxide and borax solutions suitable adsorbents could be produced, but the light emitted after the activation was considerably fainter than in the first case.

The activation of the aluminium hydroxide films prepared in the way described happened by adsorption from the absolute methanol-, resp. ethyl-alcoholic solution of sodium fluorescein. The adsorption took place on closed vessels on vertically placed plates, at equal initial dye concentration and equal adsorbent oxide surfaces. The initial concentration of the activator solution was $1,0 \cdot 10^{-3}$ mol/l sodium fluorescein. The adsorption took place in every case at room temperature and lasted from 30 minutes to 24 hours. After the adsorption and removal of the excess fluorescein by washing, the plates were dried at 110° C. The ready plates, according to the prepared adsorbent layer and the circumstances of the adsorption, were colourless, or became greyish, yellow or orange.

§ 4. Measurement of the emission of layer phosphors

The emission spectrum of the produced layer phosphors has been studied by means of an automatic spectrometer built in our Institute [17]; its construction can be seen in Fig. 2. The exciting light source was a Philips Black Light high pressure mercury vapour lamp (1), which illuminated through a UG—11 filter (2) the sample placed in the sample holder (3). In order to calibrate the energy distribution, the light of a normal lamp of determined colour temperature could be inserted in the way of the light by means of a prism (9).

The light passed through the optical system of a Zeiss monochromator and fell on a multiplier (5). Between the entrance gap and the sample there was a synchron motor-driven sector of a circle (6) with an auxiliary lamp (7) and a CdSe cell (8) on it, producing a sign synchronous with the interrupter period of the sector for the phase-sensitive rectifier.

In Fig. 3 the block scheme of the electric sensing element of the instrument can be seen. The sign given by the multiplier came through a high frequency noise suppression integrating filter to an indexing chain serving for the extension of the measuring limit. This was followed by a two-stage amplifier, then by a continuous sensitivity regulator. After another two-stage amplification the sign reached the measuring circuit of the phase-sensitive detector. A self-running multivibrator was controlled by the secondary mark of the CdSe cell, through a phase shift quadripole, after a one-stage amplification. After further amplification this sign controlled the switching circuit

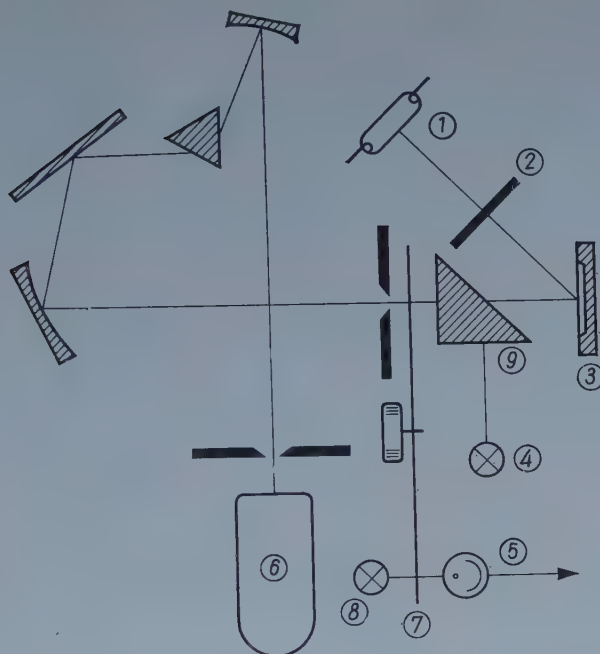


Fig. 2. The optical system of the automatic spectrometer

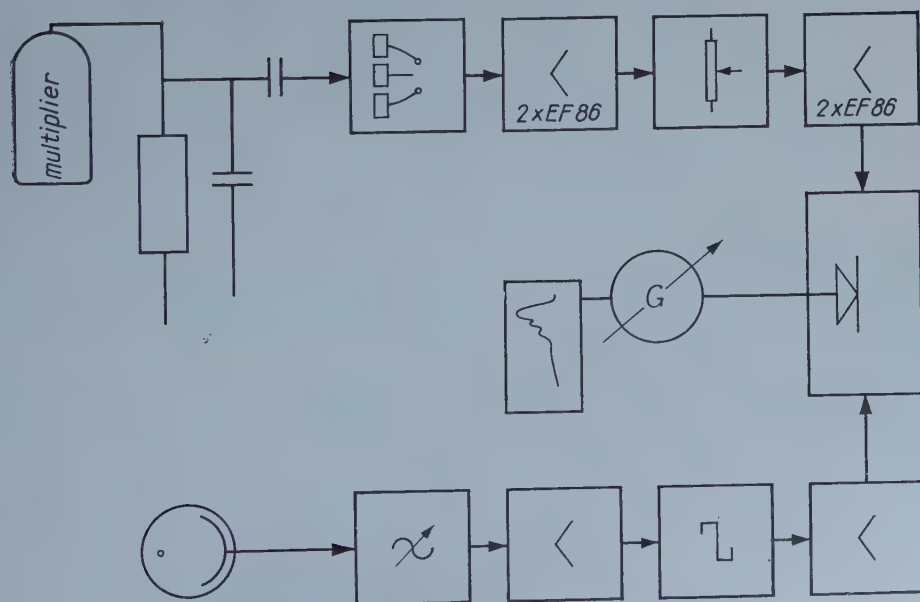


Fig. 3. The block scheme of the electric sensing element of the instrument

of the phase detector which was a four-diode system and rendered possible producing a 0.5 Hz bandwidth.

The reading part of the device consisted of a system made of a series-connected, mirror-scale precision instrument and an EKM six-point recording instrument.

The samples used for the emission measurement were $25 \times 25 \text{ mm}^2$ aluminium plates, on the surfaces of which was placed the layer phosphor to be measured.

§ 5. Emission properties of layer phosphors

According to the chemical treatment of the $\text{Al}_2\text{O}_3 \cdot \text{H}_2\text{O}$ layers we obtained spectra of various characters. Also in case of using activator solutions of the same concentration and working with same adsorption time, a

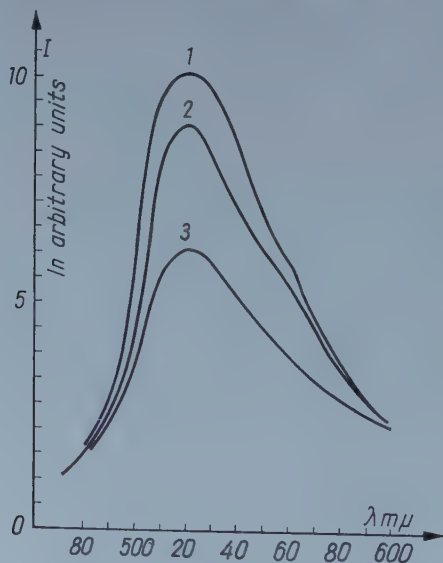


Fig. 4. The spectra of the layer phosphors which were prepared with water
Curve 1: CHOMSE's phosphor. Curves 2—3: Spectra of the layers which were treated with boiling water before the adsorption

deviation arose on the one hand in the intensity of the emitted light of one and the same frequency and on the other hand in the ratios of the measured intensities belonging to the various frequencies.

The layer phosphors obtained by the application of the CHOMSE hydrothermal after-treatment (in this case in a sealed glass-tube at 250°C by heating with water) emitted light of a very small intensity. Their emission spectra can be seen in Fig. 4. The colouration of the plates after the adsorption was only slight. The maximum intensity did not surpass 20—25% of that

of the phosphors to be discussed later. A similar result was obtained also by the simple watery boiling.

Before the adsorption of the fluorescein, boiling the aluminium oxide layers in distilled water for an hour, we obtained after the adsorption of the dye layer phosphors of the same emission peaks and of similar intensity. (See Fig. 4, curve 2.) The above statement concerns aluminium plates formed in a vitriolic electrolyte. From the watery boiling of layers formed in oxalic

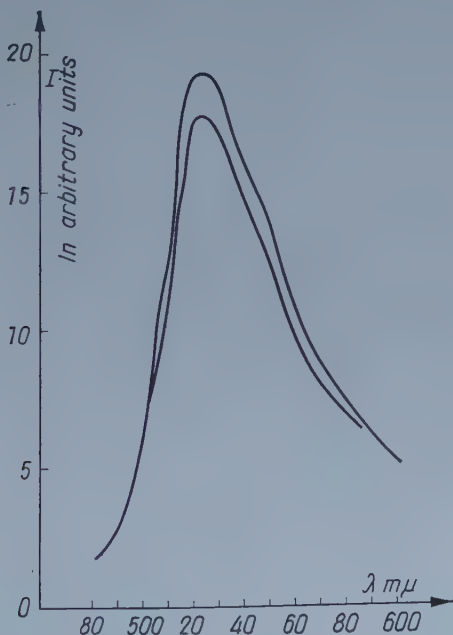


Fig. 5. Spectra of layers which were treated with 1% soda solution at 25° C before the adsorption

acid a phosphor arose lighting much more faintly, the spectrum of which can also be seen in Fig. 4 (curve 3). The maxima of all the three spectra fell to 521 mμ.

The lighting capacity of the layers rose considerably, when the oxide films were treated with alkaline solutions instead of receiving an aqueous treatment. Staying in a 25° C soda solution for 15 minutes, the adsorption capacity of the plates increased. After removal of the electrolytes by washing with boiling water, the emission of the layer phosphors after the adsorption grew about four times. Their emission spectra can be seen in Fig. 5. The plates did not change their colours during the adsorption but lost their original specular reflection. The maximum of the emission band — similarly to the formed cases — was at 521 mμ.

We succeeded to observe the long wave displacement of the emission band under a stronger alkaline influence. At 50° C during 10 minutes a treatment with 1% soda solution and then a washing with boiling water gave such aluminium oxide layers after the activation of which the peak of the emission band of the phosphor fell to 525 m μ . During the adsorption the layers took on a slightly yellowish colour. Their emission bands are shown in Fig. 6. The figure shows the spectra of layer phosphors prepared from

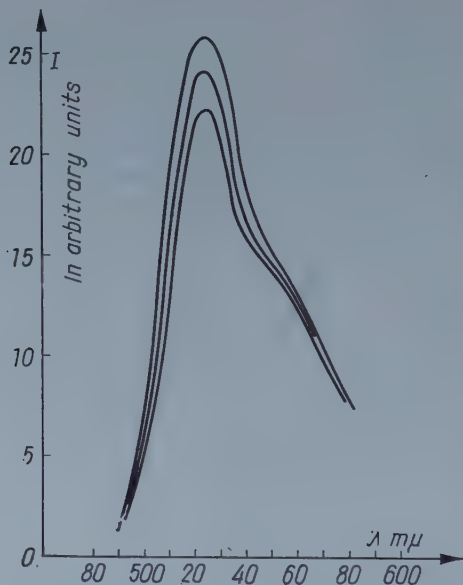


Fig. 6. Spectra of layer phosphors, which were treated with 1% Na_2CO_3 solution at 50° C before the adsorption. The different curves belong to the different oxidizing times

plates formed during various times. As can be seen, the thickness of the layer influences the emission to a small degree. The slight growth of the intensity is probably the result of the increase of the specific surface.

The treatment of the oxide film with boiling soda solution called forth the further increase of the intensity and the long wave displacement. Under the influence of a 80° C warm, 1% soda solution the maximum of the emission band migrated to 531 m μ . The plates became orange coloured after the adsorption. The spectra of layer phosphors formed during 40, 50 and 60 minutes are shown in Fig. 7.

The treatment with other alkaline chemicals was less effective. When the aluminium oxide film was softly heated with ammonium hydroxide solution (40—50° C), only a small increase of the intensity could be observed compared to the watery treatment. The maximum of the emission band

was — similarly to the other layer phosphors — at $521\text{ m}\mu$. The colour of the plate after the adsorption was slightly yellow, the light of the surface being very uniform. The spectrum is shown in Fig. 8.

From the enumerated examples it can be seen that the original oxide film after a stronger influence behaves more favourably from the point of view of producing layer phosphors.

Increasing the temperature of the soda solution treatment the intensity measured on the maximum of the emission of the layer phosphor increased

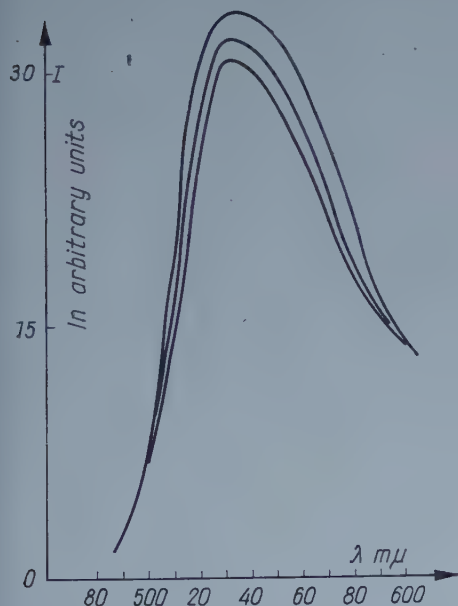


Fig. 7. Spectra of layers, which were treated with 1% soda solution at 80°C , before the adsorption. The different curves belong to the different oxidizing times

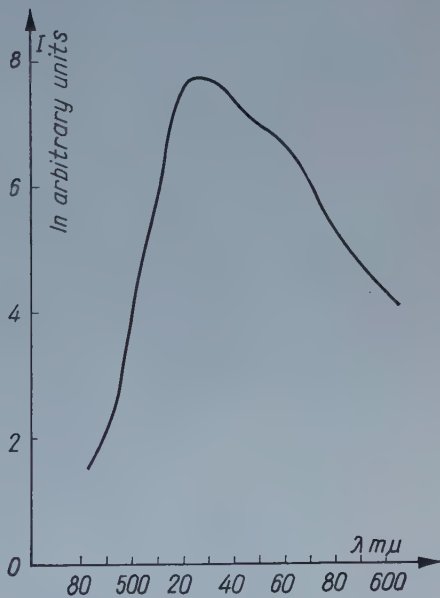


Fig. 8. The energy distribution of the layer phosphor which was treated with 1% ammonia solution at $40\text{--}50^{\circ}\text{C}$ before the adsorption

gradually. The increase of the concentration resp. temperature of the reagents was limited by the fact that the emission of the layer became, under a stronger influence inhomogeneous and the layer was very much corroded by the solution. For similar reasons the KOH and NaOH were also unsuitable. In case of the latter reagents the corrosion of the oxide layers was considerable already in case of a low concentration and temperature. Beside the above-mentioned reasons, because of the inhomogeneity of the lighting of the surface obtained after the activation, we did not use the latter reagents.

In all the cases described the adsorption time was 24 hours. In the following section we will discuss the case when the adsorbing time changes.

§ 6. Adsorption time dependence of the luminescence of adsorbed fluorescein

After the experiments described in the previous paragraphs we examined the connection between the adsorption time and the luminescent intensity. By the spectral emission measurements it could be ascertained that the luminescence originating from the layer phosphors does not only depend on the hydration of the Al_2O_3 film, but under identical conditions of preparation on the duration of the adsorption too.

The adsorbent was prepared in the same way as in the previous section. The reagent used was 1% solution of Na_2CO_3 at 25°C and the adsorption

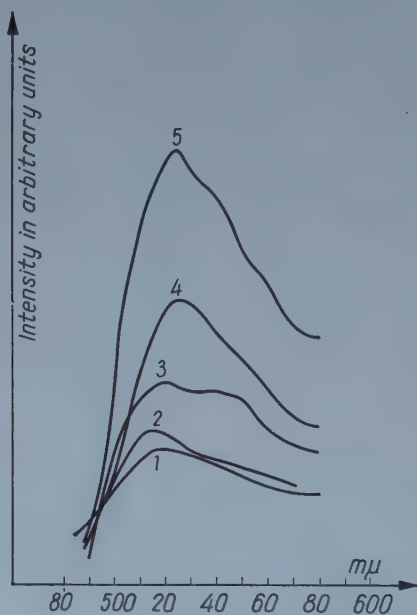


Fig. 9. The dependence of the spectra on the adsorbing time. Curve 1: 1 hour, Curve 2: 2 hours, Curve 3: 3 hours, Curve 4: 6 hours, Curve 5: 48 hours

took place in the way described in the foregoing section, from the solution of Na-fluorescein, in absolute methylalcohol as the solvent. For the measurement of the luminescence of the layer phosphors, prepared during different adsorbing times the instrument which was described previously was used. The spectra are shown in Fig. 9. From Fig. 9 it can be seen that both the form of the emission band and the wavelength of the maximum depend on the duration of adsorption. The wavelength of the maximum shifts to the longer wavelengths simultaneously with the adsorbing time and changes from $518\text{ m}\mu$ up to $524\text{ m}\mu$.

It can be shown that together with the shifting of the spectra the luminescent intensity strongly increases. The intensity tends toward a satur-

ation value, and after 30—40 hours generally does no longer change. Since the absorption equilibrium sets in slowly, we assumed, that there is a chemisorption, i. e. the amount of the adsorbat irreversibly adsorbed increases (up to a limit) with the time of contact allowed before desorption is commenced.

As it has been shown in Fig. 9, the form of the spectra depends on the adsorption time. The change of the energy distribution as function of the adsorbing time is rather complicated. This made the evaluation more difficult. In Fig. 10 the change of the intensities as the function of the duration of the adsorption at some selected wavelength can be seen.

The curves, which correspond each to one particular wavelength, are built up from some steep and some nearly horizontal sections. It can be seen

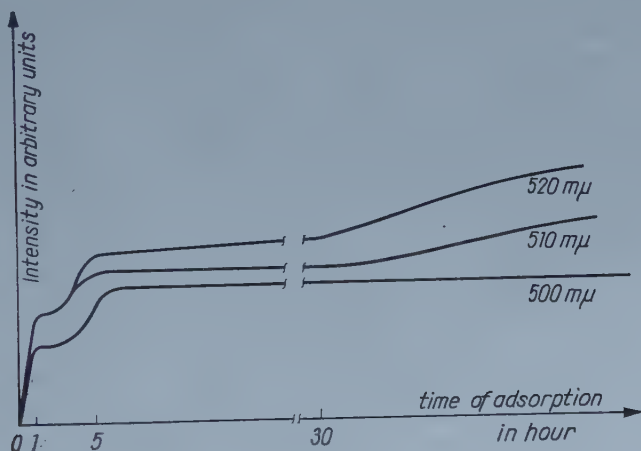


Fig. 10. The change of the intensities as the function of the duration of the adsorption at some selected wavelengths

that the character of the change is similar to that established by GOODMAN [19] in the case of the adsorption of water on ferric oxide. Similar results were obtained by the above-mentioned author and GREGG and STEPHENS with silicagel, stannic oxide gel and caolin [20].

The form of the curves, belonging to the lower wavelengths are similar and might be characterized by the curve belonging to 500 mμ. In Fig. 10 we can see that in the previously mentioned range of the wavelengths the change of the luminescent intensity is, after 6—7 hours, practically negligible. At the longer wavelengths the luminescent intensity reaches saturation only after 35—40 hours.

From this phenomenon it can be concluded that the adsorption takes place in several steps. The reaction, which takes place in the first step is pretty fast, viz. its reaction time is only 1—2 hours.

The rate of the following reactions is slower because their influence on the spectra appears only after a suitable period. These phenomena, especially the fact that the adsorption takes place in several, well distinguishable sections, verifies our supposition that in the case of the layer phosphors mentioned in the foregoing section, there are several kinds of centres of different characters on the surface termed "active sites".

Supposing that the rate of the fluorescein's adsorption, viz. the specific rate of reactions, on the different centres is different, we can simply interpret the change of the form of spectra as the function of the adsorbing time. It is evident that the adsorption is most rapid on those centres which possess the larger specific rate of reaction. If we pay attention to what was said previously, it becomes obvious that after a short adsorbing time the light originates chiefly from such luminescent centres which were formed in the first step. In this section the intensity of the luminescence increases rapidly. When the rate of adsorption in the first step decreases and tends towards zero, the increase of the intensity becomes slower, because the rate of the second and the third adsorption processes is less than that of the first one. Only after a suitable period appears the change belonging to the second resp. the third step in the spectra.

According to the suppositions mentioned above, the changes of intensities and the shift of the maximum in the spectra can thus be explained by the differences in the reaction velocities.

§ 7. Conclusions

On the basis of the experimental material reported it can be concluded that the light of the adsorbate phosphors differs from the light of the so-called "discrete centres".

The deviation is caused by the interaction of the lighting centre and the basic material (in this case $\text{Al}_2\text{O}_3 \cdot \text{H}_2\text{O}$). The fluorescein ion alone cannot be considered as the medium of the lighting. The fact that the adsorption of the dehydrated layers is inactive from the luminescent point of view shows that, in respect of the lighting centre, the interaction of the adsorbent and of the adsorbed molecule is of decisive importance. This makes the above-mentioned systems to some degree similar to the crystal phosphors. On that account the examination of the layer phosphors cannot be confined only to the organic activator, the whole adsorbatum must be treated as a uniform physical system, this similarity does not, however, mean complete analogy with the crystal phosphors. The hypothesis of CHOMSE al., according to which the organic molecule becomes during the treatment incorporated into the inorganic lattice, contradicts the experimental facts. The statement of the above-mentioned authors that the appearance of the light is closely connected with such an activator, analogous to the crystal phosphors, turned out to be

wrong. The exact examination of the lattice parameters renders in this case even the possibility of such an incorporation doubtful.

The incorporation into the crystal lattice would mean intensive perturbation of the electron system of the organic molecule because of the ionic character of the lattice. Naturally, this would result in a considerable change of the emission spectrum, but according to the measurement this does not occur.

From the wavelength displacement of the spectra one can conclude that the energy of the interaction is greater than in case of the solutions or the physically adsorbed molecules, but that it is considerably smaller than in the crystal phosphors. This proves the transient character of the examined systems between the discrete centres and the light of the crystal phosphors.

The fact that also without pressure lighting layers are obtainable with after-activation shows not the incorporation into the lattice but the adsorption to be the condition of the appearance of light. The adsorption from an alcoholic solution of the plates prepared without any chemical treatment can be compared to that of chemically treated oxide layers which are practically inactive; this shows that light is connected only with certain definite forms of the adsorption. A striking parallel can be observed between the hydration of the oxide film and the intensity of the light. The light of the oxide hydrate layers arising under the influence of a strong alkaline action is considerably more intensive than that of the layer phosphors made by hydrothermal treatment; besides, the process of the activation takes up much time. These two facts show that a chemisorption is taking place. From the wavelength displacement of the spectra it is evident that the energy of the adsorption influences to a high degree the emission of the layer phosphor. The intensity increase of the emission can be brought into connection with the change of the number of the centres and the wavelength displacement of the maximum with the change of the quality of the adsorption centres. It is obvious that the OH-groups of the adsorbent surface play an important part through the forming of hydrogen bridges. Taking into consideration that the aluminium oxide hydrate structure can contain hydroxyl groups arising from both, hydrargillite, resp. boehmit their adsorptions must be different. Further considering that the fluorescein contains also many functional groups, the difference in the emission peaks of the various layer phosphors becomes explainable.

Acknowledgements

The author expresses his thanks to Academician G. SZIGETI, the Director of the Institute, and to Dr. TH. MILLNER for reading the manuscript before publication. He also wishes to thank MR. J. SCHANDA and MR. J. WEISZBURG for carrying out the spectroscopic measurements.

REFERENCES

1. O. SCHMIDT, Ber. dtsch. chem. Ges., **74**, 987, 1941.
2. L. FLEXSER, L. P. HAMMET and A. DINGWALL, J. Am. Chem. Soc., **57**, 2103, 1935.
3. F. BANDOW, Z. Physik. Chem. (B), **34**, 323, 1936.
4. J. NASH, J. Phys. Chem., **62**, 1575, 1958.
5. G. N. LEWIS and M. KASHA, J. Am. Chem. Soc., **66**, 2100, 1944.
6. H. CHOMSE and G. HEINRICH, Naturw., **34**, 122, 1947.
7. L. GOMBAY, Kolloid Z., **101**, 157, 1942.
8. G. N. LEWIS, D. LIPKIN and TH. T. MAGEL, J. Am. Chem. Soc., **63**, 3005, 1941.
9. R. TOMASCHEK, Ann. Physik, **67**, 624, 1922.
10. H. CHOMSE, W. HOFFMANN, Z. Anorg. Chem., **296**, 20, 1958.
11. J. SCHENK, Werkstoff Aluminium und seine anodische Oxidation, A. Francke A. G. Verlag, Bern, 1948.
12. A. W. SMITH, Can. J. Phys., **37**, 591, 1959.
13. M. S. HUNTER, P. FOWLE, J. Electrochem. Soc., **101**, 514, 1954.
14. N. P. FEDOTJEV and I. KÓSA-SOMOGYI, Journ. Prikl. Chimii, XXXI., 497, 1958.
15. G. ELSSNER, Aluminium Oberflächenschutz durch elektrolytische Oxydation, Akad. Verlag, Leipzig, 1943.
16. W. J. TEGART, The Electrolytic and Chemical Polishing of Metals, The Pergamon Press Ltd., London, 1956.
17. J. SCHANDA, II. Tschechoslowakischer Spektrographischer Kongress, Tatranska Lomnica, 1959.
18. W. E. GARNER, Chemisorption, Butterworths Sci. Publ., London, 1957; p. 59.
19. J. F. GOODMAN, Thesis, London University, 1955.
20. S. J. GREGG, and M. J. STEPHENS, Clay Min. Bull., **1**, 228, 1952.

ЛЮМИНЕСЦЕНЦИЯ АДОРБИРОВАННОГО НА $\text{Al}_2\text{O}_3 \cdot x\text{H}_2\text{O}$ ПЛЕНКАХ ФЛУОРЕСЦЕИНА

Э. ЛЕНДВАИ

Резюме

На пленках Al_2O_3 , обработанных щелочными растворами, с адсорбцией флуоресцеина удалось приготовить такие слои, которые при возбуждении ультрафиолетовым светом хорошо люминесцируют.

Длина волны максимума полосы свечения зависит от метода химической обработки оксидной пленки. На основании передвижения максимумов можно сделать вывод, что мы имеем дело с хемосорбцией и что люминесцентные свойства адсорбированного флуоресцеина определяются, главным образом, химической природой поверхности адсорбента.

INVESTIGATION OF THE $^3\Pi$ STATE OF THE PH MOLECULE*

By

I. Kovács

DEPARTMENT OF ATOMIC PHYSICS, POLYTECHNICAL UNIVERSITY, BUDAPEST

(Received: 15. III. 1961)

Thorough investigations have shown that the $^3\Pi$ state belonging to the $^3\Pi_i - ^3\Sigma^-$ transition of the PH molecule does not closely follow the known triplet formula. The deviation consists in that the middle component of the $^3\Pi$ state — taken as a function of the rotational quantum number — lies in a different position from what would be expected on the basis of the triplet formula. By taking into account simultaneously the perturbation of the $^1\Pi$ terms transmitted by the spin-orbit interaction and the spin-spin interaction, the observed phenomenon can be interpreted well.

1. *Introduction.* The rotational fine structure of the 0—0 band of the $^3\Pi_i - ^3\Sigma^-$ band system of the PH molecule lying in the region of $\lambda = 3400 \text{ \AA}$ was first analysed by PEARSE [1]. At that time there was no explicit formula known for the $^3\Pi$ term, which would have held for all values of the multiplet splitting constant and the rotational quantum number, that is to say, there had been simple formulas for Hund's cases *a*) and *b*) but none for the intermediate case. For this reason PEARSE was not able to determine the constants of the initial state. A few years later, much at the same time, BUDÓ [2] and GILBERT [3] examined theoretically the behaviour of the $^3\Pi$ terms, and BUDÓ gave explicit formulas for all the three components of the $^3\Pi$ term, which hold for all the values of both the coupling constant and (apart from a few lowest values) the rotational quantum number. BUDÓ [4], on the basis of the triplet formula established by him, has compared the observed and calculated combination differences in the $v' = 0$ state of the $^3\Pi$ term of the PH molecule and has, in addition, determined the coupling constant. Subsequently, ISHAQUE and PEARSE [5], [6] published two papers on the transitions referred to of the PH and PD molecules, respectively, and, on the basis of GILBERT's formula, they determined the coupling constant once again. Quite recently LEGAY [7] has photographed and analysed the 1—0 band of the same band system lying near $\lambda = 3200 \text{ \AA}$.

The detailed investigations have resulted in the observation of deviations from the triplet formula in both states, viz. $v' = 0$ and $v' = 1$, of the $^3\Pi$ term of the PH molecule. This is most conspicuous in BUDÓ's work [4], where a systematic deviation of the order of about $0,3 \text{ cm}^{-1}$ is shown here and there

* A report of this work was given at the VI. European Congress on Molecular Spectroscopy, Amsterdam, Netherlands, 2 June, 1961.

between the observed and calculated values of the combination differences $\Delta_2 F_2(J)$ (Fig. 1a and 1b). LEGAY suggests that the multiple splitting constant determined on the basis of GILBERT's formula "changes" with the rotational quantum number. All these phenomena are of nearly the same character as the deviations found by NEVIN in the case of the $4\Pi_\mu$ term of the O_2^+ molecule [8] and by DIXON in that of the $A^3\Pi$ term of the NH molecule [9], respectively. Essentially, these deviations consist in that the two middle components of the 4Π term in the first case and the middle component of the 3Π term in the second, taken as a function of the rotational quantum number, behave differently from what would be expected on the basis of the quartet and triplet formulas, respectively. These differing behaviours can easily be interpreted if the spin-spin interaction and, at the same time, the intercombination perturbation of other Π terms of lower multiplicity [10], [11], [12] transmitted by the spin-orbit interaction, respectively, are taken into account. It is thus shown by these experiences that the interactions mentioned (above all the spin-spin interaction) play an important part not only in the interpretation of the rotational fine structure of the multiplet Σ terms but, that in certain cases, they cannot be ignored for Π term either.

From the present work it will be seen that the deviations observed on the 3Π term of the PH molecule can be easily interpreted also by taking into account simultaneously the spin-spin interaction and the perturbations of the 1Π terms.

2. *Theoretical results.* In an earlier work [12] we have shown that taking into account the spin-spin interaction as well as the perturbations of the 1Π terms the perturbed term values will be of the following form:

$$\left. \begin{aligned} F'_1 &= F_1 - \frac{\beta}{3} + \beta S_{1,J-1}^2, \\ F'_2 &= F_2 - \frac{\beta}{3} + \beta S_{1,J}^2, \\ F'_3 &= F_3 - \frac{\beta}{3} + \beta S_{1,J+1}^2, \end{aligned} \right\} \quad (1)$$

where

$$S_{1,J-1} = -\frac{\sqrt{2}(J^2-1)}{\sqrt{C_1(J)}}; \quad S_{1,J} = \frac{Y-2}{\sqrt{C_2(J)}}; \quad S_{1,J+1} = \frac{\sqrt{2}J(J+1)}{\sqrt{C_3(J)}} \quad (2)$$

and for invert 3Π terms

$$\begin{aligned} C_1(J) &= (J-1)(J+2)Y(Y-4) + 2(2J+1)(J-1)J(J+1), \\ C_2(J) &= Y(Y-4) + 4J(J+1), \\ C_3(J) &= J(J+1)Y(Y-4) + 2(2J+1)J(J+1)(J+2), \end{aligned} \quad (3)$$

and $Y = A/B$, where A and B mean the multiplet splitting constant and the rotational constant, respectively. $\beta = a - 3\varepsilon$, where a is related in a simple way to the perturbation matrix element between the $^3\Pi$ and $^1\Pi$ terms, ε being the constant of the spin-spin interaction.

BUDÓ [2] gives the following expressions for the combination differences (taking also into account the terms associated with the rotational constant D):

$$\begin{aligned}
 \Delta_2 F_1(J) &= 4B \left(J + \frac{1}{2} \right) \left[1 - \frac{2}{\sqrt{Z_1(J)}} + \frac{4}{3} \frac{Z_1(J) + 2Z_2(J)}{Z_1(J+1)Z_1(J-1)} \right] + \\
 &\quad + 8D \left[\left(J - \frac{3}{2} \right)^3 + 3 \left(J - \frac{3}{2} \right)^2 + 4 \left(J - \frac{3}{2} \right) + 2 \right], \\
 \Delta_2 F_2(J) &= 4B \left(J + \frac{1}{2} \right) \left[1 - \frac{8}{3} \frac{Z_1(J) + 2Z_2(J)}{Z_1(J+1)Z_1(J-1)} \right] \\
 &\quad + 8D \left[\left(J - \frac{1}{2} \right)^3 + 3 \left(J - \frac{1}{2} \right)^2 + 4 \left(J - \frac{1}{2} \right) + 2 \right], \\
 \Delta_2 F_3(J) &= 4B \left(J + \frac{1}{2} \right) \left[1 + \frac{2}{\sqrt{Z_1(J)}} + \frac{4}{3} \frac{Z_1(J) + 2Z_2(J)}{Z_1(J+1)Z_1(J-1)} \right] + \\
 &\quad + 8D \left[\left(J + \frac{1}{2} \right)^3 + 3 \left(J + \frac{1}{2} \right)^2 + 4 \left(J + \frac{1}{2} \right) + 2 \right],
 \end{aligned} \tag{4}$$

where

$$Z_1(J) = Y(Y-4) + \frac{4}{3} + 4J(J+1); \quad Z_2(J) = Y(Y-1) - \frac{4}{9} - 2J(J+1). \tag{5}$$

For the difference between the perturbed combination differences computed from (1) and the unperturbed ones calculated from (4) we have the following:

$$\begin{aligned}
 \Delta_2 F'_1(J) - \Delta_2 F_1(J) &= \beta [S_{1, J-1}^2(J+1) - S_{1, J-1}^2(J-1)], \\
 \Delta_2 F'_2(J) - \Delta_2 F_2(J) &= \beta [S_{1, J}^2(J+1) - S_{1, J}^2(J-1)], \\
 \Delta_2 F'_3(J) - \Delta_2 F_3(J) &= \beta [S_{1, J+1}^2(J+1) - S_{1, J+1}^2(J-1)].
 \end{aligned} \tag{6}$$

For the determination of the coupling constant the following relation is obtained from BUDÓ's formulas:

$$\begin{aligned}
 \frac{1}{4B^2} \left\{ (F_3 - F_1) - 8D \left[\left(J - \frac{1}{2} \right)^3 + 3 \left(J - \frac{1}{2} \right)^2 + 4 \left(J - \frac{1}{2} \right) + 2 \right] \right\}^2 = \\
 = (Y-2)^2 - \frac{8}{3} + 4J(J+1).
 \end{aligned} \tag{7}$$

If the spin-spin interaction and the perturbations of the ${}^1\Pi$ terms are taken into account, the left side of (7) is modified on the basis of (1) as follows:

$$\frac{1}{4B^2} \left\{ (F'_3 - F'_1) - \beta (S_{1,J+1}^2 - S_{1,J-1}^2) - 8D \left[\left(J - \frac{1}{2} \right)^3 + 3 \left(J - \frac{1}{2} \right)^2 + 4 \left(J - \frac{1}{2} \right) + 2 \right] \right\} = (Y - 2)^2 - \frac{8}{3} + 4J(J+1), \quad (8)$$

where F'_3 and F'_1 denote the perturbed term values.

To what extent the middle component, i. e. the ${}^3\Pi_1$ term, deviates from its original position, taken as a function of the rotational quantum number, is best seen if the differences of the perturbed and the unperturbed distances of the neighbouring components are considered. We obtain for this from (1):

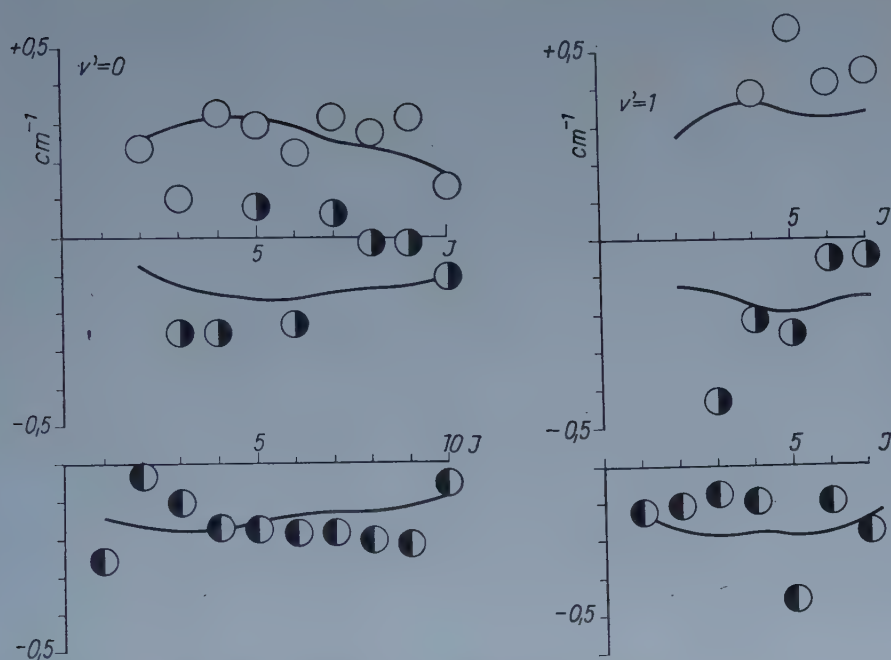
$$\begin{aligned} (F'_1 - F'_2) - (F_1 - F_2) &= \beta (S_{1,J-1}^2 - S_{1,J}^2), \\ (F'_2 - F'_3) - (F_2 - F_3) &= \beta (S_{1,J}^2 - S_{1,J+1}^2). \end{aligned} \quad (9)$$

3. *Application to the ${}^3\Pi_i$ state of the PH molecule.* The anomalies found in the case of the vibrational states $v' = 0$ and $v' = 1$ of the ${}^3\Pi_i$ term of the PH molecule can be interpreted fully by the application of the formulas (6), (8) and (9) given in the previous paragraph, if the *theoretically calculated perturbed* term values in these formulas are compared with those *observed*, and the *unperturbed* term values with those *calculated* in the usual way.

Thus, in Figs. 1/a and 1/b the circles and the curves drawn in full indicate the differences between the observed and calculated, the perturbed and the unperturbed combination differences, respectively, for all the three components in the vibrational states $v' = 0$ and $v' = 1$. It can be seen that there is considerable deviation mainly for the case of the middle ${}^3\Pi_1$ component; the deviations can be interpreted fairly well if in the formula (6) $\beta(v' = 0) = -2.0 \text{ cm}^{-1}$ and $\beta(v' = 1) = -2.40 \text{ cm}^{-1}$ is taken.

LEGAY [7] indicates that in the state $v' = 1$ the multiplet splitting constant on the basis of the GILBERT formula "changes" with the rotational quantum number, and this deviation he tries to interpret by taking into account the interaction between rotation and spin. On the basis of (8), however, the multiplet splitting constant computed with the values of β given before indicates no change whatsoever for $J > 3$ with the change of the rotational quantum number, as can be clearly seen in Fig. 2 (for $J \leq 3$ BUDÓ's formula is valid only approximatively).

If the differences between the observed and calculated distances of the neighbouring components are taken as the function of the rotational quantum number, we obtain for $v' = 0$ and $v' = 1$ the circles in Fig. 3a and 3b, re-



Figs. 1/a and 1/b. Here the differences of the observed and calculated combination differences are plotted on the basis of (6), starting from the upper part and proceeding downwards, as follows: $\Delta_2 F_{20} - \Delta_2 F_{2c} = \beta[S_{1,J}^2(J+1) - S_{1,J}^2(J-1)]$, $\Delta_2 F_{10} - \Delta_2 F_{1c} = \beta[S_{1,J-1}^2(J+1) - S_{1,J-1}^2(J-1)]$, $\Delta_2 F_{30} - \Delta_2 F_{3c} = \beta[S_{1,J+1}^2(J+1) - S_{1,J+1}^2(J-1)]$ where for $v' = 0$ $\beta_0 = -2.00 \text{ cm}^{-1}$ and for $v' = 1$ $\beta_1 = -2.40 \text{ cm}^{-1}$

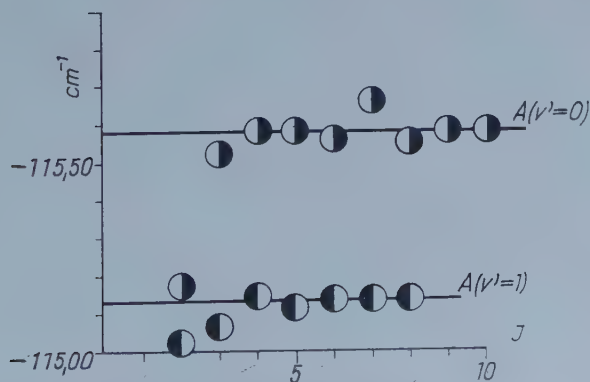
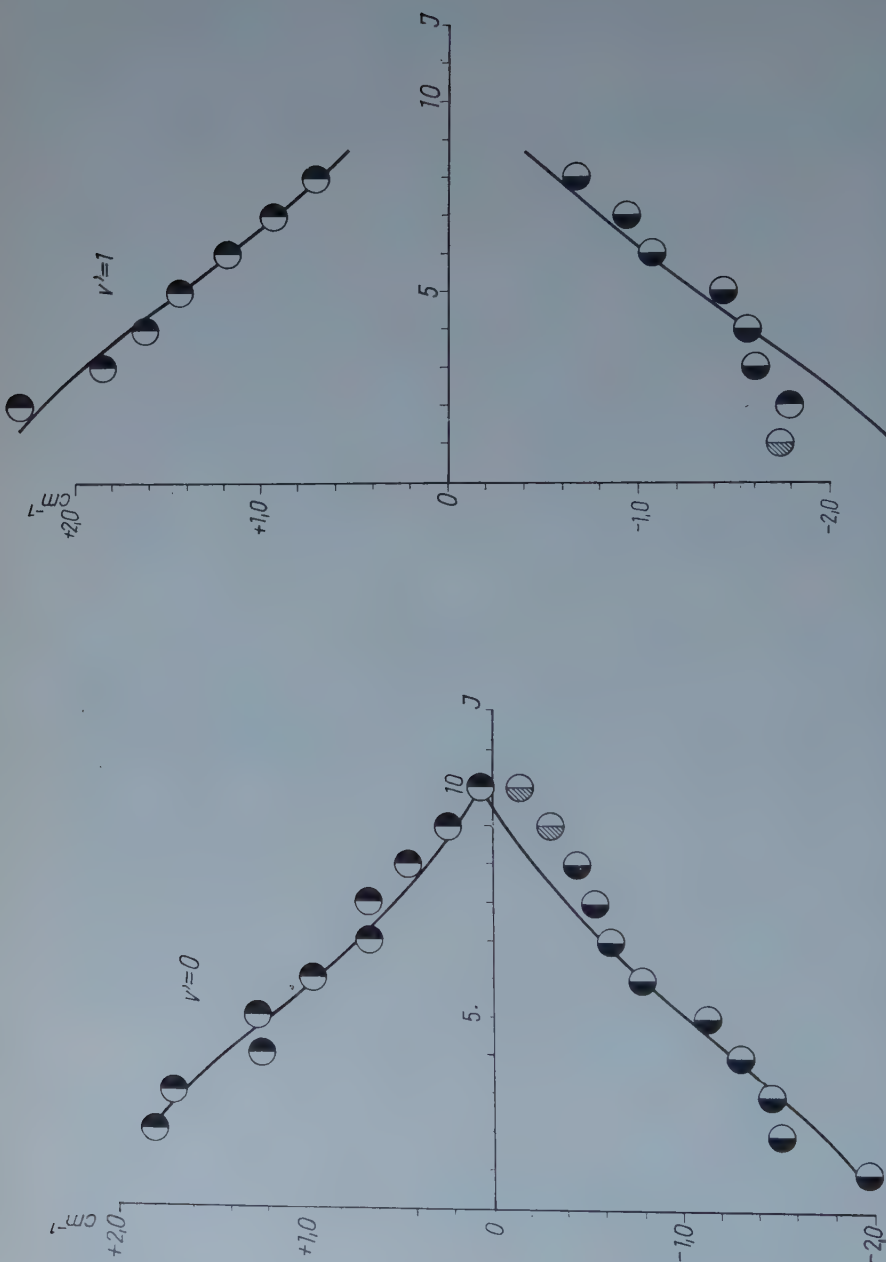


Fig. 2. In this Figure the value of the multiplet splitting constant is plotted for $v' = 0$ and $v' = 1$ on the basis of (8) for all available values of J



Figs. 3a and 3b. The empirical values indicated by the circles are calculated from the mean values of the A -doublet components. The values for the single A -doublet component are to be taken as the mean values calculated from all the branches available. The shaded circles indicate that one of the components of the A -doublet could be calculated only from a single branch. The circles denote for $v' = 0$ and $v' = 1$, respectively, the differences between the observed and calculated values of the mutual distances of the neighbouring components, the curves drawn in full show the deviations computed theoretically on the basis of (9), in the positive region $(F_{10} - F_{30}) - (F_{1c} - F_{2c}) = \beta(S_{1,J}^2 - S_{1,J-1}^2)$, whereas in the negative $(F_{20} - F_{30}) - (F_{2c} - F_{3c}) = \beta(S_{1,J}^2 - S_{1,J+1}^2)$ where for $v' = 0$ $\beta_0 = -2.00 \text{ cm}^{-1}$, and for $v' = 1$ $\beta_1 = -1.8 \text{ cm}^{-1}$.

spectively. If on the basis of (9) the differences of the perturbed and unperturbed distances of the neighbouring components are calculated, we obtain with the values of β given above the curves drawn in full. It can be seen that theory and experiment are in good agreement.

As mentioned already, LEGAY claims that it is possible to interpret the change of the multiplet splitting constant with the rotational quantum number by taking into account the interaction between rotation and spin. It has been shown, however, in the foregoing that, on the one hand, such a change does not exist, and, on the other hand, the deviations observed in the combination differences as well as those found between the differences of the observed and calculated distances of the neighbouring components can in no way be interpreted by means of the interaction between rotation and spin. For the $^3\Pi_1$ component this interaction supplies a constant term which drops out in the term differences, and for the observed and calculated differences of the neighbouring components deviations increasing with the rotational quantum number are obtained as against the observed decreasing deviations (see Fig. 3). It may be possible to assume that besides the spin-spin interaction and the perturbation of the $^1\Pi$ term the interaction between rotation and spin occurs as well, analogous to the case of the NH molecule. This would be true, provided some kind of deviation were to be found between the circles and the curves drawn in full in Fig. 3a and 3b, respectively, and this deviation were to vanish only on taking into account the interaction between rotation and spin. Since, however, there is no deviation to be observed, the latter interaction is not relevant to this issue.

Summarizing, it can be concluded that the deviations found in both the states $v' = 0$ and $v' = 1$ of the $^3\Pi_i$ term of the PH molecule can, in good agreement with the measuring results, be easily interpreted by taking into account simultaneously the spin-spin interaction and the intercombination perturbation of the $^1\Pi$ term transmitted by the spin-orbit interaction. Formula (1) for the $^3\Pi$ and similar formulas for the $^4\Pi$ terms [10], [11] indicate a character which is completely analogous to the formulas obtained for the multiplet Σ terms [13], [14], [15], [16]. The only difference is that in the latter cases the explicit form of the transformation matrix element is far simpler, as the Σ terms belong always to Hund's case b). If the Π terms belonged to Hund's case b) as well, the form of the transformation matrix element S would likewise be simple. If the similar phenomena observed on the $A^3\Pi$ term of the NH and on the $^4\Pi$ term of the O_2^+ molecule are added to the example of the PH molecule, it can be concluded that the interactions dealt with in the present paper are of far greater importance than has been thought earlier, not only for the interpretation of the fine structure of the multiplet Σ terms but also for that of the multiplet Π terms.

REFERENCES

1. R. W. B. PEARSE, Proc. Roy. Soc. A, **129**, 328, 1930.
2. A. BUDÓ, Z. Physik, **96**, 219, 1935.
3. C. GILBERT, Phys. Rev., **49**, 619, 1936.
4. A. BUDÓ, Z. Physik, **98**, 437, 1936.
5. M. ISHAQUE and R. W. B. PEARSE, Proc. Roy. Soc. A., **156**, 221, 1936.
6. M. ISHAQUE and R. W. B. PEARSE, Proc. Roy. Soc. A., **173**, 265, 1939.
7. F. LEGAY, Can. Journ. Phys., **38**, 797, 1960.
8. T. E. NEVIN, Phil. Trans. Roy. Soc. (London) **237**, 471, 1938.
9. R. N. DIXON, Can. Journ. Phys., **37**, 1171, 1959.
10. A. BUDÓ and I. KOVÁCS, Acta Phys. Hung., **4**, 273, 1954; Journ. Chem. Phys., **23**, 751, 1955.
11. I. KOVÁCS, Acta Phys. Hung., **10**, 255, 1959.
12. I. KOVÁCS, Acta Phys. Hung., **12**, 67, 1960.
13. H. A. KRAMERS, Z. Physik, **53**, 422; **53**, 429, 1929.
14. A. BUDÓ, Z. Physik, **105**, 73, 1937; A. BUDÓ and I. KOVÁCS, Hung. Phys. Acta, **1**, 1, 1948.
15. K. S. RAO, Ind. Journ. Phys., **26**, 47, 1952.
16. T. E. NEVIN, Proc. Roy. Ir. Acad., **48A**, 1, 1942; **50A**, 123, 1945.

ИССЛЕДОВАНИЕ $^3\Pi$ -СОСТОЯНИЯ РН-МОЛЕКУЛЫ

И. КОВАЧ

Резюме

Подробные исследования показали, что $^3\Pi$ -состояние, относящееся к $^3\Pi_i - ^3\Sigma$ переходу РН-молекулы, не соответствует точно известной триплетной формуле. Расхождение заключается в том, что средняя компонента $^3\Pi$ -терма, рассматривая ее в функции ротационного квантового числа, располагается не там, где это можно ожидать на основе триплетной формулы. Это явление просто объясняется, если одновременно принимаются во внимание возмущение $^1\Pi$ -термов, обусловленное спин-орбитальным взаимодействием, и спин-спиновое взаимодействие.

ON THE TIME DEPENDENCE OF IRREVERSIBLE PROCESSES

By

G. PATAKI

RESEARCH INSTITUTE FOR TECHNICAL PHYSICS OF THE HUNGARIAN ACADEMY OF SCIENCES, BUDAPEST

(Presented by G. Szigeti. — Received 29. III. 1961)

In this paper the time dependence of the so-called thermodynamic "forced" (non-spontaneous) processes is examined in homogeneous systems, when in case of $t \rightarrow \infty$ not a static equilibrium results, but a stationary process determined by external forces. The "equations of motion" are given for an arbitrary number of variables and an arbitrary generation $G(t)$ of the extensive quantities. In case of two variables we write down the differential equations holding for the components and for a constant G_0 we give also the solutions. As an application we examine in Knudsen gas the time dependence of the quotient $\frac{\Delta P}{\Delta T}$ of the thermonuclear pressure and the temperature difference. Finally, the analogy between mechanics and thermodynamics is studied taking the generation into consideration.

Introduction

The description of the approach to equilibrium in time in homogeneous systems near the equilibrium, has been given by I. FÉNYES [1]. By integrating the equations of motion a more exact picture of the process of the approach to equilibrium could be obtained. So, e. g. it could be established that because of the matrix $gL \equiv A$ being off-diagonal the forces X_i can change their signs during the decay. The relation between the reversal of signs and the initial conditions in case of two variables has in general been examined by G. FÁY and G. TÁBORI [2], while in [3] we have studied the approach to the equilibrium in Knudsen gas by means of two parameters of the conduction matrix. As a further application, we gave the thermodynamic formulation of the recombination in semi-conductors [4], on the basis of the theory of SHOCKLEY—READ.

The equations of motion given in [1] describe such processes in which, supposing an arbitrary initial state, the final state will be the static equilibrium. But, from both the theoretical and the practical point of view, the case seems to be interesting, when for $t \rightarrow \infty$ not necessarily the static equilibrium sets in, but a stationary process ensues determined by the external forced conditions.

In this paper the thermodynamic equations of motion describing the forced processes near the equilibrium in case of an arbitrary number of variables and an arbitrary generation $G(t)$ of the extensive quantities are given by

means of the formalism applied in [1]. The general equations obtained in this way are applied to the case of two variables: we write down the differential equations concerning the quantities a_i , X_i , I_i and in case of constant generation we give also the solutions.

Using the results of [3] we then examine the approach to the stationary state in Knudsen gas and determine the time dependence of the quotient $\frac{\Delta P}{\Delta T}$ of the thermonuclear pressure difference and the temperature difference.

Finally, we study the analogy between the equations of motion of thermodynamics and mechanics, with a more convenient choice of the signs of the forces and currents.

§ 1. Description of general forced (non-spontaneous) processes

Before the discussion of the forced processes we call to mind the equations referring to the spontaneous processes [1], which are obtainable from the following relations:

$$I = LX, \quad (1)$$

$$X = -ga, \quad (2)$$

$$\dot{a} = I, \quad (3)$$

where I means the column vector formed from the currents, L the symmetrical conduction matrix, X the column vector of the general forces, a the column vector formed out of the deviations of the extensive quantities from the equilibrium values and g the symmetrical matrix derived from the entropy $S(a_1, a_2, \dots)$, the elements of which are

$$g_{ik} = - \frac{\partial^2 S(a_1, a_2, \dots)}{\partial a_i \partial a_k}.$$

The equations of motion (and their solutions) will be as follows:

$$\begin{aligned} \dot{X} + gLX &= 0; & (X &= e^{-gLt} X_0), \\ \dot{a} + Lga &= 0; & (a &= e^{-Lgt} a_0), \\ \dot{I} + LgI &= 0; & (I &= e^{-Lgt} I_0), \end{aligned} \quad (4)$$

where X_0 , a_0 , I_0 are the column vectors formed from the initial values.

In forced processes each extensive quantity has its source. This fact is taken into consideration by a vector $G(t)$, the elements of which give the sources of the single a_i -s. Supposing further also homogeneity in space, instead of (3) the relation

$$\dot{a} = I - G(t) \quad (5)$$

is assumed. It is evident that the equs. (1), (2) and (5) lead to the following equations of motion:

$$\begin{aligned}\dot{X} + gLX &= gG(t), \\ \dot{a} + Lga &= -G(t), \\ \dot{I} + LgI &= LgG(t).\end{aligned}\tag{6}$$

The solutions of these inhomogeneous matrix-differential equations can be given explicitly

$$\begin{aligned}X &= e^{-gLt} \left[\int_0^t e^{gL\tau} gG(\tau) d\tau + X_0 \right]; \quad a = e^{-Lgt} \left[\int_0^t e^{Lg\tau} (-G(\tau)) d\tau + a_0 \right]. \\ I &= e^{-Lgt} \left[\int_0^t e^{Lg\tau} LgG(\tau) d\tau + I_0 \right].\end{aligned}\tag{7}$$

The equs. (6) mean the equations of motion describing the forced processes in case of an arbitrary number of variables and of an arbitrary generation. After what has been said above, it can be more precisely defined, what is meant by spontaneous and forced processes. If $G(t) = 0$, we speak of spontaneous processes while we regard the case $G(t) \neq 0$ as a forced process, i.e. also the processes leading to a static equilibrium are forced ones, if the condition $G(t) \neq 0$ is fulfilled.

§ 2. Forced (non-spontaneous) processes of two variables

The general examination of the equs. (6) and (7) is complicated. Therefore, instead of this, in case of two variables we write down the differential equations holding for the components in case of an arbitrary $G(t)$. After the separation the following equations are obtained.

For the components of X :

$$\begin{aligned}\ddot{X}_1 + T(A)\dot{X}_1 + D(A)X_1 &= \dot{m}(t) + A_{22}m(t) - A_{12}n(t), \\ \ddot{X}_2 + T(A)\dot{X}_2 + D(A)X_2 &= \dot{n}(t) + A_{11}n(t) - A_{21}m(t),\end{aligned}\tag{8}$$

where $T(A)$, resp. $D(A)$ mean the trace, resp. the determinant of the matrix $A \equiv gL$, and

$$\begin{aligned}m(t) &= g_{11}G_1(t) + g_{12}G_2(t), \\ n(t) &= g_{21}G_1(t) + g_{22}G_2(t).\end{aligned}\tag{9}$$

For the components of a :

$$\begin{aligned}\ddot{a}_1 + T(B)\dot{a}_1 + D(B)a_1 &= -B_{22}G_1(t) + B_{12}G_2(t) - \dot{G}_1(t), \\ \ddot{a}_2 + T(B)\dot{a}_2 + D(B)a_2 &= -B_{11}G_2(t) + B_{21}G_1(t) - \dot{G}_2(t),\end{aligned}\tag{10}$$

where $T(B)$, $D(B)$ is the trace, resp. the determinant of the matrix $B \equiv Lg$. For the components of the current I :

$$\begin{aligned} \dot{I}_1 + T(B) \dot{I}_1 + D(B) I_1 &= D(B) G_1(t) + \dot{v}(t), \\ \dot{I}_2 + T(B) \dot{I}_2 + D(B) I_2 &= D(B) G_2(t) + \dot{w}(t), \end{aligned} \quad (11)$$

where the following notations have been introduced:

$$\begin{aligned} v(t) &= B_{11} G_1(t) + B_{12} G_2(t), \\ w(t) &= B_{21} G_1(t) + B_{22} G_2(t). \end{aligned} \quad (12)$$

The above inhomogeneous differential equations of the second order with constant coefficients in case of a given $G_1(t)$, $G_2(t)$ can generally be solved. Further, we examine the special case, when $G(t) \equiv G_0$ is constant. Then, as can easily be seen, the solutions will be as follows:

$$\begin{aligned} X_1 &= A_1 e^{-\lambda_1 t} + B_1 e^{-\lambda_2 t} + M, \\ X_2 &= A_2 e^{-\lambda_1 t} + B_2 e^{-\lambda_2 t} + N, \end{aligned} \quad (13)$$

where λ_1 and λ_2 are the two roots of the characteristic equations

$$\lambda^2 - T(A)\lambda + D(A) = 0$$

and

$$M = \frac{A_{22} m_0 - A_{12} n_0}{D(A)}; \quad N = \frac{A_{11} n_0 - A_{21} m_0}{D(A)} \quad (14)$$

and m_0 , resp. n_0 mean the equ. (9) in case of G_{01} , G_{02} .

For the components of a we obtain:

$$\begin{aligned} a_1 &= a_1 e^{-\gamma_1 t} + b_1 e^{-\gamma_2 t} + \frac{B_{12} G_{02} - B_{22} G_{01}}{D(B)}, \\ a_2 &= a_2 e^{-\gamma_1 t} + b_2 e^{-\gamma_2 t} + \frac{B_{21} G_{01} - B_{11} G_{02}}{D(B)} \end{aligned} \quad (15)$$

and the solutions concerning the currents I_i :

$$\begin{aligned} I_1 &= c_1 e^{-\gamma_1 t} + d_1 e^{-\gamma_2 t} + G_{01}, \\ I_2 &= c_2 e^{-\gamma_1 t} + d_2 e^{-\gamma_2 t} + G_{02}, \end{aligned} \quad (16)$$

where γ_1 and γ_2 are the two roots of the equation (evidently $\lambda_i = \gamma_i$):

$$\gamma^2 - T(B)\gamma + D(B) = 0.$$

The constants A_1, B_1, A_2, B_2 , etc. figuring in the solutions must be determined on the basis of the initial conditions. The equ. (13), (15) and (16) give the time dependence of the forced processes. In case of $t \rightarrow \infty$ the quantities do not disappear, but tend to a constant value. On the basis of the equs. (13), (16) and (1), in case of $t \rightarrow \infty$ we obtain

$$\begin{aligned} G_{01} &= L_{11} M + L_{12} N, \\ G_{02} &= L_{21} M + L_{22} N. \end{aligned} \quad (17)$$

From the equ. (17) we can get the value of the necessary generations for fixed M and N and reversely, when G_{01} and G_{02} are given, we can calculate the forces belonging to the final state.

It is to be noted that the forces M and N can be expressed also by the elements of the matrices g and A , on the basis of the equ. (14).

The processes described by the equ. (17) can be considered "general stationary forced processes". Among these figures also the "stationary state" satisfying PRIGOGINE's principle of the minimal entropy production [5]. E. g. at a fixed N we obtain a minimal entropy production, if $G_{01} = 0$. Naturally, during the approach to the stationary state, temporarily also the current I_i arises, but in case of $t \rightarrow \infty$, as if $G_{01} = 0$, this current disappears. The setting in of a stationary state in the usual meaning will be discussed in the next paragraph.

§ 3. Application to Knudsen gas

One of the realizations of the processes examined above can be seen in Fig. 1. The reservoir I of finite extent is connected by the capillary c with the reservoir II of infinite extent.* In I we begin to generate with a constant

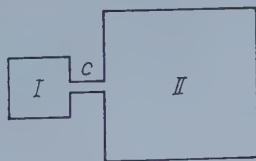


Fig. 1

G_0^{**} and examine the time-dependence of the process. This process is described by the equs. (13), (15) and (16).

In case of Knudsen gas we are generating e. g. energy. Then, in the stationary final state there will be only an energy current I_u , while the mass

* It is to be noted that it is not important that c is a capillary. It may be another connection, e.g. a semipermeable membrane, etc.

** The connection c determines the degree of the generation in I, so that the stationary state can set in, i.e. that the generated extensive quantity should not accumulate infinitely.

current I_m arises only temporarily. The forms of the solutions for the forces X_m and X_u are on the basis of (13):

$$X_m = A_m e^{-\lambda_1 t} + B_m e^{-\lambda_2 t} + M,$$

$$X_u = A_u e^{-\lambda_1 t} + B_u e^{-\lambda_2 t} + N.$$

X_m and X_u can be expressed by means of the temperature difference ΔT and the pressure difference ΔP (see e.g. [6]):

$$X_m = -v \frac{\Delta P}{T} + h \frac{\Delta T}{T},$$

$$X_u = -\frac{\Delta T}{T^2},$$

where v means the specific volume, $h = \frac{5}{2} \frac{kT}{M_0}$ the specific enthalpy. The constants A_m , B_m , A_u , B_u must be determined from the initial conditions. Taking into consideration that $X_{m0} = 0$, $X_{u0} = 0$ and on the basis of (6) $\dot{X}_{m0} = g_{mu} G_{0u}$, $\dot{X}_{u0} = g_{uu} G_{0u}$ (as $G_{0m} = 0$), we obtain the following equations for the determination of the constants:

$$A_m + B_m = -M,$$

$$A_m \lambda_1 + B_m \lambda_2 = -g_{mu} G_{0u}, \quad (20)$$

while for the constants figuring in X_u :

$$A_u + B_u = -N,$$

$$A_u \lambda_1 + B_u \lambda_2 = -g_{uu} G_{0u}. \quad (21)$$

Forming the quotient $\frac{X_m}{X_u}$ we obtain

$$\frac{\Delta P}{\Delta T} vT - h = \frac{M}{N} f(t),$$

where $f(t)$ on the basis of the equ. (20) and (21) has the following form:

$$f(t) = \frac{\frac{A_m}{M} a(t) + 1}{\frac{A_u}{N} a(t) + 1}; \quad a(t) \equiv \frac{e^{-\lambda_1 t} - e^{-\lambda_2 t}}{1 - e^{-\lambda_2 t}}. \quad (22)$$

Taking into consideration the value of h and that $\frac{M}{N} = -\frac{L_{mu}}{L_{mm}} = -\frac{2kT}{M_0}$ (see e.g. [6]), we get

$$\frac{\Delta P}{\Delta T} = \frac{1}{2} \frac{k}{M_0 v} (5 - 4f(t)) \equiv \frac{1}{2} \frac{k}{M_0 v} r(t). \quad (23)$$

The examination of the function $r(t)$ can easily be carried out. If $t \rightarrow \infty$, then $f(t) \rightarrow 1$ and thus, as has been expected,

$$\lim_{t \rightarrow \infty} \frac{\Delta P}{\Delta T} = \frac{1}{2} \frac{k}{M_0 v},$$

while in case of $t \rightarrow 0$ we may write

$$\lim_{t \rightarrow 0} f(t) = \frac{A_u + B_u}{A_m + B_m} \frac{A_m \lambda_1 + B_m \lambda_2}{A_u \lambda_1 + B_u \lambda_2} = \frac{N}{M} \frac{g_{mu} G_{0u}}{g_{uu} G_{0u}} = \frac{3}{4}, \quad (24)$$

namely on the basis of [3] $g_{mu} = -\frac{1}{mT}$, $g_{uu} = \frac{2M_0}{3mkT^2}$.

Thus we obtain

$$\lim_{t \rightarrow \infty} \frac{\Delta P}{\Delta T} = \frac{k}{M_0 v}.$$

It is easy to see that $f(t)$ (and so $r(t)$ too) is a monotonic function of time.*

In Fig. 2 the function $r(t)$ is plotted. It can be seen that the quotient $\frac{\Delta P}{\Delta T}$ changes by a factor of 2, until it attains its value valid for the stationary



Fig. 2

state. On the basis of [3] and of what has been said above, both $\Delta T(t)$ and $\Delta P(t)$ can of course be determined.

* It is enough to remark that $f(t)$ has no extreme value, because the condition $\dot{f}(t) = 0$ means the equation $\dot{a}(t) \left(\frac{A_m}{M} - \frac{A_u}{N} \right) = 0$ which for a positive t is not possible on the basis of the equs. (20), (21), (22) and (24).

§ 4. Analogy of the equations of motion of mechanics and thermodynamics

Before coming to the discussion of the analogy we make some remarks concerning the convention of the sign of the forces and currents. In the determination of the signs of the equs. (2) and (3) there is some liberty, as only the sign of the product is fixed. (See e.g. [6], Introduction, equs. (3)—(6)). In the introduction of the generation as well as in the discussion of the analogy the following choice of the signs seems to be more convenient:

$$X' \equiv -X = ga', \quad (25)$$

$$I' \equiv -I = -\dot{a}', \quad (26)$$

$$a' \equiv a. \quad (27)$$

Naturally, the form of the conduction equation remains further

$$I' = LX'. \quad (28)$$

The advantage of the introduction of the primed quantities is that $G(t)$ can be considered as positive, when the extensive quantities are increased. Namely, in this case the equ. (5) passes into

$$\dot{a}' = -I' + G(t), \quad (29)$$

while instead of (6) we obtain:

$$\begin{aligned} \dot{X}' + gLX' &= gG(t), \\ \dot{a}' + Lga' &= G(t), \\ \dot{I}' + LgI' &= LgG(t). \end{aligned} \quad (30)$$

The above choice of the signs is found to be useful also in the discussion of the analogy between mechanics and irreversible thermodynamics (see [7]). Supposing that there is as yet no generation, then the analogy given in [7] is obtained for the primed quantities introduced above with the difference that now $+X'$ corresponds to the force \mathfrak{F} , i.e. considering a point motion in a viscous medium we obtain:

$$\begin{aligned} a' &\rightarrow r; \quad (LgL)^{-1} \rightarrow m; \\ X' &\rightarrow \mathfrak{F}; \quad L^{-1} \rightarrow \kappa \end{aligned} \quad (31)$$

and the equation of motion is

$$(LgL)^{-1} \ddot{a}' + L^{-1} \dot{a}' = 0 \rightarrow m \ddot{r} + \kappa \dot{r} = 0. \quad (32)$$

If there is also generation, then the form of the equation of motion becomes

$$(LgL)^{-1} \ddot{a}' + L^{-1} \dot{a}' = \frac{d}{dt} [(LgL)^{-1} G(t)] \rightarrow m \ddot{r} + \kappa \dot{r} = \dot{p}. \quad (33)$$

The analogy remains if we examine the rotation of a rigid body. Thus, the mechanical model of irreversible thermodynamics is the rotation of the rigid body around a point in an anisotropic viscous medium, if there is no generation, while in case of generation the suitable model is the rotation of the rigid body around a point in an anisotropic viscous medium, if the impulse momentum has a source.

Acknowledgements

The author would like to express his thanks to Prof. I. FÉNYES for many helpful discussions and for his critical remarks.

REFERENCES

1. I. FÉNYES, *Acta Phys. Hung.*, **11**, 131, 1960.
2. G. FÁY and G. TÁBORI, *Acta Phys. Hung.*, **10**, 129, 1959.
3. G. PATAKI, *Acta Phys. Hung.*, **12**, 311, 1961.
4. G. PATAKI, *Acta Phys. Hung.*, **13**, 119, 1961.
5. I. PRIGOGINE, *Introduction to Thermodynamics of Irreversible Processes*. [Русское издание] ИЛ, Москва, 1960.
6. S. R. DE GROOT, *Thermodynamics of Irreversible Processes*, North-Holland P. C. Amsterdam 1952.
7. I. FÉNYES, *Soviet Phys. JETP*, **35**, 1039, 1958.

О ВРЕМЕННОЙ ЗАВИСИМОСТИ НЕОБРАТИМЫХ ПРОЦЕССОВ

ДЬ. ПАТАКИ

Резюме

В работе было исследовано временное протекание, так называемых, термодинамических вынужденных (неспонтанных) процессов, когда при $t \rightarrow \infty$ достигается не статическое равновесие, а стационарный процесс, определенный внешними условиями.

Были даны «уравнения движения» при произвольном числе переменных и при произвольной генерации $G(t)$ экстензивных переменных. В случае двух переменных написаны дифференциальные уравнения для компонентов и при постоянной генерации G_0 и даны соответствующие решения. В качестве примера применения была исследована временная зависимость отношения $\frac{\Delta P}{\Delta T}$ термомолекулярных разностей давления и температуры. Наконец, была исследована аналогия между механикой и термодинамикой, принимая во внимание и генерацию.



SEMI-CLASSICAL DESCRIPTION OF HIGH-ENERGY ELECTRON SCATTERING ON HEAVY NUCLEI

By

A. FRENKEL

CENTRAL RESEARCH INSTITUTE FOR PHYSICS, COSMIC RAY LABORATORY, BUDAPEST

(Presented by L. Jánossy. — Received 10. V. 1961)

W. K. B. phase-shift formulae for the scattering of high-energy electrons on heavy nuclei are obtained and a brief discussion of the range of their validity is given.

Introduction

Semi-classical methods are widely used in high-energy physics to describe scattering phenomena. In 1955, R. W. WILLIAMS [1] applied a semi-classical approach to calculate the reaction cross section of neutrons scattered on nuclei at 1.4 BeV and at cosmic-ray energies. On the other hand, in the past few years R. HOFSTADTER and coworkers have investigated in detail the elastic scattering of high-energy electrons on protons and on different nuclei [2]. The analysis of the scattering pattern allowed to determine the mean parameters of the charge distribution of the target particles.

For the proton and for light elements $Ze^2 \ll 1$ ($\hbar = c = 1$, $e^2 = \frac{1}{137}$ throughout), so that Born's approximation could be applied in the analysis of HOFSTADTER's results. For heavy nuclei, however, $Ze^2 \approx 1$, and the Born series converge badly. Looking for other methods, YENNIE et al. [3] calculated the differential cross section by means of the partial wave expansion. They obtained the phases by a numerical integration of the radial Dirac equations. This method allows calculation of the cross section with accuracy, but tedious numerical computations are needed.

In 1954, E. BARANGER and recently E. PREDAZZI [4] attempted to solve the problem with the help of the semi-classical W. K. B. approach. They represented the charge distribution of the nucleus by the so-called shell model ($\rho(r) = \text{const.} \delta(r-R)$) and obtained the phases in good agreement with YENNIE's numerical results for the same model. This shows that, in principle, the W. K. B. method can be used. However, as shown by YENNIE et al. in [3b], the shell model, while simple to deal with, reproduces the experimental results very poorly. For more realistic models the W. K. B.

integrals cannot be calculated in closed form without introducing new approximations in the analytic expressions of the integrands and it is an open question whether these inevitable new approximations do allow the applications of the semi-classical W. K. B. approach.

In the present paper we investigate the problem of the applicability of the W. K. B. method to a physically plausible charge-distribution model of heavy nuclei. We obtain the analytic expression for the phase shift and find an upper limit for the errors, introduced by our approximations when calculating the W. K. B. phases.* Finally, we discuss in which angular region our formulae are valid, if we require the relative error of the calculated differential cross section to be less than a given value ε .

I. Derivation of the W. K. B. phase shift formulae

The well-known W. K. B. phases can be written as follows [5]:

$$\delta_l = \frac{\pi}{2} \left(l + \frac{1}{2} \right) - pr_0 + \int_{r_0}^{\infty} (p_r - p) dr, \quad (1)$$

where

$$p_r = \left\{ [E_T - U(r)]^2 - m^2 - \frac{\left(l + \frac{1}{2} \right)^2}{r^2} \right\}^{1/2}. \quad (2)$$

In (1) and (2) the following notations are used:

n, p, E_T = mass, momentum and total energy
of the incoming particle,

l = angular momentum quantum number,

t_0 = turning point: $pr_0 = 0$,

$U(r) \equiv ev(r)$ = potential energy.

* We must point out here that, in addition to the errors mentioned in the text, our phase shifts deviate from the true quantummechanical phase shifts because of the approximation inherent in the W. K. B. method. PREDAZZI [4], comparing his exact shell model W. K. B. phase shifts with YENNIE's quantummechanical results obtained this second deviation in a pure form. Observing that PREDAZZI finds $|\Delta\delta_e| \approx 0,001$, while our errors turn out to be 0,005, and that for our charge distribution model the general condition of the applicability of the W. K. B. method $\left(\frac{\lambda}{v(r)} \frac{dv(r)}{dr} \ll 1 \right)$ is satisfied better than for the shell model, we neglect the influence of this second deviation.

Our next task is to calculate the electrostatic potential $v(r)$ from the charge distribution of the target nucleus.

HOFSTADTER's results indicate [1] that for heavy nuclei the following spherically symmetric charge distribution can be used:

$$\left\{ \begin{array}{ll} \varrho(r) = \varrho_0 u(r), & \\ u(r) = 1 & \text{for } 0 \leq r \leq c - \frac{1}{2} t', \\ u(r) = 2 \left(\frac{r-c}{t'} \right)^3 - \frac{3}{2} \left(\frac{r-c}{t'} \right) + \frac{1}{2} & \text{for } c - \frac{1}{2} t' \leq r \leq c + \frac{1}{2} t', \\ u(r) = 0 & \text{for } r \geq c + \frac{1}{2} t' \end{array} \right. \quad (3)$$

(see Fig. 1).

The physical meaning of the parameters c and t' is obvious: $\varrho(c) = \varrho_0 u(c) = \varrho_0/2$, i. e. c is the "half-density parameter", while t' is the "100%—0%

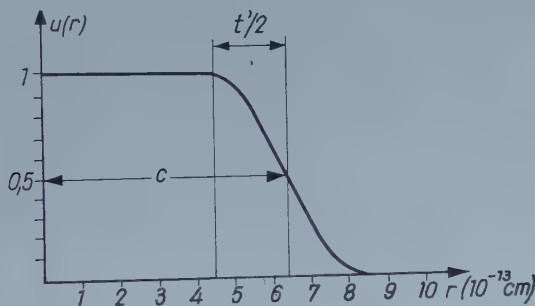


Fig. 1. The charge distribution of heavy nuclei

fall-off parameter". In HOFSTADTER's review [2] the heavy nuclei are characterized by c and t , the 90%—10% parameter. It is easy to see that in our case $t' = \frac{t}{0.6084}$. Taking the values c and t from [2] (for gold, e. g., $c = 6.38 \cdot 10^{-13}$ cm, $t = 2.35 \cdot 10^{-13}$ cm,) (3) gives the desired charge distribution for heavy nuclei.

Introducing now dimensionless units $\frac{r}{t'}$ for length and, accordingly, Et' for energy, we solve the Poisson equation $\Delta v(r) = 4\pi\varrho(r)$ with (3) and

obtain for the potential $v(r) = 4\pi\varrho_0 W(r)$ the expression (see Fig. 2):

$$W(r) = -\frac{r^2}{6} + \frac{c^2}{2} + \frac{1}{40} \quad \text{for } 0 \leq r \leq c - \frac{1}{2},$$

$$\begin{aligned} W(r) = & \frac{1}{r} \left(c - \frac{1}{2} \right)^3 \left[\frac{1}{3} - \frac{a}{3} - \frac{b}{4} \left(c - \frac{1}{2} \right) + \frac{6}{5} c \left(c - \frac{1}{2} \right)^2 - \frac{1}{3} \left(c - \frac{1}{2} \right)^3 \right] + \\ & + \left(c + \frac{1}{2} \right)^3 \left[-\frac{a}{2} + \frac{b}{3} \left(c + \frac{1}{2} \right) - \frac{3}{2} c \left(c + \frac{1}{2} \right)^2 + \frac{2}{5} \left(c + \frac{1}{2} \right)^3 \right] + \\ & + r^2 \left[-\frac{a}{6} - \frac{b}{12} r + \frac{3}{10} c r^2 - \frac{1}{15} r^2 \right], \end{aligned} \quad (4)$$

$$a \equiv \frac{1}{2} + \frac{3}{2}c - 2c^3,$$

$$b \equiv 6c^2 - \frac{3}{2} \quad \text{for } c - \frac{1}{2} \leq r \leq c + \frac{1}{2},$$

$$W(r) = \left(\frac{c^3}{3} + \frac{c}{20} \right) \frac{1}{r} \quad \text{for } r \geq c + \frac{1}{2}$$

$$\text{and } \varrho_0 = \frac{Ze}{4\pi(c^3/3 + c/20)} \quad \text{from } 4\pi \int \varrho(r) r^2 dr = Ze.$$

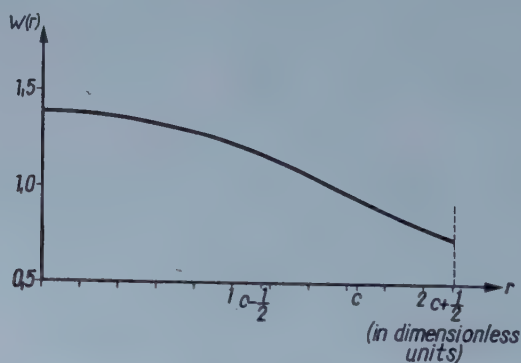


Fig. 2. The electrostatic potential of heavy nuclei

For attractive Coulomb forces the potential energy can be written now as follows:

$$U(r) = -\beta W(r), \quad (5)$$

where

$$\beta \equiv \frac{Ze^2}{c^3/3 + c/20}. \quad (6)$$

Introducing (5) in the phase-shift formula (1), we see that we have to calculate the integral

$$\int_{r_0}^r p_r dr = \int_{r_0}^r \sqrt{p^2 + 2E_T \beta W(r) + \beta^2 [W(r)]^2 - \frac{\left(l + \frac{1}{2}\right)^2}{r^2}} dr \quad (7)$$

(the limit $r \rightarrow \infty$ will be considered later).

With the $W(r)$ given in (4) the integral can be calculated in closed form only if $r_0 \geq c + \frac{1}{2}$. In the interval $\left[0, c + \frac{1}{2}\right]$ we have to approximate $W(r)$ and $[W(r)]^2$ by some such functions which make the integral analytically calculable. From several possible procedures the following turned out to be satisfactory:

In the interval $\left[c - \frac{1}{2}, c + \frac{1}{2}\right]$ we put

$$W(r) \approx \frac{A}{r^2} + \frac{B}{r} + C \equiv W'(r)$$

and, independently,

$$[W(r)]^2 \approx \frac{A'}{r^2} + \frac{B'}{r} + C' \equiv W''(r).$$

We fit the approximating functions to $W(r)$ and $[W(r)]^2$ at $r = c - \frac{1}{2}$, $r = c$ and $r = c + \frac{1}{2}$. Then the coefficients A, B, C turn out to be (with $W_1 \equiv W\left(c - \frac{1}{2}\right)$, $W_2 \equiv W(c)$, $W_3 \equiv W\left(c + \frac{1}{2}\right)$)

$$A = 2c \left(c^2 - \frac{1}{4} \right) \left[W_3 \left(c + \frac{1}{2} \right) - 2W_2 c + W_1 \left(c - \frac{1}{2} \right) \right],$$

$$B = -4 \left[W_3 \left(c - \frac{1}{4} \right) \left(c + \frac{1}{2} \right)^2 - 2W_2 c^3 + W_1 \left(c + \frac{1}{4} \right) \left(c - \frac{1}{2} \right)^2 \right],$$

$$C = 2 \left[W_3 \left(c + \frac{1}{2} \right) - 2W_2 c^2 + W_1 \left(c - \frac{1}{2} \right)^2 \right].$$

$A'B'C'$ can be obtained from a similar set of equations.

In the interval $\left[0, c - \frac{1}{2}\right]$ only $[W(r)]^2$ has to be approximated. We put

$$[W(r)]^2 \approx D' + F'r^2.$$

Fitting the curves at $r = 0$ and $r = c - \frac{1}{2}$, we obtain

$$D' = \left(\frac{c^2}{2} + \frac{1}{40}\right)^2,$$

$$F' = -\frac{\sqrt{D'}}{3} + \frac{\left(c - \frac{1}{2}\right)^2}{36}.$$

The maximum deviations δW_{\max} and δW_{\max}^2 can be found for any heavy element. For gold ($c = 1,65$ in dimensionless units) we obtain in the interval $\left[c - \frac{1}{2}, c + \frac{1}{2}\right]$ by numerical calculation

$$|\delta W_{\max}| \approx 0,005, \quad |\delta W_{\max}^2| \approx 0,024, \quad (8a)$$

while in the interval $\left[0, c - \frac{1}{2}\right]$ we find exactly

$$\delta W \equiv 0, \quad |\delta W_{\max}^2| = \frac{\left(c - \frac{1}{4}\right)^4}{144} = 0,012. \quad (8b)$$

Numerical values of the functions $W(r)$ and $[W(r)]^2$, calculated from the exact formula (4), and for comparison the approximative functions $W'(r)$ and $W''(r)$ are presented in the following Table.

r	$c - \frac{1}{2}$	1,4	$c = 1,652$	1,9	$c + \frac{1}{2}$
$W(r)$	1,1689	1,0644	0,9407	0,8341	0,7370
$W'(r)$	1,1689	1,0593	0,9407	0,8332	0,7370
$[W(r)]^2$	1,3661	1,1330	0,8849	0,6957	0,5432
$W''(r)$	1,3661	1,1094	0,8849	0,7002	0,5432

For other heavy elements similar results can be obtained.

With the help of these approximations, (7) transforms into a sum of $\int \sqrt{a_i x^2 + 2b_i x + d_i} \frac{dx}{x}$ -type integrals, which can be calculated in closed form.

If in (7) the upper limit of the integration, r , tends to $+\infty$, we get a term $\lim_{r \rightarrow \infty} pr$ which is compensated by the term $-\int_{r_0}^{\infty} p dr$ of the phase-shift formula (1), and a second divergent term, which reflects the well-known logarithmic divergence of the Coulomb phases. This divergence can be eliminated by subtracting from each phase a term $\lim_{r \rightarrow \infty} \ln 2pr$ [6].

The results of the outlined calculations are given in the Appendix.

II. The upper boundary of the deviation of the phases from the exact W. K. B. value*

YENNIE et al. [3a] elaborated a successful method for summing the partial-wave series to obtain the cross section from the phase shifts. Instead of reproducing here their considerations, we turn to the evaluation of the errors incurred by our approximations.

We have to consider the variation of the integral

$$\int_{r_0}^{c+\frac{1}{2}} \sqrt{E_T^2 + 2E_T \beta W(r) + \beta^2 [W(r)]^2 - m^2 - \frac{\left(l + \frac{1}{2}\right)^2}{r^2}} dr$$

induced by the independent variations of $W(r)$ and $[W(r)]^2$, according to our approximation procedure. r_0 is the point where the integrand vanishes, so that r_0 should be varied too. It is easy to see, however, that this variation yields a second-order correction only, which can be neglected.

Next we observe that in the interval $\left[0, c + \frac{1}{2}\right]$ (see (3) and Fig. 2).

$[\beta W(r)]_{\min} = \beta W\left(c + \frac{1}{2}\right)$; now a straightforward calculation gives

$$|\Delta \delta_l| = \left| \delta \int_{r_0}^{c+\frac{1}{2}} \sqrt{\dots} dr \right| < \frac{E_T \beta |\delta W_{\max}| + \frac{1}{2} \beta^2 |\delta W_{\max}^2|}{\sqrt{(E_T + \beta W_3)^2 - m^2}} \left(c + \frac{1}{2}\right) \equiv \Delta \quad (9)$$

for all $l \leq n$, where n is chosen so that $l > n$ belongs to the pure Coulomb phases, with $r \geq c_0 + \frac{1}{2}$.

We note for future use that, for a given target nucleus, n is proportional to the momentum p of the bombarding particle. Taking into account

* See footnote on p. 322.

that for gold with our charge distribution model $n_0 = 9$, when $p_0 = 236 \text{ MeV} = 1,18 \cdot 10^{-13} \text{ cm}^{-1}$, we obtain:

$$n = \frac{9p}{p_0}. \quad (10)$$

III. The relative error of the differential cross section

YENNIE et al. have shown [3a] that an error $\Delta\delta_l$ in the l -th phase shift leads to the following relative error in the differential cross section:

$$\frac{\Delta_l d\sigma/d\Omega}{d\sigma/d\Omega} = \frac{2 |\Delta\delta_l|}{p(d\sigma/d\Omega)^{1/2}}. \quad (11)$$

In our case the individual errors in the calculation of the phase-shifts are not independent, as they originate from the *same* approximations to $W(r)$ and $[W(r)]^2$ in each phase. Let us consider the worst case, when the full individual errors are summed:

$$\frac{\Delta d\sigma/d\Omega}{d\sigma/d\Omega} \leq \frac{2 \sum_{l=0}^n |\Delta\delta_l|}{p(d\sigma/d\Omega)^{1/2}}. \quad (12)$$

We require the relative error in the differential cross section to be less than ε . Then (9), (10) and (12) give that this requirement is satisfied, if

$$\left(\frac{d\sigma}{d\Omega} \right)^{1/2} \geq \frac{18}{\varepsilon p_0} \Delta. \quad (13)$$

As an example we evaluate the scattering angles at which our W. K. B. phases can be used for electrons of 183 MeV energy scattered by gold, if we require the relative error of the differential cross section to be less than 10%.

From (8) and (9) we obtain $\Delta = 0,0047$, and from (13) with $\varepsilon = 0,1$ we find

$$\frac{d\sigma}{d\Omega} \geq 0,52 \cdot 10^{-26} \text{ cm}^2. \quad (14)$$

Taking into account the experimental values of the differential cross section at 183 MeV [7], we find that (14) holds in the $0^\circ < \Theta \lesssim 40^\circ$ scattering angle region.

We notice that for electrons our formulae cannot be extended to energies $\geq 1 \text{ BeV}$, because of the increasing weight of the inelastic processes (bremsstrahlung) with increasing energy. For μ -mesons, however, this limitation ceases and so we conclude that the W. K. B. approach can be used in analysing the scattering of electrons up to 1 BeV and of μ -mesons for $E_T > 1 \text{ BeV}$ too.

The author expresses his thanks to Mr. G. DOMOKOS for valuable discussions and to Miss G. SZÜCS, who performed the tedious numerical calculations.

Appendix

For those values l , which lead to $r_0 \geq c - \frac{1}{2}$

$$\begin{aligned} \delta_l = & \frac{\pi}{2} \left(l + \frac{1}{2} \right) + \frac{1}{2} \left\{ \sqrt{a_1 \left(c - \frac{1}{2} \right)^4 + 2b_1 \left(c - \frac{1}{2} \right)^2 - \left(l + \frac{1}{2} \right)^2} + \right. \\ & + \frac{b_1}{\sqrt{-a_1}} \left[\frac{\pi}{2} - \arcsin \frac{a_1 \left(c - \frac{1}{2} \right)^2 + b_1}{\sqrt{b_1^2 + a_1 \left(l + \frac{1}{2} \right)^2}} \right] - \\ & - \left(l + \frac{1}{2} \right) \left[\frac{\pi}{2} + \arcsin \frac{b_1 \left(c - \frac{1}{2} \right)^2 - \left(l + \frac{1}{2} \right)^2}{\sqrt{b_1^2 + a_1 \left(l + \frac{1}{2} \right)^2 \left(c - \frac{1}{2} \right)^2}} \right] \Bigg\} + \\ & + \left\{ \sqrt{a_2 x^2 + 2b_2 x + d_2} + \frac{b^2}{\sqrt{a^2}} \ln (a_2 x + b_2 + \sqrt{a_2} \sqrt{a_2 x^2 + 2b_2 x + d_2}) - \right. \\ & - \sqrt{-d_2} \arcsin \frac{b_2 x + d_2}{\sqrt{b_2^2 - a_2 d_2}} \Bigg\}_{x=c+\frac{1}{2}} - \\ & - \left\{ \sqrt{a_3 \left(c + \frac{1}{2} \right)^2 + 2b_3 \left(c + \frac{1}{2} \right) + d_3} + \frac{b_3}{\sqrt{a_3}} \ln \left(\frac{a_3 \left(c + \frac{1}{2} \right) + b_3}{\sqrt{a_3}} + \right. \right. \\ & + \left. \sqrt{a_3 \left(c + \frac{1}{2} \right)^2 + 2b_3 \left(c + \frac{1}{2} \right) + d_3} \right) + \\ & + \left. \sqrt{-d_3} \left[\arcsin \frac{b_3}{\sqrt{b_3^2 - a_3 d_3}} - \arcsin \frac{b_3 \left(c + \frac{1}{2} \right) + d_3}{\sqrt{b_3^2 - a_3 d_3 \left(c + \frac{1}{2} \right)}} \right] \right\} \equiv \\ & \equiv \frac{\pi}{2} \left(l + \frac{1}{2} \right) + \frac{1}{2} \{1\} + \{2\}_{x=c-\frac{1}{2}}^{x=c+\frac{1}{2}} - \{3\}, \end{aligned}$$

$\{\{3\}\}$ has a different form, if $d_3 \equiv Z^2 e^4 - \left(l + \frac{1}{2}\right)^2 > 0$. This happens only for $l = 0$ and $Z \geq 64$).

For those values l , which lead to $c - \frac{1}{2} \leq r_0 \leq c + \frac{1}{2}$,

$$\delta_l = \frac{\pi}{2} \left(l + \frac{1}{2} \right) + \left\{ 2 \right\}_{x=r_0}^{x=c+\frac{1}{2}} - \left\{ 3 \right\}.$$

$$x=r_0 = \frac{-b_2 + \sqrt{b_2^2 - a_2 d_2}}{a_2}$$

For the pure Coulomb phases $\left(r_0 \geq c + \frac{1}{2} \right)$

$$\delta_l = \frac{\pi}{2} \left(l + \frac{1}{2} \right) - \left\{ \frac{b_3}{\sqrt{a_3}} \ln \frac{\sqrt{a_3}}{\sqrt{b_3^2 - a_3 d_3}} + \sqrt{-d_3} \left(\arcsin \frac{b_3}{\sqrt{b_3^2 - a_3 d_3}} + \frac{\pi}{2} \right) \right\}$$

the coefficients, a , b , c are related to the parameters used in the text in the following way:

$$a_1 = -\frac{1}{3} E_T \beta + \beta^2 F',$$

$$b_1 = \frac{1}{2} p^2 + E_T \beta D + \frac{1}{2} \beta^2 D^2,$$

$$d_1 = -\left(l + \frac{1}{2} \right)^2,$$

$$a_2 = p^2 + 2E_T \beta C + \beta^2 C',$$

$$b_2 = E_T \beta B + \frac{1}{2} \beta^2 B',$$

$$d_2 = 2E_T \beta A + \beta^2 A' - \left(l + \frac{1}{2} \right)^2,$$

$$a_3 = p^2,$$

$$b_3 = Ze^2 E_T,$$

$$d_3 = Z^2 e^4 - \left(l + \frac{1}{4} \right)^2.$$

REFERENCES

1. R. W. WILLIAMS, Phys. Rev., **98**, 1387 and 1393, 1955.
2. R. HOFSTADTER, Ann. Rev. Nucl. Sc., **7**, 231, 1957.
3. a) D. R. YENNIE, D. G. RAVENHALL and R. N. WILSON, Phys. Rev., **95**, 500, 1954.
b) D. G. RAVENHALL and D. R. YENNIE, Proc. Phys. Soc., **70**, 857, 1957.
4. E. PREDAZZI, Nuovo Cimento, **12**, 177, 1959.
5. J. A. WHEELER, Ann. Phys., **7**, 239—322, 1959.
6. Л. Ландау и Е. Лифшиц, Квантовая механика, Гос. Изд. Техн.-теоретич. Литературы, Москва, 1948г. стр. 456—457.
7. BEAT HAHN, D. G. RAVENHALL and R. HOFSTADTER, Phys. Rev., **101**, 1131, 1956.

КВАЗИКЛАССИЧЕСКОЕ ОПИСАНИЕ РАССЕЯНИЯ ЭЛЕКТРОНОВ
БОЛЬШИХ ЭНЕРГИЙ НА ТЯЖЕЛЫХ ЯДРАХ

А. ФРЕНКЕЛЬ

Резюме

Выводятся формулы квазиклассических фаз рассеяния электронов больших энергий на тяжёлых ядрах. Рассматривается вопрос о пределах применимости метода.



THE ROLE OF SURFACE HYDROXILS OF $\text{Al}_2\text{O}_3 \cdot x\text{H}_2\text{O}$ IN THE LUMINESCENCE OF ADSORBED FLUORESC EIN MOLECULES

By

E. LENDVAY

RESEARCH INSTITUTE FOR TECHNICAL PHYSICS OF THE HUNGARIAN ACADEMY OF SCIENCES, BUDAPEST

(Presented by G. Szigeti. — Received 18. IV. 1961)

Producing various surface hydroxyl concentrations on Al_2O_3 films by surface reactions it was found that there is a distinct relation between the emission and the adsorbed fluorescein and the number of $-\text{OH}$ groups. The fact that the intensity of emission is growing with the surface hydroxyl concentration indicates that the emitting centres are bound to the surface by hydrogen bonds.

§ 1. Introduction

It is known that the molecules and ions in the adsorbed state change their adsorption and emission spectra because of the adsorbing interaction [1—7]. In the case of simple physical adsorption the energy of interaction is not enough to cause any considerable shift or broadening of bands, but in chemisorption the change in the electron structure of the adsorbed ion or molecule appears in the absorption and emission spectra in a measurable manner.

There are many data in the literature concerning the inter-, and intramolecular hydrogen bonds and their influence upon the spectra of the examined materials [7—13].

Similar effects are observed in the case of layer phosphors activated by fluorescein showing that the activator molecules are bound to the surface by chemisorption, in their majority by hydrogen bonds [14].

Hydrogels were obtained by means of chemical treatment of aluminium oxide films, prepared by anodic oxidation, as they offer a possibility to study the phenomenon mentioned above. It is easy to follow in such a system the relation between the hydration state of the surface and the emission of fluorescein ions adsorbed on the hydrogels. It was found that by changing the quality of the surface not only the intensity of emission changes, but the peaks of emission shift too. It is possible to attribute these changes to the changes in the acidity of the surface of the adsorbent and the number of adsorbing centres.

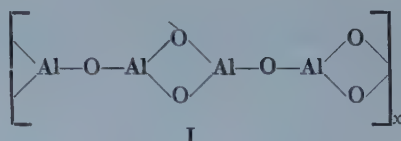
In a previous paper [14] it was examined how under the same adsorbing conditions the emission spectrum of fluorescein ions adsorbed by different $\text{Al}_2\text{O}_3 \cdot x\text{H}_2\text{O}$ hydrogels changes. It is obvious that during the chemical

treatment not only the surface of the layer is changing but that there are also substantial changes in the lower layers, therefore the data given in a previous paper [14] are not conclusive as regards the role of the surface groups. To decide how important a role the surface plays in luminescence, we need some experiments concerning the state of the surface. As the result of treatment with alcalic reagents (described in the publication quoted) is a function of different parameters, it is necessary to use reactions of other types. The present paper is dealing with the further examination of the problem of layer phosphors and with the role of surface —OH groups of Al_2O_3 hydrogels.

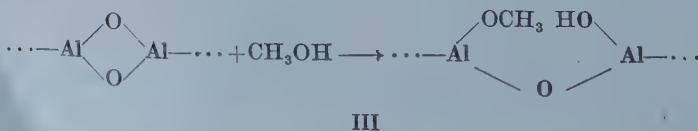
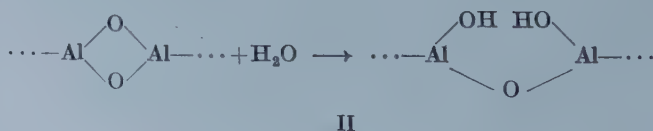
§ 2. Relation between the number of surface —OH groups and the intensity of luminescence

As is known, the structure of the upper layer of anodic oxide films examined by means of X-rays and electron diffraction patterns is amorphous or a $\gamma\text{-Al}_2\text{O}_3$ [15—21]. The transitional layer between the upper layer of the film and the metal has a boehmit-type structure [22—24].

The structure of the mentioned oxide layer is suitable for a hydrogel the water content of which is a function of the conditions existing at the time of formation of the layer. Because of this, the surface —OH concentration is very low and if the thickness of the oxide film is adequate, it may be described by structure I.



It is known that alumina as well as silica (quartz, dehydrated silicagel, microporous glass and so on) are able to bind water or methylalcohol by irreversible chemisorption [25—28]. These surface reactions may be represented in the following way:



The above formulas demonstrate that the structure II contains two hydroxyls, while the structure III (the so-called "alkylated surface") contains only one —OH group. The chemisorption process mentioned above was used to investigate whether there is a direct connection between the number of surface —OH groups and the luminescence. It is quite clear that under identical conditions

$$\alpha_{\text{OH}}^{\text{H}_2\text{O}} > \alpha_{\text{OH}}^{\text{CH}_3\text{OH}} \quad (1)$$

(where α_{OH} is the concentration of —OH groups on the surface) and so, by means of adsorbents prepared in these two ways the question can be decided.

The preparation of the aluminium oxide films, the measurements of emission spectra and the adsorption of fluorescein were described in a recent paper [14].

The oxidized aluminium plates after thorough washing were dried at 120° C for 5 hours before the chemisorption of water or methylalcohol took place. The chemisorption was carried out at higher temperatures in a suitable liquid. Some samples were treated below the boiling point of water or methylalcohol, others at the boiling point of the corresponding liquid for 4–8 hours. The surface of each sample was originally covered by a 15–18 μ thick oxide film. The dimensions of the samples were identical. There was a shift in the wavelength in the spectral energy distribution of the luminescent emission of fluorescein adsorbed on the oxide layers treated under pressure above the boiling point, therefore these were unsuitable for comparison. Transforming the layer at lower temperature (at boiling point or below it) the spectra were similar to each other.

In the previous paper [14] the close connection between the emission of the fluorescein and the quality of the adsorbing surface, more exactly the type of the adsorbing bond was pointed out.

With regard to the fact that the reaction is rather sensitive it was supposed that the emission spectra of the same type (same intensity maximum etc.) belong to the same type of luminescent centres.

Comparing the layer phosphors of identical spectral energy distributions prepared by treatment in water resp. methylalcohol it was possible to state that the water treatment gave higher intensity than the alcoholic one. Fig. 1 shows the spectra of two different layer phosphors.

The intensity of the emission of a layer phosphor after treatment with water is twice that of a phosphor treated with alcohol as Fig. 1 shows. If we suppose that the active adsorption of fluorescein [14] is accompanied by the development of hydrogen bonds, then it is evident that under identical conditions the surface treated with water contains more luminescent centres than the surface treated with alcohol. As the adsorbed fluorescein exists on the surface in a monomolecular distribution and the molecules are far enough

from each other, the quantum efficiency may be supposed to be independent of the surface concentration of the activator. For similar reasons the correction of the spectra due to the self-absorption is also negligible. In this case the intensity of emitted light is the function of the surface concentration, supposing identical adsorbing bonds.

Many experiments show that in solution in the case of organic molecules the redistribution of vibrational energy takes place among the different degrees of freedom. This process is extremely quick, its order of magnitude

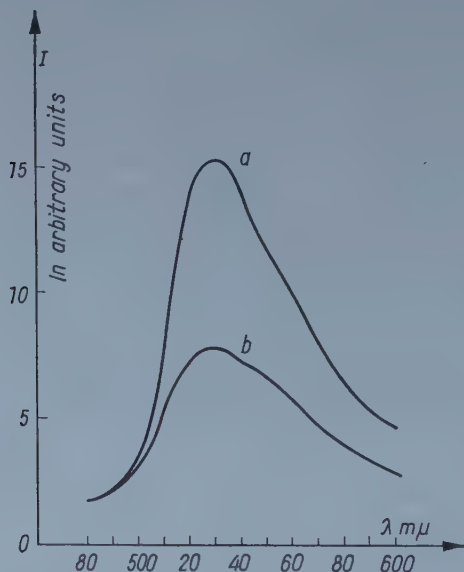


Fig. 1. Characteristic spectra of the two kinds of layer phosphors.

a — the lighting of fluorescein on $\text{Al}_2\text{O}_3 \cdot x\text{H}_2\text{O}$, which was prepared with a watery treatment.
b — luminescence of fluorescein on $\text{Al}_2\text{O}_3 \cdot x(\text{H}_2\text{O}, \text{CH}_3)$ (B was prepared with methylalcohol)

is 10^{-10} — 10^{-12} sec. i. e. essentially smaller than the average lifetime of the excited state [29]. In practice this means that an equilibrium distribution of vibrational energy develops in the excited state too. The whole process depends on the temperature of the medium.

As in the case examined there is a much greater interaction between the activator and the adsorbent than in solutions between the solvent and the solute, we may suppose that the above thermal-energy equilibrium sets in. In this case the radiation due to the frequency ν of the emission is [29—30]

$$W_{(\nu)}^L = n^* h \nu \int \varrho^*(E_R^*) A(E_R^*, \nu) dE_R^*, \quad (2)$$

where n^* is the average number of molecules in the excited state, $A(E_R^*, \nu)$

the probability of spontaneous transition from the energy level E_R^* to a lower level E_R , while the system emits $h\nu$ photons, and $\varrho(E_R^*)$ the energy distribution function of the excited states. This energy distribution function is given by

$$\varrho^*(E_R^*) = Cg^*(E_R^*) \exp\left(-\frac{E_R^*}{KT}\right) \quad (3)$$

where $g^*(E_R^*)$ is the statistical weight of the level E_R^* .

The equation (2) is of general validity, (3) is valid only if thermal equilibrium exists between the excited molecules and their environment.

The examination of equations (2) and (3) shows that in the case of identical exciting and thermal conditions and in the case of identical samples $g^*(E_R^*)$ and $A(E_R^*, \nu)$ are also identical. This means that there is a difference between the layer phosphors, produced with a treatment in water resp. alcohol only in the value of n^* , that is

$$\frac{W_{\text{H}_2\text{O}}^L(\nu)}{W_{\text{CH}_3\text{OH}}^L(\nu)} \simeq \frac{n_{\text{H}_2\text{O}}^*}{n_{\text{CH}_3\text{OH}}^*}, \quad (4)$$

where $n_{\text{CH}_3\text{OH}}^*$ and $n_{\text{H}_2\text{O}}^*$ are the number of excited molecules on a surface of alylated resp. hydrated samples of equal dimensions under the same exciting conditions. If we consider that the value of n^* under the conditions mentioned above is unique function of the number of adsorbed fluorescein molecules, then it is clear that

$$\frac{W_{\text{H}_2\text{O}}^L(\nu)}{W_{\text{CH}_3\text{OH}}^L(\nu)} \simeq \frac{n_{\text{H}_2\text{O}}}{n_{\text{CH}_3\text{OH}}} = \frac{N_{\text{H}_2\text{O}}}{N_{\text{CH}_3\text{OH}}} \quad (5)$$

and thus the value of n depends only on the number of active points, of course, if identical conditions for the adsorption of fluorescein are ensured.

According to (5) the intensity of emission changes proportionally with the surface concentration of adsorbing centres (N). If these adsorbing centres are surface hydroxyl groups, then α_{OH} determines the intensity relations of adsorbate phosphors of the same type.

In the examined case the different $-\text{OH}$ concentrations on the surface were ensured in advance (because of chemisorption of water resp. alcohol). Representing the quotient of intensities of emission of the different layer phosphors at a given frequency as a function of wavelength a straight line was obtained.

It can be supposed that the distortion of the straight line at the edges of the band is due to the inaccuracy of measurement at low intensities. The

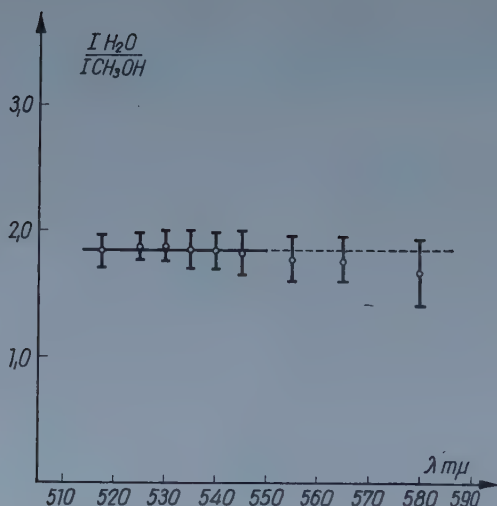


Fig. 2. The dependence of the ratio of I_{H_2O} and I_{CH_3OH} on the wavelength

value of the quotient I_{H_2O}/I_{CH_3OH} in the major part of the examined region is 1.8—2.0 which is in good agreement with structure II—III.

§ 3. Discussion

Comparing the emission spectra of two layer phosphors prepared and examined under identical conditions and varying only the liquid, we have an efficient method to study the bond of the activator. It was found that —OH groups of the adsorbing surface play an important role in the formation of layer phosphors. The relation between the surface —OH concentration and the luminescent emission makes it clear that the development of luminescent centres is connected with the formation of hydrogen bridges. The chemisorption of water resp. methylalcohol is a typical surface reaction and so these measurements mean a new experimental refutation of CHOMSE's supposition that the change of the crystal structure of an Al_2O_3 film is the primary cause of emission, thereby neglecting the chemical change of the surface [32].

As the eq. (5) shows, the quotient of intensities belonging to a given wavelength depends on the quotient of concentrations of the surface hydroxyl groups. This is true of course only in the case of molecules adsorbed on —OH groups of identical acidity. In case of different spectra we cannot make such comparisons for the $A(E_R^*, \nu)$ are not identical, because of the change of the electron structure of the molecules.

If the acceptor molecules are identical, experimental facts show that in case of hydrogen bridges the intensity of fluorescence alters with the type of donor [33]. This is in close connection with the fact that the electron density

changes on the binding atom of the acceptor. As has been mentioned, the atom is in most cases a hetero-atom which has auxochrom or chromophor character, this effect plays an important role in the formation of the physical properties of the molecule. As in view of luminescence the hetero-atom is very important to loosen the π electrons of the molecule, it is obvious that the character of the donor will influence the emission of molecules. If we pay attention to the fact that the growth or decrease of the interaction mentioned above will change the probability of radiationless transitions, it is obvious that the analysis of intensity ratios is performable only for samples being in identical surface bonds.

In the present case, having emission spectra of the same type there is no hindrance to compare the experimental results, which are in good agreement with the intensity ratio 2 : 1, expected from structure II and III.

REFERENCES

1. С. И. Кубарев, ДАН., **126**, 971, 1959.
2. Е. И. Котов и А. Н. Теренин, ДАН, **124**, 865, 1959.
3. Е. И. Котов, Опт. и Спектр., **3**, 115, 1957.
4. Г. И. Кобишев, ДАН, **127**, 375, 1959.
5. А. Н. Теренин и В. Филимонов, ДАН., **109**, 982, 1956.
6. А. И. Теренин и А. И. Сидорова, Изв. АН. СССР, **14**, 152, 1950.
7. А. И. Сидорова, Ж. Ф. Х., **23**, 525, 1954.
8. G. C. RIMENTEL, J. Am. Chem. Soc., **79**, 3323, 1957.
9. Ю. В. Набойкин и Б. А. Задорожный, Изв. АН. СССР, Сер. Физ., **24**, 758, 1960.
10. Ю. В. Набойкин, Б. А. Задорновский и Е. Н. Павлова, Изв. АН. СССР. Сер. Физ. **23**, 9, 1959.
11. N. MATAGA, J. KAIBE and M. KOIZUMI, Nature, **175**, 731, 1955.
12. Н. Д. Соколов, Успехи Физ. Наук, **57**, 205, 1955.
13. A. WELLER, Z. Elektrochem, **60**, 1140, 1956.
14. E. LENDVAY, Acta Phys. Hung., **13**, 289, 1961.
15. W. C. BURGERS, A. CLAASEN and J. ZERNIKE, Z. Physik, **74**, 593, 1932.
16. W. J. BERNARD and J. W. COOK, J. Electrochem. Soc., **106**, 643, 1959.
17. W. GEEL and B. SCHENK, Philips Res. Rep., **12**, 240, 1957.
18. M. SCHENK, Werkstoff Aluminium und seine anodische Oxidation, A. Francke AG. Verlag, Bern, p. 586, 1948.
19. E. J. W. VERWEY, Z. Kristallographie, **91**, 317, 1935.
20. A. ROTH, Z. anorg. Chem., **241**, 48, 1940.
21. G. HASS and H. KEHLER, Kolloid Z., **97**, 27, 1941.
22. TH. SKULIKIDIS, N. MASSIOS and K. KAZANTIRIS, Kolloid Z., **159**, 130, 1958.
23. R. K. HART, Trans. Faraday Soc., **50**, 269, 1954.
24. I. S. KERR, Proc. Phys. Soc. B **69**, 1056, 1956.
25. W. E. GARNER, Chemisorption, Butterworths Sci. Publications, London, 1957, p. 62.
26. D. H. EVERETT and F. S. STONE, The Structure and Properties of Porous Materials, Butterworths Sci. Publications, London, 1958, p. 209.
27. С. П. Жданов, ДАН, **58**, 99, 1949.
28. W. STÖBER, Kolloid Z., **145**, 17, 1956.
29. А. А. Бабушкин и А. В. Уваров, ДАН, **110**, 581, 1956.
30. В. И. Степанов, ДАН, **112**, 839, 1957.
31. В. И. Степанов, Изв. АН. СССР, Сер. Физ. **22**, 1367, 1958.
32. H. CHOMSE and W. HOFFMANN, Z. anorg. Chem., **296**, 20, 1958.
33. N. MATAGA and S. TSUNO, Naturwiss., **44**, 304, 1957.

РОЛЬ ПОВЕРХНОСТНЫХ ГИДРОСИЛЬНЫХ ГРУПП $\text{Al}_2\text{O}_3 \cdot \text{H}_2\text{O}$ В ЛЮМИНЕС-
ЦЕНЦИИ АДСОРБИРОВАННОГО ФЛЮОРЕСЦЕИНА

Э. ЛЕНДВАЙ

Резюме

Мы изготовили хемосорбцией метанола или воды поверхности Al_2O_3 , гидратизированные в различной мере. Ввиду того, что вследствие характера реакции возникли адсорбционные центры идентичного свойства, мы имели возможность сравнить поверхностные фосфоры, изготовленные двумя адсорбентами и активированные флуоресцеином. Опыты согласно теоретическим предположениям показали, что в случае хемосорбции воды интенсивность люминесценции удваивается. Нами сделано заключение из параллельного изменения интенсивности люминесценции и поверхностной — OH концентрации, что люминесцентные центры уранина, участвующие в эмиссии, связаны водородным мостом с поверхностью.

ON THE K-MESONIC INTERACTION OF MUONS

By

P. VÉRTES

CENTRAL RESEARCH INSTITUTE FOR PHYSICS, BUDAPEST*

(Received 26. XI. 1960)

It is known that the large mass of the muon is a serious problem in the field-theoretical interpretation of the origin of the mass of elementary particles. As far as we know the muon is subject to electromagnetic and weak interactions only. In the field-theoretical interpretation of the particle masses, however, the muon is assumed to interact also with some other field than that of the photon though this interaction has only slight effects on other processes for which it gives only small corrections.

Several attempts have been made to clarify this problem [1]. The most obvious is to assume K -mesonic interaction [2] in the form of K -meson-nucleon interaction according to GYÖRGYI's [3] formula

$$H = \frac{1}{2} g \bar{\chi} \gamma_i \chi \Phi_{\beta}^+ (\partial_i - \partial_i) \Phi_{\beta},$$

where χ is the operator of the muon, Φ the operator of the K -meson, g the coupling constant if we assume that $gM^2 = 1$, where M is the mass of the K -meson and $\beta = 1, 2$ is the isospinor index. This interaction is not renormalizable, the cut-off parameter λ , however, can be calculated from the correction for the muon's self-mass.

If we take into consideration the electromagnetic interaction too the anomalous magnetic moment of the muon can also be calculated. Finally, even the correction for the self-mass of the K -meson can be calculated. The estimation of these corrections is given in paper [4]. Here it is attempted to give more exact calculations.

Fig. 1 gives the correction for the self-mass of muons in the first order approximation:

$$\delta m = - \frac{(gM^2)^2}{12 \cdot (2\pi)^4} m Q(z).$$

* This work was carried out in the Institute for Theoretical Physics of the Roland Eötvös University, Budapest.

Here $z = \frac{\lambda^2}{M^2}$, m is the mass of the muon and

$$Q(z) = (3z)^2 \log z - (2z)^2 \log 2z - 2(2z+1)^2 \log(2z+1) + \\ + 2(z+1)^2 \log(z+1) + (z+2)^2 \log(z+2) - 4 \log 2.$$

Asymptotically $Q(z) \approx 1,5z^2$ if $z \gg 1$. We want to have $\frac{\delta m}{m} \approx 1$ and it is apparent that $z = 115$, and $\lambda = 10,7 M$ is a good value for the cut-off parameter.

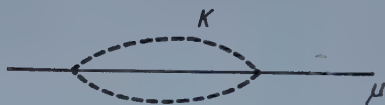


Fig. 1

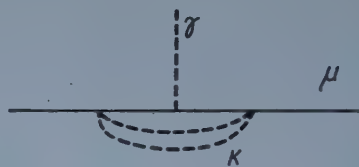


Fig. 2

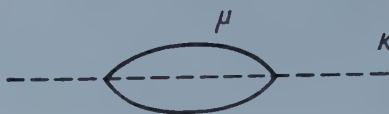


Fig. 3

Fig. 2 gives the correction for the anomalous magnetic moment :

$$\delta \mu = 10^{-5} (gM^2)^2 P(z) \text{ muon magneton,}$$

where

$$P(z) = z \log 2z - (z+1) \log(z+1) + \log 2 \approx z \log 2, \text{ if } z \gg 1.$$

For $z = 115$ we obtain $\delta \mu = 8 \cdot 10^{-4}$ which is not too large and may be consistent with the experimental facts [5].

Fig. 3 gives the correction for the self-mass of the K -meson

$$\left(\frac{\delta M}{M} \right)^2 = -1,5 \cdot 10^{-4} (gM^2)^2 R(z),$$

where

$$R(z) = [2(\sqrt{z}+z)^3 \log(\sqrt{z}+z) - (\sqrt{z})^3 \log \sqrt{z} - (2z+\sqrt{z})^3 \log(2z+ \\ + \sqrt{2})] \left(1 + \frac{1}{\sqrt{z}} \right) + (2z+1)^3 \log(2z+1) - 2(z+1)^3 \log(z+1) + \\ + \frac{1}{\sqrt{z}} [(3z)^3 \log 3z + z^3 \log z - 2(2z)^3 \log 2z].$$

For $z = 115$ we obtain $\left(\frac{\delta M}{M}\right)^2 = -10^2$. Although this correction has a negative sign it can be compensated for by some other K -mesonic interaction.

I am indebted to Dr. G. MARX for suggesting this problem and to Dr. K. L. NAGY for his help in carrying out the calculations.

REFERENCES

1. J. SCHWINGER, Ann. of Physics, **2**, 407, 1957.
2. G. MARX and K. L. NAGY, Nucl. Phys., **12**, 125, 1959.
3. G. GYÖRGYI, Nucl. Phys., **10**, 197, 1959.
4. G. MARX and K. L. NAGY, Acta Phys. Hung., **11**, 161, 1960.
5. R. A. LUNDY et al., Phys. Rev. Lett., **1**, 38, 1958.



CONFIGURATION INTERACTION FOR WAVE FUNCTIONS CONSTRUCTED FROM ORTHOGONAL MANY-ELECTRON GROUP ORBITALS

By

E. KAPUY

RESEARCH GROUP FOR THEORETICAL PHYSICS, HUNGARIAN ACADEMY OF SCIENCES, BUDAPEST

(Received 2. I. 1961)

As has been shown in [1, 2] the two-electron orbitals orthogonal in the strong sense can be derived from coupled nonlinear integro-differential equations, which highly resemble the Hartree-Fock equations. Now we shall show that the results can be easily generalized for wave functions built up of mixed one-, two-, three- and many-electron orbitals (group orbitals).

We assume that the system consists of loosely coupled $1, 2, \dots, I, \dots, M$ electron groups, each containing $N_1, N_2, \dots, N_I, \dots, N_M$ electrons ($N_1 + N_2 + \dots + N_I + \dots + N_M = N$; N is the number of electrons). If the group orbitals are antisymmetrical in the space-spin variables of the electrons

$$\psi_I(1, 2, 3, \dots, N_I) = -\psi_I(2, 1, 3, \dots, N_I) = -\psi_I(3, 2, 1, \dots, N_I) = \dots, \quad (1)$$

normalized

$$\int \psi_I^*(1, 2, \dots, N_I) \psi_I(1, 2, \dots, N_I) d(1) d(2) \dots d(N_I) = 1, \quad (2)$$

for every I ,

and orthogonal in the strong sense

$$\int \psi_I^*(1, 2, \dots, N_I) \psi_J(1, 2', \dots, N'_J) d(1) = 0, \quad (3)$$

for each pair I, J , if $J \neq I$,

the normalized complete wave function satisfying the Pauli principle is of the form

$$\Psi = \sqrt{\frac{N_1! N_2! \dots N_M!}{N!}} \sum_P (-1)^p P \psi_1(1, 2, \dots, N_1) \psi_2(N_1 + 1, \dots, N_1 + N_2) \dots \times \psi_M(N - N_M + 1, \dots, N).$$

Here P means the permutations exchanging the electrons between the group orbitals, p is the parity of the permutations.

Expanding the Hamilton operator in the usual manner

$$H = H(0) + \sum_{\alpha=1}^N H(\alpha) + \sum_{1=\alpha<\beta}^N \frac{1}{r_{\alpha\beta}}$$

and taking (1), (2) and (3) into account the following expression is obtained for the energy (see also [3, 4, 5])

$$\begin{aligned} E = H(0) + \sum_I \int \psi_I^*(1, 2, \dots, N_I) \left[N_I H(1) + \left(\frac{N_I}{2} \right) \frac{1}{r_{12}} \right] \\ \times \psi_I(1, 2, \dots, N_I) d(1) d(2) \dots d(N_I) + \sum_{\substack{I, J \\ J \neq I}} \frac{N_I N_J}{2} \int d(1) d(2) \dots d(N_I) d(\kappa) d(\lambda) \dots d(\omega) \\ \times \left[\frac{1 - P_{1\kappa}}{r_{1\kappa}} \right] \psi_I^*(1', 2', \dots, N_I') \psi_I(1, 2, \dots, N_I) \psi_J^*(\kappa', \lambda', \dots, \omega') \psi_J(\kappa, \lambda, \dots, \omega). \end{aligned} \quad (4)$$

Instead of (2) let us introduce the following auxiliary conditions

$$\begin{aligned} D_{IJ} = \int \psi_I^*(1, 2, \dots, N_I) \psi_J^*(\kappa, \lambda, \dots, \omega) \psi_I(\kappa, 2, \dots, N_I) \psi_J(1, \lambda, \dots, \omega) \\ \times d(1) d(2) \dots d(N_I) d(\kappa) d(\lambda) \dots d(\omega). \end{aligned} \quad (5)$$

If all $D_{IJ} = 0$, (3) and (5) are entirely equivalent. Varying the ψ_I 's in the energy expression (4) and taking the auxiliary conditions (2) and (5) into account we obtain with the Lagrange multipliers $-E^I$ and $-E^{IJ}$ the following system of equations

$$\begin{aligned} \left\{ \sum_{\alpha=1}^{N_I} H(\alpha) + \sum_{1=\alpha<\beta}^{N_I} \frac{1}{r_{\alpha\beta}} + \sum_{\alpha=1}^{N_I} \sum_{J \neq I} N_J \int d(\kappa) d(\lambda) \dots d(\omega) \left[\frac{1 - P_{\alpha\kappa}}{r_{\alpha\kappa}} \right] \right. \\ \left. \times \psi_J^*(\kappa', \lambda', \dots, \omega') \psi_J(\kappa, \lambda, \dots, \omega) \right\} \psi_I(1, 2, \dots, N_I) = \left\{ E^I + \right. \\ \left. + \sum_{\alpha=1}^{N_I} \sum_{J \neq I} E^{IJ} \int d(\kappa) d(\lambda) \dots d(\omega) P_{\alpha\kappa} \psi_J^*(\kappa', \lambda', \dots, \omega') \psi_J(\kappa, \lambda, \dots, \omega) \right\} \psi_I(1, 2, \dots, N_I), \\ I = 1, 2, \dots, M. \end{aligned} \quad (6)$$

We get similar equations for the complex conjugate ψ_I^* 's.

If we require that the values of the D_{IJ} 's should be exactly zero, the values of the integrals on the right-hand side of equations (6) will also be exactly zero and the variation problem has probably no solution at all. Instead, we require that the values of the D_{IJ} 's are small positive numbers $D_{IJ} \ll 1$, so that the integrals $\int \psi_I^*(1, 2, \dots, N_I) \psi_J(1, 2', \dots, N_J) d(1)$ in the energy

expression can be neglected and assume that the system of equations is correct even in the case if $D_{IJ} \rightarrow 0$ for each pair I, J ($J \neq I$). In other words when $D_{IJ} \rightarrow 0$ and $\int \psi_J^*(1, \lambda, \dots \omega) \psi_I(1, 2, \dots N_I) d(1) \rightarrow 0$ then $|E^{IJ}| \rightarrow \infty$ so that

$$E^{IJ} \int \psi_J^*(1, \lambda, \dots \omega) \psi_I(1, 2, \dots N_I) d(1) \rightarrow \mathcal{E}^{IJ}(\lambda, \dots \omega | 2, \dots N_I)$$

and the \mathcal{E}^{IJ} 's are "well-behaved" functions satisfying the following condition:

$$\int \psi_K^*(1, 2, \dots N_K) \mathcal{E}^{IJ}(\lambda, \dots \omega | 2, \dots N_I) \psi_J(1, \lambda, \dots \omega) d(1) d(\lambda) \dots d(\omega) = 0 \text{ if } K \neq J. \quad (7)$$

By means of the \mathcal{E}^{IJ} 's the system of equations (6) can be written in the following form

$$\begin{aligned} & \sum_{a=1}^{N_I} H(a) + \sum_{1=a < \beta}^{N_I} \frac{1}{r_{a\beta}} + \sum_{J \neq I} N_J \sum_{a=1}^{N_I} \int d(x) d(\lambda) \dots d(\omega) \\ & \times \left[\frac{1 - P_{a\kappa}}{r_{a\kappa}} \right] \psi_J^*(\kappa', \lambda', \dots \omega') \psi_J(\kappa, \lambda, \dots \omega) \left\{ \psi_I(1, 2, \dots N_I) = E^I \psi_I(1, 2, \dots N_I) \right. \\ & \left. + \sum_{J \neq I} \sum_{a=1}^{N_I} (-1)^{a+1} \int d(\lambda) \dots d(\omega) \mathcal{E}^{IJ}(\lambda, \mu, \dots \omega | 1, \dots a-1, a+1, \dots N_I) \psi_J(a, \lambda, \dots \omega), \right. \\ & \left. (I = 1, 2, \dots M). \right. \end{aligned} \quad (6')$$

The solutions $\psi_{10}, \psi_{20}, \dots \psi_{10}, \dots \psi_{M0}$ belonging to the lowest $E^{10}, E^{20}, \dots E^{I0}, \dots E^{M0}$ values and antisymmetrical in the electron co-ordinates, which satisfy the auxiliary conditions (2) and (5), give the group orbitals corresponding to the ground state of the system. If $N_1 = N_2 = \dots N_I = \dots N_M = 1$, N is an even number and the part of the orbitals ψ_I depending on the space coordinates is identical by pairs, the equations (6') go over into the well-known Hartree-Fock equations of the one-electron orbitals. In this case the Lagrange multipliers \mathcal{E}^{IJ} do not depend on the co-ordinates, they are bare numbers.

Keeping the ψ_{J0} 's of the ground state in the bracketed expression on the right and left-hand side of equations (6) fixed we may assume that the system of equations

$$\begin{aligned} H^I \psi_{Ii}(1, 2, \dots N_I) = & \left\{ E^{Ii} + \sum_{J \neq I} E^{IiJ0} \sum_{a=1}^{N_I} \int d(x) d(\lambda) \dots d(\omega) P_{a\kappa} \psi_{J0}^*(\kappa', \lambda', \dots \omega') \right. \\ & \left. \times \psi_{J0}(\kappa, \lambda, \dots \omega) \right\} \psi_{Ii}(1, 2, \dots N_I), \end{aligned} \quad (8)$$

$$\begin{aligned} H^I = & \sum_{\kappa=1}^{N_I} H(a) + \sum_{1=a < \beta}^{N_I} \frac{1}{r_{a\beta}} + \sum_{J \neq I} N_J \sum_{a=1}^{N_I} \int d(x) d(\lambda) \dots d(\omega) \left[\frac{1 - P_{a\kappa}}{r_{a\kappa}} \right] \\ & \times \psi_{J0}^*(\kappa', \lambda', \dots \omega') \psi_{J0}(\kappa, \lambda, \dots \omega) \left\{ (I = 1, 2, \dots M), \right. \end{aligned}$$

has besides the ψ_{I0} 's further antisymmetrical solutions ψ_{Ii} ($i = 1, 2, 3, \dots$) too (these can be regarded as the excited states of the electron groups), which, with the new Lagrangian multipliers E^{Ii} and E^{IiJ0} , satisfy the auxiliary conditions

$$\int \psi_{Ii}^*(1, 2, \dots N_I) \psi_{Ii}(1, 2, \dots N_I) d(1) d(2) \dots d(N_I) = 1, \quad (i = 1, 2, 3, \dots) \quad (9)$$

and

$$\int \psi_{Ii}^*(1, 2, \dots N_I) \psi_{Jj}(1, 2', \dots N'_J) d(1) = 0, \text{ if } I \neq J, \quad (i, j = 1, 2, 3, \dots). \quad (10)$$

In addition, taking (7) into account we obtain

$$\int \psi_{Ii'}^*(1, 2, \dots N_I) \psi_{Ii}(1, 2, \dots N_I) d(1) d(2) \dots d(N_I) = 0, \text{ if } i' \neq i, \quad (11)$$

as well as

$$\int \psi_{Ii'}^*(1, 2, \dots N_I) H^I \psi_{Ii}(1, 2, \dots N_I) d(1) d(2) \dots d(N_I) = E^{Ii} \delta_{i'i}. \quad (12)$$

$$\int \psi_{Ii}^*(1, 2, \dots N_I) \psi_{Jj}(1, 2', \dots N'_J) d(1) = 0, \text{ if } I \neq J, \text{ and both } i > 0 \text{ and } j > 0. \quad (13)$$

is, however, not necessarily true in general.

The solutions of the equations (8) form the following set of functions

$$\begin{array}{cccc} \psi_{I0}, & \psi_{I1}, & \psi_{I2}, & \psi_{I3}, \dots \\ \dots\dots\dots & & & \\ \psi_{I0}, & \psi_{I1}, \dots & \psi_{Ii}, \dots & \psi_{Ii'}, \dots \\ \dots\dots\dots & & & \\ \psi_{J0}, & \psi_{J1}, \dots & \psi_{Jj}, \dots & \psi_{Jj'}, \dots \\ \dots\dots\dots & & & \\ \psi_{M0}, & \psi_{M1}, \dots & \psi_{Mm}, \dots & \psi_{Mm'}, \dots \end{array} \quad (14)$$

Owing to the strong restrictions (10) this set of functions is not complete thus in general the exact wave function cannot be expanded in terms of it. (If we dropped the auxiliary conditions (10) each row of the set of functions (14) would be a complete set.) It is reasonable, however, to assume that the wave function of a system which consists of loosely coupled electron groups can be expressed to a good approximation as the superposition of configurations constructed from the group orbitals (14), even if the system is subject to small external perturbation. Each configuration from each row of the system

(14) contains one group orbital, i.e. it can be characterized uniquely by the second index of the group orbitals occurring in it. It should be noted that the ground state and the excited states of the same electron group are orthogonal in the usual sense

$$\int \psi_{Ii'}^*(1, 2, \dots N_I) \psi_{Ii}(1, 2, \dots N_I) d(1) d(2) \dots d(N_I) = 0, \text{ if } i' \neq i,$$

and not in the strong sense

$$\int \psi_{Ii'}^*(1, 2, \dots N_I) \psi_{Ii}(1, 2', \dots N_I') d(1) = 0, \text{ if } i' \neq i,$$

as assumed by McWEENY [4, 5].

To solve equations (8) exactly, i. e. to determine the system (14) is as yet a hopeless task. Recently, it has been proved [6] that for given two-electron orbitals $\psi_I(1, 2)$ ($I = 1, 2, \dots N$) mutually orthogonal in the strong sense there exists a complete set of one-electron spin-orbitals $u_v(1)$ which can be partitioned into N subsets

$$u_{11}, u_{12}, u_{13}, \dots; \dots u_{I1}, u_{I2}, u_{I3}, \dots; \dots u_{N1}, u_{N2}, u_{N3}, \dots;$$

such that each of the $\psi_I(1, 2)$ can be expanded in terms of $u_{I1}, u_{I2}, u_{I3}, \dots$ only

$$\psi_I(1, 2) = \sum_{i_1, i_2} c_{i_1 i_2}^I u_{Ii_1}(1) u_{Ii_2}(2).$$

This theorem can be generalized, in an analogous manner, to the case of many electron group orbitals:¹

If $\psi_I(1, 2, \dots N_I)$ ($I = 1, 2, \dots M$) are antisymmetrical and mutually orthogonal in the strong sense then there exists a complete set of one-electron spin-orbitals $u_v(1)$ which can be partitioned into M subsets

$$u_{11}, u_{12}, u_{13}, \dots; \dots u_{I1}, u_{I2}, u_{I3}, \dots; \dots u_{M1}, u_{M2}, u_{M3}, \dots;$$

such that each of the $\psi_I(1, 2, \dots N_I)$'s can be expanded in terms of $u_{I1}, u_{I2}, u_{I3}, \dots$ only

$$\psi_I(1, 2, \dots N_I) = \sum_{i_1 i_2 \dots i_{N_I}} c_{i_1 i_2 \dots i_{N_I}}^I u_{Ii_1}(1) u_{Ii_2}(2) \dots u_{Ii_{N_I}}(N_I),$$

i.e. the full space can be decomposed into mutually perpendicular M sub-

¹ Note added in proof (15th October, 1961). A theorem, somewhat more general than this, has been proved by P. O. LÖWDIN in J. Chem. Phys., 35, 78, 1961.

spaces in such a way that each of the group orbitals $\varphi_I(1, 2, \dots, N_I)$ is localized to the corresponding subspace I .

The above theorem can serve as a basis to obtain approximate group orbitals $\varphi_I(1, 2, \dots, N_I)$ like the case of two-electron orbitals [2, 7, 8]:

1) Orthonormalized one-electron spin orbitals $v_v(1)$ are divided up into M groups so that none of them occurs in two or more groups:

$$v_{11}, v_{12}, \dots, v_{1n_1}; v_{I1}, v_{I2}, \dots, v_{In_I}; \dots, v_{M1}, v_{M2}, \dots, v_{Mn_M}.$$

(Of course, it is required that $n_I \geq N_I$ for every I .)

2) Then, we build up determinants from the spin orbitals by groups, the order of which is equal to the number of electrons in the corresponding group. In the group I altogether $\binom{n_I}{N_I}$ different determinants D_{Iq} can be formed. The approximate group orbitals φ_I are of the following form:

$$\varphi_I \sim \sum_q c_q^I D_{Iq}.$$

3) We substitute the group orbitals φ_I into the energy expression (4) and vary the coefficients taking into account the auxiliary conditions (2), with the Lagrangian multipliers $-\mathcal{E}^I$. (The auxiliary conditions (3) are automatically satisfied.) So we obtain a system of equations for the coefficients c_q^I , which can be solved by iteration. For each group we obtain $\binom{n_I}{N_I}$ roots \mathcal{E}^{Ii} and the same number of different sets of coefficients of which the c_q^{I0} 's belonging to the lowest \mathcal{E}^{I0} 's are the approximations to the ground state, the other c_q^{Ii} 's are the approximations to the excited states. The orbitals φ_{Ii} so obtained conform to (9), (10), (11), (12), and besides the conditions (13) are also fulfilled.

Of course the results depend on the decomposition of the set $v_v(1)$. We can subject the $v_{Ii}(1)$ decomposed preliminarily to an unknown unitary transformation which has to be determined as to give the best approximate group orbitals.

From the φ_{Ii} 's obtained by the above approximation procedure

$$\prod_{I=1}^M \binom{n_I}{N_I}$$

various configurations Φ_K can be formed. It is easily seen that the configurations are normalized and orthogonal to each other. The matrix elements of the operator H differ from zero for only two such configurations which differ at most in two group orbitals.

Introducing the following notations (for simplicity indicating in the configurations Φ_K, Φ_L only those two indices which can be different):

$$\begin{aligned}
H_{KL} &= H_{\dots ii' \dots jj' \dots} = \int \Phi_K^* H \Phi_L d\tau = \int \Phi_K^* \dots i \dots j \dots H \Phi_{\dots i' \dots j' \dots} d\tau, \\
h_{ii'}^I &= \int \varphi_{ii'}^*(1, 2, \dots N_I) \left[\sum_{\alpha=1}^{N_I} H(\alpha) + \sum_{1=\alpha < \beta}^{N_I} \frac{1}{r_{\alpha\beta}} \right] \varphi_{ii'}(1, 2, \dots N_I) d(1) d(2) \dots d(N_I), \\
I_{ii'jj'}^{IJ} &= \frac{N_I N_J}{2} \int d(1) d(2) \dots d(N_I) d(\kappa) d(\lambda) \dots d(\omega) \left[\frac{1 - P_{1\kappa}}{r_{1\kappa}} \right] \varphi_{ii'}^*(1' 2', \dots N_I') \\
&\quad \times \varphi_{ii'}(1, 2, \dots N_I) \varphi_{jj'}^*(\kappa', \lambda', \dots \omega') \varphi_{jj'}(\kappa, \lambda, \dots \omega), \\
H_{ii'}^I &= \int \varphi_{ii'}^*(1, 2, \dots N_I) H^I \varphi_{ii'}(1, 2, \dots N_I) d(1) d(2) \dots d(N_I), \quad (15)
\end{aligned}$$

the matrix elements of the Hamilton operator different from zero can be easily written down. There are three different cases:

1) for identical configurations (diagonal elements)

$$H_{KK} = H_{\dots ii \dots jj \dots} = H(0) + \sum_I h_{ii}^I + \sum_{J \neq I} I_{ii'jj'}^{IJ}; \quad (16)$$

2) for configurations which differ in *one* group orbital

$$H_{KL}' = H_{\dots ii' \dots jj' \dots} = h_{ii'}^I + 2 \sum_{J \neq I} I_{ii'jj'}^{IJ} = H_{ii'}^I; \quad (17)$$

3) for configurations which differ in *two* group orbitals

$$H_{KL}'' = H_{\dots ii' \dots jj' \dots} = 2 I_{ii'jj'}^{IJ}. \quad (18)$$

The remaining matrix elements are all zero.

Varying the coefficients C_K in the energy expression calculated with the linear combination of the configurations $\sum C_K \Phi_K$ subject to the auxiliary condition

$$\sum_K |C_K|^2 = 1,$$

we get the system of equation

$$\sum_L H_{KL} C_L - E C_K = 0, \quad (K = 0, 1, 2, \dots) \quad (19)$$

which can be solved by well-known methods [4, 5, 9]. From the system of equations (19) we may obtain by iteration the Rayleigh—Schrödinger series for the energy up to second order in the form [4, 5, 10]

$$E = H_{00} + \sum_{K>0} \frac{|H_{0K}|^2}{H_{00} - H_{KK}}.$$

H_{00} is identical with the energy expression (4). The second term can be divided into two parts

$$\sum_{K' > 0} \frac{|H_{0K}|^2}{H_{00} - H_{K'K'}} + \sum_{K'' > 0} \frac{|H_{0K''}|^2}{H_{00} - H_{K''K''}}. \quad (20)$$

K' and K'' label the configurations containing one or two excited group orbitals, respectively. Other configurations do not appear, as the corresponding matrix elements are zero. With the notations (15), (16), (17), and (18), (20) takes the form

$$\sum_I \sum_{i > 0} \frac{|H_{0i}^I|^2}{E_{i0}^I - E^I} + \sum_{\substack{I, J \\ I \neq J}} \sum_{\substack{i > 0 \\ j > 0}} \frac{2 |I_{0i0j}^{IJ}|^2}{H_{00} - H_{\dots ii \dots jj \dots}}. \quad (21)$$

The first term is the polarization energy, the second is London's dispersion energy. In our case the first term vanishes, as the group orbitals φ_{li} are, in the sense of the variation method, approximate eigenfunctions of the operator H^I .

It should be noted that the results agree with those of McWEENY [4, 5], which can be explained by the fact that in the calculation of the matrix elements he applies instead of

$$\int \varphi_{li'}^* (1, 2, \dots N_I) \varphi_{li} (1, 2', \dots N_I') d(1) = 0, \text{ if } i' \neq i,$$

tacitly the usual orthogonality

$$\int \varphi_{li'}^* (1, 2, \dots N_I) \varphi_{li} (1, 2, \dots N_I) d(1) d(2) \dots d(N_I) = 0, \text{ if } i' \neq i.$$

REFERENCES

1. E. KAPUY, *Acta Phys. Hung.*, **12**, 185, 1960.
2. E. KAPUY, *Acta Phys. Hung.*, **12**, 351, 1961.
3. R. G. PARR, F. O. ELLISON and P. G. LYKOS, *J. Chem. Phys.*, **24**, 1106, 1956.
4. R. Mc WEENY, *Proc. Roy. Soc. A*, **253**, 242, 1959.
5. R. Mc WEENY, *Rev. Mod. Phys.*, **32**, 335, 1960.
6. T. ARAI, *J. Chem. Phys.*, **33**, 95, 1960.
7. J. M. PARKS and R. G. PARR, *J. Chem. Phys.*, **28**, 335, 1958.
8. E. KAPUY, *Acta Phys. Hung.*, **11**, 409, 1960.
9. P. O. LÖWDIN, *Advances in Chemical Physics* (Interscience Publ., Inc., New York, 1959) Vol. II, p. 270.
10. P. O. LÖWDIN, *J. Chem. Phys.*, **19**, 1936, 1951.

FÄRBUNG VON NATRIUMCHLORIDPULVER DURCH EXOELEKTRONEN

Von

L. MALICKÓ und Z. MORLIN*

INSTITUT FÜR EXPERIMENTALPHYSIK DER TECHNISCHEN HOCHSCHULE FÜR BAUINDUSTRIE
UND VERKEHRSWESEN, BUDAPEST

(Eingegangen: 10. I. 1961)

Es ist eine in der Literatur oft beschriebene Erscheinung, dass sich farblose Alkalihalogenidkristalle durch verschiedenartige äussere Einflüsse verfärben. Als äussere Einflüsse werden dabei Bestrahlung durch Röntgenstrahlen bzw. radioaktive Strahlen [1], Erhitzen in Na- bzw. K-Dampf [1] sowie Pressen bei hohen Temperaturen [2, 3] erwähnt. Als gemeinsame Folge dieser äusseren Einwirkungen gelangen, innerhalb der verbotenen Zone, Elektronen in Elektronenfallen, wodurch die sogenannten Farbzentren zustandekommen, deren Existenz makroskopisch durch die Änderung der elektrischen Leitfähigkeit, des Absorptionskoeffizienten usw. bewiesen werden kann.

Andererseits ist es bekannt, dass kaltbearbeitete Metalloberflächen Elektronen ausstrahlen. In der Literatur sind mehrere Versuche beschrieben worden, bei denen kaltbearbeitetes, gewalztes Aluminium Photoplatten bei Berührung mit diesen schwärzte [4]. Solche Aluminiumplatten lassen Spitzenzähler ansprechen. Mit Spitzenzählern durchgeführte Messungen bewiesen, dass gewalzte Aluminiumplatten, in 10 Minuten auf 350° C erwärmt, ähnlich dem Verlauf der Aufheizungskurven bei Thermolumineszenzmessungen, Elektronen ausstrahlen [5]. Die Zahl der so emittierten Elektronen kann durch vorangehende ultraviolette Bestrahlung des Aluminiums erhöht werden.

Von diesen Befunden ausgehend versuchten wir Natriumchloridkristalle durch Exoelektronen zu färben. Zu den Versuchen benützten wir 99,98 prozentige Aluminiumplättchen aus denen, zur Sicherung der guten Berührung zwischen Al und NaCl kleine Hülsen gefertigt wurden, die wir dann mit 0,5—1 g NaCl Pulver füllten. Die Hülsen wurden danach in einem elektrischen Ofen mit 35° C/Min. Heizgeschwindigkeit bis 350° C aufgeheizt und dann aus dem Ofen genommen und auf kalten Eisenplatten schnell abgekühlt. In jedem Fall entstanden gelblich-braune Pulver, die unter einem Druck von 10,000 kp/cm² zusammengepresst durchsichtige, gelbe Pastillen ergaben. Wenn wir das Aluminiumplättchen vorher bei 550° C einer thermischen

* Forschungslaboratorium für Chemische Strukturen der Ungarischen Akademie der Wissenschaften, Budapest.

Behandlung unterworfen und danach langsam, in 48—72 Stunden, auf Zimmertemperatur abkühlten, entstand keine Färbung. Bei einer solchen Behandlung lösen sich die bei der Kaltbearbeitung entstandenen Spannungen, wodurch das Metall nachher keine Exoelektronen mehr abgibt.

Die auf diese Weise gefärbten Proben wurden mit einem Zeiss-schen Spiegelmonochromator im sichtbaren Bereich gemessen. Als Lichtquelle diente

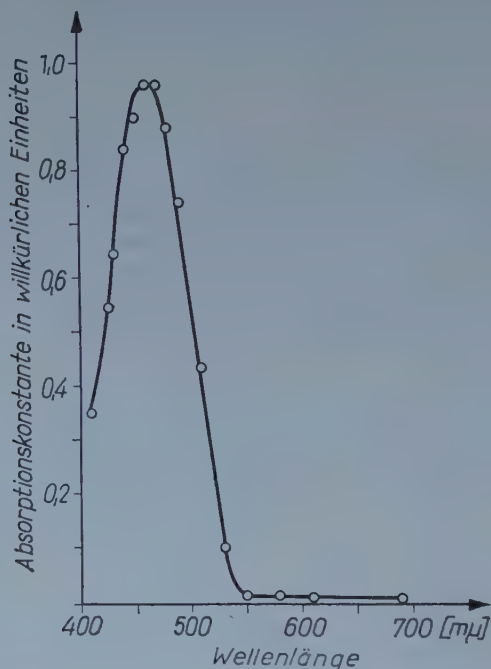


Abb. 1. Absorptionsspektrum einer aus natürlichen NaCl hergestellten und mit Röntgenstrahlen gefärbten Pastille ($k_{\max} = 0,48 \text{ mm}^{-1}$)

eine mit 12 V, 90 W Akkumulator gespeiste Tungstam Projektionsglühlampe. Die Messungen wurden mit einem durch Anodenbatterien betriebenen RCA A931 Elektronenvervielfacher und einem Lichtzeigergalvanometer mit $5,6 \cdot 10^{-9} \text{ A/s}$ maximaler Empfindlichkeit und 5000 Ohm innerem Widerstand durchgeführt. Bei 900 V Betriebsspannung war das Galvanometer sehr stabil und sein Dunkelstrom betrug nicht mehr als $1,6 \cdot 10^{-8} \text{ A}$.

Ausser uns hat noch HERSH an durchsichtigen Alkalihalogenidpastillen Absorptionsmessungen durchgeführt [6]. Sowohl unsere als auch seine Versuche beweisen, dass die Absorption der entsprechend hergestellten Pastillen gut messbar ist. Zuerst nahmen wir die Absorptionsspektren von röntgenisierten, sowie mit Kathodstrahlen bestrahlten NaCl auf. Das typische Ergebnis dieser Messungen wird durch Abb. 1 veranschaulicht. Das F-Zentrum

hebt sich scharf heraus, der Absolutwert der Absorption ist im allgemeinen grösser als bei Einkristallen. Sonst verlaufen die Absorptionskurven denen der F-Zentren enthaltenden Einkristallen ähnlich.

Das Absorptionsspektrum der nach der angegebenen Methode gefärbten Proben wird durch Abb. 2, Kurve *a* wiedergegeben. Die Pastille zeigt bei

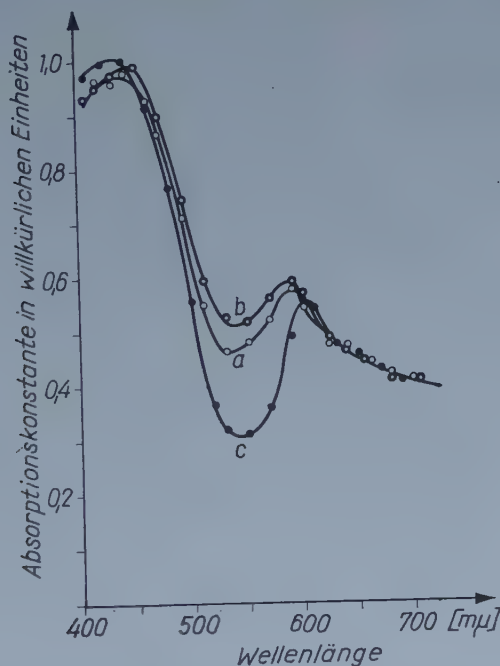


Abb. 2. Absorptionsspektren von aus NaCl-Pulver p. a. hergestellten und mit Exoelektronen gefärbten Pastillen

Kurve *a*: gemessen sofort nach der Herstellung, Maxima bei 440 ($k_{\max} = 2,89 \text{ mm}^{-1}$) und 590 $\text{m}\mu$

Kurve *b*: gemessen nach 5-stündiger Bestrahlung mit blauem Licht, Maxima bei 450 ($k_{\max} = 3,05 \text{ mm}^{-1}$) und 590 $\text{m}\mu$

Kurve *c*: gemessen nach 2-stündiger Bestrahlung mit orangem Licht, Maxima bei 440 ($k_{\max} = 3,07 \text{ mm}^{-1}$) und 590 $\text{m}\mu$

440 und 590 $\text{m}\mu$ Maxima, bei 540 $\text{m}\mu$ ein Minimum. Infolge einer 5-stündigen Bestrahlung mit einer Projektionsglühlampe von 250 W durch einen Methylblaufilter (durchlässig für $\approx 500 \text{ m}\mu$) vergrößert sich das Minimum bei 540 $\text{m}\mu$ und gleichzeitig auch das Maximum bei 590 $\text{m}\mu$ zu einem gut messbaren Wert, während das Maximum bei 440 $\text{m}\mu$ nach 450 $\text{m}\mu$ wandert (Kurve *b*). Nach einer 2-stündigen Bestrahlung bei vorgeschobenem Orangefilter vermindert sich das Minimum bei 540 $\text{m}\mu$ um 40% und, bei gleichzeitiger Verschiebung nach 600 $\text{m}\mu$ vermindert sich auch das Maximum bei 590 $\text{m}\mu$ (Kurve *c*).

Die untersuchten färbigen Pastillen können am besten mit dem natürlichen blauen Steinsalz bzw. mit dem elektrolytisch oder additive gefärbten

NaCl verglichen werden. Es ist bekannt, dass sich die additiv oder elektrolytisch gelbgefärbten Kristalle durch entsprechende thermische Behandlung blau färben lassen (Blauumschlag). Dieser Blauumschlag ist ein Zwischenzustand bei der Umwandlung der ursprünglich einfachen F-Zentren in andere

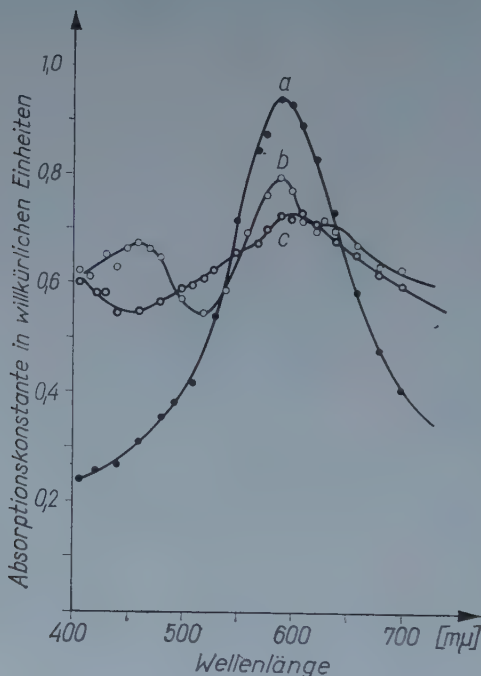


Abb. 3. Absorptionsspektren eines aus NaCl p. a. hergestellten und elektrolytisch blaugefärbten Einkristalls und der daraus gefertigten Pastillen

Kurve a: nach der Blaufärbung des Einkristalls gemessen, Maximum bei 590 mμ ($k_{\max} = 2,29 \text{ mm}^{-1}$)

Kurve b: nach Zerpulvern und Pastillieren des Einkristalls gemessen, Maxima bei 460, 590 ($k_{\max} = 1,35 \text{ mm}^{-1}$) und 630 mμ

komplexe Zentren und Na-Kolloide. Nach der Deutung von PRZIBRAM stehen wir bei diesen Erscheinungen im Falle von natürlichen Verfärbungen $F \rightarrow M \rightarrow R$ Übergängen gegenüber. Bei unseren Versuchen handelt es sich vermutlich um die gleichen Vorgänge [7].

Das Maximum bei 590–600 mμ mag mit dem F-Zentrum im Zusammenhang stehen. Darauf verweist der Versuch, wonach ein elektrolytisch gefärbter Einkristall, dessen Maximum bei 590 mμ lag (Abb. 3. Kurve a), nach Pulverisierung und Pastillieren neben einem gegenüber dem Einkristallzustand verminderten Maximum bei 590 mμ ein F-Zentrum aufwies (Kurve b), das sich bei Bestrahlung mit F-Licht abbaute, wobei sich das Maximum bei 540 mμ — geradeso wie im Falle der mit Exoelektronen gefärbten Pastillen —

erhöhte (Kurve c). Über das Maximum bei $440\text{ m}\mu$ kann man zur Zeit nicht vieles sagen. Es ist nur sicher, dass es beim blauen Steinsalz stets auftritt. Nach PRZIBRAM könnte dieses Band in Zusammenhang einer bisher unbekannten Verunreinigung [7] auftreten.

Wir danken Herrn Professor Z. GYULAI für die vielseitige Unterstützung unserer Arbeit, weiterhin Herrn J. KISS für wertvolle Diskussionen und die Überlassung elektrolytisch verfärbter Kristalle.

LITERATUR

1. F. SEITZ, *Rev. Modern Phys.*, **26**, 7, 1954.
2. Z. GYULAI und Z. MORLIN, *Fizikai Szemle*, **2**, 121, 1952.
3. Z. GYULAI, *Izvesztyija Ak. Nauk UdSSR. Ser. Phys.* **20**, 1569, 1956.
4. J. KRAMER, *Z. Physik*, **135**, 251, 1953.
5. K. SEEGER, *Angew. Chem.*, **68**, 285, 1956.
6. H. N. HERSH, *J. Chem. Phys.*, **27**, 1330, 1957.
7. K. PRZIBRAM, *Verfärbung und Lumineszenz*, Springer Verlag, Wien, 1953.



AN ANALYTICAL EXPRESSION FOR THE POTENTIAL ENERGY FUNCTION OF DIATOMIC MOLECULES

By

T. TIETZ

DEPARTMENT OF THEORETICAL PHYSICS, UNIVERSITY ŁÓDŹ, ŁÓDŹ, POLAND

(Received 10. I. 1961)

As known, the correct analytical representation of the potential energy function of diatomic molecules is of fundamental importance, e. g. for the determination of vibrational and relation levels, as also for many other important problems. Because of the importance of the above-mentioned problems many authors have given closed formulas of a potential energy function U for diatomic molecules. The best known analytical formulas for U are given by MORSE [1], HULBURT—HIRSCHFELDER [2], ROSEN—MORSE [3], RYDBERG [4], MANNING—ROSEN—NEWING [5], PÖSCHL—TELLER [6], DAVIDSON [7], MACKE—SUTHERLAND [8], LINNET [9], WU—YANG [10], PUPPI [11], LIPPINCOTT [12] and also by FROST—MUSULIN [13]. The properties and accuracy of the above-mentioned functions U have been described extensively by YATENDRA PAL VARSHNI [14].

Only some of the above U functions are convenient to solve the wave equation by the perturbation method. The purpose of this note is to give a new potential energy function for diatomic molecules. We write this function in the following form:

$$U(r) = D_e \left[\frac{B}{r(1 + Ar)} - \frac{C}{1 + Ar} \right], \quad (1)$$

where D_e is the dissociation energy, and A , B and C are three constants, which are to be determined. We require $U(r)$ to fulfil the following necessary conditions:

1. It should reach asymptotically a finite value as r tends to infinity.
2. It should have a minimum at $r = r_e$, where r_e is the internuclear distance at equilibrium.
3. It should become infinite at $r = 0$.

Besides these conditions (1), (2) and (3), we require additionally the following conditions to be fulfilled:

$$U(r_e) - U(\infty) = -D_e, \quad (2)$$

$$\left(\frac{dU}{dr} \right)_{r=r_e} = 0 \quad \text{and} \quad \left(\frac{d^2 U}{dr^2} \right)_{r=r_e} = k_e. \quad (3)$$

The first condition of eq. (2) is equivalent to the necessary condition formulated above. The remaining conditions given by eq. (2) and (3) are additional conditions. The symbol k_e appearing in eq. (3) denotes the fourth constant. By means of the physical constants r_e , D_e and k_e we can calculate our constants A , B and C appearing in eq. (1). We see that $U(r)$ given by eq. (1) fulfils the necessary conditions (1) and (3). In order to fulfil the remaining conditions we substitute eq. (1) into eq. (2) and (3). From eq. (2) follows that

$$r_e = -\frac{1-C}{2A} + \frac{1}{2} \sqrt{\left(\frac{1-C}{A}\right)^2 - \frac{4B}{A}}. \quad (4)$$

Substituting eq. (1) into the first term of eq. (3) we obtain

$$r_e = \frac{B}{C} + \sqrt{\frac{B^2}{C^2} + \frac{B}{AC}}. \quad (5)$$

As formulas (4) and (5) must be fulfilled simultaneously, we obtain the following relations:

$$C = 1 + 2Ar_e \quad \text{and} \quad B = Ar_e^3. \quad (6)$$

The last formula shows that C and B depend on the constant A which we determine using the last term of eq. (3).

Substituting eq. (1) into the last term of eq. (2) we obtain

$$k_e = \frac{2D_e}{r_e^3(1+Ar_e)^3} [B + 3ABr_e + 3A^2Br_e^2 - CA^2r_e^3]. \quad (7)$$

Taking into consideration the relation given by eq. (6) we may write eq. (7) as follows

$$k_e = \frac{2D_e A}{r_e(1+Ar_e)^3} [1 + 2Ar_e + A^2r_e^2] \quad (8)$$

or in another form

$$k_e = \frac{2D_e A}{r_e(1+Ar_e)}. \quad (9)$$

As for many diatomic molecules the physical constants r_e , D_e , k_e are well known, our constant is also known because it is possible to solve exactly the algebraic equation of the first degree. Substituting the obtained constant A into formula (6) we can calculate the remaining constants C and B . Thus we have shown that our formula for U given by eq. (1) fulfils all the required

necessary conditions given by eq. (2) and (3). This we cannot say about all functions $U(r)$ mentioned above [14].

Besides our simple formula has the merit that one can apply the perturbation method in order to solve the Schrödinger equation in the same way as has been done by the author [15] to solve the Schrödinger equation for the Thomas-Fermi potential.

REFERENCES

1. P. M. MORSE, Phys. Rev., **34**, 57, 1927.
2. H. M. HULBURT and J. O. HIRSCHFELDER, Journ. Chem. Phys., **9**, 61, 1941.
3. N. ROSEN and M. MORSE, Phys. Rev., **42**, 210, 1932.
4. R. RYDBERG, Z. Phys., **73**, 376, 1931.
5. M. F. MANNING and N. ROSEN, Phys. Rev., **44**, 953, 1933.
6. G. PÖSCHL and E. TELLER, Z. Phys., **83**, 143, 1933.
7. P. M. DAVIDSON, Proc. Roy. Soc. (London), **135**, 459, 1932.
8. R. MACKE, Z. Phys., **42**, 390, 1927; B. M. SUTHERLAND, Proc. Indian. Acad. Sci., **8**, 341 1938.
9. J. W. LINNET, Trans. Farady Soc., **38**, 1, 1942.
10. C. K. WU and C. T. YANG, J. Phys. Chem., **48**, 295, 1944.
11. G. PUPPI, Il Nuovo Cimento, **3**, 338, 1946.
12. E. R. LIPPINCOTT, J. Chem. Phys., **23**, 603, 1955.
13. A. A. FROST and B. MUSULIN, J. Chem. Phys., **22**, 1017, 1954.
14. YATENDRA PAL VARSHNI, Rev. of Mod. Phys., **29**, 664, 1957.
15. T. TIETZ, J. Chem. Phys., **25**, 789, 1956.



THE UNCERTAINTY PRINCIPLE AND THE BOHR THEORY

By

T. TIETZ

DEPARTMENT OF THEORETICAL PHYSICS, UNIVERSITY ŁÓDŹ, ŁÓDŹ, POLAND

(Received 22. II. 1961)

In the physical literature there are, as known, several illustrations of HEISENBERG's uncertainty principle, e.g. electron diffraction by a slit, determination of the position of a free electron and other examples. The purpose of this note is to show that HEISENBERG's uncertainty principle can also be formulated with the help of the BOHR theory.

On hand of two examples we shall illustrate HEISENBERG's uncertainty principle in the BOHR theory. As it is known, the particle of mass m_0 in an elastic field of force corresponding to a one-dimensional potential function $\frac{1}{2} k x^2$ is described by a simple harmonic motion of frequency $\omega_0 = \sqrt{k/m_0}$ and amplitude [1] $\sqrt{2E/k}$, where E is its energy. The square of the maximum displacement $(\Delta x)^2$ of the classical particle is just equal to the square of the amplitude, this means:

$$(\Delta x)^2 = \frac{2E}{k}. \quad (1)$$

This equation for the classical oscillator is true for every energy. As we know, the one-dimensional harmonic oscillator in the BOHR theory has the eigenvalue $E_n = \hbar\omega_0 n$, and in wave mechanics the eigenvalues are given by $E_n = \hbar\omega_0 \left(n + \frac{1}{2}\right)$. Substituting the corresponding eigenvalues into equation (1) we obtain for $(\Delta x)^2$ in the BOHR theory and in wave mechanics the relations

$$(\Delta x)^2 = \frac{2\hbar}{m\omega_0} \cdot n \quad \text{and} \quad (\Delta x)^2 = \frac{2\hbar}{m_0\omega_0} \left(n + \frac{1}{2}\right), \quad (2)$$

where $n = 0, 1, 2, \dots$. The last expression in equation (2) was obtained for the first time by REMARK [2] with the help of the wave mechanical solution of a one-dimensional harmonic oscillator. For higher quantum numbers n the wave mechanical expression for $(\Delta x)^2$ passes over into the BOHR formula for $(\Delta x)^2$. This is obvious directly from equation (2). Further it is known that the

square of the maximum momentum of a classical particle for a simple harmonic one-dimensional motion having energy E is

$$(\Delta p_x)^2 = 2m_0 E. \quad (3)$$

Substituting in equation (3) for E the eigenvalues $E_n = \hbar\omega_0 n$ of the BOHR theory or the wave mechanical eigenvalues $E_n = \hbar\omega_0 \left(n + \frac{1}{2}\right)$ we obtain

$$(\Delta p_x)^2 = 2m_0 \hbar \omega_0 n \quad \text{or} \quad (\Delta p_x)^2 = 2m_0 \hbar \omega_0 \left(n + \frac{1}{2}\right). \quad (4)$$

The second relation in the last formula was for the first time obtained quantum mechanically also by REMARK [3]. According to equations (2) and (4) the product of the maximum displacement and the maximum momentum in the BOHR theory and quantum mechanics, respectively, is given by

$$(\Delta x)(\Delta p_x) = 2 \hbar n \quad \text{and} \quad (\Delta x)(\Delta p_x) = 2 \hbar \left(n + \frac{1}{2}\right). \quad (5)$$

As another example let us consider the uncertainty principle of the hydrogen-like atoms in the BOHR theory and wave mechanics. As we know, the orbital radius r_n , the frequency ω_n and the velocity v_n of the electron are given by

$$r_n = \frac{\hbar^2}{m_0 Z e^2} n^2; \quad \omega_n = \frac{m_0 Z e^4}{\hbar^3} \cdot \frac{1}{n^3} \quad \text{and} \quad v_n = r_n \omega_n. \quad (6)$$

In equation (6) n is the principal quantum number. In the wave mechanical picture the orbits are not defined, so that the uncertainty of the displacement of the electron with respect to the nucleus according to the first relation of equation (6) is

$$(\Delta r) \simeq \frac{\hbar^2}{m_0 Z e^2} n^2. \quad (7)$$

In the particle picture the momentum p of the electron corresponding to the principal quantum number n is

$$p = m_0 v_n = m_0 r_n \omega_n = \frac{m_0 Z e^2}{\hbar n}. \quad (8)$$

Therefore the uncertainty of the momentum (Δp) according to equation (7) and (8) is

$$(\Delta p) \simeq \frac{m_0 Z e^2}{\hbar n}. \quad (9)$$

The product of (Δr) and (Δp) given by equation (7) and (9) in the BOHR theory for the electron of the hydrogen-like atoms is thus

$$(\Delta r)(\Delta p) \simeq \hbar n. \quad (10)$$

The exact calculation of (Δr) and (Δp) for the electron of the hydrogen-like atoms in wave mechanics gives according to REMARK [4] after simple modifications and calculations

$$(\Delta r) \simeq \frac{\hbar^2}{m_0 Z e^2} n^2 \quad \text{and} \quad (\Delta p) \simeq \frac{m_0 Z e^2}{\hbar n}, \quad (11)$$

thus the same result as given in equation (7) and (9) in the BOHR theory. Multiplying (Δr) by (Δp) given by equation (11) for the wave mechanical theory we obtain the same result as that given by equation (10) for the BOHR theory. PAL VARSHNI [5] has considered the connection of the uncertainty principle of the hydrogen atom with the BOHR theory for the quantum number without making any comparison with the exact results of wave mechanics. Our results given by equations (7) and (9) agree well for $n = 1$ with the results of PAL VARSHNI.

REFERENCES

1. W. MACKE, *Wellen*, Akad. Verlagsgesellschaft, Leipzig, 1958, p. 5.
2. B. REMARK, *Z. Phys.*, **69**, 332, 1951.
3. See ref. [2].
4. See ref. [2].
5. J. PAL VARSHNI, *Am. Journ. of Physics*, **22**, 568, 1954.



UNO INGARD and WILLIAM L. KRAUSHAAR, **Introduction to Mechanics, Matter and Waves** (Addison—Wesley Series in Physics; Addison—Wesley PC. Inc., Massachusetts, USA, 1960; XV + 672 pages; \$ 8,75)

The authors' aim, by this suggestive presentation of the selected topics of an introductory course of physics for the first year of a two-year sequence in general physics having in mind the students of science and engineering (as well as of an intermediate-level course in mechanics and related subjects) has been to maintain, in a balanced manner, the flavour of experiment and inductive reasoning. This means that instead of the usual deductive foundation of mechanics via a totally analytic approach — often overemphasizing the "given the force—find the motion" situation — the "given the motion or behaviour — what are the model and forces from which the phenomena can be understood" type of situation is favoured. The authors' approach emphasizes for this reason the study of interactions through observations of motions and their textbook deals with motions as influenced by all the different types of interactions in nature: electric, magnetic, nuclear, etc. as well as the traditional contact, spring, and gravitational forces. First, two-body collisions are investigated and then processes involving inertial mass, momentum and its conservation and further the center-of-mass motion are very clearly developed. The chapters on energy, angular momentum and moving coordinate systems and inertial forces are followed by chapters containing examples of forces and motions which have been very fortunately selected and arranged so as to illustrate the basic concepts as they are developed. The transition from the study of the gross motion of bodies to the inertial

motion in matter and the associated macroscopic properties of matter is accomplished in chapters on the temperature concept, on thermal interactions and on the elementary theory of the atomic structure of matter. The chapters on kinetic theory, thermodynamics and properties of matter have been woven together, and the atomic-molecular interpretation of concepts such as internal energy, entropy and properties of matter have been kept in the foreground. The classical concepts are, however, completed by a qualitative quantum mechanical interpretation of experimental results. The role of intermolecular forces in the interpretation of the equation of state of real gases is studied in some more detail, together with molecular interpretations of other gross mechanical properties of gases and liquids. Finally, through a combination of experiments and applications of conservation of momentum the mechanics of deformable bodies and waves, the behaviour of wave pulses, their wavespeed and energy content is treated, followed by the discussions of examples involving both transverse and longitudinal waves in different media. From the principle of superposition waves of arbitrary shape are then constructed and the properties of harmonic waves are studied in detail. Summarizing, we may say that the authors' introductory textbook on general physics can be regarded as an excellent selection of the classical foundations of up-to-date teaching of modern physics.

J. I. HORVÁTH

L. HERFORTH—H. KOCH: Radiophysikalisches und radiochemisches Grundpraktikum. VEB Deutscher Verlag der Wissenschaften, Berlin, 1959.

Das Buch erschien als der 31-ste Band der von FRANZ X. EDER und ROBERT ROMPE herausgegebenen Reihe der Hochschulbücher für Physik. Die Verfasser des Buches, die an dem Institut für angewandte Radioaktivität in Leipzig tätig sind, beabsichtigten, sowohl den Teilnehmern der von dem Institut veranstalteten Isotopenkurse, wie auch anderen Interessenten, die an einem solchen Isotopenkurs nicht teilnehmen können, ein Praktikumsbuch in die Hand zu geben, um damit den immer öfter auftauchenden Wunsch nach einem solchen zu erfüllen.

Den Gegenstand des Buches bilden demnach diejenigen radiophysikalischen und radiochemischen Aufgaben, die zur Zeit der Fertigstellung des Manuskriptes (Oktober, 1958) im Leipziger Isotopenpraktikum durchführbar waren. So erhebt das Praktikumsbuch in der vorliegenden Form keinen Anspruch auf Vollständigkeit.

Das Buch hat einen Umfang von 470 Seiten und gliedert sich in 13 Kapitel, von denen sich 7 Kapitel mit radiophysikalischen und 6 Kapitel mit radiochemischen Aufgaben beschäftigen. Die einzelnen Kapitel sind im allgemeinen in mehrere Aufgabengruppen gegliedert, die einzelnen Gruppen enthalten wiederum im allgemeinen mehrere verwandte Aufgaben. Diese Ordnung der Aufgaben in insgesamt 35 mit Titeln versehene Gruppen macht die Übersicht über das Material klar und leicht.

Die Verfasser verfolgten bei der Bearbeitung der einzelnen Gruppen die folgende Methode: Am Anfang jeder einzelnen Gruppe wird das Wesen der Aufgaben beschrieben, die Messmethoden werden mit anderen, inaktiven Methoden verglichen und die durch die radioaktiven Verfahren gelieferten neuen Möglichkeiten werden deutlich hervorgehoben. Danach folgen die einzelnen Aufgaben in folgender Behandlungsweise: 1) Aufgabenstellung, 2) Grundlagen, das heisst die wissenschaftliche Begründung der durchzuführenden Aufgabe, 3) Zubehör, 4) Arbeitsanleitung, das heisst eine ausführliche Beschreibung des Arbeitsganges und praktische Hinweise für den Anfänger, und 5) ein Beispiel, in dem die konkreten Messergebnisse und deren Auswertung, meistens in graphischer Darstellung, mitgeteilt werden. Schliesslich wird am Ende jeder einzelnen Gruppe ein Literaturverzeichnis gegeben.

Die Verfasser haben ihren ausgezeichneten didaktischen Sinn dadurch bewiesen, dass sie einerseits den Teilnehmern an einem solchen Praktikum den Reiz der Durchführung der Aufgaben nicht durch ausführ-

liche Beschreibung des Arbeitsprotokolles nehmen und andererseits auch die Nichtteilnehmer dadurch befriedigen, dass sie das Endergebnis jeder einzelnen Aufgabe in graphischer Darstellung oder in Tabellenform mitteilen. Die Durchführung von Fehlerrechnungen bzw. Abschätzungen wird dem Praktikumssteilnehmer selbst überlassen, in einer der ersten Aufgaben werden diese Rechnungen ausführlich behandelt.

Die Art und Weise, in der die Verfasser die Probleme angreifen und behandeln, verraten grosse Fachkenntnis und vielseitige praktische Erfahrungen. Das Buch ist klar, und einfach geschrieben und für jeden mit entsprechender Vorbildung leicht verständlich. Die Brauchbarkeit des Buches wird ausserdem durch die 182 grossen, schönen Abbildungen und durch die mehr als 50 Tabellen in grossem Masse erhöht. Der Anhang von mehr als 25 Seiten Umfang enthält ausserdem zahlreiche weitere besonders nützliche Abbildungen und Tabellen.

Im folgenden geben wir einen kurzen Überblick über die im Praktikumsbuch behandelten Aufgaben.

In der Einleitung weisen die Verfasser vor allem auf die äussere und innere Strahlengefahr und auf die Vorsichtsmassnahmen beim Umgang mit Radionukliden hin. Im weiteren behandeln sie die Methoden der Herstellung von Messpräparaten.

Das I. Kapitel enthält 6 Gruppen:

1. Gruppe: Grundmessungen an Geiger—Müller-Zählrohren. Die Charakteristik eines GM-Zählrohres, Zählrate eines Präparates, Fehlerberechnungen, Prüfung auf statistische Reinheit und relative Längsempfindlichkeit eines zylindrischen GM-Zählrohres.

2. Gruppe: Methoden der Totzeitbestimmung und Totzeitkorrekturen. Die Oszillographen-Methode, die Zwei-Präparate-Methode, die Bestimmung mit einer Totzeitstufe und Bestimmung des "over-all-correction"-Faktors.

3. Gruppe: Gammastrahlungsmessungen mit dem GM-Zählrohr. Energiebestimmung durch Absorptionsmessungen. Berechnung von Massenabsorptionskoeffizienten für beliebige Elemente.

4. Gruppe: Relative Betastrahlungsmessungen mit dem Glockenzählrohr. Geometriefaktor, Rückstreuungsfaktor, Absorptionsmessungen, die maximale Reichweite und Energie von Betastrahlen und schliesslich die Selbstabsorption von C^{14} .

5. Gruppe: Relative Aktivitätsbestimmung von Betastrahlpräparaten mit dem Glockenzählrohr. Vergleich von gleichartigen

Betastrahlpräparaten eines Radioisotopes mit geringem, grösserem bzw. grossem Aktivitätsunterschied, Vergleich von zwei gleichartigen Präparaten auf verschiedenen Unterlagen und Vergleich von zwei gleichartigen Präparaten verschiedener Radioisotope.

6. Gruppe: Zählmethoden der absoluten Aktivitätsbestimmung. Absolute Aktivitätsbestimmung mit definierter Geometrie am Glockenzählrohr nach der Koinzidenzmethode und mit dem 4 π -Zählrohr.

II. Kapitel: Szintillationszählermessungen.

7. Gruppe: Grundmessungen am Photosekundärelektronenvervielfacher. Spannungsabhängigkeit, relative Spektralempfindlichkeit.

8. Gruppe: Szintillationszähler für Alpha-, Beta- und Gammastrahlung. Aufnahme von Szintillationszählercharakteristiken für Alpha-, Beta- und Gammastrahlung. Vergleich von Gamma- und Betastrahlungsmessungen mit GM-Zählrohr und Szintillationszähler.

9. Gruppe: Alphastrahlungsmessungen. Ermittlung der günstigsten Schichtdicke eines ZnS-Ag-Leuchtschirmes, Reichweite von Alphastrahlen in Luft, Absorption in festen Substanzen.

III. Kapitel: Ionisationskammermessungen.

10. Gruppe: Betastrahlungsmessungen mit der Aluminiumionisationskammer. Spannungseichung des Elektrometers, Abstandsvariation, Rückstreuungsmessungen, Absorptionsmessungen und Aktivitätsbestimmung von Betastrahlpräparaten.

11. Gruppe: Gammastrahlungsmessungen mit der Bleiionisationskammer. Kontrolle und Spannungseichung, Abstandsvariation, Absorptionsmessungen, Bestimmung von Radiumäquivalenten, Aktivitätsbestimmung eines Gammastrahlpräparates.

IV. Kapitel: Strahlenschutzüberwachung.

12. Gruppe: Dosismessungen. Messung von Gammastrahlendosen mit Taschenkondensatorkammern und mit Filmplaketten.

13. Gruppe: Dosisleistungsmessungen. Ermittlungen der maximal zulässigen Aufenthaltsdauer, Abschirmung von Gammastrahlen.

14. Gruppe: Verseuchungsmessungen. Prüfung von Arbeitstischauflagen.

V. Kapitel: Anwendungsbeispiele aus der Technik und Industrie.

15. Gruppe: Messung dünner Schichten mit Betastrahlern. Bestimmung der Dicke von Aluminiumschichten nach der Durchstrahlungsbzw. Rückstreuungsmethode ohne Unterlage und auf dicker Bleiunterlage, Rückstreuungsmessungen zur Materialbestimmung der Dicke von aufgespritzten Lackschichten.

16. Gruppe: Messung dicker Schichten mittels Gammastrahlung. Messung nach der Durchstrahlungsmethode.

17. Gruppe: Bestimmung von Füllstandshöhen durch Gammastrahlungsmessungen. Bestimmung durch Absorptionsmessungen bei senkrechter bzw. horizontaler Durchstrahlung.

VI. Kapitel: Sonstige Aufgaben aus der Radiophysik.

18. Gruppe: Einige weitere Messmethoden. Der Funkenzähler und die Gammaradiographie.

19. Gruppe: Die kosmische Strahlung. Absorption und Einfallsrichtung der kosmischen Strahlung.

VII. Kapitel: Die Aktivierungsanalyse.

20. Gruppe: Die Aktivierungsanalyse nach der Absolutmethode. Bestimmung der Verunreinigung von Dysprosium in Holmium, Bestimmung des Neutronenflusses.

21. Gruppe: Die Aktivierungsanalyse nach der Relativmethode. Bestimmungen der prozentualen Verunreinigung, die Silberschnellanalyse.

Die Kapitel VIII—XIII behandeln die folgenden radiochemischen Aufgaben: Trennung und Anreicherung der Radioelemente, Fällungsreaktionen, Ionenaustauscherchromatographie, Solventextraktion, Radiopapierchromatographie, Trennung von Radionukliden durch Destillation, die Chemie der "heissen" Atome, Szilard-Chalmers-Effekt, Isomerentrennung, Isotopenverdünnungsanalyse, Radiometrische Analyse, Radioelemente als Leitisotope, Isotopenaustauschreaktionen, die Adsorption von Radioelementen an Glasoberflächen, Löslichkeitsbestimmungen, das Arbeiten mit Kohlenstoff-14.

LÁSZLÓ BOZÓKY

Printed in Hungary

A kiadásért felel az Akadémiai Kiadó igazgatója

Műszaki szerkesztő: Farkas Sándor

A kézirat nyomdába érkezett: 1961. VIII. 14 — Terjedelem: 10 (A/5) ív, 40 ábra, 1 melléklet

1961.53924 — Akadémiai Nyomda, Budapest — Felelős vezető: Bernát György

ÜBER KOHÄRENZEIGENSCHAFTEN DER »INKOHÄRENTEN« STREUSTRALUNG

Von

F. KÁROLYHÁZY

INSTITUT FÜR THEORETISCHE PHYSIK DER ROLAND EÖTVÖS UNIVERSITÄT, BUDAPEST

(Vorgelegt von K. F. Novobátsky. — Eingegangen: 2. III. 1961)

Bei dem Raman-Effekt bleiben die streuenden Atome nach dem Prozess im angeregten Zustand zurück. Das bedeutet aber nicht, dass es zwischen den an den verschiedenen Atomen gestreuten Photonen keine Phasenbeziehungen gibt, diese sind vielmehr im Sinne der Quantenmechanik kohärent. Diese Tatsache kann sich folgendermassen bemerkbar machen. Man lässt an den angeregten Atomen, während diese in den Grundzustand zurückkehren, eine zweite Art von Photonen streuen. Es besteht dann unter Umständen zwischen den gestreuten Photonen verschiedener Arten eine Richtungskorrelation.

I

Worin besteht die Kohärenz der kohärenten Streustrahlung? In der klassischen Theorie beantwortet man diese Frage leicht. Die von den einzelnen Streuzentren (z. B. Atomen eines Gases) ausgehenden Streuwellen haben wohldefinierte Phasenbeziehungen zueinander, sie treten daher miteinander in Interferenz. Diese Tatsache springt besonders deutlich bei dem Versuch ins Auge, an den wir im folgenden anknüpfen wollen. Wir stellen uns eine sogenannte Natrium-Resonanzlampe vor. In dieser werden die Atome eines ver-

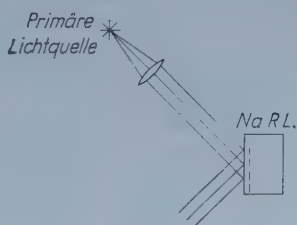


Abb. 1

hältnismässig kalten, in einem Glasgefäss befindlichen Na-Dampfes durch das Licht glühenden Natriums angeregt. Aus der primären Lichtquelle soll ein paralleles Bündel auf das Glasgefäss fallen. Wird die Dichte des Dampfes im Behälter genügend erhöht, so wird bekanntlich die sehr dünne Schicht der Na-Atome in unmittelbarer Nähe der Glaswand die Primärstrahlen spiegeln. (Abb. 1). Hält man sich die quantenhafte Natur der Emission und Absorption »heraustropfen«. Fassen wir zwei Atome *A* und *B* aus der spiegelnden Ober-

vors Auge, so wird unsere Frage etwas verwickelter. Es sei das einfallende Licht so schwach, dass die Photonen nur noch einzeln aus der Lichtquelle flächenschicht des Na-Dampfes ins Auge. In der Sprache der Quantenmechanik geht der Prozess der Absorption und Reemission des Photons durch einen Zwischenzustand durch, in welchem kein Photon vorhanden ist, dagegen das eine bzw. andere Atom sich auf dem ersten angeregten Niveau befindet. Präziser gesagt, ist der Zwischenzustand eine Superposition folgender Komponenten: a) Atom A angeregt, B im Grundzustand, b) umgekehrt. Es ist nun eben die quantenmechanische Kohärenz dieser beiden Komponenten, die die spiegelungsartige Reemission des Energiequants $h\nu$ ermöglicht. Nach der Reemission sind beide Atome mit Sicherheit im Grundzustand, so dass es ungewiss ist, an welchem die Streuung stattgefunden hat. Der Sachverhalt ist vollkommen analog zu dem in der gewöhnlichen Quantenmechanik, wo man die Wellenfunktion eines Elektrons in zwei Teile spaltet und die Teile nachher wieder vereinigt. Die Kohärenz der an der Superposition teilnehmenden Komponenten führt auch in diesem Falle zu Interferenzerscheinungen [1, 2, 3]. In Anbetracht der Interpretationsmöglichkeiten ist die experimentelle Kontrolle solcher Kohärenzen nicht ohne Wert. Im weiteren möchten wir auf eine neue experimentelle Möglichkeit in dieser Richtung hinweisen, die mit dem Raman-Effekt zusammenhängt.

II

Worin besteht die Inkohärenz der inkohärenten Streuung? Wir beleuchten wiederum die Atome eines Gases mit monochromatischem Licht. Zur Vereinfachung stellen wir uns die Atome sofort modellmässig vor. Sie sollen neben dem Grundniveau E_0 nur zwei angeregte Niveaus besitzen, mit den Energien E_1 bzw. E_2 . Die Frequenz der einfallenden Photonen sei $\nu_0 \approx (E_2 - E_0)/h = \nu_{20}$. Wir illustrieren den Prozess wieder mit Hilfe von zwei Atomen A und B . Das primäre Photon k_0 wird durch A oder B verschlungen. Nach Reemission eines Photons k_s ($\nu_s \approx \nu_{21}$) bleibt das eine oder das andere Atom im angeregten Zustand E_1 zurück, und dadurch ist es entscheidbar, an welchem Atom sich die Streuung vollzog, daher interferieren »die von den einzelnen Atomen ausgehenden Streuwellen (Frequenz — ν_{21}) nicht, sie sind inkohärent«. Wir müssen nun aber folgendes bemerken. Die quantenmechanische Entwicklung des ganzen Systems erfolgt auch hier über Zwischenzustände, die Superpositionen von kohärenten Komponenten sind. Wir wollen das durch eine Skizze veranschaulichen. Abb. 2a zeigt das Grundniveau und zwei angeregte Niveaus irgendeines Gasatoms. Durch die Pfeile werden erlaubte optische Übergänge, durch die Kreise die entsprechenden atomaren Zustände repräsentiert. Die Abb. 2b—f zeigen den Ablauf der inkohärenten Streuung an zwei Atomen. Aus der Superposition der Zustände 2c und 2d bildet sich die

Superposition der Zustände 2e und 2f aus, ohne irgendeine Beschränkung betreffs der Richtung des sekundären Photons. Dies bedeutet aber nicht — im Gegensatz zu der im Schrifttum verbreiteten Meinung —, dass es zwischen den in den beiden letzten Figuren gezeichneten Photonen »keinerlei Phasenbeziehung« gibt, im Gegenteil: nach der Quantentheorie sind die Zustände 2e und 2f streng kohärent. Dies wird ohne weiteres ersichtlich, wenn wir auf die Wahrscheinlichkeitsamplituden der Zustände, die in dieser Zerlegung des Prozesses vorkommen, die Schrödinger-Gleichung anwenden, wobei die Wechselwirkung der Atome und der Strahlung, wie gewöhnlich, als Perturbation betrachtet wird.

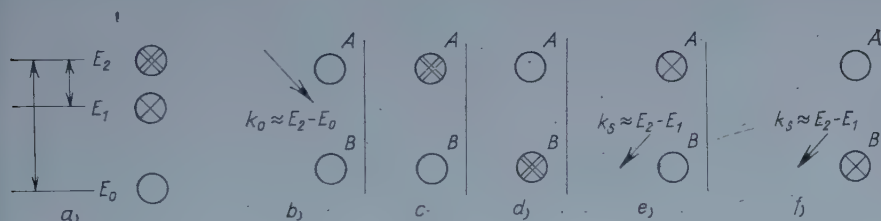


Abb. 2

Vom experimentellen Standpunkt ist diese Kohärenz »latent«, sie macht sich aber bemerkbar, wenn der Streuung die Emission eines neuen Photons nachfolgt, begleitet von dem Übergang $\oplus \rightarrow \bigcirc$ ($k_s = E_1 - E_0$). Die einfache Rechnung zeigt nämlich, dass — obwohl die Frequenzen verschieden sind — eine Richtungskorrelation zwischen k_s und k_s besteht. Diese würde nicht entstehen, wenn z. B. nur das eine Atom anwesend wäre.

In dieser Form beschäftigen wir uns nicht weiter mit den experimentellen Möglichkeiten. Wenn die Übergänge $E_0 \rightarrow E_2$, $E_2 \rightarrow E_1$ erlaubt sind, so ist der Übergang $E_0 \rightarrow E_1$ im allgemeinen verboten. Auch wenn wir dieses Verbot (z. B. durch ein Magnetfeld) aufheben, wird die Richtungskorrelation wegen der langen Lebensdauer des Zustandes E_1 sowie der thermischen Bewegung der Atome wahrscheinlich sehr verwaschen.

III

Es ist zweckmässiger, folgende modifizierte Anordnung zu betrachten (Abb. 3). Der Behälter T mit glatter, durchsichtiger Wand sei wieder verhältnismässig dicht mit Atomen im Grundzustand angefüllt, die wiederum insgesamt nur drei, nicht degenerierte Energieniveaus besitzen sollen. Bezüglich der erlaubten Übergänge wollen wir uns gesondert mit den zwei in Abbildungen 4a und 4b dargestellten Möglichkeiten beschäftigen. Im Falle 4b nehmen

wir an, dass auch der Übergang $E_1 \rightarrow E_2$ mit kleiner Wahrscheinlichkeit zustandekommen kann. Aus der Lichtquelle F bzw. F' fallen parallele, monochromatische Lichtbündel gegebener Richtung auf den Behälter, die Frequenzen sollen jedoch verschieden sein: $\nu_F \approx (E_1 - E_0)/h = \nu_{10}$, $\nu_{F'} \approx (E_2 - E_1)/h = \nu_{21}$. Wir betrachten zunächst den Fall 4b.

Was geschieht im Gase? Da die meisten Atome in T im Grundzustand sind, können die Photonen k_F , das Gas beinahe ungehindert durchdringen. Dagegen regen die Photonen $k_{F'}$ die Atome der beleuchteten Grenzschicht an der Wand zu Resonanz-Fluoreszenz an. Ist die mittlere Distanz der Atome

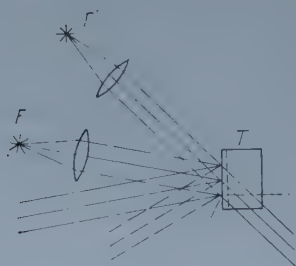


Abb. 3

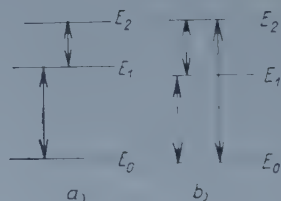


Abb. 4

genügend klein und kleiner als die Wellenlänge des Lichtes, so wird das Bündel F durch die Oberflächenschicht gespiegelt. (Grosse Gasdichte = starke Reflexionsfähigkeit und starke Absorption; das Licht kann nicht in das Innere des Gases eindringen.) Die Atome werden vorübergehend auf das Niveau E_1 gehoben. Etliche von ihnen können — noch vor der Emission von k_s — ein Photon $k_{F'}$ absorbieren; dies wird von dem Übergang $E_1 \rightarrow E_2$ begleitet und ist von der Emission eines Photons k_s gefolgt. ($\nu_{s'} \approx (E_2 - E_0)/h = \nu_{20}$, das Atom gelangt wieder in den Grundzustand.) Die Oberflächenschicht ist also schon fähig, auch das Licht des Bündels F' zu streuen. (Und zwar »inkohärenterweise« $\nu_{s'} \neq \nu_{F'}$). Wir zeigen jetzt, dass auch diese Streuung »spiegelungsartig« ist, die Strahlung der Frequenz $\nu_{s'}$, ausgehend von den verschiedenen Atomen, wird nur in einer einzigen, bestimmten Richtung »reflektiert«.

Wir wollen uns im Anfangszustand auf ein einziges Photon k_F und ein einziges $k_{F'}$, ausserdem zunächst nur auf zwei Atome der Oberflächenschicht beschränken. Der zur Bestimmung der endlichen Linienbreite verwendeten Methode von WEISSKOPF und WIGNER folgend [4], berücksichtigen wir nur diejenigen Zustände, die in der Zerlegung des Prozesses mit bemerkbarer Wahrscheinlichkeitsamplitude vorkommen. Diese und der Ablauf des Prozesses werden in Abb. 5 dargestellt. Anfänglich, zur Zeit $t = 0$, ist nur die Amplitude b_a des Zustandes a von Null verschieden. Später erscheint auch die Superposition der Zustände b und c , diese wirken wieder auf die Zustände d , e und f

unmittelbar ein. Endlich regen d und e gemeinsam den Zustand g an. (Der Zustand f entwickelt sich nicht weiter, $k_{F'}$ tritt mit den Atomen im Grundzustand in keine bemerkbare Wechselwirkung.)

Die Folge der Kohärenz der Zustände d und e kann schon mittels der gewöhnlichen Perturbationsrechnung [5] überblickt werden.*

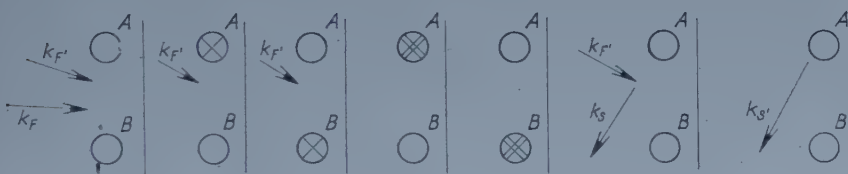


Abb. 5

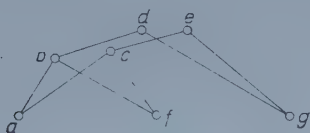


Abb. 6

Für die Amplituden b_n bestehen die Gleichungen

$$-i\hbar b_n = \sum_m H'_{nm} b_m e^{i\nu_{nm}t}, \quad \text{bzw.} \quad -i\hbar b_n^{(k)} = \sum_m H'_{nm} b_m^{(k-1)} e^{i\nu_{nm}t} \quad (2)$$

mit $b_n = \sum n_n^{(k)}$. Den Wert von H'_{nm} liefert (1). Die Verbindung der Zustände der Abb. 5a—g im Gleichungssystem (2) zeigt Abb. 6. Suchen wir sämtliche

* Wir schliessen uns den Bezeichnungen von (5) an. Die Strahlung wird durch das Vektorpotential $A = \sum (q_\lambda A_\lambda + q_\lambda^* A_\lambda^*)$ beschrieben, wo $A_\lambda(r) = c_\lambda / \sqrt{4\pi c^2} \cdot \exp \cdot (i\kappa_\lambda r)$, $\kappa_\lambda = \nu_\lambda / c$. Die Wechselwirkung eines Photons vom Impulse $k_\lambda \hbar / c$ und eines atomaren Elektrons wird durch $H' = -\frac{e}{\mu} p (q_\lambda A_\lambda + q_\lambda^* A_\lambda^*)$ dargestellt. Bei unmittelbaren Übergängen verändert sich die Anzahl der Photonen um eins, und das Atom führt einen Quantensprung $\varphi_a \rightarrow \varphi_b$ aus. Das Matricelement ist

$$\begin{aligned} H'_{an_\lambda, bn_\lambda + 1} &= -\frac{e}{\mu} \sqrt{\frac{2\pi\hbar^2 c^2}{k_\lambda}} \sqrt{n_\lambda + 1} \int \varphi_a^* (pe) e^{(i\kappa_\lambda r)} \varphi_b d\tau \approx - \\ &= -\frac{e}{\mu} \sqrt{\frac{2\pi\hbar^2 c^2}{k_\lambda}} \sqrt{n_\lambda + 1} e^{(i\kappa_\lambda r_A)} (pe) ab. \end{aligned} \quad (1)$$

Hier ist r_A der Ortsvektor des Atoms (dessen Ausdehnung klein gegen die Wellenlänge sein soll).

Amplituden b_a, \dots, b_g in der niedrigsten nicht verschwindenden Näherung, so müssen wir nach (1) und (2) die Gleichungen

$$b_a^{(0)} = 1 \quad (3a)$$

$$-i\hbar \dot{b}_b^{(1)} = H'_{ba} b_a^{(0)} e^{i\nu_{ba}t} = K \cdot e^{i\nu_{ba}t} \cdot e^{i(\kappa_F r_A)} \quad (3b)$$

$$\begin{aligned} -i\hbar \dot{b}_g^{(3)} &= H'_{gd} b_d^{(2)} e^{i\nu_{gd}t} + H'_{ge} b_e^{(2)} e^{i\nu_{ge}t} = \\ &= K' \cdot e^{-i(\kappa_{g'} r_A)} b_d^{(2)} e^{i\nu_{gd}t} + K' e^{-i(\kappa_{g'} r_B)} \cdot b_e^{(2)} \cdot e^{i\nu_{ge}t} \end{aligned} \quad (3g)$$

lösen. Die Lösungen sind der Reihe nach leicht anzuschreiben. Wir interessieren uns für (3g). Es ergibt sich

$$b_g^{(3)} = N(t) \cdot [e^{ir_A(\kappa_F + \kappa_{F'} - \kappa_{g'})} + e^{ir_B(\kappa_F + \kappa_{F'} - \kappa_{g'})}], \quad (4)$$

wo N nur vom Absolutwert von $k_F, k_{F'}, k_{g'}$ ($k = k = \hbar c \nu$) abhängt. Die Wahrscheinlichkeit der Emission des Photons $k_{g'}$ ($\sim |b_g|^2$) wird durch die Verbindung der Richtung von $k_{g'}$ mit den Richtungen von den vorher absorbierten Photonen bestimmt. Bei festem k_F und veränderlichem $k_{F'}$ (beweglicher Quellen F') muss zwischen $k_{F'}$ und $k_{g'}$ eine solche Richtungskorrelation bestehen, wie sie durch den Zusammenhang (4) beschrieben wird. Ziehen wir von der Gasschicht der Oberfläche mehr als zwei Atome in Betracht, so wächst die Anzahl der Glieder auf der rechten Seite von Gl. (4), die Korrelation zwischen $k_{F'}$ und $k_{g'}$ wird verschärft. Bei dicht liegenden Atomen tritt in der Amplitude des Zustandes, der das Photon $k_{g'}$ enthält das Integral über $e^{ir(\kappa_F + \kappa_{F'} - \kappa_{g'})}$ auf, das nach r zu integrieren ist. Das heisst: die »inkohärente« Streuung $\nu_{F'} \rightarrow \nu_{g'}$ ist spiegelungsartig; es muss also die Relation

$$k_F + k_{F'} - k_{g'} \parallel n \quad (5)$$

bestehen, wo n die Flächennormale ist. In der Abb. 7 ist die Richtung der Strahlung der Frequenz $\nu_{g'}$ in dem speziellen Fall aufgetragen, in dem $k_F, k_{F'}$ und n in eine Ebene fallen. Es ist ersichtlich, dass neben dem »reflektierten« auch ein »gebrochener« Strahl entsteht, letzterer dringt aber ebenso wenig in das Innere des Gases ein wie die Strahlung $\nu_{F'}$, er wird mittels der Resonanz-Fluoreszenz $E_0 \rightarrow E_2 \rightarrow E_0$ reflektiert und mit dem ersteren vereinigt.

Zur Beantwortung der Frage, ob diese Erscheinung tatsächlich beobachtbar ist, müssen wir noch die voraussichtliche Intensität der Strahlung bestimmen. Zu deren Berechnung ist die gewöhnliche Perturbationsrechnung nicht mehr geeignet, man kommt aber mit der Methode von WEISSKOPF und WIGNER, die auch die Dämpfung berücksichtigt, leicht zum Ziel. Wir führen die Resultate hier nicht an, die man in Bezug auf die Atome unseres Modells bekommt. Die

realen Umstände sind nämlich verwickelter, obwohl sie im Prinzip nichts Neues bringen. So können wir z. B. wenn wir an Na-Atome denken, in der Nähe der Niveaus E_1, E_2 (Abb. 4b) auch solche Niveaus E'_1, E'_2 finden, die vom Standpunkte der Übergänge der Abb. 4a entsprechen u. s. w. Ist die Theorie richtig, so scheint jedenfalls der Effekt experimentell leicht nachweisbar zu sein. Dem atomaren Übergang $E_1 \rightarrow E_2$ kann in der Wirklichkeit ein verbotener Übergang, bei dem z. B. ein äusseres Feld das Verbot aufhebt, entsprechen. Zum Schluss bemerken wir, dass die Atome sich in der obigen Anordnung jedenfalls nur kurze Zeit im angeregten Zustand befinden (die Wahrscheinlichkeit des Überganges $b \rightarrow d$ ist zwar klein, aber die des Überganges $b \rightarrow c$

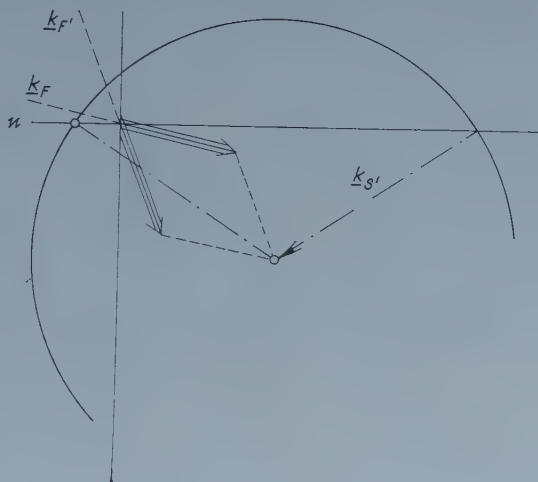


Abb. 7

sowie $d \rightarrow e$ ist gross) und daher nicht imstande sind, während des Prozesses die (eben gedachte) Grenzschicht zu verlassen und so die Richtungskorrelation zu verwaschen. Der Strahl, der zu beobachten ist, ist zwar von kleiner Intensität, er ist aber andererseits auf eine feste Richtung konzentriert, die durch (5) gegeben ist.

IV

Nun wollen wir ganz kurz den Fall *a* der Abbildung 4 betrachten. Bei unveränderten Lichtquellen geht hier der Prozess in folgender Weise vor sich: Die Atome der Grenzschicht werden die Photonen k_F im Laufe des Überganges $E_0 \rightarrow E_1 \rightarrow E_0$ reflektieren. Einige Atome gelangen aber statt durch den unmittelbaren Sprung $E_1 \rightarrow E_0$ über dem Umweg $E_1 \rightarrow E_2 \rightarrow E_1 \rightarrow E_0$ in den Grundzustand zurück, d. h. sie werden während einer sog. mehrstufigen

Fluoreszenz zunächst ein Photon $k_{F'}$ streuen ($k_{F'} \rightarrow k_{s_1}$) und erst dann die vorher aufgenommene Energie in Form eines Photons $k_{\bar{s}}$ wieder abgeben. Da der Übergang $E_1 \rightarrow E_2$ jetzt erlaubt ist, tritt dieser Prozess öfter auf als der im Abschnitt I behandelte. Nun soll das Experiment eine Richtungskorrelation zwischen den im Laufe der mehrstufigen Fluoreszenz emittierten Photonen k_{s_1} , $k_{\bar{s}}$ nachweisen. Nach der einfachen Rechnung muss nämlich folgende Relation bestehen:

$$k_F + k_{F'} - k_{s_1} - k_{\bar{s}} \parallel n,$$

die wieder in der quantenmechanischen Kohärenz der an der Streuung teilnehmenden Zustandskomponenten begründet ist. Wenn nur ein einziges Atom den Bündeln F und F' im Wege stehen würde, wäre die Richtung der Photonen k_{s_1} und $k_{\bar{s}}$ beliebig. Ist die Intensität der Lichtquelle F nicht zu gross, so können wir von der Absorption der Photonen k_{s_1} absehen, andererseits können die Photonen $k_{\bar{s}}$ nicht ins Innere des Gases eindringen. (Sie werden bei grosser Dampfdichte meistens spiegelungsartig reflektiert.) Mittels Koinzidenzmessungen sind die Aussagen der Theorie auch in diesem Falle wahrscheinlich nachprüfbar. Die Frequenzen der zu beobachtenden Photonen kommen allerdings auch in der Primärstrahlung vor, das kann unter Umständen vielleicht einen zu starken »Hintergrund« geben. Die realen Verhältnisse sind auch hier verwickelter, bringen aber prinzipiell nichts Neues. Auch dieser Prozess hat einen schnellen Ablauf, wie das zur Beobachtbarkeit der Korrelation auch wünschenswert ist.

Die oben vorgeschlagenen Experimente sind vom Standpunkte einer klassischen Strahlungstheorie von keinerlei Interesse. Wollen wir uns aber an das Quantenbild halten, so ist es wichtig zu bedenken, dass nach der Theorie das Bild der Erscheinungen wesentlich davon abhängt, ob mehrere oder nur ein einziges Atom vorhanden sind, obwohl bei den einzelnen (zusammengesetzten) Streuprozessen nach der Energiebilanz immer nur ein einziges Atom eine Rolle spielt.

LITERATUR

1. O. RANG, Zeitschr. f. Phys. **136**, 457, 1953.
2. L. MARTON, Phys. Rev., **85**, 1057, 1952.
3. G. MOLLENSTEDT, Naturwiss., **42**, 41, 1955.
4. V. WEISSKOPF und E. WIGNER, Zeitschr. f. Phys., **63**, 54, 1930.
5. W. HEITLER, Quantum Theory of Radiation, Oxford, 1954.

О КОГЕРЕНТНЫХ СВОЙСТВАХ «НЕКОГЕРЕНТНОГО» ИЗЛУЧЕНИЯ
РАССЕЯНИЯ

Ф. КАРОЛЬГАЗИ

Резюме

При эффекте Рамана рассеивающие атомы после процесса остаются в возбужденном состоянии. Однако это не означает, что между ними и рассеянными разными атомами фотонами нет никакой фазовой связи; они скорее когерентны в квантовомеханическом смысле. Данный факт можно истолковать по следующему: Пусть второй сорт фоонов рассеивается на возбужденных атомах, в то время, как атомы возвращаются в основное состояние. Кроме этого, в специальных условиях между рассеянными фотонами разных сортов имеется некоторая корреляция в направлении.



THE THEORY OF MELTING

By

T. A. HOFFMANN

CENTRAL RESEARCH INSTITUTE FOR PHYSICS, BUDAPEST

(Presented by A. Kónya. — Received: 18. IV. 1961)

The energy of a finite real crystal is expressed as that of an alloy of the atoms and vacancies. This energy is a function of the vacancy concentration and of the size of the crystal block. The mixing entropy of the crystal is a function of the vacancy concentration. For certain block sizes the energy-entropy curve shows two inflexions. In these cases the melting temperature is determined by the common tangent of the curve and the melting entropy is the interval between the two points of contact. We get as a necessary condition for normal melting a certain block size. Results for alkali and noble metals and for diamond are in good agreement with experimental data.

1. Introduction

The existing theories of melting are all unsatisfactory in certain respects. One group of these theories uses the anharmonicity of the potential curves, connecting in some way the melting properties with the tensile strength of the crystal [1]. These theories do not give a convincing explanation for the sudden melting, or they give a melting point 3—4 times too large (in Kelvin degrees). Other theories use the local and distant order-disorder phenomena to explain melting [2]. These are in good agreement with the experiment, their insufficiency being their semi-empirical structure only. There are further *thermodynamic* theories of melting, which do not give a direct connection between the properties of the atoms of the solid and the melting properties [3].

There has been a tendency in very recent times to develop the theory of melting in a direction which takes as the basis the non-ideal structure of the crystal [4]. The theories using order-disorder were in some respects already such theories, however, the theories mentioned in this paragraph extend the non-ideal behaviour beyond the order-disorder phenomena to other properties too. The present theory also follows this direction.

Summarizing the requirements which a modern significant theory of melting has to fulfil, we have collected the following list of phenomena connected with the process of melting:

1. Melting occurs discontinuously at the melting point.
2. Melting is connected with a certain latent heat, i. e. an entropy change, the melting entropy.

3. At melting there is a discontinuous change in volume.

4. Melting occurs almost exclusively without the phenomena of overheating.

5. The opposite process, freezing, is, on the contrary, sometimes connected with a considerable measure of undercooling.

6. There are some smaller anomalies in the specific heat near the melting-point, however, these anomalies do not lead to an infinite specific heat at the melting point. In addition to these the theory should show the following features:

7. It should reproduce the true quantitative connections between the thermodynamic and non-thermodynamic quantities occurring at melting.

8. The theory should make one hope, that it — or a possible extension of it — can give the absolute values of these quantities too.

9. The theory should be as nearly as possible a purely theoretical and not a semi-empirical one.

In the present work we treat the solid as a real crystal with vacancies, i. e. Frenkel-defects. We shall derive a relation between the vacancy concentration and the entropy, further between the vacancy concentration and the lattice energy of the crystal. The form of this last relation depends on the size of the crystal block as a parameter. Determining this parameter we can treat the energy as a function of the entropy only. It is essential at this point to note that when plotting this energy-entropy relationship, the curve has for certain block sizes two inflexions, and thus there exists one among the tangents to this curve, which has two points of contact. As the slope of the tangent to any point of this curve gives the absolute temperature belonging to this point, this double tangent corresponds to the melting point, the point of contact lying lower representing the solid state and that lying higher the liquid state at the melting temperature. — On these bases we get good agreement with the experimental data for the melting point, for the melting entropy, for the vacancy concentration in melting and we can form an idea of the phenomena occurring in undercooling and overheating.

The calculations were carried through in this work for one-valency metals and for diamond for atmospheric pressure only.

2. The energy of a real crystal block

The first question which arises is: What is the difference between an ideal and a real crystal? — Usually there is one respect, which is emphasized as this difference: the ideal crystal has a strict geometrical arrangement of the nuclei of the constituent atoms or ions, while in the real crystal there is the possibility of some deviation from this strict geometry. These deviations

may be vacant lattice points (vacancies) in the strict geometrical arrangement, or lattice points, which are occupied by foreign atoms or ions (impurities), or they may be atoms or ions located not at the lattice points defined by the strict geometrical arrangement (interstitials). There is another type of deviation also, in which the geometry does not repeat itself strictly periodically, i. e. there is a small deformation in the lattice.

There is, however, another possibility, which is usually not emphasized as a deviation from the ideal case and this relates to the size of the crystal block. A crystal is ideal, if besides its strict geometrical arrangement it has infinite size in all directions. The calculations made for ideal crystals were related always to such infinite crystals. We consider therefore a finite crystal as a real crystal, even if it has a strict geometrical arrangement of the constituent nuclei, in contrast to the infinite ideal one.

In our model we treat a crystal block which is finite and possesses vacancies, but no interstitials or impurities. The number of vacancies in equilibrium is well determined by the temperature. If we denote the number of atoms in the crystal block by A and the number of vacancies in the same by V , we can consider the block as a lattice of $A + V$ points. The vacancy concentration is thus:

$$p = \frac{V}{A + V} \quad (1)$$

and the concentration of the atoms

$$1 - p = \frac{A}{A + V} \quad (2)$$

The number of vacancies in the block is from (1)

$$V = \frac{p}{1 - p} A. \quad (3)$$

The energy of the crystal block may now be calculated in a very crude approximation as follows. In the lattice each lattice point has z nearest neighbours. This z , the coordination number, is given by the crystal structure under discussion. It is 6 for the simple cubic lattice, 8 for the body-centered cubic lattice, 12 for the face-centered cubic lattice and 4 for the diamond lattice. In our approximation we shall take into account additively only the contribution of the binding energy of the nearest neighbours. In a simplified phraseology we may say that all atom-atom bonds contribute E_{AA} to the energy of the block and all atom-vacancy "bonds", i. e. all atom-vacancy pairs of neighbouring position, E_{AV} . If the whole number of the atom-atom bonds in

the block is N_{AA} and that of the atom-vacancy "bonds" N_{AV} , the whole energy of the block can be written in this approximation

$$E = N_{AA} E_{AA} + N_{AV} E_{AV}. \quad (4)$$

We have to pay attention here to the circumstance that N_{AV} should contain also the atom-vacancy "bonds" on the surface of the block, where the word vacancy has lost its meaning.

To determine N_{AA} and N_{AV} we suppose that the vacancies are distributed uniformly in the block, i. e. if p is their concentration, each inner lattice point has pz vacancy neighbours and $(1 - p)z$ atom neighbours, irrespective of its being atom or vacancy.

If we denote the number of atoms on the surface by A' and that of the vacancies there by V' supposing the concentration to be the same at the surface as in the inner parts of the block, we have similarly to (3)

$$V' = \frac{p}{1 - p} A'. \quad (5)$$

We shall define a surface coordination number as the number of lattice points neighbouring a lattice point on the surface, counting only those which are within the block or on its surface. If this is z' , the number of those points, which are outside the block, is $z - z'$. These last $z - z'$ neighbours are accordingly vacancies in any case. So each lattice point on the surface has $(1 - p)(z - z')$ vacancy neighbours in addition to the pz vacancies located around the inner points of the block. We have thus a total

$$N_{AA} = \frac{1}{2} (1 - p) Az - \frac{1}{2} (1 - p) A'(z - z'), \quad (6)$$

where the factor $1/2$ prevents the bonds from being counted twice once at each end atom connected by them.

Similarly, we have for the atom-vacancy "bonds"

$$N_{AV} = pAz + (1 - p) A'(z - z'), \quad (7)$$

where the factor $1/2$ is omitted since each bond is counted only once, at the atom end.

Presently the various crystal structures will be taken into account by specifying A' and z' .

3. N_{AA} and N_{AV} for various crystal structures

We now proceed to determine the values (6) and (7) of the number of atom-atom and atom-vacancy bonds for the simple cubic, the body-centered cubic, the face-centered cubic and the diamond lattice.

In Fig. 1 parts of these four structures can be seen together with the bonds occurring on the surfaces. It can be seen that for the simple cubic lattice

$$z = 6, \quad z' = 5, \quad \text{i. e.} \quad z' = \frac{5}{6} z, \quad (8)$$

for the body-centered cubic lattice

$$z = 8, \quad z' = 4, \quad \text{i. e.} \quad z' = \frac{1}{2} z, \quad (9)$$

for the face-centered cubic lattice

$$z = 12, \quad z' = 8, \quad \text{i. e.} \quad z' = \frac{2}{3} z \quad (10)$$

and for the diamond lattice

$$z = 4, \quad z' = 2, \quad \text{i. e.} \quad z' = \frac{1}{2} z. \quad (11)$$

If we consider crystallites of cubic shape only, the crystallite can be built up of n^3 unit cells, one of which is drawn with heavy lines in each figure as the right upper cube. A unit cell contains 1 lattice point in the simple cubic lattice, 2 lattice points in the body-centered cubic lattice, 4 in the face-centered cubic lattice and 1 in the diamond lattice. (In this latter case two neighbouring cells in Fig. 1 d contain 2 lattice points, so that we have an average of 1 lattice point per unit cell.)

Thus the number A of atoms in the crystallite is determined by

$$A = n^3(1 - p) \quad (12)$$

in the simple cubic lattice,

$$A = 2n^3(1 - p) \quad (13)$$

in the body-centered cubic lattice,

$$A = 4n^3(1 - p) \quad (14)$$

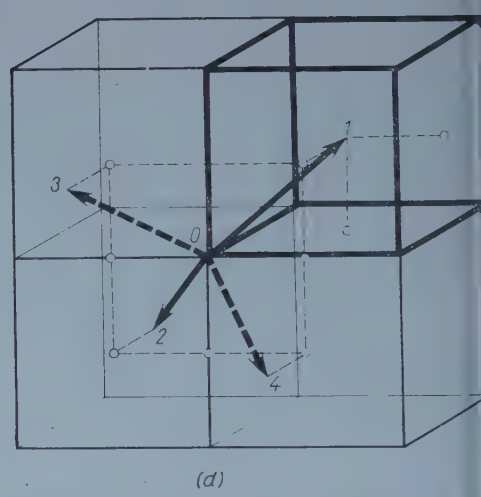
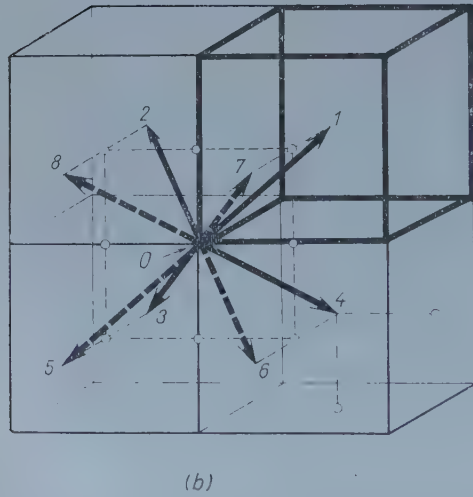
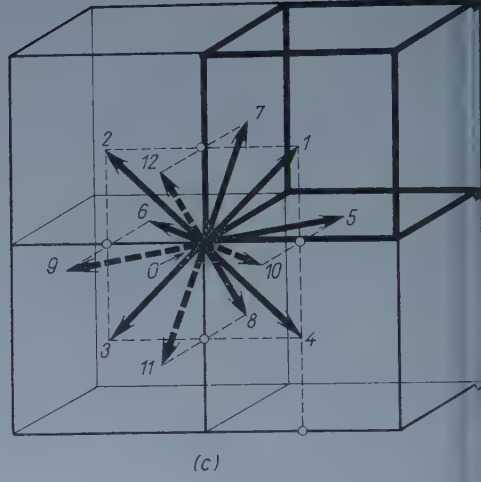
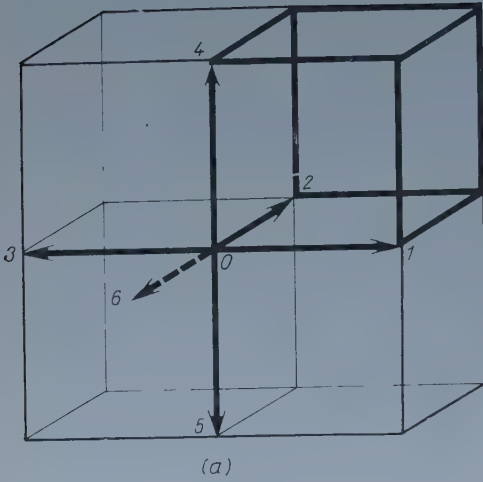


Fig. 1. Sketch of the a) simple cubic, b) body-centered cubic, c) face-centered cubic and d) diamond lattice. The full heavy lines show the bonds directed inwards from the surface (the plane of the paper), the dotted heavy lines the bonds directed outwards from the surface. In each figure one unit cell is marked in the right upper corner by heavy lines

in the face-centered cubic lattice and

$$A = n^3 (1 - p) \quad (15)$$

in the diamond lattice.

On the six surfaces of the cubes there are similarly

$$A' = 6n^2 (1 - p) \quad (16)$$

atoms in the simple cubic (s. c.) case,

$$A' = 6n^2 (1 - p) \quad (17)$$

atoms in the body-centered cubic (b. c. c.) case,

$$A' = 12n^2 (1 - p) \quad (18)$$

atoms in the face-centered cubic (f. c. c.) case and

$$A' = 3n^2 (1 - p) \quad (19)$$

atoms in the diamond-type lattice case.

Eliminating n from equations (12)—(15) and the corresponding equations (16)—(19), we have

$$A' = 6\sqrt[3]{1 - p} \cdot A^{2/3} \quad (20)$$

for the s. c. lattice,

$$A' = 3\sqrt[3]{2} \sqrt[3]{1 - p} \cdot A^{2/3} \quad (21)$$

for the b. c. c. lattice,

$$A' = 3\sqrt[3]{4} \sqrt[3]{1 - p} \cdot A^{2/3} \quad (22)$$

for the f. c. c. lattice, and

$$A' = 3\sqrt[3]{1 - p} \cdot A^{2/3} \quad (23)$$

for the diamond lattice. Substituting these values and (8)—(11) into (6) and (7) we obtain

$$N_{AA} = \frac{Az}{2} (1 - p) \left(1 - \sqrt[3]{\frac{1 - p}{A}} \right), \quad (24)$$

$$N_{AV} = Az \left[p + (1 - p) \sqrt[3]{\frac{1 - p}{A}} \right] \quad (25)$$

for the s. c. lattice,

$$N_{AA} = \frac{Az}{2} (1-p) \left(1 - 3 \sqrt[3]{\frac{1-p}{4A}} \right), \quad (26)$$

$$N_{AV} = Az \left[p + 3(1-p) \sqrt[3]{\frac{1-p}{4A}} \right] \quad (27)$$

for the b. c. c. lattice,

$$N_{AA} = \frac{Az}{2} (1-p) \left[1 - \sqrt[3]{\frac{4(1-p)}{A}} \right], \quad (28)$$

$$N_{AV} = Az \left[p + (1-p) \sqrt[3]{\frac{4(1-p)}{A}} \right] \quad (29)$$

for the f. c. c. lattice and

$$N_{AA} = \frac{Az}{2} (1-p) \left(1 - \frac{3}{2} \sqrt[3]{\frac{1-p}{A}} \right), \quad (30)$$

$$N_{AV} = Az \left[p + \frac{3}{2} (1-p) \sqrt[3]{\frac{1-p}{A}} \right] \quad (31)$$

for the diamond lattice.

4. Determination of E_{AA} and E_{AV}

The essential feature of the method will be the determination of E_{AA} and E_{AV} as functions of the vacancy concentration p and of the size n of the block. The usual theories of solids do not take into account the finiteness of the crystal block. In fact the effect of this finiteness may contribute a very small corrective term only to the total energy of the block. On the other hand, we are not interested now in the total energy, but in the — relatively small — change of this energy with p and n , and thus we have to use a model which can account for the finiteness of the block.

In previous crude LCAO MO calculations we could build up such a model in the case of a linear chain [5]. According to that work we have for the binding energy of a linear chain of k similar atoms

$$E_k = 2\beta \left[\frac{1}{\sin \frac{\pi}{2(k+1)}} - 1 \right], \quad (32)$$

if we suppose k to be even. β is the (negative) exchange integral between two nearest neighbours in the chain. For k odd we get a similar formula:

$$E_k = 2\beta \left[\operatorname{ctg} \frac{\pi}{2(k+1)} - 1 \right]. \quad (33)$$

(32) and (33) differ only very little if k is not too small. For simplicity we shall use throughout this article (32), i. e. we suppose k to be even.

Now we consider the linear analogue of a finite crystal block with vacancies. The vacancy means in the linear case that the chain is broken at the place of the vacancy. Suppose the total number of atoms in the chain to be N and the number of vacancies in it j . In this case the chain is broken into $j+1$ parts. The i -th part should contain k_i atoms. Then, obviously, we have

$$\sum_{i=1}^{j+1} k_i = N. \quad (34)$$

In the nearest-neighbour approximation this structure corresponds to $j+1$ independent chains, each containing k_i atoms. The total binding energy will be the sum of the energies of the $j+1$ chains, i. e. from (32):

$$E = \sum_{i=1}^{j+1} E_{k_i} = 2\beta \left[\sum_{i=1}^{j+1} \frac{1}{\sin \frac{\pi}{2(k_i+1)}} - j - 1 \right]. \quad (35)$$

The vacancy concentration is here

$$p = \frac{j}{N+j}, \quad (36)$$

which we suppose in the linear chain to be the same as in the three-dimensional crystal.

For given N and p , E has a well-determined range of variation, which is given by the minimum and maximum of the expression (35) for all possible variations of the k_i compatible with (34).

According to the rules of calculating the conditional extremum we have to solve the following system of equations:

$$\frac{\partial E}{\partial k_i} + \lambda = 0, \quad (i = 1, 2, \dots, j+1), \quad (37)$$

$$\sum_{i=1}^{j+1} k_i = N, \quad (38)$$

where λ is a Lagrange multiplier.

As we see from (35), E is a symmetrical function in all k_i and so using (37) all k_i are equal at the extremum. (34) gives now for the extremum

$$k_i = \frac{N}{j+1}, \quad (38)$$

and substituting this into (35):

$$E_1 = 2\beta(j+1) \left[\frac{1}{\sin \frac{\pi(j+1)}{2(N+j+1)}} - 1 \right]. \quad (39)$$

Introducing p instead of j with help of (36) we have

$$E_1 = 2\beta N \left(\frac{p}{1-p} + \frac{1}{N} \right) \left[\frac{1}{\sin \frac{\pi \left(p + \frac{1-p}{N} \right)}{2 \left(1 + \frac{1-p}{N} \right)}} - 1 \right]. \quad (40)$$

(40) gives one end of the range of variation of E . The other end of the range is given by the end of the domain of the variables, i. e. with our convention that all k should be even, by

$$k_1 = k_2 = \dots = k_j = 2, \quad k_{j+1} = N - 2j. \quad (41)$$

Substituting this into (35) we get for the other extremum of E :

$$E_2 = 2\beta \left[j - 1 + \frac{1}{\sin \frac{\pi}{2(N-2j+1)}} \right], \quad (42)$$

or expressed by p instead of by j

$$E_2 = 2\beta N \left[\frac{p}{1-p} - \frac{1}{N} + \frac{1}{N \sin \frac{\pi}{2N \left(\frac{1-3p}{1-p} + \frac{1}{N} \right)}} \right]. \quad (43)$$

The distribution of the vacancies in the chain is random and the energy of the system is established by a suitable averaging. But E_1 and E_2 do not differ very much, if N is not too small, so that it does not matter, in what way we perform the averaging. Thus we take the arithmetical mean of E_1 and E_2 as the average:

$$E = \frac{E_1 + E_2}{2} 2\beta N \left[\frac{1}{2N \sin \frac{\pi}{2N \left(\frac{1-3p}{1-p} + \frac{1}{N} \right)}} + \right. \\ \left. + \frac{\frac{p}{1-p} + \frac{1}{N}}{2 \sin \frac{\pi \left(p + \frac{1-p}{N} \right)}{2 \left(1 + \frac{1-p}{N} \right)}} - \frac{1}{N} \right]. \quad (44)$$

Expanding (44) in a Taylor-series in powers of $\frac{1}{N}$ and retaining only one term in the expansion, we have finally:

$$E = 2\beta N \left[\frac{p}{2(1-p) \sin \frac{\pi p}{2}} + \frac{1-3p}{\pi(1-p)} - \right. \\ \left. - \frac{1}{N} \left(1 - \frac{1}{\pi} - \frac{1}{2 \sin \frac{\pi p}{2}} + \frac{\pi p(1-p) \operatorname{ctg} \frac{\pi p}{2}}{4 \sin \frac{\pi p}{2}} \right) \right]. \quad (45)$$

This average energy can be interpreted according to equation (4) in the following way. The number of atom-atom bonds is in this linear case:

$$N_{AA} = \sum_{i=1}^{j+1} (k_i - 1) = N - j - 1 = N \left(\frac{1-2p}{1-p} - \frac{1}{N} \right), \quad (46)$$

since each group of k_i atoms contains $k_i - 1$ atom-atom bonds.

Similarly, each group has 2 atom-vacancy bonds, one at each end, and so we have for the number of the atom-vacancy bonds

$$N_{AV} = \sum_{i=1}^{j+1} 2 = 2(j+1) = 2N \left(\frac{p}{1-p} + \frac{1}{N} \right). \quad (47)$$

Equation (4) is therefore in the linear case:

$$E = N \left(\frac{1-2p}{1-p} - \frac{1}{N} \right) E_{AA} + 2N \left(\frac{p}{1-p} + \frac{1}{N} \right) E_{AV}. \quad (48)$$

We assume now that E_{AV} , the interaction energy between an atom and a vacancy, does not depend on N and p . E_{AA} , on the contrary, depends essentially on both these variables.

However, we can assume that in an ideal crystal, i. e. if $p = 0$, the bonds are independent of the size of the crystal, i. e.

$$E_{AA}(N, 0) = E_{AA}(\infty, 0). \quad (49)$$

With these assumptions we shall now compare (45) and (48) at the point $p = 0$:

$$\left(1 - \frac{1}{N}\right) E_{AA}(\infty, 0) + \frac{2}{N} E_{AV} = 2\beta \left[\frac{2}{\pi} - \frac{1}{N} \left(1 - \frac{2}{\pi}\right) \right]. \quad (50)$$

Since this equality holds for all N , it holds for the terms not containing $\frac{1}{N}$ and for those containing $\frac{1}{N}$ separately:

$$E_{AA}(\infty, 0) = \frac{4\beta}{\pi}, \quad (51)$$

$$-E_{AA}(\infty, 0) + 2E_{AV} = -2\beta \left(1 - \frac{2}{\pi}\right). \quad (52)$$

(51) is the well-known result for an ideal crystal. Eliminating $E_{AA}(\infty, 0)$ from (51) and (52) we get for E_{AV} :

$$E_{AV} = \beta \left(\frac{4}{\pi} - 1 \right). \quad (53)$$

Substituting this value into (48) and comparing it now with (45), neglecting powers of $\frac{1}{N}$ higher than the first one, we have for E_{AA} :

$$E_{AA} = 2\beta \left[\frac{p}{2(1-2p) \sin \frac{\pi p}{2}} + \frac{p}{1-2p} + \frac{1-7p}{\pi(1-2p)} - \frac{1}{N} \left(\frac{(1-p)(2+p)}{\pi(1-2p)^2} - \frac{p(1-p)}{(1-2p)^2} - \frac{(1-p)^2}{2(1-2p)^2 \sin \frac{\pi p}{2}} + \frac{\pi p(1-p)^2 \operatorname{ctg} \frac{\pi p}{2}}{4(1-2p) \sin \frac{\pi p}{2}} \right) \right]. \quad (54)$$

We note that in (54) N means the number of atoms present in the chain. To conform with the previous notation (equ. (12)—(15)), where n was the number of unit cells along an edge of the crystallite, we have to express N in (54) in terms of n in a way depending on the crystal structure.

5. Energies for the various crystal structures

With the results of the last two sections we can write down the energies of the crystals as functions of n and p .

In the case of a simple cubic lattice the chains containing the nearest neighbours are parallel to the edge of the cube and so the number of atoms in one chain, N , is connected with the number of cells in the same direction, n , by

$$N = n(1 - p). \quad (55)$$

Further, we have to introduce $\frac{1}{n}$ instead of $\sqrt[3]{\frac{1-p}{A}}$ in (24) and (25) using equation (12).

In this way we obtain by substituting (24), (25), (53) and (54) into (4) and neglecting terms of order $\frac{1}{n^2}$ or higher,

$$\begin{aligned}
 E = \beta A z \left[\frac{1}{1-2p} \left(p^2 + \frac{1}{\pi} (1-4p-p^2) + \frac{p(1-p)}{2 \sin \frac{\pi p}{2}} \right) - \right. \\
 \left. - \frac{(1-p)^{4/3}}{n_0(1-2p)^2} \left(1-4p+2p^2 - \frac{1}{\pi} (1-8p+2p^2) - \right. \right. \\
 \left. \left. - \frac{1-2p+2p^2}{2 \sin \frac{\pi p}{2}} + \frac{\pi p(1-p)(1-2p) \operatorname{ctg} \frac{\pi p}{2}}{4 \sin \frac{\pi p}{2}} \right) \right] \quad (56)
 \end{aligned}$$

for the s. c. lattice, where we introduced n_0 , the value of n at zero vacancy concentration by

$$n_0 = n \sqrt[3]{1-p}. \quad (57)$$

In the case of a body-centered cubic lattice the chains containing the nearest neighbours are parallel to the body diagonal of the cube. The chains are therefore of different length. As one can calculate easily, the average length of a chain is $\frac{1}{\sqrt{3}}$ -times that of the edge of the cube. Thus the average number of atoms in the chain, N , is connected with the number of cells along an edge, n , by

$$N = \frac{2n}{3} (1 - p), \quad (58)$$

where we have taken into account, that the nearest-neighbour distance is $\frac{\sqrt{3}}{2}$ -times that of the edge of the unit cell. So we have, replacing $\sqrt[3]{\frac{2(1-p)}{A}}$ by $\frac{1}{n}$ according to (13), substituting (26), (27), (53) and (54) into (4) and neglecting terms of order $\frac{1}{n^2}$, or higher:

$$\begin{aligned} E = \beta A z \left[\frac{1}{1-2p} \left(p^2 + \frac{1}{\pi} (1-4p-p^2) + \frac{p(1-p)}{2 \sin \frac{\pi p}{2}} \right) - \right. \\ \left. - \frac{3(1-p)^{4/3}}{2n_0(1-2p)^2} \left(1-4p+2p^2 - \frac{1}{\pi} (1-8p+2p^2) - \right. \right. \\ \left. \left. - \frac{1-2p+2p^2}{2 \sin \frac{\pi p}{2}} + \frac{\pi p(1-p)(1-2p) \operatorname{ctg} \frac{\pi p}{2}}{4 \sin \frac{\pi p}{2}} \right) \right] \quad (59) \end{aligned}$$

for the b. c. c. lattice. Note that (56) for the s. c. lattice and (59) for the b. c. c. lattice differ only in that the second term in the square bracket is $\frac{3}{2}$ -times as large in (59) as the corresponding term in (56).

In the case of a face-centered cubic lattice the chains of nearest neighbours are parallel to the diagonals of the faces of the cube. The chains are

again of different length. A straightforward calculation shows that the average length of a chain is in this case $\frac{1}{\sqrt{2}}$ -times that of the edge of the cube.

The average number of atoms in the chain, N , is therefore connected with the number of cells along an edge, n , by

$$N = n(1 - p), \quad (60)$$

where we have taken into account, that the nearest-neighbour distance is

$\frac{1}{\sqrt{2}}$ -times that of the edge of the unit cell. So we have, replacing $\sqrt[3]{\frac{4(1-p)}{A}}$ by $\frac{1}{n}$ according to (14), substituting (28), (29), (53) and (54) into (4) and neglecting terms of order $\frac{1}{n^2}$, or higher:

$$E = \beta A z \left[\frac{1}{1-2p} \left(p^2 + \frac{1}{\pi} (1-4p-p^2) + \frac{p(1-p)}{2 \sin \frac{\pi p}{2}} \right) - \right. \\ \left. - \frac{(1-p)^{4/3}}{n_0(1-2p)^2} \left(1-4p+2p^2 - \frac{1}{\pi} (1-8p+2p^2) - \right. \right. \quad (61) \\ \left. \left. - \frac{1-2p+2p^2}{2 \sin \frac{\pi p}{2}} + \frac{\pi p(1-p)(1-2p) \operatorname{ctg} \frac{\pi p}{2}}{4 \sin \frac{\pi p}{2}} \right) \right]$$

for the f. c. c. lattice. Note that (56) for the s. c. lattice and (61) for the f. c. c. lattice are entirely the same, except that the connection between A and n occurring in these formulas is given by (12) in the s. c. and by (14) in the f. c. c. case.

In the diamond lattice we cannot select a linear chain transversing the block. However, we can consider broken chains as seen in Fig. 2. These chains contain the same number of atoms as the chains in the f. c. c. lattice case. So the average number of atoms in the chain, N , is connected with the number

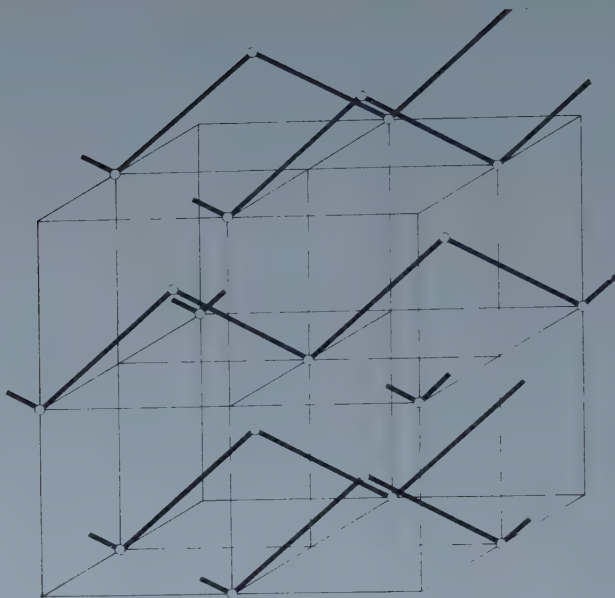


Fig. 2. Sketch of the chains in a diamond lattice

of cells along an edge, n , by the same formula (60) as in the f. c. c. lattice case.

Thus replacing $\sqrt[3]{\frac{1-p}{A}}$ by $\frac{1}{n}$ according to (15), substituting (30), (31), (53) and (54) into (4) and neglecting terms of order $\frac{1}{n^2}$ or higher, we have:

$$\begin{aligned}
 E = \beta A z \left[\frac{1}{1-2p} \left(p^2 + \frac{1}{\pi} (1-4p-p^2) + \frac{p(1-p)}{2 \sin \frac{\pi p}{2}} \right) - \right. \\
 \left. - \frac{(1-p)^{4/3}}{2n_0(1-2p)^2} \left(3 - 11p + 6p^2 - \frac{1}{\pi} (5 - 23p + 6p^2) - \right. \right. \\
 \left. \left. - \frac{2-5p+6p^2}{2 \sin \frac{\pi p}{2}} + \frac{\pi p(1-p)(1-2p) \operatorname{ctg} \frac{\pi p}{2}}{2 \sin \frac{\pi p}{2}} \right) \right] \quad (62)
 \end{aligned}$$

for the diamond lattice.

6. The mixing entropy of the crystal

The entropy of an atomic system can be built up of parts of various origin. These are of two kinds. One part of the entropy is a function of temperature, varying relatively slowly. This part is independent, or quasi-independent of the various phases existing at the same temperature. The vibrational entropy for instance is of this kind. The other part of the entropy depends, on the other hand, significantly on the respective phases. This latter part may be only a very small fraction of the total entropy, but its change is much larger than the corresponding change in the other parts of the entropy in case of a change of phase.

We consider here the vacancies as the causes of melting, thus it is obvious that we have to investigate that part of the entropy which has its origin in the vacancies. This is the same entropy of mixing which occurs in disordered alloys. In our notation this entropy is given by

$$S = k \log \frac{(A + V)!}{A! V!}, \quad (63)$$

where k is the Boltzmann constant.

In the Stirling approximation this gives

$$\begin{aligned} S &= k[(A + V) \log(A + V) - A \log A - V \log V] = \\ &= Ak \left[\frac{1}{1-p} \log \frac{1}{1-p} - \frac{p}{1-p} \log \frac{p}{1-p} \right] = \\ &= -Ak \left[\log(1-p) + \frac{p}{1-p} \log p \right], \end{aligned} \quad (64)$$

where we have made use of equ. (3).

Equation (64) gives the first approximation of the entropy only. Applying the next approximation in the Stirling formula to equ. (63) the second approximation is obtained which gives in the square bracket of equ. (64) a term proportional to $\frac{1}{A}$, that is to $\frac{1}{n_0^3}$. As the whole calculation is carried out to the first order in $\frac{1}{n_0}$ only, we can totally neglect in this approximation the change of the entropy with the block size. Similarly, the difference between the inner atoms of the block and the atoms on the surface is expressed by a term proportional to $\frac{1}{n_0^2}$, which we can again neglect in our approximation.

7. The free energy of the block structure

In the preceding section we considered a block of the crystal consisting of about n_0^3 atoms. Now the question arises, whether n_0 has or has not a finite value in the equilibrium state. In other words, the question is whether in equilibrium the crystal has a finite block size or an infinite one.

The straightforward way to decide this problem is to investigate the free energy of the system. If one could show that the free energy decreases by breaking the crystal into smaller blocks, the equilibrium state would be this latter. A natural treatment of the problem would be to show that the free energy of the crystal has a minimum at some finite value of n_0 . There has been till now no possibility of showing this in general in the three-dimensional case. The present work is not able either to show this, since here all calculations are carried through in approximations to the first power of $\frac{1}{n_0}$ only so that there is no possibility of getting a finite extreme value for n_0 .

Instead, we show in a linear case that the chain really has a minimum free energy if it is sliced into smaller chains of definite lengths and on the analogy of this we conclude that the same is true in the spatial case.

Let us suppose that we have a linear chain of N atoms as in section 4. This chain be broken into $j + 1$ parts containing k_1, k_2, \dots, k_{j+1} atoms, respectively. Then equ. (34) holds and the total energy of the chain is given by equ. (35).

As the energy (35) depends on the sum of the energies of the $j + 1$ chains, the thermodynamic probability, i. e. the number of the micro-distributions is

$$W = \frac{N!}{k_1! k_2! \dots k_{j+1}!} (j + 1)!, \quad (65)$$

since the $j + 1$ chains may be interchanged. The free energy of the system is therefore from (35) and (65):

$$\begin{aligned} F = E - TS = E - kT \log W &= 2\beta \left[\sum_{i=1}^{j+1} \frac{1}{\sin \frac{\pi}{2(k_i + 1)}} - j - 1 \right] - \\ &kT \left[\log N! + \log(j + 1)! - \sum_{i=1}^{j+1} \log k_i! \right] = \\ &= 2\beta \left[\sum_{i=1}^{j+1} \frac{1}{\sin \frac{\pi}{2(k_i + 1)}} - j - 1 \right] - \\ &- kT \left[\log \Gamma(N + 1) + \log \Gamma(j + 2) - \sum_{i=1}^{j+1} \log \Gamma(k_i + 1) \right], \end{aligned} \quad (66)$$

where $\Gamma(x)$ denotes the gamma function of argument x .

In the equilibrium state the energy has a minimum with respect to k_1, k_2, \dots, k_{j+1} and with respect to j . First we consider the minima with respect to k_1, k_2, \dots, k_{j+1} . Here we have to solve the conditional minimum problem, where the condition is given by equ. (34). We have thus in the usual manner, if λ is a Lagrange multiplier:

$$\frac{\partial F}{\partial k_i} - \lambda = \frac{\pi\beta}{(k_i + 1)^2} \frac{\operatorname{ctg} \frac{\pi}{2(k_i + 1)}}{\sin \frac{\pi}{2(k_i + 1)}} +$$

$$+ kT \Psi(k_i) - \lambda = 0, \quad (i = 1, 2, \dots, j + 1), \quad (67)$$

where $\Psi(x)$ is the logarithmic derivative of the $\Gamma(x + 1)$ -function. As the $j + 1$ equations in (67) are all of the same form, we easily obtain

$$k_i = \frac{N}{j + 1}, \quad (i = 1, 2, \dots, j + 1), \quad (68)$$

where we have made use of the condition (34). Substituting (68) into (66) we have:

$$F = 2\beta(j + 1) \left[\frac{1}{\sin \frac{\pi}{2 \left(\frac{N}{j + 1} + 1 \right)}} - 1 \right] -$$

$$- kT \left[\log \Gamma(N + 1) + \log \Gamma(j + 2) - (j + 1) \log \Gamma \left(\frac{N}{j + 1} + 1 \right) \right]. \quad (69)$$

We seek the minimum of F given by (69) with respect to j , i. e. we have to determine j from the equation:

$$\frac{\partial F}{\partial j} = 2\beta \left[\frac{1}{\sin \frac{\pi}{2 \left(\frac{N}{j + 1} + 1 \right)}} - 1 - \frac{\operatorname{ctg} \frac{\pi}{2 \left(\frac{N}{j + 1} + 1 \right)}}{\sin \frac{\pi}{2 \left(\frac{N}{j + 1} + 1 \right)}} \right] -$$

$$- \frac{\pi N}{2 \left(\frac{N}{j + 1} + 1 \right)^2 (j + 1)} - kT \left[\Psi(j + 1) - \log \Gamma \left(\frac{N}{j + 1} + 1 \right) + \right.$$

$$\left. + \Psi \left(\frac{N}{j + 1} \right) \frac{N}{j + 1} \right] = 0. \quad (70)$$

Let us denote for the moment by

$$\frac{N}{j+1} = n \quad (71)$$

the number of atoms in the short chains into which the long chain is broken. Equation (70) may then easily be solved for T and may be written

$$T = \frac{2\beta}{k} \cdot \frac{1 - \sin \frac{\pi}{2(n+1)} - \frac{\pi n}{2(n+1)^2} \operatorname{ctg} \frac{\pi}{2(n+1)}}{\sin \frac{\pi}{2(n+1)} \left[\Psi\left(\frac{N}{n}\right) + n \Psi(n) - \log \Gamma(n+1) \right]} \quad (72)$$

The temperature corresponding to any value of n may be easily calculated if we take into account, that the parameter N occurs only in one term in the denominator. The results of the calculation are shown in Fig. 3. To make the

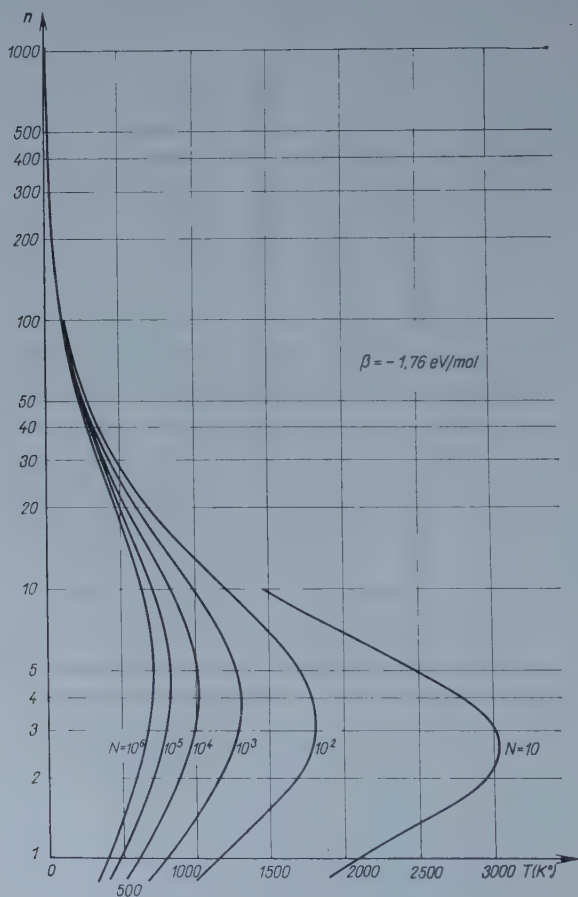


Fig. 3. Values of n for the minimum free energy at different temperatures for a linear chain built of copper atoms

order of magnitude of the temperature and n perceptible, we have taken in the Figure for β the value -1.76 ev/mol. Considering the situation at fixed temperatures there are two points of the curves at each temperature. The lower point corresponds to a maximum of the free energy and the higher to the minimum of the free energy.

Moreover from Fig. 3 one may see that at not too high temperatures (lower than 500° K in the Fig.) each n corresponds to a very narrow temperature interval in a large interval of N . This means, that approximately we have a unique relation $n(T)$ irrespective of the value of N . This would mean that at a fixed temperature all chains are broken into small chains of lengths $n(T)$ whatever the length of the whole chain.

These results show that in a linear chain the free energy has a minimum, if the chain is broken into smaller chains. To make the same calculation for the planar or the spatial case would be, however, very involved and so we restrict ourselves here to suggest that by analogy we may suppose that the free energy is lowered by the block formation even in the planar or the spatial case. For the sake of simplicity we assume further that the parameter of this block n_0 is independent of the temperature.

8. The energy — entropy curve

Formulas (56)—(62) and (64) allow us to investigate the behaviour of the energy and entropy as functions of the vacancy concentration. (56), (59), (61) and (62) can be written in a common form:

$$e(p, n_0) = \frac{E}{\beta A z} = f(p) + \frac{1}{n_0} g(p), \quad (73)$$

where $f(p)$ is for all four lattice types the same:

$$f(p) = \frac{1}{1-2p} \left[p^2 + \frac{1}{\pi} (1-4p-p^2) + \frac{p(1-p)}{2 \sin \frac{\pi p}{2}} \right], \quad (74)$$

$g(p)$ is the same for the s. c., the b. c. c. and the f. c. c. lattice:

$$g(p) = \frac{(1-p)^{4/3}}{(1-2p)^2} \left[1-4p+2p^2 - \frac{1}{\pi} (1-8p+2p^2) - \right. \\ \left. - \frac{1-2p+2p^2}{2 \sin \frac{\pi p}{2}} + \frac{\pi p(1-p)(1-2p) \operatorname{ctg} \frac{\pi p}{2}}{4 \sin \frac{\pi p}{2}} \right]. \quad (75)$$

We remark that in the b. c. c. case n_0 has to be replaced by $\frac{2n_0}{3}$. For the diamond lattice we have:

$$g(p) = \frac{(1-p)^{4/3}}{2(1-2p)^2} \left[3 - 11p + 6p^2 - \frac{1}{\pi} (5 - 23p + 6p^2) - \right. \\ \left. - \frac{2 - 5p + 6p^2}{2 \sin \frac{\pi p}{2}} + \frac{\pi p(1-p)(1-2p) \operatorname{ctg} \frac{\pi p}{2}}{2 \sin \frac{\pi p}{2}} \right]. \quad (76)$$

For the sake of completeness we re-write here the formula for the entropy too,

$$s(p) = \frac{S}{Ak} = -\log(1-p) - \frac{p}{1-p} \log p. \quad (77)$$

Our thermodynamic functions are now the following: the internal energy of the system $e(p, n_0)$, a function of the vacancy concentration, p , only, if n_0 is held constant; the entropy of the system, $s(p)$, again a function of p only if we disregard the slow change of the entropy with temperature. In our whole treatment we deal with the case of zero pressure. This is certainly admissible in the solid state and we suppose that we do not make a large error if we hold this supposition to be valid also for liquids in the neighbourhood of the melting point, i. e. we treat isobar melting at zero pressure.

The volume of the crystallite can be expressed by (12)–(15) in the form

$$v = \frac{v_0}{1-p}, \quad (78)$$

where v_0 is the volume at zero vacancy concentration, i. e. at absolute zero temperature. (73) and (77) give in addition the internal energy and the entropy of the system. The general thermodynamic relations [7] give now the following results. The absolute temperature is given by

$$T = \left(\frac{\partial E}{\partial S} \right)_{P=0} = \frac{\beta z \frac{\partial e}{\partial p}}{\frac{\partial s}{\partial p}}. \quad (79)$$

The specific heat at constant zero pressure has an additive contribution from E (the major part of it originating from the vibrational motion of the atoms, supposed to be the same in the solid and in the liquid phase). This contribution is:

$$\begin{aligned} \delta c_P &= \left(\frac{\partial E}{\partial T} \right)_{P=0} = \frac{\frac{\partial E}{\partial p}}{\frac{\partial}{\partial p} \left(\frac{\partial E}{\partial p} / \frac{\partial s}{\partial p} \right)} = \\ &= Ak \frac{\frac{\partial e}{\partial p} \left(\frac{\partial s}{\partial p} \right)^2}{\frac{\partial^2 e}{\partial p^2} \cdot \frac{\partial s}{\partial p} - \frac{\partial e}{\partial p} \cdot \frac{\partial^2 s}{\partial p^2}}. \end{aligned} \quad (80)$$

Eqs. (78)—(80) are sufficient to describe the behaviour of the system.

For a specified n_0 we can now plot the $e-s$ curve. We give here a somewhat detailed discussion of the behaviour of this curve, since it is of very great importance for the considerations further below.

According to (79) the absolute temperature is proportional to the tangent of the $e-s$ curve.

We have to note, that the n_0 occurring in the formulas after (73) are the same as the n_0 before this formula but with a reversed sign. This means that one must not attribute too great an importance to the interpretation of n_0 as the number of cells in a specified direction. Indeed, the following discussion shows that n_0 occurring in the formulas after (73) takes on positive values throughout and this would mean a negative number of cells in the system. For the moment let us disregard the meaning of n_0 and make the analysis with n_0 as a simple parameter without any specific meaning. Further we have to note that (79) holds only, if we suppose β to be independent of the temperature. This is not the case in reality. In spite of this we make our calculations independent of the variation of β and for the sake of simplicity we make a correction in the last step of the discussion only.

As β is negative, only those parts of the curve are feasible in which $\frac{\partial e}{\partial p} / \frac{\partial s}{\partial p}$ is also negative. The parts with $\frac{\partial e}{\partial p} / \frac{\partial s}{\partial p}$ positive are not points of thermodynamic equilibrium. Moreover, if the curve has a part, where $\frac{\partial e}{\partial p} / \frac{\partial s}{\partial p}$ is positive, it must have more than one minimum (the point $s = 0$ is certainly a minimum belonging to $p = 0$). This would mean that the crystal has a metastable state at some vacancy concentration different from 0. This we should exclude — at least for ordinary pure metals. Such an exclusion imposes the condition

$$\frac{\partial e}{\partial p} \bigg/ \frac{\partial s}{\partial p} \leq 0 \quad (81)$$

along the whole curve.

As

$$\frac{\partial s}{\partial p} = - \frac{1}{(1-p)^2} \log p \quad (82)$$

is always positive, taking into account (73), this means, that the inequality

$$\frac{\partial f}{\partial p} + \frac{1}{n_0} \frac{\partial g}{\partial p} \leq 0 \quad (83)$$

should hold along the whole curve. Since $\frac{\partial g}{\partial p}$ is negative everywhere, this con-

dition is fulfilled in the whole range, where $\frac{\partial f}{\partial p}$ is negative (small p -values).

In the range, where $\frac{\partial f}{\partial p}$ is positive, n_0 must be subject to an additional condition, namely

$$n_0 \leq - \frac{\frac{\partial g}{\partial p}}{\frac{\partial f}{\partial p}} \quad (84)$$

everywhere in this range. $-\frac{\partial g}{\partial p} \bigg/ \frac{\partial f}{\partial p}$ is a function of p , which has a minimum in this range. Therefore the condition (84) is fulfilled everywhere, if it is fulfilled at the minimum. The curve is given for the cubic and diamond type lattices in Fig. 4. This curve has a minimum at some value of p . According to (84) this means, that there is a maximum value for n_0 , namely the value at this minimum. This is

$$n_0 = 11,08 \quad (85)$$

for the cubic lattices and

$$n_0 = 10,75 \quad (86)$$

for the diamond lattice.

If one disregards the sign of n_0 , one obtains, using equ. (12)–(15) and (57), that the maximum value of atoms in a block of the crystallite is

$$A = 1360 \quad (87)$$

for the simple cubic lattice,

$$A = 2721 \quad (88)$$

for the body-centered cubic lattice,

$$A = 5441 \quad (89)$$

for the face-centered cubic lattice and

$$A = 1242 \quad (90)$$

for the diamond lattice.

Further investigation of the $e-s$ curve shows that for a certain range of n_0 it has two inflexion points, whereas for other values of n_0 it has no

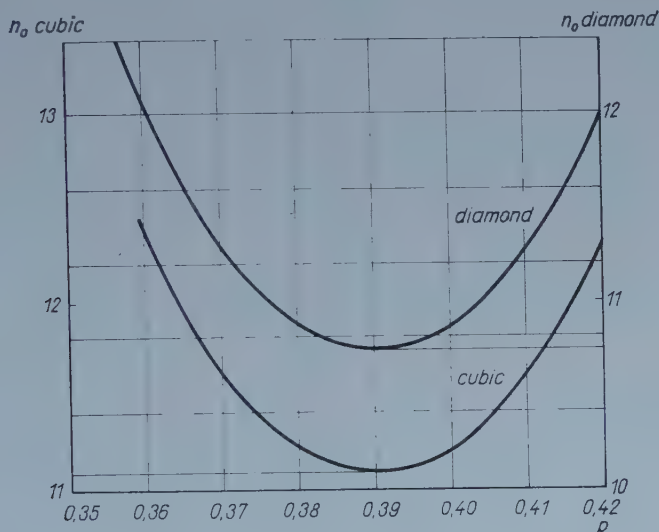


Fig. 4. The maximum value for n_0 for the cubic and for the diamond-type lattices

inflexion points at all. If the curve $e-s$ has two points of inflexion, it is possible to find a common tangent to two points of the curve, whereas in the other case each tangent has only one point of contact on the curve. We shall see later that a necessary condition for the existence of a definite melting point is the occurrence of a double tangent to the $e-s$ curve. In the case of no inflexion points we conclude that the solid-liquid transformation is a continuous one extended over a wide range of temperatures. This property characterizes the amorphous phases.

The calculations show that the two inflexion points existing in the case of n_0 not much smaller than given in (85) and (86) resp., approach each other more and more with decreasing n_0 . We can find a value for n_0 , where the two inflexion points coincide (where the second and third derivatives of e with

respect to s vanish at the same p) and if n_0 is less than this value, the curve has no inflexion points at all.

This value of n_0 is for the cubic lattices

$$n_0 = 4,5 \quad (91)$$

and for the diamond lattice

$$n_0 = 4,1. \quad (92)$$

Using equs. (12)—(15) and (57) we get for the minimum value of atoms in the crystal for a non-amorphous melting process

$$A = 91 \quad (93)$$

for the simple cubic lattice,

$$A = 183 \quad (94)$$

for the body-centered cubic lattice,

$$A = 365 \quad (95)$$

for the face-centered cubic lattice and

$$A = 69 \quad (96)$$

for the diamond lattice.

The final conclusion can be drawn that the solids having normal discontinuous melting properties have subcrystallites of the size of 91—1360 atoms for the simple cubic lattice, of 183—2721 atoms for the b. c. c. lattice, of 365—5441 atoms, for the f. c. c. lattice and of 69—1242 atoms for the diamond lattice. This relatively broad range for the number of atoms gives an uncertainty in the calculation of the melting temperature, since each subcrystallite size is connected with a well-defined melting point.

The results of equs. (87)—(96) seem to give extraordinarily low values for the size of the crystallite blocks. The idea of such intrinsic crystal blocks is familiar in the literature. Apart from the investigations of G. W. STEWART [8] about the cybotactic groups there is some theoretical and experimental evidence for the existence of small intrinsic blocks, even in the single crystals. M. BORN [9] shows that the consequent quantummechanical treatment of the dynamics of a crystal lattice leads to difficulties which cannot be solved unless an inner block structure is assumed in the crystal. BORN determines a critical number of atoms, z_0 , which is the maximum number of atoms on one edge of an ideal crystallite block at absolute zero temperature. He gets for this value $z_0 = 500$ for almost any substance. For finite temperature the number of atoms on one edge of a crystallite is according to BORN

$$z = z_0 i h \frac{\theta}{2T}, \quad (97)$$

where θ is the Debye temperature of the substance. This gives e. g. for gold with $\theta = 170^\circ \text{ K}$, at the melting point $T_m = 1336,2^\circ \text{ K}$ about $z = 30$, which is of the same order of magnitude as the value (85). However, the meaning of the block in BORN's work is not the same as in the present paper. Our block size namely is independent of the temperature, whereas BORN's block decreases with increasing temperature, further our block contains vacancies too, whereas BORN's block is an ideal one, without any lattice defects.

R. FÜRTH [10] has shown that any theory of melting, which takes into account ideal crystals and tries to explain the melting by the anharmonicity of the vibrations, gives unsatisfactory results for the melting point. He draws the conclusion that the intrinsic block structure is essential for a theory of melting. In another paper [11] he connects BRAGG's theory of the mechanical strength [12] with the theory of melting. BRAGG develops in his paper the theory of the mechanical strength of solids assuming the existence of an internal block structure in the crystal and FÜRTH, connecting the melting temperature with the existence of such a block structure concludes that the evolution of this block structure is a structure-insensitive, intrinsic property, as the melting point is also independent of the history of the sample etc. In contrast to this, the micro-crystalline mosaic structure (dealing with larger micro-crystals than those mentioned above) is a structure-sensitive property depending very strongly on the previous mechanical, thermal, etc. treatment of the sample.

As experimental evidence for the existence of subcrystallites of very small dimensions we may quote the investigations of W. A. WOOD [13]. WOOD and his collaborators made X-ray structure investigations on quenched metals. They found that deforming these metals the crystallite blocks can be broken up into smaller subcrystallite blocks, which have a well-defined minimal size, characteristic for the metal. This supports the view that this subcrystallite block structure is an intrinsic property of the solid. Recently, SIMMONS and BALUFFI [14] have shown experimentally the existence of the subcrystallite blocks in aluminium and in silver.

Considering the liquid state there is experimental evidence, evaluated by the Eötvös equation, showing that there is a tendency of association in liquid metals near the freezing point [15].

A similar tendency of association was observed in melts of selenium by Prof. RICHTER in Stuttgart with an X-ray diffraction technique [16].

In our opinion the small subcrystallite blocks given here do not constitute different units in the crystallite, observable by optical or X-ray methods, because the lattice planes of neighbouring subcrystallites are parallel and only a minute difference in the distance of planes in the same subcrystallite and of

planes in neighbouring subcrystallites (at the surface) constitutes the deviation from a larger crystallite. The subcrystallites may indicate in this sense that the lattice distance at these planes is somewhat larger than the normal one. This causes some difference in the binding energy and it is this energy which was taken into account in our calculations. This somewhat larger lattice distance however, does, not affect any essential change in the crystal dimensions and thus it is not always observed by the usual X-ray techniques.

9. The melting properties

If we take a value for n_0 between (91) and (85) or between (92) and (86)) the e — s curve has the form shown in Fig. 5. On the left of the Figure the tangent of the curve is parallel to the s -axis, i. e. the absolute temperature at this

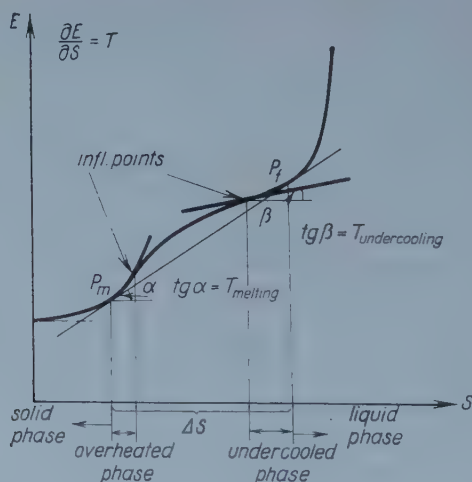


Fig. 5. Typical E — S curve for intermediate n_0

point is 0. As we proceed towards higher entropy values, the tangent becomes steeper, i. e. the temperature increases. Finally we reach a point, where the tangent to the curve has a second point of contact on the curve. In this case both points of contact represent phases at the same temperature (determined by the common tangent), the lower point representing a phase with a lower entropy, the higher one a phase with higher entropy. We attribute to the phase with the lower entropy the solid state and to the phase with the higher entropy the liquid state. The slope of the double tangent gives the melting temperature, the difference of the abscissae of the two points of contact the melting entropy, and the difference of their ordinates the latent heat of melting.

By heating the solid the temperature increases and finally we arrive at the melting point, P_m . Here there are two possibilities for the system: By receiving heat the system wanders along the straight line $P_m P_f$, i. e. the temperature does not change until reaching the point P_f . In the meantime the entropy of the system increases by ΔS . The phase with a higher entropy corresponds to the liquid phase, i. e. melting occurs in the interval $P_m P_f$ of the straight line.

The second possibility is that the system proceeds on its way along the curve in the interval $P_m P_f$. In this case the temperature further increases right up to the point P_m with a relatively small change in the entropy of the system. This way would correspond to the overheating of the solid. We shall revert later to the choice between these alternatives.

Right to the point P_f the temperature is higher than the melting temperature and the system is in a state with higher entropy, in the liquid state. With decreasing temperature arriving at P_f we again have an alternative. The system could continue along the straight line $P_f P_m$ and in this way ordinary freezing would happen at the melting temperature, or the system could proceed along the curve $P_f P_m$. In the latter case the temperature would further decrease going left from point P_f with a small change of the entropy. This corresponds to the undercooling of the liquid.

Presently we analyze under what circumstances the two alternatives occur. In the case of increasing temperature starting from the solid state it is clear that the entropy change, accompanying the absorption of a certain heat energy, is larger in the case of melting than in the case of overheating. This may be seen in Fig. 5, since the double tangent lies always on the right side of the curve. To judge which of the two alternatives will occur, we have to consider the entropy change of an adiabatic system, namely the total system consisting of the melting (or overheating) solid *and* of the heating medium. According to the second law of thermodynamics, in an adiabatic system always the process with a higher positive entropy change will be realized and never that with the lower one.

Now heating is accomplished by transmission of the energy in some way from a system of higher temperature to one of lower temperature. Usually the entropy change of the heater system is then $\frac{dE}{T}$, where T is the *higher* temperature of the heater and dE the transmitted energy. As the temperature of the heated system is always less than that of the heater system, the entropy change in the heated system is always larger than that of the heater system and thus the net entropy change is always positive. If we use a specific heating system, its negative entropy change determined by the heater, will be nearly the same in any case, whereas as we have seen above, the positive entropy change of the heated solid will be larger in the case of melting than in case of

overheating. So we conclude that by normal thermodynamic heating melting occurs in all cases and never overheating.

In the case of decreasing temperature starting from the liquid state the (negative) entropy change accompanying the development of a certain heat energy is in the case of freezing always less than in the case of undercooling, since the double tangent lies always right to the curve and so the entropy change on the straight line is less than that on the curve, reaching in the two cases the same ordinate.

In a cooling process the cooler system absorbs heat energy from the cooled system. The entropy of the cooler increases therefore by an amount $\frac{dE}{T}$, where T is the lower temperature of the cooler. The entropy change of the total system is therefore always positive, as it has to be. At first sight the freezing procedure seems to be that with a larger entropy change in contrast to the undercooling procedure, since in this case the negative change in entropy is smaller. The detailed investigation of the system shows, however, the following situation.

To examine the behaviour of the melting or the freezing system during the process, we proceed on the straight line connecting P_m with P_f . Any point of this line corresponds to a state, where a certain amount of the whole substance is in the liquid phase and the remainder in the solid phase, both at the same temperature. In P_m 100% is in the solid phase and 0% in the liquid one and in P_f just reversed. The system needs a small, but in any case finite time to get from P_m to P_f or from P_f to P_m . In the case of melting the presence of the heat needed for the process is the only necessary condition for its realization. Therefore this can be achieved homogeneously in any part of the system, however small this part is chosen. In this case the total entropy of the system discussed above may be regarded as the quantity determining the process.

In the case of freezing, however, the situation is somewhat altered. In this case the possibility of extraction of heat is only one necessary condition for the realization of the process. The other one is that the particles should reach their regular positions in the crystal. This is connected with the formation of crystallization grains. In the liquid just over the melting point there exist already some such grains distributed relatively uniformly over the whole liquid. Considering this we see that these grains have a finite average distance from each other. If we pick out of the whole system, these grains only, without the surrounding grain-free parts of the system we must conclude that in the neighbourhood of the grains all the conditions for freezing are given, whereas in the grain-free regions they are not. Any point of the straight line $P_m P_f$ corresponds therefore to a state, where some percents of the total system are already frozen and the others are not. But this is achieved in such a way that the frozen parts are concentrated on the grains and reversed. But if we

pick out a frozen region, this region is not adiabatically shut off from the other parts of the system and therefore the energy balance cannot be made for this part alone. However, the entropy of the individual parts of the total system can be discussed. This discussion shows that the entropy change in the frozen region of the system must have a very large negative value, whereas in the neighbouring undercooled regions it has less negative values, so that in total the entropy change (together with that of the cooler) is positive. That would mean that in the regions of the crystal grains the process is — at least locally — not submitted to the law of largest positive entropy change. We conclude therefore, that the natural process must be that of undercooling. The situation is somewhat altered, if we provide in some other way for the fulfilment of the second condition for freezing. We also have to furnish the freezing system with the necessary atoms in the proper positions. This is made easier if the atoms have a larger chance of finding the right place in the system, either by stirring or shaking. These operations supply always a positive entropy change and so the large negative entropy change by freezing can be counterbalanced, and freezing accomplished. Undercooling is therefore possible only under totally undisturbed conditions.

According to the above, undercooling can be accomplished in principle down to a temperature which corresponds to the tangent in the upper point of inflexion.

Therefore if the crystal structure and the binding energy are given, we have two relations between the three quantities: virtual subcrystallite size (n_0), melting temperature (T_m) and maximum undercooling temperature (T_{uc}). If any one of the three is given, the other two can be calculated.

A first approximation of the melting temperature can be calculated with the assumption that the substances may be undercooled right down to the absolute zero temperature. This assumption is not justified experimentally, but it is a well-known fact that sometimes a system can be undercooled even down to very low temperatures. The condition for such an undercooling is that the tangent in the upper inflexion point is horizontal. The condition for the horizontal tangent is

$$\frac{e'}{s'} = 0, \quad (98)$$

where the sign denotes differentiation with respect to p . The condition for the inflexion point is similarly

$$\frac{e'' s' - e' s''}{s'^3} = 0 \quad (99)$$

Since $s' \neq 0$, these give the simultaneous conditions

$$e' = 0 \quad (100)$$

and

$$e'' = 0. \quad (101)$$

According to (73) equs. (100) and (101) can be written in the form

$$f' + \frac{1}{n_0} g' = 0 \quad (102)$$

and

$$f'' + \frac{1}{n_0} g'' = 0. \quad (103)$$

Eliminating n_0 from (102) and (103) we have

$$g'' f' - g' f'' = 0. \quad (104)$$

As we stated after equ. (84), the curves of Fig. 4 give the n_0 resulting from (84), if we use there the equation sign instead of the inequality. (104) determines the minimum point of these curves and (102) the values of n_0 corresponding to these minimum values. These are the values (85) and (86): thus we conclude that the assumption of the possibility of undercooling to the absolute zero temperature implies the choice of the largest possible values of n_0 . Our assumption means $T_{uc} = 0$. Finally, T_m can be constructed from the e — s diagrams with these maximum n_0 .

As we have stated in section 7, to be consequent we would have to determine n_0 by minimizing the free energy of the system with respect to the variation of n_0 . This procedure would be, however, very involved, so that we do not follow this way. In the present treatment we approximated by taking into account the dependence on n_0 only to the first power of $\frac{1}{n_0}$ in a power series in powers of $\frac{1}{n_0}$. So in this approximation the minimization with respect to n_0 is meaningless. Consequent minimization could be carried out in a higher approximation only. That is why we have followed the inconsequent way of determining n_0 further above from some other considerations.

Fig. 6 represents the e — s curves for the cubic and for the diamond structures constructed with the maximum n_0 values (85) and (86). The melting entropy is the difference of the abscissae of the two points of contact of the double tangent. According to (77) we may evaluate this value in cal/molgrade. In Table I we give the experimental values of the melting entropy together with the theoretical values calculated here.

Table I

Calculated and experimental melting entropies in cal/molgrade

	ΔS experimental	ΔS calculated
Li.....	2,43	2,16
Na.....	1,70	
K.....	1,72	
Rb.....	1,70	
Cs.....	1,66	
Cu.....	2,29	
Ag.....	2,19	
Au.....	2,27	
average.....	2,00	2,16
C (diamond) ..	—	2,28

Table I shows that there is a connection between the crystal structure and the melting entropy. The melting entropies of the b. c. c. alkali metals (except Li) are fairly constant and so are the melting entropies of the f. c. c. noble metals. The exception, Li, shows probably a transition to molecular binding and this explains its high value. The difference in the b. c. c. and the f. c. c. structures cannot be given by the present simplified treatment.

The melting temperature can now be calculated knowing the proper values of β . Here we deal only with the simplified treatment outlined with the assumption of the possibility of undercooling to the absolute zero. In a following paper we shall discuss the complete connection between n_0 , T_m and T_{uc} .

In our particular case, $T_{uc} = 0$, we now have to fix the values we shall use in the calculations. For an ideal crystal HOFFMANN [17] could correlate the βz — values with the binding energy of the crystals. According to this we have in our notation:

$$E_b = 2,0048 \beta z, \quad (105)$$

where E_b is the binding energy per atom and we write in our notation βz for β in the paper quoted. The $A\beta_0 z$ — values determined from the experimental values of the binding energies at room temperature are given in Table II. The experimental values were taken from the compilation of BICHOWSKY and ROSSINI [18].

The values of Table II are room temperature values and since most of the melting temperatures are far from room temperature, we are for this reason compelled to make a correction in the β value. This is in contradiction

Table II

 $A\beta_0 z$ values in kcal/mol according to (97)

Li	Na	K	Rb	Cs	Cu	Ag	Au	C (diamond)
19,45	12,92	9,88	9,43	9,38	40,50	33,92	45,89	84,80

to our previous assumption of constant β , but the error made in this way is smaller than that committed by using the β_0 -value for room temperature.

To establish the temperature correction we remark that β is essentially the exchange integral of two neighbouring atoms (see e. g. reference [5]). The wave function occurring in this exchange integral is of the form

$$\psi \sim e^{-\gamma r}, \quad (106)$$

where γ is a constant, the Slater exponent.

The exchange integral is therefore in a crude approximation of the form

$$\beta \sim e^{-2\gamma d}, \quad (107)$$

where d is the distance of two neighbouring nuclei. If β_0 is the exchange integral in the case, where the two neighbouring nuclei are at the distance d_0 , we conclude from (107):

$$\beta = \beta_0 e^{-2\gamma(d-d_0)}. \quad (108)$$

Now the temperature correction consists in the correction of β for the change of the interatomic distance caused by the change of temperature. The latter is connected with the linear expansion coefficient, α of the substance by

$$\frac{d - d_0}{T - T_0} = \alpha d_0. \quad (109)$$

(108) can be written with the aid of (109) as

$$\beta = \beta_0 e^{-2\gamma \alpha d_0 (T - T_0)}. \quad (110)$$

The exponent in (110) is so small that we can expand the exponential in powers of the exponent in a Taylor-series and neglect the terms of orders higher than the first one. So we have instead of (110):

$$\beta = \beta_0 [1 - 2\gamma \alpha d_0 (T - T_0)]. \quad (111)$$

We have for the melting temperature using (73) and (77)

$$\begin{aligned} T_m &= \frac{dE}{ds} = \frac{A\beta z}{Ak} \frac{de}{ds} = \frac{A\beta z}{Ak} \operatorname{tg} \varepsilon = \\ &= \frac{A\beta_0 z}{Ak} [1 - 2\gamma a d_0 (T_m - T_0)] \operatorname{tg} \varepsilon. \end{aligned} \quad (112)$$

From (112) we can express T_m as follows:

$$T_m = \frac{\frac{A\beta_0 z}{R} (1 + 2\gamma a d_0 T_0) \operatorname{tg} \varepsilon}{1 + \frac{A\beta_0 z}{R} \cdot 2\gamma a d_0 \operatorname{tg} \varepsilon}, \quad (113)$$

where $R = Ak$ is the gas constant, $R = 1,9864$ cal/molgrade. For the cubic crystals we have from Fig. 6

$$\operatorname{tg} \varepsilon = 0,0875, \quad (114)$$

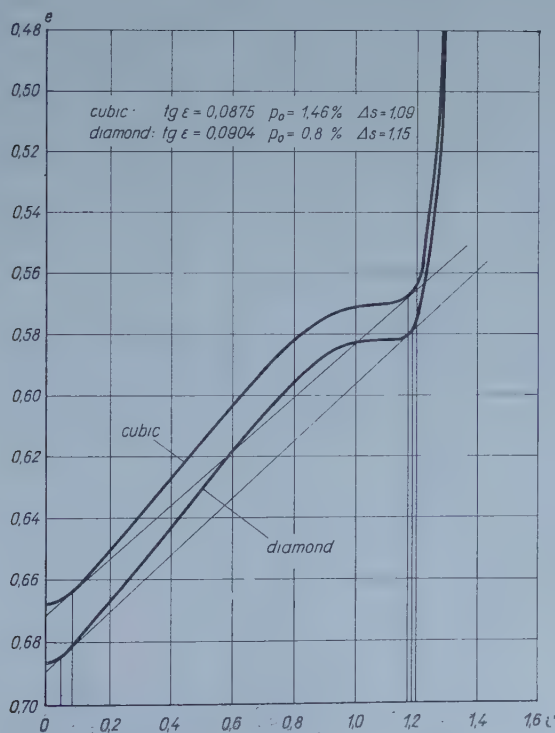


Fig. 6. $e-s$ curve for the maximum n_0 -values for cubic and diamond structures

and for a diamond-type crystal

$$\operatorname{tg} \varepsilon = 0,0904. \quad (115)$$

In Table III we summarize the values of the constants needed to evaluate T_m from (113) with $T_0 = 293^\circ \text{ K}$ (20° C).

Table III

The Slater exponent, γ , the thermal expansion coefficient at room temperature, α , the nearest-neighbour distance at room temperature, d_0 , and the value of $2\gamma\alpha d_0$

	γ (1/Å)	α (10^{-6} /grade)	d_0 (Å)	$2\gamma\alpha d_0$ (10^{-4} /grade)
Li	1,2283	58	3,040	4,3315
Na	1,3857	71	3,707	7,2942
K	1,1236	84	4,616	8,7134
Rb	1,0393	90	4,867	9,1049
Cs.....	0,9898	97	5,239	10,0600
Cu	1,8896	16,5	2,553	1,5920
Ag	1,7479	18,7	2,885	1,8860
Au	1,6647	14,2	2,878	1,3606
C (diamond) ..	3,0718	1,18	1,540	0,1116

The melting temperatures can now be calculated using (113), (114), (115) and the data of Table II and III. These values and the experimental ones are given in Table IV.

Table IV

Calculated and experimental melting points

	T_m calculated (K°)	T_m experimental (K°)
Li	704,3	575,0
Na	488,1	370,9
K	396,0	336,7
Rb	381,7	312,2
Cs.....	377,8	301,7
Cu	1454,3	1357,2
Ag	1230,3	1233,7
Au	1655,0	1336,2
C (diamond) ...	3712,0	3973

The next approximation in this theory would take into account the finite undercooling. However, as sufficient experimental data for the maximum undercooling temperature are not available, the following discussion seems to be of use. From the *known* melting temperature values we can calculate the virtual subcrystallite size and the maximum undercooling temperature at the same time. With these data the maximum undercooling temperature can be compared with the available undercooling temperatures. On the other hand, if we know the maximum undercooling temperatures exactly enough, we can calculate from these values the melting temperature and the virtual subcrystallite size.

These calculations will be given in another paper, however, we can state, that the melting points given here for $T_{uc} = 0$ will in any case increase in the case $T_{uc} > 0$.

One can see from Fig. 6 and equ. (77) that the vacancy concentration p increases at melting from a value of 1,5—2% to a value of about 40%. This would mean according to (78) a similar change in the volume at melting. However, this change in volume seems to be too large and the high percentage of vacancies in the liquid phase calls also for an explanation.

The high vacancy concentration would mean in a linear chain the total disintegration of the chain. In the planar, or even in the spatial case, however, this high vacancy concentration does not bring about the disintegration of the system. The remaining atoms, namely, may preserve a skeleton, which contains a very high number of vacancies and which all the same does not fall into pieces. The reason for this lies in the high coordination number arising in the planar and spatial cases.

The large increase in volume on account of the high vacancy concentration is partly compensated by the local shortening of the nearest-neighbour distance in the case of diminishing coordination number. The experimental data for the nearest-neighbour distance in metal and in molecules built up from two metal atoms show for instance for the alkali metals that the latter is about 0,85 that of the former. This is connected with the fact that in the metal the coordination number is 8, whereas in the molecule it is 2. This shortening would mean a decrease in the volume, i. e. $0,85^3 = 0,614$, i. e. of about 40%. In the case of melting the effective decrease in the coordination number is not so great as the decrease from 8 to 2, but it is still considerable, the decrease in volume will be therefore less than 40%. This and the increase caused by the large vacancy concentration can explain the 10—15% increase in volume at melting.

We conclude with the assertion that the theory describes quite correctly the observed anomalies in the specific heat of the alkali metals near the melting points. This will be discussed in another paper.

10. Acknowledgements

The author gratefully acknowledges the help of Mr. A. KORODI, Mrs. HEDDA HOFFMANN, Mrs. MAGDALENE KÁDÁR and Miss MONICA GROFCSIK in carrying out the numerical calculations.

REFERENCES

1. N. v. RASCHEVSKY, Z., Phys. **40**, 214, 1927; W. BRAUNBECK, Z. Phys., **38**, 549, 1926; K. F. HERZFELD and M. GOEPPERT-MAYER, Phys. Rev., **46**, 995, 1934; M. BORN, J. Chem. Phys., **7**, 591, 1939; J. H. C. THOMPSON, Phil. Mag., **44**, 131, 1953.
2. H. J. EYRING, J. Chem. Phys., **4**, 283, 1936; J. FRENKEL, Trans. Far. Soc., **33**, 58, 1937; J. E. LENNARD-JONES and A. F. DEVONSHIRE, Proc. Roy. Soc., **A169**, 317, 1939; **A170**, 464, 1939; O. K. RICE, J. Chem. Phys., **7**, 883, 1939; J. KIRKWOOD and E. MONROE, J. Chem. Phys., **8**, 845, 1940; **9**, 514, 1941; G. LEIBRIED, Z. Phys., **127**, 344, 1950.
3. H. J. EYRING and J. O. HIRSCHFELDER, J. Phys. Chem., **41**, 249, 1937; J. E. MAYER, J. Chem. Phys., **10**, 629, 1942; **15**, 187, 1947; W. G. McMILLAN, Jr. and J. E. MAYER, J. Chem. Phys., **13**, 276, 1945; J. O. HIRSCHFELDER, C. F. CURTISS and R. B. BIRD, Molecular Theory of Gases and Liquids, pp. 234–328, Wiley and Sons, New-York, 1954; R. A. ORIANI, J. Chem. Phys., **19**, 93, 1951; D. TURNBULL, Solid State Physics, Vol. 3, pp. 226–251, Academic Press, New-York, 1956.
4. N. F. MOTT and R. W. GURNEY, Trans. Far. Soc., **35**, 364, 1939; R. FÜRTH, Proc. Roy. Soc., **A183**, 87, 1944; Phil. Mag., **40**, 1227, 1949; A. OEKAWA, J. Phys. Soc. Japan, **3**, 295, 1948; **7**, 543, 1952; Bull. of the Kobayashi Inst. of Phys. Research, **2**, 45, 1952; T. A. HOFFMANN, The Theory of Melting of One-Valency Metals, Thesis, Budapest, 1956.
5. T. A. HOFFMANN and A. KÓNYA, J. Chem. Phys. **16**, 1172, 1948; Acta Phys. Hung., **1**, 5, 1951.
6. See e. g. JAHNKE—EMDE, Tafeln höherer Funktionen, 5 ed. p. 18, Teubner Verlag, Leipzig, 1952.
7. See e. g. J. C. SLATER, Introduction to Chemical Physics, pp. 23–30, McGraw-Hill, New-York and London, 1939.
8. G. W. STEWART, Phys. Rev., **30**, 232, 1927; **31**, 174, 1928; **35**, 726, 1930; **37**, 9, 1931.
9. M. BORN, Proc. Math. Phys. Soc., Egypt., **3**, 35, 1947.
10. R. FÜRTH, Proc. Roy. Soc., **A183**, 87, 1944.
11. R. FÜRTH, Phil. Mag., **40**, 1227, 1949.
12. W. L. BRAGG, Nature, **149**, 511, 1942; Report of the Conference on Strength of Solids in Bristol, 1947, p. 26.
13. W. A. WOOD, Proc. Roy. Soc., **A172**, 231, 1939; Nature **157**, 585, 1943; W. A. WOOD and W. A. RACHINGER, Nature, **162**, 891, 1948.
14. R. O. SIMMONS, Private communication; further R. O. SIMMONS and R. W. BALLUFFI, Phys. Rev., **117**, 52, 1960; R. W. BALLUFFI and R. O. SIMMONS, AEC Report AT (11–1)—182, 1960.
15. See e. g. J. R. PARTINGTON, An Advanced Treatise on Physical Chemistry, Vol. II, Longmans, London, 1952, p. 161.
16. H. RICHTER, private communication.
17. T. A. HOFFMANN, J. Chem. Phys., **18**, 989, 1950; Acta Phys. Hung., **2**, 97, 1952.
18. F. R. BICHOWSKY and F. D. ROSSINI, The Thermochemistry of the Chemical Substances, Reinhold Publ. Corp., New-York, 1936.

ТЕОРИЯ ПЛАВЛЕНИЯ

Т. А. ГОФФМАНН

Резюме

Энергия конечного реального кристалла выражается через энергии атомов и вакансий сплава. Эта энергия является функцией концентрации вакансий и размера кристаллического блока. Энтропия смешивания кристалла есть функция концентрации вакансий. Для определенного размера блока кривая энергия-энтропия имеет две точки перегиба. В этих случаях температура плавления определяется общей касательной к кривой; энтропией плавления является интервал между двумя пунктами касания. В качестве необходимого условия для нормального плавления получается определенный размер блока. Результаты щелочных и благородных металлов и для алмаза хорошо согласуются с экспериментальными данными.



INVESTIGATIONS CONCERNING THE RETENTION OF FISSION PRODUCTS ON HUMIC ACIDS

By

A. SZALAY and M. SZILÁGYI

INSTITUTE OF NUCLEAR RESEARCH OF THE HUNGARIAN ACADEMY OF SCIENCES, DEBRECEN, HUNGARY

(Received: 20. IV. 1961)

The retention of a number of fission products on humus-rich peat preparations has been investigated. At a favourable p_H (5—6) the following elements are firmly fixed: all rare earths; Y, Sr, Cs, Zr isotopes. They are firmly fixed by cation exchange on peat with an enrichment constant (distribution coefficient) of about 10.000 : 1. Some fission products are certainly not fixed by humus, such as isotopes of iodine, Nb, not to mention the inert gases. The significance of this retention is dealt with, from the point of view of the treatment of fission product contaminated waste waters of the atomic industry and the circulation or retention of fission products carried down into the humus-rich fertile soil by atmospheric precipitation.

Introduction

The retention of cations by humic acids

The senior author observed in 1951 [1] that U is very firmly fixed, *i. e.* adsorbed by humic acids and fossil forms of plant debris (peat, lignite, brown coal), which contain large amounts of humic acids. As it is well-known, they can be regarded as fossil humic acid concentrates.

The investigations of the senior author showed that this adsorption is the responsible factor for the well-known geochemical concentration of U in bioliths [2].

These investigations which were carried out in an equilibrium state between water phase and humus-rich peat phase demonstrated that the distribution coefficient of the $(\text{UO}_2)^{++}$ cation between the two phases is 1 : 10.000 in order of magnitude under favourable conditions ($p_H \sim 3-5$).

If we mix one gram of a peat preparation with a larger volume of water and add some microequivalents of a uranyl-salt solution, adjust the p_H to a value of about 5, then separate it by filtering the water from peat, we observe that U will almost completely disappear from the water and the U-content of one gram of peat will be about 10.000-times higher than that of one gram of water.

We may call this quotient of distribution between the two phases *distribution coefficient*.

If higher concentrations of $(\text{UO}_2)^{++}$ solutions are used, saturation will take place. The saturation capacity of various peat preparations amounts to

largely similar values of about 1—3 milliequivalents of $(\text{UO}_2)^{++}$ per gram of dry peat.

Further experiments were directed to clarify the fixation phenomenon itself. Radioactive tracer experiments demonstrated that the fixation process is reversible and exchangeable. The fixed cations can be easily exchanged by another isotope of the same chemical element as well as by a cation of another element. E. g. the adsorbed $(\text{UO}_2)^{++}$ cations can be replaced either by Th^{4+} cations or by H^+ cations at a $p_H < 3$. These experiments have shown that the process is actually a cation exchange process, effective at least for a number of other cations too. This property seems to be identical with cation-exchange properties of the humus of fertile soil long known for some elements of lower atomic weight (e. g. Ca^{++} etc.).

The reversibility of fixation shows that the cations are not fixed by some irreversible organic complex bond onto a polymer molecule as assumed recently by MANSKAJA et al. [3], [4]. It is a cation exchange process, even if it appears on account of the very high distribution coefficient to be something else.

In the case of cations of high atomic weight or high valence, the distribution coefficient of the cation relating to humus and water is extremely high, of the order of 10.000—30.000 : 1, at a favourable p_H of 3—5.

The exchange process is very rapid and the equilibrium sets in within a few seconds. In fact, the velocity cannot be measured. In contrast to synthetic cation exchangers, the cation exchange on humic acids takes place upon a surface and not in a volume.

Numerical characterization of cation exchange properties of a given humic acid preparation

By observing the properties of the fixation process, the necessity and possibility arose to develop a useful mathematical formalism for the numerical treatment of the observed phenomena.

The detailed deduction of the following formula — which gives a good numerical representation of the process of fixation — was previously published by the senior author [5], [6], wherefore only a short summary will be given here:

Starting from the two experimentally stated conditions:

- 1) the condition of reversibility and
- 2) the condition of saturability

one is lead to an equation similar to the Langmuir adsorption isotherm:

$$N = N_{\infty} \frac{ac}{1 + ac},$$

where c denotes the equilibrium concentration of uranium in the aqueous phase, N the concentration of uranium in the humus-rich phase (peat)

(in meq/g), N_{∞} denotes the saturation capacity of 1 gram of peat for ($\text{UO}_2/\text{meq/g}$) and a is an empirical constant.

The observed adsorption isotherms (Fig. 1) can be very well represented by this formula [5], if the experiments are carried out at a constant p_H -value. In this respect it is more suitable to speak of iso- p_H -curves instead of isotherms. The behaviour of a given humus or peat preparation can be characterized by two constants. One of them is the distribution coefficient ($N_{\infty} \cdot a$) and the other is the saturation capacity (N_{∞}).

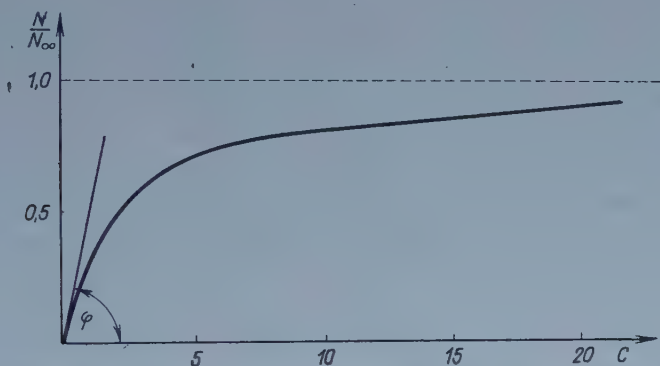


Fig. 1. The adsorption isotherm of (UO_2)** on humus-rich peat. Ordinate: equilibrium concentration of (UO_2)** on peat. Abscissa: equilibrium concentration of (UO_2)** in the water phase

After the investigations concerning (UO_2)⁺⁺, a number of other cations of high atomic weight were investigated in this laboratory [5], [7], [8].

I. SZABÓ [7] investigated a number of cations and determined their distribution coefficients and saturation capacities in a specific peat preparation (see Table 1).

Table 1

Saturation capacity and distribution coefficient of a specific peat preparation with respect to some cations measured by I. SZABÓ [7]

Cation	Saturation capacity (N) in meq/g	Distribution coefficient $N \cdot a$
Ni^{++}	0,80	$0,0451 \cdot 10^4$
Fe^{++}	0,66	$0,0910 \cdot 10^4$
Cu^{++}	0,70	$0,2380 \cdot 10^4$
UO_2^{++}	0,72	$0,8600 \cdot 10^4$
Th^{4+}	1,00	$2,1000 \cdot 10^4$
La^{+++}	0,80	$2,3000 \cdot 10^4$
Cr^{+++}	1,38	$0,0770 \cdot 10^4$
Fe^{+++}	1,35	$2,6500 \cdot 10^4$

E. BRÜCHER [8] compared the fixing of U^{4+} with that of $(UO_2)^{++}$ and stated, that quadrivalent U^{4+} is more firmly fixed than bivalent $(UO_2)^{++}$.

Prospects of the retention of fission products by humic acids

It is well known that fission products contain a great number of cations of high atomic weight, and of one or more valencies. Since it has been known for many years at this laboratory that La and other rare earth metals are firmly fixed by humus at a distribution coefficient of about 20.000, we decided to investigate in detail the fixation of the fission products by means of humus-rich peat preparations under favourable conditions.

This problem is not a simple one, because the number of primary radioactive fission products is about 90 [9], and considering their radioactive daughter-products [9] this number is raised to about 200. The number of elements of the periodic system involved is about 36 extending from $Z = 30$ up to $Z = 66$.

The importance of this problem need not be emphasized. The following significant subjects are involved:

- 1) Decontamination of the waste waters of atomic industry;
- 2) Fission products of nuclear test explosions carried down into the humus-rich soil by rain water.

Waste disposal is a great problem of the growing atomic industry. In the industrial processes of the treatment of "burnt out" fuel rods, various types of waste liquors are produced. Those of high concentration and small volume are to be concentrated and reserved. Other waste waters of medium radioactive contamination have too large volumes to be reserved and also are too contaminated to be dispersed in nature. They must be treated somehow before dispersal. The treatment is to be cheap and reliable, and it should give a high volume concentration of fission product contamination.

As we have seen above, humus-rich peat preparations seemed to be very promising for this purpose. Peat is a very cheap natural cation exchange resin for cations of higher atomic weight. The distribution coefficient of 10.000 may concentrate some of the radioactive contamination of waste waters in the proportion of 1 : 10.000. A further concentration is easily manageable by burning the peat in a special suitable incinerator, where its weight is reduced to the weight of its ash content (5—10%) and its volume is concentrated to a very small fraction. Further disposal of wastes concentrated in this way is a problem identical with the treatment of other concentrated wastes.

The following question arises now: which of the 200 or so fission products are fixed by peat, and which are not?

In our earlier experiments [10], we concentrated our attention on some long-lived or biologically dangerous fission products: Cs-137, Sr-90, J-131, Y-90, Ba-140, La-140.

We observed that the above isotopes are firmly fixed by peat with the exception of anion J-131, which is not fixed at all. We prepared a cation exchange column from humus-rich peat and observed that, in the process of elution, trivalent Yttrium is more firmly fixed than Sr-90; La-140 is more firmly fixed

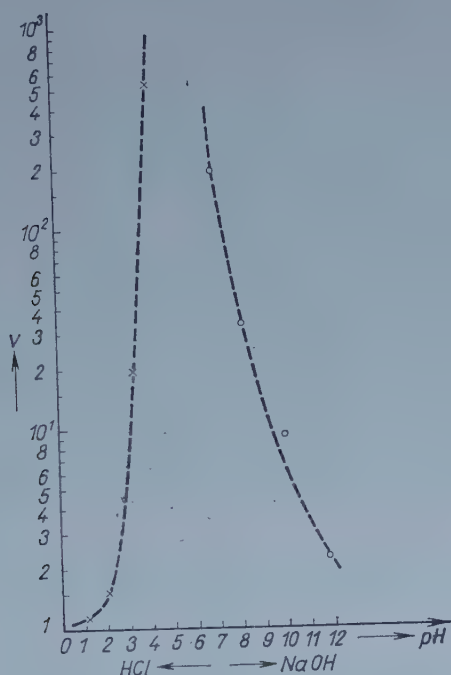


Fig. 2. The "break-through volume" of a humus-rich peat exchange column on which Ba 140 is fixed. Abscissa: p_H units. Ordinate: the volume of eluant, necessary to start the elution of fixed Ba-140, in multiples of the volume of the cation exchange column

than Ba-140; and La-140 is better fixed than Y-90. The difference between Sr-90 and Cs-137 is not very pronounced, but Cs-137 is somewhat more firmly fixed than Sr-90.

The elution can be carried out by H^+ -ions in the form of HCl, in concentrations of 0.01 n or higher. Similarly, the elution can be carried out by NaCl, $FeCl_3$ or $CaCl_2$ -solutions which are able to drive out radioactive cations if used in sufficiently high concentrations.

The influence of the p_H upon the retention of cations by humic acid is very pronounced. Fig. 2 shows the influence of p_H upon the "break-through volume" of a humus-rich peat exchange column on which Ba-140 was fixed.

The ordinate shows the volume of eluent necessary to elute the fixed Ba-140 in multiples of the volume of the cation exchange column. The curve takes on a value of 500 at $p_H = 4$ and rises to an immeasurable height at the optimum p_H of about 5. If the p_H is approaching 7, 8 or more, the humus dissolves into a yellow colloidal solution of Na-humate, and the Ba-140 cations are liberated partly by this factor and partly expelled by the surplus of Na^+ cations.

Present investigations on mixed fission products

a) Activation of fission products by n-irradiation of U_3O_8 and their electrophoretic and nuclear spectroscopic analyses

The aim of the investigations described in this paper was to inquire into the retention properties of a humus-rich preparation with respect to a large number of fission product isotopes.

Very short-lived fission products are from this point of view less important. The investigations of some of the most dangerous long-lived isotopes (Sr-90 and Cs-137) were reported in a previous paper [10]. It seemed advantageous to us to carry out an experiment in the following way:

A one gram sample of U_3O_8 was irradiated in a reactor of the swimming-pool type for 4 hours, at a thermal neutron flux of 10^{13} .

After irradiation and six months decay time, when the short-lived products practically died out, U_3O_8 was dissolved in concentrated HNO_3 and adjusted to 10 n.

The fission products were separated from uranyl nitrate by solvent extraction with aether (free of peroxide), repeated four times. The nitric acid phase was free of U, but one part of the fission product activity passed into the aether phase. The nitric acid phase containing the majority of fission products was evaporated and taken up again with 1 cc of 1 n nitric acid.

As to the fraction extracted by aether nitric acid solvent extraction, its gamma activity amounted roughly to one third of that of the total fission products as measured in Ra gamma equivalents by a GM counter. According to the paper of H. FREISER and GEORGE H. MORRISON [11], the following elements of the periodic system can be expected as partially extracted together with $(\text{UO}_2)^{++}$: Zr, As, Ce(IV).

Further investigation of this fraction is in progress.

The solution of mixed fission products was first investigated by paper electrophoresis. A drop of about 3 microliter of the solution was placed on a strip of Whatman filter-paper wetted by 1,2% NaNO_3 solution. After an electrophoresis of 2 hours at 280 V, the strip was dried and the distribution of activity along it was measured with an automatic registering beta-counting equipment. Figure 3 demonstrates the result. The activity was resolved into

four major groups. One of them (group D) migrated towards the anode and so consisted of anions. The other 3 groups were cations migrating towards the cathode. The paper strip was cut into pieces after the separation experiment, and the gamma radiations of the 4 groups were separately investigated by means of a scintillation gamma spectrometer.

No gamma radiation was detected in group "A". It seemed to consist entirely of beta emitters.

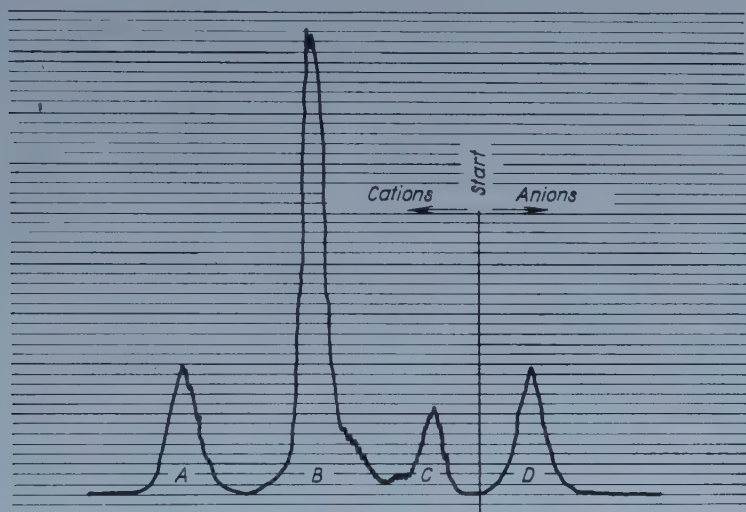


Fig. 3. The distribution of fission products after a paper electrophoretic test. The figure demonstrates an anionic group (D) and three cationic groups (A, B, C)

We investigated the beta spectrum of this fraction with a beta spectrometer of the toroid sector type constructed by SZALAY and BERÉNYI [12].

The analysis of the beta spectrum and the determination of the half period showed that most of the observed activity resulted from Sr-89. The presence of Sr-90 was not significant and could not even be expected for the short irradiation time of I_3O_8 .

The gamma spectrum of group "B" showed three characteristic peaks of 0,034, 0,080, 0,133 MeV energy and a long continuous spectrum in which no peaks could be resolved, extending up to about 1,5 MeV.

The energy of the photopeaks pointed to Ce-144 as being the most probable origin of this activity. To check up on this assumption, the gamma spectrum of a Ce-144 preparation was taken by the same scintillation gamma spectrometer, in the same geometrical arrangement. Both spectra are shown in Figure 3/B. They seem to be identical. The analysis of the beta spectrum

showed roughly one group having a maximum energy of 200 ± 100 KeV and another group having a maximum of more than 2,8 MeV.

There is no doubt that the gamma spectrum belongs to Ce-144 and to its daughter element Pr-144. Group "B" is here the fraction containing the rare-earth cations. It is sure that the rough chromatographic separation techniques used (see later) will not separate the rare-earth elements from each other. All rare earths are fixed by peat in the same manner. The short irradiation

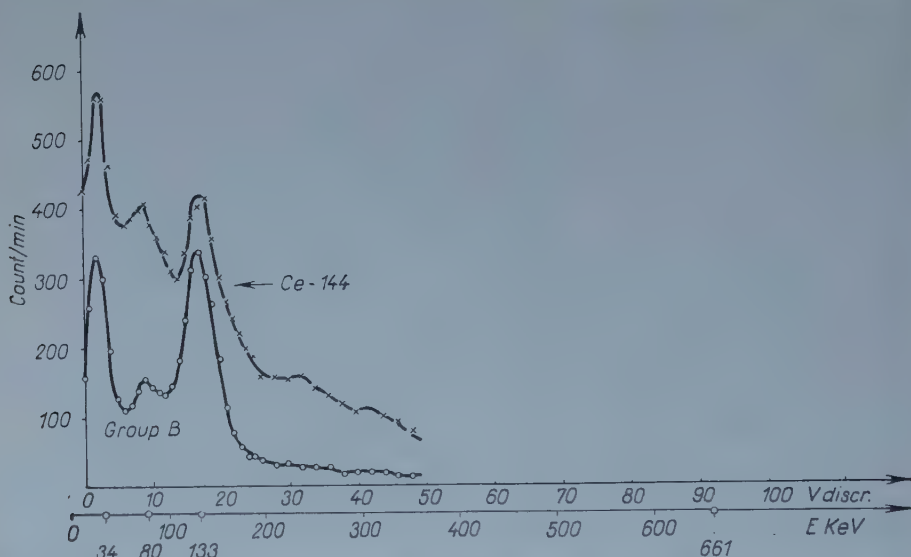


Fig. 3/B. Gamma spectrum of group "B", compared with a Ce-144 isotope preparation. Group "B" shows three characteristic peaks of 34, 80 and 133 KeV

and long cooling down time of the irradiated U_3O_8 results in the presence of other rare-earth isotopes with only insignificant activities, just as we calculated.

The gamma spectrum of group "C" showed an intense photopeak at 0,765 MeV and a complex gamma spectrum, which could not be resolved into peaks. (Figure 3/C.) The beta spectrum showed a maximum energy of about 350 ± 50 KeV.

These facts indicate that this group consists largely of Zr-95. Of course, the presence of other fission products in smaller quantities is not excluded either by the gamma spectrum or by the beta spectrum.

Group "D", which showed anionic character at paper electrophoresis, gave a strong gamma photopeak (Figure 3/D) with an energy of about 0,76 MeV and its beta spectrum had a maximum of 100 ± 50 KeV. This fact indicates that the major component of this group is Nb-95, the daughter product of Zr-95.

Our next experiment was the ion-exchange chromatographic separation of fission products on a column filled with humus-rich peat.

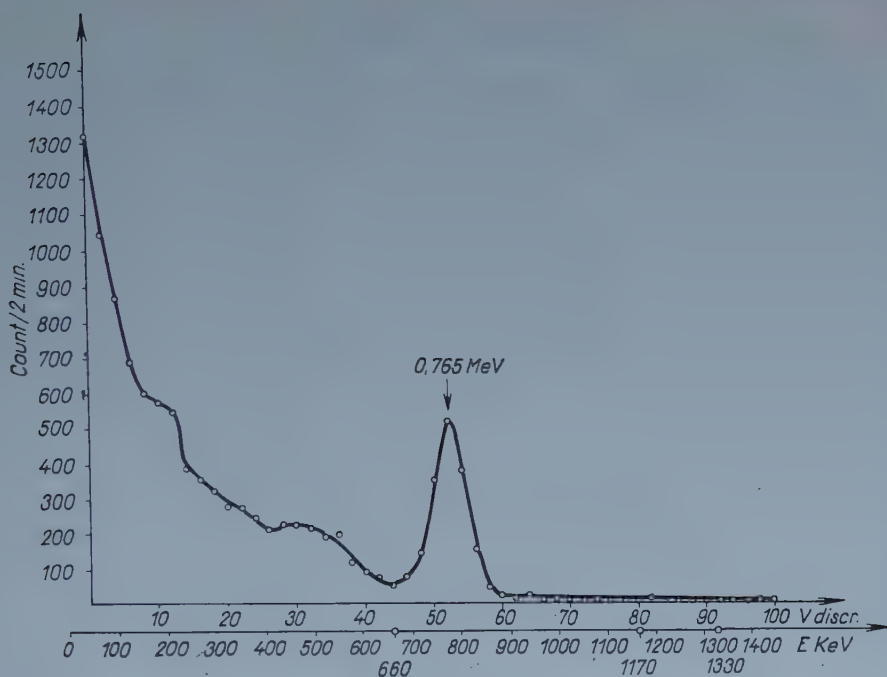


Fig. 3/C. Gamma spectrum of group "C" with an intense photopeak at 0,765 MeV

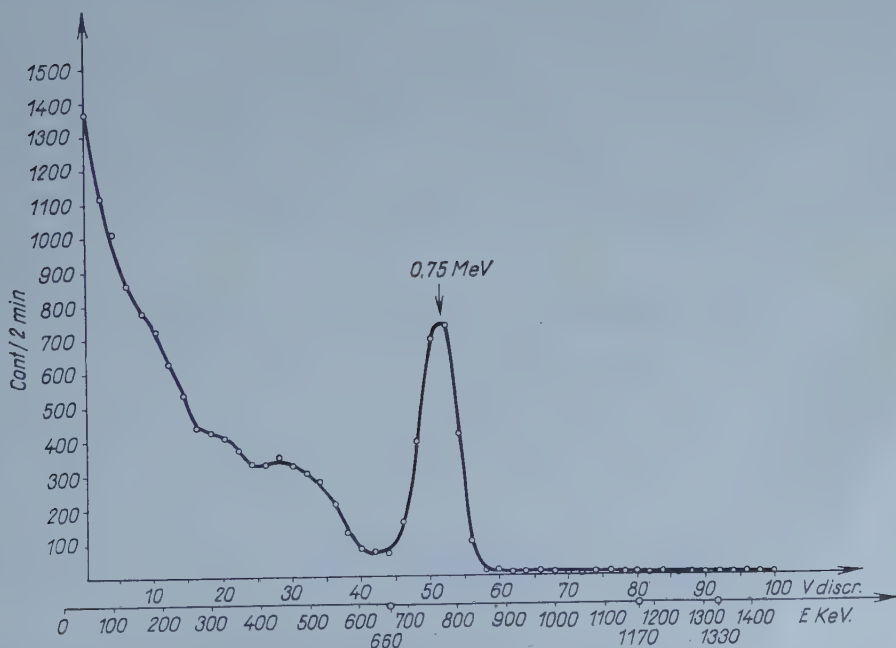


Fig. 3/D. Gamma spectrum of group "D" showing an anionic charater at paper electrophoresis. The preparation shows a strong gamma photopeak with an energy of about 0,76 MeV

b) Preparation of a humus-rich peat

Peat is a rich source of humic acids. It consists usually up to about 50% of humic acids, depending upon origin and progress in fossilization. It is easy to make a concentrated humic acid preparation from peat by extracting it with a 1% NaOH solution and reprecipitating it with dilute HCl. Earlier experience of the senior author showed that this concentration is not practicable and necessary. The concentrated humic acid extracted and precipitated in the above manner has a very fine disperse colloidal structure and it is very impracticable from the point of view of filtration, because it stops the filter paper. It is impossible, or at least impracticable, to prepare a useful chromatographic column from this preparation. Further earlier experiments of the senior author revealed that peat extracted from its humic acid content loses largely its fixation (or exchange) properties with respect to cations. This demonstrates that the fixation of cations by peat is identical with their fixation by its humic acid content. For the above reasons it is more practical both at the laboratory and possibly in industrial application to use peat as a carrier of humic acids in a modestly dispersed form. We dispersed mechanically some low-moor peat which showed an exchange capacity of about 2 milliequivalent/gr, and which was very young at an early stage of fossilization. We purified it from the bituminous and waxy substances by extraction with benzene. Resinous substances and humic acid components of low molecular weight had been extracted with ethylalcohol, and after this procedure we transformed the preparation into a hydrogenous form by treatment with dilute HCl and washed out the surplus of acid by distilled water up to a p_H of 4,5. In this way we obtained a purified peat preparation easily wettable (hydrophil) and rough-dispersed (standard mesh-size between No. 16 and 50, particle size between 0,37—0,12 mm). The preparation showed good cation-exchange properties and its dispersity enabled easy filtration and column chromatography.

c) Chromatography of fission products on a peat column

The purpose of the following experiments was to compare the strength of fixation of the different fission products on peat. A cation exchange column was prepared from the peat preparation described above. A sample of the mixed fission products from irradiated U_3O_8 was poured on it and eluted by HCl of increasing concentration.

The dimensions of the peat column were 0,8 cm in diameter and 17 cm high. The total quantity of the humus-rich peat was 0,75 gr measured in a dry state.

0,02 ccm of the fission product solution was diluted to 5 ccm. This solution was poured over the humus column, and eluted by HCl solutions of in-

creasing concentration in 100 ml steps. The total beta activity of the fission products had been measured before fixation on the humus, and in Table 2 the activity of evaporated eluent fractions was expressed in its percentage.

The fraction belonging to $p_H = 4,9$ may be regarded as non-fixed by humic acids. Between $p_H = 4,9$ and 2, no peak of outstanding intensity came down from the column. In our earlier experiments Cs and Sr started to come down at about $p_H = 2,4$ but a large volume of the eluent was necessary at this p_H . For this reason we preferred to proceed with the elution after $p_H = 4,9$ immediately with $p_H = 1$. We know from our earlier experiments [10], that alkaline cations and alkaline-earth cations must come down in this p_H range.

Table 2

Elution of fission products from a peat column by HCl solutions

Eluant $p_H/100$ ml	Beta activity (%) of the eluate
4,9	0,94
1,0	17,21
1 n	59,66
eluted:	77,81%
rest activity on the column	22,19%

Most of the activity (about 60%) is eluted by 1 n HCl.

As the table shows, a significant fraction (in this experiment about 22% of beta activity) was so firmly fixed on peat, that it could not be eluted by 1 n HCl.

The above experiment was repeated in a manner that the eluate was taken in 1 ccm steps and the beta activity of each sample was measured (Figure 4).

The Figure demonstrates that at $p_H = 4,9$ a group of non-fixed products appears. We proceeded with the elution at $p_H = 1$, where a strong activity appears with a sharp peak within the first eluate samples and afterwards a long sequence of lower activities was observed up to 200 ccm eluate. If the concentration was changed to 0,96 n HCl, a strong activity appeared with a sharp peak within the first eluate samples.

A radiometric test was carried out on the eluate samples of peak activity in the same manner as at the electrophoretic test. The test demonstrated that the peak at $p_H = 4,9$ (non-fixed products) shows the significant presence of Nb-95 and seems to be identical with group "D" (anion-group) of the electrophoretic test. The activity eluted at $p_H = 1$ consists largely of Sr-89 (group "A" of the electrophoretic test). The peak eluted with 0,96 n HCl consists

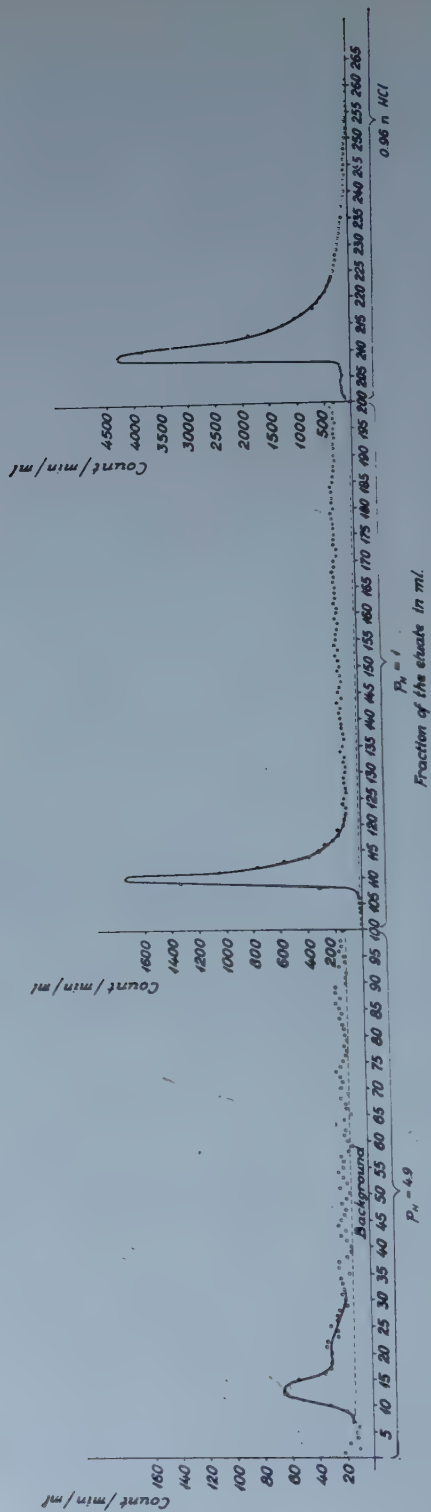


Fig. 4. The elution curve of fission products by HCl solutions

largely of Ce-144 and its daughter product Pr-144 (group "B" of the electrophoretic test). The group firmly fixed on humus and not to be eluted by 0,96 n HCl consists largely of Zr-95 (it is identical with group "C" in the electrophoretic test).

The above observations seem to demonstrate the presence of some fission products only. The total number of fission products is very large but the majority of them has either very short or very long decay periods. The short irradiation time (4^h) of the U_3O_8 sample activates the long-lived isotopes only to a very small extent. Short-lived isotopes decayed during the 6 months cooling down time.

The group eluted at $p_H = 1$ contains all the alkaline earth and Cs. The retention of Rb by humus has to be investigated in a separate experiment. The fraction eluted by 0,96 n HCl should contain all rare-earth isotopes and Y as well. The most firmly fixed group "C" may contain, in addition to the overwhelming Zr, other cations in quadrivalent form. The investigations must be extended in this direction. Group "D" (non-fixed by humus) contains probably not only Nb but also isotopes which are inclined to form complex anions under given conditions (e. g. Ru, Tc, etc.).

The junior author is carrying out further detailed investigations concerning fission products not fixed by humic acids.

Survey of the results

If we regard all the elements of fission products in the periodic chart (Table 3), and denote the cations, which are according to our investigations definitely fixed or definitely not fixed by humus, we see that from a scientific point of view many other elements have to be investigated.

A further series of investigations is necessary to clarify the fixation of some cations (e. g. Rb, Zn, Ga, Rh, Pd, Ag, Cd, In), and some amphoteric elements (Ge, As, Sn).

If we regard this problem from the point of view of public health endangered by the waste waters of a growing atomic industry, the short-lived products can be neglected.

It is practical and customary to store burnt out fuel elements for a cooling down period of about two years. During two years the fission products of a decay period of less than one month decay to less than one millionth part of their initial activity. Table 4 shows fission products with a period longer than one month. They are arranged in groups according to their behaviour with respect to the cation exchange properties of humus, so far investigated.

The results of the present investigations can be generalized for all isotopes of the same element and for all rare-earth cations from the investigated rare-earth elements.

Table 3

H																	He
Li Be																	B C N O F Ne
Na Mg																	Al Si P S Cl A
K	<u>Ca</u>	Sc	Ti	V	Cr	Mn	<u>Fe</u>	<u>Co</u>	<u>Ni</u>	<u>Cu</u>	Zn	Ga	Ge	As	Se	Br	<u>Kr</u>
Rb	<u>Sr</u>	<u>Y</u>	<u>Zr</u>	<u>Nb</u>	Mo	Tc	<u>Ru</u>	<u>Rh</u>	Pd	Ag	Cd	In	Sn	<u>Sb</u>	Te	<u>I</u>	<u>Xe</u>
<u>Cs</u>	<u>Ba</u>	<u>La</u>	Hf	Ta	W	Re	Os	Ir	Pt	Au	Hg	Tl	Pb	Bi	Po	At	Rn
Fa	<u>Ra</u>	Ac															

<u>Ce</u>	<u>Pr</u>	<u>Nd</u>	<u>Pm</u>	<u>Sm</u>	<u>Eu</u>	<u>Gd</u>	<u>Tb</u>	<u>Dy</u>	Ho	Er	Tm	Yb	Lu
<u>Th</u>	<u>Pa</u>	<u>U</u>	Np	Pu	Am	Cm	Bk	Cf	E	Fm	Mv	102	103

Table 4

Table of the fission products of a period over one month

Firmly fixed by humic acids	Not fixed	Not investigated
Sr-89	J-129	Rb-87
Sr-90	J-131	Ru-103
Y-93	Nb-95	Ru-106
Zr-91	Kr-85	Cd-115 m
Cs-135		Sn-123
Cs-137		Te-127 m
Ce-141		Te-129 m
Ce-144		Tc-99
Nd-144		Se-79
Pm-147		Pd-107
Sm-147		Sn-121 m
Sm-151		Sb-125
Eu-155		Te-125

In the light of these investigations peat or other humic acids containing natural substances are very promising for the waste disposal of the growing atomic energy industry. Peat is a very cheap natural substance and by a very simple treatment it is able to fix the majority of fission products from large volumes of waste waters. For this purpose it is necessary to adjust the p_H of the waste waters to a value of about 5—6 before contacting it with peat. A further condition is that waste waters should not contain large amounts of cations (especially those of higher valency; and high atomic weight, e.g. Ca^{++} , Fe^{+++} , Al^{+++} , Zr^{4+}) because they will saturate the cation exchange capacity of peat and expel fission products. The quantity of fission products expressed in chemical equivalents is very small. 1 Curie Sr-90 amounts to only $1,11 \cdot 10^{-4}$ g equivalents, and 1 Curie Cs-137 amounts to only $1,01 \cdot 10^{-4}$ g equivalents. The quantity of peat necessary for treating waste waters contaminated by fission products is not determined by the volume of water and its fission product content but by its content of other cations.

These investigations throw some light on the retention of fission products in fertile soil. Fission products may be carried down into fertile soil by rain following an atomic weapon test or a reactor accident. It can be assumed that the humus content of the soil is able to fix a great part of the fission products for a considerable period of time. They are probably withheld from the circulation of subsoil waters and from uptake by the roots of plants. The role of humus seems to be more significant than that of clayminerals because the distribution coefficient is very high.

Acknowledgments

We express our best thanks to the Reactor Group of the Central Research Institute of Physics of the Hungarian Academy of Sciences (KFKI) Budapest for the irradiation of U_3O_8 samples, to Mr. D. BERÉNYI and Mr. G. MÁTHÉ for their valuable help with nuclear spectroscopy and to Mr. Cs. UJHELYI for his help with the radiochemical preparations.

REFERENCES

1. S. SZALAY, MTA Műszaki Tud. Oszt. Közl., V. 167, 1952.
2. A. SZALAY, Acta Phys. Hung. 8, 25, 1957.
3. Sz. M. MANSZKAJA, T. V. DROZDOVA and M. P. EMEL'JANOVA: Geochimija, No. 4, 10, 1956.
4. Sz. M. MANSZKAJA, T. V. DROZDOVA and M. P. EMEL'JANOVA, Geochimija, No. 6, 529, 1960.
5. S. SZALAY, MTA III. Oszt. Közl., IV. 327, 1954.
6. A. SZALAY, Proceedings of the 11th United Nations International Conference on the Peaceful Uses of Atomic Energy, Geneva, 1959. Vol. 2. Geneva, United Nations p. 182.
7. I. SZABÓ, MTA Mat. és Fiz. Tud. Oszt. Közl., VIII. 393, 1958.
8. E. BRÜCHER, to be published in ATOMKI Közlemények, 1961.
9. SEYMOUR KATCOFF, Nucleonics, 18, 201, 1960.
10. S. SZALAY and M. SZILÁGYI, MTA III. Oszt. Közl. (to be published).
11. H. FREISERS and G. H. MORRISON, Annual Review of Nuclear Science, 9, 232, 1959.
12. A. SZALAY and D. BERÉNYI, Acta Phys. Hung., 10, 55, 1959.

ИССЛЕДОВАНИЯ ПО СОХРАНЕНИЮ ПРОДУКТОВ ДЕЛЕНИЯ
В ГУМУСОВЫХ КИСЛОТАХ

А. САЛАИ и М. СИЛАДЫ

Резюме

Исследовали удержание большого числа продуктов деления торфовым препаратом, богатым гумусом. При благоприятном рН ($pH = 5-6$) следующие элементы хорошо адсорбировались: все изотопы редкоземельных элементов, Y, Sr, Cs, Zr. Эти связывались на торфе катионным обменом. Фактор обогащения торфа (коэффициент разделения) 10 000:1. Имеются продукты деления, которые определённо не связываются гумусом, как например изотопы иода и Nb и разумеется, инертные газы. Это имеет большое значение для дезактивации отходных вод ядерной промышленности и также для связывания продуктов деления, попавших на гумусовую плодородную почву атмосферными осадками.

CRITICAL COMMENTS ON THE INVESTIGATION OF THE ELECTRON-NEUTRINO ANGULAR CORRELATION BY THE CLOUD CHAMBER METHOD

By

A. SZALAY, J. CSIKAI and J. BACSÓ

INSTITUTE OF NUCLEAR RESEARCH OF THE HUNGARIAN ACADEMY OF SCIENCES, DEBRECEN, HUNGARY

(Received 3. V. 1961)

This paper reports on some important problems arising from the measurement of the angular correlation between electron and neutrino by the cloud chamber method. On the ground of a critical evaluation of the method, our earlier data of measurements for $e-\nu$ angular correlation were revised. We obtained the value of $+0,278 \pm 0,243$ for the angular correlation coefficient. Because of the great statistical error it is impossible to give preference to either the tensor or the axial forms of interaction.

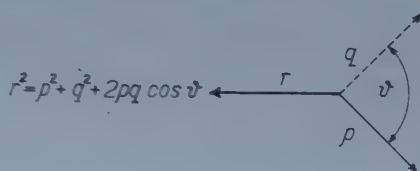
In recent years a number of angular correlation experiments have been carried out on weak interactions in order to determine the form of interaction. Recent experimental check up of earlier contradictory results confirmed more and more the supposition of SUDARSHAN and MARSHAK [1] that the possibility for a universal weak interaction between fermions of all kinds can only be realized in the form of combination VA. In the He^6 -decay, the investigation of electron-neutrino angular correlation plays an important role in the experimental check up of combination VA. In 1957, we successfully managed to take quite convincing cloud chamber photographs of the nuclear recoil effect of the neutrino from the β -decay of He^6 [2], [3]. Some of the photographs revealed such ranges for the recoil nuclei (2—3 mm in a cloud chamber of 200 mmHg filled with $\text{H}_2 + \text{H}_2\text{O} + \text{C}_2\text{H}_5\text{OH}$) which made possible the determination of the angle between β -particles and recoil nuclei and by its means the investigation of $e-\nu$ angular correlation. Our results [4] obtained by $e-\nu$ angular correlation measurement regarding the form of interaction existing in the β -decay of He^6 was in disagreement partly with the theoretical VA — combination, partly with the experimental results of ALLEN et al. [5] obtained by another method for the same decay. Therefore we thought it reasonable to review critically our applied method mainly with respect to the possible occurrence of systematic and subjective errors, first of all, when the events are to be distinguished from the background.

The measurement of $e-\nu$ angular correlation is exceedingly difficult because of the low energy of recoil nuclei and this fact results in a number of problems in the current methods. In this report we are going to give an account of problems of more importance occurring whenever the "cloud chamber method" is applied, which otherwise possesses favourable properties.

The electron-neutrino angular correlation may be measured by the cloud chamber method in the following three ways:

- (i) the energy distribution of recoil nuclei is determined,*
- (ii) the angle between β -particles and recoil nuclei as well as the impulse of β -particles are determined,
- (iii) the energy value of the recoil nuclei is determined at a given E_{β} -energy value.

The basic requirement in all the three cases which determines also the accuracy of the measurement is that the recoil nucleus of low energy should undergo a measurable displacement. In β -decay the impulse and energy of recoil nuclei are given by the following relations:



where r , p and q are the impulses of the recoil nucleus, electron and neutrino; ϑ is the angle between the directions of electron and neutrino. Expressing the impulses by the corresponding energies and making use of the relation $E_R = \frac{r^2}{2M}$, where E_R is the energy of the recoil nucleus and M is its mass, the energy of the recoil nucleus may be expressed as follows:

$$E_R = \frac{(E_{\beta} + 2m_0 c^2) E_{\nu} - E_{\nu}^2 + 2E_{\nu} [(E_{\beta} - 2m_0 c^2) F_{\beta} \cos \vartheta]}{2Mc^2},$$

where E_{β} and E_{ν} are the kinetic energies of the electron and neutrino, respectively and m_0 is the rest mass of the electron. The maximum recoil energy obviously occurs when $E_{\nu} = 0$. In the He^6 -decay $E_{\nu}^{\max} = 3.5$ MeV, $M(\text{Li}^6) = 6,017$ MU, and thus $E_R^{\max} = 1412$ eV. In order that the recoil nucleus at such a low energy may undergo a measurable displacement, a cloud chamber filled with a gas and vapour of a very low pressure and small stopping power must be used.

The determination of angular correlation from the energy distribution of the recoil nucleus with the cloud chamber method does not seem to be favourable for several reasons. Figure 1 shows the calculated energy distribution of recoil nuclei arising from the He^6 β -decay. The calculation was made by taking the whole angle ($0 \leq \vartheta \leq \pi$) and energy spectrum into consideration and by

* TOSHIKO YUASA. Étude du d'invariant de l'interaction Gamow—Teller en désintégration β^- de He^6 , J. Physique Rad., **22**, 169, 1961.

choosing an angular distribution corresponding to the forms of interaction of pure tensor and axial vectors. The energy spectrum of β -particles was taken from RUSTAD and RUBY's [6] measurement. As it can be seen in the Figure, there is a significant deviation in the shape of the energy distribution corresponding to the two forms of interaction at higher energies only.

The energy distribution of recoil nuclei can be determined by the measurement of either the range distribution or that of the droplet number.

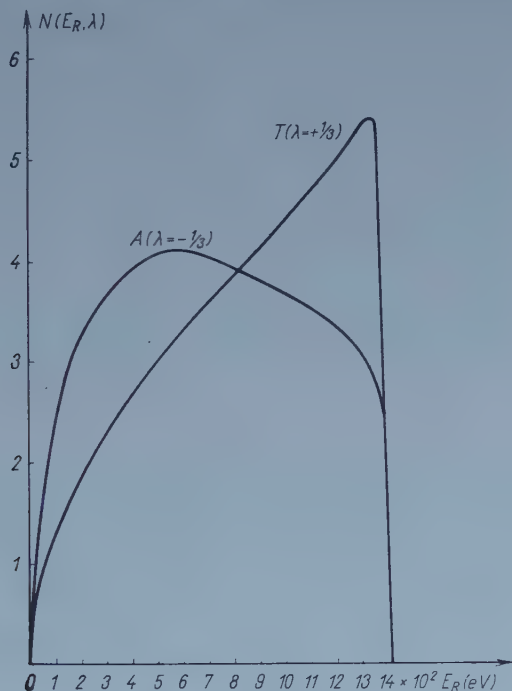


Fig. 1. The calculated energy spectrum of Li^6 -recoil nuclei from He^6 -decay

The determination of the energy of recoil nuclei by counting the droplets is uncertain for several reasons:

- (1) Inside an interval of a few hundred eV for the energy value, the energy loss per ion pair is not exactly known.
- (2) The number of droplets may be changed by molecular dissociation.
- (3) Recombination arising from high ion density decreases the number of droplets.

(4) The heat capacity available at low pressure being small, the heat released by the start of condensation will suddenly decrease super-saturation and thus the droplets enlarged by statistical fluctuation will grow to the disadvantage of the smaller ones. In this way, only a fraction of the ions grow into droplets of visible size. At random expansions, the case is similar in decays

at different points of time after expansion, as the droplets grow into visible size only on a fraction of the later arising ions. This is confirmed by photographs *a* and *b* to be seen in Fig. 2.

(a) Po — α rays emitted at different delays according to the expansion greatly vary in their number of droplets.

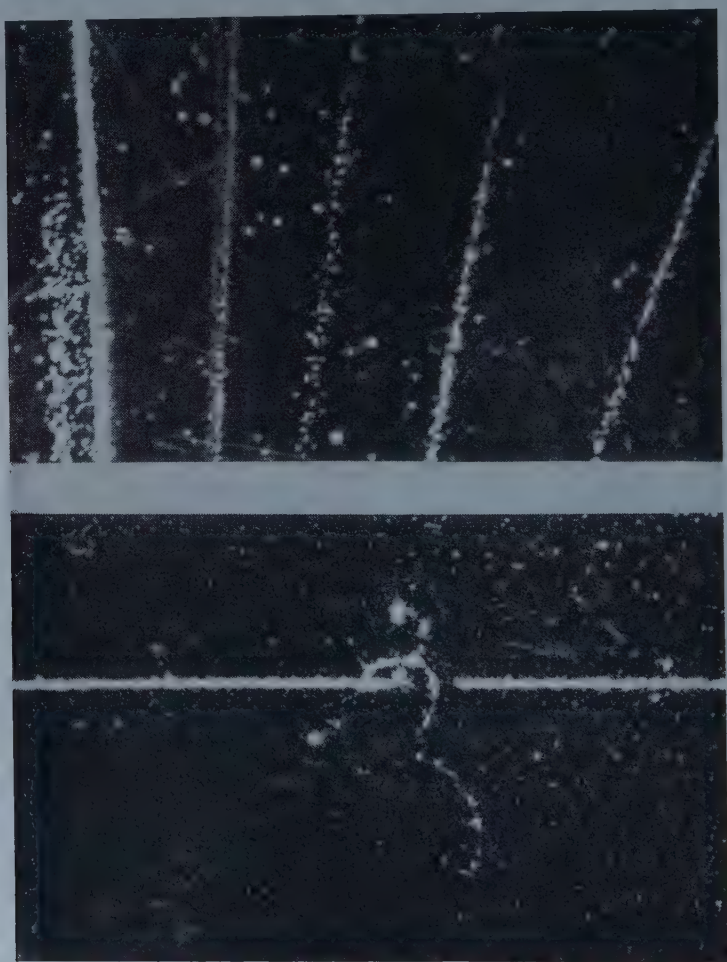


Fig. 2. (a) In a cloud chamber of low pressure, Po — α -particles emitted at different points of time after expansion. (b) The track of an α -particle crosses that of an earlier β -particle and in the area around the crossing point, on the ions produced by the α -particle the droplets have not grown into visible size

(b) The path of an earlier β -particle is crossed by the track of an α -particle, and in a considerable area around the crossing point, on the ions produced by the α -particle, the droplets have not grown into visible size because a local warming up has taken place along the path of the β -particle.

In the determination of the energy distribution of recoil nuclei by measuring the range distribution, the greatest difficulty comes from the fact that for various reasons a considerable fluctuation may occur in the range.

(1) Natural straggling.

(2) The charge of Li^6 -ion produced in the He^6 -decay may vary [7].

(3) The charge of recoil Li^6 -ion may change along its path.

(4) At random expansions, in decays occurring during expansion, a considerable change takes place in the range, considering that the expansion ratio and through it the relative change in pressure is very high at a low pressure. This change can be decreased by applying suitably chosen gas and

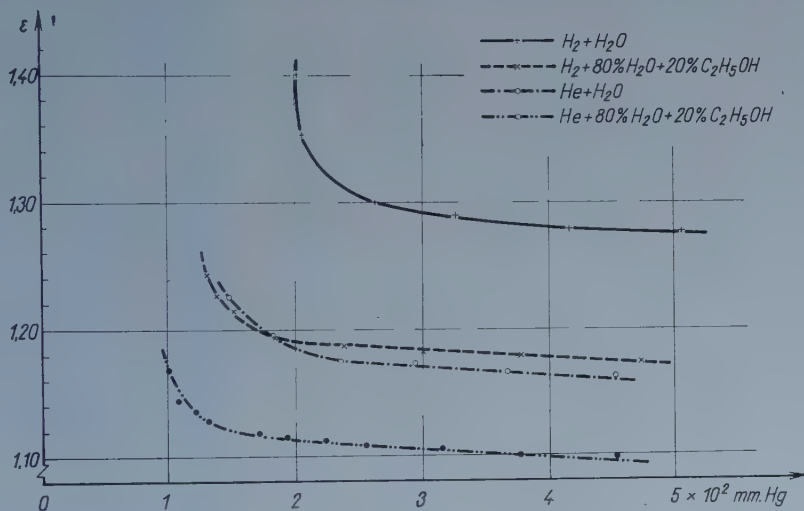


Fig. 3. The value of the expansion ratio for the ion limit as the function of the pressure preceding expansion for different gas and vapour mixtures

vapour mixtures. The value of the expansion ratio for the ion limit is presented by Fig. 3 as the function of the pressure preceding expansion, when mixtures $\text{H}_2 + \text{H}_2\text{O}$; $\text{He} + \text{H}_2\text{O}$ and $\text{He} + 80\% \text{H}_2\text{O} + 20\% \text{C}_2\text{H}_5\text{OH}$ (in the percentage of volume) are applied. As the Figure shows the best condition can be obtained by using the latter mixture. Further advantage of the alcoholic mixture is that the chamber can be operated at a considerably lower pressure.

(5) As it has been mentioned, the value of super-saturation at a given point greatly influences the size of the droplets and subsequently the range of the recoil nuclei.

(6) The diffusion of ions, which is greatly influenced by the composition of the gas and vapour mixture. At 150 mmHg total pressure, the width of the tracks of α -particles with an energy of ~ 0.1 MeV was examined in the above-mentioned three kinds of gas and vapour mixtures. As it can be seen in Fig. 4

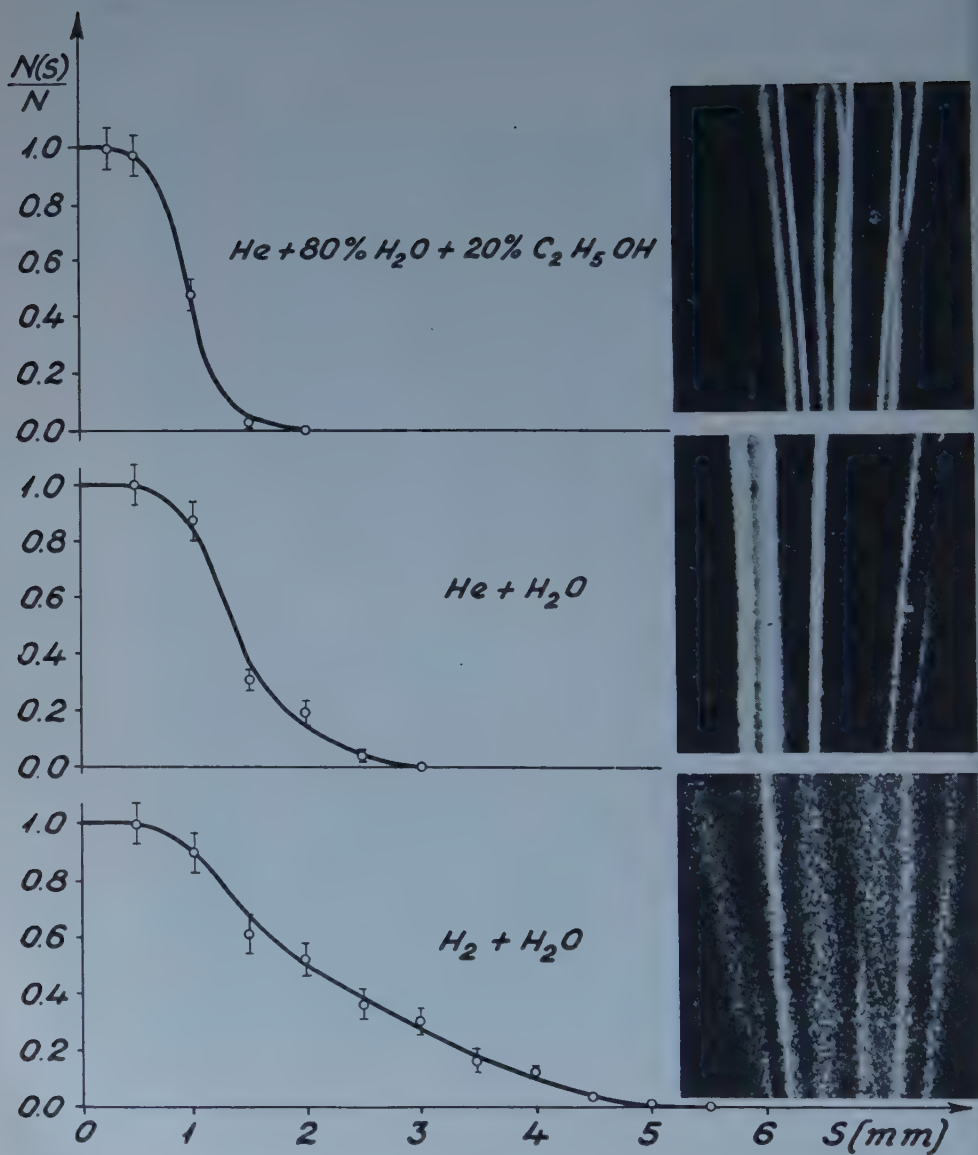


Fig. 4. The distribution of track width for Po— α -particles in the case of different gas-vapour mixtures with a total pressure of 150 mmHg

the average width of tracks and the fluctuation of width are considerable for $H_2 + H_2O$. The fluctuation of width for very short tracks becomes more and more significant in range fluctuation.

Taking the above facts into consideration, method (ii) seems to be the most reliable of the three methods used for measuring $e - \nu$ angular correlations by a cloud chamber method. In view of the fact that the choice between the two possible solutions for $p > q$ cases may be made according to the range of the recoil nucleus, only the $p < q$ energy range proves to be adequate. In this case only the direction of the impulse has to be determined for the recoil

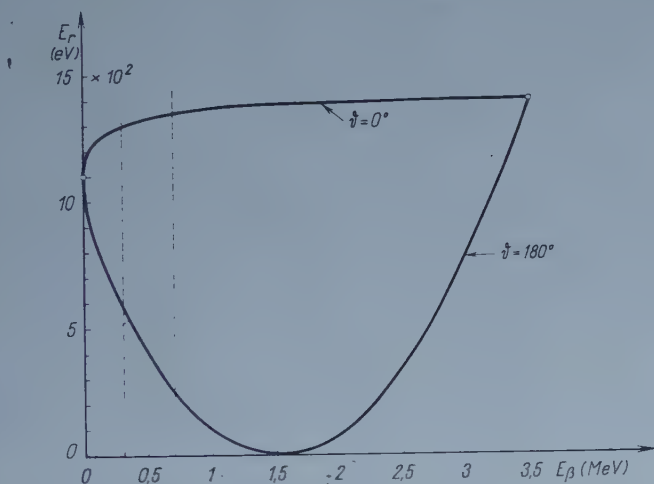


Fig. 5. The calculated energy of Li^6 -recoil nuclei arising from the β -decay of He^6 as the function of E_β at 0 and π values of ϑ

nucleus, considering that in cases $p \simeq q$, the electrons from $e - \nu$ -emissions of nearly opposite directions cannot be distinguished from background electrons of corresponding energy because the recoil nucleus cannot be observed on account of its low energy. Such events may easily escape observation and the angular correlation may undergo subjective distortions effecting unfavourably, first of all, the higher ϑ -values, that is the interaction of A-type. Thus the upper limit of the β -energy region is to be chosen so that the direction of the track of the recoil nucleus should be measurable even in $e - \nu$ -emissions of nearly opposite direction. The determination of the impulse of β -particles with a low energy is inaccurate, therefore this range also must be excluded. In view of the above, the choice of the interval $0.3 \text{ MeV} \leq E_\beta \leq 0.7 \text{ MeV}$ seems to be most suitable for He^6 . As it is shown by Fig. 5, where the energy of the recoil nucleus is plotted at values 0 and π of ϑ , the energy of the recoil nucleus in the β -energy interval of 0.3—0.7 MeV is always higher than 250 eV. On the basis of the β -spectrum, nearly 10% of He^6 -decays is included in this

region. This region is very favourable also for the observation of β -particles when a cloud chamber is operated at a low pressure.

In view of the above investigations and considerations, our earlier measurements (4) for $e - \gamma$ angular correlation in He^6 -decay have been reviewed. The following events were excluded:

- (1) those where the energy of the recoil nucleus was determined by counting the droplets,
- (2) where the energy of the β -particle is outside the energy region of 0,3—0,7 MeV.

On the basis of the 93 events thus remaining from the 381 by using the relations

$$\frac{N_1 - N_2}{N_1 + N_2} = \frac{\int_0^{\pi/2} \left(1 + \lambda \frac{\bar{v}}{c} \cos \vartheta\right) \sin \vartheta d\vartheta - \int_{\pi/2}^{\pi} \left(1 + \lambda \frac{\bar{v}}{c} \cos \vartheta\right) \sin \vartheta d\vartheta}{\int_0^{\pi} \left(1 + \lambda \frac{\bar{v}}{c} \cos \vartheta\right) \sin \vartheta d\vartheta} = \frac{1\bar{v}}{2c} \lambda$$

the following value of the angular correlation was obtained: $\lambda = +0,278 \pm 0,243$.

The value $\frac{\bar{v}}{c} = 0,849$ corresponds to the mean energy of the events obtained in the region of 0,3—0,7 MeV. The error of λ was calculated by the relation:

$$\frac{\delta\lambda}{\lambda} = \frac{\sqrt{N_1 + N_2}}{|N_1 - N_2|}.$$

Taking the limits of error into consideration, the value obtained for the correlation coefficient excludes with certainty the existence of the scalar ($\lambda = -1$) and vector ($\lambda = +1$) forms of interaction only. Because of the great statistical error it is impossible to give preference to either the tensor or the axial forms of interaction. For this very reason, our statements [4] on the existence of the tensor form of interaction has to be withdrawn because the nature of interaction cannot be definitely decided on the ground of our previous investigations, if we consider the above critical aspects.

For the purpose of getting better statistics, taking the above critical viewpoints into consideration, we go on with our investigations. We continue to produce isotope He^6 through reaction, $\text{Be}^9(n, \alpha)\text{He}^6$, but for the purpose of increasing intensity, we shall use reaction $\text{D} + \text{D}$ for neutron source (instead of $\text{Po} + \text{Be}$ so far used) which we produce by means of an impulse operating accelerator. The cloud chamber will be filled with He instead of H_2 , using a mixture of water and alcohol and decreasing the 200 mmHg so far applied to 120 mmHg.

REFERENCES

1. E. C. G. SUDARSHAN and R. G. MARSHAK, Phys. Rev., **109**, 1860, 1958.
2. J. CSIKAI, Nuovo Cimento, **5**, 1011, 1957.
3. A. SZALAY and J. CSIKAI, Padua-Venice Conference, 22—28, Sept. 1957.
4. J. CSIKAI and A. SZALAY, Proceedings of the International Conference on Nuclear Physics, Paris, July 1958.
5. J. S. ALLEN, R. L. BURMAN, W. B. HERRMANNSFELDT, P. STÄHELIN and T. H. BRAID, Phys. Rev., **116**, 134, 1958.
6. B. M. RUSTAD and S. L. RUBY, Phys. Rev., **97**, 991, 1955.
7. A. WINTHER, Dan. Mat. Fys. Medd., **27**, No. 2, 1952.

КРИТИЧЕСКИЕ ЗАМЕЧАНИЯ ПО ОТНОШЕНИЮ ИССЛЕДОВАНИЯ ЭЛЕКТРОННО-НЕЙТРИННОЙ УГЛОВОЙ КОРРЕЛЯЦИИ МЕТОДОМ КАМЕРЫ ВИЛЬСОНА

А. САЛАИ, Й. ЧИКАЙ и Й. БАЧО

Резюме

В работе приводятся несколько интересных проблем, возникающих при определении угловой корреляции между электроном и нейтрино методом камеры Вильсона. В основу критического анализа метода положен пересмотр данных, полученных нами раньше при определении угловой корреляции. Для коэффициента угловой корреляции получено значение $+0,278 \pm 0,243$. Вследствие большой статистической ошибки нельзя дать преимущества ни тензору, ни аксиальной форме взаимодействия.



A METHOD FOR MEASURING THE HALL COEFFICIENT AT HIGH TEMPERATURE

By

HUSSEIN ELKHOLY*

CENTRAL RESEARCH INSTITUTE OF PHYSICS, BUDAPEST

(Presented by E. Nagy. — Received: 9. V. 1961)

A direct method for measuring Hall voltages at high temperatures is described. As an application of the method, the temperature dependence of the Hall coefficient of Cu_3Au was investigated. It was shown that:

1. The Hall coefficient of the Cu_3Au alloy in the disordered state is temperature-independent;
2. The Hall coefficient changes its sign from a negative value in the disordered state to a positive value in the ordered state;
3. The Curie point of that alloy lies at about 385°C .

Introduction

It was my aim to investigate the kinetics of order-disorder transformations in Cu_3Au alloy by studying the Hall coefficient of that alloy. This was done by disordering the sample above the Curie point and then quench to a lower temperature below the Curie point and anneal at that temperature for several hours. Meanwhile the continuous change in the Hall voltage as a function of time of ordering was measured, i. e. the measurements of the Hall voltages were all done at high temperatures. It is much less difficult to measure the Hall voltage of a quenched specimen at room temperature than at higher temperature. This is because of the parasitic thermoelectric potentials due to the inhomogeneous temperature distribution in the specimen. These thermoelectric potentials may have a magnitude equal in order, or even greater, than that of the measurable Hall voltage, especially when the sample has a small Hall coefficient as is the case in noble metals. Therefore special care must be taken in measuring Hall potentials at high temperatures.

This paper describes the apparatus and the method used in measuring Hall voltages at high temperatures.

A dc method was used due to its simplicity and its advantages in our case.

As an application of the method, the temperature dependence of the Hall coefficient of Cu_3Au alloy has been investigated. The results are shown in Fig. 4.

* On leave of absence from the Faculty of Science, Cairo University, Cairo, Egypt, U. A. R.

Important results on the kinetics of order-disorder transformation in the same alloy were obtained by using this method. This will be the subject of a separate publication.

Preparation of the sample

An alloy of atomic composition of $25.90 \pm 0.05\%$ copper and $74.10 \pm 0.05\%$ gold served as our sample. This alloy was prepared from pure copper and gold and melted in a graphite crucible by high frequency technique. In order to make the alloy more homogeneous it was remelted twice. After remelting, the alloy was homogenized in hydrogen for 10 hours at 800°C . The resulting ingot was rolled to a thickness of 0.03 mm. After machining, the sample was annealed in vacuum for 10 hours at 600°C . The sample was in the form of a flat plate 10 cm long, 1 cm wide, and 0.003 cm thick. Three Hall probes were cut from the sample itself; two probes at one side of the sample, 4 mm apart, and one probe at the other side of the sample.

Probe contacts

Since the Hall measurements were made at high temperatures, to prevent oxidation of the sample, it was put in a glass tube evacuated up to about 10^{-5} mm Hg. Pt wires (convenient for glass sealing) were used as Hall leads and tungsten wires for current leads.

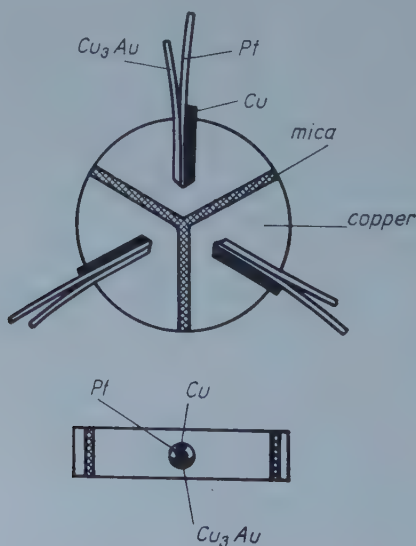


Fig. 1

Different kinds of contacts between the Cu_3Au probes of the sample and the Pt leads were tried, and all gave large thermoelectric voltages which, in some cases, were found to be larger than the Hall voltage measured. To overcome this difficulty, a disc of pure copper 5 mm diameter and 1 mm thickness was cut into three triangular segments. These segments were insulated from each other by mica. Into each segment a fine hole 0.8 mm diameter was bored, and the Cu_3Au probes and the Pt leads were inserted into each hole and brought into contact with each other by a thin pin of copper. A cross section of the contact segments is shown in Fig. 1. These contact segments proved to be very convenient, and due to their small size and the high heat capacity of copper the temperature at the three contacts was practically the same.

Sample holder

The sample was held between two mica sheets. Two copper holders served as current electrodes and helped in supporting the sample to two thick discs of mica. The two mica discs were fastened by two thin copper rods which

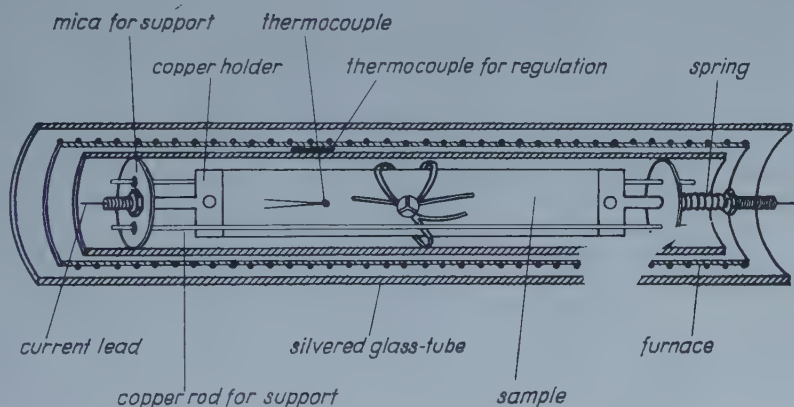


Fig. 2

gave additional support and served to connect the current electrodes to two tungsten wires used as current leads. The central part of Fig. 2 shows the essential parts of the sample and its holder. The spring shown in the Figure served to compensate for any elongation in the sample due to heat expansion, and thus making the sample always straight.

Circuit and method of measurement

Fig. 3 shows the actual measuring circuit. The Hall probes 1 and 2 were bridged by a 10 ohms resistance potentiometer, by which it was possible to balance the voltage drop in the sample due to the primary current and due to any small thermoelectric voltages appearing at the lead contacts. The Hall voltages appearing between the center tap 4 and probe 3 were measured by the aid of a Diesselhorst type compensator (U. S. S. R. make, type PPTN 1) and

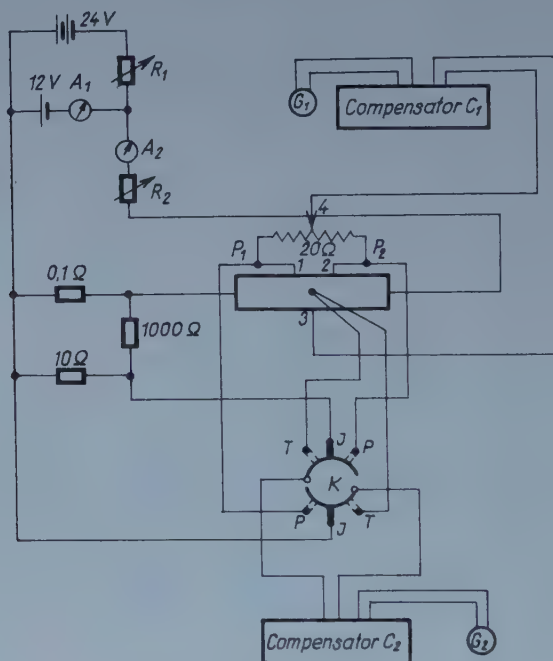


Fig. 3

a photocell galvanometer (U. S. S. R. make, type F 16). The compensator has a range of measurement from $0.1 \mu\text{v}$ to 20 mv . The galvanometer has a voltage sensitivity of 2×10^{-8} volts per one division of a scale.

The leads which are denoted as P_1 and P_2 in Fig. 3 were used for the measurement of electrical resistivity. The output potential from them, the potential of the Pt—PtRh thermocouple, and the potential appearing on the 10 ohms standard resistance, which was used to measure the current of the sample were read by the compensator C_2 and the galvanometer G_2 .

The Hall measurement at every temperature was made with the following procedure. Without applying the magnetic field, the voltage drop in the sample due to the primary current and due to any thermoelectric potentials (which

were found to be very small and constant) was balanced by means of the center tap 4. The magnetic field was then applied and the voltage appearing between the center tap 4 and probe 3 was measured by C_1 and G_1 . Four measurements were made by reversing both the magnetic field and the sample current in all possible combinations. From simple considerations [1], the Hall voltage plus the Ettingshausen voltage were calculated from these four measurements. Thermocouples [2] can be connected to each Hall probe which enable us to correct for the Ettingshausen effect. Since in metals the voltage due to the Ettingshausen effect is very small and is about one percent of that of the Hall voltage, and since the relative error in our measurement was 5%, this correction was not done and the Ettingshausen effect was neglected.

Current stabilizer

The current of the sample was supplied by using a simple circuit described by GERRITSEN [3]. The circuit in its simplest form, as it is shown in the upper part of Fig. 3, consists of one battery (12V) parallel to the main battery (two 12V batteries) and a voltage dividing resistor R_1 is introduced between, such that the voltage of the main battery equals the output voltage. The circuit can be adjusted by introducing a low resistance ammeter A_1 and varying R_1 until no current flows in A_1 . By adjusting the variable resistance R_2 , the desired current could be obtained which was read roughly by the ammeter A_2 .

A sample current of 2 amperes was used and this was found to be nearly constant throughout a period of more than 15 hours. The exact value of the current was measured by a compensator C_2 and a galvanometer G_2 by switching the key K to position 1.

Furnace

A 200 watts furnace was used in this investigation, and temperatures up to 500° C could be obtained. Manganin wires were wound on an aluminium tube 23 cm long and 2.5 cm diameter. Mica sheets were used as insulator between the aluminium tube and the manganin wire. A Pt—PtRh thermocouple was put between the inner side of the furnace and the outer side of the glass tube enclosing the sample, and this was used for regulating the temperature. The temperature of the sample was measured by another Pt—PtRh thermocouple placed at the sample.

Temperature regulator*

A proportional temperature regulator was used to regulate the temperature. The voltage appearing on the regulator thermocouple was compensated

* The temperature regulator was constructed by Mr. F. Tóth and will be the subject of a separate publication.

and then amplified by a lock-in amplifier. The output of the amplifier was connected to a grid of a thyatron tube which had the furnace connected in its anode circuit. The current of the furnace was changing proportionally with the fluctuation in the temperature. The temperature was constant within $\pm 0.1^\circ \text{C}$.

Magnet and magnetic field measurement

The electromagnet used for the Hall coefficient measurements had 10 cm diameter pole faces and a variable gap of 0–9 cm. With a current of 30 amperes and 4 cm gap, a field of 11,800 oersted was obtained. The magnet was calibrated by using a magnetic induction meter (U. S. S. R. make, type IMI-I).

Experimental results

As an application of the method, the temperature dependence of the Hall coefficient of Cu_3Au alloy was investigated. The results are shown in Fig. 4. The sample was first disordered at 485°C and annealed there for several hours.

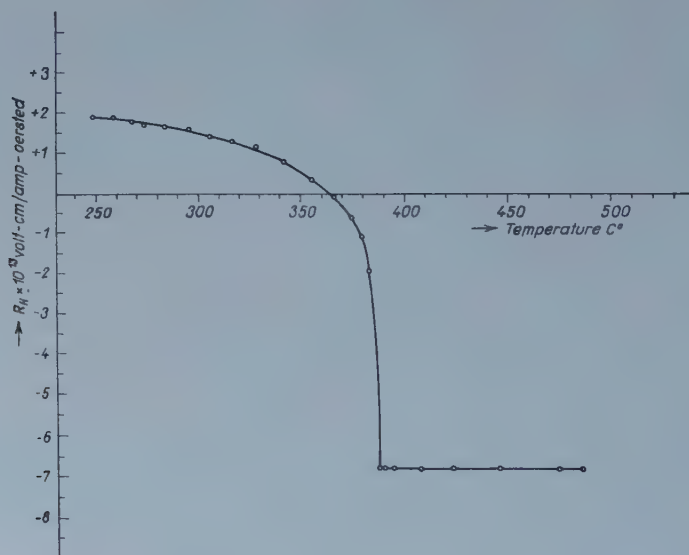


Fig. 4

The Hall voltage was measured. The sample was then cooled in steps, and annealed at every temperature until equilibrium was obtained. The Hall voltage was measured at each temperature. The graph shows the Hall coefficients measured at equilibrium at corresponding temperatures.

The Curie point determined on the basis of Fig. 4 lies at about 385°C , which lies between the value obtained by KOMAR and SIDOROV [4] and that obtained by BURNS and QUIMBY [5].

From Fig. 4 it is clear that the Hall coefficient is temperature-independent in the disordered state, i. e. above the Curie point. It is also clear from Fig. 4 that the Hall coefficient changes its sign from a negative value in the disordered state to a positive value in the ordered state, confirming the observations by KOMAR and SIDOROV [4]. The values of R_H in the disordered state obtained here coincide with the value of R_H obtained by KOMAR and SIDOROV [4].

Acknowledgement

The author wishes to express his thanks to Prof. E. NAGY and Mr. I. NAGY for their helpful assistance and advice in this work. Grateful thanks are also due to Mr. T. ANTONIGHEL for expert technical assistance without which this work would not have been possible, and to Mr. F. TÓTH for designing the electronic furnace regulator for this work and to Mr. J. TÓTH for helpful discussions.

REFERENCES

1. O. LINDBERG, Proc. I. R. E., **40**, 1414, 1952.
2. S. FONER and E. M. PUGH, Phys. Rev., **91**, 20, 1953.
3. A. N. GERRITSEN, Encyclopedia of Phys. (S. Fluegge, ed.) Band XIX, vol. XIX. 152 Springer, Berlin, 1956.
4. A. KOMAR and S. SIDOROV, J. Phys. U.S.S.R. **4**, 552, 1941.
5. F. P. BURNS and S. L. QUIMBY, Phys. Rev., **97**, 1567, 1955.

МЕТОД ДЛЯ ИЗМЕРЕНИЯ КОЭФФИЦИЕНТА ХОЛЛА ПРИ ВЫСОКИХ ТЕМПЕРАТУРАХ

ХУССЕЙН ЭЛКОЛИ

Резюме

Описывается прямой метод для измерения напряжения Холла при больших температурах. Как применение данного метода исследовалась температурная зависимость коэффициента Холла в случае Cu_3Au . Оказывалось, что

1. коэффициент Холла сплава Cu_3Au в неупорядоченном состоянии не зависит от температуры,

2. коэффициент Холла меняет знак от своего отрицательного значения при неупорядоченном состоянии к положительному при упорядоченном состоянии,

3. точка Кюри данного сплава лежит около 385°C .



ZUR HERLEITUNG DER GRUNDGLEICHUNG DER STATISTISCHEN THEORIE DES ATOMS

Von

P. GOMBÁS

PHYSIKALISCHES INSTITUT DER UNIVERSITÄT FÜR TECHNISCHE WISSENSCHAFTEN, BUDAPEST

(Eingegangen: 1. IX. 1961)

Im Anschluss an eine Arbeit von PLASKETT wird die für die statistische Theorie des Atoms grundlegende Beziehung zwischen dem maximalen Impuls und der Elektronendichte auf eine neue Weise hergeleitet, wobei sich ein Korrektionsglied ergibt, das für den Fall kleiner Elektronendichten, also am Rand des Atoms, von Bedeutung ist.

Die Grundgleichung der statistischen Theorie des Atoms, wonach der Betrag des maximalen Elektronenimpulses im Atom mit der Elektronendichte im Zusammenhang steht, wurde mehrfach hergeleitet.¹ Wir geben im folgenden auf Grund wellenmechanischer Betrachtungen im Anschluss an eine Arbeit von PLASKETT² eine neue Herleitung einer korrigierten Form dieser Beziehung. Der wesentliche Unterschied gegenüber der Arbeit von PLASKETT besteht darin, dass wir die mittlere Elektronendichte anders als PLASKETT definieren, was zu grossen Vereinfachungen führt und das ganze Verfahren sehr durchsichtig gestaltet.

Die Schrödinger-Gleichung eines Elektrons im Atom für das r -fache der radialen Wellenfunktion ψ lautet folgendermassen

$$f'' + \frac{8\pi^2 m}{h^2} (\varepsilon - U) f = 0; \quad (1)$$

hier bezeichnet r die Entfernung vom Kern, m die Masse des Elektrons, h die Plancksche Konstante, ε den Energieparameter, f das r -fache von ψ , d. h. es ist $f = r\psi$, f'' die zweite Ableitung von f nach r und U die effektive potentielle Energie des Elektrons

$$U = -eV + \frac{h^2}{8\pi^2 m} \frac{l(l+1)}{r^2}, \quad (2)$$

wo e die positive Elementarladung, l die Nebenquantenzahl und V das elektro-

¹ Man vgl. z. B. P. GOMBÁS, Die statistische Theorie des Atoms und ihre Anwendungen, Springer, Wien, 1949.

² J. S. PLASKETT, Proc. Phys. Soc. London A **66**, 178, 1953.

statische Potential bedeutet, von dem wir annehmen, dass es eine Funktion von r allein ist, dass also über die verschiedenen Richtungen hinweggemittelt wurde.

Mit dem Ansatz

$$f(r) = R(r) e^{\frac{2\pi i}{h} S(r)}, \quad (3)$$

$$S(r) = \int^r p_r dr, \quad \text{d. h.} \quad S' = p_r, \quad (4)$$

zerfällt bekanntlich die Gleichung (1) in die folgenden beiden Gleichungen

$$R'' - \frac{4\pi^2}{h^2} R p_r^2 + \frac{8\pi^2 m}{h^2} (\varepsilon - U) R = 0, \quad (5)$$

$$2 R' p_r + R p_r' = 0, \quad (6)$$

wo p_r den radialen Impuls des Elektrons bezeichnet und die Striche rechts oben neben den Symbolen R und p_r Ableitungen nach r bedeuten. Aus Gleichung (6) folgt sofort, dass $R^2 p_r$ eine Konstante ist, die wir mit a bezeichnen wollen; es ist also

$$R^2 p_r = a \quad (7)$$

und

$$R^2 = \frac{a}{p_r}. \quad (8)$$

Als klassischen Bahnbereich betrachtet man das Intervall der r -Werte, für die $p_r \geq 0$ ist. Die Grenzen r_1 bzw. r_2 des klassischen Bahnbereiches ($r_1 \leq r \leq r_2$) sind durch $p_r = 0$ determiniert. Die Eigenfunktion muss an den Grenzen des klassischen Bahnbereiches verschwinden.

Wenn R und p_r Lösungen des Gleichungssystems (5), (6) sind, dann sind die Eigenfunktionen gemäss (3)

$$f_s = R \sin \frac{2\pi}{h} \int_{r_1}^r p_r dr \quad \text{und} \quad f_c = R \cos \frac{2\pi}{h} \int_{r_1}^r p_r dr, \quad (9)$$

von denen nur f_s als Lösung in Frage kommt, denn nur diese Eigenfunktion verschwindet an den Grenzen des klassischen Bahnbereiches und zwar nur dann, wenn die Bedingung

$$2 \int_{r_1}^{r_2} p_r dr = n_r h \quad (10)$$

besteht, wo n_r eine ganze Zahl ist. Diese Bedingung ist mit der Sommerfeldschen Quantenbedingung identisch.

Die radiale Aufenthaltswahrscheinlichkeit des Elektrons wird also

$$f_s^2 = R^2 \sin^2 \frac{2\pi}{h} \int_{r_1}^r p_r dr. \quad (11)$$

Diese setzt sich aus zwei Faktoren zusammen: aus dem Amplitudenquadrat R^2 und aus dem zwischen den Werten 0 und 1 oszillierenden Faktor $\sin^2 \frac{2\pi}{h} \int_{r_1}^r p_r dr$. Dieser oszillierende Anteil wird also durch das Amplitudenquadrat moduliert. Eine mittlere radiale Aufenthaltswahrscheinlichkeit \bar{f}_s^2 lässt sich zweckmässigerweise in der Weise definieren, dass man den oszillierenden Anteil durch den Mittelwert $\frac{1}{2}$ ersetzt und für

$$\bar{f}_s^2 = R^2 \quad (12)$$

setzt, wobei wir den Faktor $\frac{1}{2}$ mit der in R enthaltenen Normierungskonstante verschmolzen haben.

Für \bar{f}_s^2 besteht die Normierungsbedingung

$$4\pi \int_{r_1}^{r_2} \bar{f}_s^2 dr = 4\pi \int_{r_1}^{r_2} R^2 dr = 1, \quad (13)$$

aus der man mit Rücksicht auf (8) für die Konstante α den Wert

$$\alpha = \frac{1}{4\pi \int_{r_1}^{r_2} \frac{1}{P_r} dr} \quad (14)$$

erhält.

Die mittlere radiale Dichte D_l der Elektronen mit der Nebenquantenzahl l in einem Atom ergibt sich mit Rücksicht auf (8) und (12) folgendermassen

$$D_l = 2(2l+1) 4\pi \sum_{n_r} \bar{f}_s^2 = 2(2l+1) 4\pi \alpha \sum_{n_r} \frac{1}{P_r}, \quad (15)$$

wo die Summierung über alle besetzten Quantenzustände auszudehnen ist. Wenn wir die Summe durch ein Integral ersetzen, so wird

$$D_l = 2(2l+1)4\pi\alpha \int_{r_1}^r \frac{1}{p_r} dn_r. \quad (16)$$

Die Integration auf der rechten Seite lässt sich folgendermassen durchführen. Aus (10) folgt

$$\frac{2}{h} \int_{r_1}^{r_2} \frac{\partial p_r}{\partial \varepsilon} dr = \frac{\partial n_r}{\partial \varepsilon}. \quad (17)$$

Mit dem klassischen Ausdruck für p_r

$$p_r = [2m(\varepsilon - U)]^{1/2} \quad (18)$$

erhält man den Zusammenhang

$$\frac{\partial p_r}{\partial \varepsilon} = \frac{m}{p_r} \quad (19)$$

und mit diesem und (14) aus (17)

$$\frac{2m}{h} \int_{r_1}^{r_2} \frac{1}{p_r} dr = \frac{2m}{h} \frac{1}{4\pi\alpha} = \frac{\partial n_r}{\partial \varepsilon}. \quad (20)$$

Man kann also in (16) dn_r durch $\frac{m}{2\pi h\alpha} d\varepsilon$ ersetzen und erhält

$$D_l = 2(2l+1) \frac{2m}{h} \int_{\varepsilon_0}^{\varepsilon_{\mu}} \frac{1}{p_r} d\varepsilon, \quad (21)$$

wo die Integration auf alle besetzten Quantenzustände zu erstrecken ist und ε_0 und ε_{μ} die Energie des tiefsten bzw. höchsten Quantenzustandes bezeichnet.

Mit (19) ergibt sich aus (21)

$$\begin{aligned} D_l &= 2(2l+1) \frac{2}{h} \int_{\varepsilon_0}^{\varepsilon_{\mu}} \frac{\partial p_r}{\partial \varepsilon} d\varepsilon = 2(2l+1) \frac{2}{h} [p_r(\varepsilon_{\mu}) - p_r(\varepsilon_0)] = \\ &= \frac{4(2l+1)}{h} (p_{r\mu} - p_{r0}), \end{aligned} \quad (22)$$

wo wir für den maximalen radialen Impuls und für den minimalen radialen Impuls der Kürze halber $p_{r\mu}$ bzw. p_{r0} setzten.³

Im allgemeinen wird angenommen, dass $p_{r0} = 0$ ist, wodurch man aus (22) zu der bekannten Beziehung

$$D_l = \frac{4(2l+1)}{h} p_{r\mu} \quad (23)$$

gelangt. Unserer Meinung nach ist jedoch die Annahme $p_{r0} = 0$ nicht zulässig, denn dies wäre damit gleichbedeutend, dass man annimmt, dass die minimale radiale Energie eines Elektrons gleich 0 sei, was, wie sich leicht zeigen lässt, nicht der Fall ist.

Hierzu teilen wir das Elektronengas des Atoms in Kugelschalen von der Dicke s ein und wählen s den Voraussetzungen der statistischen Theorie entsprechend so klein, dass in der Kugelschale U praktisch als konstant betrachtet werden kann. Die Lösungen der Gleichung (1), die den Randbedingungen — nach welchen f an den beiden berandenden Kugelflächen der Kugelschale verschwinden muss — genügen, sind die folgenden

$$f_\lambda = C \sin \lambda \pi \left(\frac{r}{s} - \frac{r_k}{s} \right), \quad (24)$$

$$(\lambda = 1, 2, 3, \dots),$$

wo C eine Normierungskonstante und r_k den Radius der inneren Kugelfläche der Kugelschale bezeichnen. Die entsprechenden Eigenwerte der Energie sind

$$\varepsilon_\lambda = \frac{h^2}{8m} \frac{\lambda^2}{s^2} + U. \quad (25)$$

Hierin ist das Glied mit λ^2 der radiale Anteil der kinetischen Energie. λ kann den Wert 0 nicht annehmen, da für diesen f_λ identisch verschwinden würde, was bedeutet, dass der Zustand mit $\lambda = 0$ nicht existiert. Hieraus folgt, dass der radiale Anteil der kinetischen Energie nicht verschwinden kann, also in unserer halbklassischen Betrachtungsweise auch p_{r0} den Wert 0 nicht annehmen kann.

Statt der bekannten Beziehung (23) erhält man also die genauere, korrigierte Beziehung (22), in der p_{r0} als Korrektionsglied auftritt. Für grosse Elektronendichten wird man p_{r0} neben $p_{r\mu}$ vernachlässigen können und die

³ Diese Beziehung wurde auch von PLASKETT auf andere Weise gefunden ohne jedoch dass von ihm die nachstehenden Folgerungen gezogen wurden.

Beziehung (23) wird eine sehr gute Näherung darstellen. Für kleine Elektronendichten — also in den äusseren Gebieten des Atoms — kann jedoch p_{r0} von gleicher Grössenordnung werden wie $p_{r\mu}$ und man kann dann p_{r0} in (22) nicht vernachlässigen, wodurch sich in diesen Gebieten eine Korrektur des statistischen Modells ergibt. Das Problem besteht in der Bestimmung von p_{r0} , was in einer folgenden Arbeit durchgeführt werden soll. Aus (25) erhält man für p_{r0} den Ausdruck

$$p_{r0} = \frac{h}{2s}, \quad (26)$$

der jedoch für unsere Zwecke nicht brauchbar ist, da in diesem die Breite s der jeweils herausgegriffenen Kugelschale eingeht. Es soll versucht werden diesen mit einem für rechnerische Zwecke brauchbaren Näherungsausdruck zu ersetzen.

К ВЫВЕДЕНИЮ ОСНОВНОГО УРАВНЕНИЯ В СТАТИСТИЧЕСКОЙ ТЕОРИИ АТОМА

П. ГОМБАШ

Резюме

В связи с работой Пласскета для статистической теории атома выводится одна основная зависимость между максимальным импульсом и плотностью электронов. Данная зависимость получается новым, отличным от упомянутого, способом, в результате появляется коррекционный член, который в случае меньшей электронной плотности значителен и во внешней области атома.

DERIVATION OF "ALMOST" ORTHOGONAL TWO-ELECTRON ORBITALS

By
E. КАРУЙ

RESEARCH GROUP FOR THEORETICAL PHYSICS, HUNGARIAN ACADEMY OF SCIENCES, BUDAPEST

(Received 30. IV. 1961)

In previous papers [1, 2], a set of coupled integro-differential equations has been deduced for antisymmetrical two-electron orbitals orthogonal in the strong sense. By varying the energy expression given in [3, 4, 5] and taking into account the auxiliary conditions

$$\int \psi_I^*(1|2) \psi_I(1|2) d\tau_1 d\tau_2 = 1, \quad (I = 1, 2, \dots, N), \quad (1)$$

$$\int \psi_I^*(1|2) \psi_J^*(3|4) \psi_I(3|2) \psi_J(1|4) d\tau_1 d\tau_2 d\tau_3 d\tau_4 = D_{IJ} \quad \text{if } J \neq I, \quad (2)$$

$$(0 < D_{IJ} < 1), \quad (I, J = 1, 2, \dots, N),$$

we have obtained the equations

$$\left\{ H(1) + H(2) + \frac{1}{r_{12}} + 2 \sum_{J \neq I} \int d\tau_3 d\tau_4 \left[\frac{1 - P_{13}}{r_{13}} + \frac{1 - P_{23}}{r_{23}} \right] \psi_J^*(3'|4) \psi_J(3|4) \right\} \psi_I(1|2) =$$

$$(3)$$

$$= \left\{ E^I + \sum_{J \neq I} E^{IJ} \int d\tau_3 d\tau_4 [P_{13} + P_{23}] \psi_J^*(3'|4) \psi_J(3|4) \right\} \psi_I(1|2), \quad (I = 1, 2, \dots, N)$$

for the two-electron orbitals ψ_I . In the limiting case, when all $D_{IJ} \rightarrow 0$, the antisymmetrical solutions $\psi_I(1|2)$ ($I = 1, 2, \dots, N$) of the equations (3) satisfying the auxiliary conditions (1) and (2), are the orthogonal two-electron orbitals to be found. When $D_{IJ} \rightarrow 0$ and $\int \psi_I^*(1|2) \psi_I(1|3) d\tau_1 \rightarrow 0$, then $|E^{IJ}|$ must tend to infinity so that $\lim E^{IJ} \int \psi_J^*(1|2) \psi_I(1|3) d\tau_1 \equiv \mathcal{E}^{IJ}$ (2|3) will be well-behaved functions. Using these, the equations can be put into the form

$$\left\{ H(1) + H(2) + \frac{1}{r_{12}} + 2 \sum_{J \neq I} \int d\tau_3 d\tau_4 \left[\frac{1 - P_{13}}{r_{13}} + \right. \right.$$

$$\left. + \frac{1 - P_{23}}{r_{23}} \right] \psi_J^*(3'|4) \psi_J(3|4) \right\} \psi_I(1|2) = E^I \psi_I(1|2) +$$

$$+ \sum_{J \neq I} \int d\tau_3 [\mathcal{E}^{IJ} (3|2) \psi_J(1|3) + \mathcal{E}^{IJ} (3|1) \psi_J(3|2)], \quad (I = 1, 2, \dots, N).$$

Even if we assume that solutions satisfying the auxiliary conditions (1) and (2) (when $D^{IJ} \rightarrow 0$) do exist, the above limiting procedure makes it more difficult to find them.

Recently it has been proved [6] that, for given antisymmetric two-electron orbitals orthogonal in the strong sense, there exists a complete set of orthonormal one-electron spin-orbitals u_i which can be partitioned into sub-sets

$$u_{11}, u_{12}, u_{13}, \dots; \dots u_{I1}, u_{I2}, u_{I3}, \dots; \dots u_{N1}, u_{N2}, u_{N3}, \dots;$$

such that each $\psi_I(1|2)$ can be expanded in terms of $u_{I1}, u_{I2}, u_{I3}, \dots$ only:

$$\psi_I(1|2) = \sum_{i, i'} C_{i, i'}^I u_{i1}(1) u_{i'2}(2),$$

etc. Hence the full space can be decomposed into mutually perpendicular N subspaces 1, 2, ..., I , ... N in such a way that each two-electron orbital $\psi_I(1|2)$ is localized to the corresponding subspace I .

In the beginning we assume that both the spin-orbitals u_i and their proper decomposition into N subspaces corresponding to the ground state of the system with Hamiltonian H are known. By requiring to satisfy, instead of the orthogonality conditions

$$\int \psi_I^*(1|2) \psi_J(1|3) d\tau_1 = 0, \quad \text{if } J \neq I, \quad (5)$$

the constraints that each $\psi_I(1|2)$ be localized to the corresponding subspace, we have the following set of equations:

$$Q^I H^I(1|2) \psi_I(1|2) = E^I \psi_I(1|2), \quad (I = 1, 2, \dots, N). \quad (6)$$

Here Q^I is a projection operator projecting on the subspace I :

$$\begin{aligned} Q^I f(1|2) &= f^I(1|2) = \sum_{ii'} f_{ii'}^I u_{i1}(1) u_{i'2}(2), \\ f_{ii'}^I &= \int f(1|2) u_{i1}^*(1) u_{i'2}(2) d\tau_1 d\tau_2, \\ H^I(1|2) &= \left\{ H(1) + H(2) + \frac{1}{r_{12}} + 2 \sum_{j \neq I} \left(d\tau_3 d\tau_4 \left[\frac{1 - P_{13}}{r_{13}} + \right. \right. \right. \\ &\quad \left. \left. \left. + \frac{1 - P_{23}}{r_{23}} \right] \psi_j^*(3|4) \psi_j(3|4) \right\}. \end{aligned}$$

The antisymmetric solutions $\psi_{10}, \psi_{20}, \dots, \psi_{N0}$ of the equations (6) belonging to the lowest values E^{10}, E^{20}, E^{N0} , correspond to the ground state of the system. Keeping the operators $H^I(1|2)$ and Q^I fixed, each of the equations (6) has further antisymmetric solutions $\psi_{I1}, \psi_{I2}, \psi_{I3}, \dots$ with Lagrangian multipliers $E^{I1}, E^{I2}, E^{I3}, \dots$ which have the following properties:

$$\int \psi_{I\kappa}^*(1|2) \psi_{I\lambda}(1|2) d\tau_1 d\tau_2 = \delta_{\kappa\lambda}, \quad (7)$$

$$\int \psi_{I\kappa}^*(1|2) \psi_{J\lambda}(1|2) d\tau_1 d\tau_2 = 0, \quad \text{if } J \neq I. \quad (8)$$

The ground state energy given by this approach lies below the energy obtained by the Hartree-Fock method and may be close to the exact non-relativistic ground state energy when the electron pairs of the system are strongly localized to different regions of the space. This can be utilized to define an exact measure for the localizability of the electron pairs in the system.

In the beginning the set u_{li} is not known, thus, in order to replace it we have to find a finite set of one-electron spin orbitals v_{li} . There are two methods to derive an approximate basis. Both resemble, to some extent, the extended Hartree-Fock equations [7, 8].

A) The approximate two-electron orbitals $\varphi_I(1|2)$ are taken in the form (see also [9])

$$\varphi_I(1|2) = \sum_{i_1, i_2} C_{i_1 i_2}^I v_{Ii_1}(1) v_{Ii_2}(2), \quad (I = 1, 2, \dots, N; \quad i_1, i_2 = 1, 2, \dots, n_I).$$

We require that

$$\int v_{Ii}^*(1) v_{Jj}(1) d\tau_1 = \delta_{IJ} \delta_{ij} \quad (I, J = 1, 2, \dots, N; \quad i = 1, 2, \dots, n_I; \quad j = 1, 2, \dots, n_J). \quad (9)$$

When

$$C_{i_1 i_3}^I = -C_{i_2 i_1}^I$$

and

$$\sum_{i_1, i_3=1}^{n_I} C_{i_1 i_2}^{I*} C_{i_1 i_3}^I = 1, \quad (I = 1, 2, \dots, N), \quad (10)$$

the approximate two-electron orbitals are antisymmetrical and normalized, respectively. With these, we get the energy expression

$$\begin{aligned} E^{(0)} = H(0) + \sum_{I=1}^N \sum_{i_1, i_2, i_3, i_4=1}^{n_I} C_{i_1 i_3}^{I*} C_{i_2 i_4}^I & \left\{ 2(Ii_1 | H(1) | Ii_2) \delta_{i_3 i_4} + \right. \\ & \left. + \left(Ii_1, Ii_3 \left| \frac{1}{r_{12}} \right| Ii_2, Ii_4 \right) \right\} + \\ + 2 \sum_{\substack{I, J=1 \\ J \neq I}}^N \sum_{i_1, i_2, i_3=1}^{n_I} \sum_{j_1, j_2, j_3=1}^{n_J} C_{j_1 j_3}^{J*} C_{j_2 j_3}^J C_{i_1 i_3}^{I*} C_{i_2 i_3}^I & \left\{ \left(Jj_1, Ii_1 \left| \frac{1}{r_{12}} \right| Jj_2, Ii_2 \right) - \right. \\ & \left. - \left(Jj_1 Ii_1 \left| \frac{1}{r_{12}} \right| Ii_2 Jj_2 \right) \right\}. \end{aligned} \quad (11)$$

Variation of the spin-orbitals v_{li} in (11) taking into account the auxiliary conditions (9) with Lagrangian multipliers $-2 e^{Ii, Jj}$ leads to the set of equations

$$\begin{aligned}
& \sum_{i_2, i_3, i_4} C_{i_1 i_3}^{I*} C_{i_2 i_4} \left\{ 2H(1) \delta_{i_3 i_4} + \int \frac{d\tau_2}{r_{12}} v_{I i_3}^*(2) v_{I i_4}(2) \right\} v_{I i_2}(1) + \\
& + 2 \sum_{J \neq I} \sum_{i_2, i_3} \sum_{j_1, j_2, j_3} C_{i_1 i_3}^{J*} C_{i_2 i_3}^I C_{j_1 j_3}^{J*} C_{j_2 j_3}^J \int \frac{d\tau_2}{r_{12}} \left\{ v_{J j_1}^*(2) v_{J j_2}(2) v_{I i_2}(1) - \right. \\
& \left. - v_{J j_1}^*(2) v_{I i_2}(2) v_{J j_2}(1) \right\} = e^{Ii, Ii} v_{I i_1}(1) + \sum_{\substack{i_2 \\ i_2 \neq i_1}} e^{Ii, Ii_2} v_{I i_2}(1) + \\
& + \sum_{J \neq I} \sum_J e^{Ii, Jj} v_{J j}(1).
\end{aligned} \tag{12}$$

Varying the coefficients $C_{i_1 i_2}^I$ and taking into account the auxiliary conditions (10) with Lagrangian multipliers $-\mathcal{E}^I$ (and the antisymmetry of the coefficients $C_{i_1 i_2}^I$ in the indices $i_1 i_2$) we obtain the set of equations

$$\begin{aligned}
& \sum_{i_2, i_4} C_{i_2 i_4}^I \left\{ (I i_1 | H(1) | I i_2) \delta_{i_3 i_4} + (I i_3 | H(1) | I i_4) \delta_{i_1 i_2} + \left(I i_1, I i_3 \left| \frac{1}{r_{12}} \right| I i_2, I i_4 \right) \right\} + \\
& + \sum_{J \neq I} \sum_{i_2, i_4} \sum_{j_1, j_2, j_3} C_{i_2 i_4}^I C_{j_1 j_3}^{J*} C_{j_2 j_3}^J \left\{ [1 - P_{I i_2, J j_2}] \left(J j_1, I i_1 \left| \frac{1}{r_{12}} \right| J j_2, I i_2 \right) \delta_{i_3 i_4} + \right. \\
& \left. + [1 - P_{I i_4, J j_2}] \left(J j_1, I i_3 \left| \frac{1}{r_{12}} \right| J j_2, I i_4 \right) \delta_{i_1 i_2} \right\} = \mathcal{E}^I C_{i_1 i_3}^I, \\
& (I = 1, 2, \dots, N; \quad i_1, i_2, i_3, i_4 = 1, 2, \dots, n_I).
\end{aligned} \tag{13}$$

(12) and (13) have to be solved simultaneously. The approximate two-electron orbitals φ_I can be constructed from solutions $v_{Ii}(i = 1, 2, \dots, n_I)$ of (12) satisfying the constraints (9), and from antisymmetrical solutions $C_{i_1 i_2}^I$ of (13) satisfying the constraints (10). Since the first order density matrix is quasi-diagonal (diagonal in the indices I, J)

$$\begin{aligned}
I(1' 1) &= \sum_I I_I(1' | 1) = \sum_I \int \varphi_I^*(1' | 2) \varphi_I(1 | 2) d\tau_2 = \\
&= \sum_I \sum_{i_1, i_2, i} C_{1 i_3}^* C_{i_2 i_3}^I v_{I i_1}^*(1') v_{I i_2}(1),
\end{aligned}$$

the submatrices $I_I(1' | 1)$ can be separately diagonalized by unitary transformations U^I [10] introducing natural spin-orbitals [7].

The approximation can be improved by increasing n (the number of the spin-orbitals v).

The main difficulty of the method A) lies in the solution of the equations (12). This is an unrealizable task as yet.

B) We choose as a basis a fixed finite orthonormalized set of one-electron spin-orbitals $w_\nu(1)$ ($\nu = 1, 2, \dots n$; $n \geq 2N$). This will be divided up into N subsets $w_{Ii}(1)$ ($i = 1, 2, \dots n_I$) so that each to the w_ν 's occurs in one of the subsets only, i.e. $n_1 + \dots + n_I + \dots + n_N = n$. We obtain with the two-electron orbitals

$$\sum_{i_1, i_2=1}^{n_I} \bar{C}_{i_1 i_2}^I w_{Ii_1}(1) w_{Ii_2}(2), \quad (I = 1, 2, \dots N),$$

an energy expression similar to (11). The only difference is that the matrix elements $(Ii_1 | H(1) | Ii_2)$, $\left(Jj_1, Ii_1 \left| \frac{1}{r_{12}} \right| Jj_2, Ii_2 \right)$ etc. are now calculated between spin-orbitals w_{Ii} , of course. Varying the coefficients $\bar{C}_{i_1 i_2}^I$ and taking into account the normalization condition (with Lagrangian multipliers $-\bar{\mathcal{E}}^I$) we obtain a set of equations identical with (12) which can be solved by iteration for the lowest roots $\bar{\mathcal{E}}^I$ and the corresponding coefficients $\bar{C}_{i_1 i_2}^I$ ($I = 1, 2, \dots N$). Of course, the results strongly depend on the choice and the decomposition of the basic set w_ν . It would be a good starting point if we knew the exclusive orbitals and some oscillator orbitals of the system [11]. However, we can subject the basic set w_{Ii} decomposed intuitively to an arbitrary unitary transformation

$$v_{Ii} = \sum_{J=1}^N \sum_{j=1}^{n_J} w_{Jj} V_{Jj, Ii}, \quad (14)$$

which has to be determined so as to give the best total energy for the ground state. Substituting (14) into the energy expression (11) and varying the matrix elements $V_{Jj, Ii}$ subject to the unitarity condition, we obtain a set of equations for the $V_{Jj, Ii}$'s which has to be solved with equation (13) simultaneously. In this way we can determine the best decomposition of the basic set w_ν into N subsets v_{Ii} of given dimension n_I .

To avoid the preliminary decomposition, $\varphi_I(1|2)$ can be taken in the form

$$\varphi_I(1|2) = \sum_{\kappa, \lambda=1}^n C_{\kappa\lambda}^I w_\kappa(1) w_\lambda(2), \quad (I = 1, 2, \dots N).$$

The orthogonality conditions (5) require that

$$\sum_{\lambda=1}^n C_{\kappa\lambda}^{I*} C_{\kappa\lambda}^I = 0, \quad \text{if } J \neq I, \quad (\kappa, \lambda = 1, 2, \dots n).$$

Taking these into account with Lagrangian multipliers $-\mathcal{E}_{\kappa\mu}^{IJ}$ (and the normalization conditions with Lagrangian multipliers $-\mathcal{E}^I$) we obtain a set of equations for the coefficients $C_{\kappa\lambda}^I$. Then the matrices $\sum_{\lambda=1}^n C_{\kappa\lambda}^I C_{\mu\lambda}^{I*}$

can be diagonalized by a unitary transformation [6]. In this way we can determine the best decomposition of the basic set w_v into N subsets v_{Ji} .

Increasing suitably n , the approximation will be better, of course. To improve convergence we introduce the idea of "almost" orthogonal two-electron orbitals $\tilde{\psi}_I(1|2)$. These are defined to be solutions of the following set of equations:

$$\begin{aligned} \{\tilde{H}^I(1|2) - \tilde{E}^I\} \tilde{\psi}_I(1|2) = \sum_{\substack{J \\ J \neq I}} [\tilde{\mathcal{H}}_{Jj}^I(1) v_{Jj}(2) + \tilde{\mathcal{H}}_{Jj}^I(2) v_{Jj}(1)] \\ + \sum_{\substack{J, J' \\ J, J' \neq I}} \tilde{\mathcal{H}}_{Jj, J'j'}^I v_{Jj}(1) v_{J'j'}(2), \quad (I = 1, 2, \dots, N), \end{aligned} \quad (15)$$

where

$$\begin{aligned} \tilde{\mathcal{H}}_{Jj}^I(1) &= \int v_{Jj}^*(2) \tilde{H}^I(1|2) \tilde{\psi}_I(1|2) d\tau_2, \\ \tilde{\mathcal{H}}_{Jj}^I(2) &= \int v_{Jj}^*(1) \tilde{H}^I(1|2) \tilde{\psi}_I(1|2) d\tau_1, \\ \tilde{\mathcal{H}}_{Jj, J'j'}^I &= \int v_{Jj}^*(1) v_{J'j'}^*(2) \tilde{H}^I(1|2) d\tau_1 d\tau_2, \end{aligned}$$

$$\begin{aligned} \tilde{H}^I(1|2) &= \left\{ H(1) + H(2) + \frac{1}{r_{12}} + \right. \\ &+ 2 \sum_{J \neq I} \int d\tau_3 d\tau_4 \left[\frac{1 - P_{13}}{r_{13}} + \frac{1 - P_{23}}{r_{23}} \right] \tilde{\psi}_J(3|4) \tilde{\psi}_J(3|4) \Big\}. \end{aligned}$$

The antisymmetrical solutions $\tilde{\psi}_I(1|2)$ ($I = 1, 2, \dots, N$) of the equations, (15) corresponding to the lowest \tilde{E}^{I0} ($I = 1, 2, \dots, N$) values and satisfying the auxiliary conditions

$$\int \tilde{\psi}_I^*(1|2) \tilde{\psi}_I(1|2) d\tau_1 d\tau_2 = 1, \quad (I = 1, 2, \dots, N), \quad (16)$$

$$\begin{cases} \int v_{Jj}^*(1) \tilde{\psi}_I(1|2) d\tau_1 = 0 \\ \int v_{Jj}^*(2) \tilde{\psi}_I(1|2) d\tau_2 = 0 \end{cases} \text{ if } J \neq I, J = 1, 2, \dots, N; \quad j = 1, 2, \dots, n_J; \quad (17)$$

are the "almost" orthogonal two-electron orbitals to be found. We may assume that the equations (15) (keeping the orbitals $\tilde{\psi}_{J0}(1|2)$ fixed in them) even have further antisymmetric solutions $\tilde{\psi}_{I1}, \tilde{\psi}_{I2}, \dots$ corresponding to excited states, which also satisfy the auxiliary conditions (16) and (17). The solutions belonging to the same operator $\tilde{H}^I(1|2)$ are orthogonal to one another in the usual sense. The strong orthogonality conditions (5) do not hold for the solutions $\tilde{\psi}_I$ exactly

$$\int \tilde{\psi}_I^*(1|3) \tilde{\psi}_J(1|2) d\tau_1 \neq 0, \text{ if } J \neq I.$$

They are, however, satisfied approximately as we shall show below. The solutions $\tilde{\psi}_I$ can be written in the following form

$$\tilde{\psi}_I(1|2) = a_I^{-\frac{1}{2}} [\varphi_I(1|2) + f_I(1|2)], \quad (18)$$

where

$$a_I = 1 + \int f_I^*(1|2) f_I(1|2) d\tau_1 d\tau_2, \quad (19)$$

$$\int \varphi_I^*(1|2) f_I(1|2) d\tau_1 d\tau_2 = 0, \quad (19)$$

$$\left. \begin{aligned} \int v_{jI}^*(1) f_I(1|2) d\tau_1 &= 0 \\ \int v_{jI}^*(2) f_I(1|2) d\tau_2 &= 0 \end{aligned} \right\} \text{ if } J \neq I, \quad (I, J = 1, 2, \dots, N; \quad j = 1, 2, \dots, n_j). \quad (20)$$

Thus

$$\int \tilde{\psi}_I^*(1|2) \tilde{\psi}_J(1|3) d\tau_1 = \int f_I^*(1|2) f_J(1|3) d\tau_1, \quad (21)$$

are of second order in the functions f_I , consequently, the energy expression

$$\begin{aligned} \tilde{E} = H(0) + \sum_I \int \tilde{\psi}_I^*(1|2) \left[H(1) + H(2) + \frac{1}{r_{12}} \right] \tilde{\psi}_I(1|2) d\tau_1 d\tau_2 + \\ + 2 \sum_{\substack{I, J \\ J \neq I}} \int d\tau_1 d\tau_2 d\tau_3 d\tau_4 \frac{1 - P_{13}}{r_{13}} \tilde{\psi}_J^*(3|4) \tilde{\psi}_J(3|4) \tilde{\psi}_I^*(1|2) \tilde{\psi}_I(1|2), \end{aligned} \quad (22)$$

is only correct up to first order. Thus, \tilde{E} may be lower than the exact non-relativistic energy of the system. To avoid this we calculate the energy with the expression

$$\mathcal{E} = \int \Psi H \Psi d\tau, \quad (23)$$

where

$$\begin{aligned} \Psi \sim \sum_P (-1)^P P \left\{ \varphi_1(1|2) \dots \varphi_I(2I-1|2I) \dots \varphi_N(2N-1|2N) + \right. \\ \left. + \sum_{I=1}^N \varphi_1(1|2) \dots f_I(2I-1|2I) \dots \varphi_N(2N-1|2N) \right\}. \end{aligned}$$

In this case \mathcal{E} is always lower than $E^{(0)}$, nevertheless the former is an upper bound to the exact non-relativistic energy of the system. In most cases \mathcal{E} is lower than the energy E obtained by the exact two-electron orbitals orthogonal in the strong sense. Suitably increasing the basic set w_p , at least in principle, the terms of (21) type can be put as small as desired, at the same time $E^{(0)}$ and \mathcal{E} will tend to E .

Instead of solving the set of equations (15) directly we can determine the two-electron orbitals $\tilde{\psi}_I$ variationally. We choose suitable antisymmetrical trial functions $g_I(1|2)$ which contain many variational parameters and are flexible enough to account for the electronic correlation. Then we orthogonalize them to satisfy the conditions (19) and (20) as was done in the case of the functions f_I . As a result we obtain functions of the form

$$\begin{aligned} \bar{f}_I(1|2) \sim & g_I(1|2) - \sum_{\substack{JJ' \\ J \neq I}} \int d\tau_3 \{ g_I(3|2) v_{JJ'}^*(3) v_{JJ'}(1) + \\ & + g_I(1|3) v_{JJ'}(3) v_{JJ'}(2) \} + \sum_{\substack{JJ', J'' \\ J \neq I}} \int d\tau_3 d\tau_4 g_I(3|4) v_{JJ'}^*(3) v_{JJ''}^*(4) v_{JJ'}(1) v_{JJ''}(2) - \\ & - \int d\tau_3 d\tau_4 g_I(3|4) \varphi_I^*(3|4) \varphi_I(1|2). \end{aligned}$$

Substituting these in the energy expression (23) and minimizing the energy we get approximate \bar{f}_I 's which belong to $\tilde{\psi}_I$ functions corresponding to the ground state. This variational procedure can be applied to determine also two-electron orbitals $\tilde{\psi}_{I1}, \tilde{\psi}_{I2}, \dots$ belonging to the excited states.

The above methods can be easily generalized to the derivation of "almost" orthogonal many-electron (group) orbitals.

REFERENCES

1. E. KAPUY, Acta Phys. Hung., **12**, 185, 1960.
2. E. KAPUY, Acta Phys. Hung., **12**, 351, 1961.
3. A. C. HURLEY, J. E. LENNARD-JONES and J. A. POPLE, Proc. Roy. Soc. A, **220**, 496, 1953.
4. J. M. PARKS and R. G. PARR, J. Chem. Phys., **28**, 335, 1958.
5. E. KAPUY, Acta Phys. Hung., **9**, 237, 1958.
6. T. ARAI, J. Chem. Phys., **33**, 95, 1960.
7. P. O. LÖWDIN, Phys. Rev., **97**, 1474, 1490, 1509, 1955.
8. R. MCWEENY, Proc. Roy. Soc. A, **232**, 114, 1955.
9. A. C. HURLEY, Proc. Roy. Soc. A, **235**, 224, 1956.
10. E. KAPUY, Acta Phys. Hung., **11**, 409, 1960.
11. J. M. FOSTER and S. F. BOYS, Rev. Mod. Phys., **32**, 300, 1960.

ON THE LUMINESCENCE OF MANGANOUS PHTALATE

By

E. LENDVAY and J. SCHANDA

RESEARCH INSTITUTE OF TECHNICAL PHYSICS OF THE HUNGARIAN ACADEMY OF SCIENCES, BUDAPEST

(Received: 2. V. 1961)

In the research into luminescence the examination of pure salts has become of ever growing importance. In connection with this we have set ourselves the task of examining the luminescent behaviour of the manganous ion, that is of great importance in luminescence, in unactivated Mn compounds.

As it is known, Mn shows as an activator a characteristic red light in several inorganic salts. Apart from the luminophors made with double activation, a typical Mn band is shown by $\text{ZnF}_2 : \text{Mn}$, $\text{ZnS} : \text{Mn}$, $\text{Cd}_2\text{B}_2\text{O}_5 : \text{Mn}$, $\text{CdS} : \text{Mn}$ etc. The emission band of these phosphors is between 560 and 640 nm.

The luminescent intensity of the pure manganous salts is considerably lower and it appears in several cases only at low temperature. So e. g. the MnSiO_3 , MnCl_2 , Mn acetate shows a weak red emission. As these materials have not been put to practical use as far as now, the characteristic properties of the Mn salts have hardly been examined and only a few references can be found in the literature concerning this topic.

Among the above-mentioned Mn^{2+} salts the Mn acetate containing the organic anion is of special interest, because the interaction between the lattice and the activator seems to be simpler than in the case of other crystal phosphors.

In the form of Mn phthalate we have found a manganic luminophor with an organic anion, but with better luminescent properties. The mentioned compound might be produced from a Na or K phthalate solution in the presence of Mn^{2+} ions on the effect of heating. The luminous properties of the resulting compound are independent of the anion of the manganous ion. Acetate, bromide, chloride as well as sulphate were used in our experiments. The pH of the medium has a strong effect on the development of the compound; probably this is why we did not succeed in producing it from phthalic acid and manganous salts. The so-produced compound is insoluble in water or organic solvents. Its X-ray diffraction pattern showed a crystalline structure. The photoluminescent spectrum of the luminophor was measured. As irradiation source we have used a medium pressure mercury lamp screened by UG-11 and BG-12 coloured Shott-

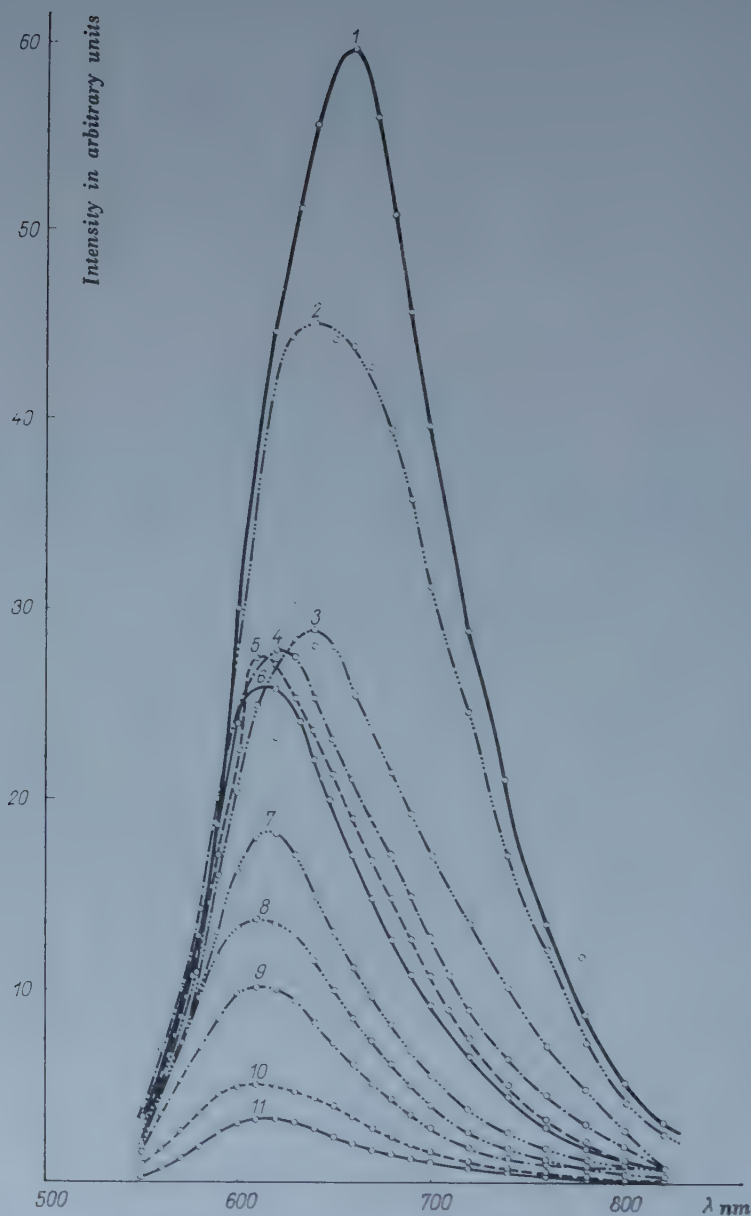


Fig. 1. Spectral energy distribution of a manganous phthalate sample at different temperatures, in arbitrary units. Curve 1: -112°C ; Curve 2: -105°C ; Curve 3: -88°C ; Curve 4: -70°C ; Curve 5: -57°C ; Curve 6: -29°C ; Curve 7: -7°C ; Curve 8: $+15^{\circ}\text{C}$; Curve 9: $+34^{\circ}\text{C}$; Curve 10: $+58^{\circ}\text{C}$; Curve 11: $+83^{\circ}\text{C}$

glasses. On irradiation with the 254 nm mercury line the phosphor does not light.

Fig. 1 shows the spectral energy distribution at different temperatures. It can be seen that the intensity of the emission as well as the wavelength of its maximum changes with temperature. With increasing temperature this maximum is shifted towards the shorter wavelengths. Further on it can be seen that as the temperature is increased an extinction takes place. Fig. 2 shows the temperature dependence of the intensity resp. wavelength of the maximum. The maximum of the emission band lies in the wavelength interval characte-

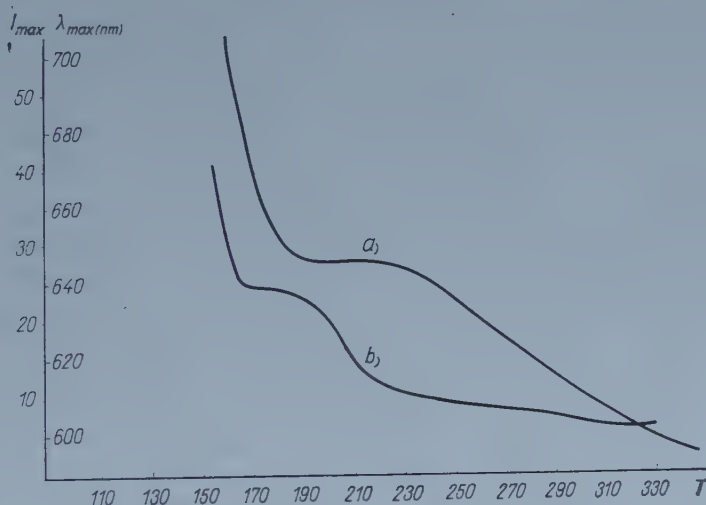


Fig. 2. Temperature dependence of the maximal intensity (curve a) and temperature dependence of the wavelength of the maximal intensity (curve b)

istic for the Mn band. The luminescent properties of this compound are similar to that of the Mn acetate, so there are good hopes that in these materials a possibility will arise for the direct investigation of the luminescent properties of the manganous (or manganic) ion.

We will revert to further experimental details resp. to the interpretation of our results in due time.



A NOTE ON THE NUCLEIC ACID — PROTEIN CODING PROBLEM

By

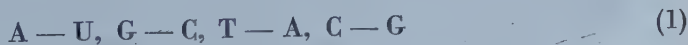
J. LADIK

CENTRAL RESEARCH INSTITUTE FOR CHEMISTRY OF THE HUNGARIAN ACADEMY OF SCIENCES, BUDAPEST

(Received: 23. V. 1961)

It is generally assumed in biochemical genetics that the genetic information carried by the deoxyribonucleic acid (DNA) molecule is determined by the sequence of the nucleotide bases in this molecule. Very likely, this information is transferred in a first step from DNA to ribonucleic acid (RNA) and in a second step the sequence of the nucleotide bases in RNA determines ("codes") the sequence of amino acids in the protein molecule [1], [2]. On the other hand, CRICK's [1] assumption that no information can be transferred from protein to nucleic acid or from protein to protein is generally accepted. Therefore, the sequences of the four kinds of nucleotide bases: adenine (A), thymine (T), guanine (G) and cytosine (C) of the DNA molecules of a cell determine through RNA molecules those proteins which can be built up in the cell under consideration. Since all possible biochemical reactions in a cell are determined by their specific protein catalysators (enzymes), the genetic information carried by the DNA molecules of a cell determines all chemical reactions in the cell in question.

The coding problem of the first step (DNA \rightarrow RNA) is the simpler. RNA also consists of four kinds of nucleotide bases: A, G, C and instead of thymine, uracil (U). Thus a four-letter alphabet must be coded with the help of another four-letter alphabet. In the literature diverse coding principles for the solution of this problem [3], [4], [5], [6] have been published. In the light of recent investigations [2] it seems probable that for unicellular organisms the coding principle of RICH [3] is valid, according to whom the base sequence of a single DNA helix determines the base sequence of the complementary RNA helix, through the well-known



WATSON—CRICK correlations [7] (here, at the left, stands the base of DNA, at the right that of RNA). For multicellular organisms it is, however, the coding principle of ZUBAY [4] which seems to be valid [2]. According to this, a nuc-

leotide base of RNA is determined by a base pair of the DNA double helix, namely:



(Here again on the left stands the nucleotide base pair of DNA and on the right the coded base of RNA.)

It is to be noted that though the molecular mechanism of this coding scheme is not clear, it was experimentally found to be in agreement with the base compositions of the DNA and RNA macromolecules of the multicellular organisms.

At present, the problem of the RNA-protein coding is far from being solved, as here the four different bases of RNA have to code the twenty different amino acids of the protein molecules [8]. The twenty different amino acids cannot be coded by dinucleotides because there exist but $4^2 = 16$ different dinucleotide combinations. As a first requirement for the coding principle it is therefore stated that at least three nucleotides can code one amino acid [8]. From the study of the known protein compositions and sequences it results further that these amino acid determining sites of RNA are independent and share no nucleotides with their neighbours. In other words, the code is not "overlapping". This second requirement follows from the fact that the amino acids have different frequencies in the proteins [8]. It is, therefore reasonable to believe that the coding principle itself imposes certain differences in frequency on the various amino acids.

When working with three nucleotides — one amino acid codes, two problems will arise: 1) Three nucleotides give $4^3 = 64$ possible combinations, but only 20 amino acids are to be coded by them. In other words, only $\log_2 20 = 4,32$ bits information content is necessary to determine one amino acid, whereas a trinucleotide has $\log_2 64 = 6$ bits information content. The coding scheme has thus $6,00 - 4,32 = 1,68$ bits /amino acid redundancy. The first problem is thus to select those 20 trinucleotides among the 64, which will really code the 20 amino acids. 2) After the solution of the first problem, it would be necessary to correlate to each amino acid the trinucleotide which codes it.

We are still very far from the solution of the second problem and consequently the whole RNA-protein coding principle is an unsolved question. As regards the first problem, however, some attempts at a solution are to be found in the literature. GAMOW [9] has recognized that by disregarding the sequences of the trinucleotides, and by taking into account only the compositions of them, we get exactly 20 different trinucleotides. These are the following:

A	G	U	C	A, A}G, or U, or C	
A	G	U	C	5—7.	
A	G	U	C	G, G}A, or U, or C	
1.	2.	3.	4.	8—10.	
				U, U}A, or G, or C	(3)
				11—13.	
				C, C}A, or G, or U	
				14—16.	
A, G, U	A, U, C	A, G, C	G, U, C		
17	18.	19.	20.		

It is to be noted that here the letters mark only the bases present in the trinucleotide and these bases can be arranged in any kind of order.

YČAS [8] showed that the advantage of this coding scheme lies in that it can impose differences in frequency on various amino acids. The amino acid namely which is coded by the trinucleotide of A, G, U composition, for instance, must be 6-times as frequent (6 being the number of different sequences with composition A, G, U) as the amino acid coded by the AAA trinucleotide, which has only 1 configuration. Here, however, the *a priori* equiprobability of each sequence of the three nucleotides is assumed. It is further to be mentioned in connection with this scheme that a scheme which disregards the sequence of the symbols can by no means be taken as a coding scheme in an information theoretical sense. From a physicochemical point of view it equally seems very improbable that the sequences of the bases in the trinucleotides should play no role in the selection of the amino acids.

CRICK [10] and his coworkers have proposed another scheme taking into account also the sequences of the bases in the trinucleotides. They assume that 20 of the possible 64 trinucleotides are "sense sites" which correspond to an amino acid, while the remaining 44 trinucleotides are "non-sense sites", which do not correspond to any amino acid. The 20 sense sites are selected with the solution of the so-called "punctuation mark problem". On the supposition that three bases determine one amino acid, the problem arises namely why the $3n + 1$, $3n + 2$, $3n + 3$ bases do determine one amino acid, while $3n + 2$, $3n + 3$, $3n + 4$ do not. These authors take as sense trinucleotides all those triplets which, when placed next to each other in any possible combination, give sense sites only at positions $3n + 1$, $3n + 2$, $3n + 3$, but not otherwise. For example, the triplet GGG is a non-sense site because when placed next to itself, it gives the sequence GGGGGG. The site is not unambiguously defined, as the GGG triplet occurs at the 1—3, 2—4, and 3—5 positions. CRICK and his coworkers have found that there are exactly 20 trinucleotides which satisfy the above criterion as follows:

A	G	A	G	C	A	G	C	A	G
G	G	C	C	C	C	C	C	U	U
A	A	A	A	A	G	G	G	A	A
1.	2.	3.	4.	5.	6.	7.	8.	9.	10.
C	U	A	G	C	U	A	G	C	U
U	U	U	U	U	U	U	U	U	U
A	A	G	G	G	G	C	C	C	C
11.	12.	13.	14.	15.	16.	17.	18.	19.	20.

(4)

In connection with this scheme it is to be noted that it has the advantage of taking into account the sequence of the bases. It has, however, the following disadvantages: a) the solution of the "punctuation mark problem" as selection criterion for the "sense" triplet seems rather artificial (this problem could be solved also if amino acids were selected in a sequential manner starting from one end of RNA and if *each* triplet is able to select an amino acid as in GAMOW's scheme). b) Assuming equiprobability for each triplet the above scheme cannot explain the differences in the frequency of the various amino acids. c) When only certain triplets of RNA are able to select an amino acid there will be other "non-sense" triplets left between the "sense sites" and so the "sense sites" of RNA will be separated in space from each other. Thus the stereochemical problem comes up: how can the amino acids coded by these separated sites react with each other in order to form peptide bonds. It is, however, to be remembered that, when instead of being in an extended or in a helical configuration the RNA molecule is but folded, this problem gets considerably reduced.

It will be shown that, when departing from the assumption of the equiprobability of all possible trinucleotides, the twenty most probable sequences can be selected in an entirely natural way. According to the WATSON—CRICK stereomodel of DNA [7] the nucleotide bases of one helix are situated at a distance of 3,36 Å from each other in parallel planes. On the basis of this stereopicture the existence of a fairly considerable interaction of the π -electrons of these bases could be shown [11]. The calculation of the quantum mechanical overlap integrals between these bases had further the result that, when a purine (Pu) type base is under¹ another Pu type base, or a pyrimidine (Py) type base is under one of the Py type, or finally when a Pu type base is under a Py type one the interaction is large, while when a Py type base is under a base of the Pu type, the interaction is small.² Since by this interaction the binding energy

¹ The DNA double helix being a right handed helix, a direction for the sequence of nucleotides can be defined.

² The Pu type bases are A and G, the pyrimidine type bases are T and C.

of the macromolecule is increased and since each system tends towards the most stable configuration, it seems plausible to suppose for the probabilities of the dinucleotides the inequality

$$P(P_U/P_U), P(P_Y/P_Y), P(P_Y/P_U) > P(P_U/P_Y). \quad (5)$$

Here $P(A|B)$ is the conditional probability for that case when the base B is under the base A (A_B). The inequality (5) is also supported by the experimental work of SHAPIRO and CHARGAFF [12], who have found that in DNA, 70 percent of the bases are arranged in PuPuPu... or PyPyPy type sequences and only 30 per cent of them are to be found in PuPyPuPy... type sequences.

Besides the criterion of great overlapping a second criterion for the strong interaction of the nucleotide bases of DNA is the maximum possible neighbourhood of the same kind of bases. Namely, from the quantum mechanical perturbation theory it is well known that in case of the same interaction potential, systems with identical eigenstates interact by the maximum amount. So the DNA molecule is the most stable when as many nucleotide bases of the same kind are adjacent as possible. Therefore we may write:

$$\begin{aligned} \mathbf{P}(\mathbf{G}/\mathbf{G}) &\approx \mathbf{P}(\mathbf{A}/\mathbf{A}) > \mathbf{P}(\mathbf{G}/\mathbf{A}) \approx \mathbf{P}(\mathbf{A}/\mathbf{G}), \\ \mathbf{P}(\mathbf{C}/\mathbf{C}) &\approx \mathbf{P}(\mathbf{U}/\mathbf{U}) > \mathbf{P}(\mathbf{U}/\mathbf{C}) \approx \mathbf{P}(\mathbf{C}/\mathbf{U}). \end{aligned} \quad (6)$$

With the aid of the inequalities (5) and (6) we may now select the most probable 20 trinucleotides of a DNA helix in the following manner: 1) Put in the GAMOW's "composition scheme" the same bases, always in adjacent positions. 2) At 5—16 compositions of (3) regard only the $\frac{P_u}{P_u}, \frac{P_y}{P_y}, \frac{P_y}{P_u}$ type sequences, but disregard the $\frac{P_u}{P_y}$ type sequences. 3) Disregard the 17—20 compositions which consist of 3 different nucleotides. In this way we arrive at the

A	G	U	C		G	A	U	C		A	G	U	C
A	G	U	C		A	A	A	A		G	G	G	G
A	G	U	C		A	G	A	A		G	A	G	G
1.	2.	3.	4.		5.	6.	7.	8.		9.	10.	11.	12.
			U	U	C	U		C	C	U	C		
			U	U	U	U		C	C	C	C		
			A	G	U	C		A	G	C	U		
			13.	14.	15.	16.		17.	18.	19.	20.		

(A, G Pu type; U, C Py type)

coding scheme.³ The trinucleotides must be read from the bottom upwards.

³ It is to be noted that when we are taking into account only condition (5) and thus allow also PuPy combinations in the triplets, we get a scheme of 28 trinucleotides, whereas disregarding condition (6) gives a scheme of 32 triplets.

From the most probable (1) and (2) DNA—RNA coding principles it is seen that each DNA base triplet of the scheme (7)⁴ gives a trinucleotide of RNA which is always a member of the scheme (7). Thus the scheme (7) gives also the 20 most probable trinucleotides of RNA. When we define these 20 most probable trinucleotide sequences of RNA as amino acid selecting sites ("sense sites") we come to a coding scheme which selects (among 64) the 20 amino acid coding triplets in a physically more plausible way than CRICK and his coworkers have done. Furthermore, since the frequency of the triplets in scheme (7) may also be very different, the scheme does not contradict the frequency differences found experimentally in the various amino acids. The estimation of the frequencies of the triplets in scheme (7) is in progress. Finally, if the 20 most probable triplets of RNA are selected as "sense sites", the redundancy of the RNA code (the frequency of "non-sense sites") is decreased and with it the above-mentioned stereochemical difficulties also are further lessened.

I wish to express my gratitude to Academician J. ERNST for calling my attention to the above problem, to Academician F. B. STRAUB and T. A. HOFFMANN, Doctor of Physical Sciences, for helpful discussions and to Prof. B. GYÖRFFY for calling my attention to valuable data in the literature.

LITERATURE

1. F. H. C. CRICK, *Symp. Soc. Exp. Biol.*, **12**, 138, 1958.
2. I. LESLIE, *Nature*, **189**, 260, 1961.
3. A. RICH, *Ann. N. Y. Acad. Sci.*, **81**, 709, 1959.
4. G. ZUBAY, *Nature*, **182**, 112, 1958.
5. G. S. STENT, *Adv. Vir. Res.*, **5**, 95, 1958.
6. R. L. SINSHEIMER, *J. Mol. Biol.*, **1**, 218, 1959.
7. J. D. WATSON and F. H. C. CRICK, *Nature*, **171**, 737, 1953.
8. M. YČAS, *Symp. on Information Theory in Biology*, Pergamon Press, London, New York, Paris, 1958, p. 70.
9. G. GAMOW, *Dansk. Biol. Medd.*, **22**, No 3, 1954; G. GAMOW, *Symp. on Information Theory in Biology*, Pergamon Press, London, New York, Paris, 1958, p. 63.
10. F. H. C. CRICK, J. S. GRIFFITH and L. E. ORGEL, *Proc. Nat. Ac. Sci. Wash.*, **43**, 416, 1957.
11. J. LADIK, *Acta Phys. Hung.*, **11**, 239, 1960.
12. H. S. SHAPIRO and E. CHARGAFF, *Biochem. Biophys. Acta*, **23**, 451, 1957.

⁴ Putting into the scheme (7) T instead of U.

NEUERE MESSUNGEN ZUR LEITFÄHIGKEIT VERFORMTER STEINSALZKRISTALLE

Von

B. JESZENSZKY und J. KISS

INSTITUT FÜR EXPERIMENTELLE PHYSIK DER TECHNISCHEN HOCHSCHULE FÜR
BAU- UND VERKEHRSWESEN, BUDAPEST

(Eingegangen 10. XI. 1961)

Wir haben die zuerst von GYULAI und HARTLY [1] beobachteten Leitfähigkeitssprünge, die an einseitig gedrückten synthetischen und natürlichen NaCl-Einkristallen zustande kommen, mit einer verfeinerten Methode untersucht. Zugleich untersuchten wir die von FISCHBACH und NOWICK [2] beobachtete Ladungsbewegung in inhomogenen gepressten Kristallen.

Die Beobachtungen haben wir mit der ursprünglichen Messeinrichtung von GYULAI und HARTLY durchgeführt, und auch die Messmethode war dieselbe: Strommessung mit Elektrometernaufladung, nur wurde jetzt die Bewegung des Elektrometerfadens nicht mit dem Auge beobachtet, sondern mittels eines Filmaufnahmeapparates zusammen mit einer Skala photographiert. Dadurch konnten 8, 16, 24 bzw. 64 Messdaten in einer Sekunde erhalten werden. Wir benutzten ein Einfadenelektrometer der Firma Zeiss. Die Auswertung der Filme geschah in bequemer Weise durch Projektion der Aufnahmen. Die Messungen wurden bei einer Temperatur von 50° C durchgeführt. Die Kristallstückchen waren 1—4 mm dick und hatten einen Querschnitt von 0,5 cm².

Die Empfindlichkeit des Elektrometers war 5—10 Skalenteile pro 1 Volt Spannung. An die Kristalle wurde 200—300 Volt Spannung angelegt.

Wir haben die folgenden Messungen durchgeführt:

1. Wiederholung der Messung des GYULAI—HARTLY Druckeffektes an natürlichen Steinsalzkristallen aus Wieliczka.

2. Ladungsfluss natürlicher Steinsalzkristalle bei asymmetrischer Belastung. Unsere Ergebnisse können wir im folgenden zusammenfassen:

1. Die Stromsprünge des schon seit langem bekannten Druckeffektes bestehen, wie die Beobachtung mit feinerer Zeitauflösung zeigt, aus mehreren Teilsprüngen.

2. In den synthetischen NaCl-Kristallen gibt es innere (mechanische und elektrische) Anisotropien, die im Falle einer plastischen Verformung auch ohne äussere Spannung das Elektrometer aufladen.

3. Bei der Wiederholung der asymmetrischen Belastungsversuche von FISCHBACH und NOWICK zeigte es sich, dass die Stromsprünge auch bei diesen Messungen in Teilsprünge aufgespalten sind.

4. Bei Anwendung paralleler Elektroden ist ein Ladungsfluss ohne äussere Spannung nur bei synthetischen Kristallen zu beobachten.

Die Versuche werden weiter fortgeführt. Wir danken Herrn Prof. Z. GYULAI für seine vielen wertvollen Ratschläge und sein stetiges Interesse an unserer Arbeit. Ebenso danken wir Herrn Dipl.-Phys. E. HARTMANN für wertvolle Diskussionen.

LITERATUR

1. Z. GYULAI und D. HARTLY, *ZS. f. Phys.*, **51**, 378, 1928.
2. D. B. FISCHBACH and A. S. NOWICK, *J. Phys. Chem. Solids*, **5**, 302, 1958.

Printed in Hungary

A kiadásért felel az Akadémiai Kiadó igazgatója

Műszaki szerkesztő: Farkas Sándor

A kézirat nyomdába érkezett: 1961. IX. 25. — Terjedelme: 9,75 (A/5) ív, 35 ábra

1961.54110 — Akadémiai Nyomda, Budapest — Felelős vezető: Bernát György

ACTA PHYSICA

TOMUS XIII

INDEX

<i>J. Levy</i> : Les trajectoires du champ unifié. — <i>Я. Лэви</i> : О траекториях объединенного поля	1
<i>I. Abonyi</i> : Classical Relativistic Motion of a Pole Particle under the Action of External and Proper Scalar Fields. — <i>И. Абони</i> : Классическое релятивистическое движение точечной частицы под действием внешнего и собственно скалярного поля	11
<i>K. L. Nagy</i> : Propagators with Dipole Ghosts for Fermion Fields. — <i>К. Л. Надь</i> : Функции распространения с дипольным духом для фермионных полей	21
<i>A. Ádám, L. Bod and L. Pál</i> : Measurement of Thermal Neutron Diffusion Parameters in Water and in Solid Diphenyl with Pulsed Neutron Source. — <i>А. Адам, Л. Бод и Л. Пал</i> : Определение параметров диффузии тепловых нейтронов в воде и в твердом дифениле при помощи импульсного метода	25
<i>R. S. Ingarden</i> : Informationstheorie, Bohr—Rosenfeldsche Unbestimmtheitsrelationen und das Problem der optimalen optischen Abbildung. — <i>Р. С. Ингарден</i> : Теория информации, соотношения неопределенности Бора—Розенфельда и проблема оптимального оптического изображения	35
<i>T. Tietz</i> : Some Practical Remarks Concerning the Calculation of the Phase Shifts of the Yukawa Potential. — <i>Т. Тимц</i> : Несколько практических замечаний относительно вычисления сдвига фаз потенциала Юкава	57
<i>J. Weiszburg</i> : Electroluminescence at Low Voltage. — <i>Я. Вейсбург</i> : Электролюминесценция при низком напряжении	61
<i>A. Lőrinczy and G. Pataki</i> : Reverse Characteristics of Germanium Junction Diodes. — <i>А. Леринци и Г. Патаки</i> : О характеристике германиевых плоскостных диодов в запиорном направлении	67
<i>Armin Uhlmann</i> : Über eine Klasse dynamischer Grössen. — <i>А. Ульманн</i> : Об одном классе динамических величин	75
<i>G. Domokos</i> : On the High Energy Behaviour of the Pion-Nucleon Elastic Scattering Amplitude. — <i>Г. Домокош</i> : О поведении амплитуды упругого п-н рассеяния при больших энергиях	89
<i>I. Biró</i> : Zur Berechnung der Grüneisenschen Konstante des metallischen Silbers. — <i>И. Биро</i> : Определение постоянной Грюнайзена металлического серебра	99
<i>T. A. Hoffmann and J. Ladik</i> : A Possible Interpretation of the Carcinogenic Effect of Radiations and Carcinogenic Hydrocarbons on the Basis of the Electronic Structure of Deoxyribonucleic Acid	103
<i>T. A. Hoffmann, J. Ladik and A. Udvardy</i> : An Attempt to Explain the Anticarcinogenic Activity of Some Nucleotide-Base Antimetabolites by the Electronic Structure of Deoxyribonucleic Acid	113

<i>G. Pataki</i> : Application of Irreversible Thermodynamics in the Theory of Recombination in Semiconductors	119
<i>J. Ladik</i> : The Ground State of the Hydrogen Molecule on the Basis of Relativistic Quantum Mechanics with the Aid of the Wang Wave Function. II. — <i>Й. Ладик</i> : Трактровка основного состояния молекулы водорода на основе релятивистической квантовой механики при помощи волновой функции Уанга II.	123
<i>J. Ladik</i> : Approximate Determination of the Most Important Radiation Correction Energy Terms for the Ground State of the Hydrogen Molecule. — <i>Й. Ладик</i> : Приближенное определение важнейших коррекционных членов энергии излучения в случае основного состояния молекулы водорода	139
<i>K. Ladányi and P. Szépfalussy</i> : An Approximate Solution of a Generalized Statistical Model. — <i>К. Ладани и П. Сепфалуши</i> : Приближенное решение обобщенной статистической модели	145
<i>M. Schubert und B. Wilhelmi</i> : Über die Möglichkeit der Bestimmung molekularer Dipolmomente aus der statistischen Theorie. — <i>М. Шуберт и Б. Вильгельми</i> : О возможностях определения дипольных моментов молекул в статистической теории	155
<i>L. Medveczky and G. Somogyi</i> : Range of Protons in the Agfa K2 Nuclear Emulsion. — <i>Л. Медвецки и Г. Шомодьи</i> : Пробег протонов в ядерной эмульсии Agfa K2	163
<i>L. Ernst</i> : Examination of Tantalum Monocrystal Tips by Means of a Field Emission Microscope. — <i>Л. Эрнст</i> : Исследование вершин танталовых монокристаллов пространственно эмиссионным микроскопом	169
<i>Э. Лендвай, Я. Шанда и Я. Вейсбург</i> : Примечания к электролюминесценции ZnS.Cu:Mn на постоянном и переменном токе — <i>E. Lendvay, J. Schanda and J. Weiszburg</i> : Some Remarks on the D. C. and A. C. Electroluminescence of ZnS. Cu : Mn	183
<i>G. Lakatos and J. Bitó</i> : On Moving Striations of Low-Pressure Mercury Discharges. — <i>Г. Лакатош и Я. Бито</i> : О движении слоев в разрядной трубке ртутных паров низкого давления	193
<i>Н. А. Измаилов, Ю. А. Кругляк, Р. Гашипар, И. Тамашши—Лентеи</i> : Квантово-механический расчёт протонного сродства — <i>N. A. Ismailov, J. A. Krugliak, R. Gáspár and I. Tamásy-Lentei</i> : Quantum-Mechanical Calculation of Proton Affinity	203
<i>Z. Füzeszy</i> : Die Bestimmung der Elektronendichte des J-Atoms auf Grund des statistischen Atommodells. — <i>З. Фюзеш</i> : Определение плотности электронов атома J на основе статистической теории	211
<i>A. Kónya</i> : Über die Reihenfolge der Besetzung der Quantenzustände in Atomen. — <i>А. Коня</i> : О порядке очереди заполнения квантовых состояний в атоме .	219
<i>P. Gombás</i> : Über die Korrelationsenergie und das Korrelationspotential eines Elektronengases. — <i>П. Гомбаш</i> : О корреляционной энергии и корреляционном потенциале электронного газа	233
<i>Zs. Csoma</i> : Die Impulsverteilung der Nukleonen im Atomkern.....	241
<i>G. Lakatos and J. Bitó</i> : The Influence of External Resistance on the Moving Striations of the Positive Column	245
<i>E. Lendvay</i> : Luminescence of Adsorbed Fluorescein	249
<i>J. Antal</i> : E. v. Angerer, Technische Kunstgriffe (Buchbesprechung)	253

G. Pócsik : Many-Body Propagators of a Self-Coupled Spinor Field in Edwards-Lieb's Approximation. — Г. Почик: Функции распространения многих тел самосвязанного спинорного поля в приближении Эдвардса-Либса	255
J. Szabó und Cs. Hargitai : Die Eindeutigkeit der magnetohydrodynamischer Strömung barotroper, leitender Medien — Й. Сабо и Ч. Харгитаи: Однозначность магнито-гидродинамического течения для баротропической, направленной среды	265
G. Lakatos and J. Bitó : Time Dependence of Some Parameters of A. C. Discharges. — Дь. Лакатош и Я. Бито: Зависимость некоторых параметров газового разряда переменного тока от времени	271
A. Szalay and A. Kovách : Fission Product Precipitation from the Atmosphere in Debrecen, Hungary, between 1958 and 1960. — А. Салаи и А. Ковач: Осаждение продуктов деления из атмосферы в г. Дебрецен в Венгрии в 1958—1960 гг.	281
E. Lendvai : Luminescence of Fluorescein Activated Layer Phosphors. — Э. Лендвай: Люминесценция адсорбированного на $Al_2O_3 \times H_2O$ пленках флуоресцеина ...	289
I. Kovács : Investigation of the $^3\Pi$ State of the PH Molecule. — И. Ковач: Исследование $^3\Pi$ -состояния PH-молекулы	303
G. Pataki : On the Time Dependence of Irreversible Processes. — Дь. Патаки: О временной зависимости необратимых процессов	311
A. Frenkel : Semi-Classical Description of High-Energy Electron Scattering on Heavy Nuclei. — А. Френкель: Квазиклассическое описание рассеяния электронов больших энергий на тяжелых ядрах	321
E. Lendvai : The Role of Surface Hydroxyls of $Al_2O_3 \cdot xH_2O$ in the Luminescence of Adsorbed Fluorescein Molecules. — Э. Лендвай: Роль поверхностных гидросильных групп $Al_2O_3 \times H_2O$ в люминесценции адсорбированного флуоресцеина	333
P. Vértés : On the K-Mesonic Interaction of Muons	341
E. Kapuy : Configuration Interaction for Wave-Functions Constructed of Orthogonal Many-Electron Group Orbitals.	345
Z. Morlin und L. Malicskó : Färbung von Natriumchloridpulver durch Exoelektronen	353
T. Tietz : An Analytical Expression for the Potential Energy Function of Diatomic Molecules	359
T. Tietz : The Uncertainty Principle and the Bohr Theory	363
J. Horváth : Uno Ingard, William L. Kraushaar, Introduction to Mechanics, Matter and Waves (Book review)	367
L. Bozóky : L. Herforth—H. Koch: Radiophysikalisches und radiochemisches Grundpraktikum (Buchbesprechung)	368
F. Károlyházy : Über Kohärenzeigenschaften der »inkohärenten« Streustrahlung. — Ф. Карольхази: О когерентных свойствах «некогерентного» излучения рассеяния.....	371
T. A. Hoffmann : The Theory of Melting — Т. А. Гоффманн: Теория плавления	381
A. Szalay and M. Szilágyi : Investigations Concerning the Retention of Fission Products on Humic Acids. — А. Салаи и М. Силадьи: Исследования по сохранению продуктов деления в гумусовых кислотах	421
A. Szalay, J. Csikai and J. Bacsó: Critical Comments on the Investigation of the Electron-Neutrino Angular Correlation by the the Cloud Chamber Method. — А. Салаи, Й. Чикаи и Й. Бачо: Критические замечания по отношению исследования электронно-нейтринной угловой корреляции методом камеры Вильсона ...	437

<i>Hussein Elkholy</i> : A Method for Measuring the Hall Coefficient at High Temperatures. — Хуссейн Элколи: Метод для измерения коэффициента Холла при высоких температурах	447
<i>P. Gombás</i> : Zur Herleitung der Grundgleichung der statistischen Theorie des Atoms. — П. Гомбаш: К выведению основного уравнения в статистической теории атома	455
<i>E. Kapuy</i> : Derivation of "Almost" Orthogonal Two-Electron Orbitals.....	461
<i>E. Lendvay and J. Schanda</i> : On the Luminescence of Manganous Phtalate.....	469
<i>J. Ladik</i> : A Note on the Nucleic Acid — Protein Coding Problem.....	473
<i>B. Jeszenszky und J. Kiss</i> : Neuere Messungen zur Leitfähigkeit verformter Steinsalz- kristalle.	479